Visit the conference website at:

http://www.icgcm.conferenceacademy.com

Your comments are welcome.
Please send your comments to:
TBarczak@cdc.gov

The papers in these Proceedings were selected by the Organizing Committee, peer-reviewed for technical content, edited in accordance with accepted standards and accepted for final publication after meeting all criteria by the Publication Committee.

Tribute to Syd Peng on 30 Years of Ground Control

Good morning. Last night at the 30th Anniversary Banquet, we celebrated in a rather light-hearted way the 30 years of this Ground Control Conference. This morning I'd like to be a little more serious.

Thirty years ago Syd Peng was dissatisfied with the way ground control technology and research and development was being applied to the coal mines of United States, and indeed the coal mines of many countries around the world. So Syd established the International Conference on Ground Control in Mining. The Ground Control Conference is well illustrated by some of the things achieved on the front cover of the beautiful Proceedings that all you have: Academic Excellence, Guidance, Good Times, Loyalty, Laughter and Friendship, Challenging Debate, and Leadership.

But ladies and gentleman, I submit to you that there is one thing missing from the front cover, and that is that the Ground Control Conference has also saved lives. This is impossible to quantify, but there is no question that the techniques that have been discussed here and introduced to the mining industries, not only in the United States, but also in Canada and Mexico and Brazil and the United Kingdom, and Germany, and Australia, India, South Africa, China, Russia, Poland, Hungary, Austria, Czech Republic, Japan, Netherlands, – all of these countries around the world who mine coal -- there is no question that the Ground Control Conference has saved lives in the four corners of the earth.

There is nothing more precious than the lives of our coal miners around the world, who work around the clock 24/7 providing inexpensive energy that increases the standard of living of countless people throughout the world. And there is nothing more noble than saving lives. I would like to pay tribute to all of the organizers, the organizing committee and the sponsors of the Ground Control Conference; but most of all, I would like to thank Syd and his co-chairs Tom, Steve, Keith, and Chris for 30 years of a wonderful and lasting contribution to the great coal mining industries of the world.

I would like all of you to please stand, stand with me and give a nice round of applause, the likes he has never heard before, to Syd for the marvelous Ground Control Conference achievements over no less than 30 years.

Syd Peng ladies and gentlemen!

TABLE OF CONTENTS

Operator Case Histories and Experiences

1. **Characteristics of Coal Bursts in the North Fork Valley of the Gunnison River Valley, Colorado,** *C. Mark, MSHA, Pittsburgh, PA, S. Phillipson, P. Tyrna, M. Gauna, MSHA, Triadelphia, WV* 1
2. **Ultra-Close Multiple-seam Mining - Analysis and Verification,** *D. Su, L. Stull, M. Jaime, J. Lu, Consol Energy Inc., Canonsburg, PA* 14
3. **Mitigation of a Massive Sandstone Channel's Impact on a 1,500-Ft–wide Longwall Face,** *D. Su, G. Hasenfus, L. Stull, J. Lu, M. Van Dyke, S. Morgan, Consol Energy Inc., Canonsburg, PA, P. Kelley, D. Teeter, Consol Energy Inc., Claysville, PA* 22
4. **Requirements and Performance of Pumpable Cribs in Longwall Tailgate Entries and Bleeders,** *P. Zhang, M. Milam, M. Mishra, W. Hudak JR., R. Kimutis, Alpha Natural Resources, Inc., Waynesburg, PA* 27
5. **Mitigating the Effects of High Horizontal Stress on Ground Control in An Underground Stone Mine: A Case History,** *J. Ellenberger, NIOSH, Office of Mine Safety and Health Research, Pittsburgh, PA, T. Miller, East Fairfield Coal Company, North Lima, OH* 38
6. **Innovation in Rock Mechanics: Iced Tailings As Structural Backfill for the Citronen Mine, Ironbark Zinc Ltd., Greenland.,** *A. Schissler, Tetra Tech Inc., Golden, CO, G. Campbell, J. McAra, Ironbark Zinc Ltd., Perth, Australia* 43

Engineering Design Tools and Developments

7. **Calibrating the LaModel Program for Site Specific Conditions,** *K. Heasley, West Virginia University, Morgantown, WV* 48
8. **CISPM-MS: A Tool to Predict Surface Subsidence and to Study Interactions Associated with Multi-seam Mining Operations,** *Y. Luo, B. Qiu, West Virginia University, Morgantown, WV* 56

New Roof Support Product Developments

9. **The Next Generation of Cable Bolts for Improved Ground Support,** *S. Tadolini, Minova USA, Bowerston, OH, J. Tinsley, Minova USA, Marion, IL, J. McDonnell, Minova USA, Grand Junction, CO* 63
10. **Improvements in Long Tendon Support with Pumpable Resin,** *T. Meikle, Minova Australia, Wyong, Australia, S. Tadolini, Minova International, Bowerston, OH, R. Hawker, D. Polack, Minova Australia, Nowra, Australia* 70
11. **The Development and Application of Polyurethane Injectable Cable Bolts,** *D. Faulkner, Jennmar Corporation, Inc., Pittsburgh, PA* 75
12. **Aspect Ratio and Other Parameters That Affect the Performance of Burrell Can Roof Supports,** *D. Gearhart, T. Batchler, NIOSH-Pittsburgh Research Lab, Pittsburgh, PA* 80
13. **J-Crete: An Engineered Cementitious Composite Rock Coating,** *A. Campoli, J. Walls, J. Mullins, D. Faulkner, Jennmar Corporation Pittsburgh, PA 15238, Pittsburgh, PA* 89

Fundamental Research Studies

14. **The Load Transfer Properties of Post-Groutable Cable Bolts Used in the Australian Coal Industry,** *R. Thomas, Strata Engineering (Australia) Pty Ltd, Charlestown, Australia* 97
15. **Comparison of the Performance of Active and Passive Roof Bolts in An Illinois Basin Coal Mine,** *A. Ray, M. Gadde, Peabody Energy, St. Louis, MO, A. Spearing, Southern Illinois University, Carbondale, IL* 107
16. **Coupon Testing for Field Assessment of Stress Corrosion Cracking of Rock Bolts,** *D. Vandermaat, The University of New South Wales (UNSW), Sydney, Australia, E. Elias, Z. Tang, P. Craig, A. Crosky, S. Saydam, B. Hebblewhite, University of New South Wales, Sydney, Australia* 117
17. **Passive Seismic Imaging for Determination of the Longwall Rear Abutment Location,** *E. Westman, Virginia Tech, Blacksburg, VA* 123
18. **Relocating Mining-Induced Seismicity at the Trail Mountain Mine,** *M. Boltz, K. Pankow, M. McCarter, University of Utah, Salt Lake City, UT* 130
19. **Effects of Transverse Isotropy on Vertical Stresses When Multi-seam Mining under Supercritical Longwall Panels,** *A. Suchowerska, J. Carter, R. Merifield, University of Newcastle, Callaghan, Australia* 136

Pillar and Mine Design

20. **Large Scale Ground Instability Caused By Failure of Underlying Pillars: A Case Study of Dynamic Multiple Seam Interaction,** *C. Mark, MSHA, Pittsburgh, PA, L. Barker, MSHA, Mt. Hope, WV* 146
21. **Investigating Abutment Load,** *I. Tulu, K. Heasley, West Virginia University, Morgantown, WV* 150
22. **Massive Pillar ColLapse: A Room-and-Pillar Marble Mine Case Study,** *S. Phillipson, MSHA, Pittsburgh, PA* 160

Roof and Rib Control Strategies

23. **The Extraction of Main Heading Pillars with a Longwall at Nre Wongawilli Colliery,** *R. Stone, Charlestown, Australia* 169
24. **Think Like a Roof Bolt - Then Make It Scream,** *G. Smith, EMS Mining, Lebanon, OH* 179

Numerical Modeling Developments and Applications

25. **A Stability Factor for Supported Mine Entries Based on Numerical Model Analysis.,** *G. Esterhuizen, National Institute for Occupational Safety and Health, Pittsburgh, PA* 186
26. **Load Transfer Distance Calibration of a Coal Panel Scale Model: A Case Study,** *M. Larson, J. Whyatt, NIOSH - Spokane Research Laboratory, Spokane, WA* 195
27. **Pillar Design Considering the Plastic Behavior of the Coal Seam,** *A. Zingano, University Federal of Rio Grande do Sul, Porto Alegre, Brazil* 206

Rock Mass Characterization and Risk Assessment

28. **A Mine Evaluation Protocol Using Applied Rock Mechanics Techniques,** *G. Petersen, Rock Mechanics Assist, Ishpeming, MI, J. Nopola, RESPEC Consulting & Services, Rapid City, SD* 211
29. **Post-Collapse Seismicity of the Crandall Canyon Mine Using Double Difference Relocations,** *T. Kubacki, M. McCarter, K. Pankow, University of Utah, Salt Lake City, UT* 217
30. **The Estimation of Ground Control Risk By Real-Time Quantitative Visual Assessments,** *A. Garcia, Golder Associates (UK) Ltd., Burton-on-Trent, United Kingdom, P. Altounyan, A. Rostocki, Golder Associates. (UK) Ltd, Burton-on-Trent, United Kingdom* 221
31. **A Management System to Develop Occupational Health & Safety in Ground Control Operations of Underground Mines,** *K. Oraee, Stirling University, Stirling, United Kingdom, N. Oraee-Mirzamani, Imperial College London Business School, London, United Kingdom, A. Goodarzi, Ministry of Labor and Social Affairs, Tehran, Iran* 227

Subsidence Evaluation

32. **Subsidence and Uplift Prediction in German and Polish Hard Coal Mining,** *A. Preusse, H. Kateloe, RWTH Aachen University, Aachen, Germany, A. Sroka, Freiberg University of Mining & Technology, Freiberg, Germany* 235

Advancements in Ground Control Instrumentation/Monitoring

33. **Knowledge Is Power: Introducing the MIDAS, a New Permissible Datalogging System for Use in Mines,** *T. Jones, NIOSH-Pittsburgh Research Lab, Pittsburgh, PA* 245
34. **New Monitoring Technologies for Measuring the In-situ Performance of Rock Bolts,** *H. Mitri, McGill University, Montreal, Canada, A. Hyett, YiledPoint Inc., Kingston, Canada, D. Guntumadugu, McGill University, Montreal, Canada* 251

Chinese Mining Practices and Solutions

35. **Is Mining Coal at a 900M Below Surface at the Xuandong Coal Mine in China Challenging or Just Interesting Rock Mechanics?,** *W. Hartman, Geohart Consultants, Melbourne, Australia, M. Everson, SIMTARS, Brisbane, Australia, B. Pang, S. Hayes, Geohart Consultants, Melbourne, Australia?* 260
36. **Applications of Microseismic Monitoring in China's Underground Coal Mines,** *X. Wu, Z. Hosseini, ESG Solutions, Kingston, Canada, C. Liu, Xi'an University of Science and Technology, Xi'an, China, C. Trifu, ESG Solutions, Kingston, Canada* 274

Poster Session Papers

37. **Track Entry Deformation Subjected to Longwall Mining in the Overlying Seam: A Case Study,** *W. Xie, S. Jing, China University of Mining & Tech., Xuzhou, China, Y. Guo, Shanxi Coking Coal Group International Development Co., Ltd., Taiyuan, China* 279

38. **Application of Chain Conveyor Cutter (CCC) to Highwall Mininig System,** *T. Sasaoka, S. Ikuta, H. Shimada, A. Hamanaka, Kyushu University, Fukuoka, Japan, H. Takamoto, MMI Coal Tech Co. Ltd, Tokyo, Japan, K. Matsui, Kyushu University, Fukuoka, Japan*.....287
39. **The Evaluation of Empirical Coal Pillar Strength Formula Based on Uncertainty Criterion,** *N. Hosseini, Islamic Azad University, South Tehran Branch, Tehran, Iran, B. Oraee-Mirzamani, Centre for Environmental Policy, Imperial College London, London, United Kingdom, K. Oraee, University of Stirling, Stirling, United Kingdom*.....293
40. **Prediction of First Weighting Distance in Longwall Coal Mining By 3D Numerical Modeling - A Case Study,** *H. Manteqi, Azad university of south of Tehran branch, Tehran, Iran, K. Shahriar, Amirkabir University, Tehran, Iran, Tehran, Iran, R. Torabi, Shahrood University of Technology, Tehran, Iran*.....297
41. **A Review of Effective Parameters on Roof Fall During Retreat Mining in Room and Pillar Coal Mines,** *E. Ghasemi, M. Ataei, Shahrood University of Technology, Shahrood, Iran, K. Shahriar, Amirkabir University of Technology, Tehran, Iran*.....306
42. **Application of Neuro-Fuzzy Technique in Mine Support System for Ground Control,** *S. Kashyap, Central Institute of Mining and Fuel Research, CSIR (Ministry of Science & Technology, Govt. of India), Barwa Road, Dhanbad, India, D. Parhi, National Institute of Technology, Rourkela, India, A. Sinha, Central Institute of Mining and Fuel Research, Barwa Road, Dhanbad, India*.....311
43. **Determination of the Strength of Powered Roof Supports According for Fatigue Life,** *M. Polak-Micewicz, Fazos Co. LW Support System The Opole University of Technology, Faculty of Mechanical Engineering, Tarnowskie Góry, Poland, T. Łagoda, The Opole University of Technology, Faculty of Mechanical Engineering, Opole, Poland, A. Khair, Department of Mining Engineering West Virginia University, Morgantown, WV*.....318
44. **Strata Management with Ground Behavior Assessment for Mass Exploitation of Coal Deposits: A Case Study of Continuous Miner,** *S. Singh, S.E.C.L.(A Subsidiary Company of Coal India Limited), Bishrampur, India, S. Jayanthu, National Institute of Technology, Rourkela, India, G. Singh, S.E.C.L.(A Subsidiary Company of Coal India Limited), Bilaspur, India*.....324
45. **Modal Testing and Dynamic Finite Element Analysis of a Roof Bolter's Drilling Boom,** *Y. Zhang, Z. Shi, J. Zhang, Xi'an Research Institute of China Coal Technology & Engineering Group Corp, Xi'an, China*.....335

AUTHOR'S INDEX.....340

Characteristics of Coal Bursts in the North Fork Valley of the Gunnison River Valley, Colorado

Christopher Mark, Principal Roof Control Specialist
Coal Mine Safety and Health MSHA
Pittsburgh, PA

Sandin Phillipson, Geologist
Paul Tyrna, Geologist
Michael Gauna, Mining Engineer Rcd MSHA
Triadelphia, WV

ABSTRACT

A coal burst is defined as the sudden, violent ejection of coal or rock into a mine opening. Coal mines in the North Fork Valley (NFV) of Colorado's Gunnison River have a long history of coal bursts in a wide variety of settings. These have included longwall and room-and-pillar, development and retreat, and single- and multiple-seam mining. In contrast to other coalfields, where bursts are typically associated with strong, massive sandstone and extremely high stress, many bursts in the NFV have occurred beneath shale roof and some distance from the most highly stressed locations.

The goal of this paper is to attempt a systematic study of the entire burst history in the NFV, in order to gain insight into their characteristics and causes. The primary sources of information are the reports of investigations conducted by the Mine Safety and Health Administration (MSHA) Roof Control Division over the past 15 years. This paper provides details on the geologic mapping conducted as part of these investigations, as well as a regional plot of burst locations using a Geographic Information System. The mapping indicates that many of the NFV bursts have been associated with structural features, including low-angled faults and well-defined zones of high-density jointing that exhibit little or no displacement. Some of these features appear to extend for several miles, impacting more than one mine.

INTRODUCTION

Coal has been mined in the North Fork Valley (NFV) of the Gunnison River for more than a century (Figure 1). Today, three longwall mines are active in the NFV, producing a combined annual total of approximately 15 million tons of high-quality, low sulfur steam coal. Located in an area of extremely mountainous topography, these mines operate under some of the deepest cover in the US, at times exceeding 2,000 ft. The deep cover, combined in some instances with multiple seam interactions, can result in high stress and very difficult ground conditions. In recent years, all three operations have experienced severe coal bursts. Figure 2 shows the location the three active mines (Mines 2, 3, and 5) and four abandoned mines whose burst experience will be discussed in this paper.

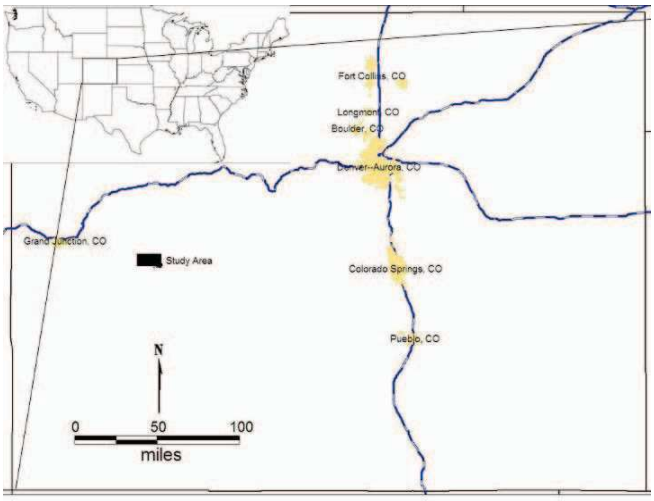

Figure 1. Location of the North Fork Valley of the Gunnison River, Colorado, USA.

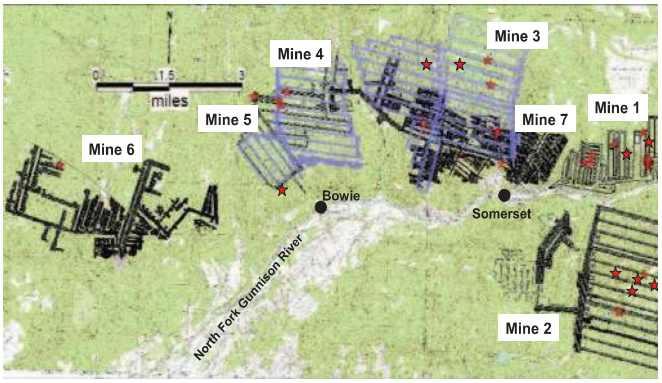

Figure 2. Location of NFV mines.

COAL BURSTS

A coal burst is defined as the sudden, violent ejection of coal or rock into the mine opening. High stress is a universal feature of burst-prone conditions, but geologic factors also contribute. The

presence of strong, massive sandstone near the seam has often been noted where bursts have occurred (Maleki, 1995; Iannacchione and Zelanko, 1995; Bräuner, 1994; Agapito and Goodrich, 1999). In the Utah coalfields, for example, miners refer to "bump sandwich" geology where the coal seam is slotted between massive sandstone roof and floor. In Germany, a study that compared rock cores from 35 areas that experienced bursts with cores from 400 burst-free areas found that the burst risk was significant when there was either a 15-ft-thick "package" of strong sandstone in the first 30 ft above the mining horizon, or a 6-ft-thick "package" within the first 15 ft of the floor (Baltz and Hucke, 2008).

Near seam geology does not wholly determine the burst risk, however. Other geologic factors that have been identified as contributing to a heightened burst risk include the following:

- Rapid changes in the depth of cover (Holland, 1958; Maleki 1995; Maleki et al., 1999)
- Sandstone channels that concentrate load (Agapito and Goodrich, 2000; Hoelle, 2008; Maleki et al., 2011)
- Seam rolls (Iannacchione and Zelanko, 1995; Maleki et al., 2011)
- Faults (Holland, 1958; Holub, 1997; Agapito and Goodrich, 2000; Alber et al., 2008; Swanson et al., 2008)

As long ago as the early 1930s, coal bursts were classified into two types according to their apparent cause (Rice, 1935). "Pressure bursts" were thought to originate in the seam itself and were associated with high stress and direct mining activity. "Shock bursts," on the other hand, were thought to be caused by "the breaking of a thick, massive, rigid strata at a considerable distance above the coal bed, causing a great, hammerlike blow to be given to the immediate roof of the mine opening, [transmitting] a shock wave to the coal pillar or pillars" (Rice, 1935). Today, we understand that the sudden, dynamic failure in the overlying (or underlying) strata releases elastic energy in the form of seismic waves. The failures include sudden downward movements of the rock above the worked-out areas, shear slip motion on faults or fractures in the overburden, or some combination of these two mechanisms (Pankow et al., 2008). Shear slip motion can occur on newly-created fractures, or on reactivated pre-existing faults (Swanson et al., 2008; Alber and Fritschen, 2008). The seismic energy released by such events can cause damage both underground and on the surface.

The "shock burst" phenomenon is well known internationally, both in hard rock mines and in burst-prone coalfields. For several decades, the deep South African gold mines have been aware that mining too near a fault can trigger a major rock burst. Researchers at the Australian Centre for Geomechanics (ACG) have recently developed a quantitative rock burst risk control method that includes the following elements (Potvin, 2009):

- Identifying sources of seismic energy, including faults and other geologic or mining structures
- Estimating the maximum likely seismic energy release from each individual seismic source
- Assessing the largest potential ground motion (peak particle velocity) in the mine as a function of the magnitude of the event and the distance of the mine workings from the event
- Assessing the potential damage to the mine resulting from the ground motions and modifying the mine plan as necessary to control the risk

The ACG approach relies on the availability of seismic source locations obtained from high quality, three-dimensional seismic monitoring systems. Such systems have been employed in some burst-prone European coalfields. In the Czech Republic, for example, researchers have been able to study the relationship between the magnitude and location of seismic events and the extent of damage underground. In one instance, extensive damage resulted from a seismic magnitude (M)event, where M=2.8, that was located more than 300 ft away from the workings (Holub et al., 2011). On the other hand, even very large events could have little impact on the mine if they occur well above the workings. During one 5-year period in Poland, there were 15 large mining-induced events with M ranging from 2.2 to 4.0 (Mutke and Stec, 1997). Only 6 of these had any effect underground. In the US, the M=4.2 event that was located approximately 500 ft above the Willow Creek longwall mine in Utah resulted in only minor damage at the mining horizon (Ellenberger et al., 2001). Seam level "mining tremors", on the other hand, are often too small to register on a regional seismic network, but they can result in serious injury if a miner is in the vicinity (Mutke and Stec, 1997).

One factor that does not seem to be strongly correlated with bump proneness is the character of the coal. Research by Babcock and Bickel (1984) indicated that a wide variety of coals can be induced to fail violently if the confining stress is suddenly reduced. Iannacchione and Zelanko (1995) noted that bursts have occurred in at least 25 different US coalbeds, varying from strong, blocky seams to very friable ones like the Pocahontas No. 3 and No. 4. Extensive German laboratory studies using large-scale specimens have also concluded that nearly all bituminous coals can burst. In these experiments, coal seams ranging in unconfined, compressive strength from 700 psi to 7,000 psi have all been shown to be burst-prone (Bräuner, 1994).

GEOLOGY OF THE NORTH FORK VALLEY

Mines in the NFV of Colorado's Gunnison River extract coal from the Cretaceous-aged Williams Fork Formation near the base of the Mesaverde Group. The Williams Fork Formation includes the coal-bearing Bowie and Paonia Shales (Figure 3). These units host the coal deposits of the Cameo-Fairfield coal zone, which extends beneath the entire Piceance Basin of western Colorado.

In the vicinity of the NFV, the Bowie Shale ranges from 164 to 525 ft thick and contains, in ascending order, the A (Old King), B (Somerset), and C (Bear) Seams. In some mines, the B Seam is subdivided into an Upper B and Lower B, or into three splits, of which the two upper splits are generally combined into a mineable height.

Overlying the Bowie Shale, the Paonia Shale ranges in thickness from 279 to 525 ft, and contains the D, E (Oliver), and F (Hawk's Nest) Seams. Where the thin Lower D Seam is separated from the Upper D Seam by interburden thick enough to preclude its incorporation in a mining horizon, it is not extracted. Mines that extract coal from the B and (Upper) D Seams are primarily discussed in this paper.

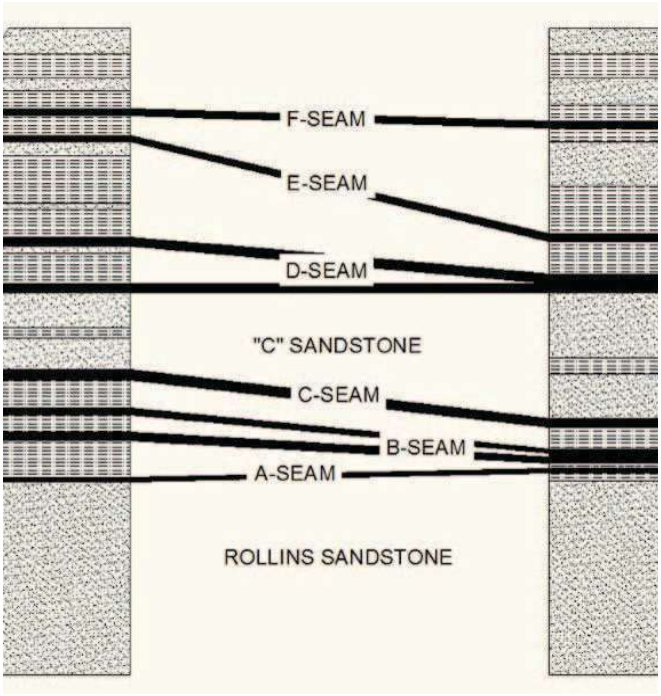

Figure 3. Typical stratigraphic sections from the NFV coalfields. (a) Southeast portion of the coalfield (after Agapito et al., 2005). (b) Northwest-central portion of the coalfield (after Robeck, 2005).

During deposition, transgressions and regressions of the seashore caused repeated grading of sandstones, shales, mudstones, and coal. Most of the sandstones thickened, thinned out, and pinched out over short distances (Agapito et al., 2005). In the NFV, only two of the sandstones are “truly tabular bodies” that are thick and extensive (Maleki et al., 2009). These are the Rollins sandstone that directly underlies the ASeam, and the marine sand that makes up much of the interburden between the C and the D Seams. This CSandstone is approximately 90 ft thick in two parts that are separated by a 10 to15-ft-thick mudstone-rich zone in the center of the unit (Maleki et al., 2009). The Rock Mass Rating (RMR) of the C-sandstone has been calculated to be approximately 65, with a measured uniaxial compressive strength (UCS) of 15,000 psi (Maleki et al., 2006).

The immediate roof of the B and D Seam mining horizons is usually composed of interbedded siltstone, fossiliferous shale, and thin layers of sandstone (Figure 4). RMR values calculated for the shale roof at one B Seam mine ranged between 40 and 60, with typical UCS values of 8,000–12,000 psi (Maleki et al., 2006; Maleki et al., 2008). The immediate floor usually contains a considerable thickness of coal.

Stress measurements have been conducted at a number of sites in the NFV. These show that the maximum horizontal stress is oriented approximately N80º E and is only slightly greater in magnitude than the vertical stress. The horizontal stress is highly anisotropic, however, with the maximum about four times greater than the minimum (Agapito et al., 2005).

The regional dip of the strata is about 3–5 degrees to the northwest. The predominant joint orientation is to the northeast.

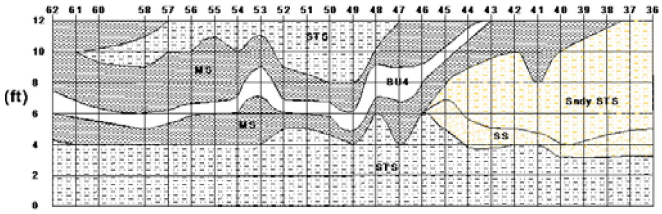

Figure 4. Cross section of the immediate roof observed in test holes along a longwall gate entry in the NFV (after Stewart et al., 2006a). The horizontal distance (crosscut 62 to crosscut 36) is approximately 3,000 ft. Abbreviations: Siltstone (STS); Mudstone (MS); Sandstone (SS); Sandy Siltstone (Sndy STS); Upper B Seam, 4th Bench, Rider Coal (BU4).

Faulting is present throughout the coalfield. In the eastern portion of the current mining area, the most prominent are strike-slip and normal faults that strike northeast and dip steeply to the northwest (Harris et al., 2002). The character of the faults varies from a single fault plane to a localized joint or deformation zone. The faults have little or no surface expression, suggesting that they were formed at depth in association with the emplacement of igneous rocks beneath the mine (Agapito et al., 2005). Based on detailed measurements of the fault dip displacement gradients, Harris et al. (2002) concluded that the most prominent faults likely originated in the major sandstone units (the Rollins and the C Sandstones).

The approximate N 70° E orientation that characterizes most of the joints, faults, and coal cleat in the NFV appears to represent a structural grain that has been imparted to the entire district. This could have influenced erosion of the North Fork of the Gunnison River in a weakened zone. Because the structural grain is uniform over a broad area, it is interpreted to be related to large-scale tectonic processes, which were responsible for uplift of various ranges of the Rocky Mountains about 50 million years ago. The N 70° Estriking joints and faults are in the expected orientation of tear faults for the northeast-directed thrusting that occurred then (Phillipson, 2005). One exception to the dominant east-northeast structural orientation is the northwest trend of several normal and strike slip faults found in the western portion of the coalfield. These structures are interpreted to represent growth faults that originally developed when the coal was deposited and were reactivated by the uplift (Robeck, 2005).

STUDY METHODOLOGY

Field visits conducted by the MSHA Roof Control Division (RCD) have documented the distribution of burst damage and geological structures at all five longwall mines over a span of nearly 10 years. These observations were supplemented with historical MSHA records from the Denver Technical Support Center for Mine 1 and Mine 7, from papers in the literature, and from the MSHA accident and injury database.

Digital mine maps obtained from each mine were displayed together in the same frame of reference using a Geographic Information System (GIS) with Colorado State Plane (Central Zone) coordinates and the NAD27 projection. In the case of a mine that closed prior to obtaining an electronic map, the existing paper copy was scanned, georeferenced to Colorado State Plane

(Central Zone), NAD27, and the traced outline of the mine workings was incorporated in the GIS. The locations of known bursts, based on RCD field investigations or documented in other records, were plotted in each respective mine. The trends of geologic structures mapped at each mine by RCD personnel were plotted on the mine maps as a separate geology layer.

Mapping was conducted generally at scales of 1 in=200 ft to 1 in=400 ft using a Brunton compass to measure the trends of structural geologic features. Geological features were plotted on field maps during the investigations and were transposed into the GIS geology layer. Incorporation into the GIS as a single layer allowed the previously isolated investigation areas to be viewed together in the same spatial context to assess the distribution of patterns.Some of the maps obtained from the mines or from the literature also show geologic structures, and these were also displayed together in order to assess the continuity of structures known or inferred in adjacent reserves.

Most of the burst events discussed in this paper were reported to MSHA and are available in the MSHA database. Appendix 1 contains a table listing 34 bursts that occurred in NFV mines between 1995 and 2011. The table includes the date of the event and the original narrative that was included with it, where available. Also included are characteristics of each burst as determined in the course of the study, including the location of the event (relative to the mining), the depth of cover, and whether a multiple seam interaction was involved. The table also states whether a fault or other geologic structure was mapped near the event, and whether a seismic magnitude (M) is known. In most instances, the seismic magnitude was obtained through a search of the US Geological Survey (USGS) National Earthquake Information Center (NEIC).

OBSERVATIONS AND MINE HISTORY

Mine 1

Mine 1 began as a room and pillar operation in the B Seam in 1991. It was overlain by workings in the C (60 ft above, in limited areas), D (230 ft above, in limited areas), and E (470 ft above, in limited areas) Seams. Roof lithology, based on brows exposed by roof falls, consisted of 1- to 6-inch-thick beds of shale interbedded with hard sandstone layers that ranged in thickness from 5–12 inches. The floor contained at least 10 ft of coal.

Prior to RCD conducting field investigations in the western coalfields, investigations were conducted by members of the former Denver Technical Support Center, which documented the occurrence of several bursts at Mine 1 in 1995. These bursts were located in five deep cover pillar recovery panels on the western side of the mine (Figure 5). Reportedly, relatively small, predictable bursts occurred on a regular basis during retreat mining, but they normally did not disrupt production. However, beginning with the second panel, much larger events would occasionally cause widespread floor heave and damage to numerous ventilation stoppings. The shaking associated with these large events, five of which were reported to MSHA (see Table 1), was clearly noticeable on the surface. The large bursts apparently became more frequent and more violent as mining progressed, even though the cover was decreasing from nearly 2,000 ft over the first panel to 1,300 ft above the fifth and last one. It should also be noted that these pillar recovery operations were conducted with relatively narrow barrier pillars that were likely incapable of carrying the abutment loads generated by the mining. Therefore, it seems likely that inadequate pillar design was a major factor contributing to the burst events.

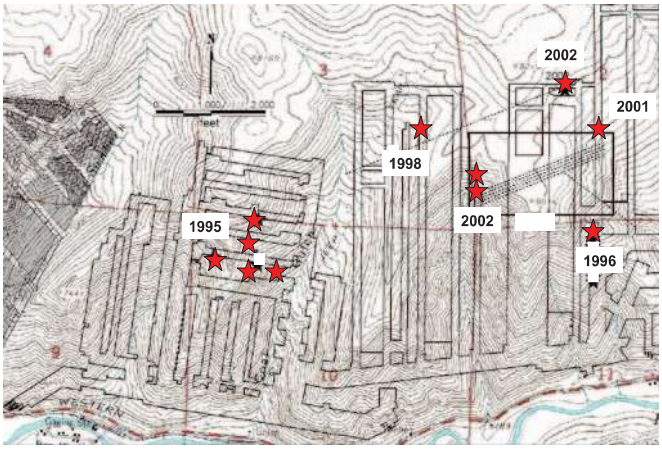

Figure 5. General outline of Mine 1, showing the locations of known bursts (red stars) in relation to structural zones (dashed, red lines) later identified by RCD.

Due, in large part,to the difficulties encountered during pillar recovery, Mine 1 shifted to the longwall method of production in the late 1990s. Six additional large bursts were reported at depths in excess of 1,500 ft between 1996 and 2003, when the mine closed. Three of these took place during development, one in a bleeder, and two in a headgate. None occurred in the tailgate or on the longwall face, where they might have been expected if high stress was the most significant factor involved.

Shortly before the mine abandonment, RCD conducted an evaluation in response to roof falls and a burst that occurred in a large pillar bounded by the bleeder and startup room (Figure 5). The 200-ft-long roof fall in the headgate development section, as well as the bleeder where bursts and closure occurred, both lay along a low-angle fault zone, defined by strongly parallel coal cleat, joints with water inflow, and low-angle bedding plane faults that strike N 70° E. Although the areas were situated beneath gob/solid boundaries in the overlying E Seam, it did not seem likely that these influenced the event because the interburden was 470 ft thick. Indeed, the multiple seam effects were not apparent in mapping conducted at depths of 1,100 ft, where the ribs were straight and the roof was smooth and unbroken.

After compiling historical burst locations on the GIS map, it was apparent that the 2002 burst pillar lies along a N 70° E trend from a 1998 burst that happened during gateroad development. The fact that the two isolated burst occurrences lie along a trend that is parallel to the identified low-angle fault zone suggests that both bursts could have been influenced by a previously unrecognized structural geologic feature.

Mine 2

Mine 2 opened in 1982 and began extracting coal from the B Seam by the longwall mining method in 1992. Mining was originally conducted in an area where overburden ranged from

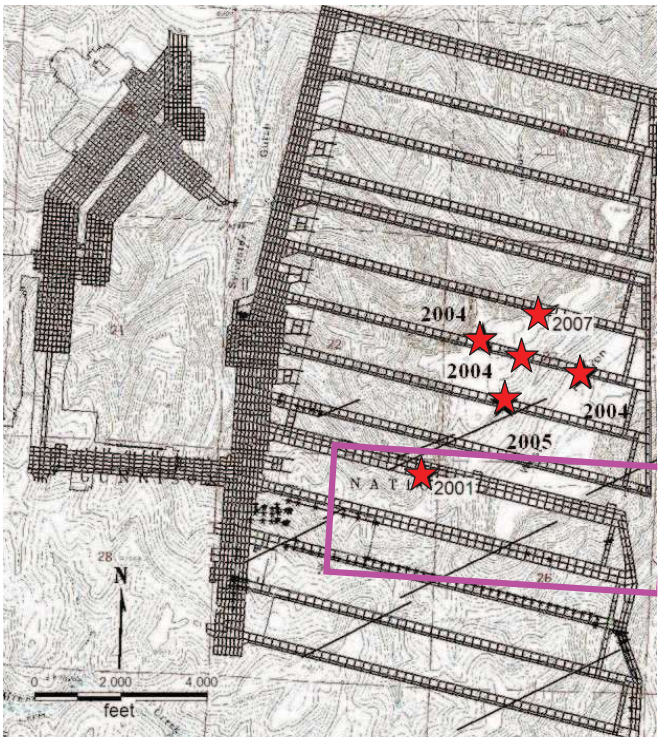

Figure 6. General outline of Mine 2, showing the locations of known bursts (red stars) in relation to structural zones (dashed, red lines) later identified by RCD.

600 ft to 1,400 ft, and, reportedly, some small "bounces" were encountered at depths exceeding 1,000 ft (Figure 6).

Subsequently, mining shifted to a reserve block where the cover exceeded 2,500 ft at its deepest points. Initially, the mine encountered a series of water and methane inflows from fault-fracture systems. The most severe of these inundated the section with 125 gallons/sec of geothermal water (~83º F). Studies showed that faults extended into the Rollins sandstone located 50 ft beneath the mining horizon (Mayo and Koontz, 2000).

The first major burst occurred in 2001 and registered as an M=3.4 event. As much as 8 ft of instantaneous heave occurred, completely closing the entry in some locations (Agapito et al., 2005). The RCD investigation found 10 damaged pillars between the No. 2 and No. 3 entries in a four-entry gateroad beneath approximately 1,650 ft of cover. The burst pillars were located in the tailgate of the first panel in the district, and they were some distance behind the face, so they were subjected only to side abutment loading from the active gob. The overburden was 500 ft less than the deepest portions of the same panel headgate where no ground instability occurred. Underground geologic mapping revealed that a prominent joint zone, which represents the extension of a scissors fault identified previously by the mine geologist, is directly adjacent to the burst area and strikes N 60° E (Phillipson, 2005). The zone is defined by closely spaced, prominent joints in the roof and intensely developed cleat swarms in the coal, as well as by an increased incidence of rib sloughing (Figure 7).

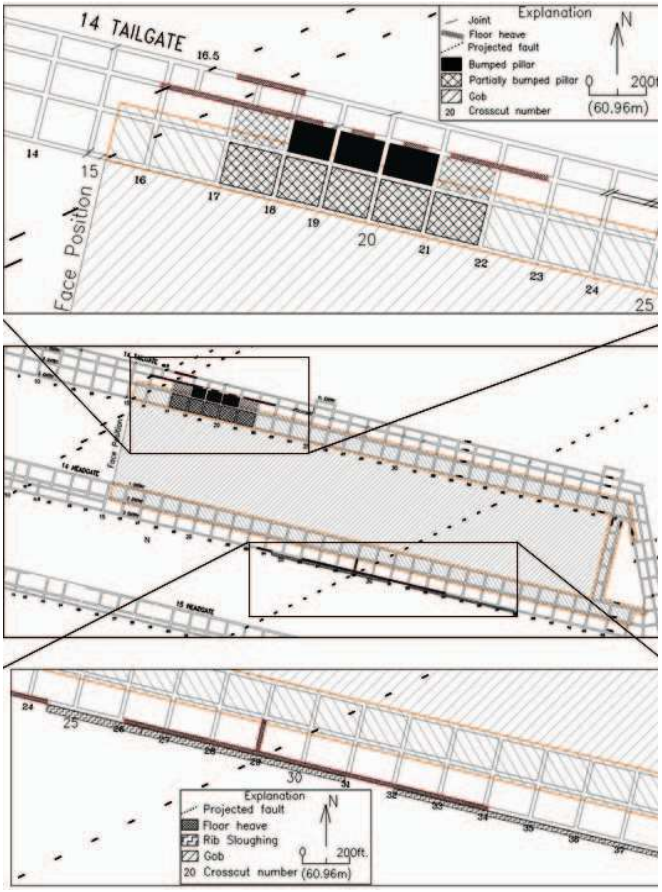

Figure 7. Detailed mapping of joint zone in relation to burst-damaged pillars on first panel tailgate at Mine 2 (Phillipson, 2005).

At the time of the 2001 RCD investigation, a 10-ft mining horizon was being extracted from the upper (B1) and middle (B2) splits, which are separated by a 2-inch-thick clastic binder. The mining horizon was overlain by 6–12 ft of thinly bedded, well-cemented sandstone. The overlying siltstone and sandstone, which was well cemented and contained faint crossbedding, hosted widely spaced joints oriented parallel to cleat. The CMRR was estimated at 50–55. Coal cleat was very well developed, occurring as vertical planes spaced 1–6 inches apart and oriented dominantly along a strike of N 62–70° E. The floor consisted of a layer of 8-inch-thick, well-cemented gray siltstone with fine shale interlaminations, separating the mined B2 split from the lower, un-mined B3 split.

Several additional bursts were reported over the next few years, all of them in or near mapped faults or prominent, discrete (generally less than 10 ft wide) joint zones that exhibited strikes of between N 60–70° E. Not all of these features were associated with bursts, however. In other cases, the joint zones controlled the shape of deep pot-outs and roof falls, particularly in intersections. Field observations also suggested a greater intensity of rib sloughing along projected joint zones.

The last significant burst in this longwall district occurred in a headgate in 2007 beneath 1,830 ft of overburden. The event, which registered M=1.9 on the local seismic network, caused pillar spall, floor heave, and roof failure, but did not significantly affect mine

operations. The damaged zone was intersected by an extension of the same fault that was associated with earlier events (Swanson et al., 2008).

Mine 3

Development of Mine 3 began in the D Seam in 2002 (Figure 8). RCD evaluations found an immediate roof consisting of at least 3 ft of sandstone with irregularly distributed pods of shale. Coal cleat was well developed, spaced 2 in. apart, and exhibited a strike of approximately N 70° E. The influence of multiple seam interactions was apparent by the presence of subsidence troughs above underlying C Seam gob areas.

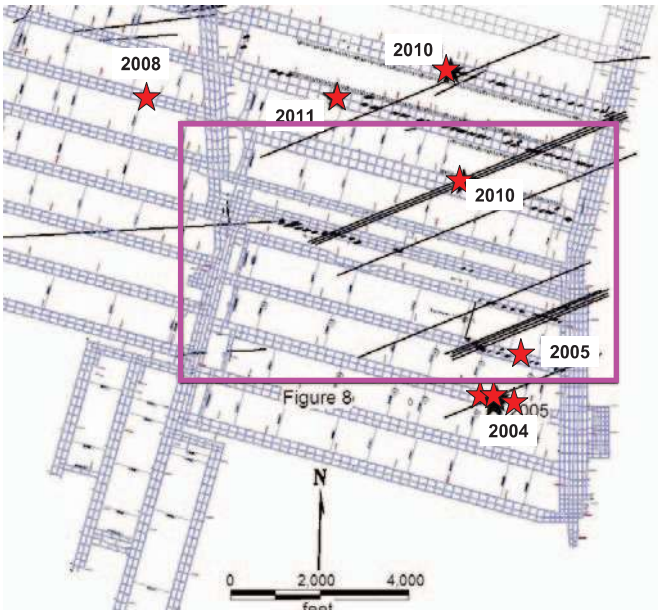

Figure 8. General map of Mine 3, showing workings in relation to faults (red lines) and bursts (red stars). Compare to Figure 2 for extent of underlying workings in the B Seam. Purple outline indicates extent of detail in Figure 8.

Geologic mapping identified a zone of strongly concentrated joints and slickensided drag folds, oriented N 67° E, which projected through two perpendicular mains and a gateroad.This zone was associated with numerous roof falls, instances of rib sloughing and floor heave, and a tailgate blockage on the active longwall panel (Figure 9). Although some major faults were shown on mine maps, those projected faults did not always correspond with structures identified by detailed geologic mapping conducted by RCD, indicating that fault projections can be unreliable and should be updated with actual underground mapping.

In 2004, a series of three bursts occurred in the tailgate of the active longwall face as it was passing over underlying works at greater than 1,500 ft of overburden. A fourth event occurred the following year in the adjacent panel tailgate in the absence of underlying workings. A fifth burst occurred three years later beneath some of the deepest overburden encountered to date (1,800 ft). No multiple seam interaction was present in this instance.

Late in 2009, the mine began longwalling in a new district, with depths of cover that consistently exceeded 2,000 ft. The first

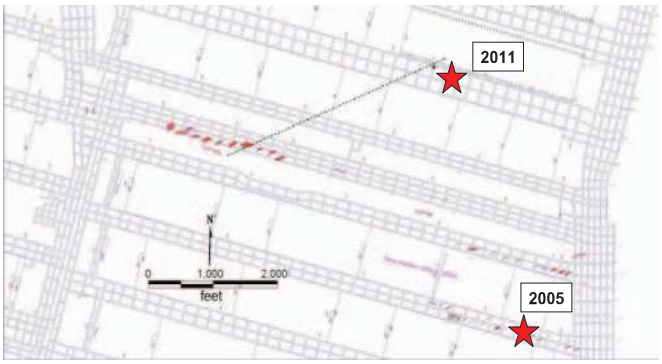

Figure 9. Section of mine map showing detailed RCD geologic mapping from 2005 and the projection of the fault zone into the 2011 tailgate burst.

panel was extracted without serious incident, but, midway through the second panel in 2011, a powerful burst that registered M=3.1 caused extensive pillar failure and floor heave over a large area in the tailgate. The burst was centered at least 500 ftoutby the tailgate corner, so it is unlikely that front abutment stresses were a significant contributing factor. The pillars were significantly larger than any that had been used at the mine in the past: three entries on 190-ft centers, and they maintained an Analysis of Longwall Pillar Stability (ALPS) stability factor (SF) of 1.12 (bleeder loading) even at a depth of 2,260 ft.

The burst did occur within the linear projection of the densely jointed and slickensided zone that RCD mapping had identified in the mains more than 3,000 ft away in 2005. Field mapping conducted by RCD in 2011 after the burst confirmed that the structural feature continued along strike across the reserve and was associated with degraded ground conditions along its length. It was one of a series of joint zones that were arrayed with roughly constant spacing across the mine reserve, exhibiting an approximate N 70° E trend.

One of these other structural features was associated with a burst that resulted in an injury during the development of the headgate for the third panel in the district. This feature was cause for concern because it crossed the tailgate of the third longwall panel in the district at about mid-panel. When another large tailgate burst occurred late in 2011, however, it was well inby this zone. While not as destructive as the burst that occurred on the second panel, the damage was extensive and forced the abandonment of the third panel.

Mine 4

Mine 4 was developed in the D Seam, using the longwall mining method, and, although mining encountered a number of faults, mine personnel indicated that the faults did not result in deleterious effects on ground conditions. RCD did not have an opportunity to conduct geologic mapping at Mine 4 prior to its closure, and no reported bursts occurred during the extraction of 12 longwall panels. Mine 4 is discussed in relation with Mine 5 because many faults encountered in Mine 4 translate vertically with depth into the underlying Mine 5.

Mine 5

Mine 5 was developed in the B Seam beneath the footprint of Mine 4, with an interburden of approximately 300 ft. The first set of three panels was mined in the southwest portion of the reserve (Figure 10). This district was bounded by two major faults, and smaller faults encountered within the panels caused some entry instability. The most severe problems included as much as 4 ft of floor heave and very difficult roof conditions that were attributed to a combination of poor roof (CMRR ~35–40) and slumps in the coal seam (Stewart et al., 2006). The D Seam overmining, stacked gateroads, and relatively small chain pillars (ALPS SF ~ 0.6) likely also contributed to the poor mining conditions. But despite the high stress and undersized pillars, no coal bursts were encountered in this district.

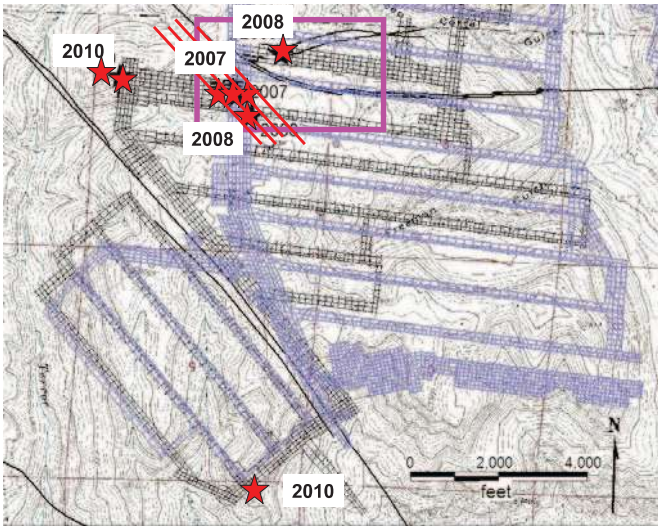

Figure 10. General mine map showing relation between faults (red) and burst occurrences (red stars), which have all occurred in the B Seam (black, Mine 5). Workings in the D Seam (Mine 4) are represented by violet.

Mining then began in a second longwall district to the east, and three longwall panels were extracted without serious incident. In this district, the gateroads were offset from the overlying D Seam gates (Figure 11). Then, in late 2007, a series of three bursts occurred while developing five-entry mains in support of a proposed northern district. The overburden was approximately 1,800 ft, and the base of the 100-ft-thick C Sandstone was 90 ft above the B Seam. The development was crossing beneath a D Seam mains located 300 ft above when the first burst occurred, causing 2–3 ft of rib failure and 1–3 ft floor heave around three pillars. It also caused an airblast and damaged ventilation stoppings for 7 breaks outby the face, and registered M=2.1 on the local seismic monitoring system.

In response to this first event, the mine attempted to ramp up into the seam and leave more coal in the floor and rock in the pillar for reinforcement. A second event occurred that required significant clean up though it measured just M=1.1. The third event was the largest of the three, registering M=2.9. It reactivated the earlier floor heave and also caused extensive new floor heave, as much as 5 ft in some places. Development ceased at this point.

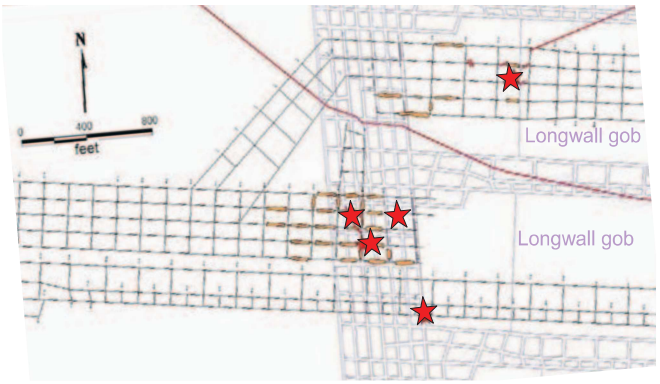

Figure 11. Detailed map of bursts (red stars) in three connected mains and longwall tailgate of Mine 5 (B Seam). Floor heave is indicated by orange swathes.

All of these events occurred beneath developed D Seam pillars, which, if they had any effect at all, should have reduced the vertical stress and transferred it to the solid coal on either side. All the events were also centered well outby the B Seam development faces, so they were not triggered directly by coal-cutting activities. It seems likely that the most significant factor was the presence of a zone of steeply dipping northwest faults that had been mined through without difficulty in the D Seam. Another hypothesis is that the D Seam pillars might have themselves failed, providing a dynamic trigger to the events encountered in the B Seam (Swanson et al., 2008).

The next event occurred one year later, in 2008, just to the southeast of the previous events. The location was a longwall headgate, and the sudden floor heave injured five miners. The event did occur above the boundary between those same abandoned D Seam mains and a barrier pillar, but several hundred ft inby the longwall had passed beneath a D Seam longwall stop line without incident. The fault zone associated with the earlier events, which was here expressed as a highly jointed zone, did extend directly through the area where the greatest damage occurred, however.

The fifth event also occurred in 2008, approximately 2,000 ft to the northeast of the first three. It was centered directly beneath a D Seam longwall stop line and within a major northeast trending fault zone. The M=2.3 event took place seven months after the area was developed and was not subject to any B Seam retreat mining stress abutments. Some limited de-stress floor blasting had even been conducted to reduce the burst hazard (Maleki et al., 2011).

Perhaps the most unusual of the Mine 5 events occurred during some small-scale room and pillar retreat mining operations that were conducted beneath relatively just 600–1,000 ft of cover in the far southwest corner of the mine. Mining in this area unexpectedly encountered a burn zone, which limited the number of pillars that could be developed. Twelve pillars had been partially extracted when four seismic events occurred within a two-minute period. While significant floor heave did occur, pillar damage dominated with voluminous coal ejected from the coal ribs encompassing multiple pillars. It appears that the burn zone could have caused the overburden to cave, imparting unexpected abutment stress to the pillars. While the additional abutment stress helps explain

why the pillars failed, it does not explain why the failure occurred so suddenly.

The most recent two events occurred in mid-2010, about 4,000 ft to the west of the first five. Room-and-pillar mining, without pillar recovery but including benching the floor, was being conducted. The pillars were substantially larger than in the nearby workings in an attempt to inhibit floor heave. Although the area was bound by two parallel faults (Figure 12), no faults or joint zones were observed in the immediate vicinity. The second of the two events was the larger, and it caused significant amounts of coal to be ejected from the ribs of four pillars and damaged ventilation controls over a large area.

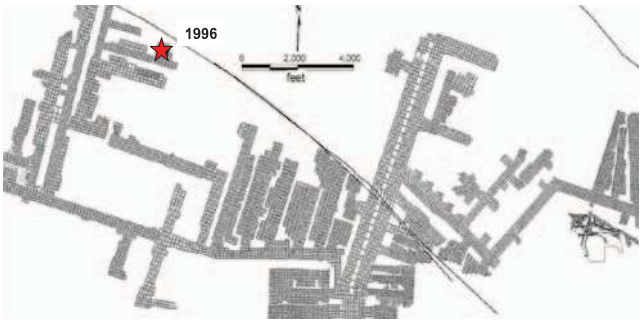

Figure 12. Map of Mine 6 in relation to the curvilinear fault and location of burst (red star) that trapped section crew.

Mine 6

Mine 6 extracted coal from the B Seam by the room-and-pillar mining method. Although it closed prior to RCD having the opportunity to conduct an evaluation of ground conditions, MSHA documents generated by the Denver Technical Support Center describe an event in which an entire section crew of 6 was trapped by a burst in 1996. The event occurred during retreat mining beneath 1,400 ft of cover. The event caused widespread roof falls, rib spall, and floor heave, and it damaged 19 stoppings. The crew was trapped for three hours, escaping only after ventilation was restored and the suspended dust cleared. Although not recognized at the time, it appears that the section was mining in the vicinity of a major curvilinear fault (Figure 13).

Mine 7

Mine 7 began extracting coal from the B Seam in the 1930s and continued operation through the 1970s. In the 1960s, mining ramped up into the C Seam, located variably 50–80 ft above the B Seam. Mining in all instances was by the room-and-pillar method. Geology of the C Seam immediate roof is unknown and has never been visited by RCD. There are no active mines currently developed in the C Seam in the NFV of the Gunnison River.

Two burst-related fatalities were recorded in C Seam workings, in 1967 and 1976, respectively. The 1967 fatality occurred during pillar-splitting operations in a large, square coal block the size of four regularly sized pillars. Mining was being conducted between retreat-mined gob and a known fault, located 400 ft away, which had terminated the advance of the section. It is unknown whether the underlying B Seam had already been mined in this area and to what extent, if any, multiple seam interactions could have been involved. However, the location of the 1967 fatal burst occurred along the projected strike of a very prominent fault zone that was identified by RCD in 2004 in the overlying Mine 3 and was related to degraded ground conditions in the mains, as well as a burst outby the active longwall face in 2011. The 1976 fatal burst occurred during the development of 5-entry mains and was located above solid coal, well away from the 1930s-era workings in the B Seam, and on the outcrop side of the mine where overburden was lowest. The available accident investigation report did not discuss any geological features, and the area is well outside the footprint of the overlying Mine 3, so no information on possible geologic structures is available for this event.

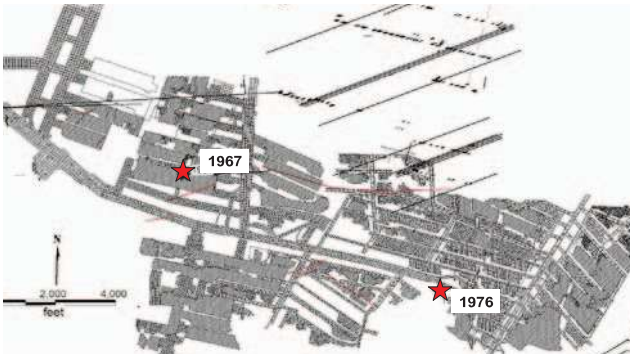

Figure 13. Extent of mine workings in the B Seam of Mine 7, in relation to geologic structures mapped by RCD in the overlying Mine 3. The C Seam workings are not shown on this map but exhibit a similar extent to the B Seam workings. For clarity, the extensive Mine 3 workings in the D Seam are not shown. The 1967 event occurs along the projection of faults mapped by the company, and later by RCD, in the overlying Mine 3.

SUMMARY AND CONCLUSIONS

The MSHA Roof Control Division has compiled an extensive history of the burst experience in the NFV, based on the published literature and its own evaluations at mines in the area. Table 1 summarizes the available data from 34 documented bursts. Some key characteristics of NFV bursts include the following:

- The immediate roof and floor seldom consists of strong, massive rock, but typically includes relatively thin beds of moderate strength or even weak material.
- The incidence of bursts clearly increases with depth. Of the 34 burst events, only 3 occurred where the overburden depth was less than 1,500 ft, and 13 occurred at depths exceeding 2,000 ft. However, bursts do not always occur beneath the maximum cover in an area.
- Although multiple seam interactions have been implicated in 10 events, the other 24 occurred where no multiple seam mining existed, or where the interburden is so thick that significant interaction seems unlikely.
- Most bursts are apparently not directly triggered by coal-cutting activities.
- Only 14 events occurred at the tailgate corner or on retreat pillar sections, where mining normally concentrates the greatest stress. The other 20 occurred at locations of lower mining stress, including 5 in headgates and 11 in development sections.

- In most cases, the pillar designs were sufficiently robust that they would have been expected to provide adequate support to the overburden.
- The bursts often have a greater effect on the floor than they do the pillar ribs.
- The bursts are often associated with known geologic structures, particularly low-angle faults and zones of high-density jointing that exhibit little to no displacement. In some cases, the joint zones transition into scissors faults, while in other cases, the joint zones represent a continuation along strike of a fault where it has curved and changed strike. Of the 28 events for which reliable geologic mapping is available, at least 21 occurred within or near a geologic structure.
- The bursts are often associated with large seismic events. Of the 26 that have occurred since 2000, 13 were large enough to be recorded in the USGS database with M>2.5.

Taken together, these characteristics imply that the most significant bursts in the NFV are largely of what Rice (1935) would have called the "shock bump" variety. In other words, they appear to be driven by large seismic energy releases occurring at some distance from the coal seam, often apparently from below. These energy releases are likely triggered indirectly when mining activity perturbs the stresses on geologic structures that must already be at near-critical levels. Given the active tectonism, which continues to occur in the NFV today (Swanson et al., 2008), it should not be surprising that there are numerous "critically stressed" structures within the crust. To hypothesize further, the main sources of the seismic energy could be the thick, strong, massive sandstones that underlie the seams at distances of 50–150 ft (the Rollins Sandstone and the C Sandstone). Hopefully,the information presented in this paper will help protect mineworkers from the hazards of coal bursts.

REFERENCES

Agapito, J.F. T., Gilbride, L.J., Koontz, W. (2005). "Implication of highly anisotropic horizontal stresses on entry stability at the West Elk Mine, Somerset, Colorado."In: *Proceedings of the 24th International Conference on Ground Control in Mining.* Morgantown, WV: West Virginia University, pp. 196–202.

Agapito J. F. T., Goodrich R. R.(2000). "Five stress factors conducive to bursts in Utah, USA, coal mines."In: *Proceedings of the 19th International Conference on Ground Control in Mining.* Morgantown, WV: West Virginia University, pp. 93–100.

Alber M., Fritschen R., Bichofff M., Meier T. (2008). "Rock mechanical investigations of seismic events in a deep longwall coal mine."*International Journal of Rock Mechanics and Mining Sciences 46*(2):408–420.

Babcock C. O., Bickel D. L. (1984). "Constraint: the missing variable in the coal burst problem." In: *Proceedings of the 25th U.S. Symposium on Rock Mechanics*.Evanston, IL: pp. 639–647.

Baltz R., Hucke A. (2008). "Rockburst prevention in the German coal industry." In: *Proceedings of the 27th International Conference on Ground Control in Mining.*Morgantown, WV: West Virginia University, pp. 46–50.

Bräuner G. (1994). *Rockbursts in coal mines and their prevention*. New York, NY: Taylor & Francis, pp. 152.

Ellenberger, J.L. and Heasley, K.A. (2000). "Coal mine seismicity and bursts: historical case studies and current field activity."In:*Proceedings of the 19th International Conference on Ground Control in Mining.*Morgantown, WV: West Virginia University, p. 112–120.

Harris R., Luthi A., Mayo A., Koontz, W. (2002). "Structural controls of hydrodynamic anisotropy in the West Elk Mine region, western Colorado."*Environmental & Engineering Geoscience8*(4): 309–318.

Hoelle J. (2008). "Coal Bumps in an Eastern Kentucky Coal Mine 1989 to 1997."In: *Proceedings of the 27th International Conference on Ground Control in Mining.*Morgantown, WV: West Virginia University, pp. 14–19.

Holland C. T. (1958). Cause and occurrence of coal mine bumps. *Mining EngineeringSeptember1958*: 994–1004B.

Holub K. (1997). "Predisposition to induced seismicity in some Czech coal mines."*Pure and Applied Geophysics 150*(3–4): 435–450.

Holub K., Rušajová J., Holečko J. (2011). "Particle velocity generated by the rockburst during exploitation of the longwall and its impact on the workings."*International Journal of Rock Mechanics and Mining Sciences 48*(6): 942–949.

Iannacchione, A.T. and Zelanko, J.C. (1995). "Occurrence and remediation of coal mine bursts: a historical review."*US Department of the Interior, U.S. Bureau of Mines, Special Publication 01-95*: 27–68.

Maleki H. (1995). "An analysis of violent failure in U.S. coal mines: case studies." *US Department of the Interior, U.S. Bureau of Mines, Special Publication 01-95*: 5–26.

Maleki H., Stewart C., Stone R., Abshire J. (2009). "Practical application of numerical modeling for the study of sudden floor heave failure mechanisms." In: *Proceedings of the International Workshop on Numerical Modeling for Underground Mine Excavation Design.*Pittsburgh, PA: NIOSH, pp. 89–100.

Maleki H., Zahl E. G., Dunford J. P. (1999). "A hybrid statistical-analytical method for assessing violent failure in U.S. coal mines." In:Mark, C., Heasley, K., Iannacchione A., Tuchman, R., eds.*Proceedings of the Second International Workshop on Coal Pillar Mechanics and Design*.Pittsburgh, PA: NIOSH, pp. 139–144.

Maleki, H., Stewart, C., Hunt, G. (2006). "Subsidence characteristics at Bowie Mines, Colorado."In: *Proceedings of the Golden Rocks 2006, 41st US Symposium on Rock Mechanics*. Alexandria, VA: American RockMechanics Association, doc ID 06–932.

Maleki, H., Stewart, C., Stone, R., Abshire, J., Whyatt, J. (2009). Analysis of sudden floor heave in US mines. SME Preprint 09-010, 9 pp.

Maleki, H., Rigby, S., McKenzie, J., Faddies, T. (2011). "Historic mine designs and operational practices used in deep mines for controlling coal bumps."In: *Proceedings of the 45th US Rock Mechanics/Geomechanics Symposium.* Alexandria, VA: American Rock Mechanics Association, doc ID 11–276.

Mayo A. L., Koontz W. (2000). "Fracture flow and groundwater compartmentalization in the Rollins Sandstone, Lower Mesaverde Group, Colorado, USA."*Hydrogeology Journal 8*(4): 430–446.

Mutke G., Stec K. (1997). "Seismicity in the upper Silesian Coal Basin, Poland: strong regional seismic events."*Geophysical Journal International 168*(2): 757–768.

Pankow K., McCarter M. C., Arabasz W., Burlacu R. (2008). "Coal mining seismicity in Utah—Improving Spatial Resolution Using Double-Difference Relocations. In: *Proceedings of the 27th International Conference on Ground Control in Mining.*Morgantown, WV: West Virginia University, pp. 91–97.

Phillipson, S.E. (2005). "Laramide orogeny-related controls on coal mine ground instability in Cretaceous coal seams, southern Rocky Mountain foreland."*International Journal of Coal Geology 64*(1–2): 20–43.

Potvin Y. (2009). "Strategies and tactics to control seismic risks in mines."*Journal of the Southern African Institute of Mining Metallergy 109*(3): 177–186.

Rice G. S. (1935). *Bumps in coal mine of the Cumberland Field, Kentucky and Virginia: causes and remedy.*Arlington, VA: US Bureau of Mines, pp. 36.

Robeck, E. D. (2005). *The effects of fault-induced stress anisotropy on fracturing, folding, and sill emplacement: insights from the Bowie coal mines, southern Piceance Basin, western Colorado.* MS Thesis. Provo, Utah: Brigham Young University, pp. 106.

Stewart C., Hunt G., Mark C.(2006a). "Geology, ground control and mine planning at Bowie Resources, Paonia, CO."In: *Proceedings of the 25th International Conference on Ground Control in Mining.*Morgantown, WV: West Virginia University, pp. 284–290.

Stewart C., Stone R., Heasley K. A.(2006b). "Mine stability mapping."In: *Proceedings of the 25th International Conference on Ground Control in Mining.*Morgantown, WV: West Virginia University, pp. 277–283.

Swanson, P., Stewart, C., Koontz, W. (2008). "Monitoring coal mine seismicity with an automated wireless digital strong-motion network."In: *Proceedings of the 27th International Conference on Ground Control in Mining.* Morgantown, WV: West Virginia University, pp. 79–86.

Table 1. Bursts that occurred in NFV mines between 1995 and 2011.

Mine	Seam	Month	Day	Year	Narrative (from MSHA accident/injury data base)	Location	Depth (ft)	Multi Seam	Fault	Magnitude
1	B	1	17	1995	Not in data base.	Retreat	1,900	No	Unknown	
1	B	3	14	1995	The 5th west section had a bounce that stopped production because 8 stoppings were leaking after the bounce around.	Retreat	1,750	No	Unknown	2.9
1	B	7	25	1995	A coal bounce occurred in the 6th west pillar section mm4-001-0 that interrupted section ventilation. The bounce caused floor heave in various locations in the section.	Retreat	1,750	No	Unknown	
1	B	8	22	1995	A coal bounce occurred in the 6th west pillar section (mmu001-0) that interrupted section ventilation. The bounce caused floor heave in various locations in the No. 4 entry outby the face areas.	Retreat	1,500	No	Unknown	
1	B	9	11	1995	A coal bounce occurred in the 6th west pillar section (mm4-001-0) that interrupted section ventilation. This condition forced all mining activities to cease for the section to be moved to another panel.	Retreat	1,300	No	Unknown	
1	B	1	22	1996	A bump/bounce occurred in the north main section (mm4002-0) of the Sanborn Creek Mine. The bump/bounce caused mining activities to cease and caused floor heaving and rib and roof deterioration in affected area. There were no injuries or equipment damage.	Development	1,500	Yes	Unknown	

Table 1. Bursts that occurred in NFV mines between 1995 and 2011.

Mine	Seam	Month	Day	Year	Narrative (from MSHA accident/injury data base)	Location	Depth (ft)	Multi Seam	Fault	Magnitude
1	B	6	1	1998	A coal outburst occurred in 19n (mmu 001-0) during mining operations. X-cut was being driven between the No. 2 entry to No. 3 entry. The entry was in 18 ft from the last row of bolts. This occurred at the No. 35 X-cut. There was no floor heave.	Development	2,200	No	Yes	
1	B	5	23	2001	A pillar bounce occurred in the 14 North development section (mmu 002-0) between 15 and 16 X-cut in the No. 2 entry. For 90 ft, 1 to 2 ft of rib line blew out on both sides of the roadway.	Development	2,100	No	Yes	
1	B	6	20	2002	A pressure bounce occurred between 16 North and 15 North bleeder for 17 North (lw, mmu 010), causing floor heave and damage to regulators in bleeder.	Bleeder	2,300	No	Yes	3.6
1	B	11	18	2002	A floor bounce occurred on the solid side of the 22 North longwall panel between 25–27 X-cut in the No. 3 entry. This resulted in floor heave along the belt line and under the mobile tailpiece. This required removal of belt structure to clean the area.	Headgate	2,050	No	Yes	
1	B	11	26	2002	A non-injury bump occurred on the solid side of the 22 North longwall panel between 24 and 25 X-cut in the No. 3 entry, resulting in floor heave under the mobile tailpiece and damage to 2 stoppings.	Headgate	1,850	No	Yes	3.1
2	B	11	5	2001	A bounce occurred in 14 tailgate, resulting in significant floor heave in entry No. 1, xc 18 to 23. Ventilation controls were damaged in entries No. 1 and No. 2 as a result of the bounce.	Tailgate	2,000	No	Yes	3.4
2	B	3	8	2004	Immediately after a bounce, the roof fell in 22 headgate, entry No. 1, crosscut 24 to 25. The roof fall was not above the anchorage zone of the bolts; however, the fallen roof material impeded the passage to the longwall face.	Headgate	2,200	No	Yes	
2	B	9	19	2004	While mining on longwall face in Panel 23, a bounce occurred. This resulted in damage to several stoppings in the bleeder system, effecting longwall face ventilation. An MSHA inspector was present on the surface when the bounce occurred.	Bleeder	2,200	No	Yes	3.5
2	B	10	10	2004	A bounce occurred, resulting in damage to several stoppings between entries No. 2 and No. 3 in Panel 23 tailgate return, affecting the ventilation system.	Tailgate	2,200	No	Yes	3.3
2	B	5	1	2005	A bounce occurred that damaged several stoppings between entries No. 2 and No. 3, 24 Tailgate outby the longwall face, and caused a tailgate blockage inby X-cut-26. This resulted in a disruption of mini ng for more than 1 hour.	Tailgate outby	2,200	No	Yes	
2	B			2007	Not in data base.	Headgate	2,200	No	Yes	1.9

Table 1. Bursts that occurred in NFV mines between 1995 and 2011.

Mine	Seam	Month	Day	Year	Narrative (from MSHA accident/injury data base)	Location	Depth (ft)	Multi Seam	Fault	Magnitude
3	D	11	9	2004	A bounce occurred in 3 west tailgate X-cut 9 inby to longwall, 4 West panel (mmu, 010) a distance of 50 ft to face. Ventilation controls were damaged, and over 1 hour was required to restore ventilation to the longwall face. MSHA was notified and investigated.	Tailgate	1,600	Yes	No	
3	D	11	13	2004	A bounce occurred in the tailgate of the 4 West panel (mmu 010) between No. 8 and No. 9 X-cut.	Tailgate	1,500	Yes	No	3.2
3	D	11	21	2004	A non-injury bump occurred in the 4 West tailgate (mmm-010) between No. 7 and No. 8 crosscut in the No. 3 exit. Ventilation controls were damaged and out 1 hour, and it was required to restore a stepping and section regulator.	Tailgate	1,400	Yes	No	
3	D	6	8	2005	Pressure bounces occurred in 4 West tailgate, resulting in floor heave between 5 and 6 X-cut No. 3 entry. This created unsafe travelway off 5th West longwall panel (mmu 010) for a distance of 50 to 75 ft.	Tailgate	1,600	No	No	3.5
3	D	9	6	2008	A bump occurred in 11 West tailgate 20 ftoutby the longwall face. The area measured 100 ft long from spad 7 + 80 to 6 + 60 in the No. 3 entry. Floor heave and rib sloughage blocked tailgate travelway. Double row of cribs installed in entry.	Tailgate	1,800	No	No	2.8
3	D	12	3	2010	Coal rib bump occurred when the miner operator had graded to the face and bumped into the coal face. The operator was standing outby the miner tail when he was hit by coal from behind the screened rib.	Development	2,500	No	Yes	
3	D	2	**17**	2010	Not in data base.	Tailgate outby	2,300	No	Yes	3.1
3	D	10	18	2011	A Non-injury mountain bump occurred in the 4 north, mmu, 010, longwall tailgate entries. From the longwall face outby for 60 feet in the #3 entry between 28 and 29 X-cut and inby 28 X-cut in t he #2 entry of 3 north.	Tailgate	2,150	No	Yes	
5	Lower B	10	2	2007	Not in data base.	Development	1,620	Yes	Yes	2.1
5	Lower B	10	20	2007	On 10/31/07, MSHA determined that a floor heave incident on 10/20/07 was a reportable “bounce.” Floor heave occurred in the First East Mains No. 4 entry crosscut 14, No.v3 entry crosscut 14 to 15.	Development	1,660	Yes	Yes	1.1
5	Lower B	11	3	2007	A bounce occurred on the First East Mains section with floor heave and rib sluffage in several areas across the section.	Development	1,660	Yes	Yes	2.9
5	Lower B	11	23	2008	A bounce occurred in the LW belt entry from the face outby the crosscuts resulting in extensive floor heave. On 5/5/09, the employee required surgery on his knee from injuries on 11/23/08.	Headgate	1,680	Yes	Yes	2.5

Table 1. Bursts that occurred in NFV mines between 1995 and 2011.

Mine	Seam	Month	Day	Year	Narrative (from MSHA accident/injury data base)	Location	Depth (ft)	Multi Seam	Fault	Magnitude
5	Upper B	12	5	2008	A floor heave event occured in Second East Mains between crosscut 6 and 7.	Development	1,700	Yes	Yes	2.3
5	Upper B	2	12	2010	An event defined as a bounce occurred in the B West Mains room area where floor coal in the bleeder entry around the second mining area heaved into the entry. Floor heave is estimated at 3 to 4 ft in the South bleeder entry.	Development	1,000	Yes	Yes	3.0
5	Upper B	4	23	2010	On 4/23/10 at about 12:30 pm, a bump was experienced in the First North Mains at the junction to the First North Rooms. The event triggered minor floor heave, rib sluffage, and ventilation structure damage.	Development	1,575	No	No	
5	Upper B	7	20	2010	A bounce type event occurred, which resulted in floor heave in areas outby and in idle areas of the First North Mains room section.	Development	1,600	No	No	2.9
6	Upper B	5	10	1996	As a result of dust liberated by a bump in the section, 6 miners temporarily became disoriented and were unable to withdraw to a safe location outby the affected area. Entries in the affected area received some heaving and or caving.	Retreat	1,560	No	Yes	

Ultra–Close Multiple–Seam Mining – Analysis and Verification

Daniel W. Su, Sr. Geomechancial Engineer
Luke Stull, Geologist
Maria Jaime, Geomechanical Engineer
Jun Lu, Geomechanical Engineer
Coal Operations Engineering
Consol Energy Inc.
Canonsburg, PA

ABSTRACT

This paper presents the results of a detailed geotechnical study on the potential multiple seam interaction between the No. 2 Gas (upper) and the Powellton seams, which are separated by an average interburden of 45 ft. The interburden consists of 4 ft of clay shale below the No. 2 Gas seam, 38 ft of massive sandstone, and 3 ft of shale above the Powellton seam. The No. 2 Gas seam was mined about 60 years ago, and many water-pooled areas were projected to be present. The deepest overburden over the No. 2 Gas seam is about 750 ft.

To evaluate the potential interaction between the two mine works and to determine the pillar safety factor, Analysis of Multiple Seam Stability (AMSS) software was initially used to determine pillar dimensions to obtain a minimum safety factor of 2.0 for areas under pooled water, as well as a minimum safety factor of 1.5 for areas not under pooled water. Furthermore, to assess the quality of the interburden rock strata, two surface core holes were drilled, and rock cores were tested in the laboratory for their strength and elastic moduli. Using the experimentally determined strengths and moduli as part of the input parameters, the RocScience Phase^2 finite element program was employed to model the stress field scenarios and estimate the safety factors of the interburden rock strata before and after Powellton seam mining. The pillar safety factors derived from the Phase^2 analysis were in excellent agreement with those obtained from the AMSS analysis. Phase^2 results also predicted that the effect of the Powellton seam mining, first mining only, would reach a maximum of 19 ft above the Powellton seam, which led to the proposal of drilling 25-ft deep test holes to detect water, instead of the 45-ft deep test holes mandated by MSHA. The proposed test-hole height was accepted by both Mine Safety and Health Administration (MSHA) District 4 and the state of West Virginia.

Mining of the Powellton coal seam commenced in February 2011 and continued for eight months. To date, no 25-ft deep hole has encountered water under the water-pooled zone, which validates the RocScience Phase^2 finite element analysis. Also, in-mine observation of excellent pillar stability and roof condition confirms the validity of the AMSS analysis.

INTRODUCTION

In late October 2010, CONSOL Energy's Central Appalachian Operations planned to reopen a room-and-pillar mine in the Powellton seam that was idled in 2005. The Powellton seam is overlain by the No. 2 Gas seam, which was extensively mined out about 60 years ago. Areas of impounded water are expected to be present in the No. 2 Gas seam mined-out areas. The average interburden thickness between the two seams is about 45 ft. Since the first two core values of CONSOL Energy are safety and compliance, Coal Operations Engineering was requested to conduct geologic and geotechnical analyses to ensure safety of underground personnel and to comply with state and federal regulations.

Citing the guidelines provided by the Bureau of Mines Information Circular 8741 published in 1977, roof control and ventilation control personnel of MSHA District 4 had requested that, as mining approaches the potential water-pooled areas in the No. 2 Gas seam, safety zones be established underneath the potential water-pooled areas and that test holes be drilled at every crosscut to penetrate the No. 2 Gas water-pooled areas to drain pooled water. In areas outside the safety zones, the drilling was to be conducted at 200-ft intervals. CONSOL Energy's Central Appalachian Operations considered drilling into the abandoned No. 2 Gas workings to be potentially hazardous and decided to avoid such a drilling plan by committing to first mining only. However, to ensure the safety of underground personnel and to comply with federal and state mining regulations, a detailed geologic and geotechnical study was conducted in order to evaluate the stability of the interburden. Results from the study have also led to the recommendation of the optimal water test hole depth to be drilled. This paper describes the methodology and results of such work. Underground observations of roof and pillar stability and monitoring of water test holes were successfully compared to the results from the geologic and geotechnical analysis.

MINING HISTORY AND SITE GEOLOGY

Location and Mining History

CONSOL Energy's Lick Branch room-and-pillar mine is located at the northern edge of Fayette County, West Virginia. The mine is positioned within the physiological province of the Appalachian

Plateau and lies above drainage with respect to the nearby Gauley River. The closest town, Gauley Bridge, is approximately 3.5 miles away (Figure 1). All coal that is produced is trucked 26 miles to the Fola preparation plant, cleaned, and then delivered to the customer by rail. Historically, coal mining has taken place since the early 1920s in this area. The Powellton seam, which is mined at Lick Branch, has been extensively mined throughout the region in addition to other seams such as the Eagle, Little Eagle, Peerless, and the No. 2 Gas. Since mining of the various seams has taken place above and surrounding the Lick Branch mine, it has led to complex mining situations related to multiple seam mining. Due to the presence of the multiple seam scenarios, a thorough geologic and geotechnical investigation was conducted prior to re-entering the mine in February 2011.

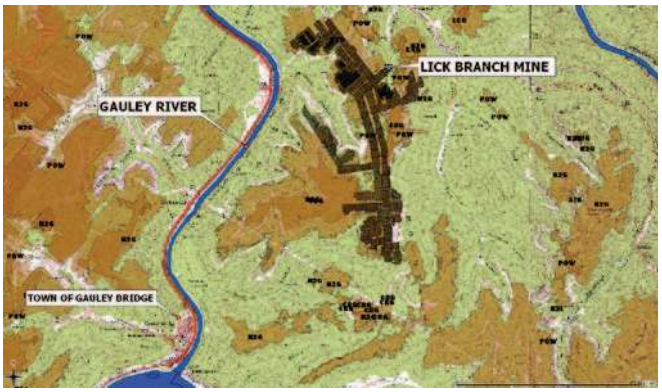

Figure 1. Location of the Lick Branch Mine. Also showing surrounding mine works in various seams.

Description of Geology

The Powellton seam, in which Lick Branch is mining, is of the Kanawha Formation within the Pottsville series. Stratigraphically, the Powellton seam lies between 40 to 80 ft above the Eagle seam and underlies the No. 2 Gas seam. The interburden thickness between the No. 2 Gas and Powellton seams ranges from 35 to 50 ft. Within the Powellton- No. 2 Gas interburden, the predominant lithology is the Brownstown sandstone (Reger et al., 1921), which can be observed in Figure 2. The interval from the top of the Powellton seam to the base of the first overlying sandstone (Brownstown) varies between zero and eight ft. The thickness for the Powellton seam ranges between 3 ft and 4.5 ft. The seam thickness varies from 2.1ft to 2.4 ft for the No. 2 Gas. Structurally, the strike and dip of the Powellton seam are N38E and 6.5 degrees, respectively. Additionally, in-mine observations within Lick Branch have provided evidence of several local rolls that were not determined through exploration drilling. Maximum overburden for the Powellton seam is 750 ft. For the interburden between the Powellton and the No. 2 Gas seams, the lithology is approximately 95 percent sandstone. However, there is little description from geologist logs about the quality of the sandstone. Sandstone thickness within the interburden is a minimum of 30 ft and as thick as 45 ft. Although there is no undermining of any seams beneath Lick Branch, the No. 2 Gas seam was mined above the Powellton reserve. Up until the late 1940s, the Midvale No. 1 mine operated by the Gauley Coal and Coke Company mined the No. 2 Gas seam and left the reserve tattered and depleted (Figure 3). Because no core was retained from previous exploration drilling, two additional holes were drilled to collect rock core samples for geotechnical testing. The interval of one of them is illustrated in Figure 4. Two sites were selected from distinct locations to avoid penetrating the No. 2 Gas mine works. In doing so, large barrier pillars were located within the No. 2 Gas works using a scanned copy of the Midvale No. 1 mine map provided from the West Virginia Mine Map Repository. The resulting cores were comprehensively logged for their geological characteristics. In addition, core samples were tested in the laboratory, as described in the finite element method (FEM) Input sub-section below.

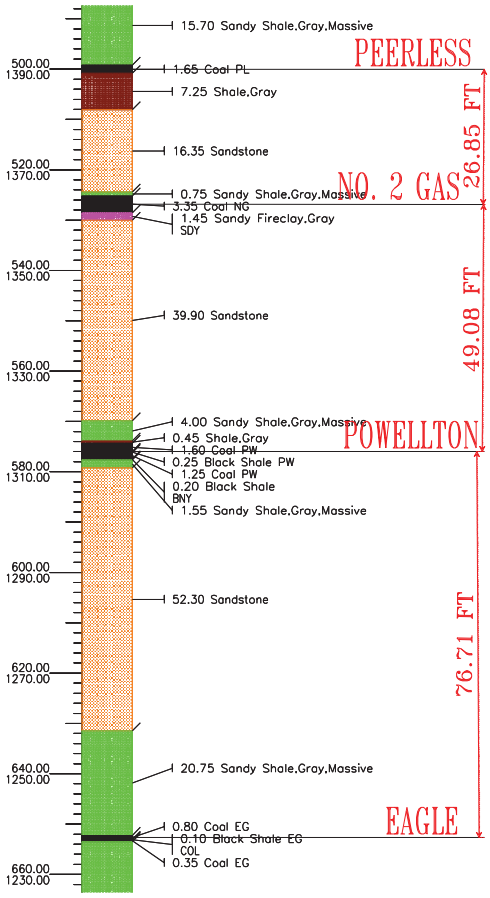

Figure 2. General Geologic Section for the Lick Branch Mine (Powellton Seam).

No. 2 Gas Gob and Potential Water-Pooled Areas

Other than the copy of the mine map, there was little information about the Midvale mine. This created several challenges. It could only be assumed that the mine was flooded and possessed the deadly atmosphere known as black damp. Therefore, safety zones were placed around dead-end rooms and panels lying down dip using the guidelines provided by Babcock (1977). Despite the deficiency of detail for the Midvale mine map, it could still be determined that there were significant isolated remnant pillars and what were considered to be gob-solid boundaries. As shown in Figure 5, by superimposing and scaling the scanned map with the Lick Branch mine map, it became possible to size the pillars

Figure 3. Scan of Midvale # 1 (No. 2 Gas Seam) mine map. Circa 1940.

Figure 4. A section of boxed rock core, having massive sandstone within the Powellton – No. 2 Gas Interburden.

of the No. 2 Gas seam. After determining the size of these pillars, it was possible to examine the surplus stresses related to the isolated remnant structures and gob-solid boundaries through the use of AMSS software, as well as finite element modeling (FEM), explained in the next section.

Recognizing the close interval between the two mines, CONSOL Energy decided to conduct first-mining only to avoid the risk of possible inundation. Therefore, the above-mentioned computer analyses were aimed at ensuring that there would be no personal injuries or damage to the mine. As part of this study, several methods were used to determine where the possibility of stress interactions could occur. One of which mapped the overburden-to-interburden ratio. Historically, when the ratio of the two factors is less than 5, no problems should occur. However, when

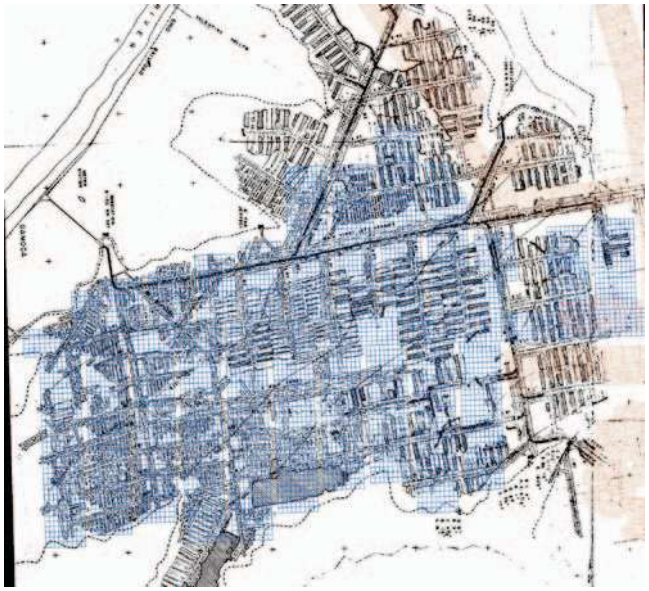

Figure 5. Showing the Lick Branch Mine and projections (Orange and Blue) with the Midvale #1 mine map superimposed.

the ratio is greater than 15, extreme ground control troubles are to be expected. In this case, the possibility of an interaction was found to depend on gob-width-to-interburden-thickness ratio, site-specific geology and horizontal-stress-to-rock-strength ratio in addition to the overburden-to-interburden ratio (Zipf, 2005). The map in Figure 6 shows the contour values of the overburden to interburden ratio. Note that the dark shaded pillars of the Midvale No. 1 mine have safety zones around each one where additional supplemental support is to be installed for increased stability. Prior to CONSOL Energy operating the Lick Branch mine, the former operator drilled test holes within the Powellton-No. 2 Gas interburden approximately every 250 ft. Drilling the test holes was done to determine if water, methane, or pillars were present at that particular location in the No. 2 Gas mine works (Figure 7).

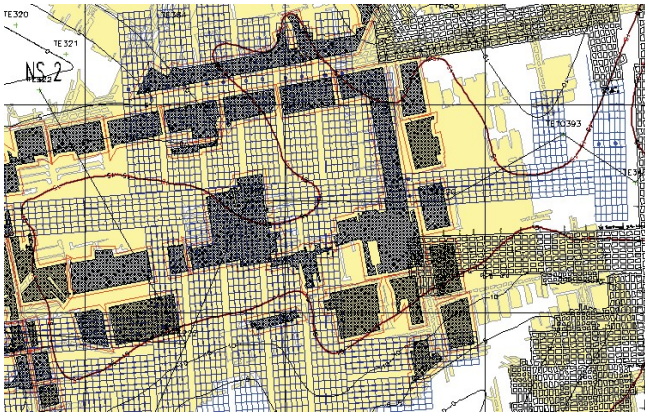

Figure 6. Contoured values of the Overburden to interburden ratio. The maximum ratio of 15 is highlighed with the red contour.

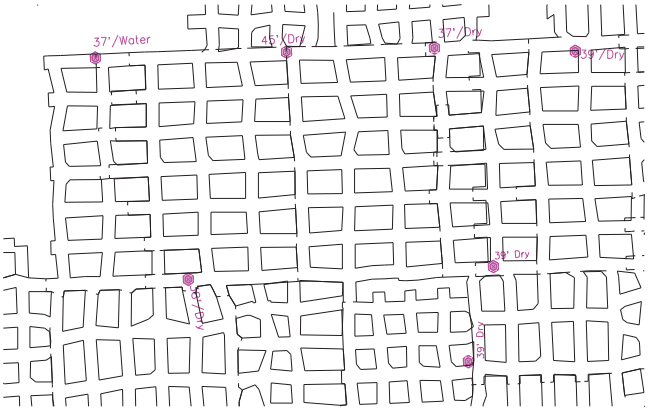

Figure 7. Map of Lick Branch showing test holes drilled into the Midvale #1 mine works. Note that each hole shows the Interburden thickness and whether water was encountered or not.

MULTIPLE SEAM INTERACTION ANALYSES

Analysis of Multiple Seam Stability (AMSS)

AMSS software was employed to analyze the multiple seam interaction between the Lick Branch Mine (Powellton seam) and the Midvale No. 1 Mine (No. 2 Gas seam). AMSS is based on more than 300 multiple seam case histories in the U.S. These case histories were analyzed with the multivariate statistical technique of logistic regression (Mark, Chase, and Pappas, 2007). Stress concentrations caused by the pillars left in the No. 2 Gas seam were the main concern for this study. In addition, water-pooled areas were also considered in this undermining condition due to the ultra-close mining scenario. Since CONSOL Energy was committed to first-mining only, only the development condition was analyzed.

As mentioned above, prior to running the computer programs, the pillars left in the Midvale No. 1 mine were identified. According to AMSS, the remnant structures were classed into two types: gob-solid boundaries with gob on one side and isolated remnant pillars that are surrounded by gob on two or more sides. It is well known that a gob-solid boundary carries a single, distributed abutment load, while an isolated remnant pillar is subjected to two, overlapping abutments. As a result, the stress concentration on an isolated remnant pillar is usually significantly larger than that on a gob-solid boundary, and its impact on underlying seams is proportionally greater (Figure 8). The remnant structures in the No. 2 Gas seam were governed by the rule described in AMSS: if the pillar width exceeds five times the square root of the depth of cover, then the pillar is so large that the abutment loads probably do not overlap, and it should be considered as two gob solid boundaries. Otherwise, the pillar should be considered as isolated remnant pillar (Mark, Chase, and Pappas, 2007).

Water-pooled areas were identified in the Midvale No. 1 mine based on the mine geometry and the bottom-of-seam structure. Since the interburden thickness between the No. 2 Gas seam and the Powellton seam is considered ultra-close, it is necessary to employ larger pillar sizes in the Lick Branch mine under the water-pooled areas to ensure pillar stability and to prevent water inflow. Accordingly, a pillar stability factor under the water-pooled areas greater than 2.0 was mandated by MSHA. For areas outside the water-pooled areas, a pillar stability factor of 1.5 was required. The stability factors were calculated for each projected panel. To meet the stability factor requirement, the pillar size and entry numbers were adjusted based on site-specific conditions (overburden depth, interburden thickness, seam thickness, width of gob, and water-pooled area extent).

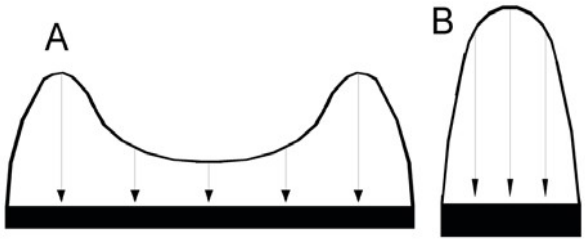

Figure 8. Stress concentrations in multiple seam mining. (A) gob-solid boundaries associated with a very large pillar and (B) remnant pillar isolated in the gob. (Mark et al., 2007b).

Results of the AMSS Analysis

Figure 9 shows an example of the AMSS calculation of a remnant pillar that is in the S-9 panel. This is the worst-case scenario; it shows the presence of an isolated remnant pillar and presence of a water-pooled area in the No. 2 Gas seam under relatively deep overburden. According to the AMSS calculation, a seven-entry panel with 70x90-ft pillar size was recommended to achieve a pillar stability factor of 2.07. In this case, the AMSS output shows that the development stability is in the yellow zone (Figure 10), which essentially indicates that a moderate interaction is possible. As a result, roof bolts one ft longer than the 5-ft minimum stated in the roof control plan were recommended for the areas within 40 ft of the safety zone (red line in Figure 9) to provide additional support to the roof. In addition, five cable bolts were also recommended for all intersections within the safety zone.

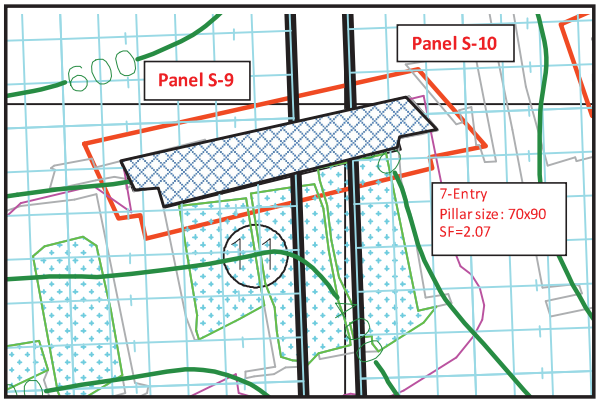

Figure 9. AMSS calculation for an isolated remnant pillar.

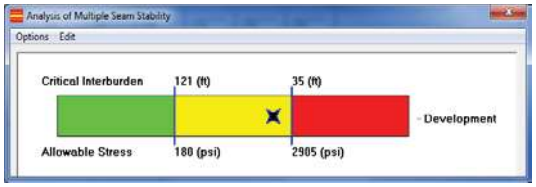

Figure 10. AMSS calculation result for an isolated remnant pillar.

NUMERICAL MODELING: FINITE ELEMENT ANALYSIS

To verify the pillar design provided by AMSS, as well as to increase understanding of the geotechnical interaction between the mined-out No. 2 Gas and Powellton coal seams, a FEM model was created using RocScience Phase^2 software. While the results of AMSS are limited to the calculation of the maximum vertical stress on the underlying pillars and the safety factor for these pillars, the FEM modeling approach offers a comprehensive picture of the field stresses, deformation, and safety factors distributed throughout the whole domain of the model.

One of the important aspects of analyzing the interaction between two coal seams is the size of the overlying pillars. The two-dimensional FEM model in Phase^2 was created to represent the most critical stress concentration condition due to an isolated remnant pillar (circled in Figure 11) located in the Midvale mine at the No. 2 Gas seam level. This isolated remnant pillar overlaid a portion of the designed room-and-pillar S-8 and S-9 panels towards the southeast of the Lick Branch mine at the Powellton seam level. Based on the multiple seam interaction theory (Mark, Chase, and Pappas, 2007), when undermining at a depth of 650 ft, an overlying pillar is considered "isolated remnant" if its width is less than 127 ft, or the pillar is considered "gob-solid boundary" if its width is greater than 237 ft.

FEM Model Input

Figure 12 shows a close-up of the FEM model domain, where a 90-ft-wide isolated remnant pillar overlays the 70 x 50-ft^2 pillars (90 ft by 70 ft center-to-center), separated by an interburden of approximately 45 ft. The FEM model covers 500 ft of the field on both sides of the remnant pillar, as well as 300 ft of rock above the gob in the Midvale mine, as depicted in Figure 14. The entire overburden is simulated by applying a uniform load distributed along the upper model boundary (308 ft above the remnant pillar), which is equivalent to the 650 ft of overburden. The rock units conforming to the interburden in the model, as well as the units below Powellton seam (up to 13 ft), were extensively tested in the laboratory in order to obtain the input parameters for the model. Compressive strength of all units was obtained, averaging the results from point load tests. Young's modulus and tensile strength of the sandstone was obtained by conducting uniaxial compression tests and Brazilian tests, respectively. Unit weight, Poisson's ratio, and moduli of the rest of the materials were estimated using typical values reported in the literature (Blair, 1955; Holland, 1941; Rusnak, 1998). Table 1 summarizes the material mechanical properties used as input to the model.

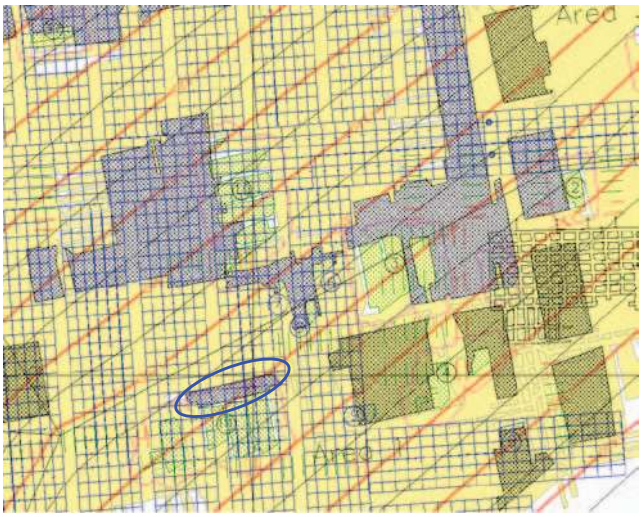

Figure 11. Detail of the superimposed mine maps: Midvale's mined out area in yellow with remnant coal blocks hashed and flooded areas in doted green. Lick Branch mine projections as the dark blue grid and its existent development with black lines. Bottom of Powellton coal seam elevation in the red intervals.

The FEM model consists of two stages. In the first stage, the geostatic stress equilibrium is calculated after applying only gravity. In the second stage, excavations are applied and, simultaneously, the unit weight of the interburden sandstone is changed from 162 to 2,000 lb/ft^3. This modification of the material property takes care of the limitation of the program to run only two-dimensional cases. A "heavier" interburden was imposed to simulate the effect that the real three-dimensional case would have on a pillar, in that, the abutment load on any pillar increases based upon the extraction of both entries and crosscuts. This implementation is carefully calibrated against the analytical calculation of pillar vertical stresses.

Moreover, the gob material in the Midvale mine is modeled taking into account the following premises: (1) there is a dome-like shape at the gob-pillar interface due to natural caving (portrayed on Figure 12 and 15), (2) the gob height reaches 3 times the mined thickness, based on a bulking factor of 1.5 for the sandstone, (3) the maximum compaction of the gob is reached approximately at a distance of H/3 from the pillar edge, where H is the mining depth. Figure 13 illustrates five different zones of the gob, which reflect an increase of the gob material strength as a function of the distance away from the pillar edge, (4) the density or level of compaction of the gob—away from the pillar edge—increases gradually until reaching maximum compaction. The values of elastic moduli and compressive strength shown in Table 2 are selected based on a comprehensive study by Pappas and Mark (1993), and (5) surrounding the gob zone, interface elements having non-cohesive frictional properties are incorporated (depicted by the blue/red line in Figure 15). This feature simulates the discontinuous nature of the gob with respect to the adjacent strata. In order to save on computational cost, half of the model is simulated due to the symmetric nature of the problem. The model boundary conditions and constraints implemented are illustrated in Figure 14.

Table 1. Mechanical properties of the materials used in the FEM model.

	g	E	sc	n
	(lb/ft^3)	(psi)	(psi)	(-)
Sandstone	162	1,500,000	14,000	0.2
Fireclay	160	1,000,000	9,400	0.3
Shale	156	875,000	7,000	0.35
Massive Sandy Shale	160	1,400,000	17,700	0.25
Gob	100	3,500 max	1,440	0.49
Coal	82	210,000	900	0.3

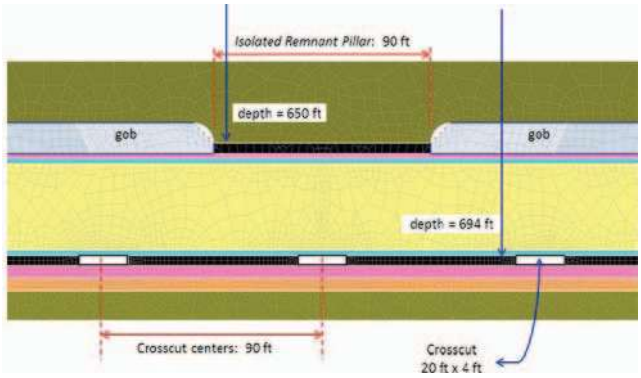

Figure 12. FEM model geometry of the worst case scenario of an isolated remnant pillar in Midvale mine overlaying the room-and-pillar Lick Branch mine.

Table 2. Variation of gob's elastic modulus and compressive strength with respect to the distance to the pillar edge.

	Gob 1	Gob 2	Gob 3	Gob 4	Gob 5
E (psi)	700	1,400	2,100	2,800	3,500
s_c (psi)	240	540	840	1,140	1,440

Results of the FEM Analysis

Figure 14 presents the vertical stress (in lbs/ft^2 or 4.79x10^{-5} Mpa) distribution after the second stage, after Lick Branch mine entries and crosscuts have been excavated. The distribution of vertical stresses shows a subtle concentration of stress (small red/orange area) at the gob-pillar interface of the No. 2 Gas seam, in contrast to the large (and expected) concentration of stress on the pillar underlying this remnant, at the Powellton seam level. Clear details on the worst-case scenario at the Lick Branch mine are shown in Figure 15. Non-colored areas next to the red stress contours represent larger values of stress, (for example, right at the pillar edge). Non-colored small areas around excavations, next to the blue contour, represent stress values less than zero(in that, the material is in tension). The crossed line along Powellton seam pillars was used to measure the vertical stress at these locations

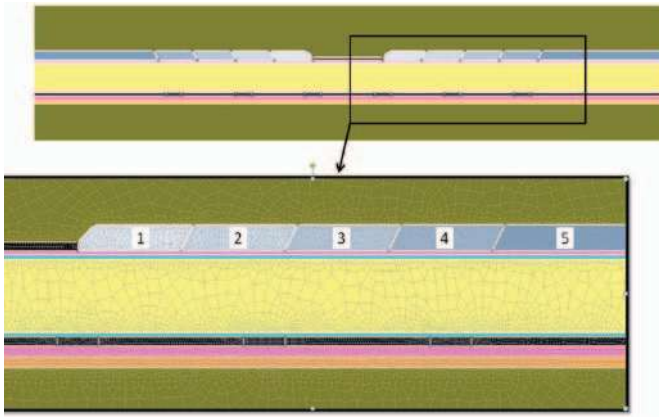

Figure 13. Discretization of the gob to represent the gradual increase of strength away from the rib.

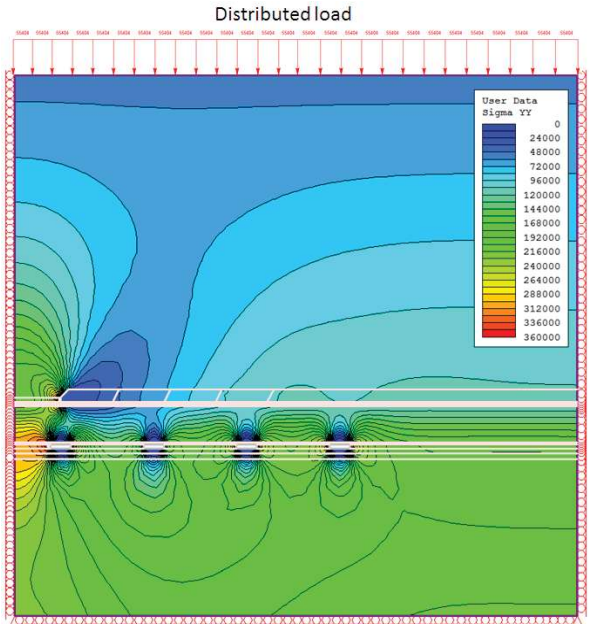

Figure 14. Whole FEM model domain and boundary conditions. Symmetry along the middle of the remnant pillar is used to save on computational cost. Colored contours correspond to the vertical stress distribution (in psf) after cross-cuts in Lick Branch mine have been excavated.

and, consequently, compare them with the results from the AMSS analysis, as can be seen in the next section.

One of the most important pieces of information from the FEM model is the distribution of strength (or safety) factors throughout the field. The strength factor in Phase^2 is defined as the ratio of the maximum strength and the effective stress (also known as Von-Mises stress). The maximum strength of the material is calculated based on the Hoek-Brown failure criterion. Figure 16 portrays the contours of strength factor from less than 0 (red) to greater than 5.5 (blue). The red zones represent the material under tension, which

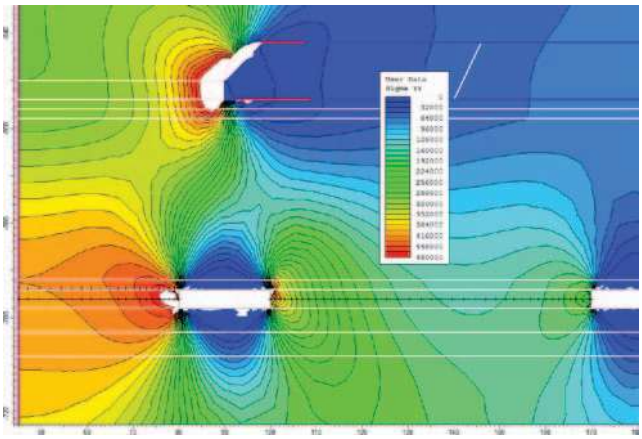

Figure 15. Vertical stress concentration in and above a 70x50 ft² pillar in Lick Branch mine overlaid by the 90-ft wide isolated remnant pillar in Midvale mine.

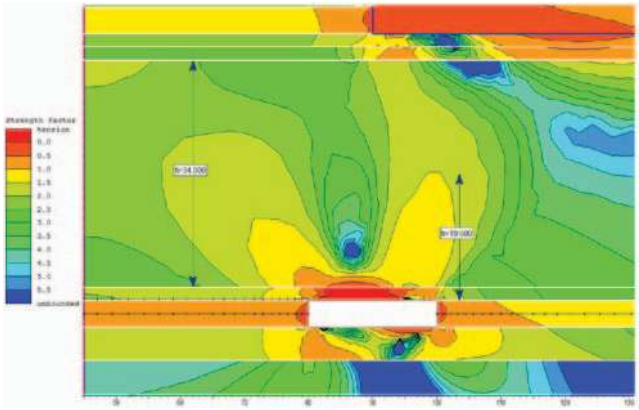

Figure 16. Distribution of strength factors surrounding the entry adjacent to the most critical pillar.

is expected to occur along the roofline of the entries. The orange and light red zones correspond to failed material. It is important to mention that this model includes no roof (man-made) support. The yellow zone has an upper bound strength factor of 1.5, which extends up to 19 ft over the entry adjacent to the most critical pillar. Above 19 ft of the Powellton seam, the strength factors are 2.0 or higher in the sandstone horizon, demonstrating safe mining conditions.

The horizontal position of the entry underneath the isolated remnant pillar was thought to cause an effect on the stresses at the Lick Branch mine level. Figure 17 depicts a variation of the entry locations with respect to the overlying remnant. Figure 17a is a zoomed-out version of Figure 16, showing the array of pillars away from the critical one and the strength factor distribution around them. Figure 17b illustrates the case where the critical pillar is shifted to a location right underneath the remnant-gob interface at the No. 2 Gas seam level. It can be seen that this case scenario improves the conditions as far as strength factor is concerned. Although there is a decrease of strength factor in the vicinity of the remnant-gob interface (yellow zone, 1.0 < SF <1.5), it never

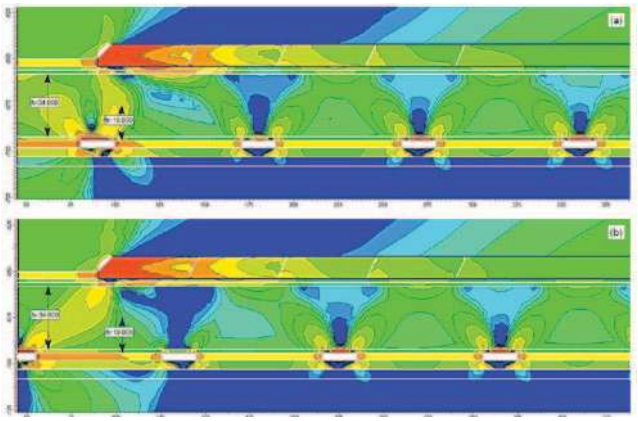

Figure 17. Distribution of strength factors with underlying entries located with respect to the critical pillar a) perfectly underneath the remnant pillar, or b) under the remnant-gob interface.

connects to the Powellton seam yellow zone, which had decreased height above the entry.

Comparison between AMSS and Phase² Results

The vertical stress variation calculated by Phase² and AMSS along the horizontal axis from the most critical pillar expected in the Lick Branch mine is illustrated in Figure 18 and Figure 19, respectively. The peak stress predicted by the FEM model is 3,657 psi, and the average vertical stress on the critical pillar is 3,083 psi; whereas, these same stresses provided by AMSS are 3,200 psi and 2,870 psi, respectively. Although the peak stresses diverge by 12%, the average stresses from both approaches compare well, with a 7% difference. This comparison serves as benchmark to validate the Phase² model results and vice versa.

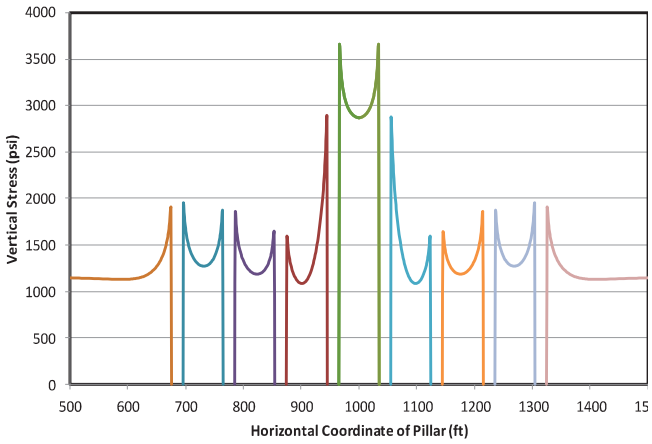

Figure 18. Prediction of vertical stress along the horizontal distance from the critical pillar (in the middle) in Lick Branch mine provided by the FEM Phase² model.

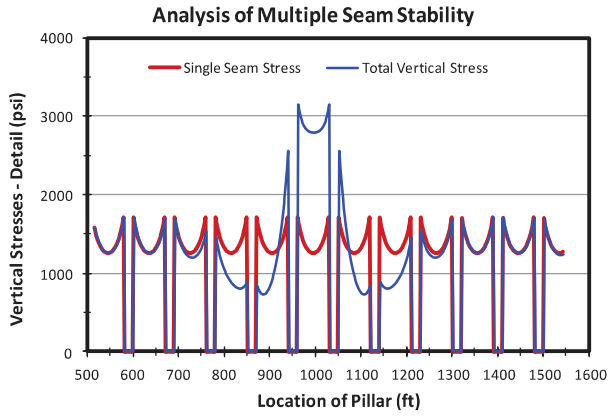

Figure 19. Prediction of vertical stress along the horizontal distance from the critical pillar (in the middle) in Lick Branch mine provided by the AMSS program.

UNDERGROUND OBSERVATIONS

Mining of the Powellton Seam by CONSOL Energy's Lick Branch Mine commenced in February 2011 and continued for eight months. To date, no 25-ft deep hole encountered water under the water-pooled zone, which validates the results from the RocScience Phase^2 FEM analysis. Also, in-mine observation of excellent pillar stability and roof condition confirms the validity of the AMSS analysis.

CONCLUSIONS

Drilling of the core hole in December 2010, along with existing core holes throughout the projected mining areas, provided detailed geologic mapping of the interburden, as well as the strength and other mechanical properties of the thick massive sandstone. This served to satisfy the guidelines outlined in the USBM IC8741 (Babcock, 1977). It stated that "where at least one competent bed of sandstone or similar material is present within the solid strata and has a thickness at least 1.75 times the maximum entry width, mining at a lesser cover than 5*s* or 10*t* may be considered", where *s* is the maximum entry width and *t* is the maximum entry height.

On the other hand, the FEM modeling effort using the RocScience Phase^2 Program provided an accurate prediction of the stress distribution and interaction, and its results were in excellent agreement with those from the AMSS analyses. Consequently, the proposal to drill only 25 ft up into the roof of the Lick Branch mine every 300 ft of development was approved by Federal and State agencies. This positive outcome fulfilled not only the compliance goal, but also CONSOL's goal of safety, because the introduction of water, black damp, methane, or any other potential hazard into the Lick Branch mine has now been avoided.

Lastly, underground observations of pillar and roof stability confirmed the validity of the AMSS analyses, and, together with the drilling results of 25-ft deep-water-test holes, confirmed the accuracy of the FEM analysis.

REFERENCES

Babcock, C. O. (1977). Results of research to develop guidelines for mining near surface and underground bodies of water. Ann Arbor, MI: University of Michigan Library, pp. 24.

Blair B. E. (1955). Physical properties of mine rock. Part III. Department of the Interior, U.S. Bureau of the Mines, pp. 69.

Holland C. (1941). "Physical properties of coal and associated rock as related to causes of bumps in coal mines." *AIME Technical Publications and Contributions 1942:17.*

Mark, C., Chase, F. E., and Pappas, D. M. (2007). "Analysis of multiple seam stability." In: *Proceedings of the 26th International Conference on Ground Control in Mining*. Morgantown, WV: West Virginia University, pp. 5–18.

Pappas D. M. and Mark C. (1993). Behavior of simulated longwall gob material. Department of the Interior, US Bureau of the Mines, pp. 39.

Reger, D. B., Price, W. A., Tucker, R. C., and Sisler, J. D. (1921). "Nicholas County." In: West Virginia Geological and Economic Survey. Wheeling, WV: Wheeling News Litho. Company, pp. 847.

Rusnak J. (1998). "Application of the coal mine roof rating, derived from drill core, in the roof support design of a coal belt conveyor tunnel." In: *Proceedings of the 17th International Conference on Ground Control in Mining*. Morgantown, WV: West Virginia University, pp. 221–230.

Zipf, R. K. (2005). "Failure mechanics of multiple seam mining interactions." In: *Proceedings of the 24th International Conference on Ground Control in Mining*. Morgantown, WV: West Virginia University, pp. 93–106.

Mitigation of a Massive Sandstone Channel's Impact on a 1,500–Ft–Wide Longwall Face

Daniel W. Su, Sr. Geomechancial Engineer
Gregory J. Hasenfus, Sr. Geomechanical Engineer
Luke Stull, Geologist
Jun Lu, Geomechanical Engineer
Mark Van Dyke, Geologist
Stephen Morgan, Geologist
Coal Operations Engineering
Consol Energy Inc.
Canonsburg, PA

Paul Kelley, Mine Engineer
Enlow Fork Mine
Consol Energy Inc.
Claysville, PA

Donald Teeter, Project Engineer
Pennsylvania Operations
Consol Energy Inc.
Claysville, PA

ABSTRACT

This paper presents the implementation and evaluation of the hydraulic fracturing technique and Longwall Visual Analysis (LVA) software to mitigate the impact of a 1,000-ft (305-meter) widemassive sandstone channel on a 1,500-ft-wide (457-m-wide) longwall face. Based on a underground roof geology reconnaissance program, four frac holes were drilled and fraced along the center axis of the sandstone channel. To further provide detailed monitoring of the longwall face, the Longwall Visual Analysis (LVA) software was installed to track the face pressure and cavity formation index. In mid-December 2011, the longwall face approached and entered into the western edge of the sandstone channel. The longwall face mined through the center axis of the sandstone channel in mid-January 2012 and advanced outby the eastern edge of the sandstone channel in early February 2012. Results from daily underground observations and production delay analysis confirmed the effectiveness of the hydraulic fracturing program and the validity of the LVA Software.

INTRODUCTION

A nearly 1000-ft wide sandstone channel was projected to run through the mid panel area of a 1,500 ft (457 m) wide longwall panel in a southwestern Pennsylvania coal mine. This sandstone channel was known to cause serious longwall face roof control problems in the mine's B-panel area in 1998 and 1999; and most recently, it induced many large face cavities and caused substantial production delay in the preceding panel. For the two B panels mined in 1998 and 1999, hydraulic fracturing of the massive sandstone was conducted to facilitate better caving, thus relieving cantilever compressive stress at the longwall face. Vastly improved longwall face condition was observed and four weeks of mining delay due to bad roof condition was eliminated. The implementation of hydraulic fracturing technique, results of underground observation and measurement, and results of numerical modeling were summarized in a paper presented in the 20th International Conference on Ground Control (Su et al., 2001).

This paper presents a summary of the activities that took place over a 4-month period (October 2011 through February 2012) at the CONSOL Energy longwall mine mentioned aboveto improve face condition and safety of underground personnel during mining of the 1,500 ft (457 m) wide longwall panel. The elevated concern for safety was driven by adverse face conditions encountered while mining the preceding longwall panel. Many of the problems were attributed to a thick and massive sandstone channel. A joint task force consisting of Coal Operations Engineering, Pennsylvania Operations Engineering, and CNX Gas personnel was formed in August 2011, which recommended drilling four hydraulic fracturing holes along the center axis of the sandstone channel to reduce pressure and improve face conditions at the 1,500 ft (457 m) wide longwall face. To further provide detailed monitoring of the longwall face and to evaluate the effectiveness of the hydraulic fracturing program, the Longwall Visual Analysis (LVA) software (Hoyer, 2011) was installed in early December 2011 to track the face pressure and cavity formation index along the longwall face.

In mid-December 2011, the 1,500 ft (457 m) wide longwall face entered the western edge of the nearly 1,000 ft (305 m) wide sandstone channel, and the face cleared the eastern edge of the sandstone channel on February 3, 2012. To evaluate the effectiveness of the hydraulic fracturing program and the validity of the LVA software, the Geomechanical Group of Coal Operations Engineering conducted daily face monitoring over a four-week period. The correlations among the observed face conditions, the hydraulic fracturing hole locations and LVA cavity formation prediction will be discussed in this paper.

GEOLOGIC RECONNAISSANCE, SANDSTONE CHANNEL AND GEOTECHNICAL EVALUATION

Upon encountering the massive sandstone channel in the preceding panel in February 2011, a detailed underground geologic mapping program and a detailed underground roof scoping program, which employed a 20 ft (6.1 m) long fiberscope, were initiated in the track entries of the preceding and the current1,500 ft (457 m) wide longwall face. In addition, a sandstone channel projection over the past and current mining areas was constructed from available surface core hole information. Figure 1 shows the projection of the massive sandstone channel (double red lines) over the preceding and current 1,500 ft (457m) wide longwall panels.

To determine the exact location of the sandstone channel and its properties, in-mine roof coring was also conducted by CONSOLCoal Operations Engineering's Geologic, Geomechanical

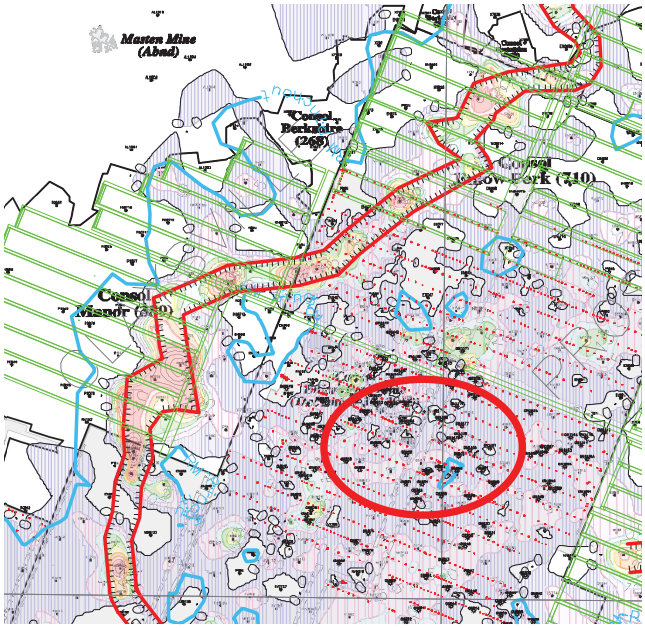

Figure 1. Projection ofmassive sandstone channel.

and Degas groups, which showed that the sandstone channel was nearly 1,000 ft (305 m) wide and more than 60 ft (18.3 m) thick, and the center axis of the sandstone channel is between crosscuts 30 and 29 (Figure 2). The extracted cores were logged and tested for uniaxial compressive strength. As expected, the cores from the center axis of the sandstone channel showed that the sandstone was rather massive and medium- to coarse-grained. Table 1 lists the mechanical properties of the sandstone, which are very similar to the strength results obtained in 1998 and 1999 (Su et al., 2001). Note that although the sandstone was not exceptionally strong (~8,000 psi (~55 MPa) compressive strength), it was medium-to-coarse grained and rather massive and possessed very high flexural rigidity due to its 60 feet (18.3 meters) thickness.

Based on the stress ellipsoid of 5,000 psi (34 MPa) East–West and 3,500 psi (24 MPa) North–South obtained from a prior stress measurement programusing the CSIRO MINIFRAC technique (Su and Hasenfus, 1995), under a cover depth of 700 ft (219 m), horizontal pancake fractures are expected at the selected hydraulic fracturing locations. Due to surface topography and property ownership constraints, four frac wells were planned along the center axis of the sandstone channel (Figure 3).

HYDRAULIC FRACTURINGOFTHE SANDSTONE CHANNEL

Mine management was very concerned over the face width because the 1,500 ft (457m) wide face possesses 400 ft (122 m) more mid-face area compared to the previously employed 1,100 ft (335 m) wide face. Also, due to a shield rotation program, 262 PM4 shields, which were designed for limestone geology and possessed low set load density, were employed at the 1,500 ft (457 m) wide face. As mentioned above, a joint task force consisting of Coal Operations Engineering and Pennsylvania Operations personnel recommended drilling four hydraulic fracturing (frac) holes along the center axis of the sandstone channel.

A drilling program was initiated in mid-October 2011 to drill four boreholes 300 ft (92 m) apart across the 1,500ft (457m) wide longwall panel (Figure 3). The boreholes were drilled from the surface to 5 ft (1.5 m) above the bottom of the sandstone channel. The drill holes were purposely stopped at 5 ft (1.5m) above the bottom of the sandstone channel to avoid penetrating the coal seam, which would then speed up the permitting process. After drilling and setting casing, perforations were shot into the casing at the targeted horizons to pre-fracture the sandstone. The perforation tool was about 4 ft (1.22 m) long and had 4 shot per foot (0.3 m). The estimated shot penetration into the borehole surface was about 26 to 30 inches (0.66 to 0.76 m).Water fracing, as opposed to the nitrogen foam fracing used in 1998, was employed, since enough surface area was present for the water trucks. During the 1998 fracing operations, very limited surface area was present which led to the choice of the more expensive and dangerous nitrogen foam fracing.

The four holes were successfully fraced on November 13 and 14, 2011. Two-stage hydraulic fracturing was conducted in Hole #1, located about 300 ft (92 m) from the tailgate, at 24 and 42 ft (7.3 and 12.8 m) above the bottom of the sandstone channel (Figure 4). Note that the intended frac horizons were initially set at 15 and 30 feet (4.6 and 9.2 m) above the bottom of the sandstone channel. However, due to a 10 ft (3.1 m) discrepancy in measuring the hole depth where the driller measured hole depth from their drill platform instead of the ground surface, the boreholes were actually stopped at approximately 15 ft (4.57 m) above the bottom of the sandstone channel. Similar hole depth measuring discrepancy also occurred at Hole #2. To reduce water usage, one-stage hydraulic fracturing was conducted in Hole #2 at 28 ft (8.5 m) above the bottom of the sandstone, in Hole #3 at 15 ft (4.57 m) above the bottom of the sandstone, and in Hole #4 at 14 ft (4.27 m) above the bottom of the sandstone. The average fracture initiation pressure was about 5,000 psi (34.5 MPa). The average shut-in pressure was about 500 psi (3.45 MPa), indicating the creation of horizontal pancake fractures (Figure 5). Also, the bottom hole frac gradient was large than 1.0, typically indicating the creation of horizontal pancake fractures. The estimated horizontal pancake fracture ellipsoid in each hole was about 250 ft (76.2 m) in the E–W direction and 150 ft (45.7 m) in the N–S direction. The pancake fracture ellipsoid was estimated based on the amount of water used, which averaged about 4,200 gallons per frac initiation and propagation. Well perforations and hydraulic fracturing were conducted by Weatherford and Superior Well Services, respectively. The project was conducted under the supervision of CONSOL PA Operations Engineering and CNX Gas.

FACE MONITORINGAND EVALUATION

To further provide detailed monitoring of the longwall face and to enable the prediction of excessive face pressure and cavity formation, the Longwall Visual Analysis (LVA) software was installed in early December 2011 to track the face pressure and cavity formation index.The LVA software has been used successfully in Australian coal mines to predict roof weighting and longwall face cavity formation over the past few years (Hoyer, 2011). In mid-December 2011, the 1,500 ft (457 m) wide longwall face entered the western edge of the nearly 1,000 ft (305 m) wide sandstone channel, and the longwall face cleared the eastern edge of the sandstone channel on February 3, 2012.

Table 1. Test results from in-mine core samples.

Sample (#)	Rock Type Sandstone Coal	Distance Below / Above BOC / TOC (ft)	Axial Tests Estimated Avg. Uniaxial Compressive Strength (psi)	Diametral Tests Estimated Avg. Uniaxial Compressive Strength (psi)
R24	SS GRY	51.9	8,900	4,600
R23	SS GRY	51.8	6,500	2,400
R22	SS GRY	45.9	10,800	7,200
R21	SS GRY	45.8	10,600	7,800
R20	SS GRY	41.8	11,100	5,400
R19	SS GRY FGR MIC STK	41.7	13,800	3,600
R18	SS GRY	37.8	9,700	5,600
R17	SS GRY	37.7	8,500	5,200
R16	SS GRY FGR MIC STK	33.8	11,000	1,400
R15	SS GRY FGR MIC STK	33.7	8,400	1,000
R14	SS GRY	29.5	8,500	5,800
R13	SS GRY	29.4	9,000	5,000
R12	SS GRY	24.4	6,000	4,800
R11	SS GRY	24.3	8,000	5,200
R10	SS GRY	19.9	8,000	5,000
R9	SS GRY	19.8	4,600	5,000
R8	SS GRY	15.9	3,900	5,100
R7	SS GRY	15.8	5,400	5,300
R6	SS GRY	11.1	7,000	5,400
R5	SS GRY	11.0	6,400	5,000
R4	SS GRY	7.6	8,400	3,500
R3	SS GRY	7.5	6,600	1,900
R2	SS GRY MGR FEW MIC STK WBD	3.6	9,700	6,800
R1	SS GRY MGR FEW MIC STK WBD	3.5	8,000	10,500
P8 COAL				
		Sandstone Average	8,283	4,938
		Sandstone Maximum	13,800	10,500
		Sandstone Minimum	3,900	1,000

To evaluate the effectiveness of the hydraulic fracturing program and the validity of LVA software, with assistance from CONSOL Energy's I.E. Group, the Geomechanical Group of Coal Operations Engineering conducted daily face monitoring over a 4-week period. The correlations among the observed face conditions, the hydraulic fracturing hole locations and the LVA cavity formation prediction were recorded daily and are shown in the attached map (Figure 6). Note that the red shaded areas show the locations of the large-chunk sandstone falls at the face, while the brown shaded areas show the locations of the roof coal pot out without sandstone failure. Clearly, Figure 6 indicates that there is a strong correlation between the hydraulic fracturing hole locations and the locations of the large-chunk sandstone falls at the face. Prior to entering into the influence zones of the four frac ellipsoids, severe face pot outs and sandstone failure were present at the 1,500 ft (457 m) wide longwall face, which caused about one week of face downtime in late December 2011. Once the longwall face entered the influence zones of the four frac ellipsoids, roof conditions along the 1,500 ft (457 m) wide longwall face improved considerably.However, face pot outs and minor sandstone failure were still present along the gaps between the frac ellipsoids.

Figure 6 also illustrates that there is a very strong correlation between the LVA cavity index and the observed sandstone falls at the 1,500 ft (457m) wide face.It is important to note that, while the standard LVA cavity index warning is preset at 80%, due to the large tip-to-face distance and low set load density employed by the PM4 shields, the LVA cavity index warning was reset to 40%

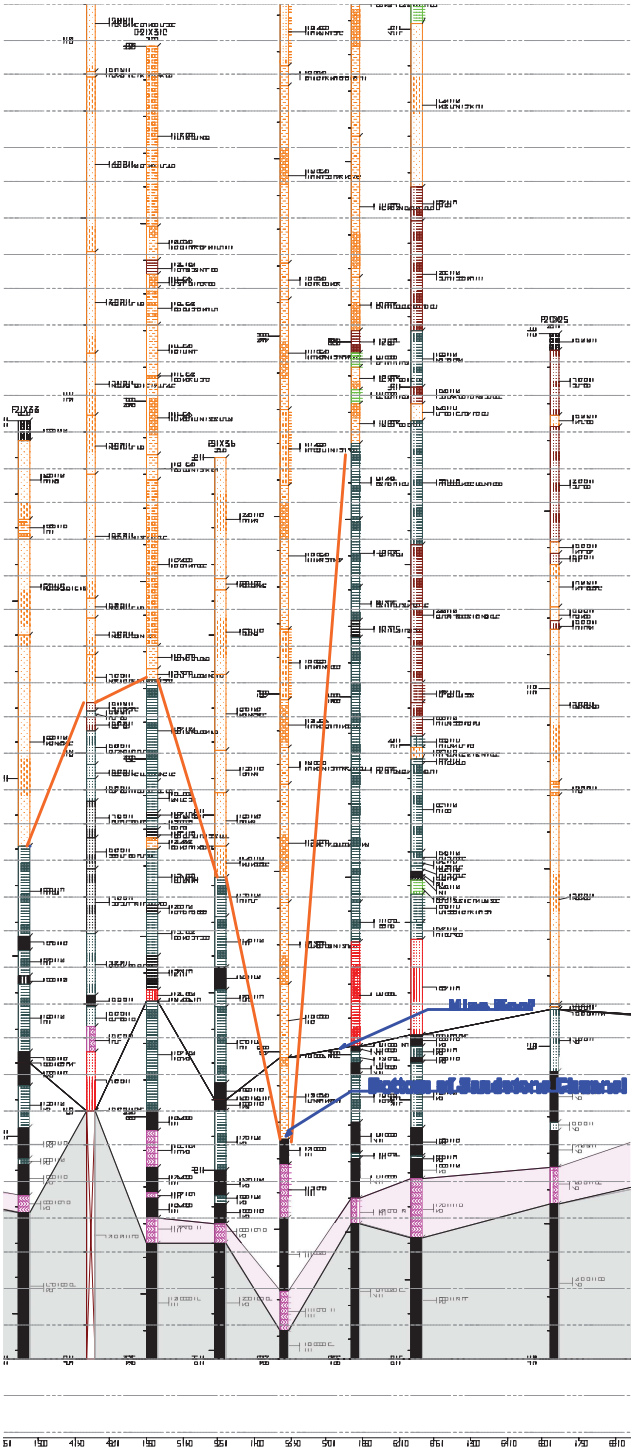

Figure 2. Cross-section of in-mine core and scope holes.

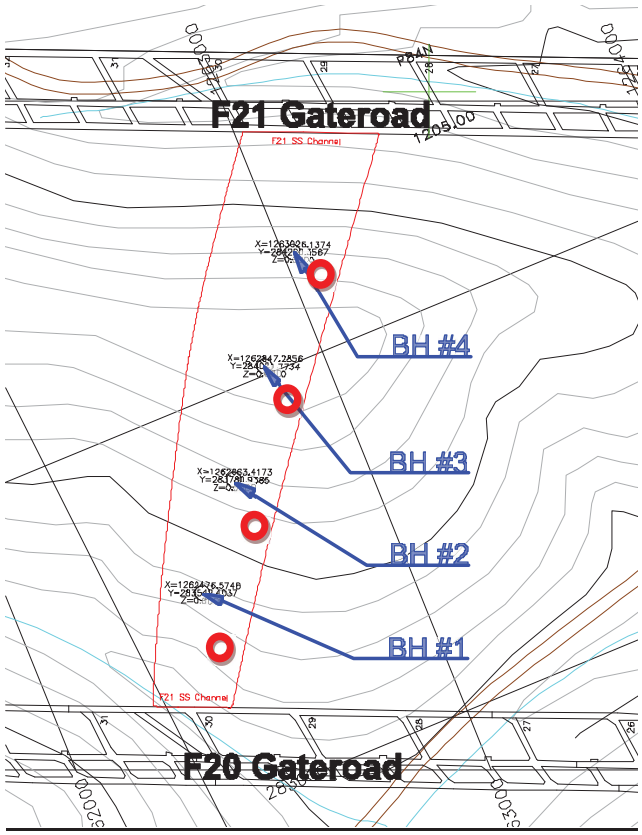

Figure 3. Location of boreholes over the 1,500-ft-wide longwall panel.

for this PM4 face. With this lower cavity index warning, Figure 6 shows that the correlation between the LVA 40% cavity index and the sandstone falls at the 1,500 ft (457 m) wide face is about 80%. After observing the strong correlation and gaining confidence, the LVA information was used by the Mine Longwall Coordinator to successfully guide the longwall face crew to institute double-pull behind the shearer drum to reduce the tip-to-face distance at the critical spots along the longwall face.

CONCLUSIONS

This paper presents the successful implementations of the hydraulic fracturing technique and LVA software to mitigate the impact of a 1,000 ft (305 m) wide massive sandstone channel on a 1,500 ft (457 m) wide longwall face.Based on the results of a month-long monitoring shown in Figure 6, it is apparent that three additional frac holes may be needed to fill the gaps. Alternatively, more water could be pumped into each frac hole to propagate the individual horizontal pancake fractures to enable them to overlap one another. Pumping more water in each frac hole would be much cheaper than drilling three additional frac holes. Sandstone fracing over the next panel, which is scheduled to start on August 15, will adopt the more cost effective method by pumping more water to propagate the pancake fracture in each hole.

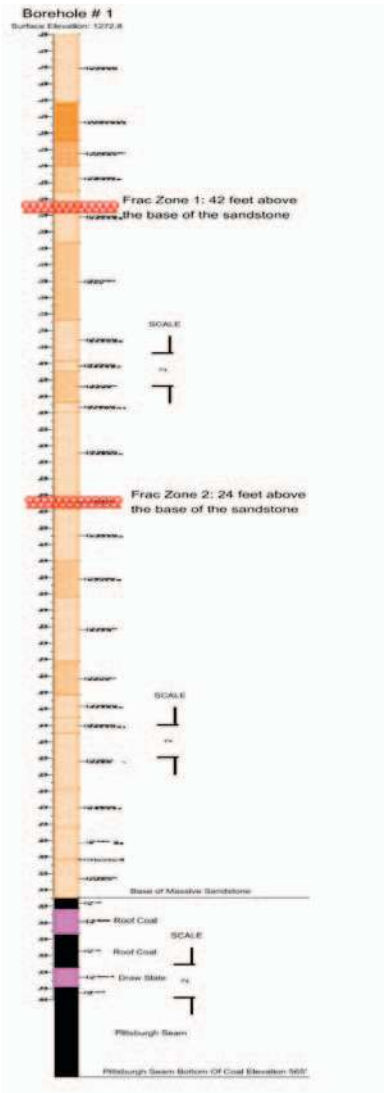

Figure 4. Schematic showing the frac horizons in the sandstone for borehole #1.

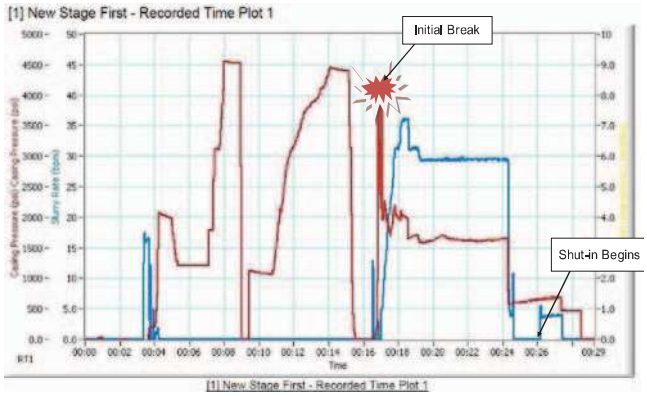

Figure 5. Graph of pressure and water injection rate vs. time for borehole #1, frac 1.

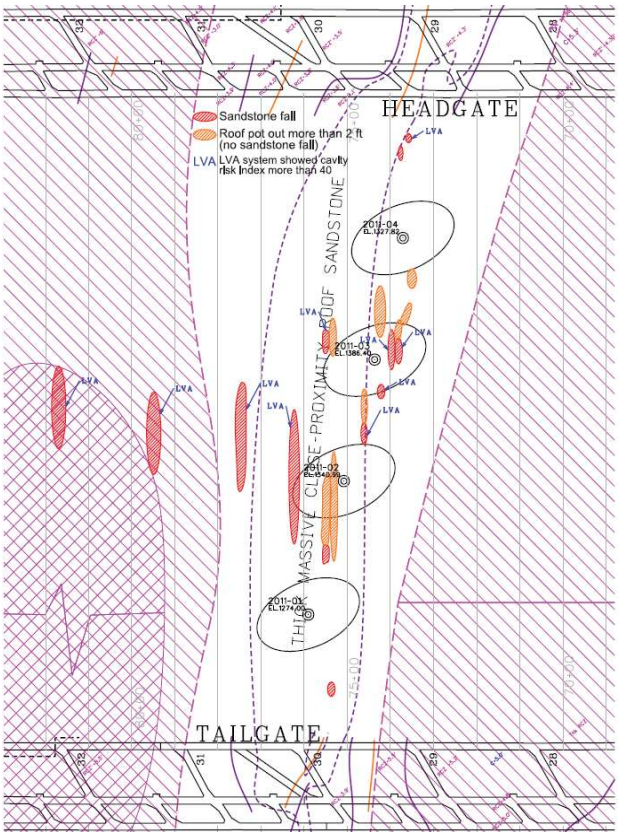

Figure 6. Correlation among the observed face conditions, the hydraulic fracturing hole locations, and LVA cavity formation prediction.

As stated before, the primary purpose of the hydraulic fracturing program is to improve safety for CONSOL underground personnel, since large chunks of sandstone laying on the face conveyor creates tremendous safety hazards. In the end, the hydraulic fracturing program and the application of LVA software have achieved their intended goals of improving safety and increasing productivity at the 1500 ft (457 m) wide longwall face.

REFERENCES

Hoyer, D.(2011). "Early warning of longwall weighting events and roof cavities using LVA software." In: *Proceedings of the 30th International Conference on Ground Control in Mining*. Morgantown, WV: West Virginia University, pp.207–213.

Su, D., Hasenfus, G. (1995). "Regional horizontal stresses and its effect on longwall mining in the northern Appalachian coal field." In: *Proceedings of the 14th International Conference on*

Ground Control in Mining. Morgantown, WV: West Virginia University, pp.39–45.

Su, D., McCaffrey, J., Barletta, L., Thomas, E., Toothman, R. (2001). "Hydraulic fracturing of sandstone and longwall roof control – implementation and evaluation." In: *Proceedings of the 20th International Conference on Ground Control in Mining*. Morgantown, WV: West Virginia University, pp.1-10.

Requirements and Performance of Pumpable Cribs in Longwall Tailgate Entries and Bleeders

Peter Zhang, Senior Geotechnical Engineer
Alpha Natural Resources Services
Alpha Natural Resources, Inc.
Waynesburg, PA

Mike Milam, Senior Director Engineering
Mike Mishra, VP Projects, Engineering and Geology
Alpha Natural Resources Services
Alpha Natural Resources, Inc.
Waynesburg, PA

William J. Hudak, Jr., Senior Mining Engineer
Robert Kimutis, Manager of Engineering
Cumberland Coal Resources, LP
Alpha Natural Resources, Inc.
Waynesburg, PA

ABSTRACT

Pumpable cribs are being increasingly used in longwall tailgate entries and bleeders for roof support under abutment pressure. Their high peak capacity and confinement-controlled yield characteristics from reinforced-bags make them relatively safe and reliable standing supports for highly productive longwall panels. The pumpability of crib material over a long distance from the surface greatly reduces material handling and makes the underground installation more efficient and flexible. However, the performance of pumpable cribs is dependent upon crib properties, crib pattern, quality of installation, and geological and mining conditions. For proper crib selection and safe support design, it is critical to understand the basic technical requirements and performance of pumpable cribs in longwall tailgate entries and bleeders.

Based on more than 10 years of experience using pumpable cribs for longwall standing support, the requirements and performance of pumpable cribs in longwall tailgate entries and bleeders under different mining conditions are presented. Experience shows that the load-displacement curve from full-scale lab testing is a good indicator of pumpable crib suitability for certain applications. Crib peak capacity, stiffness, and residual characteristics define its applicability to certain gate entries and bleeders under different cover depth. Crib pattern and spacing can be determined by abutment pressure level, roof, floor, and rib conditions, local roof stability, and ventilation requirements. To achieve proper in-situ performance, quality control of crib installation is also important.

INTRODUCTION

Pumpable cribs were developed in the late 1990s and were first used to replace wood cribs or concrete cribs in longwall tailgates in Cumberland and Emerald Mines (Mucho, 1999; Chen 2003). Because pumpable cribs are stiffer than wood cribs and Cans, their load-displacement characteristics make their capacity to be used more efficiently in the tailgate within the front abutment pressure zone. Their residual strength and high residual convergence also help make the tailgate inby the face partially open for ventilating the return air to the second entry. Pumpable cribs are also used to support and maintain other gate entries and bleeders for long-term ventilation. Compared to other standing supports in longwall gate entries, the advantages of pumpable cribs are not only their strength and stiffness but also the pumpability of crib material over long distance and the flexibility of installation. The economics of using pumpable cribs can be justified by significant reduction of material handling and substantial improvement of roof stability and longwall safety.

Over the years, several studies have been done on pumpable crib support design, including design methodologies, design criteria, in-situ measurements, and numerical modeling (Mucho, 1999; Chen, 2003; Barczak, 2003; Barczak, 2008; Dolinar, 2010). These studies have helped the development and application of pumpable cribs under different mining conditions.

Since their development, pumpable cribs have been increasingly used in longwall tailgate entries and bleeders for roof support under various conditions (Chen, 2003; Barczak, 2008; Dolinar, 2010). The high peak capacity and confinement-controlled yield characteristics make them a relatively safe and reliable standing support for highly productive longwall panels. The performance of pumpable cribs is dependent upon crib properties, installation pattern, quality of installation, and geological and mining conditions. For proper crib selection and safe support design, it is critical to understand the technical requirements and performance of pumpable cribs in longwall tailgate entries and bleeders.

Therefore, based on more than 10 years of experience in using pumpable cribs for longwall standing support in the Pittsburgh seam, the requirements and performance of pumpable cribs in longwall tailgate entries and bleeders under different mining conditions are presented in this paper.

GEOLOGICAL AND MINING CONDITIONS

Two longwall mines in Western Pennsylvania have been using pumpable cribs for secondary support in gate entries and bleeders since 1998. They are also the pioneers in using pumpable cribs in the United States. Over the years, several products have been tested in the NIOSH Pittsburgh lab and then tried in these mines. To date, four or five crib products have been used in the gate entries and bleeders for secondary support. Experience has shown that the requirements and performance of pumpable cribs are largely dependent on roof and floor geology and overburden

depth. When overburden depth is less than 950 ft, the entries can be well supported by a single row of pumpable cribs. But when overburden depth is greater than 950 ft, crib support has to take into account local roof failure, floor heave, and rib slough age.

The two longwall mines are mining Pittsburgh seam with overburden depth ranging from 500 ft to 1,200 ft. The immediate roof consists of shale, rider coal, and clay stone, while the floor can be clay stone, shale, or limestone. Longwall panels are developed by 3-entry systems with 90–110-ft-wide and 160-200 ft long (center-to-center) gate pillars. The entry height is about 7–8.5 ft, and entry width is 16 ft. The roof is primarily supported by three 8-ft 7/8-in tension bolts with steel straps on 4-ft spacing. Pumpable cribs are used in gate entries and bleeders for secondary support.

PERFORMANCE AND FAILURE OF PUMPABLE CRIBS IN LONGWALL TAILGATES AND BLEEDERS

Load-Displacement Curve from Lab Testing

A pumpable crib is formed by pumping a two-component grout into a reinforced plastic bag. With a high liquid-to-solid ratio, the crib material can be pumped about 12,000–15,000 ft from a surface borehole site to an installation location underground. The strength of a crib is achieved by the intrinsic strength of the cured mixed material and the confinement provided by the reinforced plastic casing of the bag. The strength of the bag, wire spacing, and gauge contribute to the peak and residual capacity of the crib. Pumpable cribs usually achieve full strength four weeks after being pumped. There are several suppliers of crib materials and bags, but the final products give similar load-displacement characteristics. Figures 1-3 show the load-displacement curves from three crib suppliers. Generally, for a 72-in. high and 30-in. diameter crib, the load-displacement curve has a linear portion up to a 1-in. convergence with 150–250 tons of peak load, and about an 8–12-in. convergence with 100–150 tons of residual load. Depending on the crib material and bag reinforcement, the peak load could quickly drop to residual load or sustain a certain period of plastic displacement before reducing to residual load. The failure of a crib begins when shear fractures develop in the crib material, but with bag reinforcement, a crib can maintain peak load for a certain convergence before shedding to residual load. The residual strength is maintained by the confinement of the bag until the bag is broken, and the crib material falls out. With the plastic wrap reinforcement, a crib can take significant residual convergence under compressive loading but could completely lose its supporting capacity under bending or shear loading.

Functions of Pumpable Crib Support

Figure 4 shows the layout of pumpable cribs installed in longwall gate entries with a 3-entry gate pillar system. New cribs are pumped in the head gate entries (second entry and the tailgate for the next panel) close to the face line as the longwall retreats. The cribs pumped for the next tailgate are subjected to slight side abutment pressure inby the current face and to both side and front abutment pressure when the next panel is being mined. The cribs in the current tailgate are loaded under small side abutment pressure from the previous longwall panel and front abutment pressure to about 100–150 ft out by the face. The main function of the cribs in the tailgate is to support the roof within the front abutment pressure zone out by, and to maintain an opening inby the

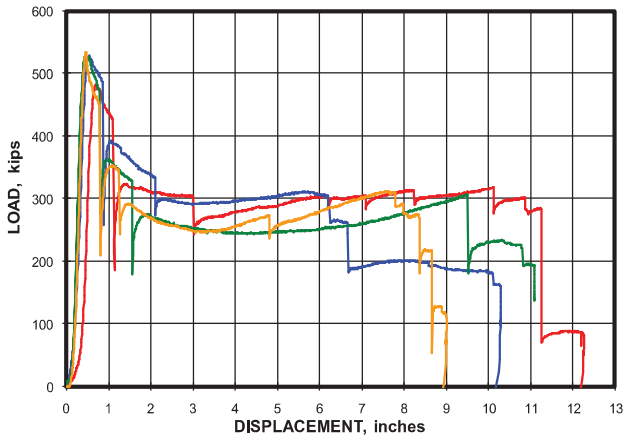

Figure 1. Load-displacement curve for the cribs from supplier I.

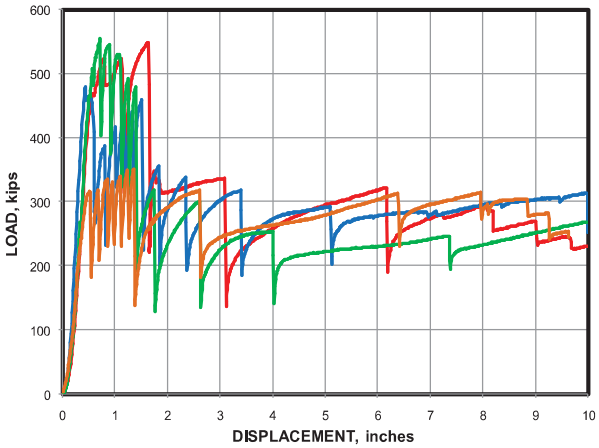

Figure 2. Load-displacement curve for the cribs from supplier II.

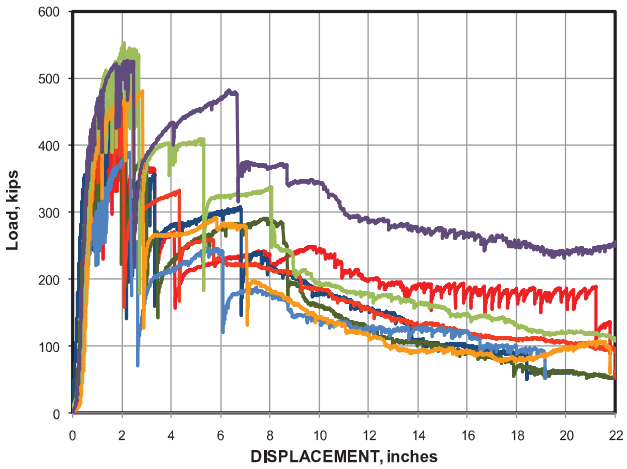

Figure 3. Load-displacement curve for the cribs from supplier III.

face at the edge of the gob to provide a conduit for the ventilation air to the second entry. The cribs pumped in the middle entry will be subjected to side abutment pressures of two gobs inby the current face and to one side abutment pressure of a previously mined panel. The main function of the cribs in the second entry is to keep the middle entry open for ventilation until both panels are mined.

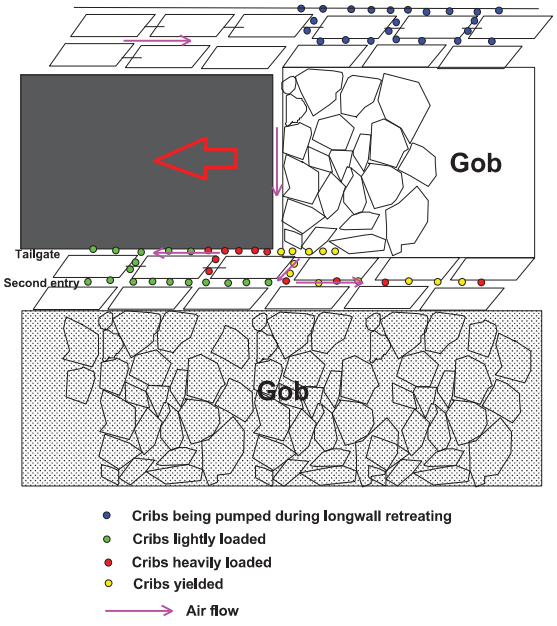

Figure 4. Layout of pumpable cribs in longwall gate entries.

Pumpable cribs are installed in bleeders, typically a four entry system, to establish long-term support for reliable ventilation. In a typical longwall setup area, the second entry inby the setup entry is not required to be supported after the face starts. The third and fourth entries inby the set up entry are bleeder entries. Cribs are pumped in the third and fourth entries prior to or soon after the longwall production face starts. The third entry may be subjected to slightly higher abutment pressure compared to the fourth entry.

Pumpable Cribs in Bleeders

Bleeder entries are mainly subjected to development load, and, even though the bleeder entries are within abutment pressure zone, experience has shown that the abutment pressures transferred to these entries are not significant. Crib loading in bleeder entries is caused mainly by time-dependent roof sagging and floor heave. No floor heave issues are seen when overburden is less than 900 ft, but minor floor heave is seen in some places in bleeder entries under around 1,000+-ft overburden depth.

Pumpable Cribs in Tailgate

The optimal performance of pumpable cribs in the tailgate is for the cribs to take peak load within the front abutment pressure zone to fully use crib capacity. To better maintain the roof stability in the tailgate, the cribs in the tailgate out by the face are not designed to yield; however, minor crib yielding close to the face may not significantly affect the roof stability at the tailgate T-junction. The cribs inby the face mostly yield under the pressure of the cantilevered roof in the gob. As long as the yielded cribs can maintain their residual strength, an opening between the cribs and pillar rib can be kept open, at least to the last open crosscut along the gob edge for ventilation. Figure 5 shows yielded cribs inby the face line.

Figure 5. Cribs inby the face line in yield condition.

The cribs in the tailgate within the front abutment pressure zone are loaded as a result of roof-to-floor convergence, which largely depends on overburden depth. Although weak claystone floor in the tailgate heaves under high cover depth, floor heave is mostly time-dependent and generally does not develop quickly enough to cause severe crib loading in the tailgate in a fast-moving longwall panel.

To obtain roof-to-floor convergence in the tailgate, in-situ measurement of crib convergence has been measured with different overburden depths from 700 ft to 1,000 ft. Figures 6 through 8 show the crib convergence in the tailgate in by and out by the face under different overburden depth. It can be seen that, generally, crib convergence starts about 200–300 ft out by the face and accelerates within about 150 ft out by the face. The maximum crib convergence at the face line is less than 2 in., but less than 1 in. about 10–15 ft out by the face. The crib convergence tends to increase with overburden depth. The crib convergence inby the face line ranges from 1 in. to 8 in., which indicates that mostly the cribs inby the face line have yielded.

Pumpable Cribs in the Second Entry

Cribs in the second entry are lightly loaded inby the face after the first panel is mined. Figure 9 shows the crib convergence inby the face with the gob on one side under 1,000 ft overburden depth. It can be seen that the maximum crib convergence is less than 0.4 in.

Crib convergence in the second entry is mostly caused by abutment pressure with high overburden depth and floor heave of weak claystone or shale. Generally, no significant floor heave occurs in the second entry even during the mining of the second panel when overburden depth is less than 900 ft. When overburden depth is greater than 950 ft, a minor to severe floor heave can occur in the second entry. If the floor is strong, cribs can be intact

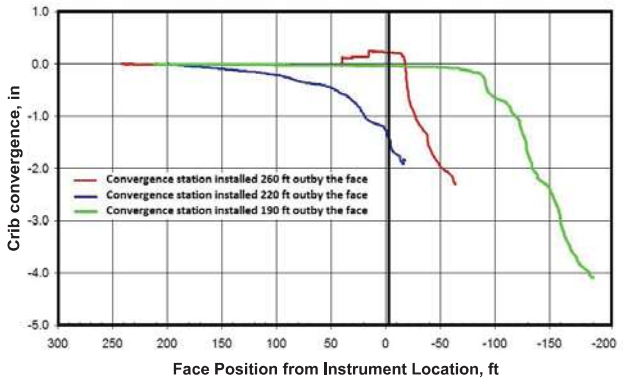

Figure 6. Crib convergence at tailgate under 700 ft overburden depth (average crib height = 7 ft; 30-in cribs with single row on 8 ft row spacing with shale floor).

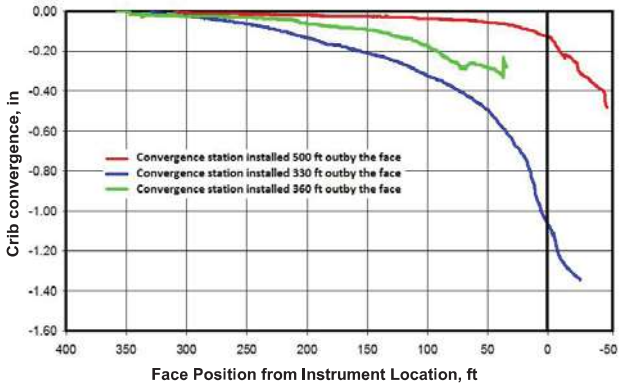

Figure 7. Crib convergence at tailgate under 825 ft overburden depth (average crib height = 7 ft; 30-in cribs with single row on 8 ft row spacing with shale floor).

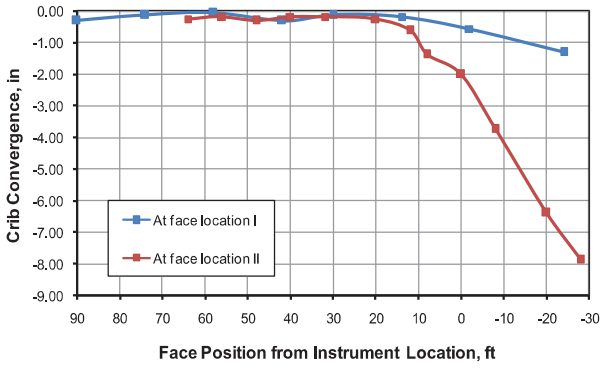

Figure 8. Crib convergence at tailgate under 1000 ft overburden depth (average crib height = 7 ft; 27-in cribs with double row and 8 ft row spacing with silt shale floor).

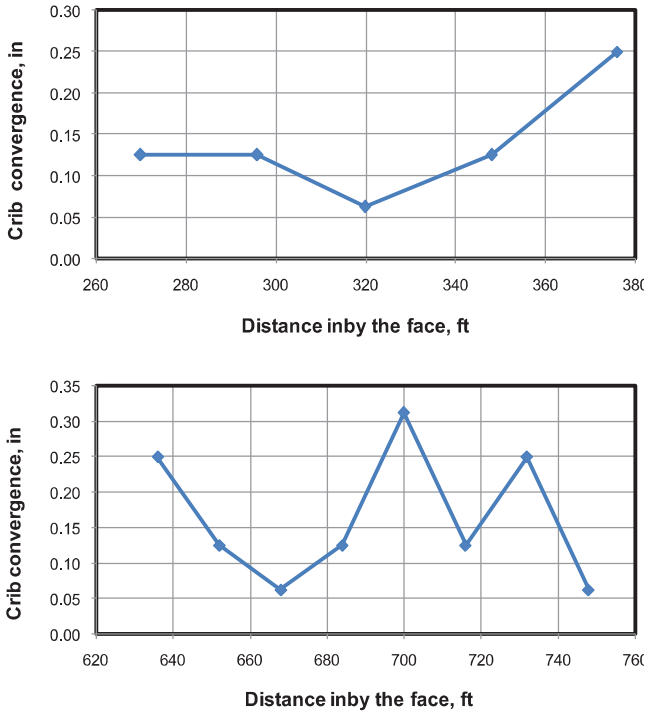

Figure 9. Crib convergence at the second entry under 1,000 ft overburden depth with gob on one side (average crib height = 7 ft; 27-in cribs with double row on 12 ft row spacing with gray clay shale floor).

without yielding (Figure 10). If the floor is weak and wet, cribs can punch into the floor without yielding (Figure 11). If the floor is weak but dry, cribs can be broken by shearing due to a buckling failure of the floor (Figure 12) and completely lose their support capacity.

As the second entry experiences the first and second side abutment pressure, roof cutters and rib slough age can occur with increasing abutment pressure and time. Severe cutters and rib slough age can impair the support efficiency of pumpable cribs (Figure 13). In the worst case, a roof fall can occur with the cribs remaining intact underneath the fall cavity (Figure 14). Figure 15 shows rib slough age and floor heave measurement information in a second entry after the first panel is mined. The amount of rib slough age and floor heave is strongly correlated with overburden depth and existence and thickness of a claystone floor. The overburden depth is about 1,000 ft around crosscuts #30–40, and 700–900 ft in other areas. There is about 4–6 ft of claystone floor around crosscuts #60–70, while the floor in other areas is competent shale.

Figure 10. Intact cribs without floor heave in the second entry.

Figure 11. Cribs punched into the floor without yielding.

Figure 12. Claystone floor heaved up for about 3 ft and cribs were broken by shear load.

Figure 13. Roof cutter and rib sloughage in the second entry.

Figure 14. A Roof fall in the second entry with the crib underneath the fall cavity intact.

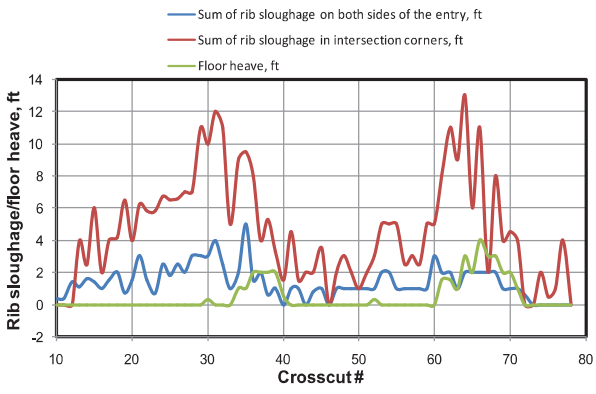

Figure 15. Rib sloughage and floor heave in a second entry with one side gob.

REQUIREMENTS FOR PUMPABLE CRIBS

Operational Requirements

For crib material pumped from the surface to underground, when the longwall panel is long, it is required that crib material be pumped to a minimum distance of 12,000 ft, and preferably 15,000–18,000 ft. To ensure pumpability and reduce cost, a high water-to-solid ratio for the material mix is desired. As crib material is pumped into a flexible bag hung from the roof, it is beneficial for the material to have a short gel time for quick crib installation.

For installation efficiency, low-line maintenance and a high-pumping rate (cribs pumped per shift) are desired. For a high production longwall with an advancing rate of 50–100 ft per day, cribs should be pumped at a rate of 20–25 cribs per shift minimum.

Geotechnical Requirements

The applicability of pumpable cribs to longwall gate entries and bleeders is determined by the characteristics of a crib load-displacement curve. The important parameters are stiffness, peak load, residual load, and residual convergence. The stiffness of a crib is defined by how fast the crib can be loaded by roof and floor deformation. Though the Young's modulus of the crib material is a good indication of the crib stiffness, the crib stiffness can be determined by the peak load and the maximum convergence at the peak load. The stiffness requirement for different entries can be illustrated by the ground reaction curves. Figure 16 shows the ground reaction curves for gate entries and bleeders under 1,000 ft cover depth. The operating point of the cribs are marked by + on the curves. The single crib support curve is for illustrating the stiffness requirement.

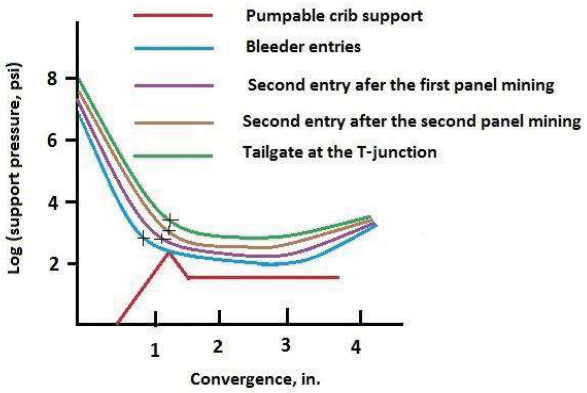

Figure 16. Ground reaction curves for gate entries and bleeders under 1,000 ft overburden depth.

Bleeder entries mostly take the development load and crib convergence is minimal after crib installation. Depending on the allowable roof sag, bleeder entries can accommodate a wide range of crib stiffness without crib and entry failure. However, if the cribs in bleeder entries are soft, their support efficiency would be is low because their peak capacity may never be utilized. Considering the characteristics of current crib products in the market, a minimum requirement for 30-in. cribs in bleeders can be defined by the load-displacement characteristics shown in Figure 17. The chart illustrates that, in lab testing, a 72-in. high and 30-in. diameter crib should take at least 150 tons of peak load at a displacement of no more than 1.5 in. and 100 tons of residual load for up to 6-in. displacement. It should be pointed out that this requirement is applicable to bleeders under less than about 1,000 ft cover depth. As overburden depth and potential floor heave increases, the requirement can change.

The tailgate takes side and front abutment pressure, and the crib stiffness requirement can be based on the convergence in the tailgate out by and close to the face. Based on the previous convergence measurements under up to 1,000 ft cover depth, the convergence in the tailgate out by the face is less than 2 in. at the face line, and less than 1 in. 10–15 ft out by the face. The minimum requirement for 30-in. cribs in the tailgate under 1,000 ft cover depth can be defined by the load-displacement characteristics shown in Figure 18. The chart indicates that, in lab testing, a 72-in. high and 30-in. diameter crib should take at least 150 tons of peak load at about 1-in. displacement, maintained through at least 1.5-in. displacement at the peak load, and then take 100 tons of residual load for up to 6-in. displacement.

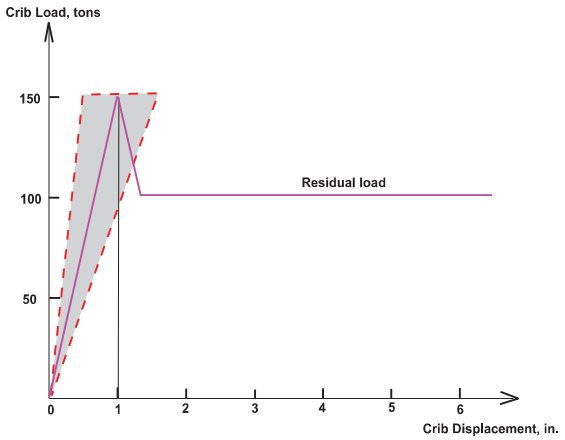

Figure 17. Required load-displacement characteristics for 72-in high and 30-in diameter cribs in bleeders under less than 1,000 ft cover depth.

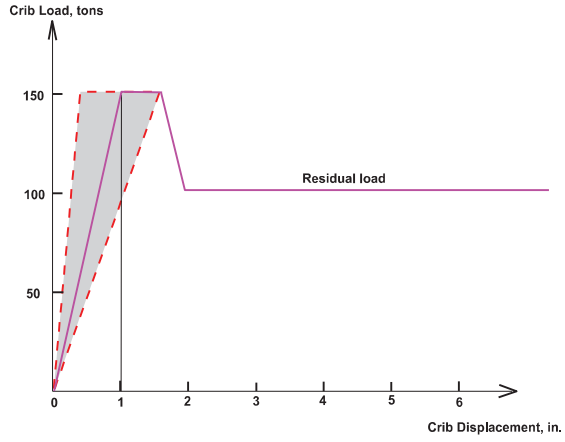

Figure 18. Required load-displacement characteristics for 72-in high and 30-in diameter cribs in tailgate under less than 1,000 ft cover depth.

For the cribs in the second gate entry, the crib operating points marked in Figure 16 are for medium to strong floor conditions without significant floor heave. In this case, the requirement for the cribs in the second entry can be the same as for the tailgate. However, as the second entry experiences two periods of side abutment pressure, the entry deformation is highly time-dependent, especially when the floor is weak claystone and overburden depth is greater than 900 ft. If floor heave is severe, cribs can fail under shearing load and completely lose supporting capacity.

Quality Control

Quality control is important to ensure desired crib performance. Quality control consists of two parts: testing and installation. The following quality control measures have been used by Alpha Natural Resources over the past years to ensure that cribs are properly selected and installed.

- Any new type of cribs should be tested at the NIOSH Pittsburgh Research Mine Roof Simulator Laboratory before they can be used underground. Then, any cribs meeting the technical specifications must be trialed in an underground test area before they have wide spread use for a specified application.
- Additional crib testing can be requested whenever there are changes in crib material and concerns with crib qualities and strength.
- Cribs should cure and achieve 90% strength within 2 weeks after pumping.
- The cribs should be set as vertical as possible, and a crib with an offset of more than 3 in. is unacceptable for both a tilted crib and a bowed crib.
- The cribs should have good contact with the floor and the roof.
- All defective cribs should be corrected once identified. New cribs should be set up within 1 ft from the defective cribs.
- Crib curing should be checked by the pumping crew every day for the cribs pumped the day prior. Crib pattern and installation quality should be checked by mine management every 2–3 weeks.

CONSIDERATIONS OF PUMPABLE CRIB SUPPORT DESIGN

Numerical Modeling of Crib Support in Tailgate and Second Entry

The required support in gate entries and bleeders is largely dependent on stress level and roof and floor geology. Numerical modeling is a useful tool to help understand the stress level and potential failures in gate entries and bleeders for proper design of crib support.

LaModel is used to obtain the pillar stress distribution in gate entries and bleeders. Figure 19 shows the vertical stress distribution in two longwall panels under 1,000 ft of overburden depth. Figures 20 and 21 show the vertical stress distribution across the gate pillars out by the tailgate T-junction and across the gate pillars with gobs on both sides, respectively. It can be seen that the tailgate is subjected to more abutment pressure than the second entry with gobs on two sides.

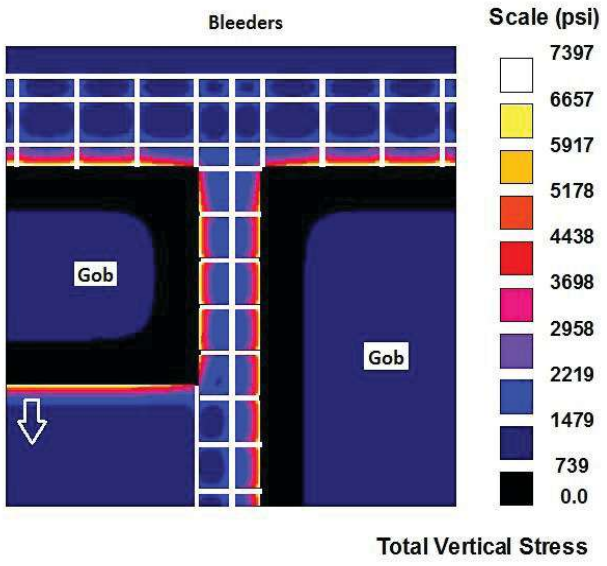

Figure 19. Vertical stress distribution in the coal pillars alongside extracted longwall panels under 1,000 ft overburden depth.

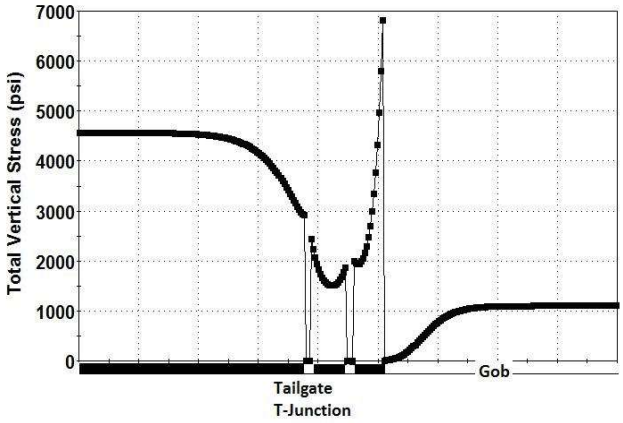

Figure 20. Vertical stress distribution across the gate pillars outby tailgate T-junction under 1,000 ft overburden depth.

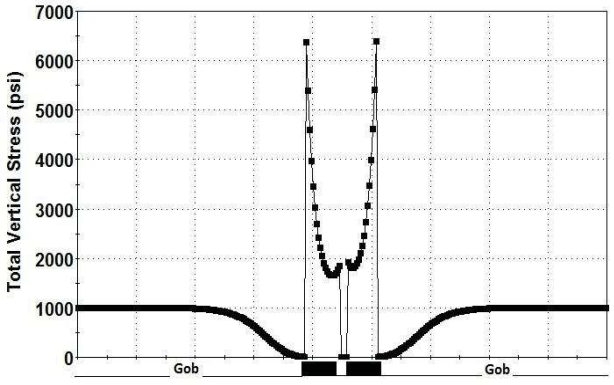

Figure 21. Vertical stress distribution across gate pillars under 1,000 ft overburden depth with gobs on two sides.

Table 1. Rock Properties Used in the FLAC3D Model.

Rock Type	Young's Modulus ($\times 10^6$ psi)	Poisson's Ratio	UCS (psi)	Tensile Strength (psi)	Cohesion (psi)	Internal Friction Angle (degree)
Clay shale	1.42	0.25	2,100	210	606	30
Shale	2.00	0.20	3,600	360	998	32
Coal Seam (Pittsburgh)	0.30	0.30	900	40	270	28
Clay Stone (floor)	1.30	0.3	800	80	240	28
Crib Material	0.04	0.35	566	56	180	25

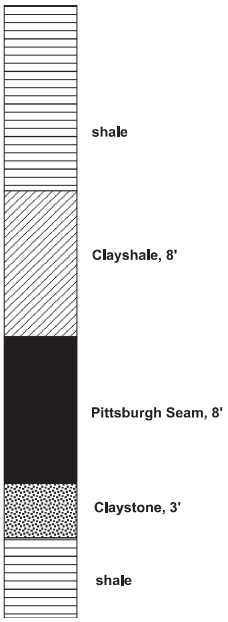

Figure 22. Generalized geologic column used in the model.

The entry deformation and failure can be modeled with FLAC3D by taking abutment pressure distribution from LaModel as the input of the loading condition. Figure 22 shows a generalized geologic column used in the model, and Table 1 shows the rock properties in the model. Figure 23 shows the yield zone around the tailgate out by the T-junction. It can be seen that yielding occurs in the roof, rib, and floor, indicating that potential roof cutters, rib slough age, and floor heave could occur in the tailgate out by the T-junction when overburden depth is 1,000 ft. Figure 24 shows the tailgate deformation out by the T-junction. The floor heave, rib convergence, and crib bulging in the model are also observed in the tailgate out by the face under similar overburden depth. Figure 25 shows the yield zone around the second entry with gobs on both sides. It can be seen that yielding occurs in the rib and floor. Figure 26 shows the deformation of the second entry with gobs on both sides. Though the roof and floor yielding in the second entry is less than those in the tailgate in the model, the actual yielding and deformation in the second entry could be more severe when a weak floor exists because the model does not consider the time-dependent failure in the second entry.

Based on modeling results, the tailgate has more roof yielding than the second entry, so double row of cribs in the tailgate and single row in the second entry should be the first consideration for the crib support design under 1,000 ft cover depth. However, if cribs are needed to control cutters and rib slough age in addition to floor heave, a double row may also be considered in the second entry. For better crib support design, numerical modeling together with underground observation and measurements should be used to predict potential entry failure and anticipated crib performance.

Determination of Crib Pattern and Size

Crib pattern is determined by the roof, floor, and rib condition, as well as safety requirements. When overburden depth is small (less than 950 ft) and no significant roof cutter, floor heave, or rib slough age would occur, a single row of cribs can be used. Under higher cover (over 950 ft), a double row of cribs is helpful to control roof cutters and floor heave. With severe rib slough age, a double row of cribs is also helpful to maintain an open walkway for safe entry inspection. At intersections, double row or additional cribs could be needed if the intersection span is large. In bleeders, a single row is generally sufficient, but a double row may be used for support reliability or in the areas that experience high horizontal stresses.

Pumpable cribs come in different sizes, and the selection of crib size mainly deals with crib capacity and pattern. If a double row is used, 27-in. or 24-in. diameter cribs rather than the larger diameter cribs should be used to reduce cost.

Determination of Crib Spacing

The primary function of pumpable cribs is to provide additional support to the roof to prevent bolted roof collapse either locally or regionally. For regional stability, the total capacity of the pumpable cribs installed should be sufficient to support the dead weight of the roof strata within the highest potential roof fall height. The following equation can be used to calculate the crib spacing:

$$S = \frac{n \times C \times 2000}{S_h \times \left(W - \frac{S_h}{\tan(\alpha)} + 2 \times \mathrm{B}\right) \times i_f \times \gamma}$$

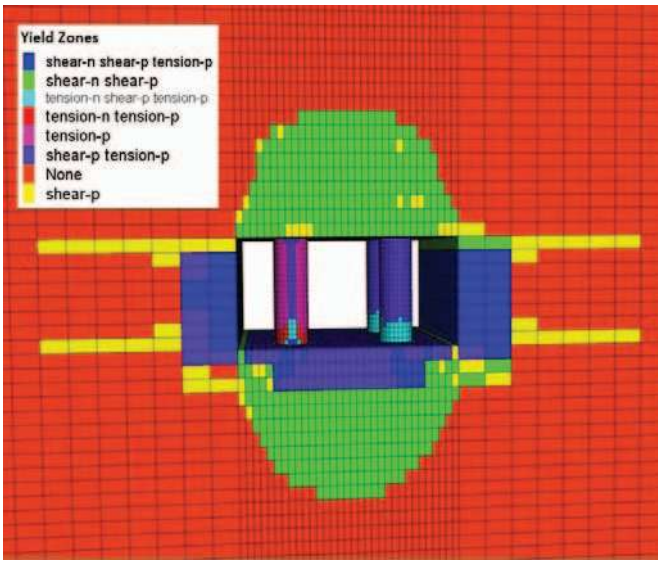

Figure 23. Yield zone outby the tailgate T-junction under 1,000 ft overburden depth.

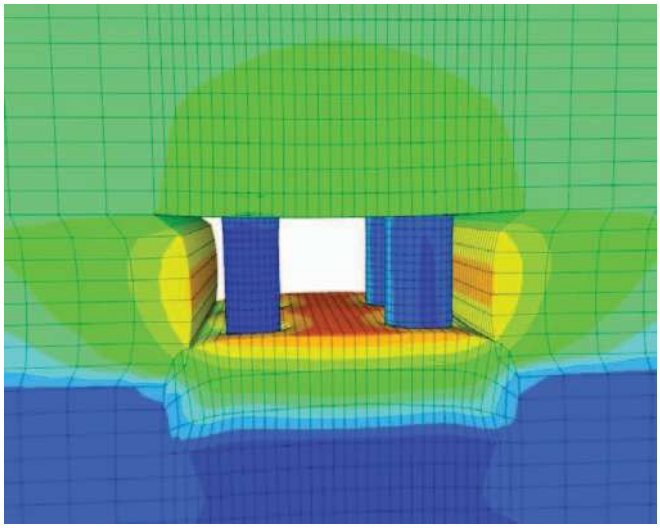

Figure 24. Entry deformation close to Taigate T-junction under 1,000 ft overburden depth.

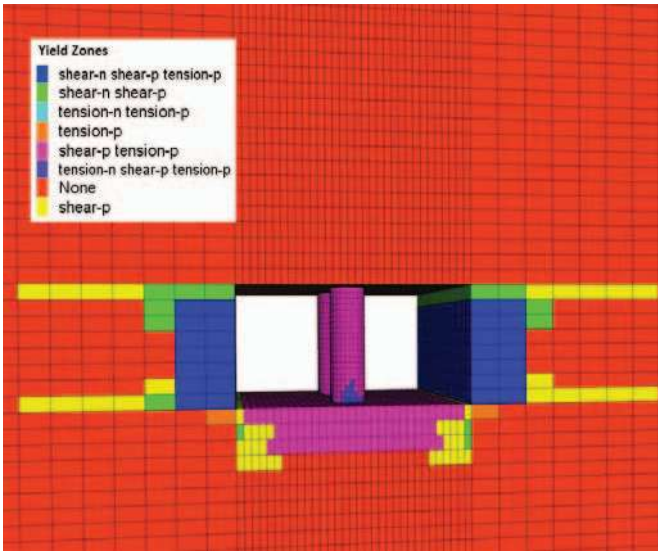

Figure 25. Yield zone in the second entry under 1,000 ft overburden depth.

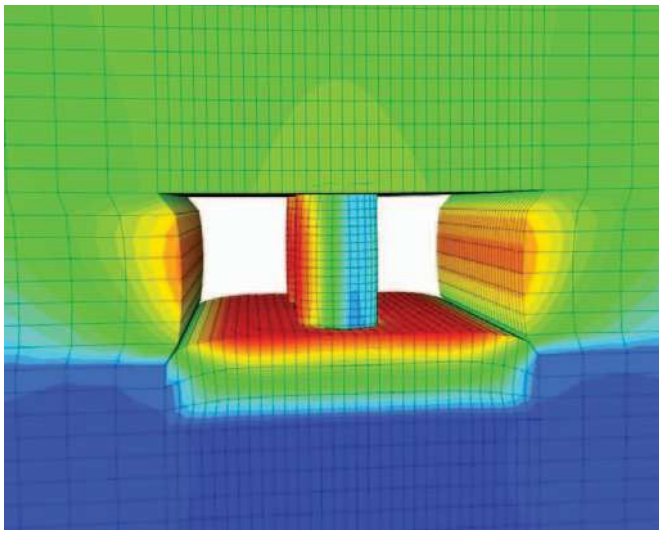

Figure 26. Entry deformation in the second entry under 1,000 ft overburden depth.

where:

S = crib row spacing, ft

n = number of cribs per row

C = designed capacity of the cribs, tons. If cribs are not designed to yield, crib peak capacity should be used. If cribs are anticipated to yield, crib residual capacity should be used.

S_h = potential roof fall height, ft

B = depth of rib slough age at each side of the entry, ft

W = entry width, ft

α = roof breaking angle above entry corners, 70-–85° for laminated roof

i_f = intersection reinforcement factor. i_f=1 for entries/crosscuts. i_f can be calculated as

$$i_f = \frac{D_s}{2\sqrt{2}W}$$

where:
D_s = sum of the intersection diagonals, ft
γ = average rock density in the immediate roof, lbs/ft^3

Table 2. Maximum crib spacing requirement under 900 - 1,000 ft cover depth.

Location	Crib Diameter, in	Min. Crib Peak Load, tons	# of Rows	Row Spacing, ft
Tailgate	30	150	single	8
	27	120	double	12
	24	100	double	10
Mid-Entry	30	150	single	12
	27	120	single	12
	24	100	single	8
Bleeders-Outmost Entry	30	150	single	8
	27	120	double	12
	24	100	double	10
Bleeders-Second Entry	30	150	single	12
	27	120	single	12
	24	100	single	8
Intersection			double	Additional cribs based on roof intersection span

The potential roof fall height can be determined by analyzing historical roof falls in the mine. Figure 27 shows the roof fall height histogram in one longwall mine in the Pittsburgh seam. For crib spacing determination, 12 ft roof fall height is used for entries and 15 ft roof fall heights for intersections. It should also be pointed out that the row spacing calculated by the above equation is the maximum spacing. The actual spacing used should consider potential development of roof cutters, the local roof stability between cribs, floor heave, primary roof support, and the importance of the entries. Table 2 shows the minimum spacing requirements for the longwall entries under 900- 1,000 ft cover depth. When overburden depth is less than 900 ft, a single row of 27-in or 30-in cribs on 8–12 ft spacing is generally sufficient for both gate entries and bleeders.

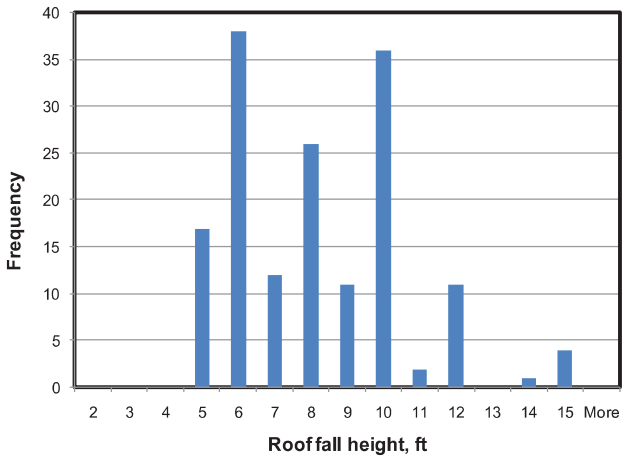

Figure 27. Histogram of historical roof fall height.

Interactions between Roof Bolting and Pumpable Crib Support

Pumpable cribs are installed under the bolted roof with at least the primary bolts in place. Supplementary cable bolts or other secondary support systems are generally not installed if pumpable cribs will be installed later. Pumpable cribs are set up to prevent the roof with the primary support from falling. In an entry with crib support, two types of roof failure could develop: local failure and global failure. Local failure includes roof cutters at entry corners, roof skin failure, and roof cavities due to slicken-sides, joints, geologic features, or local roof weakness. Global failure is a roof collapse up to a certain height above the primary roof bolting horizon. Together, with the existing bolting system, the cribs must be sufficient to support the roof against global failure. A local failure can be tolerated in some circumstances in longwall gate entries, but, if not controlled properly, it could become a global failure. Local failures can also reduce crib support efficiency as the crib may not be in full contact with the roof. Because the roof is supported by the combination of roof bolts and cribs, the two types of support interact with each other. If roof bolting is sufficient to prevent local roof failures, the cribs only need to support the roof against global failure. If local failure is anticipated under the support of the existing bolting system, crib spacing and pattern have to be designed to control both local and global failures. In entries with heavy abutment pressure under deep cover, a higher capacity bolting system with straps and wire mesh may be considered during development to better maintain roof stability during or after the panel is being mined.

CONCLUSIONS

Based on a study of performance and requirements of pumpable cribs in Pittsburgh seam longwalls under less than 1,000 ft cover depth, the following conclusions can be made:

Pumpable crib peak capacity, stiffness, and residual characteristics are applicable to longwall gate entries and bleeders

under certain overburden depth. The load-displacement curve from full-scale lab testing is a good indicator of the suitability of the pumpable crib in certain applications.

Performance of pumpable cribs in longwall tailgate entries and bleeders are largely dependent on overburden depth, abutment pressure, entry life, and floor geology.

The requirement for crib stiffness can be determined by ground reaction curve and field measurements. Crib pattern and spacing are largely dependent on overburden depth, roof, floor and rib conditions, and ventilation and safety requirements.

Quality control of crib installation is important for crib performance.

REFERENCES

Barczak, T., Chen J., Bower J. (2003). "Pumpable roof supports: developing design criteria by measurement of the ground reaction curve." In: *Proceedings of the 22nd International Conference on Ground Control in Mining*. Morgantown, WV: West Virginia University, pp. 283-293.

Barczak, T., Esterhuizen, G., Ellenberger, J., Zhang, P. (2008). "A first step in developing standing support design criteria based on ground reaction data for Pittsburgh seam longwall tailgate support." In: *Proceedings of the 27th International Conference on Ground Control in Mining*. Morgantown, WV: West Virginia University, pp. 347-357.

Barczak, T., Tadolini, S. (2008). "Pumpable roof supports: an evolution in longwall roof support technology." *Transactions of the Society for Mining, Mettallurgy, and Exploration, Inc. 324*: 19–31.

Chen, J., Mishra M., Beck K., Barczak T., Bower J., Huff C. (2003). "Design considerations of the secondary roof support for longwall tailgate entries." In: *Proceedings of the 22nd International Conference on Ground Control in Mining*. Morgantown, WV: West Virginia Univeristy, pp. 294-299.

Dolinar, D., 2010, "Ground and standing support interaction in tailgates of western U.S. longwall mines used in the development of a design methodology based on the ground reaction curve." In: *Proceedings of the 29th International Conference on Ground Control in Mining*. Morgantown, WV: West Virginia University, pp. 152-160.

Heasley, K. (2011). *LaModel, Version 3.0.05*. Morgantown, WV: West Virginia University.

Itasca Consulting Group, Inc. (2009). "FLAC3D, Fast Lagrangian Analysis of Continua in 3 Dimensions, version 4.0, user's manual." Minneapolis, MN: Itasca, pp. 12.

Mucho, T., Barczak, T. Dolinar, D., Bower, J., Bryja, J. (1999). "Design methodology for standing secondary roof support in longwall tailgates." In: *Proceedings of the 18th International Conference on Ground Control in Mining*. Morgantown, WV: West Virginia University, pp. 136-148.

Mitigating the Effects of High Horizontal Stress on Ground Control in An Underground Stone Mine: A Case History

John Ellenberger, Geologist
Ground Control Branch
NIOSH, Office of Mine Safety and Health Research
Pittsburgh, PA

Tim Miller, Geologist
East Fairfield Coal Company
North Lima, OH

ABSTRACT

The nature of a stone deposit is rarely defined through exploration and engineering design, but more through the actual experience encountered as the mine develops; hence, issues with ground control are often at the forefront for a new mine. Ground control problems account for over 15 percent of lost-time injuries in underground stone mines. The objective of this work is to present actions taken during early development of a stone mine to mitigate the obvious effects of high horizontal stress on ground control. The mine was developed from a box cut with relatively little cover, and high horizontal stresses were not anticipated. Early recognition of possible high horizontal stress resulted in mapping of the mine using the NIOSH-developed Roof Fall Risk Index (RFRI) to provide a baseline to objectively analyze roof conditions. A program of borescoping the mine roof provided valuable roof beam thickness data and found that the roof beam was of minimal thickness, approximately 10 percent of drift width. As the mine developed, it became apparent that ground control problems related to high horizontal stress existed. A concentrated effort was made to improve ground conditions by implemeting a number of mitigation techniques. Actions taken by the mine included systematic roof support, reorientation of mining direction, a lower roof horizon, reduced span widths and reduced mining height in crosscuts to prevent running falls. These strategies resulted in signifcantly improved ground stability.

INTRODUCTION

In underground stone mining, a mine design is usually developed based on the exploration and engineering data obtained through experience and test drilling. Experiences of a nearby mine may contribute significantly to a mine design. The primary site-specific tools for ground control design during the pre-mining investigation are geologic logs and physical property test results. Once the mine is operational, actual experience and other tools become available to assist mine personnel in refining mine design to optimize safety and productivity. This study presents actions that were taken during early development years of a stone mine to mitigate the effects of abnormally high horizontal stresses that were also of an unusual orientation. The study mine is the Subtropolis Mine, an underground limestone mine owned by East Fairfield Coal Company. It is located near Petersburg in Mahoning County, Ohio. Mahoning County is in eastern Ohio and has relatively flat terrain, and the mining horizon is generally from 125 to 180 feet (38-55 meters) below the surface. Normally, one does not anticipate high horizontal stress in coal mines when overburden is less than 275 ft (84 m) (Dolinar, 2003), and high horizontal stresses are not normally encountered in stone mines with less than 500ft (150m) of overburden (Iannacchione et al., 2002). Further, topographic features can affect the stresses observed underground (Molinda et al., 1992; Hasenfus and Su, 2006), but given the flat terrain overlying the mine, topographic influences would not be expected. The World Stress Map indicates that the maximum horizontal stress in the vicinity of the mine would be expected to be oriented in the range of N50-80°E (Mark and Gadde, 2008; Zoback and Zoback, 1989).

SITE DESCRIPTION

The mine is developed from a box cut, with portals into the Vanport Limestone with slightly less than 150 ft (45 m) of overburden. To date, overburden for the area mined is less than 160 ft (49 m). The surface is gently rolling, and the Vanport remains near horizontal with maximum grades of less than three degrees. Geologically, the Vanport limestone is a part of the Allegheny Formation within the Pennsylvanian System. The Lower Kittanning coal overlies the Vanport and is typically 30 to 40 ft (9 to 12 m) above the top of the limestone.

The initial underground mine development consisted of 40 ft (12 m) wide drifts driven directly west with north-south crosscuts that were also 40 ft (12 m) wide. The pillars were 25 ft (8 m) wide by 60 ft (18 m) long. The resultant mine plan consisted of crosscuts on 100 ft (30 m)centers with drifts on 75 ft (23 m) centers. The mining height of the initial mine area was approximately 18 ft (5.5 m), and a 4 ft (1.2 m) beam of limestone was left in the mine roof, representing approximately 10 percent of the drift width.

MINE DEVELOPMENT PROBLEMS

It was assumed that the strong limestone beam in the roof would be self-supporting; consequently, the roof was unsupported during the initial development of the mine. As development progressed in a westerly direction, roof cutters and a fall developed along the northern edge of the mine area. The initial fall was oval with

less than 1 ft (0.3 m) failing and a cutter extended beyond the end of the roof fall area as illustrated in Figure 1. This was the first obvious evidence of abnormal magnitude and orientation of horizontal stress. A number of publications have described conditions that are indicative of high horizontal stresses in mines (Mark and Gadde, 2008; Kuhnhein and Ramer, 2004; Iannacchione et al., 2003; Dolinar, 2003; Iannacchione et al., 2002; Mucho and Mark, 1994; Parker, 1973). The anticipated stresses in this region would be in a range of N50-80°E, but the fall indicated maximum stresses to be nearly North South in this area. It was also unusual to encounter abnormally high stresses with overburden of 150 ft (45 m). Several measures were utilized in efforts to regain roof control after the initial stress-related failures. A systematic pattern of roof bolting was initiated, which helped reinforce the limestone roof beam and prevent large falls from developing. From the time the mine opened until the first area of roof began to show signs of high horizontal stress, no bolts were used. The transition was made to installing 8 ft (2.4 m) grouted and tension bolts on 8 ft (2.4 m) by 8 ft (2.4 m) centers as supplemental support, and most of the mine area that was developed without bolts was bolted. When the developed areas were bolted, the mine began to fully bolt all faces within one cut of the face. The bolting is now maintained one cut away from the face using grouted bolts. Experience demonstrated that roof bolts tended to be damaged by development when they were installed closer than one cut away from active faces. In areas where the roof began to fail in an oriented pattern, the most effective measure for arresting a running fall was the use of concrete cribs shown in Figure 2.

Figure 1. Initial oval-shaped stress-related fall of less than 1 foot (0.3meter) thickness with cutter extension in foreground.

Roof damage mapping: As development continued west, more cutters developed along an East West trend, and efforts were undertaken to map the mine using the Roof Fall Risk Index (RFRI) (Iannacchione et al., 2007). RFRI is a qualitative method

Figure 2. Cribbing to resist continued extension of stress-related roof failure.

for determining risk of roof failures. Roof defects are examined in 10 different categories, and a weighted value is calculated for the roof in a given area. The areas are usually intersections, crosscuts and the drift between two intersections. Figure 3 shows the roof fall areas that occurred during early mining. It is readily apparent that the majority of the problems were developing along the East West trend. Figure 4 shows the same area shown in Figure 3, with RFRI colors ranging from green (relating to a relatively low risk index) to red and magenta, indicating a high roof fall probability.

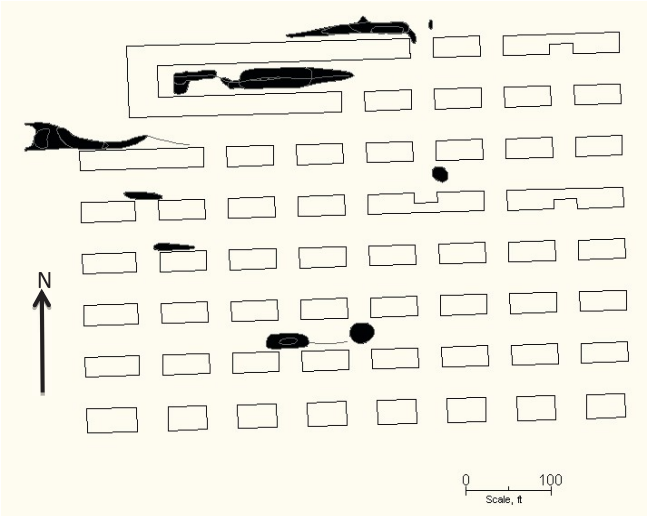

Figure 3. Map showing roof falls (in black) in an early mining area.

Roof Borescoping: The mine roof in the area developed in the mine's early life did not have a smooth bedding plane that generated an even surface. The uneven surface made it difficult for the drillers and blasting crew to maintain a uniform roof beam. Therefore, test holes were routinely drilled in the roof to assess roof conditions near active faces, and they were left open to use for roof borescoping and continued observation. The borescoping provided both information on the thickness of stone left in the roof to assess roof beam quality (Ellenberger, 2009), and an opportunity to identify any separations or cracks in the roof.

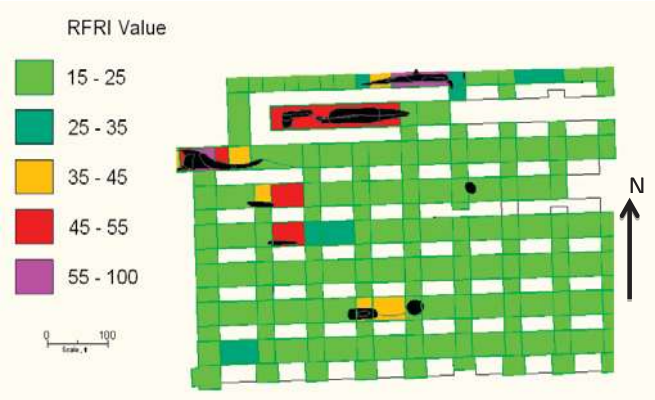

Figure 4. Map showing RFRI and roof falls for area shown in Figure 2 (after Bohan, 2008).

The test holes also proved to be valuable to detect offset in the holes (horizontal displacement) with a cap lamp. Extra test holes were drilled near a hole that was offset by approximately 50 percent of the hole diameter. However, a borescope examination of freshly drilled nearby test holes revealed little evidence of shearing as a result of horizontal movement. Drilling test holes as soon as the mining cycle permits can provide an additional tool to observe and evaluate conditions in active work areas.

Observation of test hole offsets: As mine development progressed, the test holes were also found to have an additional purpose: the ability to track movement activity with observation holes. Figure 5 shows one of the test holes where a slip plane developed in the roof. The hole shown was offset by 60 to 70 percent of the hole diameter. Such a visible displacement that can be observed simply by looking up the hole from the mine floor has obvious value from a roof assessment perspective.

Figure 5. Visible offset due to lateral movement in test hole.

As offsets were observed in test holes, one immediately wonders what damage is occurring along the slip surface. In order to examine the damaged zone, several test holes were drilled near a hole that exhibited an approximate 50 percent offset. The holes were drilled approximately 3 ft (1 m), 10 ft (3 m) and 25 ft (8 m) from the hole that showed the offset plane. Figure 6 shows two photographs taken with the borescope. The first photograph (Figure 6(a)) is taken at the slip plane in the offset hole, and the overhanging surface is apparent. The second photograph (Figure 6(b)) shows the corresponding plane in the test hole that was drilled approximately 3 ft (1 m) away. Surprisingly, the zone shows only minor cracks, but no significant aperture on the cracks, shearing or other evidence of movement. Experience at the mine indicates that complete offset of a hole indicates sufficient movement to initiate a roof failure.

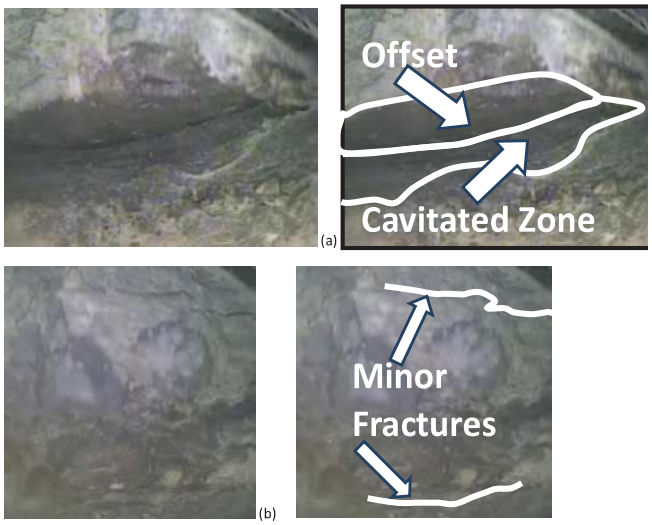

Figure 6. Borescope photographs showing (a) offset plane in a borehole, and (b) the same plane in another hole drilled after movement at (a) three feet away.

MINE DESIGN MODIFICATIONS

A number of mining design parameters may be altered to reduce the effects of horizontal stress (Iannacchione et al., 1998; Esterhuizen et al., 2007). A common corrective action to reduce the impact of horizontal stress is to reorient and align the long axis of rectangular pillars parallel to the major horizontal stress. Other options are to stagger crosscuts, reduce mining width or reduce mining height. Roof cutters and elongated roof falls tend to develop at right angles to the primary stress direction.

At the Subtropolis Mine, the orientation of the cutters and roof failures indicated that the maximum horizontal was nearly North South instead of the normal regional stress of N50 to 80°E. The best orientation to exploit the reserve with regard to reducing the impact of the horizontal stress would be to mine north and south. Horizontal stress-related roof falls have a tendency to elongate in a direction perpendicular to the orientation of the stress, and this may be mitigated by the use of rectangular pillars and/or offsetting crosscuts. Rectangular pillars were already in use with the long axis oriented East West and this was altered to North South. Figure 7 shows the area seen earlier in Figure 4, and an additional area that was developed with the long axis of the pillars rotated 90 degrees. The RFRI is also shown on the map, and it should be noted that the RFRI is less than 35 over the area that was developed with the long axis of the pillars oriented North South. The RFRI of less than 35 implies the roof in those areas has a low risk of potential failure (Iannacchione et al., 2007).

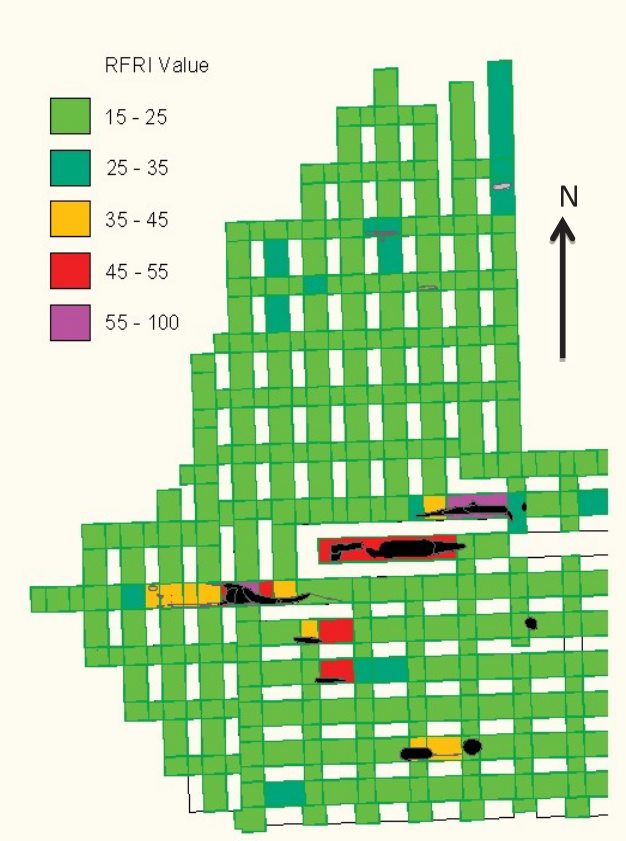

Figure 7. Map showing mining and RFRI after reorienting pillars (after Bohan, 2008).

While the long axis of the pillars was rotated from East West to North South, other changes were also implemented to reduce the impact of the horizontal stress. The normal crosscut width during early operations was 40 ft (12 m), and this dimension was reduced to 30 ft (9 m). The roof horizon over the entire mining area was lowered by 2 ft (0.6 m) to provide a thicker and stronger main roof. Finally, the roof beam was thickened even more in some crosscuts to provide a thicker and stronger beam that would resist the tendency of falls to grow across several drifts (Figure 8). In the case shown, the roof was lowered by an additional 3 ft (1 m) to produce an even thicker and stronger beam to prevent the possibility of running falls. Although the lowered roof in the crosscuts produced a brow which is generally avoided, the unit was sufficiently massive to reduce those concerns. The disadvantage in this situation was that the clearance was reduced to less than the minimum clearance for roof bolting. The option to use staggered crosscuts was also considered, but was not implemented because of the already reduced crosscut width.

SUMMARY AND CONCLUSIONS

Mines seldom develop identical to their pre-mine design. This is largely because most engineering data is derived from a few core holes. The geologic and engineering data that serves as the basis for the design is usually widely spaced, and nearby mining experience in the same horizon often proves to be very different. This case history demonstrates that, as mining progresses, there are specific tools that can be applied to assess conditions; the results may provide the impetus to alter mine design and mining approach.

Figure 8. Arch/brow produced by leaving the thicker roof beam to control stress-related failure (note: crosscut width is also reduced). (a) (b).

Within a year of beginning underground development at the Subtropolis Mine, actual conditions revealed not only that the mine had unusually high horizontal stresses, especially for a mine with relatively little overburden, but also that the stress field was not oriented similarly to stresses that had been measured in the region. RFRI and borescoping were used to assess conditions, two tools that are applicable in mine workings but not possible in a pre-mining design. RFRI served to highlight problem areas and the oriented nature of stress-related ground control issues, and borescoping permitted the mine to map the main roof beam thickness while simultaneously identifying areas of roof with cracks that contributed to weakening the main roof beam.

The final and likely most important actions are those that relate to the day-to-day operation of the mine. The initial mine development was based on the premise that the mine roof would be self-supporting. When the problems associated with horizontal stress were identified, roof bolting was initiated and additional bolting was installed when conditions warranted extra support. Concrete cribs have also been added to control any running roof falls. One lesson learned is that it is better to monitor and control the roof through an appropriate design as conditions become known than to expend the effort to regain control of the roof once a running fall is initiated.

DISCLAIMER

The findings and conclusions in this report are those of the authors and do not necessarily represent the views of the National Institute for Occupational Safety and Health.

REFERENCES

Dolinar, D.R. (2003).“Variation of horizontal stresses and strains in mines in bedded deposits in the eastern and midwestern United States. ”In: *Proceedings of the 22nd International Conference on Ground Control in Mining*. Morgantown, West Virginia. 178-185.

Ellenberger, J.L. (2009). “A roof quality index for stone mines using borescope logging ”In: *Proceedings of the 28th International Conference on Ground Control in Mining*. Morgantown, West Virginia. 143-148.

Esterhuizen, G.S., Dolinar, D.R., Ellenberger, J.L., Prosser, L.J., Iannacchione, A.T. (2007). “Roof stability issues in underground limestone mines in the United States. *“*In: *Proceedings of the 26th International Conference on Ground Control in Mining*. Morgantown, West Virginia. 320-327.

Hasenfus, G.J., Su, D.W.H. (2006). “Horizontal stress and coal mines: twenty-five years of experience and perspective. ”In: *Proceedings of the 25th International Conference on Ground Control in Mining*. Morgantown, West Virginia. 256-267.

Iannacchione, A.T., Prosser, L.J., Esterhuizen, G., Bajpayee, T.S. (2007). “Technique to assess hazards in underground stone mines: the roof-fall-risk index (RFRI).”*Mining Engineering* 59(1): 49-57.

Iannacchione, A.T., Marshall, T.E., Burke, L., Melville, R., and Listenberger (2003). “Safer mine layouts for underground stone mines subjected to excessive levels of horizontal stress.” *Mining Engineering* 55(4): 25-31.

Iannacchione, A.T., Dolinar, D.R., Mucho, T.P. (2002). “High stress mining under shallow overburden in underground US stone mines.”In: *Proceedings of the First International Seminar on Deep and High-Stress Mining*. Nedlands, Australia: Australian Centre for Geomechanics Section 32. 1-11.

Iannacchione, A.T., Dolinar, D. R., Prosser, L. J., Marshall, T.E., Oyler, D.C., Compton, C.S. (1998). “Controlling roof beam failures from high horizontal stress in underground stone mines. ”In: *Proceedings of the 17th Conference on Ground Control in Mining*. Morgantown, West Virginia. 102-112.

Kuhnhein, G., Ramer, R. (2004) “The influence of horizontal stress on pillar design and mine layout at two underground limestone mines. ”In: *Proceedings of the 23rd International Conference on Ground Control in Mining*. Morgantown, West Virginia. 311-319.

Mark, C., Gadde, M. (2008).“Global trends in coal mine horizontal stress measurements. In: *Proceedings of the 27th International Conference on Ground Control in Mining*. Morgantown, West Virginia. 319-331.

Molinda, G.M., Heasley, K.A., Oyler, D., Jones, J.R.(1992). “Effects of horizontal stress related to stream valleys on the stability of coal mine openings. ”*USBM RI9413*. 26.

Mucho, T.P., Mark, C. (1994) “Determining horizontal stress direction using the stress mapping technique. ”In *Proceedings of the 13th International Conference on Ground Control in Mining*. Morgantown, West Virginia. 277-289.

Parker, J. (1973) “How to design better mine openings: practical rock mechanics for miners.” *Engineering and Mining Journal,* Part 5, December. 76-80.

Zoback, M.L., Zoback, M.D. (1989). *Tectonic Stress Field of the Continental United States Geological Society of America Memoir 172*. 523-539.

Innovation in Rock Mechanics: Iced Tailings As Structural Backfill for the Citronen Mine, Ironbark Zinc Ltd., Greenland.

Andrew P. Schissler, Principal Mining Engineer
Mineral Resources
Tetra Tech Inc.
Golden, CO

Gregory C. Campbell, Executive Director
Jacqueline Mcara, Project Engineer
Ironbark Zinc Ltd.
Perth, Australia

INTRODUCTION

The Citronen Zinc-Lead Project is one of the world's largest undeveloped zinc-lead resources, containing more than 13 billion pounds of zinc and lead metal. The project is located in northern Greenland, a self-governed region of the Kingdom of Denmark (Figure 1).

Figure 1. Citronen Project Location.

Citronen is the northern-most mine in the world, operating at a latitude of 83° 3' N. In excess of 67,000 meters of diamond drilling have been completed to delineate the resource. As of January 2012, the measured, indicated, and inferred reserves for the Citronen project totaled 70.8 million tonnes, consisting of 5.7% zinc + lead (3.5% zinc cut-off) (Ironbark, 2012).

For the underground mine plan, room-and-pillar and long hole-stoping mining methods were selected. The beneficial application of structural fill was considered for increased recovery, efficient tailings disposal, and ground control. Three types of fill were compared - paste fill, cemented rock fill, and iced tailings. An environmental and economic feasibility study concluded that iced tailings was the preferred alternative provided it met the ground control requirements. The purpose of this paper is to explain the investigatory steps that led to the possibility for the use of iced tailings as structural fill.

Geologic Setting

The zinc-lead mineralization at the Citronen project is formed within a sedimentary exhalative (SEDEX) deposit. The mineralization is in the proximity of a volcanic flow, whereby the host is layered in a sedimentary rock regime of mudstones and siltstones interbedded with carbonate debris flows of the Ordovician Amundsen Land Group of the Franklinian Basin (Figure 2).

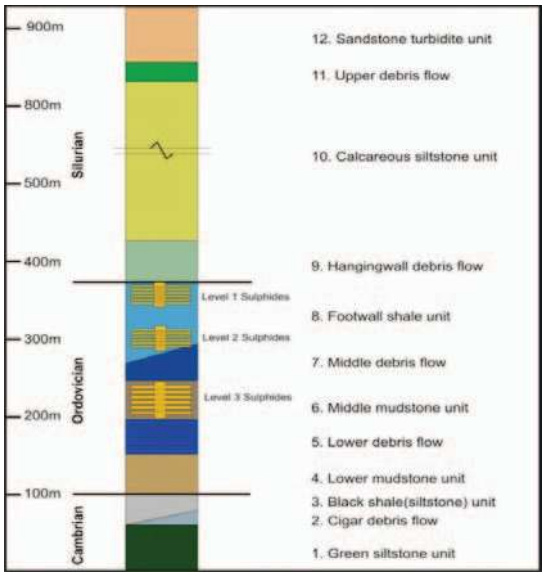

Figure 2. Generalized Lithologic Cross Section for the Citronen Project.

Three mineralized stratigraphic horizons (Levels 1, 2, and 3) are located within three major stratiform mineralization bodies (the Beach, Esrum, and Discovery ore bodies). Although the Discovery ore body can be mined using surface methods, the deeper lying Beach and Esrum ore bodies must be mined using underground mining methods.

The structural geology of the Citronen deposit consists of strike slip near vertical liniments with additional structure and folding of the SEDEX depositional environment. During exploratory drilling, no squeezed bits were experienced, and the drill holes tended to remain open. These field conditions indicate a lack of high horizontal stress at the project site. Any additional mining-induced stress will more than likely be carried in the greater strength rock, which in this case, is the sulphide ore. Because of the mountain and valley topography and pitching sulphide mineralization layers, the depth of cover for the level II ranges from 96 to 259 m and for level II from 161 to 510 m.

FIELD DATA COLLECTION PROGRAM

Field data collected for a detailed rock mechanics investigation program in 2010. The data collection included seven geotechnical drill holes totaling 1,456 meters targeting the underground Beach and Esrum deposits. The drilling program was done to establish rock mass characteristics for rock mass rating (RMR). Using the obtained core from the drilling, specimens were extracted and sent to a laboratory for physical testing. To assess rock jointing, two scan lines were done in the field. Finally, because the site is near the end most northing land, thermistors were placed in drill holes to measure geothermal gradient.

Rock Mass Rating

Rock Mass Rating (RMR) used in the analysis was based on using the 2010 geo tech drill holes with comparison of results from prior field studies. The RMR assesses the rock on a scale of 0 to 100 based on compressive strength, joint spacing and condition, water presence and other parameters. Table 1 shows the results of the RMR measurements.

(list these i.e., give # samples from which horizon). The core was sent from Citronen to Advanced Terra Testing in Lakewood, Colorado. A total of seventy-two tests were completed to determine the physical characteristics of the rock units. The average test results, which were used for mine design are listed in Tables 2A and 2B.

In general, the metallic -bearing sulphides are stronger than the surrounding roof and floor rock. From the footwall shale unit down through the Level 2 and 3 sulfides, the rock is typically strong, having an average unconfined compressive strength (UCS)>100 MPa.

Structural Geology Analysis

In previous studies, the geological structure for the potential mining districts at Citronen was mapped along two 8-m scan lines. One of these scan lines was located at a debris flow outcrop near the portal site (Figure 3), and the other scan line was located on a hanging wall debris flow above the Level 1 sulphides at the Discovery surface mine site.

Using the portal site scan line, a major fracture set was identified having a strike of 255°, a dip ranging from 81° to 90° to the southeast, and an average fracture frequency of 3.3 m. A secondary fracture set having an orientation of 310° with a nearly vertical dip and an indeterminate fracture frequency was also identified at the portal site. With the Discovery scanline, a primary fracture set was noted at an orientation of 267°, a dip of 75° to the south, and a fracture frequency of 7 to 8 m. A secondary fracture set was also noted having a bearing of 145°, a dip of 80° to the northeast, and a fracture frequency of 2.6 m. In addition to these fracture sets, a major fault was also identified at a bearing of 290°. This

Table 1. Rock Mass Rating - 2010 Results.

Rock	UCS (MPa)	RMR	Notes
Footwall Shale	133	60	RMR rating primarily a result of weak planes of carboniferous separation every 0.1 to 0.3 m
Level II Sulphide	172	82	Stronger rock due to metallic content
Middle Debris Flow	120	79	Can have localized low bond strength between matrix and pebble
Middle Mudstone	118	72	Can be gradational in metallic content constituting ore
Level III Sulphide	144	84	Ore
Lower Debris Flow	80	75	At 80 MPa, has sufficient strength for floor bearing capacity for equipment

The immediate back of the Level 2 ore zone is the footwall shale unit. This has a distinctive and repeating fracture pattern with pronounced carboniferous planes of weakness. These carboniferous planes are either filled with calcite or they have semi-polished surfaces that produce clean breaks in the drill core. The carboniferous planes have minimal tensile strength when they are not filled with calcite.

Physical Core Testing

A complete core testing program was performed on drill core specimens for each of the major rock units at the Citronen deposit

fault based on field mapping and lineament studies is projected to extend through all mineralization. Considering the orientations of this fault and the fracture sets mentioned above, the main laterals in the mine plan were oriented in a north-south direction at an oblique angle to the primary geological structure. This orientation enhances the stability of these entries by mitigating the effect of ground movement along these geologic features as a result of horizontal stress.

Table 2A. Physical Characteristics of Citronen Rock Units - 2010 Testing Results.

Rock Unit	# Samples	Cohesion (MPa)	Friction Angle (deg)	Unconfined Compressive Strength (MPa)	Brazilian Tension (MPa)	Young's Modulus (x 10^6 MPa)	Poissons Ratio Ratio	Density (mg/cc)
Glac Till	1			0		0	0	2.80
HW DF	4			68		0.048	0.141	2.74
L I Sul	1			68		0.046	0.138	3.74
FW Sh	8	0.1	31.1	133	19	0.082	0.194	2.86
L II Sul	18			172	15	0.083	0.140	3.24
Mid DF	17	0.2	21.6	120	10	0.062	0.172	2.86
Mid MS	13			118		0.062	0.167	2.94
L III Sul	8			144	18	0.102	0.220	3.41
Lower DF	2			80				

Table 2B. Triaxial Test Results with Citronen Sulphides.

Compressive Strength (MPa)			
Mineralized Horizon	Confining Pressure (MPa)		
	3.45	6.90	10.34
Level 1 Sulphides	169	272	222
Level 2 Sulphides	270	248	309
Level 3 Sulphides	220	262	301

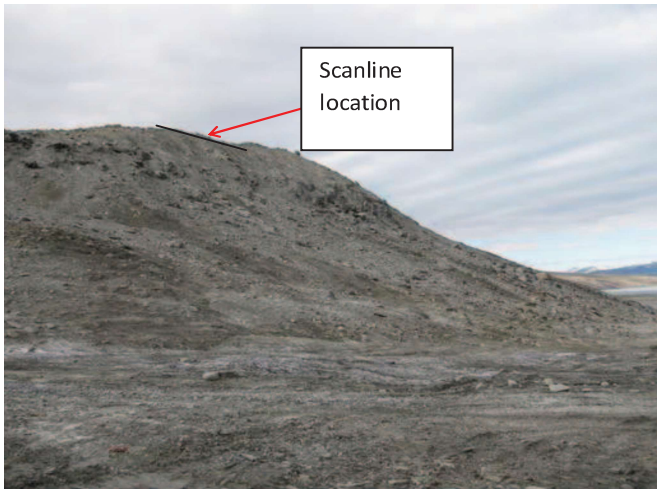

Figure 3. Citronen Portal Site with Scanline.

Permafrost Analysis

The depth of permanently frozen ground (permafrost) is key to maintaining frozen tailings as iced backfill. The depth of permafrost at the Citronen site was determined through down hole thermistor measurements and historical drilling observations. Campbell Scientific 107-L thermistors were installed in two NQ (47.6 mm) drill holes within 300 m of the fjord. Readings from the thermistors were recorded using a Campbell Scientific CR 850 data logger. Approximately eight days were required for the thermistors to reach equilibrium with the ground temperature. Thermistor readings were collected from July 1 to August 15, 2010, the warmest time of the year. Typical temperature measurements are listed by depth in Table 3.

An average geothermal gradient of 29.4 m per 1°C or 88.2 m per 3°C was determined from an analysis of the thermistor data (not including the first 12 m of depth).These values appear to be reasonable given the standard assumption of 100 m per 3°C for an arctic permafrost temperature gradient. At the center of the Beach ore body, the depth of cover to the mine floor ranges from about 116 m for the Level 2 sulphides to 211 m for the Level 3 sulphides. Using the above measured thermal gradient, the rock temperature in the mine at these two depths will be -9.6°C and -6.3°C, respectively. The depth of cover in the Esrum ore body ranges from 275 m in the northern part of the Level 2 sulphides to 592 m in the southwest portion of the Level 3 sulphides. In the deepest parts of the Esrum ore body, the ground temperatures are projected (use geothermal gradient equation developed earlier) to reach 0°C. Iced tailings are not planned to be used in these areas of the mine. As shown in Table 4, the permafrost at Citronen appear to agree with data collected from other arctic locations for depth.

TAILINGS BACKFILL TEST RESULTS AND DESIGN

The feasibility of using iced tailings as structural fill at Citronen was evaluated from the standpoint of strength, transport characteristics, and freeze time.

Iced Tailings Strength

Strength tests were conducted with tailings that had been used during bench scale metallurgical testing for process mill design at the Burnie Research Laboratory in Tasmania, Australia. A 12-kg sample of tailings was sent to the Earth Mechanics Institute (EMI) at the Colorado School of Mines where strength tests were conducted with the material during August and September of 2010. The tailings has a size consist of approximately P80 of 250 mesh. Tests were conducted with frozen tailings samples to determine

Table 3. Thermistor Measurements of Ground Temperature- July 2010.

Depth Below Surface (m)	Temperature (°C)
0	-13.6
4	-13.4
8	-13.1
12	-13.1
14	-13.0
70	-10.5
100	-9.7
150	-8.4

their water retention, UCS, and mechanical behavior under load. The results of these tests are summarized in Table 5.Frozen tailings specimens were formed by mixing tailings with water at a 55% solids ratio by weight and then freezing the resulting mixture in cardboard cylinders to specific temperatures. During unconfined compression tests, strain softening was observed with all of the frozen tailings samples beginning at approximately 50,000 micro strain. The failure loads reported in Table 5 were based on either loading peaks when failure occurred or at the onset of significant additional strain softening. Some of the samples continued to take load above the failure loads listed in Table 5.

A shown in Figure 4, a plot of the test results provides a nearly linear relationship between strength and temperature. The strength values in the table are peak.

Time to Freeze

Two different stope sizes (7 m high by 10 m wide by 150 m long and 14 m high by 10 m wide by 150 m long) were considered for determining the time required to freeze a decanted tailings slurry that had been pumped to a stope at Citronen. A two-dimensional analysis of this problem was conducted using the general form of Fourier's heat conduction equation (Cassie, et al., 2005). Complicated explanation of using 2-d solution that is representative of plane strain condition that exist near room length centers. Transient models were run for five years to determine the length of time necessary for the slurry to freeze completely in these stopes. The models indicate that the slurry in the 7-m high stope would freeze completely in 75 days, whereas the slurry in the 14-m high stope would not freeze completely until 200 days. Both of these models represent worst case scenarios. The actual time to completely freeze these stopes will be substantially less because of the sheeting action of the flowing material freezing over itself.

Application of Iced Backfill

Given a surface temperature of -13.6°C and a geothermal gradient of 88.2 m per 3°C, the ambient ground temperature at a depth of 211 m, the lowest point in the Beach ore body, is calculated to be -6.4°C. At this temperature, the iced backfill is projected to have a compressive strength of 2.6 MPa (377 psi). Most mining structural fills fall in the range of 2 to 4 MPa. However, most of the Beach resources will be mined at depths between 116 m and 170 m. Consequently, the strength for a majority of the Beach backfill will range from 3.3 MPa (479psi) to 3 MPa (435psi), respectively. These strengths fall into reported UCS strengths.

Table 4. Permafrost Depth at Selected Arctic Locations.

Location	Latitude, elevation	Depth of Permafrost	Reference
Fort McPherson NWT, Ca	67.85° N, 10.7 m	107 m	Mackay
Arctic Red River, NWT, Ca	67.45° N, 76.2 m	107 m	Mackay
Fort McPherson NWT, Ca	67.43° N, 396 m	122 m	Mackay
Well #3, South Barrow, Alaska	71.29° N, ~ 50 m	> 181 m, temp at 181 m = -6.5° C	Kutasov
North Slope Alaska West Fish Creek #1	70.33° N, 27 m	258 m	Kutasov
North Slope Alaska Put River N-1	70.32° N, 8 m	610 m	Kutasov
North Slope Alaska Drew Point #1	70.88° N, 5 m	> 210 m, temp at 210 m = -4.0° C	Kutasov
Ellesmere Island Well 175	79.98° N, +100 m	510 m	Kutasov
Meliadine Mine 25 km NW Rankin Inlet, Hudson Bay	63.00° N, 65 m	450 m	Micon

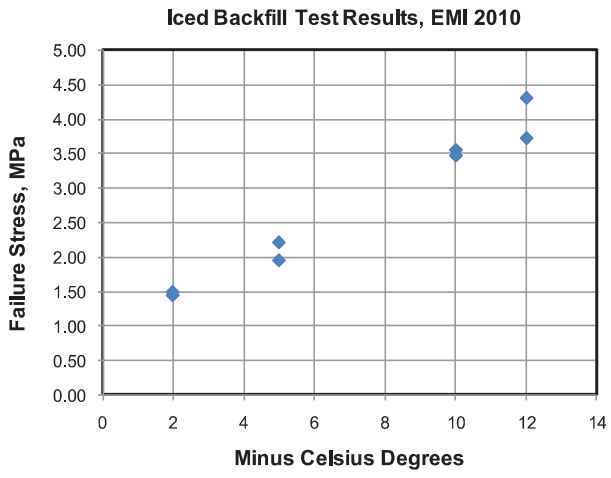

Figure 4. Compressive Strength versus Temperature for Frozen Tailings Specimens.

Because the Esrum ore body is located under the side of a mountain, it will have a much different surface temperature and thermal gradient than the Beach deposit. The rock temperature is expected to be more consistent under the mountain with more widely spaced thermal isolines. (distracting evidence, not needed here to defend temp used in analysis) As a result, the thermal gradient for the Esrum ore body is estimated to be 100 m per 2.5°C. Using this parameter, the rock temperature at Esrum will range from -8.1°C (negative or positive temp) at a depth of 275 m to -0.2°C at a depth of 592 m. Therefore, the compressive strength of the iced tailings backfill in the Esrum ore body will be highly dependent on its depth beneath the surface ranging from 3.1 to 0 MPa (450 to 0 psi).

Mine Case Histories Strength of Structural Fill

To investigate the use of iced tailings at Citronen, a literature search was conducted to identify mining operations where paste fill or cemented rock fill (CRF) with a UCS of between 2 to 4 MPa was used to provide ground support. Brady, et al. (2003) (ref) surveyed 13 mines using structural fill and reported backfill compressive strengths ranging from 0.7 to 2.5 MPa. Furthermore, two other underground gold mines in Nevada have successfully used CRF having a UCS of 2.75 MPa (Schissler, 2010).

The initial lithologic unit of the Beach deposit is frozen glacial till from zero to 70 m thick. Bandopadhyay (2004) performed unconfined compressive strength tests with this type of material and reported compressive strengths versus temperature that are similar to the Citronen tests.

The Svea North Mine on Spitsbergen was visited to review their ground control program for a decline that was successfully excavated through glacial rock, sandstones, and shales. Located at a latitude of 77° 51' N, this long wall coal mine is one of the northern-most mines in the world. The decline is 5 m high by 8 m wide by 6 km long and supported by 0.6-m rebar bolts installed on 1.20-m centers along with a 50-mm thick layer of shotcrete. Should this green highlighted section be in literature survey section, not results section.

CONCLUSION

The use of iced tailings as structural mine fill has possible application to the proposed underground operations at the Citronen Zinc-Lead Project.. Field data and laboratory data show compressive strength similar to other structural fill mine applications. Further study is required to determine the depth temperature and strength correlation.

REFERENCES

Bandopadhyay, S. (2004). "Ice-cemented backfill for underground support in Arctic mines." *SME Preprint 04-23*.

Brady, T, Martin, L., Pakalnis, R. (2003). "Empirical Approaches for Weak Rock Masses." 98th annual AGM-CIM conference, Montreal, QC.

Cassie, J, Mehling, P, Porter, M. (2005). "Thermal Conductivity of Sulphidic Tailings." *BGC Engineering Inc.*

GeoStudio 2007: Thermal Modeling with TEMP/W 2007 - an Engineering Methodology, 3rd Edition by Geo-Slope International Ltd. Ironbark. "January 2012 JORC resource." www.inronbark.gl, Perth Australia, 2012.

Kutasov, I. M., Eppelbaum, L. V. (2003). "Prediction of formation temperatures in permafrost regions from temperature logs in deep wells – field cases." *Wiley InterScience, Permafrost and Periglac*. 14: 247-258.

Mackay, R. J. (2010). "Permafrost depths Lower Mackenzie Valley, Northwest Territories." *Arctic Institute of North America, ASTIS database*, pp. 21-26.

Micon. (February 20, 2009). "Independent Technical Report, Meliadine Project, Nunavut, Canada." In: Micon International Limited, www.complex.com, 222 p.

Schissler, Andrew P. "Personal communications with operating mines in Nevada". Andrew P. Schissler, 2010.

Calibrating the Lamodel Program for Site Specific Conditions

Keith A Heasley, Professor
West Virginia University
Morgantown, WV

ABSTRACT

The LaModel program has been used successfully in the United States for many years to design pillars to ensure global stability of pillar recovery operations. However, the recent Crandall Canyon Mine collapse showed that further research was required to improve the design of pillar recovery under deep cover. Toward this end, a new calibration procedure was implemented in LaModel. This calibration procedure prescribes techniques for calibrating the critical LaModel input parameters based on empirical abutment loading and pillar strength, as utilized in the time-tested ALPS and ARMPS programs. The calibration procedure is intended to help guide a novice modeler in choosing calibrated input parameters that produce a standard model that fits within the verification database. However, the rigid parameter specification incorporated in the calibration procedure also removes most of the flexibility in LaModel for specific calibration to the unique conditions at a given mine site. In this paper, a number of the LaModel input parameters are varied outside the bounds of the suggested calibration and the effects on the model results are analyzed. Ultimately, it is shown how the LaModel user might vary certain input parameters to adjust the model to site-specific conditions, while still maintaining the general accuracy and philosophy of the recommended calibration.

INTRODUCTION

After the collapse of the Crandall Canyon Mine in Utah on August 6, 2007, several questions were raised concerning the accuracy of the currently available analysis tools and methods for the design of deep-cover, pillar-retreat mining sections (MSHA, 2008). One of the analysis tools used in the original design of the mine plan at Crandall Canyon was the LaModel boundary-element program. This program has a long history of successful application at coal mines in the United States and around the world. So, why was the mine design unsuccessful?

As with any numerical method, the success and accuracy of the LaModel program is largely dependent on the accuracy of the input parameters. Also, the user must be sure that the problem is appropriate for the laminated displacement-discontinuity formulation of LaModel, typically large single or multiple-seam areas with broad stress and displacement impacts. To effectively design a specific mining plan and pillar layout, the LaModel input parameters need to be specifically calibrated to the unique conditions at the mine. However, at the time of the Crandall Canyon Mine design, a standardized process for calibrating the LaModel program for a specific mine site was not available. In the last few years, as a direct result of the Crandall Canyon Mine collapse, a standard method of calibrating LaModel has been developed and verified against actual case studies (Heasley et al., 2010; Heasley, 2008).

When using the suggested calibration method with LaModel, the values of the critical input parameters are rigidly specified. This rigid parameter specification is good for (1) producing a standard model that fits within the verification database, (2) guiding a novice modeler in the correct direction, and (3) serving as a standard for discussion of the model design. However, the rigid parameter specification also removes most of the model flexibility for specific calibration to the unique conditions at a given mine site. This paper examines how varying the critical LaModel parameters outside the bounds of the suggested calibration affect the model results and shows how some parameter variation can be used for site-specific calibration while still maintaining the general philosophy of the recommended calibration.

BACKGROUND

LaModel Introduction

The LaModel program is used to model the stresses and displacements on thin tabular deposits such as coal seams. It uses the displacement-discontinuity (DD) variation of the boundary-element method, and because of this formulation, it is able to analyze large areas of single or multiple-seam coal mines (Heasley, 1998). What makes LaModel unique among DD codes is that the overburden material includes frictionless laminations that give the model a more realistic flexibility for stratified sedimentary geologies and multiple-seam mines.

Since LaModel's original introduction in 1996, it has continually been upgraded (as need arose) and modernized as operating systems and programming languages have changed. The present program is written in Microsoft Visual C++ and runs in the Windows operating system. It can be used to calculate

convergence, vertical stress, overburden stress, pillar safety factors, intra-seam subsidence, etc., on single and multiple seams with complex geometries and variable topography. Presently, the program can analyze a 2000 x 2000 grid with 6 different material models and 52 different individual in-seam materials.

LaModel uses a forms-based system for inputting model parameters, a spreadsheet-type interface for creating the mine grid, and a graphical post-processor for analyzing the output. Recently, the LaModel program has been interfaced with AutoCAD; it can take an AutoCAD map of the pillar plan and overburden and automatically convert these into the appropriate seam and overburden grids. Also, the output from LaModel can be downloaded into AutoCAD and overlain on the mine map for enhanced analysis and graphical display (Heasley, 2008).

LaModel Calibration

A detailed formulation of the process for calibrating the LaModel program for deep-cover pillar retreat and the verification against a database of case histories was previously presented at this conference (Heasley et al., 2010; Heasley, 2008). In the background section of this paper, only the key components of that previous work are briefly introduced. More details of the calibration or verification process can be found in the previous publications.

For the LaModel calibration process, it was desired that the model output be as realistic and accurate as possible; therefore, it was desired that the calibration process be based on field measurements, observations, and/or empirical formulas as much as possible. Ultimately, the calibration process was primarily derived from the empirical formulas for overburden loading and pillar strength, as implemented in ARMPS and ALPS. These programs (and their underlying "empirical mechanics") have been verified against hundreds of case studies with good results and have practically become design standards in many situations.

In LaModel, the most critical input parameters with regard to controlling the mechanical response of the program and for accurately calculating stresses and pillar safety factors were determined as follows:

1. The Rock Mass Stiffness
2. The Gob Stiffness
3. The Coal Strength

In the laminated model, the rock mass stiffness is primarily controlled by the thickness and elastic modulus of the laminations. In the recommended calibration process, the rock mass elastic modulus is held constant and the rock mass stiffness is calibrated by adjusting the rock mass lamination thickness to produce an extent of abutment zone at the edge of the gob areas that matches the empirical abutment extent used in ALPS and ARMPS. The equation for this lamination thickness (t) was derived previously (Heasley, 2008) and is shown below:

$$t = \frac{2E_s\sqrt{12(1-\upsilon^2)}}{Eh}\left(\frac{5\sqrt{H}-d}{\ln(0.1)}\right)^2 \quad (1)$$

where

t = the lamination thickness in the rock mass

E_s = the elastic modulus of the seam

E = the elastic modulus of the rock mass

υ = Poisson's Ratio of the rock mass

h = the seam thickness

H = the seam depth

d = the width of the yield zone

In a LaModel analysis with gob areas, the interaction between the overburden stiffness and gob stiffness determines how the overburden load above the gob is distributed between the gob and the adjacent pillars. With the overburden stiffness initially calibrated to match a desired extent of the abutment stress, the gob stiffness then becomes the parameter that functionally determines the overburden load distribution. Therefore, a calibrated gob stiffness is critical for accurately calculating the pillar stresses and safety factors. In the recommended calibration process, the gob stiffness is calibrated by adjusting the gob modulus until the two-dimensional gob loading matches the empirical gob load (Heasley et al., 2010) as determined by a 21° abutment angle and as used in ALPS and ARMPS (Mark, 1992; Mark and Chase, 1997).

Accurate in situ coal strength is the final critical parameter in LaModel that needs to be calibrated to determine accurate pillar safety factors. However, it is very difficult to get a representative sample of coal for laboratory testing, and it is also difficult to scale the lab strength to accurate in situ strength. Therefore, in the recommended LaModel calibration process, a default empirically determined coal strength of 900 psi is used in conjunction with the Mark-Bieniawski pillar strength formula (Heasley et al., 2010). This is the same default coal strength used in ALPS and ARMPS (Mark, 1999).

The three calibration techniques mentioned above for the rock mass stiffness, the gob stiffness and the coal strength have all been implemented into the new LamPre3.0 as the following:

1. A Lamination Thickness Wizard
2. A Gob Stiffness Wizard
3. A Coal Strength Wizard

These new wizards make it very quick and easy for the LaModel user to apply the suggested calibration techniques.

Calibration Verification

In order to verify the recommended calibration method for LaModel, a database of deep-cover retreat mining case studies

was developed. In this database, there were 47 deep-cover, pillar-retreat case studies from 11 different mines. Seven of these mines were in Central Appalachian coal fields, and four were in the Western coal fields (Heasley et al., 2010). The depths at the case study sites ranged from 750 to 2,200 ft, with an average of 1,256 ft. The number of entries in the sections ranged from 3 to 13, with an average of 6.2 entries. Pillar widths ranged from 50 to 100 ft (center-to-center), and crosscuts spacing ranged from 80 to 150 ft (center-center), with the average pillar size being 78 ft by 101 ft. With seam heights that ranged from 3.6 to 9.0 ft witn an average of 6.9, the pillar width-to-height ratios ranged from 6.0 to 16.7 with and average of 9.0. The panel widths ranged from 160 to 940 ft, with an average of 410 ft.

For each of these case studies, the LaModel mine grid was built directly from the mine map, and the true topography from the mine map was gridded into the LaModel overburden grid. The critical input parameters, as discussed above, were calibrated exactly as recommended. The safety factors for the detailed case study analysis were calculated by using the average stress-based pillar safety factor for the area within the Active Mining Zone (AMZ) as defined by ARMPS (Mark and Chase, 1997).

The results of the database analysis using the recommended calibration method are shown in Figure 1. When the separation between the successes and failures is examined, it can be seen that the bulk of the safety factors have been fairly well separated. Most of the successes are towards the higher safety factors and most of the failures are at the lower safety factors. The area where the successful and failed designs overlap (or the "grey" area) goes from a safety factor of 0.86 to a safety factor of 1.50. This grey area encompasses a safety factor deviation of ± 0.22 and compares very well with an ARMPS analysis of the case studies that had a grey area that encompassed ±0.41 (Heasley et al., 2010). In the calibration analysis, only 4 failures (and middlings) out of 19 total occurred with an idealized safety factor above the recommended design line at 1.40, and only one success occurred with an idealized safety factor below 1.00. Therefore, if a safety factor of 1.40 is used as a design objective, there would be only an 8.5% (4 out of 47) chance of misclassifying a potential failure as a successful design.

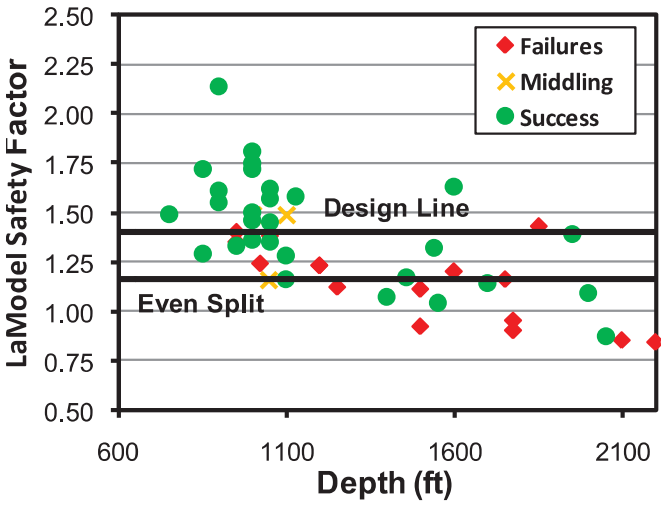

Figure 1. The LaModel safety factors for the calibration verification case histories.

SENSITIVITY ANALYSIS OF THE INPUT PARAMETERS

As seen in Figure 1 and discussed above, the recommended calibration method for LaModel produces fairly good results when compared to ARMPS. However, when using this calibration method, the values of the critical input parameters are rigidly specified. This rigid parameter specification is good for (1) producing a standard model that fits within the verification database, (2) guiding a novice modeler in the correct direction, and (3) serving as a standard for discussion of the model design. However, the rigid parameter specification also removes most of the model flexibility for specific calibration to the unique conditions at a given mine site.

In this section of the paper, a number of the LaModel input parameters are varied outside the bounds of the suggested calibration and the effects on the model results are analyzed, Specifically,

1. The lamination thickness is varied, but the gob modulus is still calibrated.
2. The rock mass modulus is varied, but the lamination thickness and gob modulus are still calibrated.
3. The coal seam modulus is varied, but the lamination thickness and gob modulus are still calibrated.
4. The Poisson's Ratio is varied

These numerical exercises show how a user might adjust the LaModel input to calibrate for multiple-seam stresses, surface subsidence, etc. and still remain consistent with the calibration procedure.

These analyses are performed for both single and multiple seam situations (where appropriate). For the single seam analysis, a "standard" mine geometry is used (overburden depth = 700 ft, panel width = 360 ft, mining height = 5 ft, center to center pillar width = 60 ft, center to center crosscut length = 80 ft, and entry width = 20 ft). For the multiple seam analysis, a 5-ft-thick solid coal seam is inserted 50 ft under the standard mine geometry.

Lamination Thickness

In LaModel, the overburden loads are distributed by the laminated overburden model based on the failure strength of the coal and the relative stiffness between the coal seam, gob, and overburden strata (rock mass). All of these parameters play an equally important role by interacting with each other during the overburden load distribution process. However, in the recommended calibration process, the lamination thickness is the first parameter calibrated. Once the lamination thickness is determined, the subsequent determination of the gob stiffness properties to provide a desired gob loading is highly dependent on the predetermined lamination thickness.

When the standardized calibration method, as briefly explained above, is used for calibrating the standard single seam model (Heasley et al., 2010), the lamination thickness is calculated as 407 ft and the associated final gob modulus for this lamination

thickness is calculated as 1,948,000 psi. These values of lamination thickness and final gob modulus are quite large when compared to values that have traditionally been used (lamination thickness ≈ 50 ft and final gob modulus ≈ 300,000 psi). When using these larger values, the amount of seam convergence and multiple-seam stress transfer will be significantly reduced from those previously seen.

The calibration process for the lamination thickness is designed to produce a stress abutment extent that matches the value observed in the field and used in ALPS and ARMPS. However, what if the user is more interested in obtaining accurate multiple-seam stresses and/or seam convergence as opposed to stress abutment extents? How does using thinner lamination thicknesses than suggested by the recommended calibration method affect model results?

To investigate this question, the lamination thickness in the standard model was varied between 100 and 500 ft, while the desired gob load was still calibrated using the suggested method. Thus, for each different value of lamination thickness, a different final gob modulus value was calibrated so that the magnitude of the gob and abutment load was held constant to match the recommended 21° abutment angle gob loading. This process produced final gob modulus values that increase with increasing lamination thicknesses (see Table 1).

Table 1. The effect of changing the lamination thickness on the calibrated gob modulus and the abutment extent (D90).

Lamination Thickness (ft)	Final Gob Modulus (psi)	Abutment Extent (ft)
100	581,866	74
200	1,099,349	97
300	1,540,916	115
407	1,948,005	132
500	2,255,853	149

The reason for the increase in the final gob modulus value with an increase in lamination thickness can be seen in Figure 2. As the lamination thickness increases, the overburden becomes stiffer and the convergence over the gob naturally decreases. To compensate for the decreasing convergence and still maintain the same average load on the gob, the final gob modulus must also increase.

The effect of changing the lamination thickness on the vertical abutment stress can be seen in Figure 3, which shows the vertical stress where the gob is adjacent to the solid coal rib in essentially a 2-D situation. As the lamination thickness decreases, the peak abutment stress increases, and the abutment extent decreases (see Table 1). In all cases, since the gob modulus has been calibrated to provide a constant abutment load, the total abutment load is the same; just the load distribution is changing.

The concentration of the vertical stress near the edge of the panel is even more pronounced in the multiple seam stress transfer below the panel (see Figure 4). In the case of multiple-seam stress transfer, the thinner laminations not only concentrate the stresses at the edge of the abutment zone in the active seam, but they also cause the multiple-seam stresses to be more concentrated as they

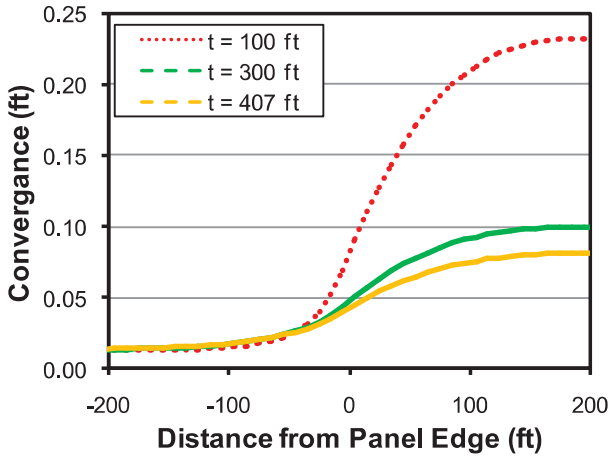

Figure 2. The effect of changing the lamination thickness on the convergence over the gob.

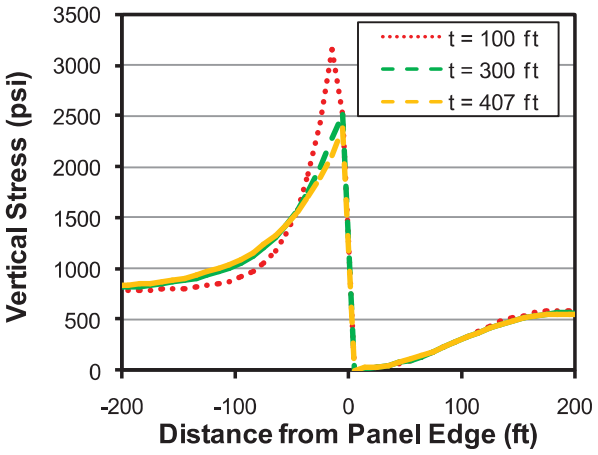

Figure 3. The effect of changing the lamination thickness on the vertical abutment stress.

are vertically transmitted to the sub-adjacent seam. Therefore, if the user is interested in accentuating the multiple-seam stress transfer, using a thinner lamination greatly increases the multiple-seam stress concentration, while leaving the overall abutment load or multiple-seam load magnitude unaffected.

However, the LaModel user must be careful in lowering the lamination thickness to increase the multiple-seam stress concentration. If a smaller lamination thickness than recommended is used as an input, the calculated load transfer over a barrier pillar onto the active mining zone may be less than reality, and an artificially high safety factor on the active mining zone may result.

Rock Mass Modulus

The fundamental partial differential equation of the laminated model is shown below as Equation 2 (Heasley, 1998):

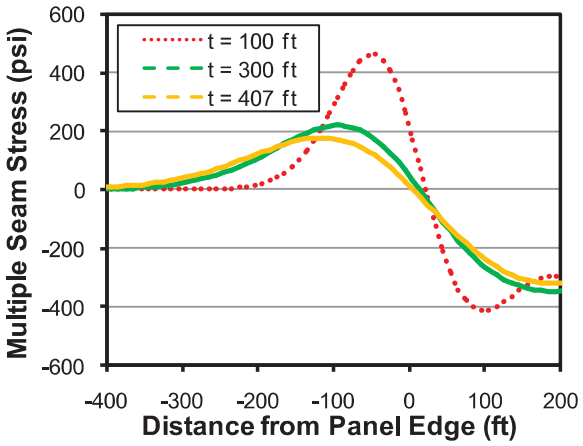

Figure 4. The effect of changing the lamination thickness on the multiple seam stresses.

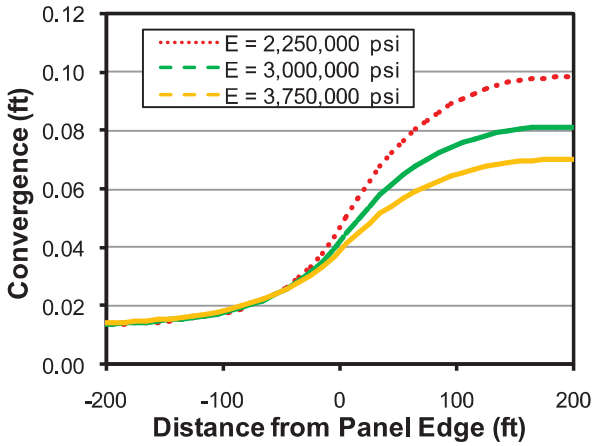

Figure 5. The effect of changing the rock mass modulus on the convergence over the gob.

$$\left(\frac{\partial^2}{\partial x^2}s(x,y)+\frac{\partial^2}{\partial y^2}s(x,y)\right)=\frac{4\sqrt{3(1-\nu^2)}}{Et}\sigma_i \qquad (2)$$

In this equation, the two primary parameters that control the stiffness of the overburden are the elastic modulus (E) and the lamination thickness (t), and it can be seen in the equation that they are multiplied together in the denominator of the induced stress function. Therefore, similar to the lamination thickness, increasing the rock mass modulus (all other parameters held constant) will decrease the convergence over the gob, decrease the peak abutment stress, and increase the extent of the abutment zone (see Table 2, Figure 5, and Figure 6). In the calibration process, it is recommended to fix the rock mass modulus and then only vary the lamination thickness to obtain the desired extent of the abutment stress. However, what would be the effects on the calibrated parameters and model results if the rock mass modulus is varied and then the lamination thickness is calibrated as recommended?

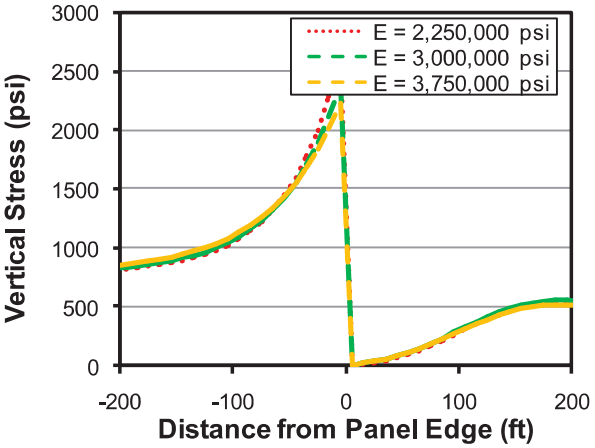

Figure 6. The effect of changing the rock mass modulus on the vertical abutment stress.

Table 2. The effect of changing the rock mass modulus on the abutment extent.

Rock Mass Modulus (psi)	Lamination Thickness (psi)	Abutment Extent (ft)
2,250,000	407	
3,000,000	407	
3,750,000	407	

In the calibration process, the rock mass stiffness is calibrated to match a desired abutment extent. Considering that only one value of rock mass stiffness can match a given abutment extent and that the rock mass modulus and lamination thickness are multiplied together in the fundamental equation to determine the rock mass stiffness (see Equation 2), it is clear that the product of the rock mass modulus and lamination thickness has to remain constant for the laminated model to match a desired abutment extent. Therefore, any increase in rock mass modulus will be compensated by an equal decrease in the lamination thickness in the calibration process. This is indeed the case, as seen in Table 3. Once the rock mass stiffness has been calibrated to a desired abutment extent, the resulting single-seam convergence and vertical stress are identical between the different rock mass modulus/lamination thickness pairs.

Table 3. The effect of changing the rock mass modulus on the calibrated lamination thickness.

Rock Mass Modulus (psi)	Lamination Thickness (psi)	Abutment Extent (ft)
2,250,000	543	132
3,000,000	407	132
3,750,000	326	132

However, changing the rock mass modulus/lamination thickness pairs does have a profound effect on the multiple seam stresses.

The laminated model influence function used to calculate the multiple-seam stresses on the adjacent seam is shown in Equation 3 (Heasley, 1998):

$$F = \frac{E}{8\pi Z^2}\left(\frac{12(1-v^2)}{t^2}\right)\left(\frac{X^2+Y^2}{4|Z|}\right)e^{-\sqrt{\frac{12(1-v^2)}{t^2}}\left(\frac{X^2+Y^2}{4|Z|}\right)} \quad (3)$$

In this equation, the rock mass modulus (E) is in the numerator and the square of the lamination thickness (t) is in the denominator. Therefore, increasing the rock mass modulus or decreasing the lamination thickness will increase the multiple-seam stress. When the rock mass modulus and lamination thickness were calibrated for a single seam, it was seen that an increase in rock mass modulus resulted in a corresponding decrease in lamination thickness; therefore, increasing the rock mass modulus, which decreases the lamination thickness, has a compound effect on increasing the peak multiple-seam stress. This effect is clearly seen in Table 4 and Figure 7.

Table 4. The effect of changing the rock mass modulus on the multiple seam stress.

Rock Mass Modulus (psi)	Calibrated Lamination Thickness (psi)	Multiple Seam Stress Extent (ft)	Maximum Multiple Seam Stress (psi)
2,250,000	543		
3,000,000	407		
3,750,000	326		

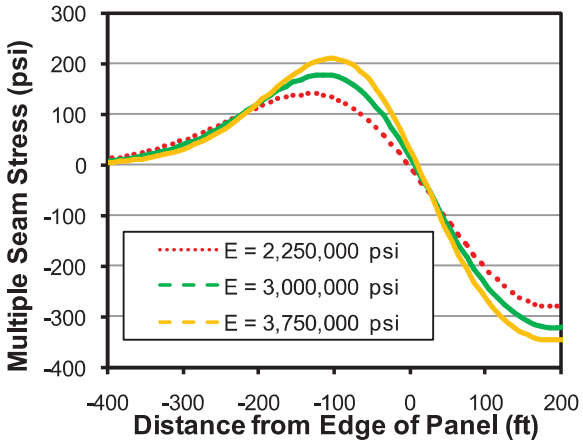

Figure 7. The effect of changing the rock mass modulus on the multiple seam stresses.

So, by increasing the rock mass modulus yet still calibrating the lamination thickness to the desired abutment extent, the single seam displacements and stress stay the same; however, the multiple-seam stress influence increases. Therefore, in essence, by increasing the rock mass modulus in the calibration process, the LaModel user can get increased multiple-seam stresses and convergence, while the single seam stresses stay constant. This result provides the user with a technique to calibrate multiple-seam stress and displacements while keeping the model consistent with the recommended calibration technique.

Coal Seam Modulus

Another input parameter to LaModel that is not often considered in any detail (and that is in Equation 1) is the elastic modulus of the coal seam. Obviously, the modulus of the coal seam directly affects the amount of convergence of the seam, but how does the seam modulus affect the calibration process and the calibrated parameters?

In Equation 1, it can be seen that the elastic modulus of the coal seam is in the numerator of the equation. Therefore, an increase in seam modulus directly causes an increase in the calibrated lamination thickness in order to keep the desired abutment extent. This increase in lamination thickness then results in a corresponding increase in the final gob modulus to keep the abutment load constant (see Table 5).

Table 5. The effect of changing the coal seam modulus on the lamination thickness and the final gob modulus.

Coal Seam Modulus (psi)	Lamination Thickness (psi)	Final Gob Modulus (psi)
250,000	339	1,575,074
300,000	407	1,948,005
350,000	475	2,329,534

When the coal seam modulus is changed but the abutment extent and load are calibrated, the single seam vertical stress does not change (see Figure 8). However, as might be expected, as the coal modulus increases, the single seam convergence over the solid coal decreases. And because the increase in the coal modulus causes an increased lamination thickness and increased final gob modulus, the convergence over the gob also decreases (see Figure 9). Therefore, increasing the coal modulus in a calibrated model will decrease the seam convergence without affecting the seam stresses.

Poisson's Ratio

As part of this research, the effect on the LaModel output of varying the Poisson's Ratio of the rock mass was also investigated. If Equations 1, 2, and 3 are examined, it can be seen that the Poisson's Ratio (v) is always in the general form of

$$\sqrt{1-v^2} \quad (4)$$

In this form, if Poisson's Ratio changes from 0.25 to 0.40 (a 60% increase) the factor in the equations only changes from 0.968 to 0.916 (a 5% decrease). Therefore, as a result of the underlying equations, the effect of a change in Poisson's Ratio of the rock mass is generally greatly muted.

This small impact of changing Poisson's Ratio can be seen in the application of the LaModel program. In the initial standard model, the default Poisson's Ratio of 0.25 was used for the rock mass. Then, the value of Poisson's Ratio was changed to 0.30 and 0.40,

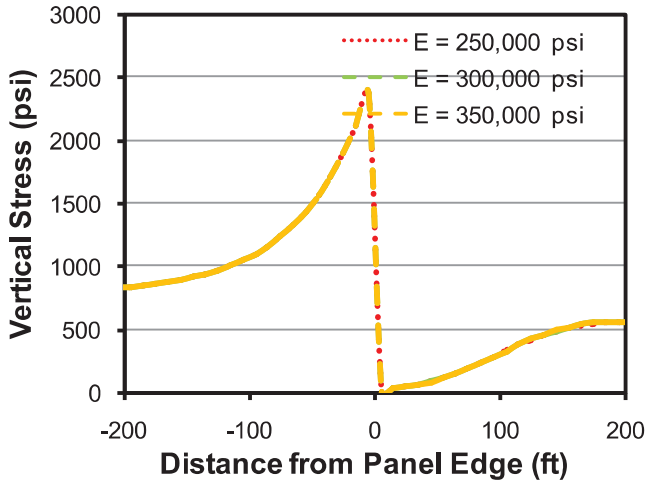

Figure 8. The effect of changing the coal seam modulus on the calibrated vertical stress.

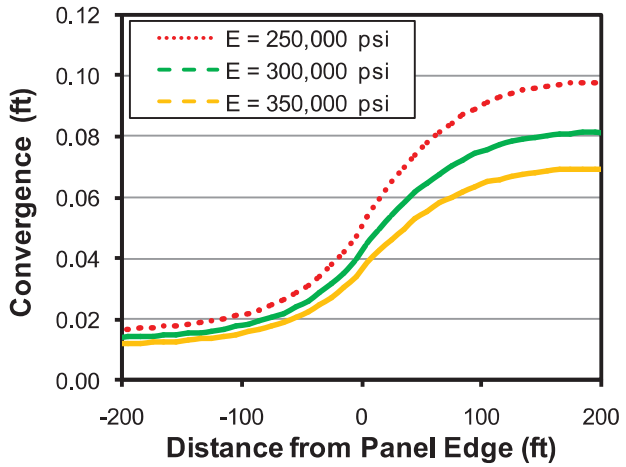

Figure 9. The effect of changing the coal seam modulus on the calibrated convergence.

and the model was re-run while all of the other parameters were kept constant. Table 6 shows the functional values of the abutment extent (D_{90}) and the abutment load that resulted from this change. It can be seen that increasing the Poisson's Ratio essentially increased the stiffness of the overburden and resulted in a greater abutment extent and a greater abutment load. However, the 60% increase in the Poisson's Ratio only increased the abutment extent by 3.0% and the abutment load by 3.9%.

Table 6. The effect of changing the Poisson's Ratio.

Poisons Ratio	Abutment Extent (ft)	Abutment Load (%)
0.25	132	66.5
0.30	133	67.9
0.40	136	69.1

Similarly, Figure 10 shows the effect of changing the Poisson's Ratio on the convergence of the strata over the gob. In this figure, the change is so small that it cannot be seen very well. Changing the Poisson's Ratio from 0.2 to 0.4 (100%) only changed the maximum convergence from 0.0812 ft to 0.0807 ft (0.6%). In general, changing the Poisson's Ratio of the rock mass has a very minor effect on the LaModel output, and accurately calculating the input Poisson's Ratio is generally not necessary.

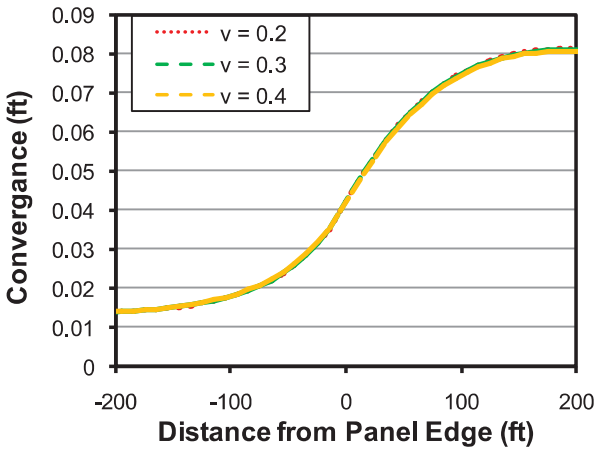

Figure 10. The effect of changing the Poisson's Ratio on the convergence over the gob.

SUMMARY

After the Crandall Canyon Mine collapse, a new calibration procedure was implemented in LaModel for deep-cover retreat mining. This calibration procedure prescribed techniques for calibrating the critical LaModel input parameters (rock mass lamination thickness, final gob modulus, and coal strength) based on empirical abutment loading and pillar strength as utilized in the time-tested ALPS and ARMPS programs. Also, this new calibration procedure produced very good results when applied to a database of 47 deep-cover case histories.

The calibration procedure has been implemented into wizards in the new LamPre3.0, and it is intended to (1) produce a standard model that fits within the verification database, (2) guide a novice modeler in choosing optimum input parameters, and (3) serve as a common basis for discussion of the model design. However, the rigid parameter specification incorporated in the calibration procedure also removes most of the flexibility in LaModel for specific calibration to the unique conditions at a given mine site.

However, in a sensitivity analysis of a number of the LaModel input parameters, it is shown how the LaModel user might vary certain input parameters to strategically adjust the model output and still maintain the general philosophy and validity of the recommended calibration. By making the lamination thickness smaller but still calibrating the magnitude of the abutment load, the user can greatly accentuate the multiple-seam stress transfer, while only slightly affecting the abutment stress distribution. If the rock mass modulus is increased at the same time the lamination

thickness is decreased, the single-seam displacements and stress remain the same, while the multiple-seam stress influence is increased.

In addition, it was shown how increasing or decreasing the coal modulus in a calibrated model can be used to decrease or increase the seam convergence without affecting the seam stresses. Finally, the Poisson's Ratio of the rock mass was analyzed, and it was ultimately demonstrated that changing the Poisson's Ratio of the rock mass has a very minor effect on the LaModel output, and accurately calculating the Poisson's Ratio is generally not necessary.

REFERENCES

Heasley, K.A. (1998). "Numerical modeling of coal mines with a laminated displacement-discontinuity code" [Dissertation]. Golden CO: Colorado School of Mines. p. 187.

Heasley, K.A. (2008). "Some thoughts on calibrating LaModel." In: *Proceedings of the 27th International Conference on Ground Control in Mining.* pp. 7–13. [http://icgcm.conferenceacademy.com/papers/detail.aspx?subdomain=icgcm&iid=335].

Heasley, K.A., Sears, M.M., Tulu, I.B., Calderon-Arteaga, C.H., Jimison, II, LW. (2010). "Calibrating the LaModel program for deep cover pillar retreat coal mining." In: *Proceedings of the 3rd International Workshop on Coal Pillar Mechanics and Design*. Department of Health and Human Services, Centers for Disease Control and Prevention, National Institute for Occupational Safety and Health. pp. 47–57.

Mark, C. (1992). "Analysis of longwall pillar stability (ALPS); an update." In: *Proceedings of the Workshop on Coal Pillar Mechanics and Design*. United States Bureau of Mines, IC 9315. pp. 238–249.

Mark, C. (1999). "Empirical methods for coal pillar design." In: *Proceedings of the Second International Workshop on Coal Pillar Mechanics and Design.* National Institute for Occupational Safety and Health, IC 9448. pp. 145–154.

Mark, C., Chase, F.E. (1997). "Analysis of retreat mining pillar stability (ARMPS)." In: *Proceedings of New Technology for Ground Control in Retreat Mining.* National Institute for Occupational Safety and Health, IC 9446. pp. 17–34.

MSHA. (2008). "Fatal underground coal burst accidents August 6 and 16, 2007, Crandall Canyon Mine." Department of Labor, Mine Safety and Health Administration. RI. p. 472.

CISPM–MS: A Tool to Predict Surface Subsidence and to Study Interactions Associated with Multi–Seam Mining Operations

Yi Luo, Associate Professor
Biao Qiu, Graduate Research Assistant
Mining Engineering
West Virginia University
Morgantown, WV

ABSTRACT

Multiple-seam mining operations induce surface subsidence basins different from those caused by mining in a single coal seam, and also disturb the mining operations in the other coal seams. A computer program, CISPM-MS (Comprehensive and Integrated Subsidence Prediction Model for Multiple Seam Mining), has been developed to predict the final surface movements and deformations as well as the interactions associated with multi-seam coal mining operations. The program applies a newly developed subsurface subsidence prediction model that is able to consider the geological stratification variations. In predicting surface subsidence, the surface movements and deformations caused by the individual mining operations as well as the interactive effects are all considered. A case study is conducted in this paper for validating the program.

INTRODUCTION

It is estimated that the multiple-seam coal reserves account for about 70% of the total reserves in the United States (Mark, Chase and Pappas, 2007). Particularly in the central Appalachian and Western coal fields, the majority of today's coal mines are operating above and/or beneath previously mined seams. The effects of mining one coal seam on the other coal seams, referred as the interactions of multi-seam mining, present one of the major ground control challenges in the coal mining industry. The severity of the multi-seam mining effects depends on the inter-burden thickness and properties, mining sequence, seam heights and mining method applied, time interval between the mining activities in neighboring seams, and sometimes local topographic and hydrographic features.

The mining activity in one coal seam can cause strata movements and stress redistribution in the coal seams both above and below. The mining-induced stress and deformations can affect the stability of the mine structures in neighboring seams. For example, the subsurface strain induced by an underlying active mine may reduce the pillar confinement and the frictional resistance along the pillar-roof and pillar-floor interfaces in the overlying seam. Such effects reduce the pillar strength and may potentially cause pillar failure. When the pillar failure occurs in a sufficiently large contiguous area, it could induce additional surface and subsurface subsidence other than that caused by the active mine alone. This unexpected additional subsidence may influence surface and subsurface structures and water bodies.

In order to make accurate subsidence predictions for multi-seam mining operations, the multiple seam mining interactions should be taken into consideration. A previously developed subsurface subsidence prediction model (Luo and Qiu, 2012) will be used to assess the subsidence effects of an active mine on the mine structures in the neighboring seams. In that model, a new deformation term - void intensity is defined to express the severity of expansion or shrinkage of a volume of rock strata under the influence of subsidence process. The void intensity around the mine pillars can be determined by the subsurface subsidence prediction model (Luo and Qiu, 2012).

The subsidence-induced void intensity in the subsurface strata changes the confinement to the pillar-roof and pillar-floor interfaces, and subsequently affects the strength of the pillars. Particular attention will be paid to areas with positive void intensity (expansion) that could reduce pillar strength. The possibility for pillar failure can be judged using the reduced pillar strength and safety factor. The failure of the pillars can cause additional subsurface and possibly surface subsidence.

This void intensity-pillar strength model is then incorporated into the newly developed multi-seam mining subsidence prediction program, CISPM-MS. This program has a user-friendly working environment. It allows the user to draw the mine panels and prediction points in AutoCAD, and it provides convenient tools for data output and post analysis.

ENHANCED SUBSURFACE SUBSIDENCE PREDICTION MODEL

The subsurface deformation caused by mining activities in an underlying coal seam could affect the pillar stability in the upper seam(s) as both the load and the strength of the pillar are changed. Change in the pillar load can be resulted from the differential subsidence between the roof and floor of the pillars. Pillar strength decreases with the confinement pressure as a result of the increased void intensity caused by the strata subsidence process. Therefore,

the stability of the upper seam pillars can be determined based on the predicted subsurface movements and deformations.

The concept of the influence function method, proven to be reliable and versatile for surface subsidence prediction, has been employed to develop an enhanced subsurface subsidence prediction model (Luo and Qiu, 2012). The model is capable of considering the varying overburden stratification. This model mimics the subsidence propagation process layer-by-layer from the strata immediately above the coal seam to the ground surface to predict the subsurface subsidence as shown in Fig. 1. The subsidence of a given layer in the overburden strata is caused by the subsidence of the layer immediately below. The final subsidence at a subsurface point of interest is determined by integrating the defined influence function within the proper horizontal interval. To apply the influence function method in developing a subsidence prediction model, the influence functions for subsidence and horizontal displacement along a major cross-section should be defined first and they are shown in Eqs. 1 and 2, respectively.

$$f_s(x', z_i) = \frac{S(x+x', z_{i-1}) \cdot a_i}{R_i} e^{-\pi\left(\frac{x'}{R_i}\right)^2}$$

$$i = 1, 2, \ldots, n \qquad (1)$$

$$f_u(x', z_i) = -2\pi \frac{S(x+x', z_{i-1}) \cdot a_i \cdot n}{R_i \cdot h} x' e^{-\pi\left(\frac{x'}{R_i}\right)^2}$$

$$i = 1, 2, \ldots, n \qquad (2)$$

The final subsidence and horizontal displacement at a prediction point in the overburden are determined by integrating the respective influence functions within the computing zone, as shown in the following two equations.

$$S(x, z_i) = \frac{a_i}{R_i} \int_{d_{i1}-x}^{W_i-d_{i2}-x} S(x+x', z_{i-1}) \cdot e^{-\pi\left(\frac{x'}{R_i}\right)^2} dx'$$

$$i = 1, 2, \ldots, n \qquad (3)$$

$$U_i(x, z_i) = -2\pi \frac{a_i \cdot n}{h \cdot R_i} \int_{d_{i1}-x}^{W_i-d_{i2}-x} S(x+x', z_{i-1}) \cdot x' \cdot e^{-\pi\left(\frac{x'}{R_i}\right)^2} dx'$$

$$i = 1, 2, \ldots, n \qquad (4)$$

In these equations, a_i, R_i, d_{i1}, and d_{i2} are the final subsidence parameters for the i^{th} layer in the overburden strata and are very important for subsidence prediction. Among them, a_i is the subsidence factor, R_i is the radius of major influence, d_{i1} and d_{i2} are the offset distances of inflection points on the left and right sides of the panel, respectively. These parameters are dependent on the layer thickness, the overburden load, the percent of hard rock in each layer, etc. The methods to determine these final subsidence parameters have been discussed in a previous publication (Luo and Qiu, 2012).

The differential strata movements in both horizontal and vertical directions will cause deformations in the subsurface strata. In surface subsidence studies, the surface deformations long a major cross-section are traditionally described by slope, strain, and curvature. However, for applications dealing with subsurface subsidence, the distributions of horizontal, vertical, and total strains in the overburden strata could be much more valuable for assessing the subsidence influences to subsurface mines structures, hydrology, and degasification wells. The horizontal strain (e_x) is defined as the first derivative of horizontal displacement with respect to x (Eq. 5). Sufficient horizontal strain could cause vertical fractures or even cracks in the strata. The vertical strain (e_z) is defined as the first derivative of subsurface subsidence with respect to z (Eq. 6). Sufficient vertical strain could cause bed separations along the strata bedding planes or even step cracks. The total strain (e_t), defined in Eq. 7, is an indicator of the severity of expansion or shrinkage of a volume of rock strata under the influence of subsidence process. It should be noted that the expansive type of total strain (in positive value), reflecting the average intensity of voids, is an indicator of the increase in porosity and permeability for seepage flows of gases or water in the subsurface strata. It can be an indirect indicator for reduction in confining pressure to underground mine structures. For simplicity, the expansive volumetric strain is also called void intensity.

$$\varepsilon_x(x, z) = \frac{dU(x, z)}{dx} \qquad (5)$$

$$\varepsilon_z(x, z) = \frac{dS(x, z)}{dz} \qquad (6)$$

$$\varepsilon_t(x, z) = \varepsilon_x + \varepsilon_z + \varepsilon_x \cdot \varepsilon_z \qquad (7)$$

MULTIPLE-SEAM MINING INTERACTIONS

The subsurface deformations due to mining operations in underlying seams have the potential to cause stability problems to mine structures (i.e., coal pillars, entry floor, and roof) in the upper seams (Fig. 2). Unstable pillars, roof, and floor can not only cause significant problems to mining operations but also can create hazardous working conditions as well as addition subsurface and surface subsidence.

Multiple-Seam Interactions on Roof and Floor Stability

Roof falls are the number one safety threat to underground miners. Common roof falls in coal mines are tensile failures and roof cutters. When an underground coal mine is affected by mining

activities conducted in the underlying coal seam, the originally stable mine roof could become unstable. Roof tension cracks could be induced in zones with high void intensity, while roof cutters are more likely to occur in high shear areas. The interactions could also result in unstable mine floors problems such as floor cracks in high tension zones and floor heaves in high compression zones. The subsurface subsidence could also cause mine safety problems. For example, the connected fracture zone between the mined coal seams induced by the subsurface subsidence process could allow the accumulated methane in the sealed mine areas to rush into the active working areas to create a dangerous condition. Because of its capability to predict the magnitude and distribution of various subsurface deformations, the subsurface subsidence prediction model can be used to guide mine design to avoid excessively disturbed zones and to plan ahead on any mitigation measures to minimize such influences.

For assessing the stability of the mine roof and floor, the predicted horizontal strain along the mine roof and floor should be compared to their respective critical strain for initiating cracks. For example, a tensile strain higher than 2×10^{-3} ft/ft is capable of causing cracks in the immediate roof and floor that are made up by shale type of rocks.

Multiple-Seam Interactions on Pillar Stability

The stability of a coal pillar depends on its strength and the load applied on it. The pillar strength is a function of its confinement that is indirectly reflected by the pillar width to height ratio in a single seam mining setting. However, when a pillar is disturbed by mine subsidence, both the pillar load and its strength could be affected.

Change in pillar load can be related to the differential subsidence between the roof and floor line of the pillar. The pillar load under the influence of multi-seam influence, σ'_p, can be calculated by Eq. 8. In the equation, s_p is the pillar load prior to the multi-seam mining effect (normally determined using the tributary load method), E_c is the Young's modulus of the coal pillar, and e_v is the subsidence-induced vertical strain at the pillar location (sign convention: positive for tensile strain and negative for compression).

$$\sigma'_p = \sigma_p - E_c \cdot \varepsilon_v \tag{8}$$

The pillar strength would decrease with the confinement pressure that is related to the increased void intensity in the subsurface subsidence process. The pillar strength under the influence of subsurface subsidence, S'_p, is calculated by the following equation.

$$S'_p = \lambda S_p \tag{9}$$

The subsidence-influenced pillar strength is related to the pillar strength prior to the multi-seam mining influence S_p which can be determined by the Bieniawski's formula (Eq. 10), and λ is the pillar strength reduction factor. The determination of this factor will be discussed in a later section.

$$S_p = \sigma_1(0.64 + 0.36\frac{W}{H}) \tag{10}$$

In the equation, s_1 is the in-situ coal strength (900 psi), W and H are the pillar width and height, respectively. Subsequently, the safety factor of a pillar under the disturbance of subsurface subsidence can be determined by Equation11.

$$SF' = \frac{S'_p}{\sigma'_p} \tag{11}$$

If the pillar safety factor under the disturbance of mine subsurface subsidence is less than a critical value, the pillar could fail. Based on the published investigation cases (Morsey, Yassien and Peng, 2006), it is proposed that a critical safety factor for pillars to fail in a large area is 1.0.

Void Intensity and Pillar Strength

The Bieniawski's formula (Eq. 10) is widely used to estimate the pillar strength in the process of pillar design and pillar stability analysis. The pillar width to height ratio (W/H) contained in the formula is an indirect measure of the confinement level of the pillar. However, the pillar strength is also affected by other factors, such as the structure and surface conditions of the discontinuities inside the pillar and the roof and floor conditions. In order to account for the effects of subsurface subsidence on the pillar strength, the Hoek-Brown failure criterion is adopted here to evaluate the pillar strength. The generalized Hoek-Brown (1997) failure criterion for jointed rock masses is defined as

$$\sigma'_1 = \sigma'_3 + \sigma_{ci}(m_b\frac{\sigma'_3}{\sigma_{ci}} + s)^a \tag{12}$$

In Eq. 12, σ'_1 and σ'_3 are the major and minor effective principal stresses at failure, s_{ci} is the uni-axial compressive strength of the intact rock material, and m_b, s, and a are the material constants. When considering the strength of a pillar, it is useful to have an estimate of the overall strength of the pillar rather than a detailed knowledge of the extent of fracture propagation in the pillar. This leads to the concept of a global "rock mass strength" that could be estimated by the following Mohr-Coulomb relationship, as proposed by Hoek et al (2002).

$$S_p = \frac{2c'\cos\phi'}{1-\sin\phi'} \tag{13}$$

In Eq. 13, c' and ϕ' are the cohesion and angle of internal friction. It can be further derived into Eq. 14 in the stress range of $s_t < \sigma'_3 < s_{ci}/4$.

$$S'_p = k\sigma_{ci} \tag{14}$$

$$k = \frac{[m_b + 4s - a(m_b - 8s)](m_b/4 + s)^{a-1}}{2(1+a)(2+a)} \tag{15}$$

$$\lambda = \frac{S'_p}{S_p} = \frac{k'\sigma_{ci}}{k\sigma_{ci}} = \frac{k'}{k} \tag{16}$$

The terms k and k' in the previous equation are the pillar strength reduction factors when the pillar is undisturbed (k) and disturbed (k') by multi-seam mining. The reduced material constant m_b is a function of the unaffected material constant m_i, the rock's geological strength index (*GSI*), and the degree of disturbance (D) as shown in Eq. 17. The coefficients s and a for the rock mass are determined by Eqs. 18 and 19.

$$m_b = m_i \cdot e^{\left(\frac{GSI-100}{28-14D}\right)} \tag{17}$$

$$s = e^{\left(\frac{GSI-100}{9-3D}\right)} \tag{18}$$

$$a = \frac{1}{2} + \frac{1}{6}(e^{-GSI/15} - e^{-20/3}) \tag{19}$$

Coefficient D is a factor reflecting the degree of disturbance to which the rock mass has been subjected by blasting damage and stress relaxation. It varies from zero for undisturbed in-situ rock masses to 1 for very disturbed rock masses. The significance of the parameters and their values can be found in Hoek, 2004. The Geological Strength Index (*GSI*), introduced by Hoek (1994) and Hoek et al. (1995), provides a system for estimating the reduction in rock mass strength for different geological conditions. The *GSI* takes into account the geometrical shape of intact rock fragments as well as the condition of joint faces. For underground structures, such as tunnels, slopes, and mine openings that are easy to access and observe the geological conditions, the *GSI* is determined using the method proposed by Hoek and Brown (1997). However, in this research, the geological conditions of the subsurface structures under the disturbance of the subsurface subsidence are very hard to observe. The subsurface total strain in the rock mass can be considered as a mining-induced geological condition of the rock mass. An empirical formula is established here to estimate the *GSI* for the subsurface structures based on the subsurface total strain distribution.

$$GSI = 75 - 0.95(\varepsilon_t \cdot 10^3) \tag{20}$$

Numerical Study of the Effect of Subsurface Deformation on Pillar Strength

In order to calibrate the empirical formula, numerical simulations are also performed. The Fast Lagrangian Analysis of Continua (FLAC) program package, capable of elasto-plastic analysis of rock excavations with strain softening using the linear Mohr-Coulomb failure criterion, was used in the simulation. A FLAC3D model was developed to study the coal pillar strength under the influence of subsurface subsidence. The model consists of 8 ft coal seam, 30 ft roof strata, and 30 ft floor strata (Fig. 3). The entry and crosscut are 20 ft wide. The elastic-perfectly-plastic Mohr-Coulomb model is assigned for the rock strata, and the strain softening Mohr-Coulomb model is assigned for the coal seam. Roller boundary conditions are used along the sides and bottom of the model. In order to establish the peak load for the pillar to carry, the velocity of vertical displacement on top of the model is fixed at a constant value of -1×10^{-5} ft/sec. The sum of reaction forces at the base of the model is obtained via a FISH function (Itasca, 2006) to estimate the average vertical stress developed in the pillar. The input geo-mechanical properties are the same as those used by Lu et al. (2008). Four pillar widths (24, 40, 56, and 80 ft) for pillar width to height ratios (W/H) of 3, 5, 7, and 10 are simulated. The resulting stress-strain relationships are plotted in Fig. 4. The pillar strengths based on the simulation are comparable to the Bieniawski equation.

To simulate the subsurface subsidence effect on the pillar strength, the subsidence-induced horizontal strain and vertical strain are simulated by applying the displacements on the side and the top of the model, respectively, at a constant value of -1×10^{-5} ft/sec. Different subsurface deformation values are simulated with this model. The numerical simulation results are compared to the results of the previous analytical model for validation purposes in Fig. 5. It shows that the proposed pillar strength formula to consider the subsurface subsidence effects agrees well with the numerical simulation results.

CASE STUDY

To demonstrate the capability of CISMP-MS program in the studies of multi-seam interactions, a multi-seam mining case (Fig. 6) that caused damages to both subsurface mine structures and to surface structures is modeled using the program. In this case, an active room-and-pillar mine was developing its mains in the Sewickley coal seam over a portion of the closed coal mine in the Pittsburgh seam. The inter-burden between these two coal seams was about 90 ft. The mine in the Pittsburgh seam had been mined in the 1960s using the room-and-pillar method and then closed afterwards. Pillaring operation was performed in a large portion of the mine. The most noticeable mine structure left in the Pittsburgh seam under the problems areas was an irregularly shaped support area (about 250 ft long and 150 ft wide) left around a gas well.

The spatial relationship among the two residential structures and the layout of the active mine in the Sewickley seam are shown in Fig. 6. The boundary between the pillared area and the area with development mining only in the Pittsburgh seam mine are also shown in Fig. 6.

The surface subsidence damages including a ground crack and a depression zone were reported near the surface structures. The damages occurred on the mine structures in the active mine in the Sewickley seam included rib spallings, cutter roof, floor cracks and minor floor heave. The occurrence of all these surface and subsurface structural damages coincided with an event in which the raising mine water in the closed mine in the Pittsburgh seam reached under the problem area. Underground observations made in the active mine indicate that rib spalling and cutters are more prevalent in the area above and around the boundary line in the Pittsburgh seam. The large roof fall in the entries in the active mine appeared to coincide with the edge of the support pillar area.

In order to study the subsurface subsidence effects of the Pittsburgh seam on the Sewickley seam mine pillars and entries, predictions were performed along the cross-section A-A' and in a rectangular area of BCDE as shown in Fig. 6. The predicted subsurface subsidence and subsurface void intensity distribution over the rectangular area BCDE in the Sewickley seam are plotted in Figs. 7 and 8, respectively. The subsurface subsidence along the prediction line A-A' at the Sewickley seam around the support pillar area of the Pittsburgh seam is predicted using CISMP-MS and the results are shown in Fig. 9.

The subsurface subsidence prediction indicates that the subsurface deformation can reduce the average safety factor of the upper Sewickley seam pillars by 11%. The original pillar safety factor for the Sewickley seam mine is about 8.6, and the pillar safety factor under the subsurface subsidence influence is 7.6, which agrees well with the underground observation that the pillars in the active mine were still intact. The resulting high pillar safety factors and the fact that no pillar failure in the active mine strongly suggested that the mining operation in the Sewickley seam is not the cause for the reported surface subsidence events.

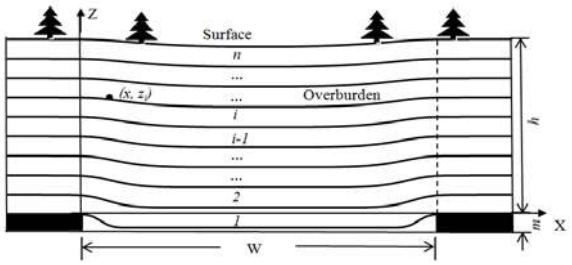

Figure 1. Subsurface subsidence prediction model (h = overburden depth; m = mining height; W = panel width; n = number of overburden layers).

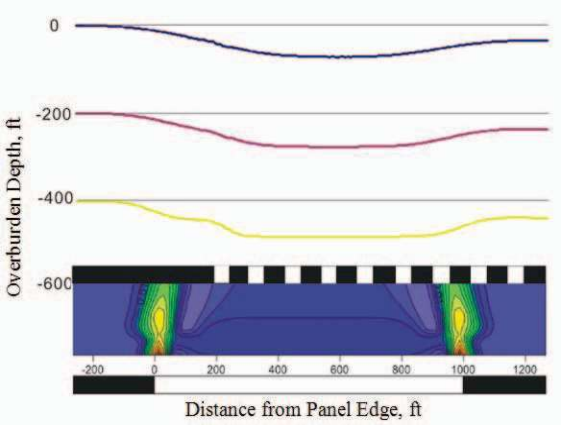

Figure 2. Subsurface subsidence profile and multi-seam mining interactions.

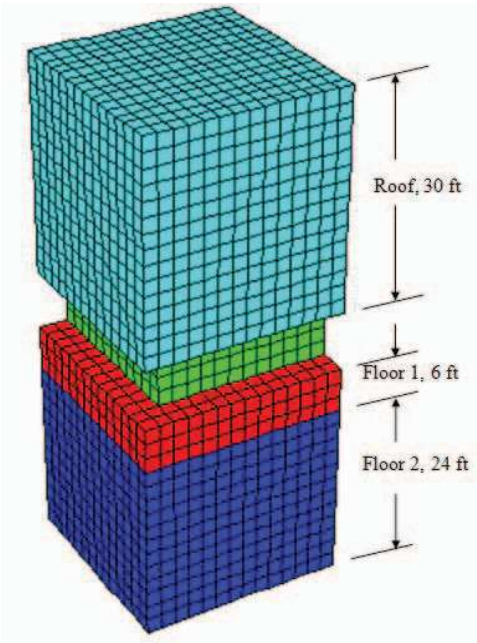

Figure 3. The three-dimensional discretized view of quarter pillar (w/h=5).

The maximum strain on the mine roof in the Sewickley seam at the location near the edge of the support pillar was1.96×10^{-2} ft/ft. This is significantly higher than the proposed critical tensile strain for roof cracking, 2×10^{-3} ft/ft, and more than sufficient to cause the roof failure at in the active mine. Figure 8 shows most of the observed massive roof falls (in cross hatch pattern), and roof cracks in the active mine in the Sewickley coal seam are located in the zones of high void intensity.

CONCLUSIONS

The enhanced subsurface subsidence prediction model can be used to analyze the interactions in multi-seam mining operations. A number of important parameters to quantify the subsurface

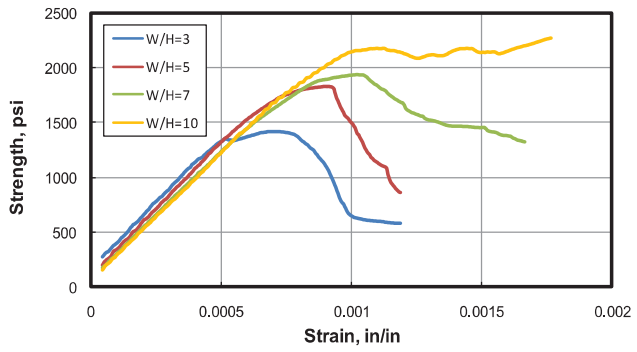

Figure 4. Stress-strain curves under different W/H ratios.

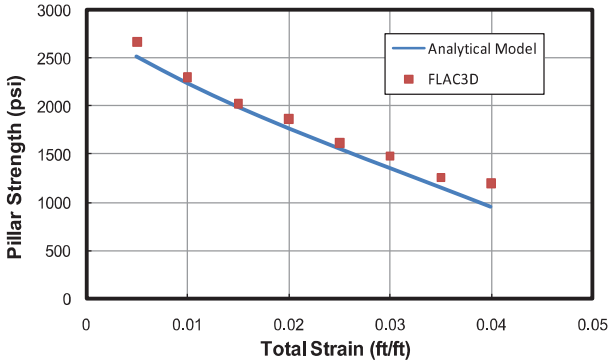

Figure 5. Comparison between proposed pillar strength formula and FLAC modeling results.

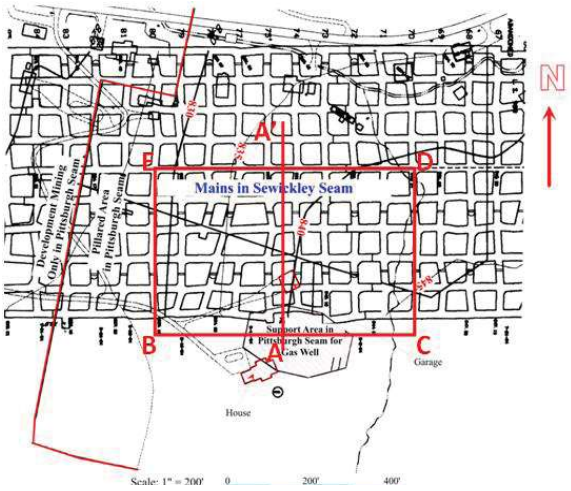

Figure 6. Spatial relationship among surface structures and mains in the mines in the Sewickley and Pittsburgh Seams.

subsidence influences to subsurface mine structures have been proposed. They include (1) the critical strain for causing tensile cracks in the mine roof and floor, (2) the method to determine subsidence-induced pillar load, and (3) the failure criteria based method to determine pillar strength under the influence of subsurface subsidence. The methodology to assess the multi-seam

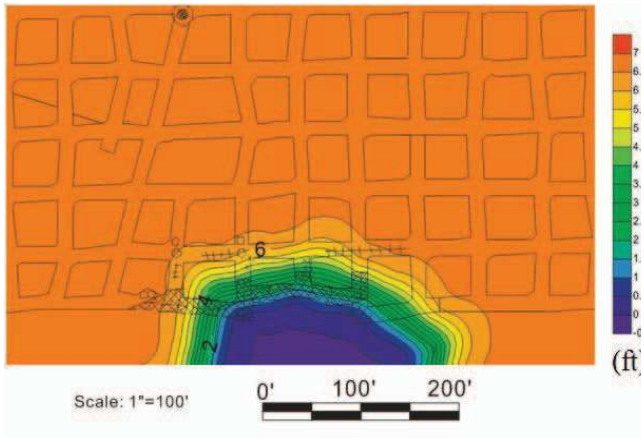

Figure 7. Predicted subsurface subsidence in the Sewickley seam in rectangular area BCDE.

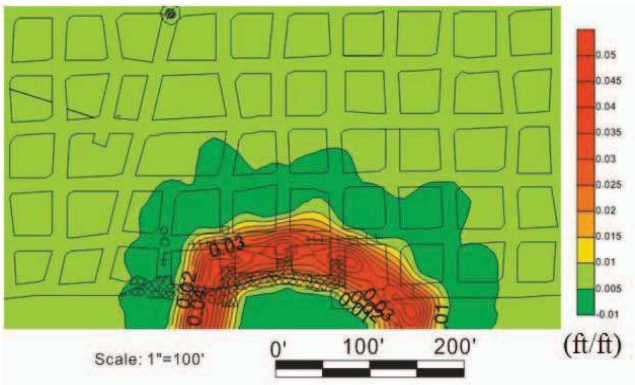

Figure 8. Predicted subsurface void intensity in the Sewickley seam in rectangular area BCDE.

mining interactions has been incorporated in the subsidence prediction model CISPM-MS for multi-seam mining operations. A case study to illustrate its capability to assess the multi-seam mining actions showed agreement with the field observations.

REFERENCES

Hoek, E., 1994, "Strength of rock and rock masses," *ISRM New Journal*, *2*(2), pp. 4–16.

Hoek, E., 2004, "Practical rock engineering—an ongoing set of notes," Rocscience, www.rocscience.com/hoek/corner/Practical_Rock_Engineering.pdf.

Hoek, E. and E.T. Brown, 1997, "Practical estimates of rock mass strength," *International Journal of Rock Mechanics & Mining Science, 34*(8), pp. 1165–1186.

Hoek, E., C. Carranza-Torres, B. Corkum, 2002, "Hoek-Brown failure criterion—2002 edition," *Proceedings of the 5th North American Rock Mechanics Symposium,* Toronto, Ontario, Canada, University of Toronto Press.

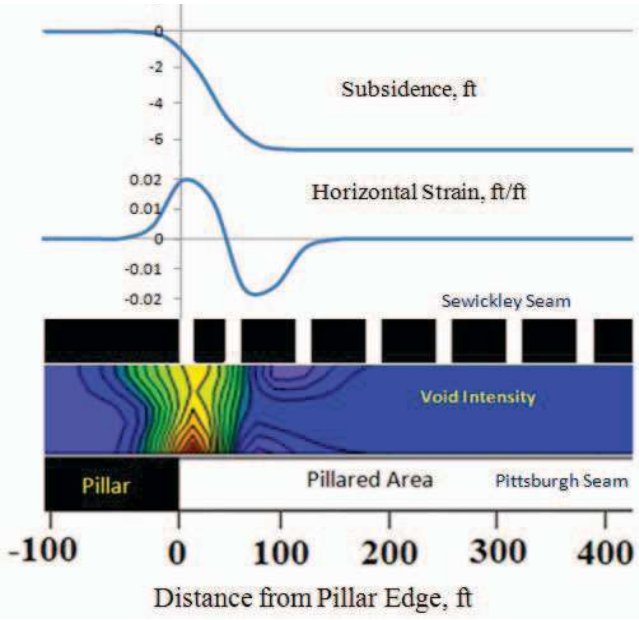

Figure 9. Predicted subsurface subsidence and horizontal strain along A-A' cross-section in the Sewickley seam above the Pittsburgh seam.

Hoek, E., P.K. Kaiser, W.F. Bawden, 1995, "Support of underground excavations in hard rock," Rocscience, rocscience.com/hoek/corner/ Support_of_Underground_ Excavations_in_Hard_Rock.pdf.

Itasca Consulting Group, Inc., 2006, *Flac 3D Version 3.1 Example Applications*, Minneapolis, MN, Itasca Consulting Group, Inc., pp. 2-1– 2-17.

Jaiswal, A. and B.K. Shrivastva, 2009, "Numerical simulations of coal pillar strength," *International Journal of Rock Mechanics & Mining Science*, *46, pp.*779–788.

Lu, J., K. Morsy, A. Ray, S.S. Peng, 2008."Effects of rock/coal interface properties on coal pillar strength," *Proceedings of the 27th International Conference on Ground Control in Mining*, pp. 262–267. [http://icgcm.conferenceacademy.com/papers/detail.aspx?subdomain=icgcm&iid=369]

Luo, Y., 1989, Integrated computer model for predicting surface subsidence due to underground coal mining–CISPM, Dissertation, West Virginia University, UMI order No. 9020385, Morgantown, WV, 168 p.

Luo, Y. and S.S. Peng, 2000, "Prediction of subsurface subsidence for longwall mining operations," *Proceedings of the 19th International Conference on Ground Control in Mining*, pp. 163–170.

Luo, Y. and S.S. Peng, 2010, "Subsurface subsidence prediction model and its potential applications in the study of longwall subsidence effects on hydrologic system," *SME Transactions*, Vol. *326,* pp. 458-465.

Luo, Y. and B. Qiu, 2012, "Enhanced subsurface subsidence prediction model considering overburden stratifications," Paper submitted to SME Publication (under review).

Mark, C., F.E., Chase and D.M. Pappas, 2007. "Multiple-seam mining in the United States: design based on case histories," *Proceedings: New Technology for Ground Control in Multiple Seam Mining*. Ed. C. Mark and R.J. Tuchman, National Institute for Occupational Safety and Health, (NIOSH) 2007-110, pp. 15–28.

Morsy, K., A. Yassien and S. S. Peng, 2006, "Multiple Seam Mining Interactions – A case Study," *Proceedings of the 19th International Conference on Ground Control in Mining*, pp. 308–314.

Qiu, B. and Y. Luo, 2011, "Subsurface subsidence prediction model and its potential applications for longwall mining operations," *Journal of Xi'an University of Science and Technology*, Vol. *11*(6), pp. 823–829.

The Next Generation of Cable Bolts for Improved Ground Support

Stephen C. Tadolini, Chief Technology Officer
Minova USA
Bowerston, OH

Jason Tinsley, Mid-West Engineering and Sales Manager
Minova USA
Marion, IL

John P. McDonnell, Western Engineering and Sales Manager
Minova USA
Grand Junction, CO

ABSTRACT

PC-Strand tendons, commonly referred to as cable bolts, have become a major rock reinforcement device for underground mining and civil applications. The most common configuration is a 1+6 strand, which designates a center king-wire, with six outer wires wound around it to form a 0.6-in (15-mm) diameter cable. The capacity of this tendon approaches 30 tons, but the performance is largely dependent on the anchorage medium and the ability of the system to transfer stresses back into the rock mass while reinforcing and suspending the immediate roof. Recent developments to improve the transfer mechanisms of the PC-strand via the anchorage medium by impregnating the individual wires with uniquely designed deformations have resulted in improved anchorage and subsequent cable bolt performance. This paper describes a series of laboratory tests used to develop the initial indentation patterns and numerical modeling simulations that were undertaken to refine and optimize the final designs. The new, indented PC-Strands, offered in both bright and properly galvanized, have been tested in the field and are being used effectively in two new cable bolt products. The results of the laboratory, computer modeling, field testing and in-situ installations provide a glance at the next generation of cable bolts. This suite of testing shows how they will improve the safety and serviceability of openings under adverse ground conditions.

INTRODUCTION

Maintaining safe underground openings has always been a challenge in underground mining. Intrinsic systems, which are installed into boreholes drilled with conventional mining equipment, started with wedge systems and slowly evolved into the mechanical anchor (shell) systems that are still used in some applications today. In the 1970s, resin systems were introduced that used a threaded or headed rebar bolt that could be forced into a borehole, thereby breaking a cartridge containing polyester resins that mixed and cured to form mechanical interlocks along the borehole walls. These two systems have been mixed, matched, and combined to create today's resin-assisted and combination bolting systems.

The primary bolting system used in underground mines remains the headed rebar system, which accounts for over 65% of the nearly 100 million bolts installed in the United States annually. However, those bolting systems, and the systems described above, are often supplemented with high-capacity PC-Strand or cable bolt systems.

Cable bolting systems date back to the early 1940s, when old wire-rope systems were degreased and anchored in boreholes post-grouted with cements. Resin-grouted systems were introduced into the U.S. MSHA Roof Control Plans in 1992 when Rocky Mountain Bolt Company developed and patented a technique for integrating the barrel and wedge system into a mixing device that allowed the cable to be inserted into a resin column, mixed, and anchored with a head capable of developing the capacity of the system (Tadolini and Koch, 1994). Cable bolts have become standard support practice using both cement and polyester resin systems. The cable bolt system, in the U.S., primarily used consists of seven-wire, high-strength steel cables that are 30- to 40-ton nominal capacities and measure 0.6 and 0.7 inches (15 and 18 mm) in diameter. The cables' characteristics provide a large amount of deformation and resistance to shear at a high degree of loading and ultimate tensile strength. During the initial development of cable support systems, it was quickly realized that if cables were installed in either cement or resin systems and loaded axially from the end, the tendon has the tendency to dilate and "unscrew" from the anchorage medium. Additionally, when the cable started screwing or pulling out of the borehole without resistance, the high-strength tensile capacity of the system was not recognized or used. Several designs were evaluated and tested in both laboratory and field conditions. As shown in Figure 1, these designs ranged from epoxy coating impregnated with small sand particles to actually unwinding the strand to create voids for the anchorage materials to flow and form mechanical bonds with the individual wires. Large steel buttons were swaged onto the strands at specific locations that also facilitated resin mixing during insertion. Garford Bulbs (shown in Figure 2) are the most common anchorage element due to easy fabrication and proven performance (Martin, Girard, and Curtin, 1996). As shown, the king-wire (center or middle wire) is actually deformed so the anchorage material can form around all seven strands.

For a cable support system to be effective, the loads have to be successfully transferred from the rock to the cable through the grouting materials. These axial forces can be applied via the bearing plate (i.e., for non-post-grouted cables) or as a result

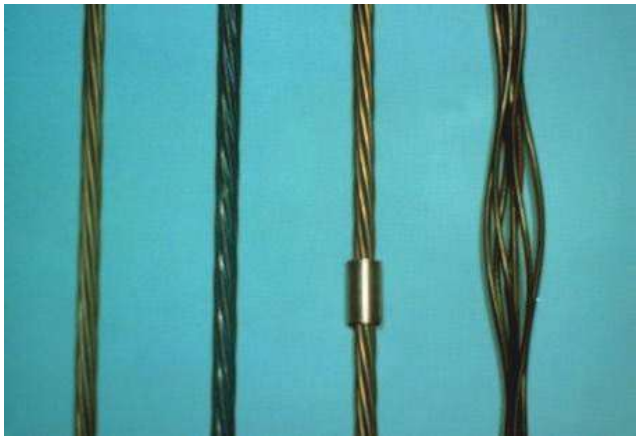

Figure 1. Various types of cable anchorage systems: Left to Right, smooth PC-strand, epoxy coated, steel button, and birdcage.

Figure 2. Garford bulbed 7-wire, .6-in (15-mm) PC-Strand.

of horizontal movement of the rock mass at shear planes and bed separations. The anchorage, applied at the top of the hole, was enhanced by applying buttons, opening the strand—called birdcages—or using Garford Bulbs. Figure 3 shows a series of Garford Bulbs uniformly applied to 16-ft (5-m) cables.

New technology in strand design has resulted in an innovative process to anchor the PC-strand bolts and effectively transfer the loads back into the rock mass. The strand has indentations or deformations along the entire length that form interfaces where mechanical interlock is enhanced at the bolt-resin interface. The physical design and placement of these deformations were the result of a large laboratory investigation that provided the physical data required to calibrate sophisticated numerical models to refine and enhance the indentation designs. The result is a high-strength PC-strand cable bolt that has been field-tested and is now being used in several underground mining applications.

PC-STRAND DESIGN AND TESTING

PC-Strands are traditionally seven-wire configurations, where the king-wire or center wire is wrapped or covered with the

Figure 3. Garford bulbs applied to 16 ft (5 m). The cable bolts will be anchored with polyester resin.

remaining six outer wires. While it can vary by design, the king-wire can be slightly larger in diameter to ensure the outside wires contact each other. A preliminary process was developed to indent the individual wires before they were wound in the final stranding process. The deformations, along the entire length of the cable, provide irregularities in the strand to form mechanical interlock features which can improve anchorage and enhance stress transfer from the cable bolt to the rock mass. A sample of the indented PC-Strand under magnification is shown in Figure 4. The indented cables must still pass the rigorous testing requirements established in the ASTM 432-10 Standard Specification for Roof and Rock Bolts and Accessories.

Figure 4. Individual indented wires under magnification. Note the vertical ridges where resin or cementateous material can form locking (anchorage) mechanisms.

Laboratory Testing Protocol

Three different indentation designs were manufactured for testing. The indented samples depths were documented using

Figure 5. The indented PC-strand samples H, S, L and R-regular smooth strand.

microscope measurement systems and designated H, S, and L. Figure 5 shows the three indented PC-Strand samples and R, a regular, smooth strand.

The strand samples were cut into 4-ft (1.25-m) lengths and anchored in 6-in (15.2-cm) long steel pipes with an internal hole diameter of 1 in (25.4 mm). The anchor material used was a Minova Anchor tite, Mix-and-Pour resin so the quality of mixing would not be a variable (Hyett, Bawden, and Reichert, 1992). The individual cables were rotated and centered into the pipe and allowed to cure seven days prior to testing. Figure 6 shows the samples positioned for curing in the laboratory after the pour was completed.

Figure 6. The samples, designated with colored tape, were allowed to cure seven days.

The samples were tested in a high-capacity tensile testing machine and the data was captured using a high-speed data acquisition system. The cable was gripped at the top of the sample and force was applied to the pipe, allowing the cable to be loaded and "pulled" from the resin. The steel pipe length was selected by design to help ensure that the resin would shear at the resin/cable interface (Mosse-Robinson and Sharrock, 2010). The lower platen and the testing hardware are shown in Figure 7. The deformations and loads were plotted and analyzed to determine the anchorage capacity and anchorage system stiffness.

Figure 7. Steel platens were fabricated to ensure the pipe edge was loaded during tensile testing.

Testing Results

The anchorage testing results are shown in Figure 8. The regular or "smooth" PC-Strand averaged 19,795 lbs (88 KN) before being pulled out of the steel pipe. The "L," "S," and "H" averaged 23,700 lbs (105 KN), 34,440 lbs (153 KN), and 37,500 lbs (167 KN), respectively. The "H" samples indicated an 89% increase in anchorage capacity compared to the smooth, conventional PC-Strand cable.

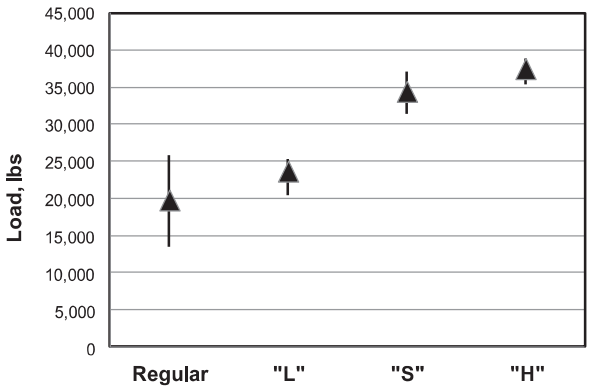

Figure 8. Anchorage capacity test results. The minimum and maximum bands describe the range for the value (n=5).

While anchorage is an important indication of load capacity, a significant parameter is the stiffness of the cable-resin system. In this case, the stiffness is characterized by the amount of force (lbs) required to move the cable a known distance (in inches) from the pipe. The stiffness is presented in lb/inch and the results

are shown in Figure 9. The regular strand resulted in an average stiffness of 66,500 lbs/in (11,638 KN m), while sample "H," which had an average stiffness of 168,500 lbs/in (29,506 KN/m), increased the stiffness 2.5 times. This parameter relates directly to the performance that can be expected in underground mines and tunnels in transferring the applied loads from the cable bearing plates back into the rock mass.

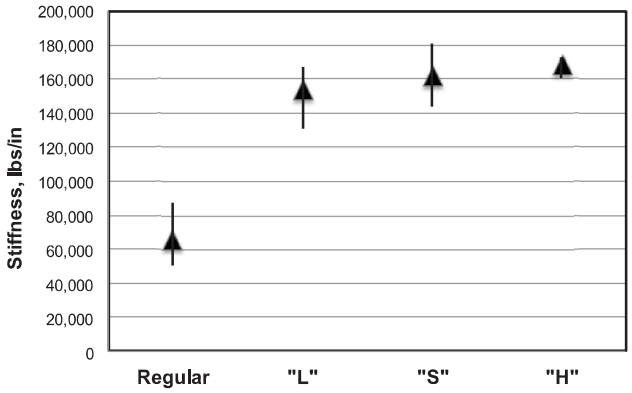

Figure 9. Stiffness test results. The minimum and maximum bands describe the range for the value (n=5).

The anchorage capacity and stiffness values presented represent the fabricated PC-Strand, similar to those currently used for ground support. To provide input and calibration input values for numerical simulation, experiments on single strands of the outside wires were also conducted. The individual strands were simply isolated and prepared in the steel tubes using the same laboratory protocol. The individual wires were tested, and anchorage capacity and stiffness were determined.

The single strand anchorage results are presented graphically in Figure 10. The average for the five samples tested with each indentation pattern and smooth wire were very consistent. The smooth strand slipped at 2,250 lbs (10 KN), and the indented strands, L, S, and H, slipped at 8,550, 8,550, and 8,325 lbs (38, 38, and 37 KN), respectively. This represents increased pull-out anchorage of 3.8 times that of a smooth wire over a relatively short encapsulation length of 6 in (15 cm).

The data was evaluated to determine the single strand stiffness, shown in Figure 11, and increased from a smooth wire average value (n=5) of 13,040 lbs/in (2,283 KN) to 15,290, 15,680 and 15,170 lbs/in (2,677, 2,746 and 2,656 KN/m), respectively (an increase of approximately 17%). Positive combinations of enhanced anchorage and stiffness, coupled with the specific indentation measurements, were used in the finite element modeling and calibration cycles.

FINITE ELEMENT MODELING

The objective of the finite element modeling was to analyze the effect of single indentations obtained from the laboratory testing program and then alternate the indentation depth, spacing, and profile.

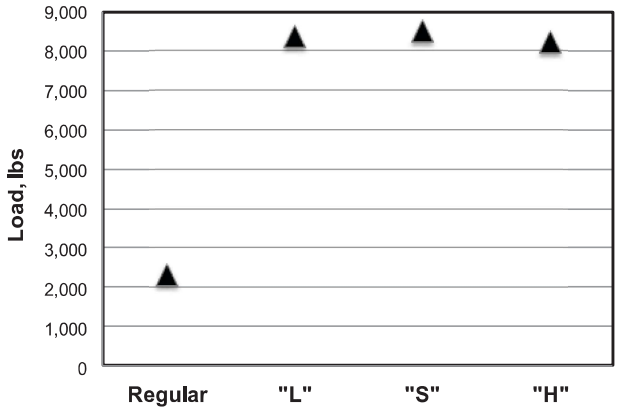

Figure 10. Single wire anchorage capacity results for Regular, L, S, and H indented PC-Strand (n=5).

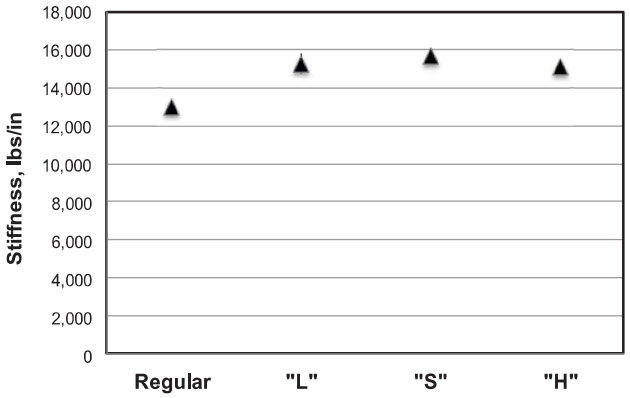

Figure 11. Single wire stiffness values for Regular, L, S, and H indented PC-Strand (n=5).

Model Parameters and Results

The model was constructed with a an outside steel wire with a diameter of 0.21 in (5.3 mm) that contained three longitudinal rows of indents. The initial indentation shape was identical to those analyzed in the laboratory testing program, which started with available indentation cartridges. The indentations in the simulation were perpendicular to the strand lay or 90 degrees.

The mechanical properties of the resin were as follows: 6,181 psi (42.6 MPa) compressive strength, Young's modulus of 254,682 psi (1,756 MPa), and a tensile strength of 1,249 psi (8.6 MPa).

The model "build-up" consisted of a mesh for a single wire with four indentations and developing the mirror image in the resin shell (Figure 12).

As the wire is pulled from the right side of the model (shown in Figure 13), you can observe the red elements with high strain and the elements that eventually collapse.

The initial model results aligned well with the laboratory results so the next phase of the analysis was to increase the depth of the

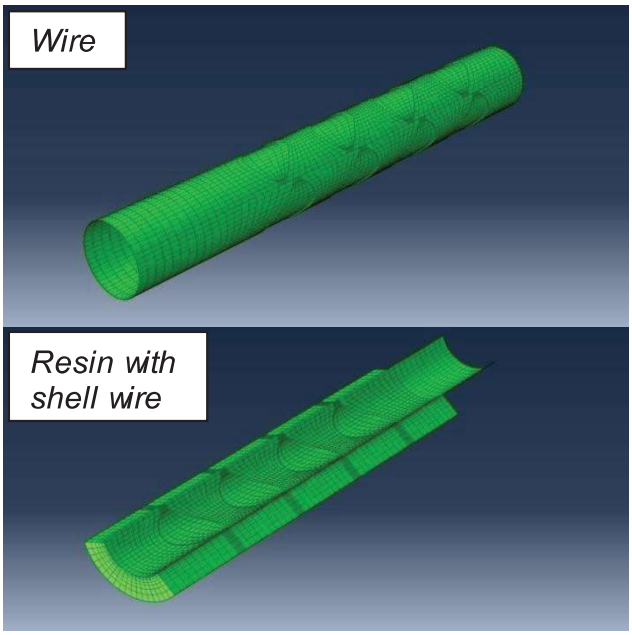

Figure 12. Model build-up of single wire (top) and the mirror image in the resin with wire (bottom).

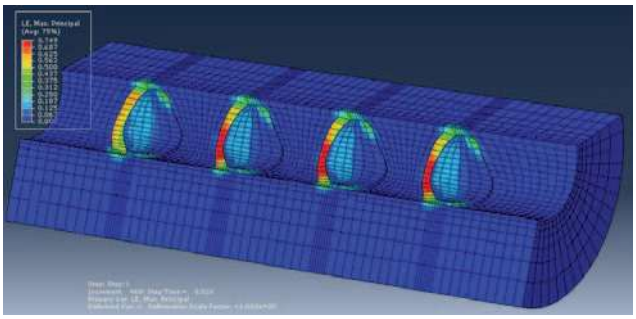

Figure 13. Single wire loaded from the right, illustrating high strain areas in the resin (red) and collapsing elements.

indentations from 80µ to 180µ in 20µ increments. The results of the maximum principal strains, shown in Figure 14, indicated that there was only a slight increase in pull-out force as the depth of the indentations were increased.

The numerical modeling results, calibrated with the laboratory experiments, provided valuable insight into the effectiveness of the depth of the indentations. Once mechanical interlock has been created at the steel wire and resin interface, it is simply a matter of the shear strength of the resin that will control anchorage and deformation. Additional modeling is being conducted on variations of the inclination of the wall to increase compression forces at the interface. The hypothesis is that reduced surface angles should optimize loads and minimize deformations.

FIELD EVALUATION

Evaluations were conducted at several mines to examine the anchorage capacity and stiffness results under field conditions

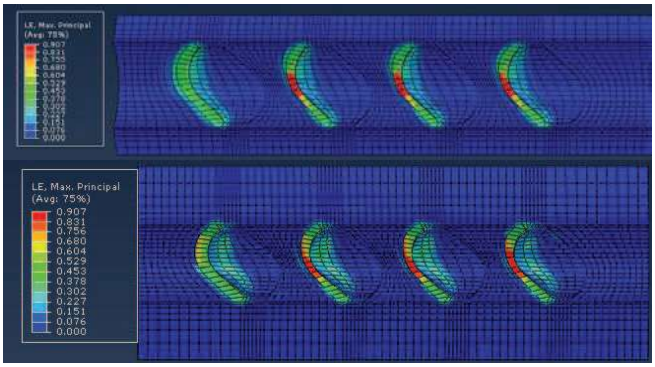

Figure 14. The maximum principal strains for 80µ (top) and 180µ (bottom).

to complete the evaluation of the indented PC-Strand. Anchorage capacity tests, also called pull tests, were completed in several underground coal mines. In the presented example, the immediate mine roof consisted of a typical competent inter bedded shale roof. For the comparison tests, standard cable bolts were configured to have three 0.9 in (23 mm) diameter bulbs located at 6, 18, and 30 in (15, 45, and 76 cm) from the end of the cable. The 10-ft (3.2-m) cables were encapsulated in 4 ft (1.25 m) of resin and pull-tested using a hydraulic ram approximately 60 minutes after installation. The normalized results, shown in Figure 15, indicate that the indented PC-Strand performed better than the standard cables with respect to anchorage. To help illustrate this performance, the deflection data at 10 tons of applied load were averaged for the four indented and standard samples. The average deflection for the indented samples was 0.209 in (5.31 mm) and the average for the standard cables was 0.287 in (7.29 mm). This illustrates that the anchorage along the entire length of the resin grouted cable bolt for the indented PC-Strand exceeded the anchorage for a smooth PC-Strand with three Garford Bulbs applied as a resin anchorage system.

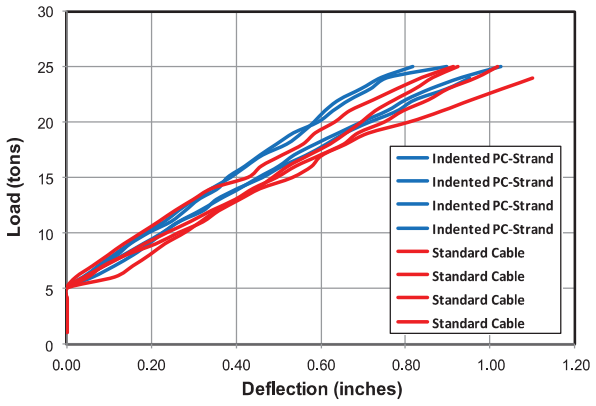

Figure 15. Anchorage capacity testing results of standard versus indented PC-Strand.

HOW CAN INDENTED PC-STRAND BE APPLIED?

The indented PC-Strand has already been combined with new cable support products, taking advantage of the superior anchorage

and subsequent performance. The basic application has been the Low Profile Square Head (LPSQ) offered in a bright (black) or properly galvanized strand. The entire "Low Profile" series, introduced by Minova, was designed to conform tightly into an embossed bearing plate. The latest incremental improvement was designing the integrated steel cast head, used to spin the bolt and will mix the resin and develop the installed cable capacity. The 1-1/8" (29 mm) square head, will fit drilling pods and typical wrench designs. While a couple of inches of additional head height may not sound significant, it makes a huge difference when extracting low seams. Figure 16 shows a LPSQ cable bolt installed in a coal mine roof. These cable bolts are designed to work in metal and non-metal mines, as well. The indented PC-Strand lowers the back pressure created during insertion, which facilitates longer resin columns if a stiffer support system is desired by the ground control engineer.

Figure 16. Low Profile Square Head (LPSQ) installed with an embossed bearing plate in a coal mine roof.

The newest application for the indented PC-Strand is the Tensionable Cable Bolt (TCB), which was designed to provide rapid and superior anchorage of the resin column. The TCB system, which is used as both primary and secondary support, develops cable tension from the bearing plate to the bottom of the resin column, placing the roof in compression for beam building and suspension. The resin column will not slip or "bleed-off" at the low shear strength values of the immediate roof materials. The patented slotted tube system allows for the cable to be pulled straight down, without twisting or wrapping the PC-Strand, which can cause spring-back and damage the wires (Figure 17). Figure 18 shows the TCB product installed between rows of primary support in a critical entry adjacent to a pillar mining (extraction) section. The TCBs have been used in longwall panel set-up rooms as well as recovery chutes and entries. The bolts install quickly during primary bolt support scenarios and can be a critical component of a single support pass mining cycle.

SUMMARY AND CONCLUSIONS

PC-Strand supports, called cable bolts, continue to be used for ground control in mining and civil applications. Laboratory experiments and finite element modeling confirmed that the indentation patterns on the high strength PC-Strand can increase the anchorage capacity and stiffness of the support. Field evaluations of manufactured cable bolts used for supporting mining roofs showed that the indentations along the entire anchorage length of 4 ft (1.25 m) developed more anchorage than three traditional Garford Bulbs in a 1-in (25-mm) diameter hole. The bolting systems were also stiffer, which can be a support advantage

Figure 17. Tensionable Cable Bolts (TCB) during production. The cables are color coded for length in accordance with the ASTM 432-10.

in minimizing downward movements of the strand within the anchorage zone. Refinements in the engineered design of the indentations are already underway and optimization of the patterns will continue to improve the cable bolting system performance. The Low Profile Square Head (LPSQ) and Tensionable Cable Bolt (TCB) are just two of the new Minova products that are improving cable support system performance and reliability. The indented PC-Strand is available in bright or properly galvanized and when coupled with these and several new support designs and concepts, will be the next generation of Minova's cable bolt products.

Figure 18. Tensionable Cable Bolts (TCB) supporting heavily loaded ground during pillaring mining cycle.

ACKNOWLEDGEMENTS

The authors would like to acknowledge the laboratory support of Jeremy Sell and Travis Wilson, Minova International, USA, and Stijn Defossez, NV Bekaert SA, Belgium for assisting with the numerical model simulations.

REFERENCES

Tadolini, S.C., Koch, R.L. (1994). "Resin-grouted cables for longwall tailgate support systems." In: *Proceedings of the*

13th International Conference on Ground Control in Mining. pp. 175–184.

Martin, L., Girard, J.M., Curtin, D. (1996). "Laboratory pull tests of resin-grouted cable bolts." In: *Proceedings of the 15th International Conference on Ground Control in Mining*. pp. 455–468.

Hyett, A.J., Bawden, W.F., Reichert, R.D. (1992). "The effect of rock mass confinement on the bond strength of fully grouted cable bolts." International Journal of Rock Mechanics and Mining Sciences & Geomechanics Abstracts. *29*(5): 503–524.

Mosse-Robinson, S. Sharrock, G. (2010). "Laboratory experiments to quantify the pull-out strength of single strand cable bolts for large boreholes." In: *Proceedings of the Second Australasian Ground Control in Mining Conference*. Australian Institute of Mining and Metallurgy, pp. 201–209.

Improvements in Long Tendon Support with Pumpable Resin

Tom Meikle, General Manager - Operations
Minova Australia
Wyong, Australia

Stephen C. Tadolini, Chief Technology Officer
Minova International
Bowerston, OH

Robert Hawker, Technology Manager
Daniel Polack, Mining Engineer
Minova Australia
Nowra, Australia

ABSTRACT

Long tendon support systems provide several challenges when used in-cycle as part of the secondary or primary support cycle. A two-component pumpable resin, Carbothix, has been in development for use with self-drilling rock bolts, but many of the attributes of this new resin system make it ideal for grouting long tendon support systems.

While neat Portland cement grouts or polyester resin capsules have been used with long tendon support systems for many years, two-component pumpable resin systems overcome many of the shortcomings in these systems. The two-component systems dramatically improve the set-time to enable mining face advance with fewer delays, enable longer pumping distances, improve quality control, and enhance load transfer mechanisms.

This paper describes the key benefits associated with a new pumpable resin and details the Australian Department of Mines and Petroleum department atmospheric testing results and cable load testing completed by Minova personnel to date. It also details the results of the Australian mine site trials and the introduction of these systems into production use.

INTRODUCTION

Resin-grouted cable systems have been in use for many years. Tadolini (1994) detailed the development of these systems with the use of resin capsules for enhanced coal mine roof support, but the length of the tendons described were short (6 m) in comparison to long tendon systems used in Australia (13 m).

Long tendon cable support systems are used in both coal and metal mines. Resin capsules are only used with long tendons (6 m to 8 m in length) for point anchoring to enable pre-tensioning of the cable prior to full encapsulation of the cable with a cement grout. Also, resin capsules can only be used with single strand cable systems, due to mixing and anchorage issues with twin-strand systems. These issues make them unsuitable for the majority of hard rock cable systems, which are twin-strand in configuration. In addition to the mixing and quality of anchorage issues, resin capsule anchoring is often difficult where variation in borehole size is experienced.

Initially, Portland cement cable bolts were “bottom up” grouted, using a Portland cement/water mixture. In more recent years, with advanced grout technology, grouts with low shrinkage and high strength properties have been introduced.

Low slump grouts have also been developed to allow “top down” grouting of cables, particularly those cables that are point anchored and pre-tensioned using resin capsules.

However, current cement grouting systems (grout and equipment) have some disadvantages:

1. Quality of grout has always been an issue; very rarely do operators mix grout to manufacturer’s specification, often relying on the operators visual observations to determine whether the grout was of the correct mixture.
2. Low slump grouts require pumps that can pump a thick grout; choice of suitable pump is limited.
3. Pumping distance is limited with current grout pumps; operators often add more water to allow pumping long distance, which adversely impacts the quality and strength of the material.
4. Grout is mainly supplied in 20 kg bags; therefore, grout waste is excessive when a small number of cables are to be grouted (for example, a row of cables in a continuous miner heading).
5. Grout strength development is relatively slow in comparison to resin systems, thus making tensioning of cable system only possible after hours of cure rather than minutes.

Carbothix Two Component Resin

Carbothix can best be described in the following bullet points:

- Two component grouting resin, Organomineral Pre-polymerized Methylene Diphenylene Diisoycynate (PMDI) based, primarily used for grouting long tendon cables and strata reinforcement bolts, e.g. Wiborex and Glass Reinforced Polymer (GRP) Bolts
- Carbothix is a pre polymer; therefore, it has lower volatility than Toluene Di-Isocynate (TDI) or Hexamethylene Di-Isocynate (HDI) and contains less free isocyanate, thus reducing the vapor hazard
- Used in self-drilling rock bolts (SDRB)

- Delivered via two component pump and hoses
- Mixed in volume ratio from 1(Part A):1(Part B) or 1(Part A):2(Part B) depending on the application needs and strength requirements
- Mixed at grouting site
- Reacts to form thick paste for "top down" grouting within seconds of mixing and sets within minutes to provide early load transfer between steel tendon and strata
- Early set time allows cables to be fully tensioned in less than 60 minutes
- No reaction with borehole water
- Low application pressures (< 60 bar)
- Cured resin is highly resistant to acidic and alkaline environments

Using the Minova pumping system, Carbothix resin has been supplied a distance up to 2.5 km in Germany.

History of Carbothix Use for Long Tendon Grouting

Xstrata Nickel first trialed the use of Carbothix in 2006 at the Craig Mine as part of its Sudbury Basin operations support plan (Pritchard and McClellan, 2011). The resin was initially used for grouting hollow core fibreglass rebar but was soon investigated for use with long tendon support systems. Cable bolts up to 10 m in length have routinely been fully grouted at the operation with great success, achieving full encapsulation by using Carbothix materials.

Other cable applications at the mine have enabled cycle times to be reduced by up to 24 hours compared to Portland cement cable systems. This is because the resin sets within one minute of cable grouting, and tensioning can occurs in less than 10 minutes later. The initial resin used was a fast setting 1:1 formulation to accommodate the cool rock conditions. Some difficulty was experienced with this resin when using longer cables, which required the development and use of a slower setting version.

Surface Trials of Long Tendon Carbothix Grouting

Prior to carrying out underground trials, several surface trials were undertaken to achieve the following:

- Ensure that the pumping system chosen could handle the product and deliver it at a consistent 1:2 ratio
- Ensure that the feed pipe system chosen could cope with system pressure
- Prove that 6 m and 8 m cables of various types could be fully encapsulated

Initial results in laboratory environment, with Carbothix at 24 °C, were very encouraging; the pump delivered material at a consistent 1:2 ratio. Once the grout had set, cables were cut into sections to prove that full encapsulation had occurred. Figure 1 shows fully encapsulated twin-strand cables. Figure 2 shows a cross section of the Carbothix material fully encapsulating a Megadowel strand bolt. The Megadowel bolt is a 9 strand cable with a grout tube located in the center of the outside or sheath wires. The pump, shown in Figure 3, is configured to deliver material at 1:2 ratios but that can be easily modified depending on specific requirements.

Figure 1. Cross sections of fully encapsulated twin-strand cable bolts.

Figure 2. Cross section of a fully grouted Megadowell strand bolt.

LABORATORY TESTING

Prior to the use of Carbothix resin with long tendon supports, various tests were completed to compare the Carbothix's strength against both polyester capsule resin and also Portland cement cable grouts.

Initial Punched Shear testing, indicated the Carbothix resin was able to achieve one hour Punched Shear strengths of 26 MPa. This was compared to fast Lokset polyester resin, which achieved 24 MPa and Carbothix, which achieved 30 MPa at 24 hours. It is also comparable with other Lokset Resins as shown in Figure 4. The

Figure 3. Pumping system for Part A and Part B components.

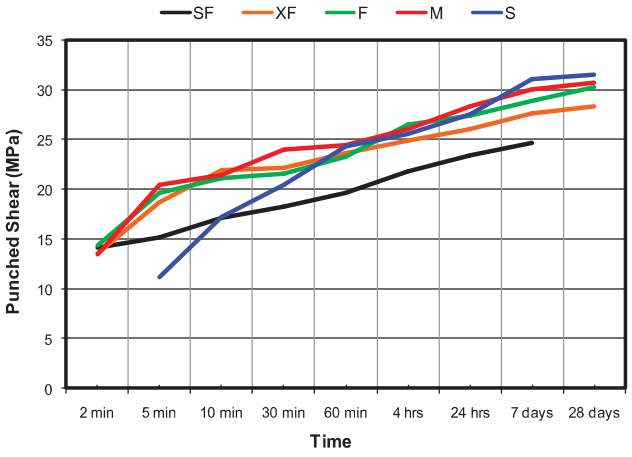

Figure 4. Punched Shear tests at various times for five different speeds of Carbothix materials. (SF = Superfast, XS = Extra Fast, F = Fast, M = Medium, S = Slow).

Uniaxial compressive strength data for Carbothix was 70 MPa after 24 hours, which is comparable to Portland cement cable grouts.

To provide further confidence of the load transfer ability of Carbothix, further testing was done using various cable designs and related borehole diameters. The laboratory testing method is shown in Figure 5. The cables were installed centrally then grouted in a steel pipe with 170 mm of anchorage medium and then "pulled" with a hydraulic jacking system. For a twin-strand bulbed cable, the Carbothix material reached anchorage strength of 7 kN in one hour. This compares with the identical style cable installed with General Portland (GP) cement that did not reach the 7 kN strength after 24 hours. This faster cure time makes it possible to post-tension the cables, which dramatically improves mining cycle times.

Figure 5. Laboartory setup with hydraulic ram and pump.

INTRODUCTION OF CARBOTHIX TO AUSTRALIAN HARD ROCK MINES

Initial trials at Cosmos Mine, owned by Xstrata, where underground air and product temperatures were around 40 °C, were less than promising. Carbothix 1:2, at 24 °C, has a set time of 90 seconds; at 40 °C this time is greatly reduced to 25 seconds. Furthermore, the cables were installed in 62 mm holes. This would require approximately 16 L of product, but the pump output was set at 10 L/minute.

Due to the temperature of the product, excessive pump pressures were seen—up to 200 bar. Typically, this indicated that the Carbothix was setting faster than anticipated and that the pump was attempting to push solidified Carbothix down the annulus of the borehole. Due to these conditions and some safety concerns, the trial was terminated prematurely.

Developing a Slow Set Carbothix

Following the less than successful first trial at Cosmos Mine, Minova and Xstrata Nickel drew up a set of actions before commencing the next trial. Minova would formulate a slow set resin; Xstrata Nickel would review their current cable bolt drilling process and make the necessary operational changes in order to drill a 52–55 mm hole. With this in mind, Minova had to develop a resin that (1) would work within a wider range of temperatures and (2) had the same or similar mechanical characteristics as the current formulation.

Minova Australia's technical department commenced developing a slow set resin in March 2011, and finalized the formulation in May 2011. Laboratory testing showed that Carbothix Slow Set would provide slower gel time in a higher temperature environment

but still enable sufficient strength development for tensioning the cable whether the resin temperature was 20 °C or 40 °C. Note the gel time is the time required for Carbothix to become thick, and this occurs very quickly. The set time is the when the final hardening reaction starts to generate heat and hardening is initiated. This is different than conventional resin capsule terminology where the gel time occurs after mixing and the set-time is when the material has completed "curing". Figure 6 shows the gel strength and set time comparisons for Carbothix at selected temperatures. The slower setting material took 10 seconds longer to set at 40 °C and 25 seconds longer to set at 20 °C. The slower setting materials were also able to sustain adequate shear strength properties, as shown in Figure 7. Finally, short Mega Strand (Megabolt) anchorage testing was completed in the laboratory to ensure that adequate anchorage capacity could be achieved throughout a range of times. The MegaStrand is a 60 Tonne capacity cable which has the ability to be post grouted after tensioning. Figure 8 shows the results of bulbed and non-bulbed systems as a comparison to standard polyester resin and FB400 which is a standard cement grout for cable bolting.

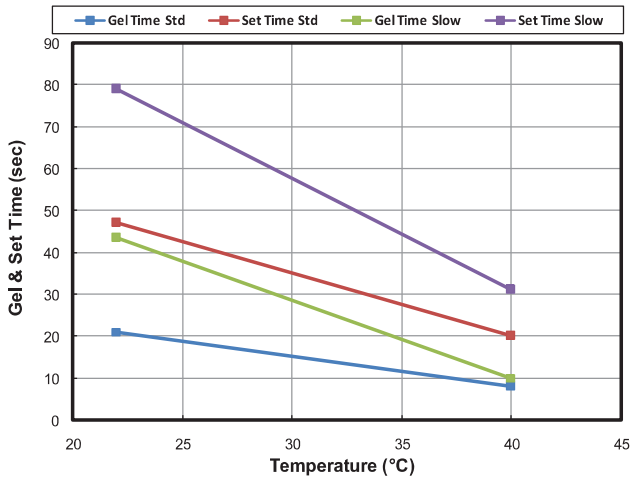

Figure 6. Gel and set times for materials at various temperatures.

Further Trials at Cosmos Mine

Two further trials were carried out at Cosmos Mine using the new slow set formulation. In these trials, four different cable types were grouted in different ground conditions. The four types included single strand smooth cables, single strand bulbed cables, single strand de-bond cables, and twin-strand cables. The mine temperature varied between 31.8 °C and 36.1 °C due to various locations and ventilation conditions in the mine. All of the cables were tensioned in excess of 20 tonnes in less than 60 minutes. Subsequently, Xstrata Nickel Cosmos Mine has entered into a commercial arrangement with Minova Australia to supply Carbothix and accessories for long tendon grouting.

Four additional hard rock mines have commenced using Carbothix for cable grouting, and all of the mines are seeing substantial reductions in cycle times and outstanding support performance. Figure 9 shows a double strand cable installed and waiting for tensioning and plating.

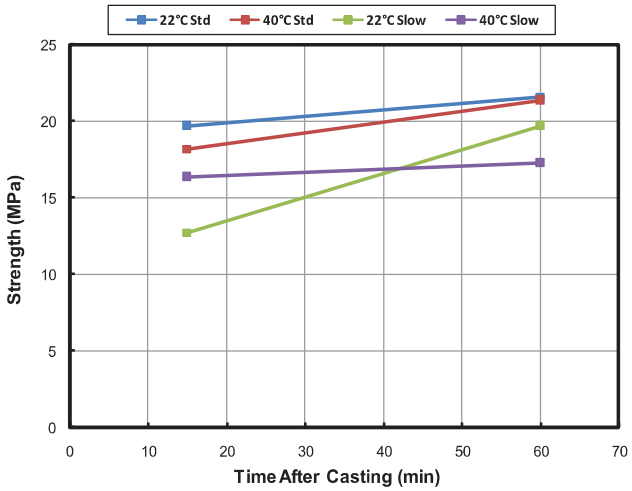

Figure 7. Carbothix material strenghts at varing times and temperatures.

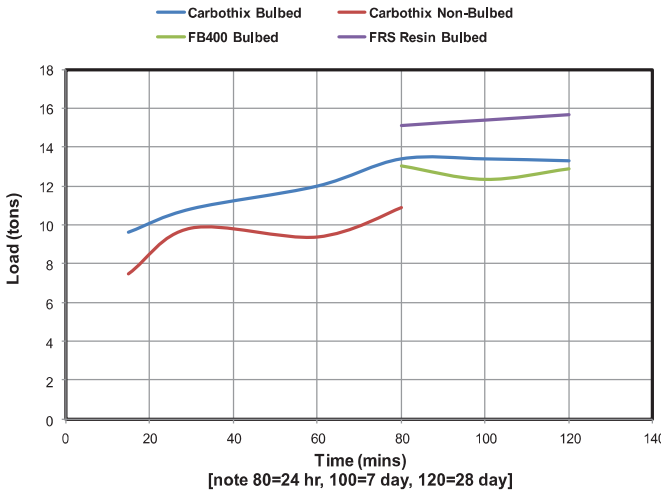

Figure 8. Short MegaStrand anchorage strengths for bulbed and non-bulbed cables anchored in Carbothix and traditional cements.

INTRODUCTION OF CARBOTHIX TO AUSTRALIAN COAL MINES

In Australia, the use of polymer materials that react in situ in underground coal mines is regulated under the Coal Mines Health and Safety Regulations 2006. These products are controlled using a license system, and the only systems exempt from these controls are traditional resin capsules.

Prior to the processing of the license application, the product must pass certain characterization tests, which include flash point, fire resistance, flame propagation, reaction temperature, oxygen indexing, and electrical resistance. Carbothix is the only pumpable resin approved currently for use with cable and bolt systems.

Figure 9. Twin-strand cable bolt installed and pumped with Carbothix anchorage material.

Minova Australia commenced the application process to the New South Wales (NSW) Department of Industry and Investment (DII) for Carbothix to be used in self-drilling rock bolts in 2010, and a limited "trial" license was granted that same year. The trial was limited to Tahmoor Mine, part of Xstrata Coal NSW Group. During these trials, air sampling was carried out by Coal Services Health to determine if Isocyanate was produced by the pumping process. Results showed that Isocyanate was not detected at any stage during the trial.

Following these trials, Minova Australia applied for an extended license to include the grouting of long tendon supports at any mine in NSW. This trial license was granted in November 2010

Underground Trials

The first underground trial was carried out at the Centennial Coal Mandalong Mine. Ten 8-m-long cable trusses were installed to provide additional support in the LW12 tailgate, #3 cut through area. All 20 cables were grouted with Carbothix Standard Set Formulation due to the low underground temperature (18 degree Celsius), and cables were trussed and tensioned after 30 minutes. Air analysis monitoring was carried out by Coal Services Health, and no MDI was detected.

Further underground trials were carried out at Centennial Coal Angus Place Mine, where several 8 m Megadowels were grouted successfully using standard set resin. Again, air analysis was carried out by Coal Services Health, and zero MDI was detected.

Minova Australia has now applied to the NSW DII for a full license and are confident that restrictions will be lifted or at least reduced to allow full implementation of the system in coal mines in NSW.

CONCLUSIONS

There are several significant advantages of using Carbothix 1:2 resin for grouting long tendon cables with pumpable resin:

- Fast set allows early tensioning of cable bolts
- Post-groutable cables can be grouted immediately after tensioning
- Ability to grout single cables, particularly in boggy or high shear ground
- High early load transfer
- Rapid resin set time; allows "in cycle" bolting, and
- System can be adapted to be used with most post-grouted cables

New developments of Carbothix grouting systems offer the advantage of safety, speed and reliability in a range of temperature conditions. The strengths are comparable to traditional cement-based anchorage systems while reducing mining cycle times. The recent acceptance of the material for coal mine applications is bringing forward several unique solutions for difficult ground conditions.

Use of Carbothix in the grouting of long high-capacity cables and truss systems have become routine at a number of operations leading to increase in development rates. Additionally, Carbothix is being used in the self-drilling rock bolts (SDRB) currently being tested in a full-scale program. The ultimate goal is to make the ground conditions safer for workers while improving operational efficiencies.

ACKNOWLEDGEMENTS

The authors would like to acknowledge the effort of the Minova Australia support teams in the development of this innovative solution. Special thanks are extended to Michael Rockhoff, Minova, for assisting with initial underground trials in Western Australia and Rob Hawker's team for developing the new slow set, low viscosity Carbothix 1:2 resin for these applications. We would also like to recognize the mine site personnel at Xstrata Nickel Cosmos Mine, Centennial Coal Mandalong and Angus Place Mines for providing underground trial sites and operational support.

REFERENCES

Tadolini, S. (1994). "Resin grouted cables for enhanced coal mine roof support." *Technology News*. U.S. Bureau of Mines, United States Department of the Interior. No. 433.

Pritchard, C.J., McClellan, R.S. (2011). "Injectable resin—a highly adaptable ground support anchoring system." CIM Conference and Exhibition.

The Development and Application of Polyurethane Injectable Cable Bolts

Dakota D. Faulkner, Research & Development Engineer
Keystone Mining Services, LLC
Jennmar Corporation, Inc.
Pittsburgh, PA

ABSTRACT

Cable bolts have been very effective in mine ground control. Non-tensioned and tensioned cable bolts are now used for both primary and supplemental bolting (Suder, 2001; Mirabile, 2010). In the United States, cable bolts are typically installed in either 1 or 1-3/8 in. (25 or 35 mm) diameter drill holes and, if point anchored only, are utilized with 4 - 5 equivalent feet (1.2 - 1.5 m) of resin. Cable bolts can be tensioned by various methods such as using an expansion shell mounted on the cable or post-tensioned with a hydraulic cable tensioning unit. In recent years there has been a desire to completely encapsulate the cable bolt for corrosion protection. Fully encapsulating a cable bolt with traditional resins can be very difficult. Keystone Mining Services, LLC (KMS) and Jennmar Corporation have developed a new cable bolt that can be fully encapsulated during installation or post-installation with polyurethane (PUR). The Fully-Grouted Cable Bolt (FGCB)* is equipped with a special head that allows the injection of PUR up through the cable bolt head and cable strands, completely encapsulating the cable and filling the drill hole. Although the FGCB was initially developed to fully encapsulate the cable for corrosion protection, it was also found that by modifying the cable bolt head and injection pressure, PUR could be injected into cracks and fissures of the strata to stabilize the roof. This paper details the development of this system and three underground applications under different ground conditions.

INTRODUCTION

The Fully-Grouted Cable Bolt (FGCB), as shown in Figure 1, was recently developed by Keystone Mining Services, LLC (KMS) and Jennmar Corporation through key customer input and extensive lab and field testing. The FGCB allows for a standard cable bolt to be fully encapsulated during installation or post-installation with polyurethane (PUR). Cable bolts have been very effective in mine ground control; however, one limitation has been their inability to be fully encapsulated with traditional resins. A fully encapsulated cable bolt is better protected than a traditional bolt from corrosive elements that may be in a mine roof which could affect the cable bolt's structural properties, especially if the cable bolt is subjected to these elements for long periods of time. Although initially developed for corrosion protection, early field trials demonstrated that the FGCB can act as a traditional PUR injectable bolt. The FGCB is proving to be a very versatile roof support due to its ability to control many different ground conditions, from increasing the lifespan of standard cable bolt supports in long-term main entry systems to stopping the ingress of water and allowing access to previously unattainable reserves. The FGCB is becoming a very effective and economical option.

*The Fully-Grouted Cable Bolt (FGCB) is the subject of a pending U.S. Patent and is the proprietary property of FCL Holdings Delaware, Inc.

Figure 1. Jennmar FGCB with new packer.

DEVELOPMENT OF THE FGCB

The development of the FGCB initially began when mine operators expressed concern over the effects of corrosion on ground control supports. Since it is costly to install new slopes and portals, mine operators have to maintain their underground travel ways for longer periods of time. An area of key concern has been the effect of corrosion on the longevity of roof supports, particularly cable bolt roof supports. Typically, a headed rebar or torque tension bolt is fully encapsulated with traditional resins, which provide a barrier between the corrosive elements and steel support. Cable bolts on the other hand, can be difficult to fully encapsulate with traditional resins due to the longer bolt lengths, and the low stiffness characteristics of the cable. In addition, cable bolts can be more susceptible to corrosion due to the increased surface area of the multi strand cable when compared to a standard head rebar bolt. They are commonly limited to 4 - 5 equivalent feet (1.2 - 1.5 m) of resin encapsulation, which can leave an unprotected section of cable. To address this, the FGCB was developed to provide the added reassurance to the mine operator that their cable bolt roof supports are adequately protected for long-term applications.

The FGCB was initially designed based on Jennmar's Non-Tensioned Cable Bolt (NT). However, it incorporates a few modifications that allow the bolt to be injected. The key component is the special cable bolt head. The head is similar to the standard

1-1/8 in. (28.5 mm) square head on a normal cable bolt, but it is modified to accept a special fitting to inject the PUR (Figure 2). Later versions have allowed this design to be applied to Jennmar's INSTáL® cable bolt systems (Stankus, 2000), which allow for a tensioned, fully grouted cable bolt.

Figure 2. Specially designed FGCB head.

The bolt is installed in the normal manner as a basic cable bolt with resin cartridge. However, at any time after installation, the injection is conducted with a portable pump. During injection, the PUR flows through the housing and wedge assembly and directly into the stiffener tube, completely filling the drill hole and encapsulating the exposed cable. Additionally, a new component, the packer, is located 4 - 8 in. (10 - 20 cm) from the bottom of the drill hole, and it creates a seal between the drill hole and stiffener tube (Figure 1). This newly designed packer allows the PUR to rapidly fill and pressurize the drill hole from the packer up to the cable resin along with any fractures or voids. With this addition, the FGCB is able to act as a traditional PUR injectable bolt with the added strength of a cable bolt.

Polyurethane

A wide variety of PURs with vastly different material properties can be injected into the FGCBs. Jennchem® (Jennmar affiliate) provides MARITHAN® E, a non-foaming polyurethane with high compressive and bonding strengths (Table 1), is commonly used with the FGCB. Jennchem's MARITHAN® N, which still incorporates high strength properties but has an expansion ratio of 2:1 when properly injected, is another option. The type of PUR used is dependent on the application and user preference.

Laboratory Testing

Ultimate tensile strength tests were performed on several FGCB samples that were injected with MARITHAN® E to validate that the PUR would not have any negative effects on the housing and wedge assemblies when subjected to load. Cable samples 36 in. (914 mm) in length were made out of standard grade 270,000 psi (1,862 MPa) cable in 0.6 in. (15 mm) and 0.7 in. (18 mm) diameters with a FGCB housing assembly set on one end and a standard housing assembly set on the opposite end. The 0.6 in. (15 mm) diameter cable has a minimum ultimate tensile capacity of 58,600 lbf (261 kN), and the 0.7 in. (18 mm) diameter cable has a minimum ultimate tensile capacity of 79,400 lbf (353 kN). The samples were placed in a tensile tester and the load was steadily increased until cable strand failure occurred. The load versus deflection results are shown in Figures 3 and 4.

Table 1. MARITHAN® E Material Properties.

COMPONENT DATA RESIN CATALYST	RESIN	CATALYST
Density at 77°F (25°C), (g/cm³)	1.03	1.23
Viscosity at 77°F (25°C), mPa.s	200	210
Mixing ratio (in volume)	1	1
REACTION DATA	**60°F (15°C)**	**77°F (25°C)**
Start of reaction	0:45	0:20
Expansion ratio	1	1
Compressive strength at 10% deformation, psi (MPa)	>2,900 (20)	>2,900 (20)
Adhesion test on concrete Bond strength at 86°F (30°C) after 30 minutes, psi (MPa)	>145 (>1)	>145 psi (>1)

CASE APPLICATIONS

The FGCB's original design was for corrosion protection. However, it has proven very versatile in being able to control many different ground conditions. The following case studies will detail some uses of the FGCB under different ground conditions.

Case Study 1 – Pittsburgh 8

The first case study takes place in the Pittsburgh 8 seam, where the original concept for the FGCB was initiated. Several mine operators in this region were concerned about the effects of corrosion on their cable bolts in long-term mains, belt entries and slopes, as well as the weathering that occurred on the roof surrounding the cable bolt drill holes. Strata in underground mine openings is often subject to gradual weathering over time due to moisture absorption and air contact. Moisture sensitive strata such as weak shale, black shale, clay stone, clayey shale, fireclay, etc., may deteriorate, lose strength and fall unexpectedly.

These mines began installing the FGCB in early 2011, using a typical 4 ft polyester resin column as the anchor. The bolts were injected with PUR either directly after installation or up to several months later (Figure 5). The bolt lengths ranged from 12 - 16 ft (3.65 - 4.87 m), resulting in an 8 - 12 ft (2.43 - 3.65 m) injection zone in the drill hole.

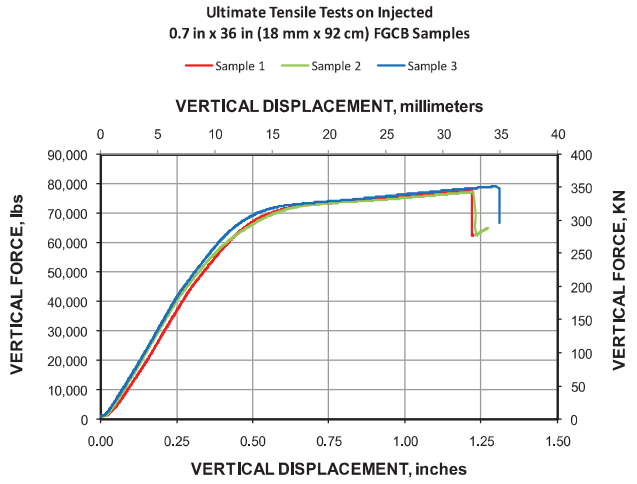

Figure 3. Ultimate tensile tests on injected 0.7 x 36 in. (18 x 914 mm) FGCB samples.

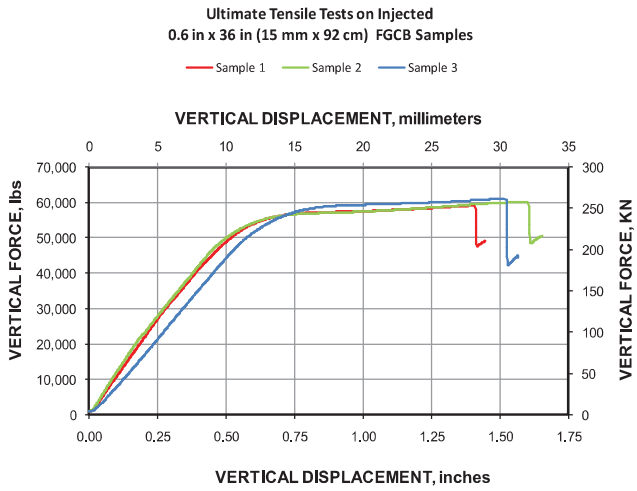

Figure 4. Ultimate tensile tests on injected 0.6 x 36 in. (15 x 914 mm) FGCB samples.

In this case, the FBCBs were not being used to inject the strata. Jennchem personnel developed a special pumping technique to pump only enough PUR to fill the drill hole and protect the cable (Figure 6). This prevented an unnecessary amount of PUR from being injected into the mine roof, a cost saving measure for the mine. In some instances, the FGCBs were installed in areas where the roof began to deteriorate before they were injected. The FGCBs were quickly injected, which consolidated the strata and prevented further roof movement.

Overall, the mine engineers described the FGCB as a way to cost effectively extend the lifespan of their roof supports while improving the safety of their mine well into the future. The added stiffness the PUR provided to the cable was also noted as an added benefit. The stiffness created a rigid roof support system, preventing premature movement of the roof.

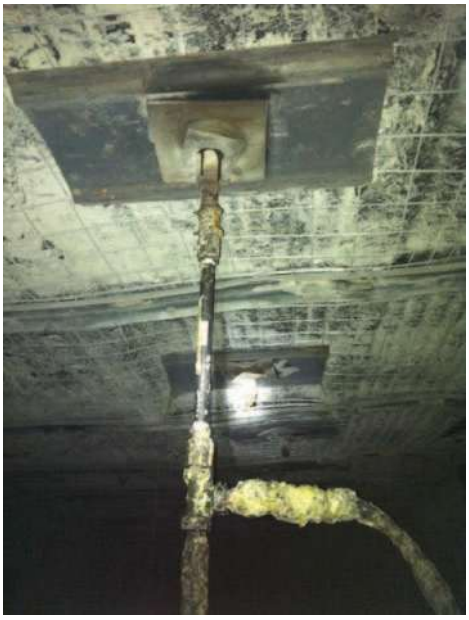

Figure 5. FGCB during injection.

Figure 6. Jennchem personnel injecting the FGCB.

Case Study 2 - Winifiede/Coalburg

This case study takes place in the Winifiede/Coalburg seam. A mine was making a second attempt at crossing under a local stream valley with less than 100 ft (30 m) of overburden. The operator previously mined a short-term panel under this stream using 6 ft (1.8 m) torque-tension bolts and two 0.6 in. x 12 ft (15 mm x 3.65 m) cable bolts as support. Ground conditions

tended to deteriorate after 3 - 6 months due to the action of ground water on the shale roof.

This new stream crossing was designed to be a long-term corridor to access reserves in the northern section of the property. Mine management was very interested in using PUR to control water in the mine roof. The mine uses two super sections with two continuous miners per section. Typically, each section develops 500 ft (152 m) of entry per shift.

Jennmar recommended continued use of 6 ft (1.8 m) fully grouted torque-tension bolts on a 4 ft (1.2 m) spacing for primary support. For supplemental support, Jennmar recommended the FGCBs in conjunction with a 16 ft (4.9 m) T5 channel. The recommended bolting pattern for the FGCBs is shown in Figures 7 and 8. Immediately after the bolting cycle, the cable bolts were injected with PUR, which filled the fractures and fissures and stopped the migration of water. This can been seen in Figures 9 and 10, which show a drill hole before injection and a new drill hole after injection. Figure 11 shows a complete roof channel after installation and injection.

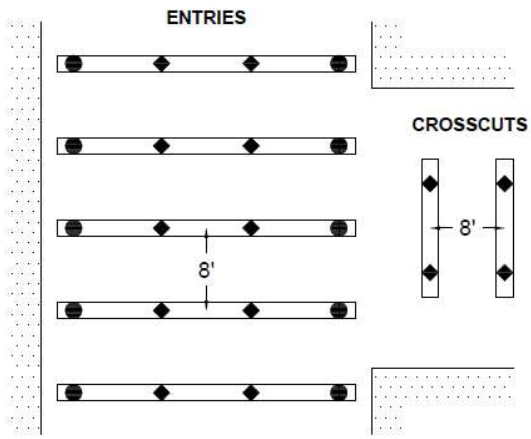

Figure 7. Recommended FGCB bolting pattern with roof channel.

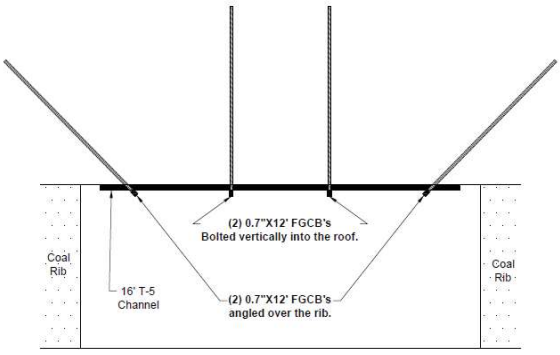

Figure 8. Profile view of FGCBs and roof channel in entries.

Figure 9. Drill hole before grouting.

Figure 10. New drill hole after grouting.

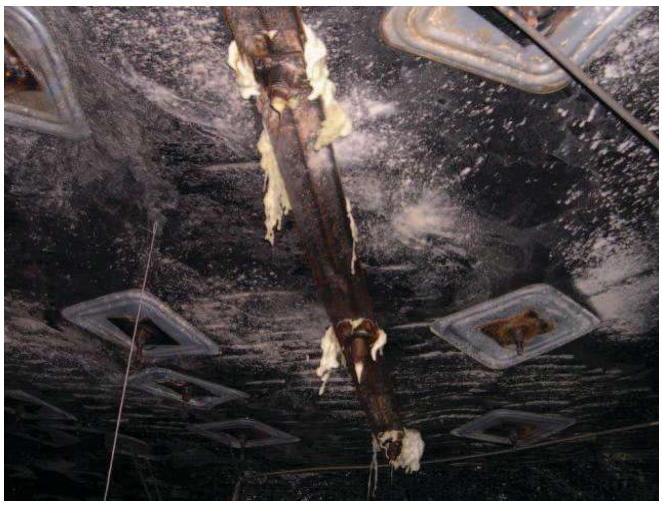

Figure 11. Complete roof channel with FGCBs after injection.

The FGCBs presented multiple injection locations across the section, enabling Jennchem personnel to quickly move pumping activities from entry to entry across the section. The pump's mobility allowed pump personnel to stay out of the way of section production equipment minimizing interruptions to the mining cycle.

The FGCBs were effective in controlling roof water in the low-cover area, allowing the mine to successfully cross the stream valley. In addition, the PUR provides long-term corrosion protection for the supplemental cable bolts. To date, there have been no issues reported in the area where the FGCBs were used.

Case Study 3

The third case study is a low-coal, room and pillar operation in the Upper Freeport seam. The average mining height is 48 in. (1.2 m) and the roof bolting consists of four 6 - 8 ft (1.8 - 2.4 m) fully grouted rebar bolts on 4 ft (1.2 m) spacing and two 0.6 in. x 12 ft (15 mm x 3.65 m) non-tensioned cables every 8 ft (2.4 m). As the mine advanced, they would periodically run into areas where several of their cable bolt drill holes would intercept fractures in the roof strata that connected to a source of entrapped water. This water could rush out of the drill holes at an estimated rate of up to 10 gallons (38 L) per minute for several days or weeks before the source of water was mitigated.

Since the rebar bolts were fully grouted, the resin created a "plug" in the drill hole, stopping the water from reaching the mine. However, the cable bolt drill holes were not fully grouted with resin and allowed a direct path for the water to make its way into the mine. This created adverse working conditions, reducing the mine's productivity until the flow of water diminished and excess water was pumped out of the mine.

To counteract these conditions, the mine decided to use FGCBs. When the conditions returned, the bolter operator was instructed to install the FGCBs in the drill holes that were emitting a large volume of water. Mine personnel would then use a portable pump on third shift to inject the cable bolts. The PUR stopped the flow of water from the drill holes, improving mining conditions and eliminating production slowdowns caused by the additional water.

SUMMARY

The capabilities of Jennmar's Fully Grouted Cable Bolts (FGCB) are just now being realized. The three case studies cited here demonstrate the FGCB's versatility along with offering an economical option, to improve mining conditions and increase the longevity of current roof support. The FGCB also allows mine operators to safely access new areas of reserves that were previously restricted by geologic features such as streams or sub-terrain fault lines. With the addition of FGCBs to a mine operator's available roof support systems, the future safety of the underground miner will be greatly enhanced.

*The Fully-Grouted Cable Bolt (FGCB) is the subject of a pending U.S. Patent and is the proprietary property of FCL Holdings Delaware, Inc.

REFERENCES

Suder, T., Stankus, J.C., Williams, D. (2001). "Tensioned cable bolts as primary support: update." *Proceedings of the 20th International Conference on Ground Control in Mining*, pp. 252–258. [http://icgcm.conferenceacademy.com/papers/detail.aspx?subdomain=icgcm&iid=737].

Mirabile, B., Poland, R., Campoli, A. (2010). "Application of tensioned cable bolts for supplemental support." *Proceedings of the 29th International Conference on Ground Control in Mining*, pp. 128–133. [http://icgcm.conferenceacademy.com/papers/detail.aspx?subdomain=icgcm&iid=308].

Stankus, J.C., Taylor, K.L. (2000). "INSTAL CableOx: a new tensionable & corrosion resistant cable bolt." *Proceedings of the 19th International Conference on Ground Control in Mining*, pp. 261–265.

Aspect Ratio and Other Parameters That Affect the Performance of Burrell Can Roof Supports

David F. Gearhart, Lead Research Engineer
Ground Control Branch
NIOSH-Pittsburgh Research Lab
Pittsburgh, PA

Timothy J. Batchler, Research Engineer
NIOSH-Pittsburgh Research Lab
Pittsburgh, PA

ABSTRACT

The Burrell Can[1] is a thin, steel, tubular shell filled with aerated concrete that is used as a roof support in coal mines. The Can height is always shorter than the mining entry, so it is capped with wooden timbers and wedges when it is installed. This combination of the Can and the wooden header is a standing support system that is designed to yield in a controlled manner and exhibit a constant yield, or elastic-plastic behavior. The Burrell Can is capable of withstanding 20 in or more of vertical convergence and 15 in or more of horizontal displacement. Because of this exceptional ability to sustain load through extended convergence and displacement, it is one of the most robust standing supports in use today.

The National Institute for Occupational Safety and Health (NIOSH) conducted testing on seventeen Burrell Cans in 1995, during development of the support where the ratio of the height to the diameter, or the aspect ratio, was between 2:1 and 4:1. Based on the results of that testing, it was suggested that the standard aspect ratio of the Can be less than 5:1. This suggestion is intended to preserve the overall stability of the Can, which will help to maintain the initial stiffness and prevent load shedding. Recently, the necessity of the aspect ratio has been questioned, and this issue will be addressed in this paper.

Since the initial development and introduction, more than 130 tests of the Can have been conducted at the NIOSH Mine Roof Simulator (MRS), and 25 of those specimens had aspect ratios greater than 5:1. The 18-in-diameter by 10-ft-tall specimens had the largest aspect ratio, 6.67:1.However, the aspect ratio is not the only parameter that affects the performance characteristics of the Can. Multiple factors, such as the use of different wood species, the use of different header or footer configurations, and the use of pedestals, as well as biaxial loading conditions can also decrease the stiffness and capacity of the Can. Data from full-scale tests that include these other factors are analyzed to show that the initial stiffness is primarily affected by the roof and floor contact configurations. Furthermore, load shedding is more likely to occur or begin earlier when the aspect ratio is greater than 5:1 and one or more of the other factors are present.

This investigation confirms that the 5:1 aspect ratio rule-of-thumb should still be used for longwall tailgate applications although Cans with larger aspect ratios have been stable under some conditions. It also shows that the initial stiffness of the support is affected by the roof and floor contact conditions created during installation and must be considered in the support system design.

INTRODUCTION

Standing roof supports in longwall tailgates provide the last line of defense against roof falls that can block the secondary escapeway or disrupt ventilation. Therefore, it is important that the design and installation of the standing roof support systems ensure the highest probability of preventing these roof falls. One feature that is critical to the performance of standing support systems is the initial stiffness, which enables a passive support to generate capacity in response to the movement of the roof. Because the Can height is always shorter than the mine entry, the effect the capping material has on the support stiffness is important and must be considered in the system design. The rule-of-thumb for the header is that the first layer of wood material should completely cover as much of the top of the Can as possible and the height of the materials used to install the Can should not be greater than the diameter of the Can (Burrell Mining Products, 2012).NIOSH also recommends that the capping materials should be designed not to yield before the Can yields (STOP, 2010).

Another feature that affects the overall performance of all standing roof supports is the aspect ratio, defined as the height of the support divided by the width or diameter. The aspect ratio is the simplest measure for the overall stability of a standing support, which is the ability to maintain capacity and stiffness, and to resist load shedding through a given displacement. A support that is too tall or too narrow will have a high aspect ratio that can reduce the initial stiffness and may allow the support to shed load during convergence of the entry.

Rules-of-thumb for the aspect ratio of all crib-type standing supports have been proposed based on results from testing

[1] Mention of a company name or product does not constitute endorsement by the National Institute for Occupational Safety and Health.

conducted in the Mine Roof Simulator (MRS) Laboratory. Rule-of-thumb values are not intended to be strictly accurate or reliable for every situation; they are intended as guidelines. The suggestion for the Burrell Can is 5:1, a recommendation that was made after conducting testing on 17 supports (Barczak, 2001) where the aspect ratio of the specimens ranged between 2:1 and 4:1. Recently, this rule-of-thumb suggestion has been questioned by some users, and regulators; therefore, NIOSH has undertaken a reevaluation of the performance of Burrell Can supports when the aspect ratio is at or above 5:1. Since the original testing that proposed the recommended aspect ratio, more than 130 Cans have been tested, with 25 specimens having aspect ratios greater than 5:1. This paper presents the results of tests on Cans with aspect ratios from 2:1 to 6.7:1. Both initial stiffness and observed load shedding are evaluated. Other factors that affect the performance of Cans with larger aspect ratios, including the height of the wood cap, the species of wood, the use of pedestals, and the direction of the applied load, are examined and discussed in the paper.

BACKGROUND

The Burrell Can roof support is a thin steel tube filled with aerated concrete. It is a yielding support that can absorb a large amount of vertical convergence and withstand large shear displacements. Because of this exceptional ability to sustain load through extended convergence and displacement, the Can is one of the most robust and stable standing supports in use today. The diameter of the Can ranges from 18 to 36 in and its capacity is the combination of the local buckling strength of the steel shell and the compressive strength of the fill material. Burrell Cans are rated by the manufacturer based on the diameter, ranging from 120 kips (60 tons, 1 kip equals 1,000 lb) for an 18-in-diameter unit, up to 400 kips (200 tons) for a 36-in-diameter Can. If the support configuration is stable, then its behavior when subjected to vertical convergence is elastic-plastic with a small degree of strain hardening. The support has an initial, stiff elastic response that allows for a rapid build-up of load through yield followed by a plastic, strain-hardening phase, where the voids in the aerated concrete collapse and local, axisymmetric wrinkles form in the steel tube.

The original 17 MRS tests conducted on Can supports included 18-, 24-, and 36-in-diameter specimens and heights that ranged from 64 in up to 132 in. This resulted in aspect ratios ranging from 2:1 to 4:1. Each specimen used a single layer of either 8-in-thick western softwood or 5-in-thick eastern hardwood for the header. Twelve tests were conducted with only a vertical displacement applied, and five used a 3:1 vertical-to-horizontal biaxial displacement ratio. None of the specimens shed load through 22 in of convergence during the tests, including the 2:1 aspect ratio specimen that was placed on a 7.5 degree tilted fixture to simulate an uneven roof, and the 4:1 aspect ratio specimen that used two softwood timbers for the header and had a 3:1 biaxial displacement applied. Since there was no load shedding during the tests on the specimens up to the 4:1 ratio, a rule-of-thumb for the aspect ratio of 5:1 was proposed for the Can support. Therefore, an 18-in-diameter Can could be up to 7.5 ft tall, a 24-in-diameter Can could be up to 10 ft tall, and a 36-in-diameter Can could be up to 15 ft tall.

The purpose of the 5:1 rule-of-thumb for the aspect ratio of the Burrell Can is to help ensure the stability and the maximum performance of the support when other factors that may affect the performance are unknown (Barczak, 2001). The stability of the wood cap is one of these factors. Therefore, according to the rules-of-thumb for the header, the first layer of wood on top should completely cover as much of the Can as possible, the total height of the wood layers should not exceed the diameter of the Can, and the wood should be stronger than the average yield strength of the support. These three rule-of-thumb recommendations help ensure the stability of the wood cap, and therefore, increase the initial stiffness of the support and prevent load shedding.

The calculation of the aspect ratio for the Can is also different from any other crib-type support. It is calculated using only the height of the Can itself, while all other crib-type standing support systems use the height of the mine opening. This difference occurs because the Can requires capping material to complete the installation, whereas other crib-type standing supports are the same material from bottom to top. The height of the header or footer is not included in the calculation of the aspect ratio for the Can, which presumes that the header and footer will be completely stable and will not degrade the performance of the Can. Therefore, the comparable aspect ratio for a Can installation with a 5:1 aspect ratio and including the maximum recommended amount of wood in the header would be 6:1. This is larger than any other rule-of-thumb aspect ratio for crib-type standing supports and validates how robust and stable the Can support is, as long as the recommendations to preserve the stiffness and stability are followed. Furthermore, there are many successful Can installations with the aspect ratio greater than 5:1.

ROOF SUPPORT PERFORMANCE EVALUATION

The performance of Burrell Cans or any standing supports are evaluated during convergence tests conducted in the NIOSH Mine Roof Simulator (MRS). From these tests, load-displacement curves are developed, and from these curves, the support capacity and elastic stiffness are calculated. Load shedding, which is an indication of instability, can also be identified from the load-displacement curves.

Capacity

Burrell Cans are available in five standard diameters, as listed in Table 1. The capacity is assigned by the manufacturer based on the results of tests using the standard steel shell and standard density fill material (STOP, 2010). Figure 1 shows the load-displacement curves for the four main sizes. Each Can in Figure 1 had a single, 6-in-thick layer of poplar wood for a header. The test specimens were unaffected by the aspect ratio, end conditions, or other factors and were completely stable with no load shedding through 20 in of displacement.

Initial Stiffness

The initial stiffness of a support is the slope of the elastic portion of the load-displacement curve before the support yields. The stiffness is calculated as the change in support load divided by the change in displacement and is measured in pounds per inch or kips per inch. The initial stiffness of each support shown in Figure 1 is listed in Table 2. The squat supports with the larger diameters and smaller aspect ratios are stiffer than the narrower supports because they develop load more quickly in response to convergence than the narrower supports.

Table 1. Can diameter and capacity rating.

DIAMETER in	CROSS SECTIONAL AREA sq in	RATED CAPACITY kips (tons)	AVERAGE STRENGTH psi
18	254	120 (60)	472
22	380	160 (80)	421
24	452	180 (90)	398
30	707	280 (140)	396
36	1,018	400 (200)	393

Table 2. Initial stiffness of four different diameter Cans.

DIAMETER in	ASPECT RATIO	DEFLECTION at Yield Load in	YIELD LOAD kips	STIFFNESS kips per in
18	4.00:1	2.06	135	65.6
24	3.25:1	1.76	190	107.9
30	3.60:1	1.73	282	162.5
36	2.00:1	1.36	351	258.5

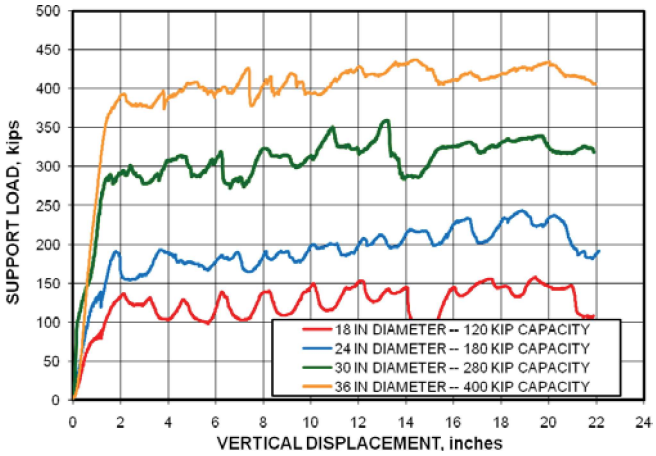

Figure 1. Load-displacement curves for four different diameter Cans.

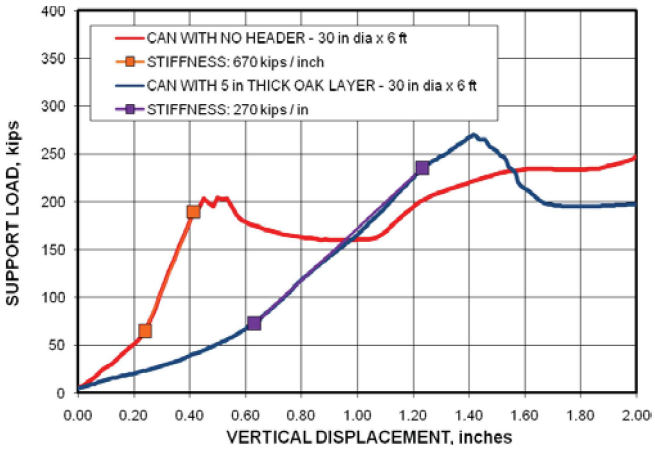

Figure 2. Comparison of 30-in by 6-ft Can tests. The stiffer Can has no header, and the softer Can has one layer of oak timbers.

The first 2in of the curves for the 18-, 24-, and 30-in-diameter Cans in Figure 1 show the interaction between the open top of the Can and the header when the edge of the steel Can cuts into the first wood cap layer. The effect of the interface between the header and the Can on the total stiffness of the support is important.

Figure 2 shows the results of tests on two different 30-in-diameter by 6-ft-high Cans, one with no header and the other with a single, 5-in-thick oak header. The stiffness with no header is 670 kips per inch and the stiffness with the single layer of oak is 270 kips per inch. Additionally, the stiffness of the 30-in-diameter Can listed in Table 2 using a single layer of poplar is 162.5 kips per inch. Thus, a single layer of oak resulted in a 60 percent reduction of the Can system stiffness, and a single layer of poplar resulted in a 76 percent reduction.

This behavior is explained by series stiffness (Barczak and Tadolini, 2005), where the stiffness of the timbers and Can add proportionally as shown in Equation 1:

$$\frac{1}{K_{System}} = \frac{1}{K_{Can}} + \frac{1}{K_{Crib}} \quad (1)$$

where

K_{System} = total system stiffness, kips per inch,

K_{Can} = Can stiffness, kips per inch, and

K_{Crib} = wood crib stiffness, kips per inch.

Rearranging the equation yields:

$$K_{System} = \frac{K_{Can}K_{Crib}}{K_{Can} + K_{Crib}} \quad (2)$$

and $$K_{Crib} = \frac{K_{System}K_{Can}}{K_{Can} - K_{System}} \quad (3)$$

Using 270 kips per inch for the stiffness of the entire specimen, K_{System}, and 670 kips per inch for the stiffness of only the Can, K_{Can}, then solving for the stiffness of the oak layer, $K_{C\ rib}$, results in a value of 452 kips per inch. Likewise, the 30-in-diameter Can from Table 2 had a measured stiffness of 162.5 kips per inch with a single layer of poplar timbers for a header. Calculating the stiffness of the poplar header alone results in a value of 215 kips per inch. These stiffness values are for the first layer of wood that is against the edge of the steel Can. The stiffness of a single layer of oak that is 5-in-thick with the same area as the Can but with the load distributed uniformly over the entire surface (rather than concentrated against the steel edge) can be estimated using Equation 4.

$$K = \frac{AE}{L} \quad (4)$$

where

K = stiffness, kips per inch,
A = area, in^2,
E = modulus of elasticity, ksi, and
L = length, in.

The area of a 30-in-diameter Can is 707 in^2, and the average modulus is 159.3 ksi for Northern Red Oak (Forest Products Laboratory, 1999). If the layer is 5 in thick, then the stiffness is about 22,500 kips per inch, and the stiffness of the 270 kip per inch Can with the added layer of oak would only be reduced to about 267 kips per inch. Additional wood layers are much stiffer than the first layer because the loading conditions are different. Therefore, additional solid layers will not seriously degrade the support system stiffness, but the number of wood layers should be minimized to preserve the system stiffness and to prevent other affects.

Indications of Instability

The load-displacement curve for a stable Can installation will exhibit a definite, linear region of elastic stiffness, then a slightly increasing capacity in the plastic region. This behavior is clearly shown by the load-displacement curve for the 36-in-diameter Can in Figure 1. If the performance curve shows decreasing stiffness, or exhibits load shedding in the plastic region, then the stability of the specimen is probably being affected by some other parameter or combination of parameters, such as the aspect ratio being too large, the species of wood being too soft, or the header configuration causing instability. The curve for Test D in Figure 3 shows load shedding at about 18 in of convergence when the Can started to bend at the upper circular weld. The curve for Test E shows yielding of the wood header during more than 5 in of convergence before the Can started to yield.

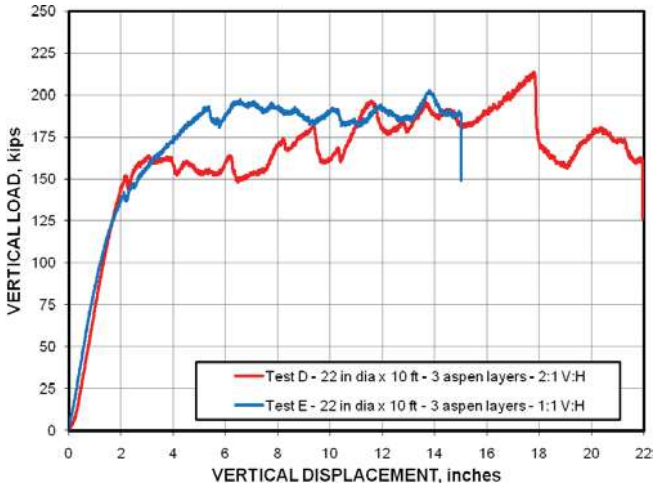

Figure 3. Load-displacement curves showing indications of instability.

CONDITIONS ALLOWING FOR STABLE PERFORMANCE WITH ASPECT RATIOS GREATER THAN 5:1.

The curves for Cans with aspect ratios from 2:1 to 4:1 and just a single layer of poplar timbers for a header demonstrate both consistent elastic stiffness and increasing plastic capacity (Figure 1).Figure 4 shows the results from tests on specimens with aspect ratios from 3.82:1 to 5.45:1 that also demonstrate consistent elastic stiffness and increasing plastic capacity. There are load-displacement curves for four 22-in- and two 24-in-diameter samples shown that were tested using a single layer of mixed hardwood for a header. Notice that the initial stiffness of the specimens is similar and there is no load shedding, even when the aspect ratio is greater than 5:1, indicating that all the supports were stable.

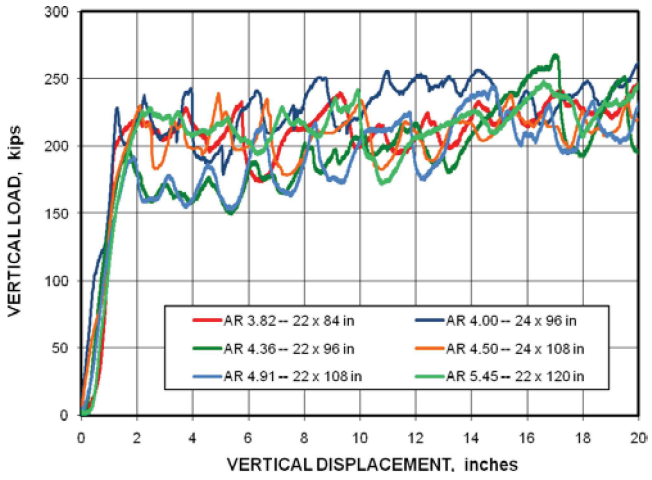

Figure 4. Load-displacement curves from 22- and 24-in-diameter Cans with a single layer header of mixed hardwood and with aspect ratios (AR) from 3.82 to 5.45.

Figure 5 shows the load-displacement curves for Cans with aspect ratios of 6.7:1. These 18-in-diameter by 10-ft-tall specimens

were tested with a single layer of hardwood for a header and used vertical only, 3:1, and 2:1 vertical-to-horizontal ratios of displacement. The results indicate that it is possible for Cans with aspect ratios as large as 6.7:1, using a single layer of hardwood for a header and with minimal lateral loading, to behave in a stable, consistent manner.

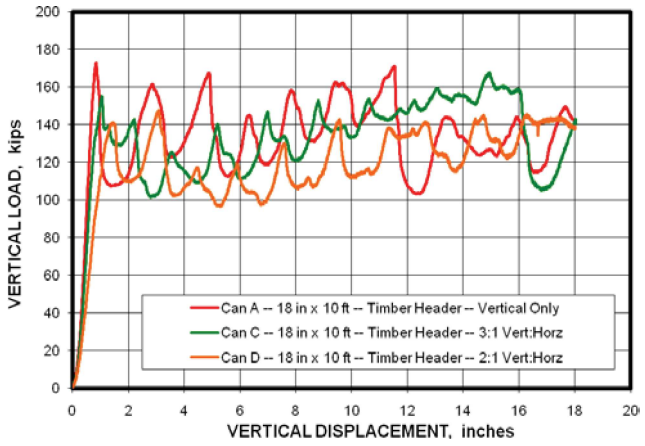

Figure 5. Load-displacement curves for stable Can supports with an aspect ratio of 6.67:1.

The capacity, stiffness, and stability of Cans are important for predicting the effectiveness of the supports installed underground and for identifying the factors that can degrade the performance. It has been shown here that the Burrell Can support can provide stable and consistent behavior in the laboratory, even at aspect ratios greater than 5:1, but the effect on the performance by multiple factors must be understood. This understanding is needed to establish the guidelines for the safe and effective application of the supports underground.

TESTS WITH ASPECT RATIOS GREATER THAN 5:1 INCLUDING OTHER FACTORS THAT DEGRADE PERFORMANCE

The factors that can degrade Can performance include the aspect ratio, the species of wood, the height of the header or footer, the wood stack configuration, and the application of a biaxial displacement. It has been demonstrated that Burrell Cans with aspect ratios greater than 5:1 can meet their performance specifications during closure, as long as the presence of these other factors is minimized or eliminated. This Can behavior is shown in Figure4, where the aspect ratio ranged from 3.82:1 to 5.45:1 and the header was limited to a single layer of hardwood for all of the specimens. Figure 5 shows that even with an aspect ratio of 6.67:1 where the header was a single layer of timber and the biaxial displacement was limited to a 2:1 ratio, the performance specifications can be met. For aspect ratios above 5:1, any single factor including the aspect ratio by itself may not degrade the performance of the Can. However, the following examples will show how combinations of factors can affect the support performance. Some comparisons will be made to tests conducted under similar conditions but with aspect ratios less than 5:1.

The purpose of the aspect ratio of 5:1 is to preserve the stability of the Can, which will allow the supportto withstand the existence of the other factors with minimal impact on the performance. A single factor usually has little or no impact on the performance of the support, but when multiple factors are present, the performance may be less than expected.

Example A—Aspect Ratio and Biaxial Displacement

Figure 6 shows the performance curves for two 12-ft-tall units that had diameters of 24 and 30 in. The yield load of each specimen was below the normal rated capacity because these specimens were not fully cured and therefore the overall performance may be different than standard Cans. However, because they were the same age, these test results can be compared. Both specimens had a single layer of mixed hardwood timbers as a header and were subjected to a 2:1 biaxial displacement. The only difference between the specimens is the aspect ratio. For the 30-in-diameter Can, the aspect ratio is 4.8:1, and for the 24-in-diameter Can, the aspect ratio is 6:1. As expected, the capacity and stiffness of the Cans is proportional, but there is a difference in performance during the plastic section of the curves. After yielding begins on the 4.8:1 aspect ratio Can, the trend is an increasing load, which indicates stable behavior. Conversely, the 6:1 aspect ratio Can began to shed load after the peak load was reached at about 10.5 in of convergence, which indicates instability. Nearly 25 percent of the peak load was shed during the remaining convergence.

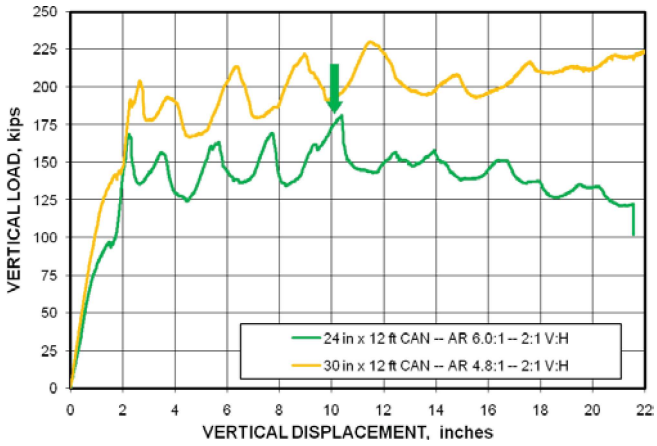

Figure 6. Load-displacement curves comparing the performance of 4.8:1 and 6:1 aspect ratio Cans.

When the aspect ratio was less than 5:1 and the 2:1 biaxial displacement was applied, the support was stable and the capacity of the support was maintained, but when the aspect ratio was 6:1 and the 2:1 displacement was applied, the stability of the support was marginal and load shedding occurred.

This example demonstrates that when the compressive strength of the fill material is lower than normal, the aspect ratio should be less than 6:1 to prevent load shedding.

Example B—Biaxial Displacement and Height of Headers and Footers

Figure 7 shows the load-displacement curves from four tests conducted on 24-in-diameter Cans. Three of the supports were 12 ft tall and one was 10 ft tall. The capacities of these Cans werehigher

than the normal rated load because the density of the cement fill was higher than the standard mix. Table 3 shows the aspect ratio of the Can, the displacement ratio, and the number of wood layers used for each test. The oak timbers used for the headers and footers were 6 x 6 x 30 in.

Table 3.Multiple factors influencing Can performance and length of stable behavior.

TEST	ASPECT RATIO	V:H Displacement RATIO	HEADER LAYERS	FOOTER LAYERS	INITIAL PEAK-TO-ULTIMATE PEAK DISPLACEMENT, ins
A	6:1	1:0	1	0	14.24
B	6:1	3:1	1	0	10.56
C	5:1	3:1	4	0	5.81
D	6:1	3:1	4	1	5.36

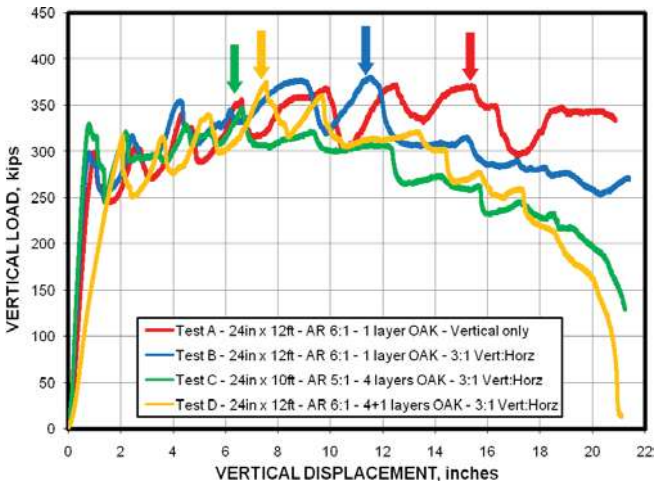

Figure 7. Load-displacement curves showing the effect of the wood configuration and biaxial convergence.

There was a slight increase in the initial stiffness of the support with the change from a vertical only convergence to biaxial displacement. Stiffness also increased slightly when the height of the Can was reduced to 10-ft and the oak header was increased from a single layer to four layers. However, there was a significant decrease in the stiffness when the Can was increased to 12-ft and the wooden footer was included. The initial stiffness for the specimen with four layers of oak was 557 kips per inch. The stiffness was reduced to about 176 kips per inch when the single layer of oak timbers was added for the footer. This reduction was mainly the result of the circular Can-to-wood contact created at the bottom of the support.

The effect of the multiple factors on load shedding during the yielding phase is shown in Figure 7. Each color-coded arrow points to the peak load of the matching color curve. The difference in displacement between the initial peak and the ultimate peak load for each curve is given in Table 3. Load shedding begins at less convergence as the number and severity of the factors increase from Tests A to D. Even at a 5:1 aspect ratio there is some load shedding when there are multiple layers of wood with a biaxial displacement. This example clearly demonstrates the effect of combinations of factors, such as the header height and biaxial loading along with the higher aspect ratio on load shedding performance. The only difference between Test A and B is the addition of biaxial loading. This caused the onset of load shedding to start 3.68-in earlier. Between Test B and C, the aspect ratio was reduced and the header height was increased. The smaller aspect ratio would theoretically delay the onset of load shedding and the increased header height would cause an earlier onset of load shedding. The result of the combined changes was that the load shedding started 4.75-in earlier; therefore the header height has a much larger effect than the aspect ratio. Between Test C and D the aspect ratio increased and the footer was added. This combination resulted in the onset of load shedding 0.45-in earlier.

Example C—Wood Header Strength and Stability Effects

The strength and stability of the header stack also affects the performance of the Cans when the aspect ratio is greater than 5:1.Figure 8 shows a comparison of load-displacement curves from three tests on 22-in-diameter by 10-ft-tall Cans and Figure 9 shows a photograph of the wood headers. The cap for Test A used three solid layers of three 6x8x36inaspen timbers on top of the Can (Figure 9a) as specified by the mine that requested the tests. Because each layer was nominally 24 in wide, the entire cap is essentially a 24-in-square by 18-in-tall block of wood. The width of the header was only 2in wider than the diameter of the Can. The contact area with the Can was 380 in^2, and the interlayer contact area of the wood layers was 576 in^2.

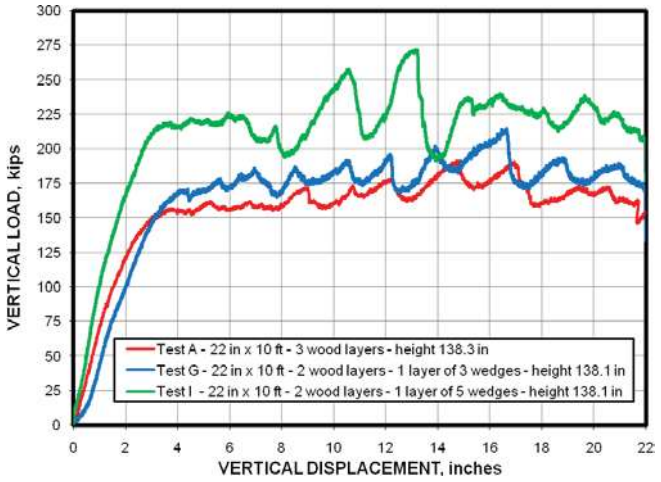

Figure 8. Wooden header stability comparison.

The header for Test G used two layers of three 6 x 8 x 36 in timbers with three wedge blocks as the third layer (Figure 9B). This configuration was also specified by the mine that requested

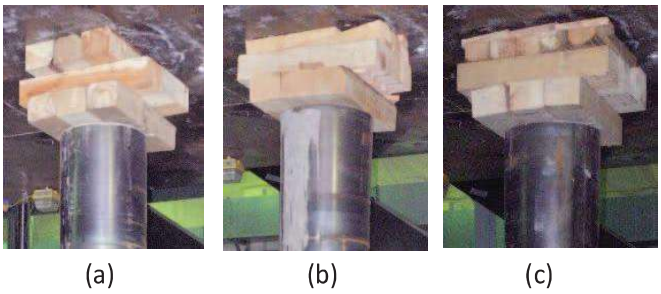

Figure 9. Wooden header arrangements for (a) Test A, (b) Test G, and (c) Test I.

these tests. The wedge blocks are 6 x 6 x24in blocks cut along a diagonal to create two large wedge pieces that are 2 to 4 in thick. The wedges were aligned parallel with the second layer of timbers. For this configuration, the contact area with the Can was 380 in^2, and the interlayer contact area between the two layers of timbers was 576 in^2. Referring to Figure 9B, the contact area between the timbers and the wedges was 648 in^2 (18 in by 36 in), but it is narrower by 4 in than the 22 in diameter of the Can.

The performance of specimens A and G were nearly identical because the only difference between the two specimens was the replacement of one layer of three aspen timbers in Test A with three large wedges for Test G. The reduced stability for the test G arrangement was mainly caused by the 18-in dimension of the wedges across the 22-in-diameter Can. If the wood is not perfectly centered on the Can, the loading becomes eccentric. The load shedding that occurred after about 16 in of closure was caused by the instability of the wooden caps that caused the top section of the Cans to bend over at the circular weld (Figure 10).

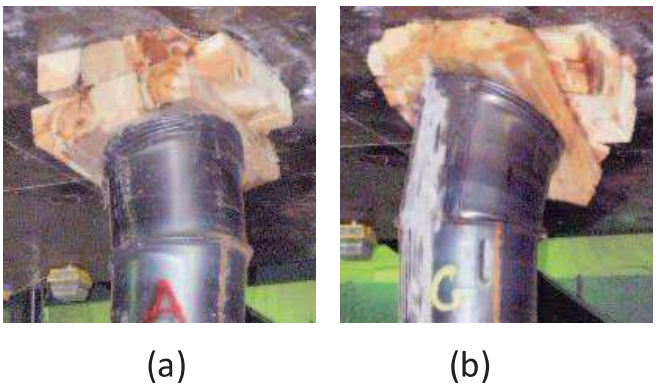

Figure 10. Unstable wood headers that allowed load shedding on (a) Test A and (b) Test G.

The performance of Test I was significantly different from the other two tests due to the improved capacity, stiffness, and stability of the wood header. This was due to the addition of a fourth timber in the second layer and two additional large wedges in the third layer above the Can. The increased contact areas provided more stability and a more uniformly distributed load for the Can throughout the test and resulted in a 50 percent increase in the elastic stiffness and a 50-kip improvement in the support capacity over the other two header configurations.

Example D—Use of a Pedestal to Increase Height

Pedestals are used when the total height of a Can with the maximum recommended amount of wood on top is not tall enough to reach the roof of the mine. The load-displacement curves shown in Figure 11 are for 22-in-diameter by 10-ft-tall Cans using pedestals (Figure 12). The pedestals were 24 in in diameter, with a 24-in-tall shell and filled to a height of 22 in with aerated cement. For test C, the Can was placed directly on top of the pedestal with a header that was identical to the specimen for Test A (Figure 9a). Comparing the performance of Test C to Test A, the elastic stiffness at 2in of convergence was reduced from 61.0 to 57.5 kips per inch. This reduction is caused by the Can crushing the fill material inside the pedestal. Both sample A and C began to shed load after about 17 in of convergence.

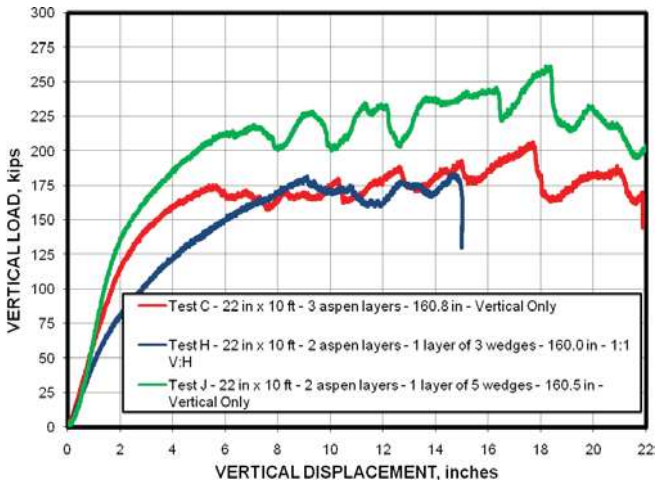

Figure 11. Comparison of 22-in-diameter Cans using pedestals.

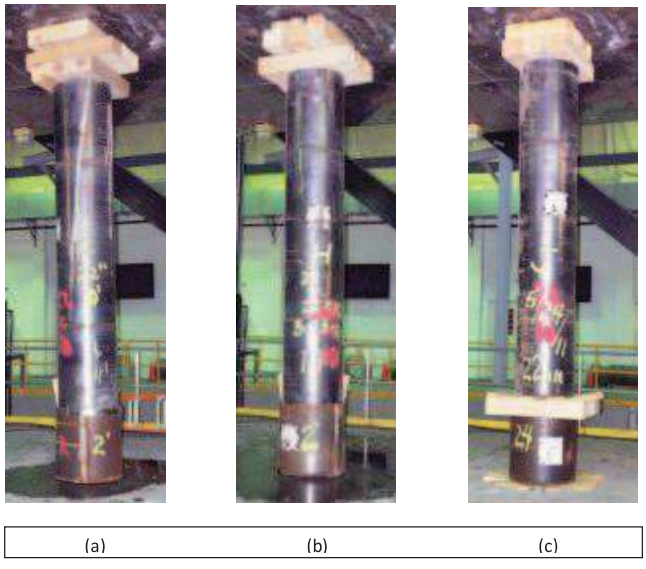

Figure 12. Test configurations using pedestals for (a) Test C, (b) Test H and (c) Test J.

Test H had the same header configuration as test C except it used wedges in the third layer and an applied biaxial displacement

with a 1:1 vertical-to-horizontal ratio instead of a vertical only convergence. With the horizontal displacement, the load was concentrated on one edge of the Can, which resulted in the Can punching deeper into the top surface of the pedestal. This reduced the elastic stiffness of the support by 30 percent, from 57.5 to 40.5 kips per inch. Because of this softer response, the 160 kip rated capacity of the Can was not reached until more than 6.75 in of convergence had occurred. The test was ended before the occurrence of load shedding could be verified.

Test J used the same amount of wood as tests C, except one layer of timbers was placed directly on top of the pedestal and under the closed end of the Can, to help prevent the Can from pushing into the aerated fill. The upper edge of the pedestal was also bent over the fill to allow transfer of the Can load onto the steel pedestal shell. Only a vertical convergence was used for this test. The elastic stiffness of Test J compared to Test C was improved by more than 19 percent from 57.5 to 68.5 kips per inch. Thus, the rated load for the support was achieved in less than 3 in of convergence. The capacity of the support increased to more than 200 kips at about 5 in of convergence due to the improved stability of the pedestal and header. The support did begin to shed load after more than 18 in of closure.

These tests show that the use of pedestals to extend the height of a Can generally decreases the elastic stiffness but placement of the wood can improve the performance.

Example E—Wood Species Effects

Figure 13 shows the load-displacement curves for Cans where three different wood species were used for the header: aspen, oak, and poplar. The Cans were either 10 or 11 ft tall with diameters of 22 or 24 in. This resulted in aspect ratios that range from 5:1 to 5.5:1. The 18-in-tall aspen header clearly shows the behavior of soft wood with an elastic response to about 120 kips, and then plastic yielding of the wood up to 225 kips when the 24-in-diameter Can yielded. The support did not reach its 180 kip rated capacity until 3.3 in of convergence because of the soft wood header.

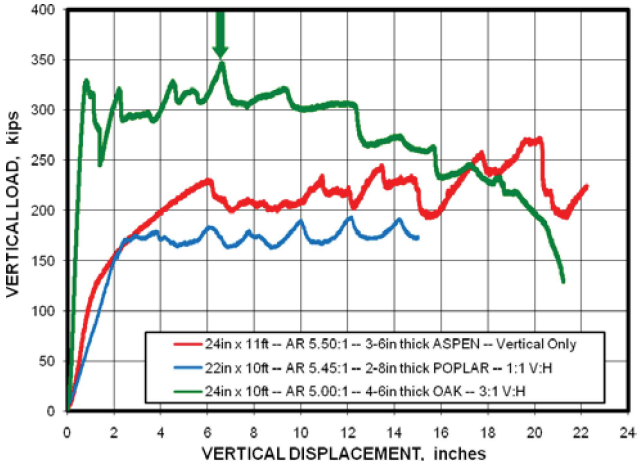

Figure 13. Load-displacement curves showing the behavior of different wood species.

For the 22-in-diameter support with the 16-in-tall poplar header, the Can yielded rather than the header after only 2.2 in of convergence because the wood did not reach its yield stress. The 24-in-tall oak header did not yield either, even with the 24-in-diameter Can capacity of over 300 kips due to its high fill density. This Can support reached its initial peak load at only 0.4 in of convergence.

In the test with the oak header, load shedding did occur. For the test with the aspen and poplar headers, load shedding cannot be verified because the peak load occurred too close to the end of the convergence. The specimen with the oak header shed load from a combination of factors. The aspect ratio was 5:1, a 3:1 ratio biaxial displacement was applied and the height of the header was the diameter of the Can. The support shed load when the Can bent over at one of the circular welds.

The differences caused by the strength of the wood species used for the header has its biggest effect on the initial stiffness and the displacement when the initial peak capacity of the support was reached. The effects of the wood species on load shedding could not be determined because of multiple confounding factors including the higher aspect ratios, the header height, and the biaxial displacement.

SUMMARY AND CONCLUSIONS

Burrell Can roof supports can absorb large vertical convergence and horizontal shear displacement. This makes them one of the most robust and stable roof supports used in coal mines. Nevertheless, the initial stiffness and the load shedding performance of the Can may be affected by other factors when it is installed, and support system designers and installers should be aware of these conditions.

The initial stiffness of the Can is primarily influenced by the interface between the top of the Can and the wood header. Therefore the rule-of-thumb recommendations for header installation should be followed for optimal performance. The first recommendation is for 100 percent coverage of the Can with the first layer of wood. The second is that the compressive strength of the wood be stronger than the average strength of the Can, and the third is that the height of the header should be shorter than one diameter of the Can. Failure to follow these guidelines may lead to conditions where the yield load is lower than the rated capacity of the Can and extended convergence is required to reach the rated capacity. The same sub-optimal performance effects can result from the use of footers and pedestals.

The load shedding behavior of the Can is primarily affected by the aspect ratio and the combination of installation factors or load conditions, like the stability of the header or biaxial loading. This is because the aspect ratio represents the stability of the support, which is a measure of how well it can resist the bending caused by other factors. Therefore, as the aspect ratio increases, the sensitivity of the support to the presence of the other conditions also increases. One example comparing Cans with 6:1 aspect ratios showed that load shedding occurred after 14.24 in of vertical only convergence and after 10.56 in of the vertical component of a biaxial displacement.

Therefore, the rule-of-thumb for the aspect ratio of Cans used in tailgates should remain at 5:1 where the presence of the other factors that may affect the performance may be unknown. A rule-of-thumb is not intended to be strictly accurate or reliable for every situation, but is intended as a guideline. This suggestion is based on the tests conducted in the MRS with aspect ratios greater than 5:1 and the presence of other contributing factors such as header thickness and configuration, wood strength, and biaxial displacement. Local experience from a particular mine may permit the installation of the Can at aspect ratios higher than 5:1.

The designer of the standing support system and the personnel responsible for installation should be completely familiar with all of the factors that can affect the performance of the Can support and take precautions to avoid diminished behavior.

DISCLAIMER

The findings and conclusions in this paper are those of the authors and do not necessarily represent the views of the National Institute for Occupational Safety and Health.

REFERENCES

Barczak, T. M. (2001). Mistakes, misconceptions and key points regarding secondary roof support systems."In: *Proceedings of the 20th International Conference for Ground Control in Mining,* pp. 347–356.

Barczak, T.M., Tadolini, S.C. (2005), "Standing support alternatives in Western Longwalls." Preprint 05-78. Littleton, CO: Society for Mining, Metallurgy and Exploration.

Burrell Mining Products. (2012). Suggested Guidelines for the Purpose of Installing The CAN® Cribbing System

Forest Products Laboratory.(1999). "Wood handbook—wood as an engineering material."General Technical Report FPL—GTR, 113. Madison, WI: U.S. Department of Agriculture, Forest Service, Forest Products Laboratory, 463 p.

STOP.(2010). Support technology optimization program. Pittsburgh, PA: National Institute for Occupational Safety and Health, Office of Mine Safety and Health Research,.

J–Crete: An Engineered Cementitious Composite Rock Coating

Alan A. Campoli, Vice President
Jennchem
Jennmar Corporation Pittsburgh, PA 15238
Pittsburgh, PA

Jason Walls, J-Crete Manager
Jennchem, LLC
Jennmar Corporation Pittsburgh, PA 15238
Pittsburgh, PA

Joshua Mullins, Project Engineer
Jennchem
Jennmar Corporation Pittsburgh, PA 15238
Pittsburgh, PA

Dakota Faulkner, R&D Engineer
Keystone Mining Services, LLC
Jennmar Corporation Pittsburgh, PA 15238
Pittsburgh, PA

ABSTRACT

The mining industry has long been searching for an effective structural application that prevents weathering and falls of loose rock, debris, and sediment. J-Crete is a fiber-reinforced, engineered, cementitious composite rock application that is designed, tested, and successfully utilized as such a material. Laboratory evaluation of J-Crete material properties has shown the final compressive strength to be in excess of 7,300 psi (50.34 MPa), with 24 hour strength in excess of 1,500 psi (10.34 MPa). The flexural tensile strength is in excess of 600 psi (4.1 MPa) and is provided through a unique combination of polyvinyl alcohol (PVA) fibers activated by a proprietary liquid additive that prevents them from clumping and enables even distribution throughout the grout. Tensile bond strength in excess of 350 psi (2.4 MPa) at 28 day cure tightens the strata and holds loose material in place. Practically impervious to gas and liquids, J-Crete protects strata against long-term weathering, does not require screening to be effective, and has proven to be a successful waterproofing material. J-Crete has demonstrated the potential to alleviate coal mine roof cutters in soft, wet clay formations. J-Crete reinforces coal mine ribs by bonding directly to the rib, conforms to the strata, strengthens the rib, and eliminates sloughing due to long-term weathering; stabilizes coal mine entries by bonding directly to the brow and roof, and creates a monolithic shell with double reinforced corners.

INTRODUCTION

J-Crete (patent pending) is an engineered, cementitious, fiber-reinforced composite rock coating material designed to be applied as thin as 0.25 in (6 mm) and as thick as 8 in (203 mm) in a single application. The unique proprietary technology employs specifically engineered PVA (polyvinyl alcohol) fibers of a specified length and denier that are optimized for the application and activated by the liquid additive. The additive disperses the fibers evenly and consistently, facilitating a homogenous, isotropic, and interwoven thin layer. The interaction between the additive and the PVA fiber results in a strong interactive bond between the fiber and the cement matrix, thereby rendering the fiber to function as a true structural component of the engineered cementitious composite. The full bonding of the material with the strata creates a monolithic shell in which the rock strata becomes an integral part, thereby resisting lateral and vertical movement, assisting to prevent keystone movement that can lead to unraveling, and making the entire structure more stable.

J-Crete material cures quickly and achieves 80% of full strength after 7 day cure. Figures 1 and 2 show that the material develops more than 1,500 psi (10.3 MPa) compressive strength and 339 psi (2.3 MPa) flexural strength within 24 hours, and it achieves more than 7,300 psi (50.34 MPa) compressive strength and 995 psi (6.9 MPa) flexural strength upon 28 day cure. Four-point flexural bending tests (ASTM C1399) indicate that the material achieves more than 750 psi (5.2 MPa) flexural tensile strength and 91 psi (0.63 MPa) average residual strength upon 14 day cure. Shear bond strength per ASTM D4501 is in excess of 291 psi (2.0 MPa) upon 7 day cure. Tensile bond strengths per ASTM C1583 are 300 psi (2.1 MPa) and 358 psi (2.5 MPa) upon 7 day and 28 day cure respectively. Table 1 summarizes the material properties of the J-Crete product.

J-Crete adheres to wet coal, fireclay, black shale, limestone, shale, and even galvanized metal. It forms a durable impermeable shell that permanently prevents weathering. The product is practically impermeable to gas and liquid, and demonstrates an extremely low permeability (10^{-12} m/sec), which is equivalent to that of the highest strength concrete. J-Crete sprayed as surface control does not require mesh or other reinforcement because of its very high strength levels and its load bearing capacity. J-Crete was derived from a specially engineered material designed for hot and wet environments. However, it can withstand numerous freeze and thaw cycles without losing its flexural strength. Freeze thaw testing pursuant to ASTM-1186 indicated that the material retained its initial strength after fifty freeze/thaw cycles. The product has a flame spread index less than 0.67 and is practically fire-proof, demonstrates an excellent insulating heat transfer characteristics, and has been accepted and recommended in United Kingdom for products of combustion testing. The material is safe to apply and chemically stable. According to lab test results by Pace Analytical, an accredited laboratory, potable water in contact with the J-Crete material meets or exceeds EPA standards. Thus the product is suitable for repair of drinking water, reservoir, and pipeline infrastructures.

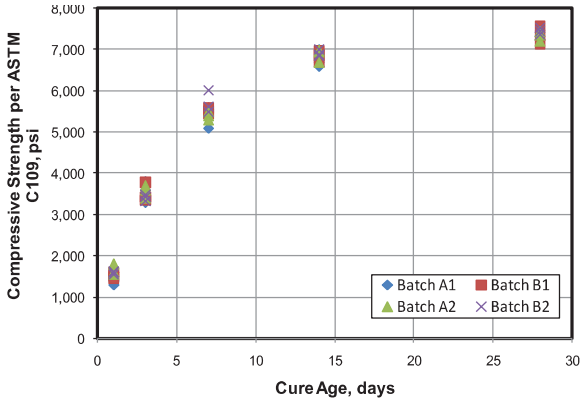

Figure 1. Compressive strength vs. cure age.

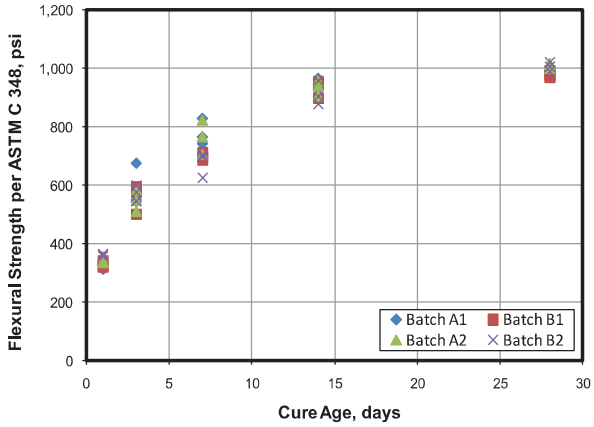

Figure 2. Flexural strength vs. cure age.

Table 1. Summary of J-Crete material properties.

Properties	Test Standard	Results	Cure Age
Compressive strength	ASTM C109-08	1,548 psi (10.7 MPa)	24 hour
		3,513 psi (24.2 MPa)	3 day
		5,489 psi (37.9 MPa)	7 day
		6,845 psi (47.2 MPa)	14 day
		7,362 psi (50.8 MPa)	28 day
Flexural strength (3 point bending)	ASTM C348-08	339 psi (2.3 MPa)	24 hour
		567 psi (3.9 MPa)	3 day
		728 psi (5.0 MPa)	7 day
		930 psi (6.4 MPa)	14 day
		995 psi (6.9 MPa)	28 day
Average residual strength	ASTM C1399	750 psi (5.2 MPa) Peak	14 day
		91 psi (0.63 MPa) Residual	
Flexural tensile strength	ASTM C78 - 04	600 psi (4.1 MPa)	28 day
Shear bond strength	ASTM D4501	291 psi (2.0 MPa)	7 day
Tensile bond strength in lab(high strength concrete as substrate)	ASTM C1583-04	244 psi (1.7 MPa)	3 day
		300 psi (2.1 MPa)	7 day
		351 psi (2.4 MPa)	10 day
		358 psi (2.5 MPa)	28 day
Flammability	ASTM E162	Flame spread index 0.67	
Heat transfer insulation		Result acceptable, suggested for applications in UK coal mine	
Freeze / Thaw	ASTM C1186	50 cycles no damage	
Permeability	ASTM D5084-03	10^{-12} meters per second	
Potable Water	TNI and EPA	Meets or exceeds EPA standards.	

TENSILE BOND STRENGTH TEST

Research at the National Institute for Occupational Safety and Health (NIOSH) concluded that conventional cement coatings fail primarily in adhesion and that this initial debonding from the underlying substrate is followed by subsequent failure in flexure and tension (Seymour et al., 2010). Values reported for adhesion strength of shotcrete in underground mines range from 29 to 218 psi (0.2 to 1.5 MPa). The wide range of values was attributed to the surface preparation and variation in formulation. The crown or roof presents the worst-case condition for shotcrete stability, because the shotcrete is rebounded during spray and affected by its own weight from the moment it is applied. When applied overhead at the recommended ¼ inch thickness, J-Crete's high adhesion characteristic minimizes such worst-case conditions.

J-Crete's tensile bond strength has been rigorously evaluated in the laboratory and in the field. Laboratory tests were conducted following American Society for Testing and Materials (ASTM) C1583. To reduce possible substrate failure, the J-Crete was sprayed on high strength concrete slabs (over 7500 psi (52 MPa) compressive strength) with a naturally cured smooth surface at a thickness of approximately .75 in (19 mm). Figure 3 shows a schematic of the test setup.

A 2-in (51-mm) diameter hole is core drilled through the J-Crete at least 0.5 in (13 mm) into the high strength concrete substrate. A steel pull disk was then attached to the cored J-Crete with an epoxy adhesive. Upon different curing age of the J-Crete, a measured pull force was applied until the specimen failed in tension at the epoxy, J-Crete, interface, or substrate. Table 2 summarizes the laboratory tensile bond strength of J-Crete along with high strength concrete. The laboratory test results indicate that the J-Crete develops high bonding strength to the substrate, over 1/3 of specimens tested broke the high strength concrete substrate.

To evaluate applicability of the product to field substrate, a series of tensile bond strength tests were conducted in a coal mine in the mid-western United States using a test setup designed and

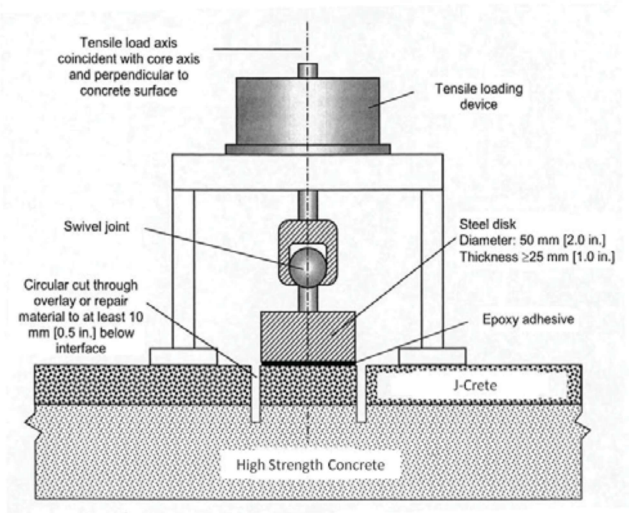

Figure 3. Schematic of bonding strength test in lab per ASTM C1583.

Table 2. Summary of laboratory tensile bond strength test results.

Sample #	Curing Age	Pull stress, psi	Failure location
1	3	244.4 (1.7 MPa)	J-Crete
2	3	200.2 (1.4 MPa)	Epoxy
3	3	220.6 (1.5 MPa)	Interface
4	7	300.2 (2.1 MPa)	J-Crete
5	8	237.4 (1.6 MPa)	Substrate
6	8	244.0 (1.7 MPa)	Substrate
7	10	351.7 (2.4 MPa)	J-Crete
8	10	320.5 (2.2 MPa)	Interface
9	10	305.6 (2.1 MPa)	Substrate
10	10	335.8 (2.3 MPa)	J-Crete
11	10	272.5 (1.9 MPa)	J-Crete
12	28	358.0 (2.5 MPa)	J-Crete
13	28	308.5 (2.1 MPa)	Substrate
14	28	333.4 (2.3 MPa)	Substrate
15	28	328.0 (2.3 MPa)	Substrate

assembled with the assistance of NIOSH, especially Mr. Brad Seymour. The testing methodology closely followed ASTM C1583 standard and the test procedure developed and implemented by Seymour, 2010.

Three test sites were selected on the rib side of a few stable pillars (Figure 4). The sites represent substrate (sandstone, medium gray shale, and coal) that J-Crete is typically sprayed on in a coal mine. To cover the uneven surface of the substrate and ensure proper attachment of the pull plate to the sample, approximately .75 in (19 mm) of J-Crete was sprayed on. A series of bonding strength tests were conducted at the sites selected. Figure 5 shows a simplified schematic drawing of the tensile bond strength test.

Figure 4. Test sites selected.

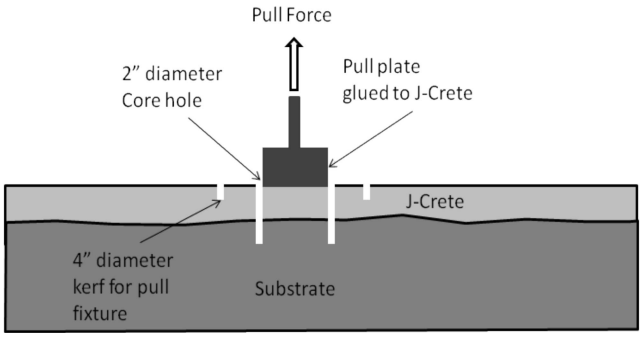

Figure 5. Simplified schematic of a tensile bond strength test.

After securing the drill stand to the rib wall with rock anchors, a dry coring bit is used to drill the 2-in (51-mm) diameter coring hole through the J-Crete coating approximately 0.5 in (13 mm) into the substrate (Figure 6), and then a 4-in (102-mm) diameter shallow kerf is drilled (Figure 7). The shallow kerf is used for seating the base of the pulling fixture. The cored specimen is cleaned, and a pull plate is attached to the J-Crete using a quick-setting, two-part, high strength epoxy adhesive (Figure 8). After the epoxy adhesive is fully cured (12–16 hours), a pulling fixture assembly is placed over the core specimen with the base of its reaction ring positioned in the kerf of the outer drill hole; the pulling fixture is secured against the rib strata with straps in three directions (Figure 9). To eliminate bending effect, the pulling force is applied through a chained connection from the specimen to the hydraulic unit. During the test, a tensile force is increasingly applied to the core specimen in a slow and steady manner until the core breaks. Listed in Table 3 is the summary of the field tensile bond strength test results. As shown by the results, the bond strength of the J-Crete exceeded the tensile strength of the sandstone, coal, and shale, and all the samples broke at the substrate. Shown in Figure 10 is a representative sample that broke at sandstone substrate. Note that the J-Crete bonding strength exceeded the tensile strength of the coal measure strata at an age of only 6 days.

Table 3. Summary of field tensile bond strength test results.

Substrata	Age, days	Pull stress, psi	Failure location	Average strength, psi
Sandstone	6	159 (1.10 MPa)	Substrate	125.3 (0.86 MPa)
Sandstone	6	91 (0.63 MPa)	Substrate	
Sandstone	6	126 (0.87 MPa)	Substrate	
Shale	6	114 (0.79 MPa)	Substrate	128.0 (0.88 MPa)
Shale	6	126 (0.87 MPa)	Substrate	
Shale	6	144 (0.99 MPa)	Substrate	
Coal	8	108 (0.74 MPa)	Substrate	100.0 (0.69 MPa)
Coal	8	96 (0.66 MPa)	Substrate	
Coal	8	96 (0.66 MPa)	Substrate	

Figure 6. Test specimen coring.

To determine flexural tensile strength of the J-Crete material, several prism specimens were prepared (Figure 11) and cured in the field. Upon 28 day cure, testing for four-point flexural bending per ASTM C78-04 resulted in 600 psi (4.1 MPa) (Table 1). Prior laboratory 28 day three-point flexural bending pursuant to ASTM 348-08 indicated 995 psi (6.9 MPa) of flexural strength (Table 1). The four point bending test estimates the tensile strength of the outermost fiber of the beam, and is expected to yield a lower value.

MINE ENTRY REHABILITATION

Strata in underground mine openings is often subject to gradual weathering over time due to moisture absorption and air contact. Moisture sensitive strata such as weak shale, black shale, clay stone, clayey shale, fireclay, etc., may deteriorate, lose strength, and fall unexpectedly. Figure 12 shows a belt entry in an underground coal mine. The skin between the roof bolts, roof channel, and roof pan has weathered over time and collapsed. Therefore, prevention of the strata deterioration by moisture, air, and gradual weathering are imperative for effective surface control.

The short-term benefits of J-Crete are the immediate alleviation of cutters, sloughing, flaking, and surface saturation. The long-term benefits are the same regarding pillar protection and roof control. However, using J-Crete in a preventative rather than reactionary application will increase personnel safety and productivity. These benefits have been demonstrated by the tensile bond strength tests described above and with the application of over 150,000 ft^2 (14,000 m^2) of J-Crete. The J-Crete demonstrated a very positive effect on surface control and has the potential to reduce cutter roof deterioration (Figure 13).

WATER SEALING

Water damage control aspects of J-Crete have also been demonstrated in a coal mine in the Midwest. The mine extracts a 4.2-ft (1.3-m) thick coal seam that is covered by a dark gray or black shale immediate roof and underlain by approximately 2-ft (0.6-m) thick fireclay immediate floor strata. A portion of the mine under a surface stream valley where the four main entries were developed was an especially challenging situation. The area has approximately 80 ft (24 m) of overburden strata due to the valley topography. Cracks exist in the overburden strata underneath the creek. Surface water seeps through the cracks and flows into the main entries of that area at an approximate rate of 75 gallons (284 liters) per minute as reported by mine management. Water presence in the mine entries created severe damage to the fireclay floor strata. Fireclay in the entry floor turned into mud, and the same material was squeezed out from pillar base (Figure 14). The fireclay under the coal pillars lost strength due to excessive water and deterioration. The effective pillar size was reduced significantly due to the loss of the rib base (Figure 15), which may be a precursor to pillar failure and possible roof collapse.

Figure 7. Shallow kerf preparation.

Figure 8. Pull plate attachment.

Figure 9. Field tensile bonding strength test.

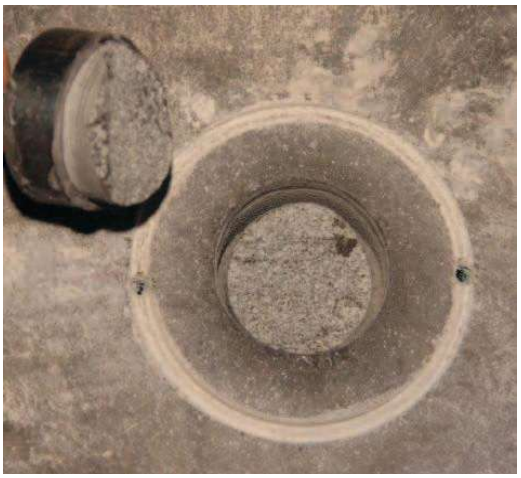

Figure 10. Failure on sandstone substrate.

Figure 11. Flexural (ASTM C78) samples prepared in the field.

Figure 12. Example of deteriorated mine entry.

In this particular case, Jennchem was called to remedy the problem of deteriorating pillars due to excessive air and water exposure onto the fireclay that was exposed on the lower 2 ft (0.6 m) of the pillars. This created a significant concern for the mine, as the fireclay was throughout the four main entries. Fireclay in its natural state is a strong material, however, when exposed to water, it loses significant strength and the resultant mud impedes the movement of mining equipment.

Figure 13. J-Crete applied in a mine entry.

Figure 14. Fireclay strata in presence of water.

Figure 15. Close view of the base of a pillar corner.

The Jennchem recommendation was to install the J-Crete product from top to bottom of the rib at a .25 in (6 mm) thickness. The J-Crete technicians arrived and working with the mine personnel and contractors, all four main entries were sprayed within seven weeks. The application of J-Crete to the ribs stopped the flow of water through the ribs and allowed the fireclay to dry and stiffen significantly, thus making the fireclay an integral part of the structure rather than a decaying component. Figure 16 shows the belt entry after the J-Crete installation.

Figure 16. Wet area remedied by J-Crete.

OTHER APPLICATIONS

In another instance, Jennchem was called to evaluate rib sloughing in a maintenance area. The engineers had determined that high-pressure water hoses were being used to wash down mining equipment, and the previously installed material was re-emulsifying, softening, and delaminating. J-Crete was installed from a height of 8 ft to the bottom of the rib. Within 48 hours, the maintenance crew was washing down their mining equipment under high pressure and the J-Crete protected the ribs, resulting in no further deterioration. Over a year after J-Crete installation, the mine reports outstanding performance of the material with no signs or indications of weakening in any area of performance or strength.

Multiple highwalls have been successfully protected from weathering and deterioration (Figure 17). A ventilation shaft into a coal mine was likewise protected with J-Crete (Figure 18). In a novel application, J-Crete was used to support the roof and exposed high areas, to strengthen strata integrity, and to beautify a cave designed as a public attraction (Figure 19).

In other areas, Jennchem engineers have been called upon to evaluate deteriorating pillars and cutter roof in coal mines (Figure 20), trona mines, and lime rock mines. The deterioration consisted of weak coal, such as Blue Creek, in the coal mines; excessive air causing the trona to flake in the trona mines; or preventative maintenance in a lime rock mine.

GENERAL METHODOLOGY

J-Crete is applied with either diesel (Figure 21) or electric hydraulic (Figure 22) pumping equipment. The electric unit is capable of being utilized in low vein mines and for higher clearance or surface applications, whereas diesel equipment is utilized where permissible. The low vein electric hydraulic J-Creter has its own on board air compressor that provides a constant 130 cfm /100 psi (3.7 m^3/min / 0.7 MPa) at the nozzle. This air supply is a key component to a high production application as well as ensuring that the J-Crete is applied with force into the small cracks in the strata and for proper verification of the mixture, which facilitates curing and proper fiber distribution. The entire unit is 6 ft (1.8 m) wide, 10 ft (3 m) long, and only 40 in (1 m) high, and it runs off one 480 v 3-phase motor.

Figure 17. Highwall protection.

Figure 18. Ventilation shaft application.

Figure 19. Public cave support application.

Figure 20. Claystone cutter support.

Figure 21. Diesel mixer and pump.

Figure 22. Electric mixer, pump, and air compressor.

SUMMARY AND CONCLUSIONS

The mining industry has long been searching for an effective structural material that prevents weathering and falls of loose rock, debris, and sediments, and that provides additional structural integrity. J-Crete is an engineered, cementitious, fiber-reinforced composite rock coating mixture specifically designed, tested, and successfully utilized as such a material. Rigorous laboratory and field evaluations have resulted in a solid understanding of J-Crete capabilities. Success in various engineering applications to date has demonstrated the potential of J-Crete. However, each project is different, requires specific engineering consideration, and should be evaluated on a case by case basis.

REFERENCES

ASTM C109 / C109M - 08 Standard Test Method for Compressive Strength of Hydraulic Cement Mortars . American Society for Testing and Materials.

ASTM C348 - 08 Standard Test Method for Flexural Strength of Hydraulic-Cement Mortars. American Society for Testing and Materials.

ASTM C1399 Standard Test Method for Obtaining Average Residual-Strength of Fiber-Reinforced Concrete. American Society for Testing and Materials.

ASTM C78 / C78M - 4 Standard Test Method for Flexural Strength of Concrete (Using Simple Beam with Third-Point Loading). American Society for Testing and Materials.

ASTM D4501 Standard Test Method for Shear Strength of Adhesive Bonds Between Rigid Substrates by the Block Shear Method. American Society for Testing and Materials.

ASTM C1583 /C1583M-04 Standard Test Method for Tensile Strength of Concrete Surfaces and the Bond Strength or Tensile Strength of Concrete Repair and Overlay Materials by Direct Tension (Pull-off Method). American Society for Testing and Materials.

ASTM E162 Standard Test Method for Surface Flammability of Materials Using a Radiant Heat Energy Source. American Society for Testing and Materials.

ASTM C1186 Standard Specification for Flat Fiber Cement Sheets. American Society for Testing and Materials.

ASTM D5084-03 Standard Test Methods for Measurement of Hydraulic Conductivity of Saturated Porous Materials Using a Flexible Wall Permeameter. American Society for Testing and Materials.

Clark, C.C., Stepan, M.A., Seymour, J.B., Martin, L.A. (2010). “Report on early strength performance of modern day weak rock mass shotcrete mixes.” SME Preprint 10-138, SME Annual Meeting. Society for Mining, Metallurgy and Explorations.

Kuchta, M. (2003). “Shotcrete adhesion tests at NIOSH’s Lake Lynn Laboratory (TR4-2),” Project Report, National Institute for Occupational Safety and Health.

Seymour, B., Martin, L., Clark, C., Stepan, M., Jacksha, R., Pakalnis, R., Roworth, M., Caceres, C. (2010). “A practical method of measuring shotcrete adhesion strength.” SME Preprint 10-137, SME Annual Meeting. Society for Mining, Metallurgy and Exploration.

The Load Transfer Properties of Post–Groutable Cable Bolts Used in the Australian Coal Industry

Rob Thomas, Principal
Strata Engineering (Australia) Pty Ltd
Charlestown, Australia

ABSTRACT

Adequate load transfer is considered essential for optimum ground support and is increasingly important in weak roof and/or high stress environments. If adequate load transfer is achieved not only can this have a positive impact on the resulting roof behavior, but it may also allow the use of lower and hence more economic densities of roof support.

A wide variety of post-groutable cable bolts are currently in use in the Australian coal mining industry, each of varying capacity, design, and grouting methodology. Though all of the cables are supplied with the appropriate steel specification, strength, and modulus data, the Australian coal mining industry does not have access to a comprehensive and comparative database on the corresponding load transfer performance, which is a critical problem.

On the basis of the above, this paper describes the methodology and results of a laboratory pull testing program that aims to assess the impact of cable bolt design on load transfer, and specifically, the impact on the capacity and stiffness of the anchorage.

As part of the testing program, 19 cables were tested including (1) plain-strand cables installed in holes drilled with 28 to 55 mm diameter drill bits and (2) bulbed and nutcaged cables installed in holes drilled with 42 to 64 mm diameter drill bits. Other parameters assessed included the significance of smooth and profiled wire, wire packing, and expanded geometry bulbs.

The main results of the testing indicate that in comparison to plain-strand cables, if the cable is bulbed or nutcaged, the capacity of the anchor can increase by up to 400%, and the peak stiffness by between one and two orders of magnitude. The results also indicate that increasing hole diameter may have a positive impact on load transfer in the case of bulbed or nutcaged cables and a negative impact on plain-strand cables. No conclusive results were obtained with regard to the impact of grout strength on load transfer.

INTRODUCTION

There are many factors to consider when selecting the most appropriate cable bolt for a specific geotechnical application: cost, ease of installation, availability, quality control, desired support mechanism, capacity, grouting method, and collar arrangement. However, fundamental to the success or failure of a cable bolt is its ability to transfer load, and in doing so, provide resistance to bed separation. Therefore, while all of the above factors will still need to be considered, it is nonetheless imperative that the load transfer properties of cable bolts are understood. If applied correctly, this knowledge will increase the likelihood that the most appropriate cable bolt will be installed for the anticipated range in ground conditions.

In Australia, this decision making process is complicated by view of the fact that currently there are around 15 different types of groutable cable bolts available (14 of which are assessed in this paper), each with different strand designs, capacity, grouting method, and hole size.

In addressing the above, this paper therefore aims to provide a database on the load transfer properties of the various cable bolts currently available to the Australian underground coal industry.

FUNDAMENTAL ASPECTS OF CABLE BOLT LOAD TRANSFER

In its simplest terms, when rock fractures, load is transferred from the unit of rock located below the fracture plane to the unit of rock located above the fracture plane through tension in the cable bolt (see Figure 1). This transfer in load is a result of the mechanical interlock achieved between the irregular surface profile of the cable bolt and the side of the borehole wall. Critically, the adhesive property of grout is insignificant and in the range of 10 kN per 200 mm of bond length on a 15.2mm diameter plain strand cable (Hutchinson and Dierdrichs, 1996).

As illustrated in Figure 2, there are several means (depending, for example, on the strength of the rockmass and grout) by which a cable bolt can fail. However, for the purpose of this assessment if it is assumed that the “weak link” in the system is the cable to grout interface, the cable to rock load transfer mechanism can best be described in the following steps (see Figure 3):

Step 1— The rock fractures and in doing so, a separation plane develops in the rockmass.

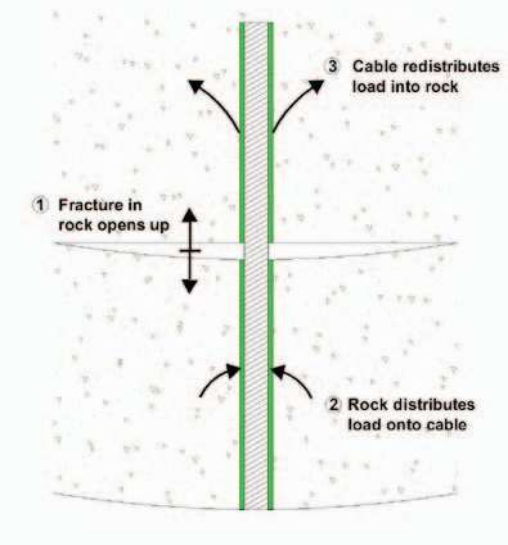

Figure 1. Schematic illustration of the load transfer concept.

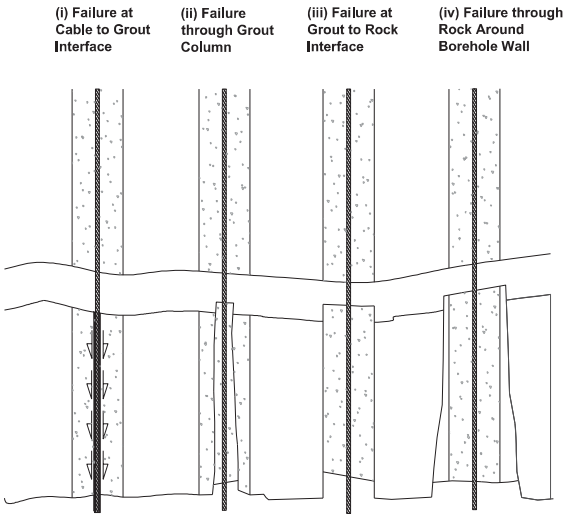

Figure 2. Schematic illustration of the four modes of load transfer related failure in a cable bolt.

Step 2—After the adhesive capacity of the cable to grout interface has been exceeded, the rock and grout slip around the cable.

Step 3—As the irregular surface profile of the cable creates a mirror, and therefore irregular impression in the grout, with ongoing roof displacement, the ridges of grout (or flutes) will ride up and over the cable wires.

Step 4—As the grout ridges try to ride up and over the cable wires, the grout compresses against the wall of the borehole and in doing so, generates confining stress along the cable to grout interface.

Step 5—As a result of the confining stress, the shear strength of the cable to grout interface increases and in doing so, the cable locks into the rockmass and starts to load up.

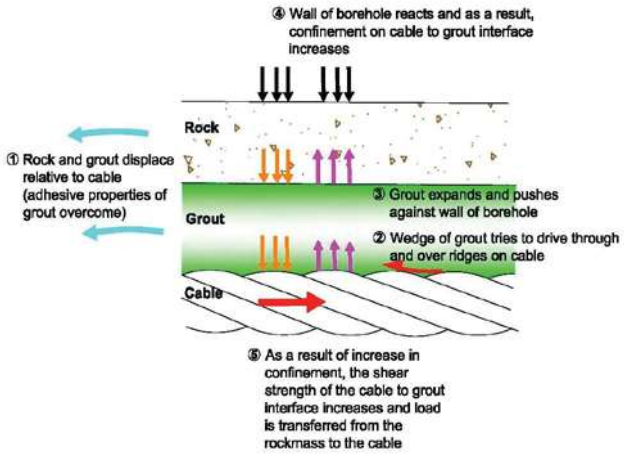

Figure 3. Detailed illustration of theload transfer concept.

Step 6—As the cable loads up, the length of cable located above the fracture plane slips relative to the grout and by the same expansion and compression process described above, the load that has been accumulated in the cable is transferred back to the rockmass.

The process described above is called dilation. As shown in Figure 4, the more the rock displaces, the greater the dilation and as such, the more load is transferred onto the cable i.e., until such a point that the build-up in stress exceeds the strength of the cable to grout interface and the cable starts to lose load.

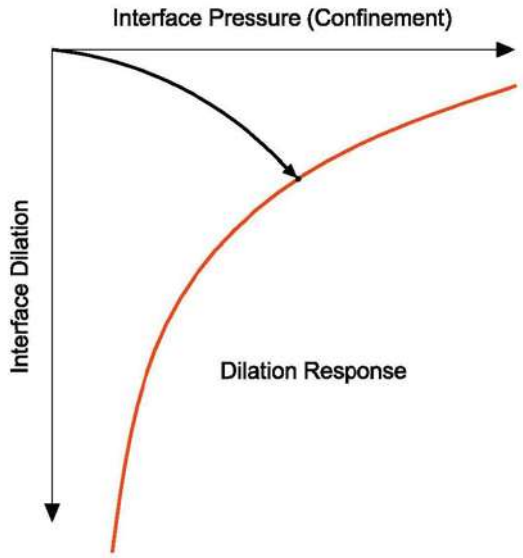

Figure 4. Schematic illustration of inferred relationship between interface dilation and borehole confinement.

Although it is generally agreed that the magnitude of dilation (and hence the magnitude of mechanical interlock) is controlled by numerous factors including grout strength, grout stiffness, and rock stiffness (Hutchinson and Dierdrichs, 1996)—as will

be discussed in this paper—the geometry of the cable is also of particular importance.

TESTING PROCEDURE

The typical method for assessing cable bolt performance in a laboratory is to install a sample of the cable into two adjoining steel tubes and load the tubes axially in tension. This is commonly referred to as a Double Embedment Pull Test (DEPT). The apparatus used for the DEPT is shown in Figure 5. Though this test offers a repeatable means of assessment, due to the use of steel tubes, it does not include any means of assessing the grout to rock interface.

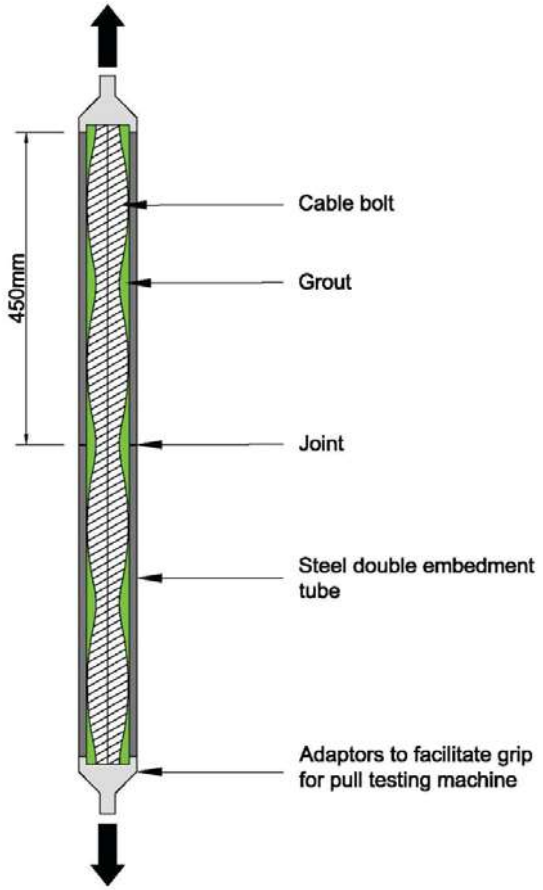

Figure 5. Double Embedment Pull Test (DEPT) setup.

A variation to the DEPT is the Laboratory Short Encapsulation Pull Test (LSEPT) developed by RMT Ltd (Clifford et al., 2001), which allows an assessment of the grout to rock interface and hole rifling, and as such, better simulates the underground environment. As shown in Figure 6, the LSEPT involves the installation of the test sample into a sandstone core, which itself is locked into a biaxial pressure cell. One of the main benefits of this method therefore is the perceived ability of the biaxial cell to simulate the underground environment through the application of 10 MPa confining pressure to the sandstone core.

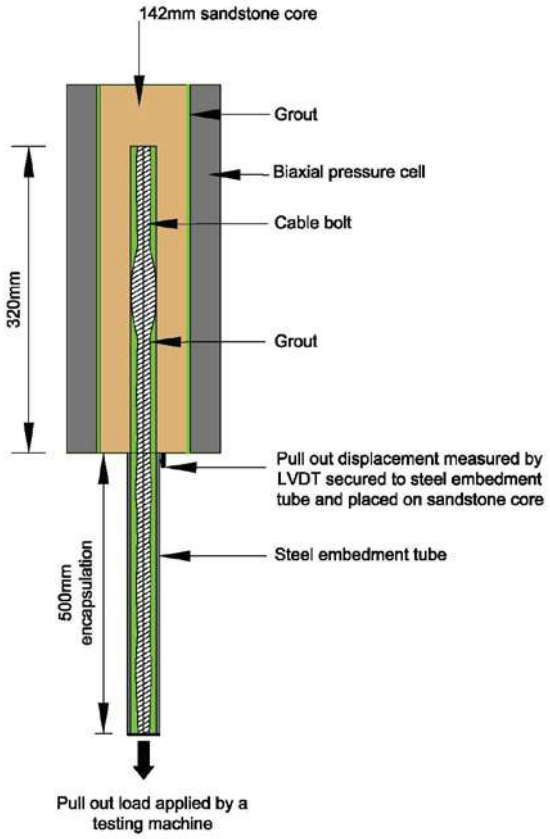

Figure 6. Laboratory Short Encapsulation Pull Test (LSEPT) setup.

As part of this study, however, modifications were required to the LSEPT testing procedure, because it was found that the biaxial cell setup could not resist cable rotation, which caused some of the plain-strand cables tested to unwind out of the core under load, thereby giving anomalously low pull out load and stiffness results.

In addition to the above, it was also assessed that the 10 MPa confinement imparted onto the core through the biaxial cell is not necessarily a true and consistent reflection of the underground environment in that (1) very little is known in regard to the *in situ* magnitude of borehole closure in underground coal mines and (2) it is almost certainly a dynamic variable that will vary both along the length of the cable and during the "life" of the cable.

Further to this, it was also found that the applied confining pressure has a very significant impact on the strength and stiffness of the cable and as such, it was a concern that almost any variation in the applied pressure could have a misleading or masking impact on the measured results. Note in Figure 7 the increased strength and stiffness of the cable tested in the biaxial cell compared to that tested in a passive steel cylinder.

On the basis of the above, the sandstone core was therefore grouted into a thick-walled steel cylinder and the whole assembly locked with an anti-rotation device so as to prevent the cable from unwinding out ofthe core when the load was applied (see Figure 8).

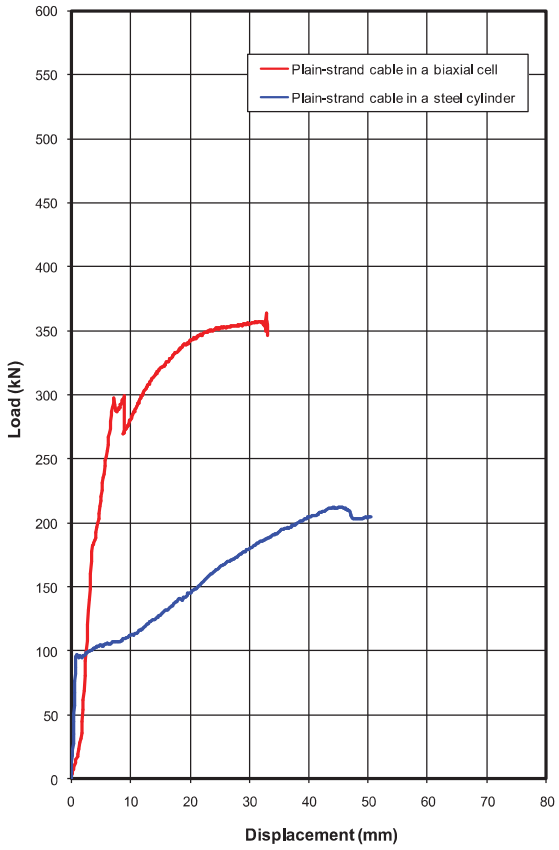

Figure 7. Load vs.displacement curves for two plain-strand cables showing the impact of active (i.e., biaxial cell) and passive (i.e., steel cylinder) versions of the LSEPT.

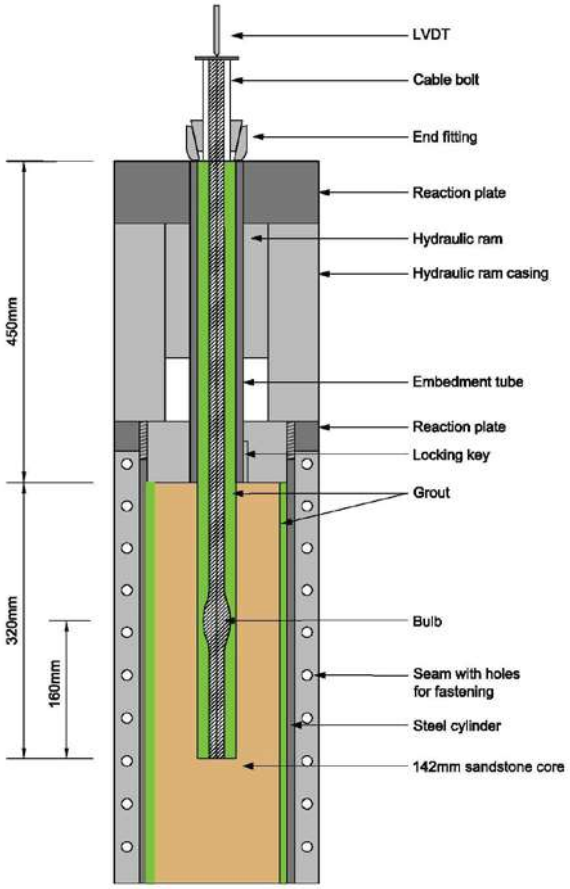

Figure 8. Modified version of the Laboratory Short Encapsulation Pull Test incorporating a steel cylinder.

Other points of note with regard to the testing procedure used in this assessment are summarized below:

- The diameter of the sandstone core was 142 mm and the Unconfined Compressive Strength (UCS) of the sandstone typically ranged between 19 and 25 MPa.
- The cables tested were between 770 and 1000 mm long: (1) 320 mm of the cable was grouted into the sandstone core, and (2) 450 mm of the cable was grouted into the steel tube. If the cable included a bulb, the center of the bulb was positioned 160 mm from the bottom of the hole drilled into the sandstone core.
- In order to ensure the cable did not slip in the steel tube, (1) where appropriate, a bulb was also positioned in the steel tube, and in all cases (2) the appropriate barrel and wedge or nut fitting was fixed to the cable.
- In order to better simulate the underground environment, where applicable, the appropriate grout tubes and breather tubes were also fixed to the cable and grouted into the sandstone core.
- The drill rod used was slightly bent so as to create a rifling effect in the hole and in all cases, twin-wing tungsten carbide bits were used.
- Depending on the cable used, one of six different sized drill bits were used. In some cases the same cable was tested in different sized holes.
- In regard to the resulting size of the holes drilled into the sandstone, (1) the 28 mm drill bits generally resulted in 28.5 to 30 mm diameter holes; (2) the 42 mm bits, 45 to 47 mm diameter holes; (3) the 45 mm bits, 50 to 51 mm diameter holes, (4) the 52 mm bits, 56 to 58 mm diameter holes, (5) the 55 mm bits, 59 to 61 mm diameter holes, and (6) the 64 mm bits, 69 to 71 mm diameter holes.
- CBG grout (manufactured by Tarmac Ltd in the UK) was used for all tests. CBG grout is a non-shrink, high flow grout comprising Portland Cement, pulverized fuel ash, and selected additives. The grout was mixed with a water to cement ratio of 0.3 and achieved a nominal UCS of 80 to 100 MPa.
- Once the core and steel tube was filled with the pre-mixed grout, the cable was then inserted into the core and the steel tube. Following installation, the cable was then rotated to ensure full grout coverage and as far as is practically possible, located centrally within the core.
- The hydraulic ram was powered by a compressed air powered pump, and in the initial stages of the tests (i.e., before the anchor started to yield), the load was applied at an approximate rate of 10 kN per second.
- Where possible three tests were conducted for each cable.

CABLES TESTED

Four types of cable are currently used in Australian coal mines: (1) plain-strand cables, (2) bulbed cables where during manufacture the cable is clamped between two hydraulic grips and crimped in the intervening section to form a deformed bulb, (3) nutcage cables where a plain-strand cable is unwound and the resulting space filled with a spacer of some form to create a deformed bulb, and (4) modified plain-strand cables where some form of indentation is cut or rolled onto the surface of the cable (see Figure 9).

The cables tested as part of this assessment and their relevant parameters are summarized in Table 1.

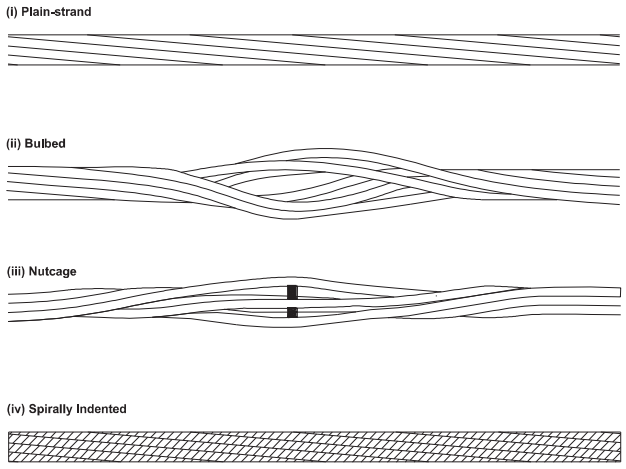

Figure 9. Schematic illustration of the various cable types used in Australian coal mines.

RESULTS

The main points of note from the testing can be summarized as follows:

- All cables reached their peak elastic load after 1 to 5 mm of displacement (see Table 2 and Figures 10 to 12). The elastic load was determined as the point when the system stiffness reduced to less than 20 kN/mm.
- The plain-strand cables typically result in a reasonably low peak elastic load and following the onset of inelastic behavior and/or a corresponding sudden reduction in load, (1) the load either starts to increase at a steady but decreasing rate or (2) in the case of the Hilti spirally indented cable and plain-strand Megastrand, maintains a reasonably high residual load (see Table 2 and Figure 10). Because the indented cables have a more irregular surface profile and the plain-strand Megastrands are made out of large (i.e., around 7 mm diameter) individual wires between which the grout is able to permeate, it is assumed that the peaks and troughs in the load/displacement profile reported in these tests is related to the ability of these more aggressively profiled cables to repeatedly shear and lock up against the ridges (or flutes) of grout formed around the cable. This is best explained as a "slip/lock" mechanism.
- Compared to the plain-strand cables, the bulbed and nutcaged cables typically result in higher peak elastic loads and following the onset of inelastic behavior, a further and more significant increase in load after around 10 to 20 mm of displacement (see Table 2 and Figures 11 and 12). The reduction in load recorded following the peak load with the bulbed and nutcaged cables was however unexpected and is probably related to the magnitude of load retained on the anchor immediately prior to it yielding and the associated generation of high shear stresses at the cable to grout interface. Although a more controlled cyclic residual loading profile was anticipated with the bulbed and nutcaged cables (i.e., as per the "slip / lock" mechanism discussed above and shown in Figure 13), it is assessed that this "stripping" of the anchor may at least in part explain how cables behave in very high deformation environments and may therefore serve to "protect" the cable.
- The majority of the cables failed at the cable to grout interface. The only exceptions to this being the HLT Megastrand cables where on some (not all) occasions the cable located below the bulb failed at the grout to rock interface and the cable located above the bulb, at the cable to grout interface.
- As it appears almost inevitable that the anchor will yield and that cables are more often than not installed in aggressive geotechnical conditions where the roof is expected to displace several 10s of millimeters, of most relevance is the peak load and the magnitude of displacement required to achieve this peak load.
- In order to provide a combined value or rating for both the magnitude of the peak load and corresponding peak stiffness of the cable, the following Load Transfer Index is proposed:

$$\text{Load Transfer Index} = \frac{\text{Peak Load}}{\text{Displacement at Peak Load}} \quad (1)$$

- This formula therefore indicates that the higher the peak load and the lower the corresponding amount of displacement required to achieve the peak load, the higher the Load Transfer Index, and by implication therefore, the greater the load transfer.
- The Load Transfer Indices are summarized in Table 3 and from this data it is evident that the bulbed and nutcaged cables report values that are generally an order of magnitude higher than those achieved on the plain-strand cables.
- The peak loads are ranked in Table 4 and from this data it is evident that the triple-strand cables achieve the highest peak loads, followed by the standard and HLT Megastrands, the twin-strand cables and lastly, the plain-strand cables. Of theplain-strand cables, the MB9 Megastrand and TG cable retain the highest loads.
- Similarly, the Load Transfer Indices are ranked in Table 5 and from this data it is evident that the MW9 HLT Megastrand achieves the highest value, followed by the remaining Megastrands (including the plain-strand MB9 cable), the spirally indented Hilti cable, the triple-strand cables, twin-strand cables and the remaining plain-strand cables. Of the plain-strand cables, the MB9 Megastrand and Hilti spirally indented cables report the highest values.

- Accepting that there does not appear to be a conclusive relationship between peak load and Load Transfer Index, and grout strength, it is nonetheless of note that (1) despite measuring some of the highest loads and stiffness values, the MW9 and MW10 HLT Megastrands were encapsulated with 63 to 71 MPa grout and (2) despite being encapsulated with 103 to 107 MPa grout, the MB12 HLT Megastrand did not report significant and consistently higher peak loads or peak stiffness values than the MW9 and MW10 HLT Megastrands (see Tables 4 and 5 and Figure 12). As a means of comparison, all of the remaining cables were anchored in grout which reported UCS values of between 80 and 100 MPa. It is also of note that grout strength may explain why the 19 wire plain-strand Hilti cable reported a higher peak load and Load Transfer Index than the 19 wire plain-strand JSS cable, as even though both cables were installed in holes drilled with a 28 mm bit, compared to the JSS cables which were encapsulated with 80 to 90 MPa grout, the Hilti cables were encapsulated with 94 to 99 MPa grout (see Tables 4 and 5 and Figure 10).
- Although not conclusive, in regard to the significance of hole diameter, it is nonetheless of note that (1) the peak load and Load Transfer Index values measured on the twin and triple-strand cables are higher in the larger hole diameters and (2) conversely, with the plain-strand JSS and HI-TEN cables, the peak load and Load Transfer Index values reduced in the larger hole diameters (see Tables 4 and 5 and Figure 10).
- Other points of note from the testing include the low peak load and Load Transfer Index values reported for the Mambo cable. Although it is not possible in view of the limited number of tests conducted to provide a definitive answer in this regard, it is assumed that this is related to the large number of wires (i.e., 21) in a Mambo cable and the consequent inability of the grout to permeate into the “weave” of the cable. This also probably explains the low peak load and Load Transfer Index results obtained for the 21 wire HI-TEN cable (see Tables 4 and 5 and Figures 10 and 11).

Table 1. Summary of cable bolts tested.

	Axial Capacity	Strand Type	Cable Diameter	Drill Bit Diameter
TG	620 kN	Plain-strand	28 mm	42 mm
JSS - 19 wire cable	590 kN	Plain-strand	21.8 mm	28 mm
JSS - 19 wire cable	590 kN	Plain-strand	21.8 mm	42 mm
JSS - 19 wire cable	590 kN	Plain-strand	21.8 mm	55 mm
HI-TEN - 21 wire cable	610 kN	Plain-strand	23.5 mm	45 mm
Hilti - 19 wire plain-strand	590 kN	Plain-strand	21.8 mm	28 mm
Hilti - 19 wire spirally indented strand	590 kN	Spirally indented plain-strand	21.8 mm	28 mm
MB9 Megastrand	590 kN	Plain-strand	31 mm	42 mm
Bowen - 19 wire cable	590 kN	Nutcage	21.8 to 32 mm	42 mm
Mambo - 21 wire cable	610 kN	Nutcage	23.5 to 34 mm	42 mm
Garford twin-strand	530 kN	Bulbed	15.2 to 28 mm x 2 cables	52 mm
Garford twin-strand	530 kN	Bulbed	15.2 to 28 mm x 2 cables	55 mm
Garford twin-strand	530 kN	Bulbed	15.2 to 28 mm x 2 cables	64 mm
Garford triple-strand	795 kN	Bulbed	15.2 to 28 mm x 3 cables	55 mm
Garford triple-strand	795 kN	Bulbed	15.2 to 28 mm x 3 cables	64 mm
MW9 Megastrand	590 kN	Nutcage	31 to 36 mm	42 mm
MW9 HLT* Megastrand	590 kN	Nutcage	31 to 46 mm	52 mm
MW10 HLT* Megastrand	685 kN	Nutcage	31 to 46 mm	52 mm
MB12 HLT* Megastrand	785 kN	Nutcage	31 to 46 mm	52 mm

Note:* HLT = High Load Transfer

Table 2. Summary of pull test results.

	Avg Peak Elastic Load	Avg Displacement at Peak Elastic Load	Avg Peak Load	Avg Displacement at Peak Load
Plain-strand Cables				
TG - 19 wire cable in a 42mm hole*	208 kN	2mm	325 kN	48 mm
JSS - 19 wire cable in a 28 mm hole	61 kN	1 mm	161 kN	47 mm
JSS - 19 wire cable in a 42 mm hole	77 kN	1 mm	144 kN	50 mm
JSS - 19 wire cable in a 55 mm hole	55 kN	1 mm	134 kN	57 mm
HI-TEN - 21 wire cable in 45 mm hole	50 kN	1 mm	87 kN	35 mm
Hilti - 19 wire plain-strand in a 28 mm hole	142 kN	3 mm	215 kN	40 mm
Hilti - 19 wire spirally indented strand in a 28mm hole	323 kN	5 mm	323 kN	5 mm
MB9 Megastrand in a 42 mm hole	360 kN	3 mm	378 kN	5 mm
Bulbed Cables				
Bowen - 19 wire cable in a 42mm hole	182 kN	2 mm	309 kN	19 mm
Mambo - 21 wire cable in a 42mm hole	73 kN	1 mm	201 kN	47 mm
Garford twin-strand in a 52 mm hole	176 kN	2 mm	308 kN	15 mm
Garford twin-strand in a 55 mm hole	289 kN	3 mm	383 kN	14 mm
Garford twin-strand in a 64 mm hole	251 kN	2 mm	400 kN	14 mm
Garford triple-strand in a 55 mm hole	337 kN	3 mm	504 kN	13 mm
Garford triple-strand in a 64 mm hole	309 kN	3 mm	479 kN	12 mm
Nutcaged Cables				
MW9 Megastrand in a 42 mm hole**	402 kN	2 mm	458kN	5 mm
MW9 HLT Megastrand in 52 mm hole	410 kN	3 mm	429 kN	3 mm
MW10 HLT Megastrand in a 52 mm hole	364 kN	4 mm	449 kN	12 mm
MB12 HLT Megastrand	313 kN	2 mm	453 kN	15 mm

Note:
* average value based on two successful tests.
** only one successful test obtained.

CONCLUSIONS

A short encapsulation laboratory based pull testing methodology has been developed which more accurately reflects the underground environment, in that it prevents cable rotation and does not include a biaxial cell which through the applied confinement, can result in misleading results.

The results of the testing indicate that in comparison to plain-strand cables, if the cable is bulbed or nutcaged, the capacity of the anchor can increase by up to 400% and the peak stiffness by between one and two orders of magnitude. Although not conclusive, the results also indicate that increasing hole diameter may have a positive impact on load transfer in the case of bulbed or nutcaged cables and a negatve impact on plain-strand cables. No conclusive results were obtained with regard to the impact of grout strength on load transfer.

Lastly, in regard to areas of future research, additional work is recommended on (1) the post-peak performance of high load transfer capacity cables and (2) the role of hole size and grout strength on load transfer, particularly in weak rockmasses.

ACKNOWLEDGMENTS

The author would like to thank the following for their support and help in this project: (1) Megabolt (in particular Ron McKenzie and Joe Hetherington), Jennmar (in particular Peter Craig), DSI, and Hilti for supplying the cables and part-funding the project, (2) the many Australian coal mines for funding the project, (3) Golder Associates for the testing, and (4) Mr. Michael Callan (LDO Mining) for his initial contribution to the project.

REFERENCES

Clifford, B., Kent, L., Altounyan, P., Bigby, D. (2001). Developments in Long Tendon Systems used in Coal Mining Reinforcement. In: *Proceedings of the 20th International Conference on Ground Control in Mining.* pp. 235–241.

Hutchinson, D.J., Diedrichs, M.S. (1996). *Cablebolting in Underground Mines*. BiTech Publishers Ltd.

Hyett, A.J, Bawden, W.F and Hedrick, N. (1994). *The 25mm Garford Bulb Anchor for Cable Bolt Reinforcement - Part 1: Laboratory Results.* CIM Bulletin, May 1994.

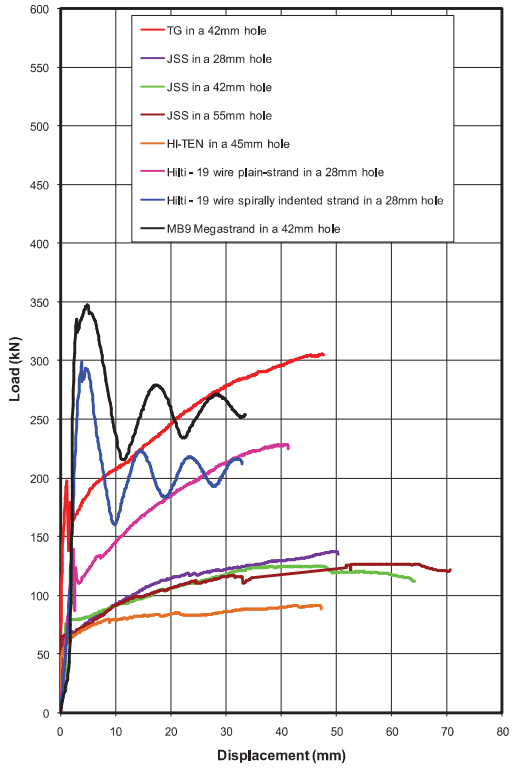

Figure 10. Median plain-strand cable results.

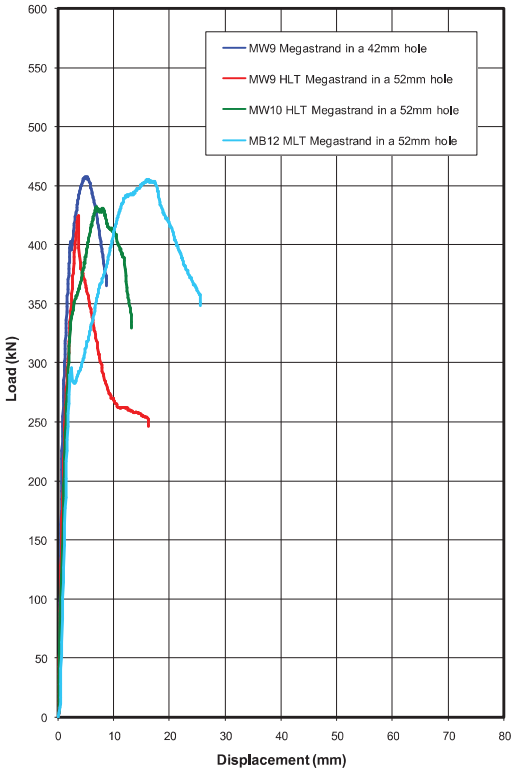

Figure 12. Median nutcage cable results.

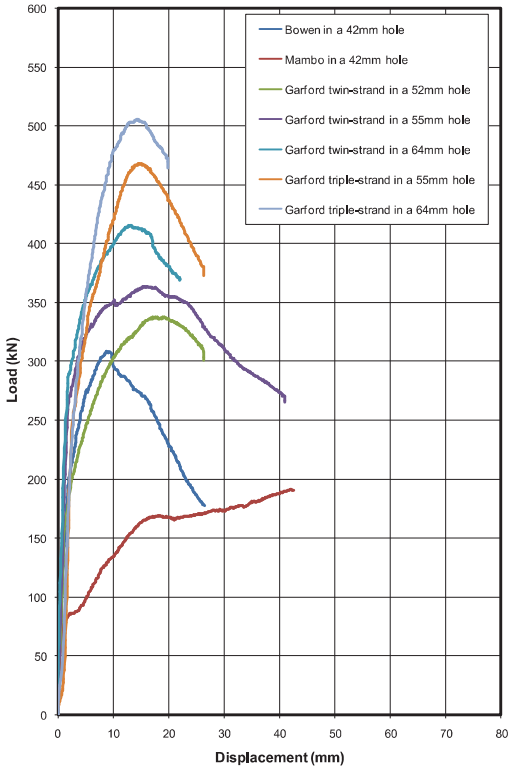

Figure 11. Median bulbed cable results.

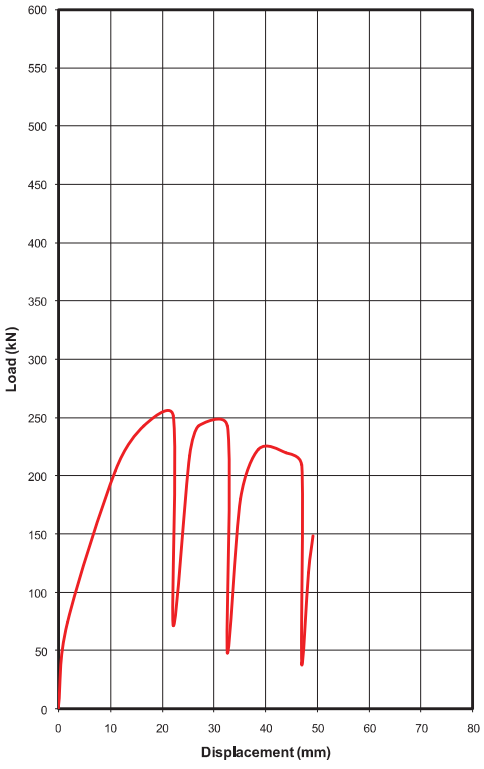

Figure 13. Load vs. displacement curve for a single-strand bulbed Garford cable (Hyett et al., 1994).

Table 3. Summary of pull test results showing calculated average peak load transfer indices.

Plain-strand Cables	
TG in a 42mm hole*	7
JSS - 19 wire cable in a 28 mm hole	4
JSS - 19 wire cable in a 42 mm hole	3
JSS - 19 wire cable in a 55 mm hole	2
HI-TEN - 21 wire cable in a 45 mm hole	3
Hilti - 19 wire plain-strand in a 28 mm hole	5
Hilti - 19 wire spirally indented strand in a 28mm hole	69
MB9 Megastrand in a 42 mm hole	85
Bulbed Cables	
Bowen - 19 wire cable in a 42mm hole	22
Mambo - 21 wire cable in a 42mm hole	4
Garford twin-strand in a 52 mm hole	22
Garford twin-strand in a 55 mm hole	27
Garford twin-strand in a 64 mm hole	28
Garford triple-strand in a 55 mm hole	38
Garford triple-strand in a 64 mm hole	39
Nutcaged Cables	
MW9 Megastrand in a 42mm hole**	92
MW9 HLT Megastrand in a 52mm hole	126
MW10 HLT Megastrand in a 52mm hole	43
MB12 HLT Megastrand in a 52mm hole	33

Note:
* - average value based on two successful tests.
** - only one successful test obtained.

Table 4. Order of load capacity performance.

Rank	Cable Type	Load
1	Garford triple-strand in a 55 mm hole	504 kN
2	Garford triple-strand in a 64 mm hole	479 kN
3	MW9 Megastrand in a 42mm hole**	458 kN
4	MB12 HLT Megastrand in a 52mm hole	453 kN
5	MW10 HLT Megastrand in a 52mm hole	449 kN
6	MW9 HLT Megastrand in a 52mm hole	429 kN
7	Garford twin-strand in a 64 mm hole	400 kN
8	Garford twin-strand in a 55 mm hole	383 kN
9	MB9 Megastrand in a 42 mm hole	378 kN
10	Garford twin-strand in a 52 mm hole	341 kN
11	TG in a 42mm hole*	325 kN
12	Hilti - 19 wire spirally indented plain-strand in a 28mm hole	323 kN
13	Bowen - 19 wire cable in a 42mm hole	309 kN
14	Hilti - 19 wire plain-strand in a 28mm hole	215 kN
15	Mambo - 21 wire cable in a 42mm hole	201 kN
16	JSS - 19 wire cable in a 28 mm hole	161 kN
17	JSS - 19 wire cable in a 42 mm hole	144 kN
18	JSS - 19 wire cable in a 55 mm hole	134 kN
19	HI-TEN - 21 wire cable in a 45 mm hole	87 kN

Note:
* - average value based on two successful tests.
** - only one successful test obtained.

Table 5. Order of load transfer performance.

Rank	Cable Type	Load Transfer Index
1	MW9 HLT Megastrand	126
2	MW9 Megastrand in a 42 mm hole**	92
3	MB9 Megastrand	85
4	Hilti - 19 wire spirally indented strand	69
5	MW10 HLT Megastrand	43
6	Garford triple-strand in a 64 mm hole	39
7	Garford triple-strand in a 55 mm hole	38
8	MB12 HLT Megastrand	33
9	Garford twin-strand in a 64 mm hole	28
10	Garford twin-strand in a 55 mm hole	27
11	Garford twin-strand in a 52 mm hole Bowen - 19 wire cable	22
13	TG in a 42mm hole*	7
14	Hilti - 19 wire plain-strand in a 28 mm hole	5
15	Mambo - 21 wire cable JSS - 19 wire cable in a 28 mm hole	4
17	JSS - 19 wire cable in a 42 mm hole HI-TEN - 21 wire cable in a 45 mm hole	3
19	JSS - 19 wire cable in a 55 mm hole	2

Note:
* - average value based on two successful tests.
** - only one successful test obtained.

Comparison of the Performance of Active and Passive Roof Bolts in An Illinois Basin Coal Mine

Anil K. Ray, Senior Engineer, Ground Control
Murali M. Gadde, Director, Geotechnical Services
Peabody Energy
St. Louis, MO

Anthony J.S. Spearing, Associate Professor
Southern Illinois University
Carbondale, IL

ABSTRACT

This paper discusses in situ studies conducted at an Illinois Basin room-and-pillar coal mine to evaluate the performances of three different types of bolts under similar geologic conditions. The bolt types considered were the fully grouted passive rebar (FGPR), the resin-assisted mechanical anchor (RMAB), and the fully grouted tension rebar (FGTR). During the evaluations, the three types of bolts were installed in a single entry covering a span of three contiguous pillars with almost identical geologic conditions. The performances of the three types of bolts were investigated by instrumentting the bolts prior to installation as primary supports on cycle. Additional data on roof behavior was collected with extensometers and shear meters placed near the instrumented bolts. Excluding some time lapse right after installation, the performance evaluation of the three bolt systems was based on the data collected for over a year. Based on this study, it was found that the axial loads measured in the different bolt types did not show any identifiable patterns under the prevailing geological conditions at the mine. Therefore, the assumption that active bolts must be superior to passive ones is not always valid. Even though the studied mine did not have any thinly laminated, weak rocks in the immediate roof, the passive bolts performed as well as the active systems.

INTRODUCTION

Underground coal mines in the United States and many other countries use roof bolts as the primary support. The roof bolts are mainly of three types: fully grouted passive rebar (FGPR), resin-assisted mechanical anchor (RMAB), and fully grouted tension rebar (FGTR). The most common type used among the three is the fully grouted passive bolt. The other two types of bolts are considered active because tension is applied during their installation. It is commonly postulated that due to the pre-tension, active bolts provide better roof support than the passive type especially when the immediate roof is highly laminated. However, limited field data exist to support this hypothesis. Within the knowledge of the authors, even among the available in situ bolt studies, no comprehensive study has been carried out to investigate the relative performance of active and passive bolts under "similar" geological conditions. A survey by Tadolini and Mazzoni (2006) revealed that 26% of total bolts used in the United States were active bolts. Additionally, practical experience shows that when roof falls occur with passive bolts, the tendency of the stakeholders has been to switch to active bolts as one corrective measure. Given this "perceived" superior performance of the active systems, it is desirable to have some in situ data to shed light on the differences in the performance of these different bolts under comparable geologic conditions.

In the past, several researchers have used instrumentation as a means to monitor the performance of active and passive bolts. In chronological order, Parker and Caverson (1951) were one of the first to instrument roof bolts underground. But Sawyer and Karabin (1975) were the first to use strain gauges fitted on bolts to measure the axial loads for resin bolts. After that, Lundy, Karmis, and Haycocks (1983) used the same type of strain gauge fitted bolts to study the axial, bending, and shear strain distributions on fully grouted bolts. In the early 1990s, a major study was conducted by Signer and Jones (1990) at a two-entry gate road of a longwall mine. They used 12 6-ft-long fully grouted instrumented bolts in the study. These studies were able to explain the load transfer mechanism for passive bolts and their performance under certain conditions. However, it was not until 1993 that some effort was made to compare the performance of active and passive bolts under similar geo-mining conditions. It was Signer etal. (1993) who performed a comparative study at a longwall mine using two different bolt systems: fully grouted passive rebar and resin-assisted mechanical anchor bolts. This study indicated slightly better performance of the active bolts in comparison to passive bolts. However, because the yield capacities of the active bolts used were much higher than the passive bolts, the comparison might have had some bias. Subsequently, no further in situ studies were conducted in the United States to study the performance of active and passive bolts under similar geological conditions.

Considering the current popularity of three different bolt types in the U.S. coal industry, the need to investigate field performance of these systems under comparable geologic conditions was highly warranted. Towards this end, a NIOSH-funded research project was undertaken in September, 2009, by the Southern Illinois University, Carbondale (SIUC) in cooperation with Peabody Energy. The study was conducted at two room-and-pillar mines and one longwall mine. Spearing et al. (2011) discussed some data on the initial performance of the three types of bolts covering all three locations.

Based on these initial readings, it was reported that the "installed" loads were much lower than expected for the active bolts despite following the best installation practices under the supervision of a roof bolt vendor, researchers from NIOSH, and the project team. As a continuation to the Spearing etal. (2011) study, in this paper, field data obtained during a span of over a year are reported for one room-and-pillar coal mine in Indiana. This paper reports not only the roof bolt load data for the three different bolt systems, but also covers the extensometer and shearmeter output from the instrumentation sites.

SITE GEOLOGY

The study mine was a room-and-pillar operation located in southwestern Indiana with mining being conducted in the Springfield No. 5 coal seam of the Petersburg Formation. A typical exploration borehole cross-section near the test sites is shown in Figure 1. The immediate roof consists of mainly shale and some sandy shale. The immediate floor is made up of a relatively weak underclay/claystone bed. The coal seam is around 5 to 5.5 ft thick and the overburden depth is around 330 to 350 ft. To understand the exact geology at the instrumentation sites, borehole scoping was conducted to a depth of about 14 ft in the roof (Spearing et al., 2011). The lithologies in the immediate roof from bore scope observations indicate consistency in rock types around the test sites. The scoping showed that the immediate roof was made up of a medium gray silty shale with thickness ranging from 0.0 to 1.0 ft. Overlying the gray shale was a black carbonaceous shale. The thickness of the black shale unit appears to range from 1 to 2 ft in the test area. Further up, there was a dark gray to medium gray shale 7 to 8 ft in thickness along with 0.3-ft-thick limestone lenses. The uppermost unit was a medium brown to medium gray shale.

INSTRUMENT LAYOUT

The main emphasis in the design of instrument layout and the selection of a test site was to install all three different types of bolts in similar geo-mining conditions. Hence, it was originally planned to install the instrumented bolts in three adjacent entries. But due to some practical mining constraints in conjunction with the unavailability of three adjacent intake air courses, it was necessary to use a single entry for the instrumentation. However, considering that all the instruments were installed around three pillars right next to each other in the same entry, the variability of geo-mining conditions was considered to be minimal. This conclusion was further supported by the bore scoping results near the test sites. The layout of instrumentation is shown in Figures 3 through 6. In order to capture complete loading history, all the instrumented bolts were installed as primary supports. Even though not shown in the layout, all the primary bolts surrounding the instruments were of the same type as the instrumented bolts.

The mine normally uses 6-ft-long fully grouted, #6, Grade 60 rebar for primary support. Due to the slotting on the instrumented bolts to mount strain gauges, it was decided to use #6, Grade 75 rebar for the instrumented bolts to match the capacity of the primary supports. However, laboratory testing of the slotted #6, Grade 75 bars produced slightly lower yield capacity than desired. Therefore, to achieve higher or comparable capacity as the normal pattern bolts at this mine, it was finally decided to use 6-ft-long, 0.804-in-diameter, Grade 75 bars for *all* the instrumented bolts.

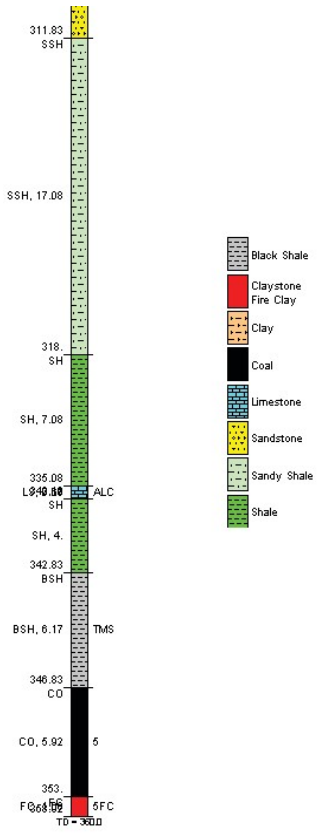

Figure 1. Typical lithology above Springfield number 5 seam near the test site.

Figure 2 shows the general location of all the instruments while Figures3 through 5 show the details around the fully grouted passive rebar bolts (FGPR), resin-assisted mechanical anchor bolts (RMAB), and fully grouted tension rebar bolts (FGTR). In the enlarged figures, the nomenclature used for instrument identification is as follows. The first letter indicates the type of instrument (B-bolt, S-shearmeter, E-extensometer), the second letter indicates the type of bolt (F- FGPR, D-RMAB, T-FGTR), the third letter indicates the location of the instrument (M-near mid-pillar, I-intersection), and the fourth letter indicates the serial number of the instrument. For example, BTM4 represents the fully grouted tension rebar bolt located near mid-pillar with serial number 4. Similarly, SFI1 identifies the shearmeter with serial number 1 located in the intersection where fully grouted passive rebar bolts were installed.

The instrumentation at this mine was planned such that roof bolt loading and displacement data were obtained for each bolt type at the mid-pillar as well as around the intersection areas. A closer look at Figure 2, however, shows that such planned instrument distribution was not achieved for the RMAB bolts. At the time of entry #3 development, the RMAB bolts were installed as planned such that after the area around the pillar was completely developed, the instruments would be in the mid-pillar region and within the intersection with crosscut (XC) 13. But when the crosscut was finally developed and got connected with entry #3, the intersection was formed with an offset from the projected one. It appears the

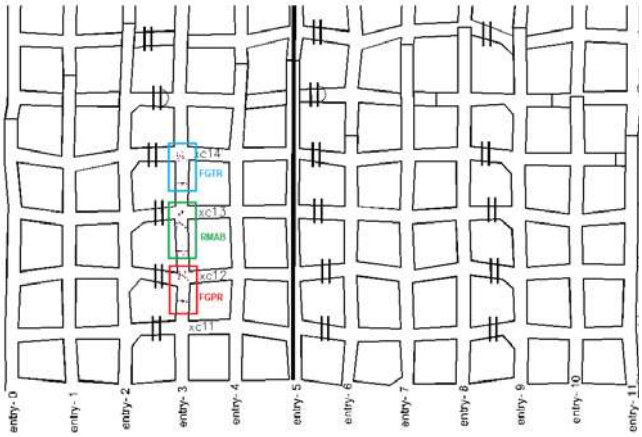

Figure 2. Layout of instruments in entry #3 between XC 11 and 14.

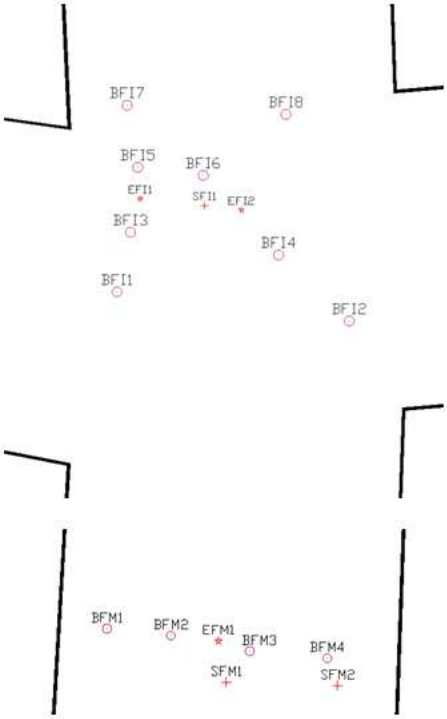

Figure 3. Enlarged view of installation of instruments (FGPR) at intersection and mid pillar between XC 11 and 12.

offset was due to some operational problems that resulted in a larger pillar and slightly altered orientation of the crosscut. Consequently, some of the instrumented RMAB bolts were not positioned strictly within the intersection. The planned pillar size was 60 ft by 60 ft, rib-to-rib, but between XC12 and 13 the actual pillar length was 72 ft, while the pillar length between XC11 and 12 was 50 ft. The pillar length between XC 13 and 14 was 60 ft. The pillar width was around 60 ft for all the pillars near the test site. The actual entry widths varied from 17 to 19.3 ft between XC11 to 14. The crosscut width also varied from 17 to 18.6 ft in the test zone. The overburden depth was around 350 ft, whereas the actual mining height was 8.5 to 8.75 ft near the test sites.

DATA COLLECTION

At this mine, four instrumented bolts of each type were installed at mid pillar and eight bolts were installed in the intersection (Figures 2 to 5). Three shearmeters and three extensometers were installed along with each type of bolt. Altogether, 36 instrumented bolts, 9 shearmeters, and 9 extensometers were installed. However, not all the instruments yielded usable data. A few bolts got damaged by equipment movement around the test sites even before taking initial readings. When the initial readings were being taken, a few instruments were found to be malfunctioning and showed abnormally high strain. Such extreme strains might be due to damage to sensors or because of improper installation. Despite this, during the period of almost a year after installation, 28 instrumented bolts out of 36 have been working well, and 8 shear meters and 7 extensometers also provided satisfactory data. It may be noted that in some functioning instruments, a few sensors provided abnormal readings, but these were excluded from the analysis.

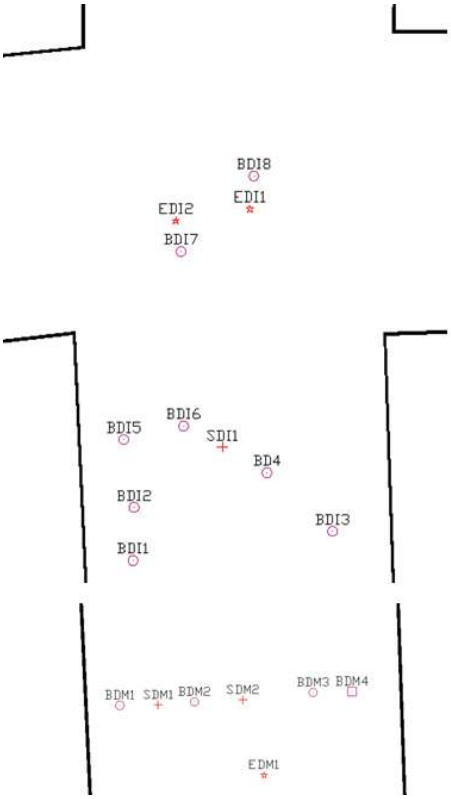

Figure 4. Enlarged view of installation of instruments (RMAB) at intersection and mid pillar between XC 12 and 13.

The slug4 dataloggers were used for the data collection from all the instruments. These dataloggers could not be used until fresh air was established because they were not intrinsically safe as required by the Mine Safety and Health Administration (MSHA). Consequently, there was a delay between the time the instrumented bolts were installed as primary supports and the

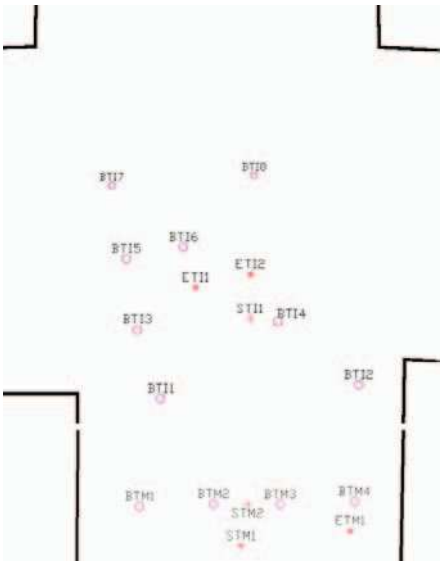

Figure 5. Enlarged view of installation of instruments (FGTR) at intersection and mid pillar between XC 13 and 14.

time the first readings were taken. It took considerable time to read the first set of data because only one entry could be utilized for instrumentation. The average delay was 10 days between installation and the first data reading.

Figure 6 shows the actual cut sequence used around the tests and the position of the face when the first set of observations was recorded. As shown in Figure 2, the FGPR bolts were installed between XC 11 and 12, the RMAB between XC12 and 13, and the FGTR between XC 13 and 14. The pink solid line in Figure 6 shows the face position when initial observations were recorded for all FGPR and RMAB bolts at mid pillar, and the green solid line shows the face position when initial reading were taken for all the remaining instruments. It is obvious from Figure 6 that by the time the first set of data was recorded, significant mining related loading was induced in the different types of instrumented bolts. Because of this, direct estimation of the pre-tension loads on RMAB and FGTR bolts was not possible. While the pre-installed loads could not be measured, the cumulative bolt loads were not affected by the time lag in data collection. Thus, in terms of the primary objective of comparing the overall performance of the different types of bolts under similar geologic conditions, the data's utility has not been compromised.

After the initial readings, the data was continuously recorded for a period of five months (up to February 5, 2011). After that, due to some ventilation modifications, the entry had been changed to a return entry. Because the dataloggers were not intrinsically safe, no further observations were taken following the ventilation change. After another six months, however, this entry was converted back to an intake entry in the third week of August, 2011. Following this change, readings were taken for all the instruments on August 26, 2011, and the dataloggers were reinstalled for all the instruments that were still functional. Though the data collection is still going on, this paper only includes data up to August 26, 2011.

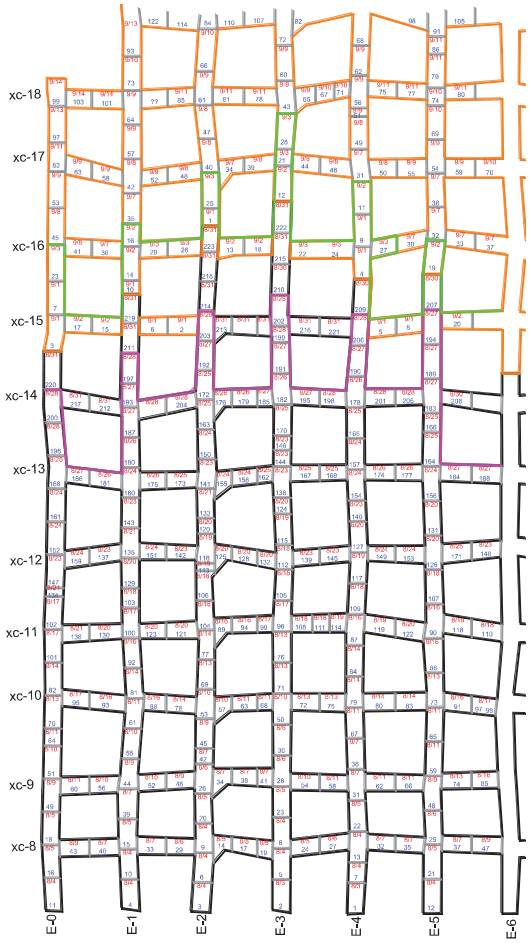

Figure 6. Cut sequence used at mine and installation of instrumented bolts (pink and green solid lines are the face positions when the first set of observations was recorded; red numbers are dates, and the blue numbers are cut numbers).

AXIAL LOADS IN BOLTS

At this mine, all instrumented bolts were fitted with gauges on stacked configuration, and the rock bolt loads were estimated as described by Spearing et al. (2011). The bolt loads in this paper are in ***metric tons*** and not short tons. From the strain gauge data, the axial load and axial stretch of the bolts were obtained. The axial loads in the different types of bolts installed at mid-pillar and at intersection were obtained for different times. Even though the data was logged on one-hour intervals, due to the negligible change on a daily basis and for the sake of clarity, the results were plotted on an interval of about a month.

Given the extensive amount of data collected, it is difficult to include the plots for all the instrumented bolts in this paper. To illustrate the nature of loading obtained, however, one bolt each at mid pillar and intersection was selected for the three types of bolts. Figures 7, 8 and 9 show the development of load in one of the FGPR, RMAB and FGTR bolts respectively. The plots for all the instrumented bolts can be found in the final report submitted to NIOSH (Spearing and Gadde, 2011). From the bolt load trends

obtained, the following observations were drawn about the bolt axial loads:

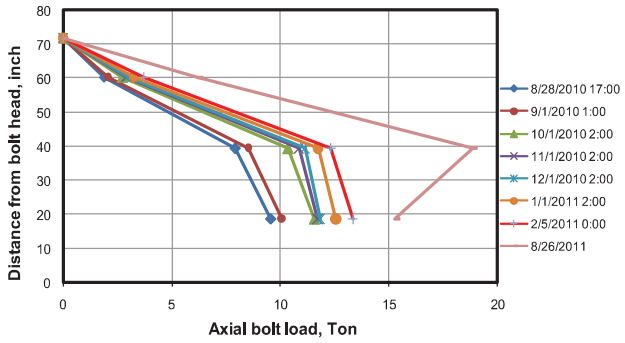

Figure 7. Development of load in FGPR (BFM2) at mid pillar.

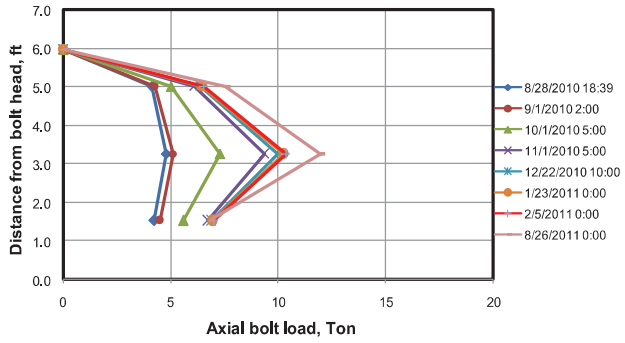

Figure 8. Development of load in RMAB (BDI5) at entry-intersection edge.

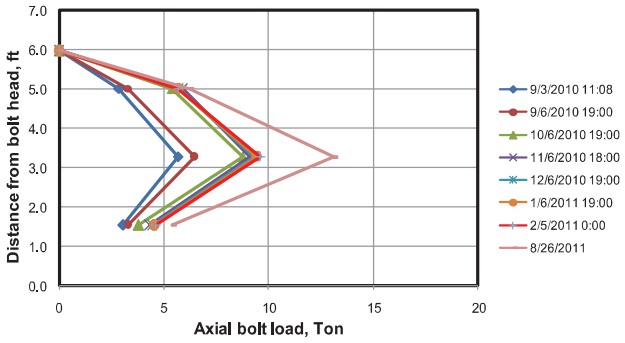

Figure 9. Development of load in FGTR (BTI4) at intersection.

- The passive bolt system provided the most resistance to roof movement. The axial loads developed in the FGPR bolts were the highest among the three systems used at the mine.
- For the FGPR bolts, there was no significant difference between the axial loading in the mid-pillar region versus the intersection.
- The highest axial load among the FGPR bolts was noticed in BFM2 bolt, which was about 19 tons. It was also noted that the bolt loads in the mid-pillar region were essentially asymmetric with higher loading induced towards the left rib when looking inby.
- Excluding the two bolts near the ribs in the mid-pillar region, all the FGPR bolts displayed a distinct peak axial load some distance inside the roof.
- Among the three bolt types, the RMAB instrumented bolts performed the best in terms of providing response data, with all the bolts except one providing useful data.
- Given that only the top 4ft of the RMAB bolts was grouted, the axial load in these bolts was either uniform within the first 3–4ft in the roof or it displayed some peak at about 3ft into roof. A few bolts also had peak load around a 5-ft depth.
- In contrast to FGPR, the RMAB bolts showed clear differences in the loading of the mid-pillar and intersection regions with the later exhibiting higher axial bolt loads.
- For RMAB, asymmetric bolt loading was also noticed in the mid-pillar region with higher loads towards left rib looking inby.
- For FGTR bolts, data could be obtained from only two bolts in the mid-pillar region. Despite this limit, it appears that in general the intersections were loaded a little more than the mid-pillar region.
- Even though the pre-tension values could not be captured due to the unavailability of permissible dataloggers, when the total loads measured in the active bolts are noticed—especially in comparison to the FGPR bolts—it was clear that much of the pre-installed load was lost before the first set of readings were taken. At this point, the exact reasons for such a loss are not clear. It is possible that some installation errors could have caused some tension bleed-off, but such errors are considered negligible considering the extreme care taken in installing the instrumented bolts. To ensure best installation practices were followed, representatives from a reputed bolt vendor were constantly present throughout the installation time. Additionally, the best available roof bolter operators at the mine were used for the instrumented bolt installation.
- This mine is a room-and-pillar operation with no pillar retreat. Despite the lack of mining activity in the immediate vicinity of the instrument sites, the roof bolt loads continued to increase with time. This shows that some time-dependent deformations were occurring in the roof. It is not clear whether source of the creep was in the roof, the coal pillar, or the soft floor. However, given the very soft and friable nature of the underclay floor and the historical data on its time-dependent movements, the most likely dominant source of the time-dependent axial bolt load change is the floor. This conclusion is supported by numerical modeling analyses which are beyond the scope of this paper.
- The small overloading (but not yielding) in the FGPR bolts may perhaps be due to the smaller coal pillar around these bolts as compared to the other two bolt types.

In order to decide if one bolt system performed better than the others, the axial loads were compared for the three different systems at similar “geometric” locations within the entry or intersection. Such comparative plots are shown in Figures 10

through 15. It may be noted that in Figure 11 and Figure 13, the *average* axial loads are plotted for the two rib and two center bolts, respectively, in the mid-pillar region. Even though at one or two locations it may be seen that one bolt system clearly outperformed the others, in general, there is no clear trend in the data. Based on this, it appears that under the geo-mining conditions such as those at this mine, all the bolt systems provided comparable performance and no single system was superior to the others. This was a rather surprising finding given the conventional belief that the tensioned systems should perform better than passive bolts due to their better "clamping"action. Unless more in situ studies of the nature described here are conducted, it appears the perceived benefits of the active bolting systems based on pure theory may not exist in reality. The logical conclusion seems that extensive field instrumentation is required to understand if and under what conditions active systems will provide superior performance over the passive system. Without such validation studies, the higher costs of active bolting systems are hard to justify in light of the findings in this research. It may be reminded that within the knowledge of the authors, field studies like those in this paper were not conducted in the past to compare the performance of the *three* popular bolt systems under *similar* geologic and mining conditions and in such close proximity.

ROOF MOVEMENT

As shown in Figure 2, in addition to the instrumented roof bolts, some extensometers and shearmeters were also installed to monitor the vertical and horizontal movement of the rock beds in the immediate roof within and above the bolting horizon. Because of the operational constraints, the extensometers and shearmeters were installed after a time lapse of 10 to 17 days from the date of bolt installation. These instruments were installed when the site was free from any major mining operation, which normally occurred after the face moved about two crosscuts inby. All the displacement instruments were zeroed before their installation. Because of the different delays in the actual data logging, the first set of data from the displacement monitors was recorded after a time gap of 2 to 7 days in comparison to the bolt load data. As a consequence of the delay in the installation, the initial movement of the roof right after excavation and in the interim period was not captured. Further, due to the slight delay in recording the data before automatic dataloggers were installed, the *trends* of displacement within this delay period were not captured.

In order to make sense of the roof movements in relation to the bolt axial loads, a comparison of was made of the extensometer data with the "axial stretch"calculated for the nearest instrumented roof bolt. By combining the axial stretch of the bolt along with extensometer data, it may be possible to estimate the "pick up"and "anchor" lengths of the bolt (Freeman, 1978). For the sake of brevity, in the following discussions the vertical movement of the rock beds and the axial stretch in the bolts were compared on some select days covering the total observation period. The three time periods selected were the day of initial readout (9/5/2010), after about 5 months (2/5/2011), and after about a year (8/26/2011). As noted before, not all installed extensometers worked during this timeframe. The data obtained by functioning extensometers along with the nearest instrumented bolt axial stretch are plotted for a few extensometers in Figures 16 and 17. Similarly, the horizontal movements for a few of the shearmeters along and across the entry are shown in Figures18 and 19.

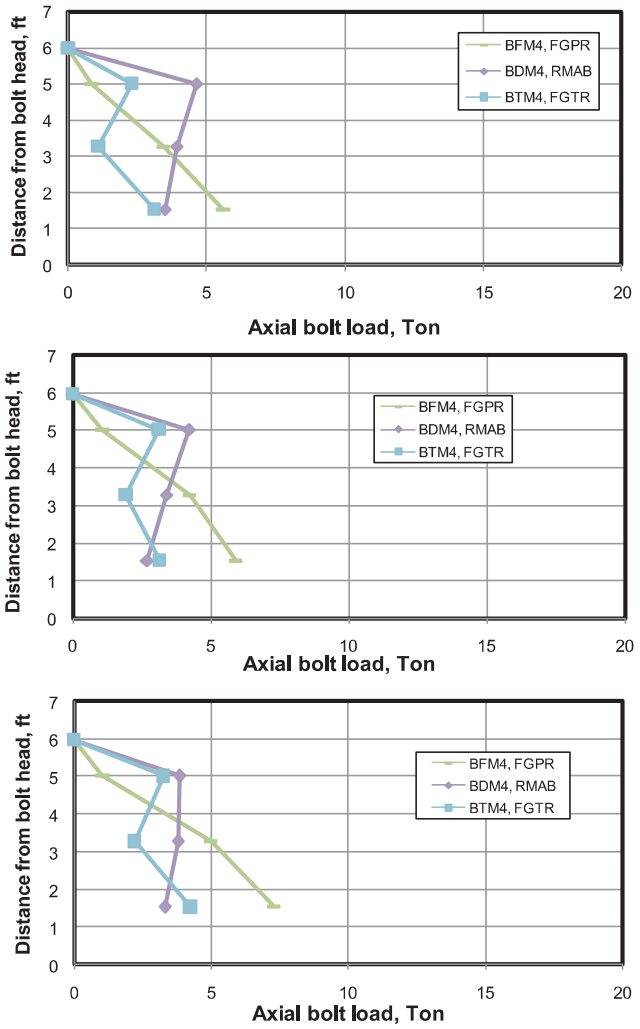

Figure 10. Comparison of axial loads in different types of bolt installed near the rib at mid pillar (the bolts used for comparison are noted in the legend) after (a) 15 (b) 160 and (c) 365 days from installation.

Before proceeding to the interpretation of the extensometer data vis-à-vis axial bolt stretch (and hence axial loading), some discussion on a few basic concepts is in order. Freeman (1978), in a pioneering work published in the late 1970s introduced the concepts of neutral point, pick-up length, and anchor length for a fully grouted passive bolt. According to Freeman, within the pick-up length zone of the bolt, the rock moves more than the bolt, thus transferring some axial load to the bolt. The opposite happens in the anchor length portion. The bolt moves more than the rock, thus enabling the bolt to transfer the load picked up within the pick-up length zone to the surrounding rock mass. At the neutral point, there is no relative movement between the bolt and the rock mass. If Freeman's model is considered universal, then it may be interpreted that in an ideally designed fully grouted passive roof bolt, both the pick-up length and the anchor length must exist in such way to balance the loads picked up with those transferred by the bolt. At the extremes, if the bolt only has pick-up length then

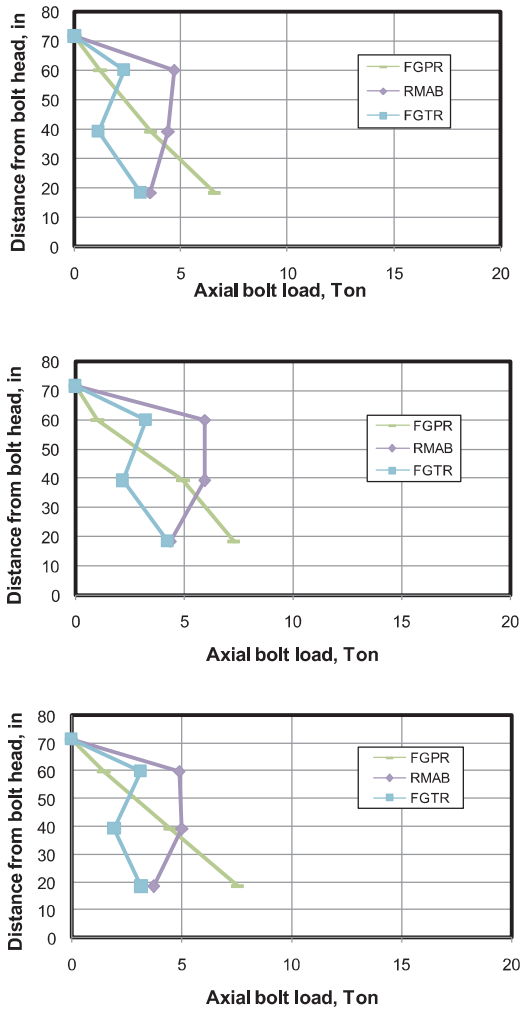

Figure 11. Comparison of average axial loads in different types of bolts installed near the rib at mid pillar after (a) 15 (b) 160 and (c) 365 days from installation (the axial loads are averaged for the two bolts closest to either rib).

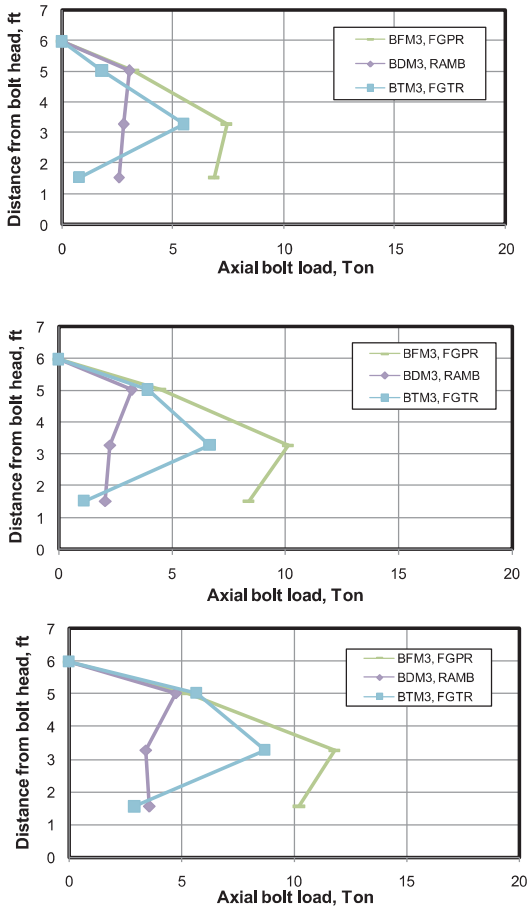

Figure 12. Comparison of axial loads in different types of bolt installed in center of the entry at mid pillar (the bolts used for comparison are noted in the legend) after (a) 15 (b) 160 and (c) 365 days from installation.

the bolt is perhaps overdesigned and existence of only anchor-length shows an underdesign. However, the smaller rock movement along the entire bolt length as compared to bolt's axial stretch by itself will not tell if the rock mass is going to experience instability or not. Such a trend only indicates that the bolt is functioning in a purely "beam building"or in a purely "suspension"mode. On the same token, it may be inferred that the existence of both anchor and pick-up length shows a combination of beam building and suspension mode of bolt action. It is not clear how Freeman's concepts apply to active fully grouted or active partially grouted bolts.

Given Freeman's fundamental model, when the extensometer data was compared with the axial stretch of the nearby bolts, the following trends could be identified:

- Among the fully grouted bolts, both pick-up and anchor lengths exist. These lengths changed over the monitoring period from pure anchor length to a combination. However, the peak axial load location in the bolts did not exactly match with the neutral point because of the use of longer (18-inch) strain gages and the resulting averaging of axial loads in the bolts.
- Overall the amount of vertical movement in the roof is extremely small.
- Interestingly, Freeman's concepts appear to be extendable to both types of active bolts used. The plots in Figures 16 and 17 show existence of pure pick-up length to a combination of pick-up and anchor lengths.
- The roof movement around all three types of bolts is very small. Notwithstanding the extremely small magnitude, it also seems the roof movement extended to some distance above the 6-ft bolts.
- The roof movement continued long after completion of mining around the instrument sites.
- The vertical displacement trends clearly show the adequacy of any of the three types of bolts for the geo-mining conditions at this mine.

Though the extensometer data provided some meaningful interpretation, the shearmeter data at this stage did not reveal any major trends. However, the data does show significant horizontal

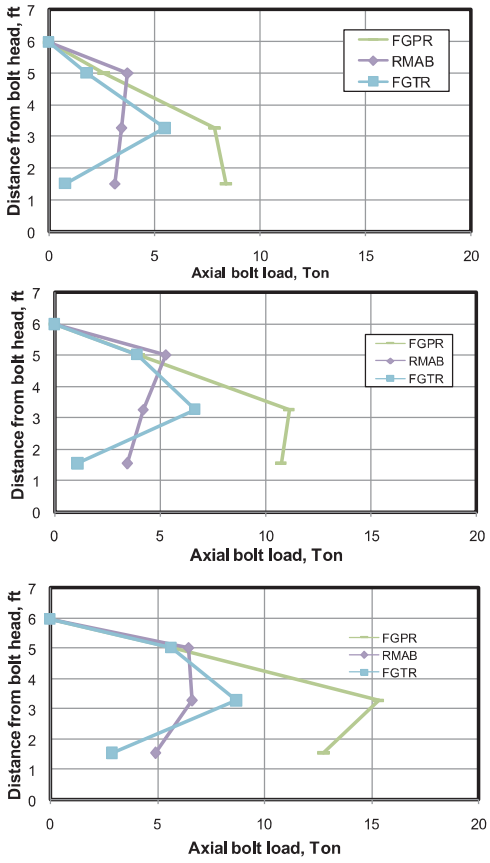

Figure 13. Comparison of average load in different types of bolts installed in center of the entry at mid pillar (the axial loads are averaged over the two center bolts) after (a) 15 (b) 160 and (c) 365 days from installation.

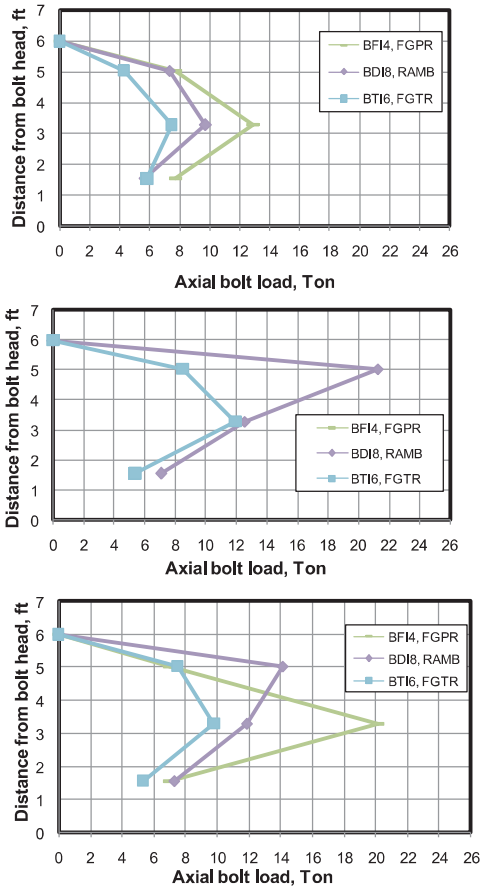

Figure 14. Comparison of axial load in different types of bolts installed at the center of intersection (the bolts used for comparison are noted in the legend) after (a) 15 (b) 160 and (c) 365 days from installation.

movements occurred within the roof, and the magnitude of the movement changed over time. The data also showed that the location of peak horizontal movement changed over time. Interestingly, no significant difference in the lateral movement existed between the intersections and the mid-pillar regions. Finally, some lateral movement occurred both across and along the entry. This final conclusion has a profound effect on some of the modeling approaches used in coal mine ground control. When heterogeneous rock materials that exhibit high spatial variability are involved, the plane-strain assumption in modeling may not always be valid. Further research is required to fully understand the implications of the dual directional horizontal movements measured in this study.

CONCLUSIONS

The extensive instrumentation carried out at the study mine led to several useful insights on the behavior of different systems of roof bolts in situ. Even though the pre-installed loads on the active bolts could not be explicitly measured, given the total loads measured, it appears that much of the pre-tension was lost due to unknown reasons. Therefore, the utility of the pre-tension has become highly questionable in conditions like those at this mine. The axial loads measured in the different bolt types did not show significant differences. Further, the loads experienced by the bolts around the mid-pillar region did not differ substantially when compared to the data from the intersections for same bolt types. Based on this data, it seems for the geo-mining conditions like those at this mine, any of the three bolt types would perform well. The extra investment in the active bolting systems did not appear worth it in light of the in situ data obtained for conditions like those at this mine. Excluding the elastic movements right after the excavation, the extensometer data showed that subsequent roof displacements were negligible at this mine. Comparison of the bolt axial stretch with the extensometer data revealed several types of bolt behavior within the Freeman type interpretation model. It appears significant horizontal movements occur in the roof both along and across the entry. Further work is required to completely understand the significance of such movements. The shearmeters used in this project appear to yield useful data and perhaps are the only instruments that capture displacements both along and across the entry.

ACKNOWLEDGEMENTS

The funding and support provided by NIOSH (under BAA number 2008-N-10989) is greatly acknowledged. The support of graduate students from SIUC, particularly Todd Kostecki for data collection, and the help extended by the mine management is highly appreciated.

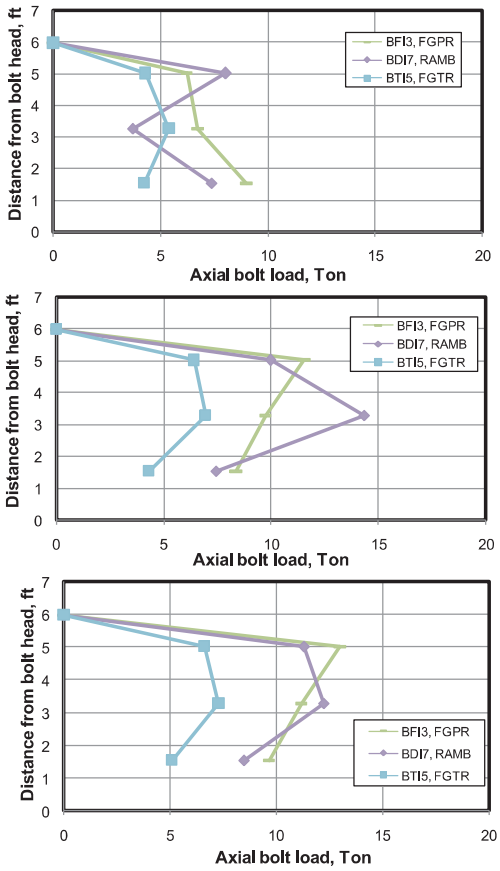

Figure 15. Comparison of axial load in different types of bolts installed at the edge of intersection (the bolts used for comparison are noted in the legend) after (a) 15 (b) 160 and (c) 365 days from installation.

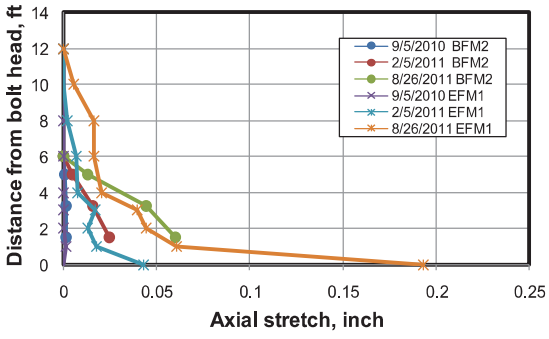

Figure 16. Variation in roof movement and axial bolt stretch for FGPR at mid-pillar.

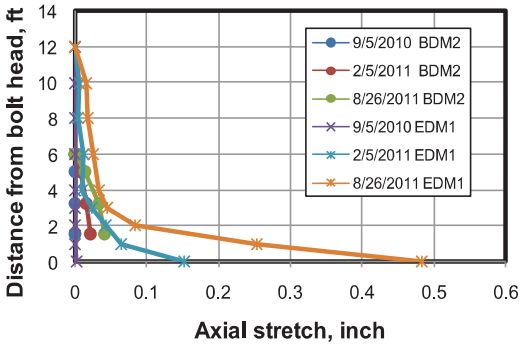

Figure 17. Variation in roof movement and axial bolt stretch for RMAB at mid-pillar.

REFERENCES

Freeman, T.J. (1978). "The behavior of fully-bonded rock bolts in the Kielder experimental tunnel." *Tunnels and Tunneling*. (June):37–40.

Lundy, D.G., Karmis, M., Haycocks, C. (1983)."An in situ study of the interaction between resin bolts and the surrounding strata."In: *Proceedings of the First International Conference on Stability in Underground Mining*. Society of Mining Engineers of AIME, pp. 674–700.

Parker, J., Caverson, B. (1951). "Resin bolts hold best with resins." *Mining Engineering.23*(5).

Sawyer, S.G., Karabin, G.J. (1975). "The development and use of resin instrumentation for the in-situ measurement of axial loads in fully resin-grouted roof bolt." In: *Proceedings of the First Symposium on Underground Mining. NCA/BCR Coal Conference & Exposition II*(Louisville, KY, Oct. 21-23, Vol. 2pp. 90–103.

Signer, S., Jones, S. (1990). "A case study of grouted roof bolt loading in a two-entry gate road." In: *Proceedings of the 9th International Conference on Ground Control in Mining*,pp. 35–41.

Signer, S.P., Mark, C., Franklin, G., Hendon, G. (1993). "Comparisons of active versus passive bolts in a bedded mine roof." In: *Proceedings of the 12th International Conference on Ground Control in Mining*,pp.16–23.

Spearing, A.J.S., Gadde, M.M. (2011). "Final report on NIOSH funded project 'Improving underground safety by understanding the interaction between primary rock bolts and the immediate roof strata". NIOSH Project BAA number 2008-N-10989.

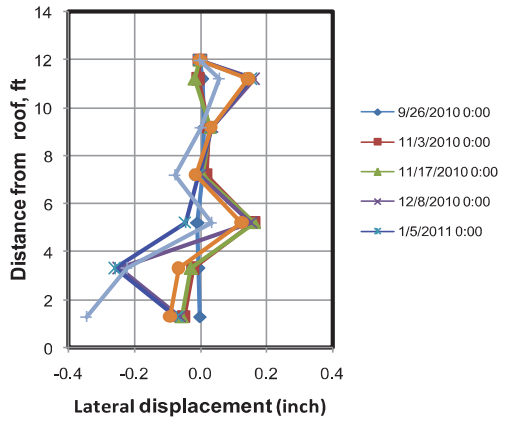

Figure 18a. Horizontal movement of rock bed along X-axis near rib at mid pillar \(SFM2\).

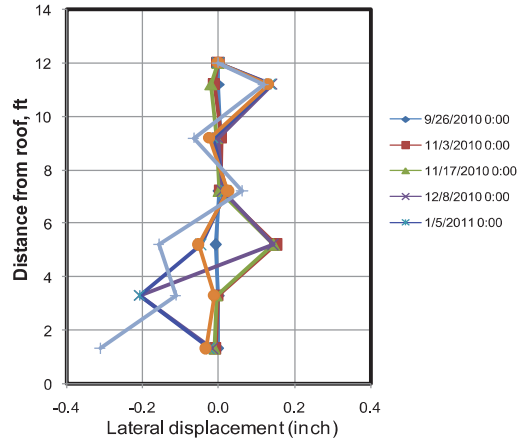

Figure 18b. Horizontal movement of rock bed along Y-axis near rib at mid pillar \(SFM2\).

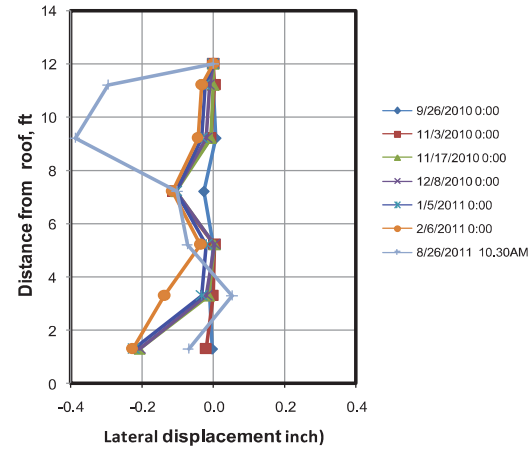

Figure 19a. Horizontal movement of rock bed along X-axis near at intersection \(STI1\).

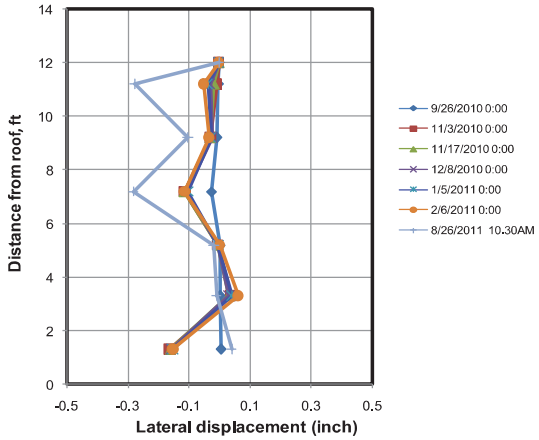

Figure 19b. Horizontal movement of rock bed along Y-axis near rib at mid pillar \(STI1\).

Spearing A.J.S., Gadde, M.M., Ray, A.K., Reisterer, J., Lee, S. (2011). "The initial performance of commonly used primary supports in US coal mines." In:*Proceedings of 30th International Conference on Ground Control in Mining*, pp.80–91.

Tadolini, S.C., Mazzoni, R.A. (2006). "Twenty-four conferences: more than one-hundred and seventy papers; understanding roof bolt selection and design still remainspriceless." In:*Proceedings of 25th International Conference on Ground Control in Mining*, pp. 382–389.

Coupon Testing for Field Assessment of Stress Corrosion Cracking of Rock Bolts

Damon P Vandermaat, Mr
The University of New South Wales (UNSW)
Sydney, Australia

Elias Elias, Mr
University of New South Wales
Sydney, Austria

Alan Crosky, Mr
The School of Materials Science and Engineering
University of New South Wales
Sydney, Australia

Zileng Tang, Mr
Peter Craig, Mr
The School of Mining Engineering
University of New South Wales
Sydney, Australia

Serkan Saydam, Mr
Bruce Hebblewhite, Mr
The School of Mining Engineering
University of New South Wales
Sydney, Australia

ABSTRACT

Coupon testing allows for the rapid understanding of a material's likely behavior in service conditions, allowing engineers and operators to make informed decisions about the likely service-life of parts when subjected to field conditions.

Bend testing has been identified as the best approach for exploring rock bolt susceptibility to stress corrosion cracking (SCC) in underground mining. The bend test specimens used were 2–3 mm thick slivers of steel, cut from the outer edge of a rock bolt. For the specimens, 1350 grade steel was chosen due to its wide use in the industry. The jigs themselves are small assemblies made of stainless steel that are capable of imparting a bending load on the specimens.

The jigs were installed at a coal mine located in the Western Coals West of Sydney, Australia, in such a way as to expose the test specimen to water dripping from the mine roof.

It is expected that this approach will yield results pointing to the likely SCC mechanisms affecting the service life of rock bolts, as well as demonstrate the jigs' usefulness as an early warning system for SCC. Furthermore, the coupon tests will be correlated against the results of large-scale laboratory tests.

INTRODUCTION

Stress corrosion cracking (SCC) is a failure mode that is induced by the combination of an applied stress and an appropriately corrosive environment. SCC can result in the catastrophic, brittle failure of the material as a result of crack growth (Vandermaat et al., 2012).

SCC of rock bolts has been recently identified in the Australian underground coal mining industry as an issue that leads to the premature failure of bolts in situ. The issue was first reported to occur in the late 1990s by Gray (1998), and it has been an active area of research since. An Australian Coal Association Research Program (ACARP) report published in 2002 (Crosky et al., 2002) reported SCC was an issue in at least three Australian coal mines; however, this number has since grown. SCC has been noted to occur in the following situations: the bolting horizon intersects clay bands; there is a thick coal roof;corrosive ground water is present; and shearing between the strata is active (Crosky et al., 2002).

Hydrogen embrittlement is sometimes referred to in the literature as a mechanism for rock bolt failure. It should be noted that hydrogen embrittlement is a subset mechanism of the greater SCC family (Villabla and Atrens, 2009). Gamboa and Atrens (2003; 2005) produced SCC failures in rock bolt steels in the laboratory and concluded that hydrogen embrittlement was the mechanism of failure. However, these tests were carried out in a pH 2.1 test solution, which is not representative of typical underground mine ground water conditions (Craig et al., 2010).

This coupon testing programs is a part of a larger Australia Research Council project, aiming to determine the cause of SCC and develop SCC-resistant rock bolt systems. This project aims to determine the environmental and metallurgical factors affecting SCC. A new environmental controlled laboratory has been developed to simulate the underground environment. Experiments will be carried out in this new lab to assess SCC properties on both full sized, and coupon specimens (Vandermaat et al., 2012).

COUPON TESTING

Coupon testing is designed to generate rapid understanding of the way a material will behave in as given environment, in this case with regards to SCC. The small cross sections used in the test mean that significantly less force is required to generate the desired stress, and the time to failure is considerably reduced. By measuring the time taken to fail, an understanding of crack growth velocities in situ can be gained. This will provide engineers with an insight into the likely life of an installed rock bolt in SCC-generating conditions.

There is currently very little understanding of how long it takes for SCC to affect a bolt in situ. Sampling of SCC-affected bolts in situ is limited to those that have fallen to the ground. These bolts may lay unnoticed for some time before they are found. Also, strata shear may cause a failed bolt to hang in the roof for a period of time before it might be dislodged and fall to the ground—if they fall at all (Crosky et al., 2002). This introduces bias into any sampling done, making it difficult to build a reliable database.

Bend testing was identified as the best coupon testing method for this project. In situ, rock bolts are subjected to both tensile and shear stresses. Shear stressing generates a tight radius bend in the bolt, inducing massive tensile stresses on the outer radius of the curve. The bend test was identified as working by a similar mechanism, where tensile stresses are built up in the outer radius of the curve.

Because reduced sized specimens were to be used, there could only be a rib profile on one side of the specimen. This ruled out the direct tensile method (ASTM G49, 2005), because it would produce a stress in both the ribbed and non-ribbed sides of the specimen. This would mean that SCC could grow from either of the surfaces. To get valid results, it was deemed necessary to limit crack initiation to the outer layer of the bolt specimen. By using the bend test, the crack initiation point could be controlled.

Other tests, such as the C-ring test (ASTM G38, 2005), were also ruled out, because they do not generate stress in the required direction (i.e., axially along the specimen length).

Part of this test work involves identifying the most appropriate testing method for the underground environment to create SCC. For this reason, the three point and the four point tests will be examined. An analysis of the results will be done to verify the most appropriate arrangement.

Additionally, the project will explore the possibility of using coupon testing as an early warning system for SCC detection. The idea behind this is that an engineer could have a number of these jigs installed in a roadway that is suspected of having issue with SCC. If a number of the samples fail, it could likely be expected that installed bolts may also be subjected to SCC. This could then be coupled with a non-destructive testing (NDT) device to randomly sample installed bolts to assess their integrity.

THREE POINT BEND TEST

The three point bend test is outlined in ASTM G39 (2005). The testing jig has two support posts at both ends and a loading point in the center. Load is applied to the specimen by tensioning the bolt in the center. This raises the center loading point and creates a simply supported beam. The three point loading jig and the dimensions can be seen in Figure 1.

In the three point bending arrangement, the tensile stress on the outer fibers of the specimen ranges from zero at the outer support posts, to a maximum at the center loading point. The amount of stress generated at the center point is directly proportional to the amount of displacement generated by the central loading point.

FOUR POINT TEST

The four point test works on the same mechanism as the three point test, though there are two contact points in between the outer support posts. This generates a slightly different stress regime within the specimen. In the four point test, the stress develops from zero at the outer support, to a maximum at the inner support. Between the two inner supports, the stress is constant at this maximum value. The four point loading jig can be seen in Figure 2.

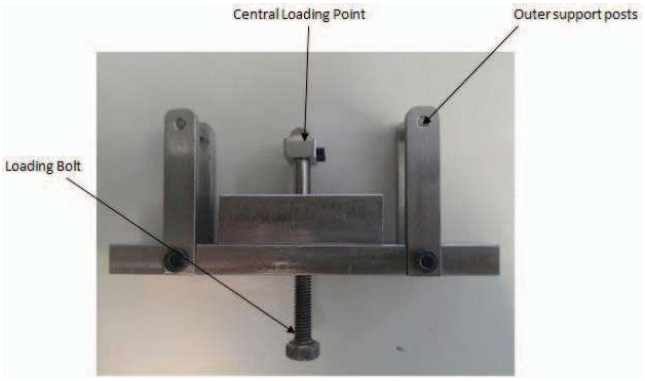

Figure 1. The three point bend test loading jig (After, Vandermaat et al., 2012).

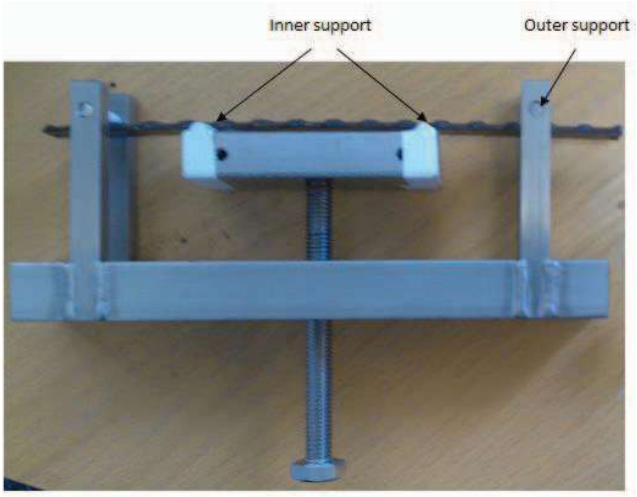

Figure 2. The four point bend test with specimen placed to the rig.

Concurrent testing that has been undertaken by the authors at the University of New South Wales is examining the generation of SCC failures in full sized rock bolt specimens (Vandermaat et al., 2012). The four point test will double as an in situ validation of the proposed full scale test design.

SAMPLE PREPARATION

The specimens were prepared by cutting a thin slice from the length of the rock bolt to produce a long, thin specimen with a rib profile on one side, seen in Figure 3. The samples were then ground flat using a surface grinder. The testing jigs are made out of stainless steel, and to prevent any galvanic corrosion between the specimen and the jig, the back of the samples were coated with black tar paint. In addition, when the samples were loaded into the jig, Teflon tape was used to wrap around the contact points. The specimens were stamped for identification and tied to the jigs using zip ties to prevent them falling to the ground and being destroyed or lost when they failed. Since the ground surface of the specimen will be in compression for the duration of the test, it is unlikely that it will experience SCC, as SCC tends to be a tensile driven failure mechanism.

Table 1. Steel specimen chemical analysis conducted in accordance with AS 3641.1.

%C	%Mn	%Si	%Ni	%Cr	%Mo	%S	%P	%Cu	%V	%W	%Ti	%Al
0.54	1.63	0.27	0.06	0.06	0.010	0.024	0.012	0.2	0.001	0.024	0.001	0.004

Figure 3. Specimens prior to coating with black tar paint.

Table 2. Specimen dimensions.

	Average Thickness (mm)	Length (mm)
Three Point Specimen	2.0	120
Four Point Specimen	3.0	200

The specimens were machined from 1350 grade steel rock bolts. This grade was chosen for its wide use in the industry (Crosky et al., 2002). The alloy chemistry for this specimen can be seen in Table 1. Because the three point and four point jigs are different sizes, the specimen sizes varied as well, as seen in Table 2.

ASTM G39 (2005) recommends the use of flat, polished specimens; however, it was decided that the surface abnormalities such as the ribs, as well as decarburization and scale generated through the manufacturing process, were important to the final results. This required the use of a non-flat specimen, outlined in Figure 4. As a result, the equations specified for analytically

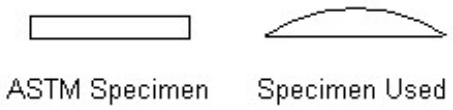

Figure 4. Cross section of the suggested ASTM specimen and the specimen used.

determining the tensile stress in the outer fiber of the specimen had to be recalculated to take into account the curved profile. Although the specimen geometry has changed, the basic premise of the test (i.e., to induce a tensile stress in the material through the use of a bending force) remains intact. All guidelines within the standard with regards to specimen placement, data collection and reporting have been adhered to.

STRESS CALCULATIONS

As stated, the equations given by ASTM G39 (2005) are not applicable to specimens with a non-rectangular cross section. Justification and modification needed to be made to the formulas from ASTM G39 (2005) to suit the arced cross section. Equations (1) and (2) were derived to replace the formulas given by ASTM G39 (2005):

$$\text{3-point test: } \sigma = 12Edy/L^2 \quad (1)$$

$$\text{4-point test: } \sigma = 24Edy/2.75L^2 \quad (2)$$

Where:

σ = maximum tensile stress at outer extreme fiber

E = Modulus of elasticity

d = distance from neutral axis to extreme fiber

y = maximum deflection (between outer support), and

L = distance between the outer support points.

The specimen's second moment of inertia of is required to calculate the induced bending stresses as well as the applied load. The second moment of inertia (I_{xx}) was calculated numerically by Simpson's rule for various specimen thicknesses (Table 3). Expressions for the bending moment generated at the center of the sample, as well as the force required to deflect the specimen, are given below. All equations given are only true for elastic deformation.

Table 3.Second moment of inertia for coupon specimens.

	Thickness (mm)	$I_{xx}(mm^4)$
Four Point Specimen	2	23.01
Three Point Specimen	3	24.69

3-point test: Bending Moment = $12EyI_{xx}/L^2$
Displacing Force = $48EyI_{xx}/L^3$

4-point test: Bending Moment = $24EyI_{xx}/2.75L^2$
Displacing Force = $192EyI_{xx}/2.75L^3$

Prior to installation, all specimens were deformed by 5 mm. This amount of deflection placed the specimens in a zone of plastic deformation, ruling out any of the derived equations for determining the stress in the sample. This was done to ensure the best chance of inducing SCC in the specimens and to validate the testing method. Future testing will aim to control the stress in the specimen.

Further work on the project will explore the use of numerical methods to analyze the stress in plastically deformed specimens, as well as the stress state around the ribs.

INSTALLATION

The two testing jigs were installed at Centennial Coal's Springvale Colliery, an underground mine in the western coal fields, approximately 120km west of Sydney. The jigs were installed under dripping ground water in a particularly wet heading of the mine. Flow rates of 50mL/min have been recorded to be dripping from some of the bolts in this heading. This roadway suffers from poor ground conditions, and a large number of bolts have been found lying on the ground after having failed by SCC. All failed bolts found at this mine have been collected and tagged, and they are currently being analyzed by the research team at the University of New South Wales.

At the time of installation, an extensive water collection regime, outlined by Vandermaat et al., (2012) was carried out to classify the mine environment. Due to testing lead times, not all the samples have been analyzed; however, some of the results can be found in Table 4.

Table 4. Water testing results gathered at time of installation.

Test	Result
Dissolved Oxygen	1.0 mg/L
Water Temperature	22°C
pH	7.5
Conductivity	844 µS
Dissolved Solids	415 PPM

The jigs were placed so that the water dripping from the rock bolts would land on the most highly stressed part of the specimen. The jigs were attached to the roof meshing with plastic zip ties. Care was taken to ensure that there was no galvanic connection between any dissimilar metals to prevent aqueous corrosion. A schematic of the test rig placement can be seen in Figure 5. Figures 6 and 7 show the three and four point rigs installation in the roof, respectively.

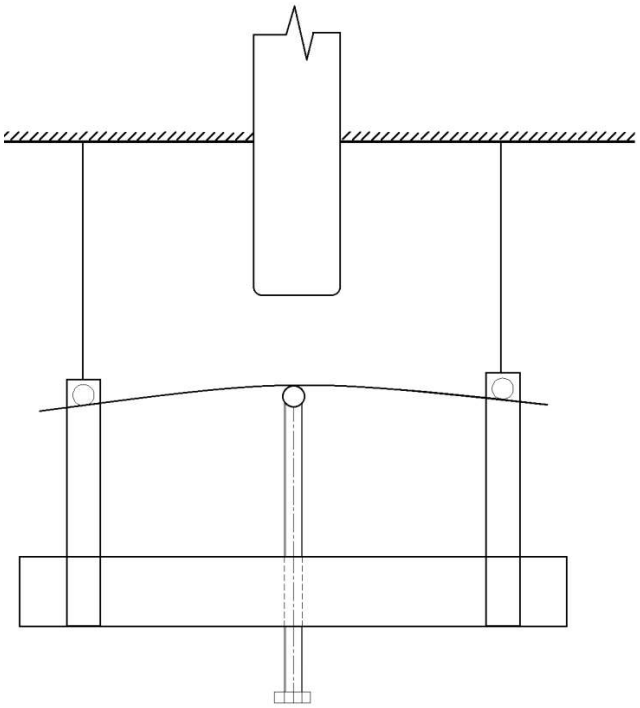

Figure 5. Schematic of testing jig placement in roadway tunnel (After, Vandermaat et al., 2012).

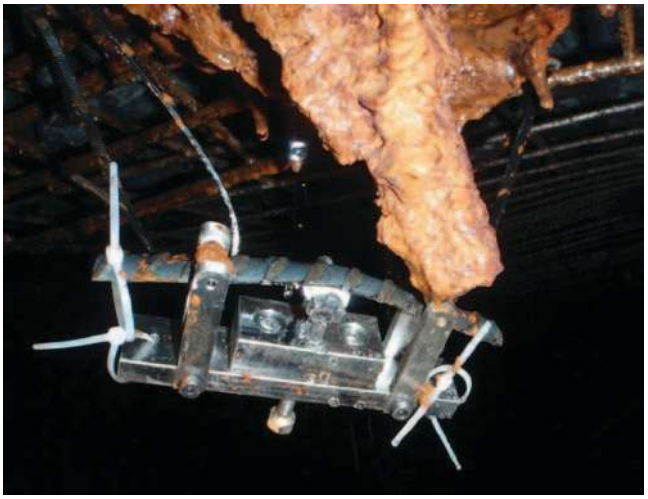

Figure 6. Three point jig installed with water dripping onto specimen.

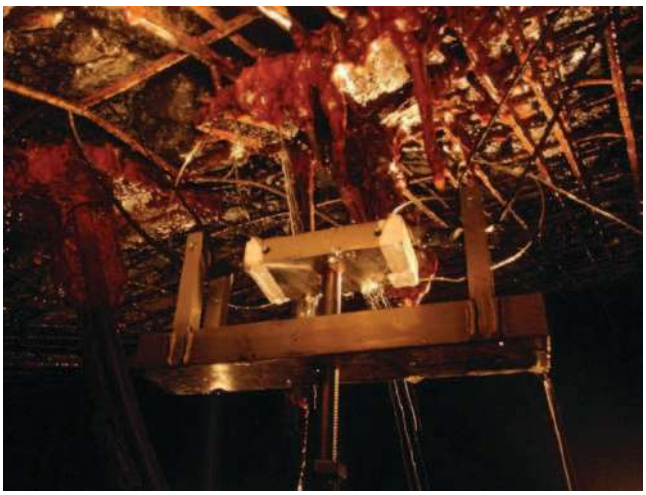

Figure 7. Four point jig installed with water dripping on specimen.

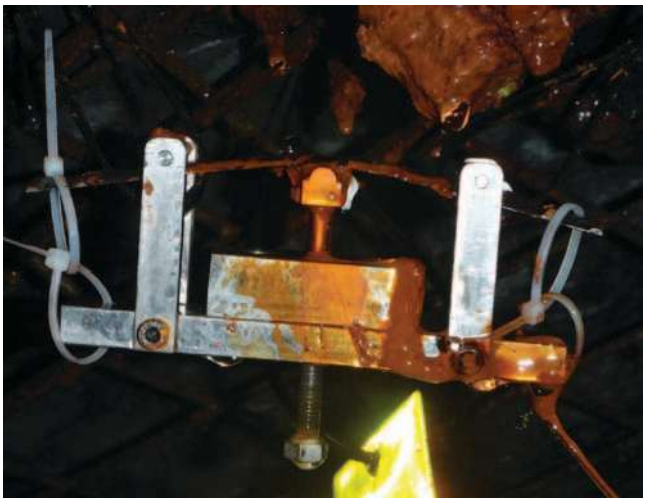

Figure 8. Three point test after 7 days showing accumulation of brown/orange substance.

A thick, brown/orange, almost gelatinous substance has accumulated on the mesh and bolts protruding from the roof. This substance was collected and is currently being analyzed for its chemical makeup and possible microbiological origins.

Microbiology can play an important role in the corrosion process. An accumulation of a biofilm on specimens may result in significantly different chemical conditions on the surface and crack tip compared to what is found in the bulk ground water solution (Little, 2011).

DATA GATHERING

The main aim of the experiment is to use coupon jigs to measure SCC velocities in the environment. To do this, the samples are visually inspected on a weekly basis to determine a time frame for failure. This visual inspection includes an assessment of changing water flow rate to determine if wetting and drying cycles are experienced, as well as noting any discoloration and/or visible cracking on the specimen.

Preliminary observations after one week in situ have shown that the brown/orange substance has begun to accumulate on the surface of the specimen and fixture (Figures 8 and 9). It is likely that this has accumulated from deposits on the mesh and bolts, falling onto the specimen. It is unclear how this will affect the results of the test.

Once the specimens have failed in the field, they will be returned to the laboratory so the failed surface can be inspected under a scanning electron microscope (SEM), as well as tested for products of corrosion. This will allow for a determination of the specific SCC process in the underground environment and weigh in on the proposed hydrogen embrittlement hypothesis (Villabla and Atrens, 2009; Gamboa and Atrens 2003; 2005).

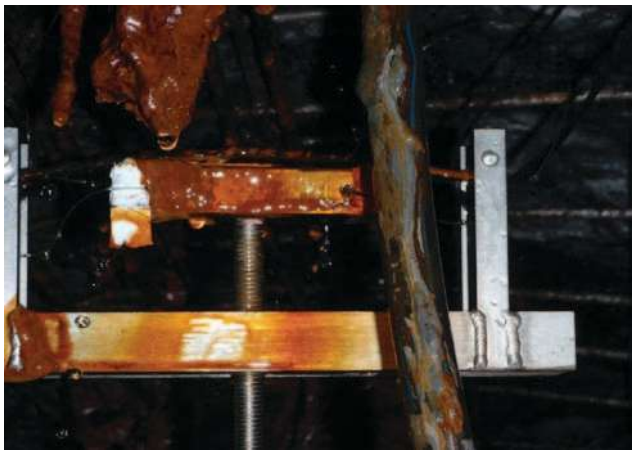

Figure 9. Four point test after 7 days showing accumulation of brown/orange substance.

CONCLUSIONS

Coupon testing has been identified as potential platform for investigating SCC in the mining environment. Specifically, ASTM G39 (2005) Bend Test has been selected as the most relevant form of coupon testing due to the nature of the tensile stresses generated in the specimen.

This type of testing produces stresses in a specimen that are comparable to those experienced by servicing bolts in situ. As result, it is feasible to conclude that any SCC experienced by the test specimens is likely to be indicative of the behavior of installed bolts. Coupon testing is expected to harvest an insight into the time frame and susceptibility of rock bolt steel to SCC within the mine environment. Further work will be conducted at other

partner mine sites and will be coupled with an extensive laboratory testing regime, as well as numerical modeling of stresses. At the conclusion of the project, it is expected that these experiments will indicate the possibility of using this testing as an early warning detection system for SCC in underground mines, allowing operators to gauge their potential exposure to the issue.

ACKNOWLEDGMENTS

The authors would like to acknowledge the Australian Research Council, as well as Anglo American, Centennial Coal, Xstrata Coal and Whitehaven Coal, for their generous funding of the project Coal. The authors would also like to extend their sincere gratitude to Brett Murnane and Springvale Colliery for allowing access to conduct experiments at their site.

REFERENCES

ASTM G38 (2005). "Standard practice for making and using c-ring stress corrosion test specimens." In: *Annual book of ASTM standards*. vol.3. Philadelphia, PA: American Society for Testing and Materials,) pp. 84–90.

ASTM G39 (2005). "Standard practice for making and using bent-beam stress corrosion test specimens." In: *Annual book of ASTM standards*. vol. 3. Philadelphia, PA: American Society for Testing and Materials, pp. 91–97.

ASTM G49 (2005). "Standard practice for preparation and use of direct tension stress-corrosion test specimens." In: *Annual book of ASTM standards*. vol. 3. Philadelphia, PA: American Society for Testing and Materials, pp. 151–157.

Craig, P, Saydam, S, Hagan, P, Crosky, A, and Hebblewhite, B, 2010. Australian Rock Bolt Steel Chemistry and Stress Corrosion Cracking. In: Hagan P, Saydam S, editors. The Second Australasian Ground Control in Mining Conference, Sydney (2010), publisher AusIMM. pp. 79–84.

Crosky, A., Fabjanczyk, M., Gray, P., Hebblewhite, B., Smith, B. (2002). "Premature rock bolt failure." Final Report Australian Coal Association Research Program, ACARP Project No. C8008.

Gamboa, E., Atrens A. (2003). "Laboratory testing of rock bolt stress corrosion cracking."In:Aziz, N., Kinnimoth, B., eds. *Proceedings of the Fourth Underground Coal Operators Conference*. Institute of Mining and Metallurgy, pp. 132–153.

Gamboa, E., Atrens, A. (2005). "Material influence on the stress corrosion cracking of rock bolts." *Engineering Failure Analysis*. *12*(2): 201–235.

Gray, P.(1998). "Stress corrosion cracking of rock bolts." In: Aziz, N., Kinnimoth, B., eds. *Proceedings of the Underground Coal Operators Conference*. Institute of Mining and Metallurgy, pp. 206–212.

Little, B.(2011). "Microbiologically influenced corrosion: causative organisms and mechanics." In: Camper, A., Feron, D., eds. *Proceeding of the Symposium on Microbiologically Influenced Corrosion*. Perth, Australia: The Australian Corrosion Association, pp. 1–8.

Vandermaat, D., Elias, E., Craig, P., Saydam, S., Crosky, A., Hagan, P. and, Hebblewhite, B. (2012). "Experimental protocol for stress corrosion cracking of rockbolts." In: Aziz, N., Kinnimoth, B., eds. *Proceedings of the Twelfth Coal Operators Conference*. Institute of Mining and Metallurgy, pp. 130–137.

Villabla, E., Atrens, A.(2009). "Hydrogen embrittlementand rock bolt stress corrosion cracking." *Engineering Failure Analysis*. *16*(2009): 164–175.

Passive Seismic Imaging for Determination of the Longwall Rear Abutment Location

Erik Westman, Associate Professor
Mining & Minerals Engr.
Virginia Tech
Blacksburg, VA

ABSTRACT

Few studies have been conducted regarding the location, movement, and relative magnitude of the rear abutment of a longwall coal mine. The rear abutment, or the abutment pressure arch in the gob area, is controlled primarily by the quality of pack of the gob; the more compacted the gob is, the larger the stress would be theoretically. While there is no definitive location for the rear abutment, early studies showed that it could be located as far back in the gob as 300 m (1,000 ft). Like the location of the rear abutment, there has been little research conducted and very few answers as to the exact magnitude of the rear abutment load.

Due to the fact that the rear abutment has been studied considerably less than the front or side abutment, the need for further studies is evident. From a ground control standpoint, the location and magnitude of a rear abutment could reveal information on the caving process associated with longwall mining, such as when the initial cave could be expected to occur in future panels. Besides the possible importance of the rear abutment from a ground control perspective, evidence related to the longwall rear abutment could be vital from a ventilation standpoint. The peak rear abutment location could serve as an area for harmful gases, such as methane, to accumulate because forcing air through repacked rock is more difficult than through loose rock.

The objective of this study is to determine whether passive seismic tomography could image the location, movement, and relative magnitude of the rear abutment as the longwall face retreated, in addition to the forward abutment and gob.

The results of a passive seismic imaging study at a western US longwall show evidence for the location, movement, and relative magnitude of a rear abutment. A clear zone of highly-stressed strata is shown where the forward abutment is expected and a low-velocity, damaged zone is shown behind the face where the gob is located. These two zones retreat with the face over a three-week period. In addition, the images show a return to stress levels behind the gob that are slightly higher than overburden stress levels, which is presumably the rear abutment. This occurs at a distance behind the face that is approximately the same as the face width for this mine.

We can conclude that passive seismic imaging can be used to identify the location, movement, and relative magnitude of the rear abutment of a longwall mine. This conclusion is dependent on the use of appropriate data collection and processing methods. The information provided can benefit the both ground control and ventilation engineers as they strive to improve the safety and efficiency of longwall mines. The knowledge associated with the rear abutment of a longwall could not only help increase production through proper initial planning and reduce down time, but it could also make positive strides in improving the overall safety surrounding a longwall mining operation.

INTRODUCTION AND BACKGROUND

Rear Abutment Location and Magnitude

In the early 1980's, longwall mining techniques were in their infancy in the United States. Advancements over the past thirty years have made longwall mining an integral portion of the United States coal industry, with nearly fifty percent of all underground coal produced in 2009 obtained through longwall methods (Weir International, 2010). Longwall mines have high production rates due to their continuous production, design simplicity, and their high recovery rates. Although longwall mines are extremely productive, there are only a few mines utilizing the method because the system itself demands specific seam qualities. As such, longwall mines accounted for only eight percent of the underground coal mines in the United States in 2009, but produced about half of the total underground coal tonnage (Young, 2010). Longwall mines require nearly horizontal seams with the ability to be extracted in a single slice (Hartman, 1992). If longwall mining is the selected extraction method in spite of unfavorable mining conditions, the mining process is likely to become more difficult due to the addition of numerous dangers accompanying the hazards inherent to underground mining.

There are many safety issues that may arise in longwall mines even with ideal seam conditions that are characteristic of underground coal mining in general. In underground coal mines, gas emissions are a common occurrence; continuous movement across the face causes gas to be a constant hazard on a longwall. Stress on the active workings is another concern with any underground mining operation, but unlike typical room and pillar

mining where ground response can be better anticipated from past experience, longwall mining ground response is difficult to determine due to the dynamic loading nature (Yasitli, 2005). The key for longwall mining success lies in the ability to deal with these safety concerns, as well as the overall capability to cope with rock pressure induced from longwall mining (Stefanko, 1963).

Rock pressure manifests itself primarily in the front and to the side of the longwall face, although a less discussed area of high stress is located behind the longwall face, in the caved zone (Stefanko, 1963). These three areas surrounding a longwall are each considered abutment zones. An abutment, or the highly stressed zone that develops to support an arch, occurs as weight from the overburden is shifted away from broken material and on to nearby solid material. These abutment loads can begin forming hundreds of feet in front of the longwall face, eventually coming to a peak near the face. These abutment loads can lead to dangerous conditions along the longwall face in the form of rock bursts, collapses in locations other than the gob, increased difficulty in ventilation controls caused by collapses, and even the continuous release of known firedamp gases, such as methane, due to increased pressure. While all these issues can arise due to the abutment pressures, knowledge of the known locations, approximate values, and anticipated times when the abutment loads form allow for planning and prevention to problems.

Of the two commonly discussed abutment stresses, front and side, the side abutment has not been evaluated to the extent of the front abutment. The side abutment refers to the pressure abutment arch on the headgate side of the longwall panel. The maximum side abutment is located to the rear of the face (Chang, 2011), approximately 3 to 9 m (10 to 30 ft) from the longwall side of the panel. The maximum pressure can be up to 3.5 times the in situ overburden pressure with pressures decreasing to as low as 0.4 times that of the overburden pressure at a lateral distance from the longwall of 0.25 to 0.33 the depth of the overburden (Hartman, 1992).

The front abutment, or the stress abutment arch ahead of the longwall face in the virgin coal (Stefanko, 1963), is the most researched and discussed abutment stress related to longwall mining. Numerous studies have been performed relating to the front abutment ranging from underground stress monitoring to numerical modeling. Through different studies, it has been shown that there is a defined front abutment zone located ahead of the face, with the greatest area of influence approximately between 18 and 36 m (60 and 120 ft) wide (Stefanko, 1963). While the area of influence is typically only 1/10 to 1/20 of the width of the longwall panel, it has been shown that largest front abutment loading occurs on the tailgate side of the panel and can extend for hundreds of feet preceding the longwall face (Chang, 2011).

Though the front abutment loading extends hundreds of feet in front of the face, the maximum front abutment is typically located between 4 and 9 m (13 and 30 ft) ahead of the face (Hartman, 1992); exact location is largely dependent on the Young's modulus of the host rock (Stefanko, 1963). The peak value has been measured at five times the overburden pressure (Hartman, 1992). From the peak of five times the overburden pressure, the front abutment decreases in advance of the longwall face, eventually leveling to the overburden stress (Alehossein, 2010). Hanna and others indicate that abutment pressure is present at 0.25 times the depth ahead of the longwall face, while significant increases can be seen at 0.1 times the depth for the mine (Hanna, 1991). Tailgate abutment pressure patterns were similar with the peak stress measuring approximately 1.5 times the headgate stress. They also indicate that these values are in agreement with data from other mines in the western United States. Personnel with the US Bureau of Mines conducted studies at the mine to measure the forward abutment stress location (Kneisley and Haramy, 1992). Borehole pressure cells in the panel rib showed that the peak forward abutment stresses occurred within 5 m (16 ft) of the longwall face, and stresses were not evident at a distance of 30 m (100 ft) from the face.

Exact locations, loads, and times have been observed in the field on numerous occasions for the front abutment, ranging from shallow longwall mines in the Appalachian basin to deep longwall mines in the western United Sates, as well as longwall mines with seams up to 9 m (30 ft) around the world. Utilizing borehole pressure cells, convergence recorders, and horizontal roof strain indicators in the Pittsburgh seam of the Appalachian basin, a front abutment ranging up to 370 m (1,200 ft) ahead of the face with a peak of four times the overburden pressure has been observed (Kalia, 1982). Using borehole pressure cells and observing entry convergence on a 2.7m (9 ft) thick seam in Colorado, an entry stress profile of a current longwall panel was mapped showing both side and front abutment loads (Chen, 2002). Alehossein mapped a full stress profile through field measurements that show not only the standard front and side abutment, but also an extremely low stressed zone above the longwall itself at a top coal caving longwall operation in China. From the low stressed zone above the longwall, a gradual increase in pressure was observed throughout the gob until a peak was reached showing the peak of a rear abutment stress (Alehossein, 2010).

While Alehossein's study was not the first to discuss or identify the location of a rear abutment peak, there are only a few studies that do. Few studies have been conducted in relation to the rear abutment due to initial thoughts by numerous scholars in the 1960s that a rear abutment did not exist. In the 1960s, Atkinson stated that any proof of the rear abutment existed was merely a source or instrumentation error (Stefanko, 1963). In conjunction with initial thoughts of a rear abutment only existing due to measurement errors, further proof of the rear abutment is difficult to obtain due to the inability to test for a rear abutment. Dangers that exist in the gob prevent accurate measurement and location of a rear abutment.

Even with limited ability to locate or identify the peak rear abutment, enough research has been conducted to detail the basics of a rear abutment. The rear abutment, or the abutment pressure arch in the gob area, is controlled primarily by the quality of pack of the gob: the more compacted the gob is, the larger the stress would be, theoretically. While there is no definitive location for the rear abutment, early studies showed that it could be located as far back in the gob as 300 m (1,000 ft). Like the location of the rear abutment, there has been little research conducted and very few answers as to the exact magnitude of the rear abutment load. This limitation exists due to the difficulty in placing and monitoring pressure cells in the gob. In one study, it was determined that the rear abutment load was greater than the overburden stress (Stefanko, 1963), while in another study it was determined that the rear abutment could only have a maximum load of the overburden pressure (Hartman, 1992).

With the lack of field testing in relation to the rear abutment, the best source of evidence for it lies in lab testing and numerical modeling analysis. Numerical modeling of a lignite seam in the Kutahya Province of Turkey that focused on the stress distribution of a longwall with top coal caving yielded results that not only supports the idea of a rear abutment, but also the location and load of the rear abutment. The numerical model, which began as a solid block of coal and then excavated to simulate the longwall mining process beginning with tailgate and headgate development for a 90 m (300 ft) wide face, successfully modeled the typical front abutment at a location 6 m (20 ft) ahead of the face. In addition to the front abutment, a rear abutment was identified following the same general trend of increasing stress. As such, the broken material exhibited a stress of zero, and the stress increased with distance from the face, reaching a maximum point nearly 60 m (200 ft) into the gob (Yasitli, 2005).

Besides numerical modeling analysis, lab testing conducted by Harris in the mid-1970s has generated a great deal of interest in furthering knowledge of longwall abutment stresses. Harris created a sandbox model of a typical longwall mine with the floor of the sandbox representing a coal seam and the overlying sand representing the roof strata; both the floor and sand were of similar scale up qualities in density and material properties to real material. Utilizing different depths of sand to represent differing overburden depths, as well as pressure measurements from highly sensitive diaphragm cells, it was concluded, for this test, that a rear abutment did exist and was a function of face position and depth. Harris concluded that the rear abutment was located at a lateral distance equal to 1.25 times the overburden depth from the front abutment for the sandbox model; with this distance Harris noted that it was possible the rear abutment had not been observed in the field because research had never been conducted far enough into the gob to locate it. Aside from showing a rear abutment, Harris stated that, since the rear abutment seems to be a function of front abutment and depth, it would be possible for the rear abutment to completely disappear (Harris, 1974). In tests based on Harris' research, Park used an improved sandbox model and obtained similar results to Harris related to the front abutment stress and strata reaction to mining; Park did not focus on a rear abutment (Park, 1985).

Due to the fact that the rear abutment has been studied considerably less than the front or side abutment, the need for further studies is evident. From a ground control standpoint, the location and magnitude of a rear abutment could reveal information on the caving process associated with longwall mining, such as when the initial cave could be expected to occur in future panels. In addition to caving information, specific knowledge related to the rear abutment could lead to information about when the gob area transforms from a dynamic loading process to a static load; theoretically, the location of the rear abutment peak would be that transitional point.

Besides the possible importance of the rear abutment from a ground control perspective, evidence related to the longwall rear abutment could be vital from a ventilation standpoint. From previous research, it has been noted that the rear abutment is dependent on the repack of caved material with a magnitude ranging anywhere from virgin stress to some multiple of that. If the rear abutment stress were that of the overburden, or more, then, at that point, the material would be repacked to approximate intact rock with little void space. The peak rear abutment location could then serve as an area for harmful gases, such as methane, to build up because forcing air through repacked rock is more difficult than through loose rock. With the possible location of high methane concentrations, it could then be possible to determine the amount of ventilation required through the gob to reduce the concentrations to non-harmful levels.

Passive Seismic Tomography

Seismic tomography is the method where a rock mass is non-destructively imaged by analysis of the velocity at which the seismic waves travel through the rock mass. Central to this research is the change that a rock mass undergoes as it is loaded. Figure 1 shows a typical stress-strain curve on an unconfined compression test with three regions marked. During initial loading (region I), many microfractures within the sample are closed, resulting in a rapid increase in the velocity with which an elastic wave travels through a rock sample. As the sample is loaded elastically (region II), the wave velocity continues to rise, but not as rapidly. As macrofractures nucleate and grow (region III), the velocity at which the wave travels is reduced (Paterson and Wong, 2005). Thus, the velocity with which a seismic wave travels through a rock mass is related to relative stress changes within the rock mass, and relative stress changes can be imaged using seismic tomography.

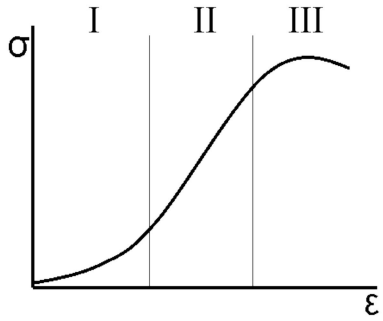

Figure 1. Typical stress-strain curve for unconfined rock sample with three regions in which elastic wave propagation velocity changes due to stress-induced changes to the rock.

Tomography techniques can be divided into two different approaches, active tomography and passive tomography. Active tomography employs a seismic source at a known location, which acts at a prescribed time, for example a hammer blow or an explosive blast. Active tomography was used at the field scale as far back as 20 years ago in the mining industry to image geologic- and stress-related features (Buchanan, et al., 1981; Kormendi et al., 1986; Mason, 1981). It was not until the past several years that it has been readily accepted within the geosciences for petroleum reservoir characterization and for geotechnical applications. Passive tomography, also known as local earthquake tomography, has been used by the geoscience community to develop images of earth structures, including volcanoes and earthquake fault zones, by passively monitoring existing seismicity with multiple receivers (Kissling, et al., 1994; Power, et al., 1998; Thurber and Eberhart-Phillips, 1999). In the case of monitoring a longwall panel, the existing seismicity is that which has been induced by the mining process. These induced seismic events were used as the sources for passive seismic tomography in the current study.

STUDY SITE

NIOSH personnel collected the data for the study site over an 18-day period in 1997 (Swanson, 2002). Average overburden at the mine is 350 m (1,150 ft), with coal seam height ranging from 2.6 to 3 m (8.5 to 10 ft). The seam is overlain by 2 to 7 m (6.5 to 23 ft) of sandstone and underlain by 35 m (115 ft) of sandstone. The mine had experienced bumps in the past, mainly in the tailgate entry.

The panel under investigation is 250 m (820 ft) wide with a previously-mined panel to the tailgate side and an unmined panel to the headgate side. Over the course of the study, the face retreated 430 m (1,400 ft), averaging about 25 m (80 ft) per day. Sixteen geophones were assembled on the surface above the panel to monitor and locate microseismic events. Figure 2 displays the panel geometry and receiver locations. The face retreated through a series of backfilled entries about halfway through the study. These entries were mined for escapeway purposes and are evident in the figure. The raw data include 172,632 P-wave arrival times from 11,696 microseismic events. There was an average of 650 events per day with a maximum of 1,450 events. The area of interest is 0.34 square km (0.13 square mi.).

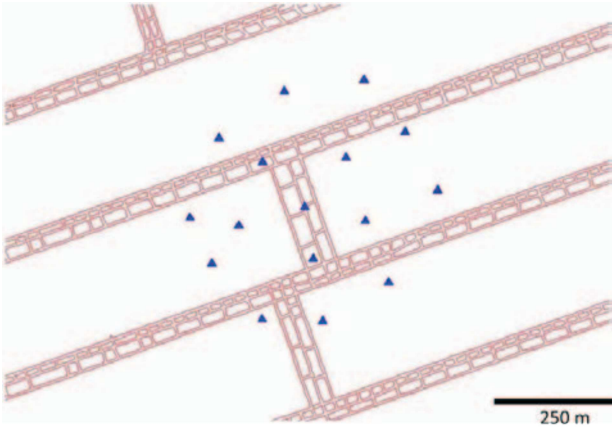

Figure 2. Panel geometry and receiver locations.

DATA PROCESSING

The data set consists of event locations, station locations, arrival times at stations, event magnitudes, and error magnitudes. Only events that reported arrival times by at least 10 of 16 stations were included in the set. A layered initial velocity model, determined from measurements at the site, was included. To convert arrival times to travel times, the ray that arrived to the station array first was propagated through the layered initial velocity model and assigned a travel time. This travel time was then added to the remaining arrival times for that event. Also straight ray path velocities were examined, and any velocities above 10,000 m/s (32,800 ft/s) were removed from the data sets. These velocities are likely the result of poor arrival time picks and could produce high velocity artifacts in the tomograms. Figure 3 shows a scatter plot of the travel times versus the separation distance between the event and the station at which it was recorded. Examination of the plot shows that the background velocity is approximately 4,500 m/s (14,800 ft/s), the lowest observed velocities are approximately 3,000 m/s (10,000 ft/s) and that the travel times above 10,000 m/s (32,800 ft/s) have been removed from the data set.

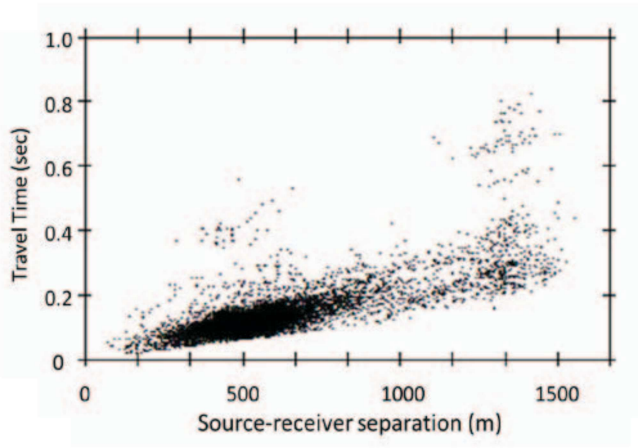

Figure 3. Scatter plot of the travel times versus the separation distance between the event and the station at which it was recorded.

The double-difference algorithm, TomoDD, written by Haijiang Zhang and Clifford Thurber, was developed for use in earthquake tomography. It is based on the double-difference relocation algorithm, HypoDD (Waldhauser, 2001). TomoDD is a double-difference method that jointly relocates events and determines a velocity model (Zhang and Thurber, 2003). There are several examples in the literature of its use in earthquake relocation and tomography (Waldhauser and Ellsworth, 2000; Zhang and Thurber, 2003); however, there are no applications to mining. The assumption behind double-difference tomography is that, if the distance between two seismic events is small compared to the distance from the events to a receiver, they will have similar travel times. The difference between calculated and measured travel times between two events at one receiver can then be used to adjust the position of the events, as well as the velocity model used to locate the events (Waldhauser and Ellsworth, 2000). TomoDD allows for variable gridding; the interval between the x, y, and z nodes in the inversion grid can be varied so that a finer grid may be applied in areas that are well sampled and a courser grid in areas that are not as well sampled. This is especially useful for passive sources because ray path density is rarely consistent, and areas of high microseismic activity can be imaged with a fine grid. Important parameters in TomoDD include damping, weighting, and number of iterations. The damping factor damps the hypocentral adjustments so that the adjustment vector does not become large or unstable. In TomoDD, examination of a condition number output by the program is used to determine the damping value. The condition number, the ratio of the smallest to largest eigenvalue, should be between 40 and 80 with damping values between 1 and 100 (Waldhauser and Ellsworth, 2000). For this data set, damping factors between 120 and 150 were used resulting in condition numbers from 45 to 66.

RESULTS AND DISCUSSION

The knowledge associated with the rear abutment of a longwall could not only help increase production through proper initial

planning and reduce down time, but it could also make positive strides in improving the overall safety surrounding a longwall mining operation. Plan-view velocity tomograms at seam level were generated by the passive seismic tomography to map the redistribution of the abutment stresses and are shown in Figure 4. Pixels not traversed by rays are shown in purple, and the daily face position is shown by a heavy black line.

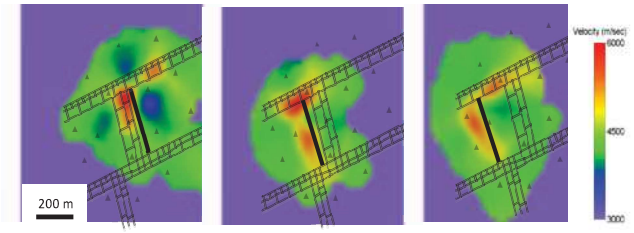

Figure 4. Plan-view velocity tomograms at seam level. Pixels not traversed by rays are shown in purple. Face locations shown by solid black line.

Abutment stress occurs in underground mines as ore is extracted along the boundary where the material is removed (Peng and Chiang, 1983). In longwall mining, this stress is transferred immediately in front of the face and to the sides of the panel. Formation of gob behind the advancing face allows for stress relief. Abutment stress is generally larger on the tailgate side, assuming it is adjacent to a mined-out panel. At the seam level, front abutment pressure is detectable at a lateral distance approximately equal to the overburden thickness. The front abutment becomes evident about 30 m (100 ft) outby the face and from there the stress starts to increase to its peak at 1 to 10 m (3.28 to 32.8 ft) outby the face (Peng and Chiang, 1983; Yasitli and Unver, 2005). In weak roof, the maximum abutment stress along the faceline occurs at the corners of the face, while, in stronger roof, it often occurs midface (Peng and Chiang, 1983). In addition to vertical stress redistribution, joints faults and horizontal stress orientation may contribute to larger or smaller abutment stresses and more erratic failure.

Several consistent features are clearly shown in the images generated by the passive seismic tomography study while other features are present but less obvious. The high velocity region caused by the forward abutment stress associated with movement of the longwall face is clearly shown moving with the face location on the three days shown in Figure 4. Additionally, higher velocities are seen near the tailgate side of the face and along the tailgate entry. The lowest velocities seen in the images are located in the gob inby the longwall face. While it is unlikely that seismic waves were transmitted directly through the gob, it is likely that the first arriving seismic energy had traveled from its source, around the gob, and to the receiver, resulting in a long travel time and indicting a relatively low velocity through the gob. These low-velocity regions also clearly move with the face position. Less easily observed is a return to velocity levels that are approximately the same as, or slightly above, the background levels further inby the longwall face (i.e., inby the low-velocity gob region). These features are consistent for each of the three days and are approximately the same distance from the face, but they vary in magnitude. It is presumed that these features correlate to the location of the rear abutment.

To make the magnitude and location of the abutment zones more clearly visible, velocity cross sections were generated parallel to the gateroads and in the middle of the longwall face. Both the images and the cross sections display smoothed results. Nodes in the tomograms are located at 20 m intervals. Nevertheless, the smoothed results are useful for examining the magnitude and location of the abutment zones.

Figure 5 shows the distribution of velocities from the panel outby the abutment loading (toward the left) through the high-velocity region caused by the peak forward abutment, through the low-velocity gob region, then to a slightly elevated velocity zone and a return to background velocities (on the right). The plots are all oriented so that the face is positioned at a value along the x-axis of zero, so the x values indicate a distance inby the face. Cross-sections for each of the three days are shown, along with an average value for the three days. For each of the three days, the peak forward abutment stress is located approximately 30 m (100 ft) outby the face, the lowest velocity is located from 65 to 90 m (213 to 295ft) inby the face, and the presumed rear abutment occurs 190 to 240 m (623 to 787ft) inby the face.

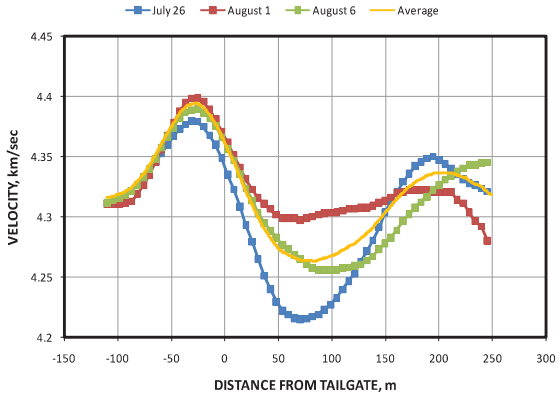

Figure 5. Distribution of velocities parallel to gateroads and at mid-face. The plots are all oriented so that the face is positioned at a value along the x-axis of zero, so the x values indicate a distance inby the face (meters). Values on y-axis are velocity, with units of km/sec.

The distribution of velocity parallel to the face and approximately 100 m (330 ft) inby the face is shown in Figure 6 and is provided as a basis for developing confidence in the tomography results. The y-axis has been placed in the middle of the tailgate pillars, and the values along the x-axis indicate the distance into the gob, then into the headgate, and eventually into the next, unmined panel (at the right of the figure). A very low velocity is shown on the left side of the figure, which corresponds to the gob of the previously mined panel. At the y-axis, the velocities peak indicating the loading of the tailgate pillars. The velocities reach their lowest value at a distance of 80 to 90 m (262 to 295 ft) from the tailgate, in the lowest velocity, least consolidated portion of the gob. The velocities increase toward the headgate, reach another peak at the headgate pillars, and then drop to a background level in the adjacent, unmined panel. The measured velocities agree with expected stress redistribution, providing a measure of confidence in the results obtained by the current study.

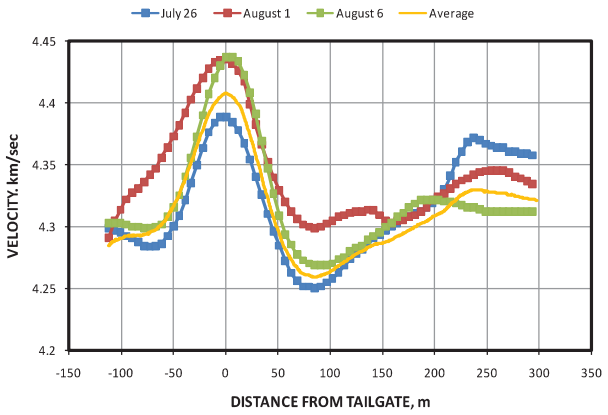

Figure 6. Distribution of velocity parallel to the face and approximately 100 m inby the face. The plots are all oriented so that the tailgate is positioned at a value along the x-axis of zero, so the x values indicate a distance from the tailgate toward the headgate (meters). Values on y-axis are velocity, with units of km/sec.

The results can be compared to prior studies on the forward abutment location and magnitude, as well as the location and relative magnitude of the rear abutment. By comparing the current results to the well-studied forward abutment location, a measure of the reliability of the current results can be obtained. The passive seismic tomography results show a peak forward abutment located approximately 30 m (100 ft) outby the face and starting approximately 100 m (330 ft) outby the face. The study by Chen et al. (2002) provides field measurements that are likely the best comparison as the mining conditions were comparable. Their borehole pressure cell measurements in the active panel show an increased loading that initiates 85 m (279 ft) outby the face for one panel and 120 m (394 ft) outby the face for the subsequent panel, which is in close agreement with the results obtained by the current study. The field measurements show the peak forward abutment stresses were measured in close proximity to the face, at a distance of less than 10 m (33 ft). This is less than what is observed by the passive seismic tomography, which is probably a result of the smoothing inherent in the tomography calculations.

The current study indicates a rear abutment that is located approximately 200 m (656 ft) behind the face and is slightly greater in magnitude than the overburden stresses, although the results indicating the rear abutment were not as consistent as those for the forward abutment. The face width at the mine was 260 m (853 ft) at the time that the data were collected and the overburden was a fairly consistent 350 m (1,148 ft). The observed location of the rear abutment at a distance approximately equal to the face width supports the adage that the full cave occurs in a longwall panel when the gob has "squared up," (i.e., when the length of the gob is equal to its width). Additionally, the current results agree somewhat with measurements made by Maleki (1984) using Gloetzl cells located in the gob. At a Western US semi-caving panel coal mine having a 150 m (500 ft) wide face, Maleki measured a rear abutment at a distance of 180 m (590 ft) behind the face.

Based on the observed correlation between the current results and the expected forward abutment stress redistribution and gateroad loading, a moderate level of confidence can be placed in the ability of passive seismic tomography to indicate the location and relative magnitude of the rear abutment, although additional studies at other mines are recommended. Additionally, future research could include comparison to subsidence data to determine whether the location of the rear abutment can be correlated to the location of completed subsidence.

SUMMARY AND CONCLUSIONS

The knowledge associated with the location and magnitude of the rear abutment of a longwall will not only help increase production through proper initial planning and reduce down time, but it can also make positive strides in improving the overall safety surrounding a longwall mining operation. A passive seismic tomography study at a Western US longwall coal mine was conducted to determine whether the location and relative magnitude of the rear abutment could be identified. Sixteen geophones on the surface above the mine recorded mining-induced seismicity over an 18-day period, and more than 11,000 events were recorded. The recorded arrival times were converted to travel times, and double-difference passive seismic tomography was completed with the data. Double-difference tomography provides the most precise results and is used routinely in earthquake seismology studies. The fundamental concept linking seismic velocity tomography to stress redistribution is that as rock is stressed, seismic waves travel through it at a higher velocity due to its increased modulus. Velocity tomograms at seam level were plotted for three days, and cross sections were generated.

Based on the results observed, several conclusions are drawn:

1. Passive seismic tomography provides consistent and reasonable results for interpreting the location of the abutment loads associated with a longwall coal mine.
2. The forward abutment peaks approximately 30 m (98 ft) outby the face and initiates approximately 100 m (330 ft) out by the face, which agrees relatively well with measurements by others.
3. Analysis of the cross-sections parallel to the face and approximately 100 m (330 ft) inby the face clearly shows loading on the headgate and tailgate pillars as expected, providing confidence in the tomography results.
4. The cross sections parallel to the gateroads indicate that the gob extends from 65 to 90 m (213 to 295 ft) inby the face, and that the presumed rear abutment occurs 190 to 240 m (623 to 787 ft) inby the face.

The results seem reasonable although additional mine studies are recommended. The ultimate goal of the research must be to increase the safety and efficiency of underground the underground miner.

ACKNOWLEDGEMENTS

The authors are grateful to the National Institute for Occupational Safety and Health for providing the raw data for this study and to Dr. Haijiang Zhang for sharing the passive seismic tomography code. This research was funded by a National Science Foundation EAGER Grant (CMMI-1051111).

REFERENCES

Alehossein, H. and Poulsen, B.A. (2010). "Stress analysis of longwall top coal caving." *International Journal of Rock Mechanics and Mining Sciences 47*(1): 30–41.

Buchanan, D.J., Davis, R., Jackson, P.J., and Taylor, P.M. (1981). "Fault location by channel wave seismology in United Kingdom coal seams." *Geophysics 46* (7): 1065–1073.

Chang, J. (2011). "Distribution laws of abutment pressure around fully mechanized top-coal caving face by in-situ measurement." *Journal of Coal Science and Engineering (China) 17*(1): 1–5.

Chen, J., Mishra, M., Zahl, E.,Dunford, J., and Thompson, R. (2002). "Longwall mining induced abutment loads and their impacts on pillar design and entry stability." In: *Proceedings of the 21st International Conference on Ground Control in Mining*. Morgantown, WV: West Virginia University, pp. 11–17.

Hanna, K. (1991). "Automated longwall mining for improved health and safety and the Foidel Creek Mine." *Preprint Number 91-165*.Denver, CO:SME, pp. 9.

Harris, G. W. (1974). "A sandbox model used to examine the stress distribution around a simulated longwall coal-face." *International Journal of Rock Mechanics and Mining Sciences and Geomechanics 11*(8): 325–335.

Hartman, H. L., ed. (1992). *SME Mining Engineering Handbook*. 2nd Ed. Englewood, CO: Society for Mining, Metallurgy, and Exploration, pp. 2161.

Kalia, H. N. and Jones, J.C. (1982). "Monitoring mine stability." *First International Conference On Stability In Underground Mining*. Vancouver, British Columbia: AIME, pp. 25.

Kissling, E., Ellsworth, W.L., Eberhart-Phillips, D., and Kradolfer, U. (1994). "Initial reference models in local earthquake tomography." *Journal of Geophysical Research 99*(B10): 19,635–19,646.

Kneisley, R. O. and Haramy, K. (1992). *Report of investigations 9427: Large-scale strata response to longwall mining: a case study*. Washington, DC: US Department of the Interior, Bureau of Mines, pp. 25.

Kormendi, A., Bodoky, T., Hermann, L., Dianiska, L., and Kalman, T. (1986). "Seismic measurements for safety in mines." *Geophysical Prospecting 34*(7): 1022–1037.

Maleki, H. (1984). "Pressure measurements in the gob." In: *Proceedings of the 25th US Symposium on Rock Mechanics*. Evanston, IL, American Rock Mechanics Association, pp. 533–545.

Mason, I. M. (1981). "Algebraic reconstruction of a two-dimensional velocity inhomogeneity in the High Hazles Seam of Thoresby Colliery." *Geophysics 46*(3): 298–308.

Park, D. and Kicker, D.C. (1985). "Physical model study of a longwall mine." *Mining Science and Technology 3*(1): 51–61.

Paterson, M.S. and Wong, T. (2005). *Experimental rock deformation – the brittle field*. 2nd ed. New York, NY: Springer, pp. 358.

Peng, S. S. and Chiang, H. S. (1983). *Longwall Mining*. Hoboken, NY: Wiley and Sons, pp. 720.

Power, J.A., Villaseñor, A., and Benz, H. M. (1998). "Seismic image of the Mount Spurr magmatic system." *Bulletin of Volcanology 60* (1): 27–37.

Stefanko, R. (1963). "Stress distributions in longwall mining." *AIME Preprints 63F13*. Englewood, CO: AIME, pp. 13.

Swanson, P., Kenner, B., and Krahenbuhl, T. (2002). "Seismic event data acquisition and processing: distribution and coordination across PC-based networks." In: *Proceedings of the 30th International Symposium of Application of Computers and Operations Research in the Mineral Industry*. Littleton, CO: SME, pp. 637–647.

Thurber, C. and Eberhart-Phillips, D. (1999). "Local earthquake tomography with flexible gridding." *Computers & Geosciences 25*(7): 809–818.

Waldhauser, F. (2001). "HypoDD—a program to compute double-difference hypocenter locations." *US Geological Survey Open File Report 01-113*, pp. 25.http://geopubs.wr.usgs.gov/open-file/of01-113/

Waldhauser, F. and Ellsworth,W. L. (2000). "A double-difference earthquake location algorithm: method and application to the Northern Hayward Fault, California." *Bulletin of the Seismological Society of America 90*(6): 1353–1368.

Weir International, Inc. (2010). *United States longwall mining statistics: 1989–2010*. Downers Grove, IL: Weir, pp. 8.

Yasitli, N. E. and Unver, B. (2005). "3-D numerical modelling of stresses around a longwall panel with top coal caving." *Journal of the South African Institute of Mining and Metallurgy 105* (May/June): 287–300.

Young, P. (2010). Annual *Coal Report 2009*. Washington, DC:US Energy Information Administration, Office of Oil, Gas, and Coal Supply Statistics, US Department of Energy, pp. 79.

Zhang, H. and Thurber, C. H. (2003). "Double-difference tomography: the method and its application to the Hayward Fault, California." *Bulletin of the Seismological Society of America 93*(5):1875–1889.

Relocating Mining–Induced Seismicity at the Trail Mountain Mine

Meagan S. Boltz, Student
Department of Mining Engineering
University of Utah
Salt Lake City, UT

Kristine L. Pankow, Associate Director
University of Utah Seismograph Stations
University of Utah
Salt Lake City, UT

Michael K. McCarter, Professor
Department of Mining Engineering
University of Utah
Salt Lake City, UT

ABSTRACT

From October 2000 to April 2001 a local array of fourteen seismograph stations was deployed at the Trail Mountain Mine (TMM), an underground coal mine in Emery County, Utah, to locate mining-induced seismicity (MIS). Original analysis of the data provided epicentral locations that coincided closely with the active longwall panel. The original analysis yielded poor quality hypocenters, however, preventing a useful relation from being made between mining activity and the event depths. For the original analysis, only stations at elevations above mine level were used for locating MIS. As a result, P- and S-arrival times from four of the stations in the local array were not used: an in-mine station and three stations at elevations below mine level. This study compares mine workings and active mining to a revised TMM dataset that included P- and S-arrival times from the lower elevation stations that were not used in the previous study. In the revised locations, a modified master event methodology was used to calculate station delays. These station delays correct for errors in the shallow layers of the velocity model. The resulting hypocentral locations have improved depth resolution, determined by a lower root mean square (RMS) for the locations, compared to the original study. Most of the events occur in the roof of the mine and follow the longwall panel. When located using the velocity model determined in the original study, the elevations of the events increase as the longwall panel progresses. One possible explanation for the elevation increase is that it may be related to geology or the caving process. As presented here, a 10% decrease in the shallow velocity structure results in a more plausible location for the hypocenters. Consequently, it is hypothesized that progressive development of the TMM longwall panel(s) may have resulted in a progressive change in the velocity model.

INTRODUCTION

In a previous study by Arabasz et al. (2002), a local mine-scale network, as seen in Figure 1, was installed at the Trail Mountain Mine (TMM). The TMM is an underground, longwall coal mine located in Emery County, Utah. At this location, a 2.5 m coal seam was mined at a depth of approximately 0.67 km. The goal of the study was to provide an analysis of the effect of mining-induced seismicity (MIS) on the Joes Valley Dam. During this study, 1,906 MIS events were located over a seven-month period from October 2000 to April 2001. Figure 2 shows a time-magnitude distribution plot for the dataset. The MIS is coincident with the mining of the 1st right longwall panel (Figure 3a), which was started shortly after the 2nd right panel was abandoned after 366 m due to unexpectedly numerous bounces.

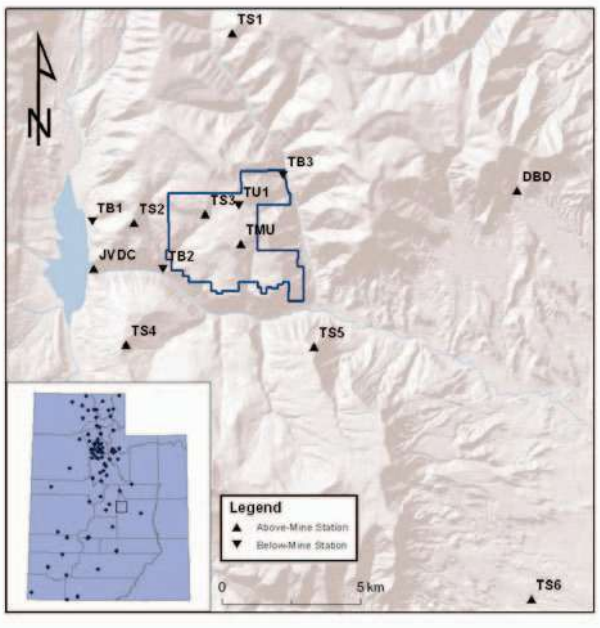

Figure 1. Map showing stations within the vicinity of the Trail Mountain Mine. Triangles represent stations at elevations above the mine while inverted triangles represent stations below the mine. TU1 is an in-mine station. The inset shows the regional seismic network (diamonds) and the location of the enlarged map (box).

The local mine-scale network at the TMM consisted of fourteen stations embedded into the larger Utah regional network (Figure 1). The local network provided increased coverage, which allowed for the improved detection and analysis of small magnitude events. The majority of the stations were located at elevations above the

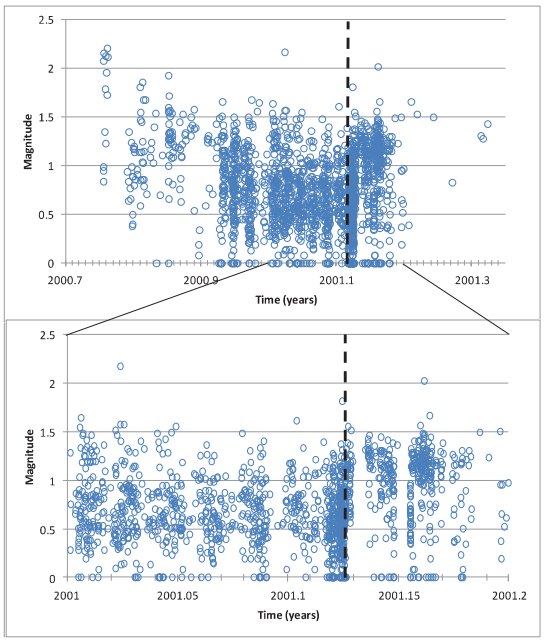

Figure 2. Plot of magnitude vs. time. The time scale is given in decimal years and the dashed line shows the time when seismic activity increases.

mine, though there were four stations below the level of mining. Three of these below-mine stations were located on the surface, but at lower elevations because of the topography of the area. The fourth station was an in-mine station that was placed at the end of the 1st right panel.

The velocity model used for locating the MIS in the original study, known as the Trail Mountain Composite velocity model (Pechmann et al., 2002), consists of two separate velocity models. The first model is for stations located in the eastern Basin and Range province of Utah and the second model is for stations located in the Colorado Plateau province of Utah. The two models differ at depths below 4.14 km to account for differences in crustal structure between the two physiographic provinces. The shallow portion of the models was derived from sonic logs recorded about 60 km away from the mine. Logs closer to the mine were available, but were not used because there were no data for the first 0.8 km of the stratigraphic column. A comparison done as part of this study showed that the Trail Mountain Composite velocity model agrees with a sonic log from the TMM property (Wagner, 1984) at the depths where the log is available.

The original study used a location algorithm known as Hypoinverse (Klein, 1978) to determine the locations of the MIS. The below-mine stations were not used in the original study because the location algorithm would incorrectly calculate the ray paths to these stations. Even with the reduced station coverage, Hypoinverse provided epicentral locations that coincided closely with the longwall panel; however, the quality of the hypocenters was poor, making it difficult to discern a useful relation between the mining activity and location depths. The calculated depths for the majority of the events clustered around the datum, which is a predefined depth at the top of the velocity model that represents the average elevation of the surface stations (2.6 km above sea level).

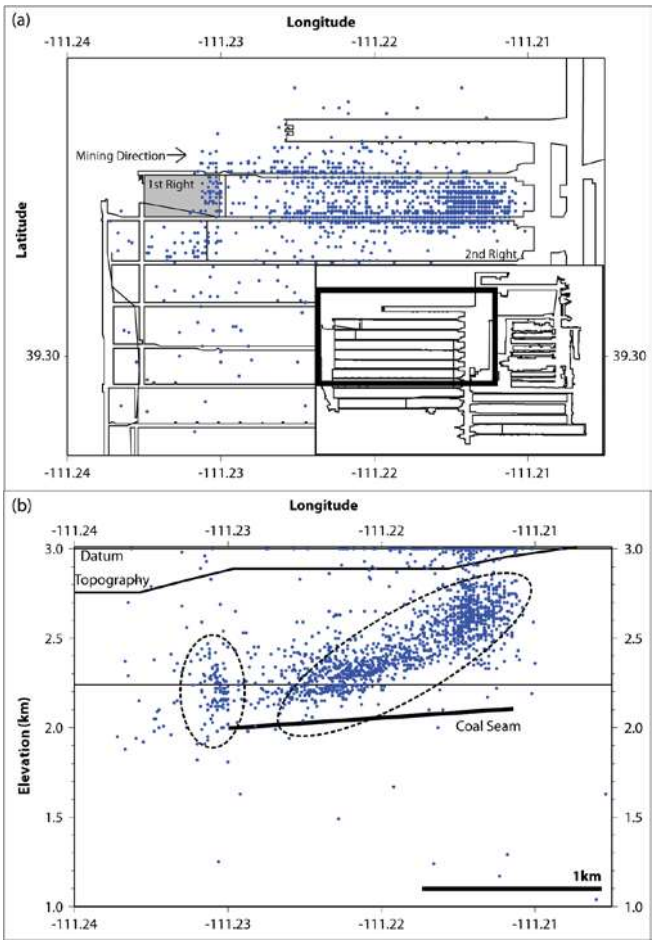

Figure 3. Plots of revised locations of the MIS using Hypoellipse and the station delays showing (a) plan-view locations and (b) a cross-section of the locations. The ellipses in the cross-section locations show the two event clusters. The line at 2.24 km depth marks a change in the velocity model. The shaded region on the 1st right panel indicates a barrier between the 1st right and 2nd right panels.

Boltz et al. (2011) relocated the MIS from the TMM using 1) Hypoellipse (Lahr, 1979), an algorithm that allows the use of both above- and below-mine stations and 2) station delays calculated using a modified master event methodology. In this study, the revised hypocenters are compared to the geologic structure around the mine and the mining sequence.

LOCATING THE MINING-INDUCED SEISMICITY

Unlike Hypoinverse, which calculates ray paths to a datum and applies elevation corrections to determine the hypocenter, Hypoellipse calculates ray paths directly to the station elevation. This enables the program to find ray paths to stations located below the seismicity, as well as those above the seismicity. As a result, all stations can be used in the locations, creating a three-dimensional station array and improving depth resolutions.

As was shown by Boltz et al. (2011), using Hypoellipse improved the depth resolution, seen by a decrease in root mean square (RMS), for the events that were located with all stations.

Unfortunately, as a result of poor data quality, it was only possible to make P-arrival time picks at the below-mine stations for 179 of the 1,906 events using standard data processing methods. The remaining events were located using only the above-mine stations and, as in the original study, the depths cluster around the datum, as shown in Figure 4. In order to improve the hypocenters, a master event technique (Johnson and Hadley, 1976) was used to generate station delays. The delays are applied primarily to correct for possible errors in the upper layers of the velocity model as a result of weathering in the rock mass. Using a slightly modified approach to the master event technique, Boltz et al. (2011) selected twenty "well-located" events, events that had the most picks from both above- and below-mine stations. These twenty events were used to find the median travel time residual (the difference between the calculated and observed travel times) at each station, which was applied as the station delay.

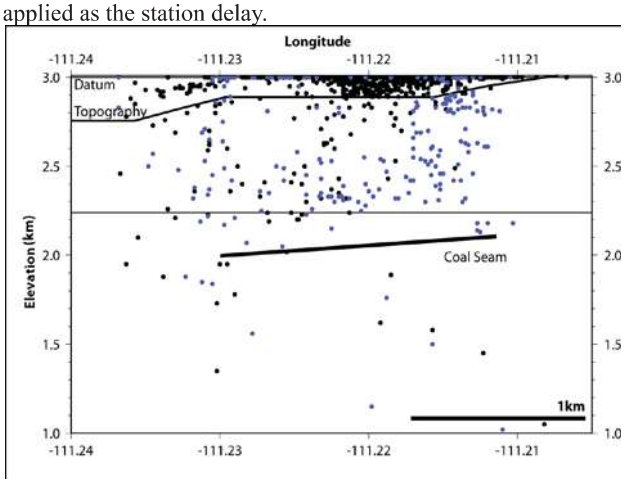

Figure 4. Cross-section of the original Hypoellipse locations. Blue events are located with below-mine stations. The line at 2.24 km depth marks a change in the velocity model.

TRAIL MOUNTAIN LOCATIONS

Figure 3 shows the revised locations of the MIS using Hypoellipse and the station delays calculated using the modified master event technique. In plan-view (Figure 3a), most of the events follow the 1st right longwall panel, with a small portion of the events scattered through older mine workings. In the cross-section of the Hypoellipse locations with station delays (Figure 3b), there is a significant increase in depth resolution compared to the Hypoellipse locations without station delays (Figure 4). In the trial with station delays, the seismicity locates closer to mine level and is concentrated in the roof.

There are two distinct event clusters in the final locations, seen by the dashed ellipses in Figure 3b. The first cluster is a small group of events that occur immediately before the start of mining of the 1st right panel. These events are located at the beginning of the 1st right panel and in the mined-out portion of the 2nd right. The second cluster includes the majority of the events and is above the 1st right. The elevations of the events in this cluster increase as time and the panel progress.

Despite the increased depth resolution there are still 280 air quakes, or events that occur above the topography. The air quakes are determined by plotting a cross-section of the topography over the length of the longwall panel and tabulating the number of events that occur above this line. This provides a reasonable estimate of the air quakes because the event depths and topography elevation change very little across the width of the longwall panel.

DISCUSSION

The events that occur before the mining of the 1st right panel are in the small barrier between the 2nd right and the beginning of the 1st right (shaded area of Figure 3a), possibly due to the start-up room for the 1st right. There are also a few events in the end of the mined-out portion of the 2nd right. Most of the activity in this cluster occurs immediately before the panel begins to advance, though some of the events occur shortly after advance begins, and exhibit the largest magnitudes of the events recorded during this study (Figure 2). The depths of these events span over roughly 500 m, but there is no good explanation for the varying depth at this time. During this pre-mining period there were also a number of events that locate in older mine workings.

Animations were generated that show the seismicity with the position of mining in the 1st right panel. The slides for the animation are rendered in 12-hour increments and show both the events that occur during that 12-hour period and the cumulative activity. Slides from the animation are presented in Figure 5. The black events are events that occur during the 12-hour period covered by the slide. The colors of the events fade as time progresses. The black bar represents the current face position. The animation shows the seismic activity following the headgate and tailgate as mining of the panel progresses, from approximately December to mid-February. Figure 5a shows this occurring on December 16 and December 17, 2001. The animations also show that most of the events closely follow the face position, with about one-half of the most recent events (black events) occurring ahead of the face and one-half behind the face (Figure 5b). This was determined assuming that the face progresses at a uniform rate between known positions of the face, which were given in one-week increments. Examining the activity on dates when the position of the face is known suggests that there is more activity behind the shearer than ahead of it. In mid-February, the seismic activity increases and the events merge across the longwall panel (Figure 5c). The cause of this increased activity is still being investigated, though it is observed that there is a slight increase in magnitude for these events (Figure 2). The median magnitude of all events is 0.77. During the three-week period prior to the increase in activity, the median magnitude is 0.6, and it increases to 0.89 for the next three weeks.

As seen in Figure 3b, the majority of the seismicity occurs in the roof of the mine, at least 125 m above the coal seam. As the panel progresses, the elevations of the events greatly increase until they are within approximately 100 m of the surface. Figure 6 shows a stratigraphic cross-section of the seismicity. The roof of the mine is made up of several sandstone layers. The seismicity appears to begin in the Blackhawk Formation and Castlegate Sandstone, approximately parallel to the coal seam, but as the panel progresses the seismicity is no longer constrained to those layers. Instead the seismicity increases in elevation, cutting through all of the layers until it reaches the surface.

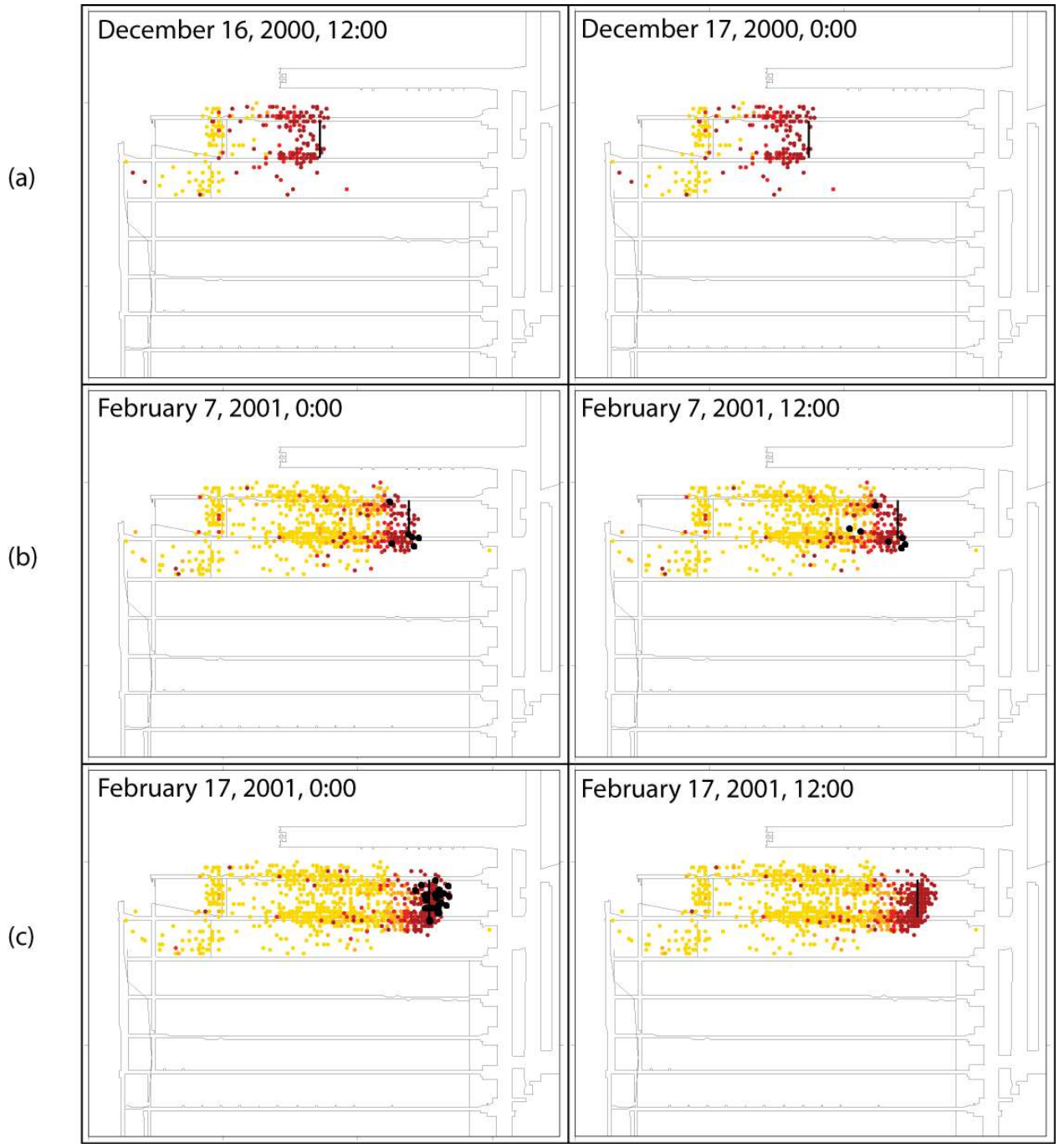

Figure 5. Plan-view of seismic events locations and longwall location for two sequential 12-hour time frames for (a) December, (b) early February, and (c) mid-February. The black events are events that occur during the 12-hour time frame of the slide. The colors of the events fade from red to yellow over 3 weeks.

Alternate Velocity Model

One possible explanation for the upward trend in event locations as the face advances is an inaccurate velocity model. One hypothesis is that the velocity model has been altered as a result of mining. The Trail Mountain Composite velocity model was based on sonic logs taken 60 km away from the mine in an area undisturbed by mining activity. While a log taken on mine property verifies the velocities at lower depths, it could not confirm the shallow velocities because the log does not have data for the upper 0.8 km of the stratigraphic column. The velocities for the shallower layers may have been lowered by the mining process. To test this, the upper layers of the Trail Mountain Composite velocity model were reduced by 10%. This simulates a low-velocity area above the mine. Figure 7 illustrates the difference in velocity between the models.

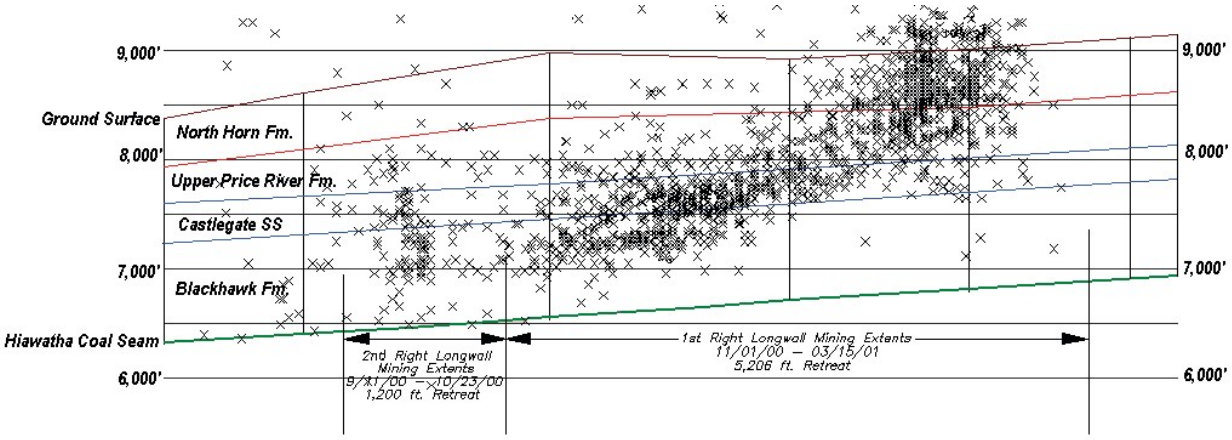

Figure 6. Stratigraphic cross-section of the master event locations.

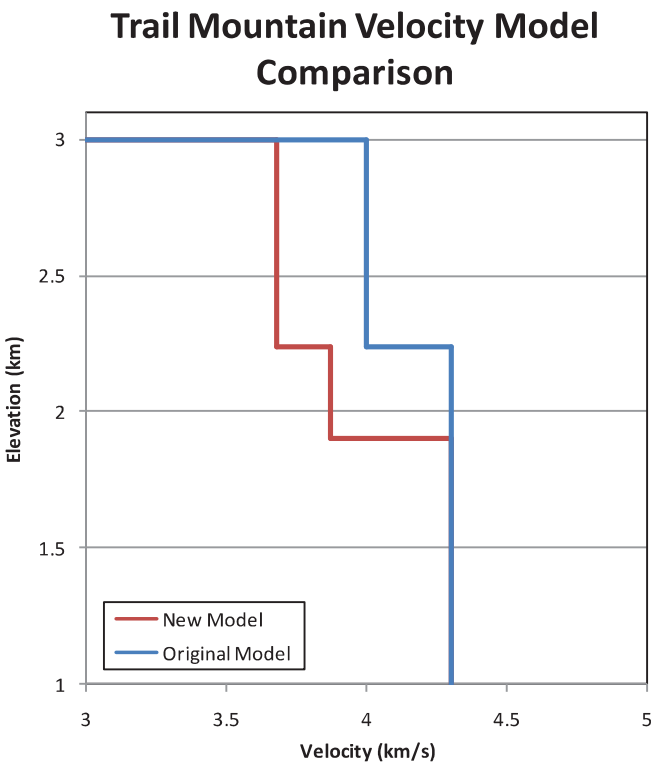

Figure 7. Comparison of the Trail Mountain composite velocity model and the modified Trail Mountain velocity model for the first 2 km of the stratigraphic column.

Figure 8 shows the resulting cross-section from this alternate velocity model. The cross-section provides a more plausible representation of the seismicity. The events are still occurring in the roof, though closer to mine level. The event depths range from about 80–530 m above the coal seam, rather than ranging from 125 m above the seam to the surface as determined by the original velocity model. Additionally, the seismicity is at the same dip as the coal seam and occurs in the Blackhawk Formation and Castlegate Sandstone until the end of the panel. At the end of the panel, the elevation of the seismicity once again increases, though it does not reach the surface, as in the previous model. The elevation increase indicates that the velocity structure is still more complicated than the model that was used in this study.

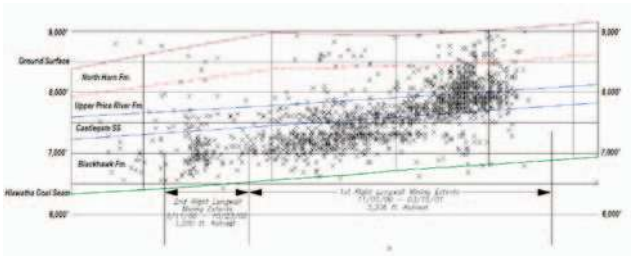

Figure 8. Stratigraphic cross-section showing the alternate velocity model locations.

CONCLUSIONS

The revised MIS locations using Hypoellipse and station delays (Boltz et al., 2011) provide higher quality hypocentral locations when compared to the original locations (Arabasz et al., 2002). These revised locations allow for the observation of previously unseen features of MIS at the TMM. The revised locations show the activity grouping around the headgate and tailgate of the 1st right panel for approximately three-fourths of the panel, at which point it forms a single cluster spreading across the panel.

The relocations also reveal that the seismicity is occurring in the roof of the longwall panel. The event elevations may increase as the longwall progresses. If this is the case, the increase could be related to an unmapped geologic structure or could be a product of the caving process. A more probable explanation is that the development of the mine workings lowered the seismic velocity of the stratigraphic column above the mine. Assuming this hypothesis is true, the MIS locates in the roof of the mine, in the Blackhawk Formation and Castlegate Sandstone, with an elevation increase at the end of the panel. The increase indicates that the velocity structure in the Trail Mountain area is more complicated than what can reasonably be developed using the available information.

ACKNOWLEDGEMENTS

The authors of this paper would like to thank Andrew King, James Pechmann, William Pariseau, and Tex Kubacki for their insights and opinions on this project. The authors would also like to thank the University of Utah Seismograph Station for the use of their facilities and equipment. Additionally, they would like to thank the state of Utah and NIOSH for funding this project. Finally, the authors would like to thank Energy West Mining Company, a subsidiary of PacifiCorp, for their willingness to provide information about the Trail Mountain Mine for this study.

The views and conclusions contained in this document are those of the authors and should not be interpreted as representing the opinions or policies of NIOSH or other sponsors of this research.

REFERENCES

Arabasz, W.J., Nava, S.J., McCarter, M.K., Pankow, K.L. (2002). "Ground-motion recording and analysis of mining-induced seismicity in the Trail Mountain area, Emery County, Utah." Technical Report. University of Utah Seismograph Stations, Salt Lake City. [www.quake.utah.edu/Reports/sitla2002a/TMSITLARept.pdf].

Boltz, M.S., Pankow, K.L., McCarter, M.K. (2011). "Relocating mining-induced seismicity at the Trail Mountain Utah coal mine with a three-dimensional seismic array." (Abstract S33A-2299). Presented at the AGU Fall Meeting 2011. San Francisco, CA: December 5–9.

Johnson, C.E., Hadley, D.M. (1976). "Tectonic implications of the Brawley Earthquake Swarm, Imperial Valley, California." *Bulletin of the Seismological Society of America*, 66(4): 1133–1144.

Klein, F.W. (1978). "Hypocenter location program HYPOINVERSE." U.S. Geological Survey. Open-File Report 78-694.

Lahr, J.C. (1979). "HYPOELLIPSE: a computer program for determining local earthquake hypocentral parameters, magnitudes, and first motion pattern." U.S. Geological Survey. Open-File Report 79-431.

Pechmann, J.C., Arabasz, W.J., Pankow, K. L., Jensen, M. E. (2002). "Seismic velocity model for the Trail Mountain area." In: Arabasz, W.J., Nava, S.J., McCarter, M.K., Pankow, K.L., with Pechmann, J.C., Jensen, M.E., McKenzie, J.D. "Ground-motion recording and analysis of mining-induced seismicity in the Trail Mountain area, Emery County, Utah." Technical Report, University of Utah Seismograph Stations, Salt Lake City. B1–B9. [www.quake.utah.edu/Reports/sitla2002a/TMSITLARept.pdf].

Wagner, A. (1984). "High resolution seismic survey, Trail Mountain Project, Emery County, Utah." Technical Report for Natomas Coal Company. Austin, TX: Emerald Exploration Consultants, Inc.

Effects of Transverse Isotropy on Vertical Stresses When Multi–Seam Mining under Supercritical Longwall Panels

Anastasia M. Suchowerska, Ph. D. Student
John P. Carter, Prof.
Richard S. Merifield, Ass. Prof.
Centre For Geotechnical and Materials Modelling
University of Newcastle
Callaghan, Australia

ABSTRACT

The design of effective ground support requires a sound understanding of the pre-mining state of stress in the stratum to be mined. Irregularities in the stress field encountered during multi-seam mining are governed primarily by the previous mining in the surrounding strata. The aim of this study is to quantify the effects of rock mass transverse isotropy on the vertical stress redistribution in the rock strata beneath supercritical longwall panels. Wilson's equations for determining the stress distribution induced in and beyond a single longwall panel after it has been mined have been adopted, and a plane strain finite element analysis of an elastic medium, together with the stress changes predicted by Wilson, was used to calculate the final pre-mining stresses in the underlying strata. Values of the independent shear modulus ($G¢$) of the rock strata, ranging from 0.1 to 1 times the isotropic shear modulus (G_{iso}) in the plane of the strata, and a Poisson's ratio (ν) of 0.25 have been investigated. The key finding of this study is that the predicted magnitude of vertical stress in the transversely isotropic strata beneath a mined supercritical longwall panel is larger and changes more quickly with horizontal distance than is the case for an isotropic rock mass. This finding is of significance for the design of ground support measures in multi-seam mining operations.

INTRODUCTION

Multi-seam longwall coal mining is considered to be the future means of extracting a large portion of the underground coal in Australia (Gale, 2004a, Howarth and Monger, 2009). This is because technological advances over the last two decades have enabled longwall mining to supersede room-and-pillar mining in terms of both safety and production levels for both single and multi-seam operations.

Multi-seam coal mining has been conducted for many decades around the world. Many types of investigations have been conducted to understand what generates adverse mining conditions, including empirical investigations(e.g., Haycocks, Karmis and Ehgartner, 1982, Chase, Worley and Mark, 2005); analytical derivations(e.g., Salamon and Oravecz, 1976, Salamon, 1990); numerical modeling studies(e.g., Chekan and Listak, 1993, Gale, 2004b, Morsy, Yassien and Peng, 2006, Zipf, 2006, Wittles, Reddish and Lowndes, 2007, Esterbuizen, Mark and Murphy, 2010); and published summaries of what generates adverse mining conditions(Hsiung and Peng, 1987a, Hsiung and Peng, 1987b, Haycocks and Zhou, 1990, Hill, 1995). Most of these studies have commented that there are still many aspects of multi-seam mining instability that are not well understood. In particular, most of the focus has been on multi-seam mining where at least one of the seams has been extracted using room-and-pillar mining. Only a select few studies have considered the situation where each seam has been mined using longwall panels (Chekan and Listak, 1993, Gale, 2004a).

Understanding the in situ stress environment is required for effective ground control during mining. The in situ stresses encountered when second and subsequent seams are extracted in a multi-seam mining operation are not the same as for virgin conditions, prior to any mining at all. Although a lot of research has been conducted to understand what governs multi-seam interactions, there is still a limited understanding of the stress fields in which multiple seam mining is conducted. Understanding the stress field around a longwall panel and its gateroads is what enables mine designers and engineers to predict potential failures and design appropriate ground control measures.

Underground coal mine designers are often under pressure to propose "less-conservative" designs, in an environment where failures are not tolerated. Many mine designers use computer models to help estimate how the ground will redistribute stresses and deform. There are two main means of represent a rock mass stratum using continuum modeling technique: individual structures of the rock mass and how they behave and interact are modeled; and the overall behavior of the rock mass is modeled as an equivalent continuum material (Gerrard and Pande, 1985). The development of more sophisticated computer software packages matched by the increase of computer processing power in the last decade has enabled many modelers of underground coal mining to favor the use of the former (e.g., Gale, 2004a, Gale, 2004b, Zipf, 2006, Esterbuizen, Mark and Murphy, 2010). The methods of this type of modeling have become very sophisticated: modeling in 3D, representing elasto-plastic constitutive behavior with non-associated flow rules, incorporating strain softening models for coal, ubiquitous joint modeling, and even simulating the caving process behind a longwall face. Modeling of the individual structures in a rock mass is extremely useful because it can

provide more detailed information at a local level than equivalent continuum material modeling (e.g., stresses and displacements along discontinuities). However, direct modeling of the structures within a continuum is usually a very time consuming process to setup. Furthermore, a large number of input parameters are often required, and quite often their values are not immediately available and must be assumed. Many modelers of underground coal mining have considered modeling the rock mass stratum as an equivalent continuum material (e.g., Morsy and Peng, 2002, Badr et al., 2003). Modeling a rock mass as an equivalent continuum material is advantageous when all the individual material properties of the discrete structures in a stratum are not available, and the analysis is not as labor intensive as modeling each of the individual structures. However, the difficulty is to select properties for the equivalent continuum material that will effectively represent the behavior of the essentially discontinuous rock mass. Irrespective of the level of intricacy of the computer model all computer models still necessarily include assumptions, because our understanding of rock mass behavior and the essential properties is incomplete. Obviously, these assumptions are warranted if their effects are insignificant or able to be quantified.

Previous authors (Su, 1991, Seedsman, 2011) have mentioned that stratification in coal measure rocks gives rise to transverse isotropic behavior of the rock mass, and that this property should not be ignored in analysis of coal extraction because it can significantly affect the resulting stress distributions. However, to date, the effects of transverse isotropic behavior have not been extensively quantified. This paper presents results from a much larger study, which has investigated the stress changes in rock strata under supercritical longwall panels. The larger study (Suchowerska, Merifield and Carter, 2012) aimed to identify the parameters that most influence vertical stress redistribution around supercritical longwall panels. Parameters that have been considered include: the abutment angle, overburden depth, pillar width, unconfined compressive strength of the coal, and the friction angle of the coal.

THEORY

Mining of subsequent coal seams is usually considered once there is no more coal to be safely removed from a seam that is being or has recently been mined. What is left behind from a seam that has been mined using the longwall technique is usually approximately equally spaced chain pillars with goaf material in between. Analysis of the stresses that are present in an underlying seam can be understood by considering a typical plane strain section parallel with the longwall face (Figure 1).

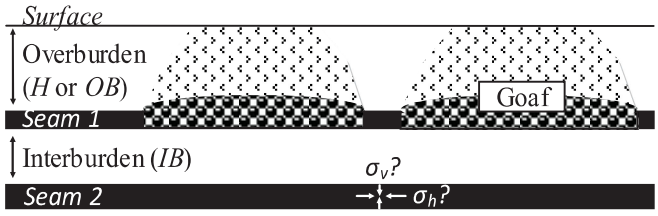

Figure 1. Schematic representation of the structure of the strata before multi-seam mining commences.

Vertical Stress Distribution In A Chain Pillar

A theoretical solution for the vertical stress redistribution after a longwall panel has been mined was first presented by Whittaker (1974) (Figure 2). For a single longwall panel, this theory shows that the abutment stress in the ribs dissipates to the original overburden stress with increasing distance from the rib-edge. The final peak stress induced in the ribs is offset from the rib-edge. The loading in the goaf area returns to a maximum vertical stress at some distance behind the longwall face, after the goaf material has undergone consolidation and hardening.

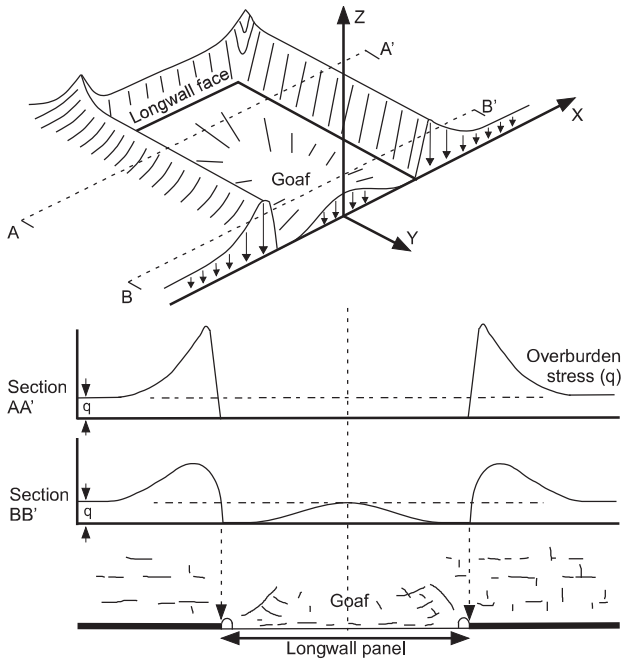

Figure 2. Strata pressure redistribution in the plane of the seam around a longwall face. Figure is based on the schematic diagram by Whittaker (1974).

There have been several theoretical models presented to describe the vertical stresses in conventional chain pillars as a result of mining a series of longwall panels: e.g., Wilson (1972, 1983), Choi and McCain (1980), Hsiung and Peng(1985), and Mark (1990). A comprehensive review of each of these methods and their associated assumptions was presented in a paper by Mark (1990). The study by Mark (1990) also made comparisons of the predictions of each of these models with case studies in order to assess their robustness and make recommendations on appropriate input parameters. The models suggested by Wilson (1983) and Mark (1990) were judged to be the most flexible for any longwall design project, because they can consider a variable number of gateroads and mined seam heights. The Wilson model also considers yielding of the pillar at the rib-edge and the potential for yield to occur only in the seam (i.e., in the pillar) or also in the roof, seam, and floor of the longwall panel. The equations of this model require a relatively large number of input parameters, which means the model can be difficult to use for specific projects when there is limited information available. For the purpose of the present study, Wilson's analytical model provides equations that contain enough flexibility to consider all the possible potential

variables that may affect vertical stress redistribution around a longwall panel. These equations also have the advantage of ensuring that vertical equilibrium is maintained at seam level. Wilson's general stress distribution in a pillar consists of a yielded zone and an elastic zone in the pillar, for which the vertical stress equations are provided in Figure 3.

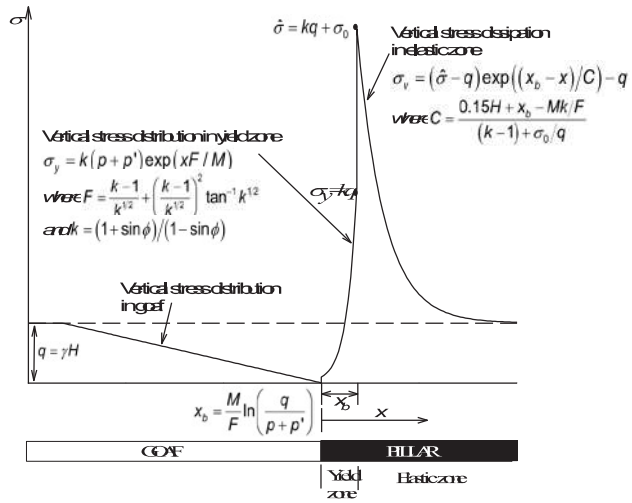

Figure 3. Wilson's (1983) equations for vertical stress in the vicinity of the rib-edge (x = 0) of a longwall panel for conditions of yield in seam only, for rigid roof and floor boundary condition. Where p is the lateral restraint applied to the rib-edge boundary, $p'=\sigma_0'/(k-1)$, σ_0' is the uni-axial (residual) compressive strength of yielded coal, M is the extracted seam height (thickness), H is the depth of the overburden, and φ is the friction angle of the material.

Wilson (1983) assumed that a distance from the rib edge of 0.3 times the depth of cover was required to return to overburden stress in the goaf. This implies that the extra loading on the pillar would correspond to an abutment angle (β) of 16.7 degrees. The abutment angle is used to define a wedge of material above the goaf, whose load is supported by the chain pillars (King and Whittaker, 1971, Wilson and Ashwin, 1972). The abutment angle assumed by Wilson (1983) together with the associated pressure rise in the caved waste have been queried by Salamon (1992). Therefore, a study was conducted to assess the effect of variation in the abutment angle to the stresses in the strata underlying supercritical panels (Suchowerska, Merifield and Carter, 2012). Mark (1990) deduced from stress measurements in chain pillars that an abutment angle of 21 degrees should generally be used, as it would yield conservative estimates of the abutment load. The Analysis of Longwall Pillar Stability (ALPS) computer program developed by NIOSH therefore uses an abutment angle of 21 degrees in its calculations. The abutment angle for Australian coal fields was confirmed also to be about 21 degrees, with a few exceptions (Colwell, 1998). Therefore, for the purpose of the present study, Wilson's equation for the parameter *C* (see Figure 3) was changed to allow for the inclusion of the widely accepted and used abutment angle of 21 degrees (Equation 1):

$$C = \frac{0.5H\tan\beta + x_b - Mk/F}{(k-1) + \sigma_0/q}$$

Transverse Isotropy

Coal measure rocks, being sedimentary in origin, usually contain sub-horizontal bedding planes in conjunction with one or more sub-vertical joint sets. These joint sets in the coal measure stratigraphy often give rise to transversely isotropic deformation behavior. Figure 4 shows a schematic representation of a transversely isotropic material.

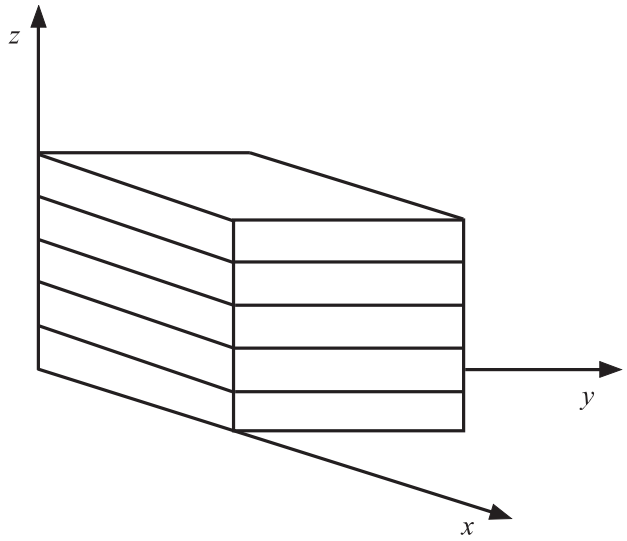

Figure 4. Schematic diagram of a transverse isotropic material, where the xy plane is the plane of isotropy (adapted from Brady & Brown (1992)).

As identified by Lightfoot and Liu (2010), an isotropic elastic medium does not represent coal measure rocks accurately, because the bedding in coal measure stratigraphy inhibits lateral spread of stress. For the purpose of stability analysis of underground coal extraction, it has been claimed that considering the transverse isotropic behavior of the rock mass is more significant than considering its nonlinear behavior (Seedsman, 2011). A study conducted by Su (1991) confirmed that considering the planes of weakness in coal measure rock was more important than the nonlinear material behavior to predict magnitudes of subsidence above a longwall panel.

In general, a transverse isotropic material requires five independent variables to describe its elastic constitutive behavior, but in many cases this number may be reduced to just three independent variables. For plane strain analysis, as considered in this study, the stiffness matrix for a general transversely isotropic material is as given in Equation 2, where E and ν are properties in the plane of isotropy, and E', ν', and G' are in planes perpendicular to the plane of isotropy.

$$\begin{pmatrix}\varepsilon_{xx}\\ \varepsilon_{zz}\\ \gamma_{zx}\end{pmatrix}=\begin{pmatrix}1/E & -\upsilon'/E & 0\\ -\upsilon'/E & 1/E' & 0\\ 0 & 0 & 1/G'\end{pmatrix}\begin{pmatrix}\sigma_{xx}\\ \sigma_{zz}\\ \tau_{zx}\end{pmatrix}$$

For the transversely isotropic material shown in Figure 4, E and ν govern the behavior in the xy plane, while E' and ν′ are relevant to deformations in the xz and yz planes. As previously indicated, in many cases it is assumed that $E = E'$

For isotropic materials, the shear modulus (G_{iso}) is defined by Equation 3:

$$G_{iso}=\frac{E}{2(1+\nu)}$$

In a transversely isotropic medium, the shear modulus in the planes perpendicular to the plane of isotropy is independent of the values of Poisson's ratio and Young's modulus relevant to the plane of isotropy. Thus it is called the independent shear modulus (G').

Independent shear moduli have been measured for many different rock types in laboratory tests, and some of these results have been summarized by Gerrard (1977). Most of the laboratory measurements involved testing intact triaxial rock samples. Generally published values of the independent shear modulus normalized by the Young's modulus (i.e., G'/E) from this type of laboratory testing are in the order of 0.3 to 1.

However, the independent shear modulus is likely to be smaller for bedded and jointed coal measure strata when those strata are represented as a single continuum. Back analysis of the heights of failures in the roof at the Donkin Morien tunnel was used by Seedsman(2009, 2011) to estimate the independent shear modulus of the rock mass. In this case, Seedsman proposed that the value for Young's modulus normalized by the independent shear modulus (E/G') to be between 15 and 20. This corresponds to a value of shear modulus normalized by Young's modulus (G'/E) of 0.06 to 0.05. Therefore, Seedsman's proposed independent shear modulus corresponds to a ratio of G'/G_{iso} range from 0.1667 to 0.125. This is calculated by dividing the G'/E ratio by a ratio of G_{iso}/E of 0.4, which arises by assuming that a stratum has a Poisson's ratio of 0.25.

Transversely isotropic rock mass properties have also been represented by incorporating the shear and normal stiffnesses of the bedding planes into the derivation of constitutive relations of the rock mass (e.g., Goodman and Duncan, 1969). For a plane strain problem, the stress-strain relationships can be written as shown in Equation 4 (Alehossien and Carter, 1990). These equations assume that the discontinuities are equi-spaced and parallel to the xy plane.

$$\begin{pmatrix}\varepsilon_{xx}\\ \varepsilon_{zz}\\ \gamma_{zx}\end{pmatrix}=\frac{1}{E}\begin{pmatrix}1-\nu^2 & -\nu(1+\nu) & 0\\ 0 & 1-\nu^2+R_n & 0\\ 0 & 0 & 2(1+\nu)+R_s\end{pmatrix}\begin{pmatrix}\sigma_{xx}\\ \sigma_{zz}\\ \tau_{zx}\end{pmatrix}$$

where

$$R_s=E/(SK_s) \quad \text{and} \quad R_n=E/(SK_n)$$

K_s and K_n represent the relative shear and normal stiffness of the joint set, and S represents the joint spacing. The relative shear and normal stiffness values obtained from experimental testing of joints have been collated by Bandis et al. (1983). The shear stiffness (K_s) values primarily range from 0.1 to 100 MPa/mm. Equation and show the derivation to relate shear stiffness of the joints to the normalised independent shear modulus (G'/G_{iso}).

$$\frac{1}{G'}=\frac{2(1+\nu)}{E}+\frac{R_s}{E}=\frac{1}{G_{iso}}+\frac{1}{SK_s}$$

$$\frac{G'}{G_{iso}}=\frac{1}{1+G_{iso}/SK_s}=\frac{1}{1+E/(2SK_s(1+\nu))}$$

The value of the independent shear modulus will vary between sites depending on geologic conditions. The independent shear modulus values considered in this study range from 0.1 to 1 times the isotropic shear modulus (G_{iso}) which encompasses Seedsman's proposed values.

PROBLEM DEFINITION

The aim of this study was to identify the effect of transverse isotropy on the changes of in situ vertical stresses in the strata underlying a longwall-mined seam, assuming the plane strain model shown in Figure 1. Only the case where the first seam has been extracted as a series of supercritical longwall panels has been considered here. Analysis of the problem has also been simplified by considering only those areas where the vertical stress in the mined coal seam differs significantly from the magnitude of the initial overburden stress. This corresponds to the pillar region and parts of the left and right goaf, as shown schematically in Figure 5.

For the cases studied here it was assumed that the pre-mining stress state in the ground was initially isotropic, i.e., at any location the vertical and horizontal stress components are initially equal. The vertical stress changes imposed on the underlying strata due to mining of the first seam were applied to a finite element model using Wilson's equations (Wilson, 1983). Key assumptions of this study were that the magnitude of the unit weight of the overlying

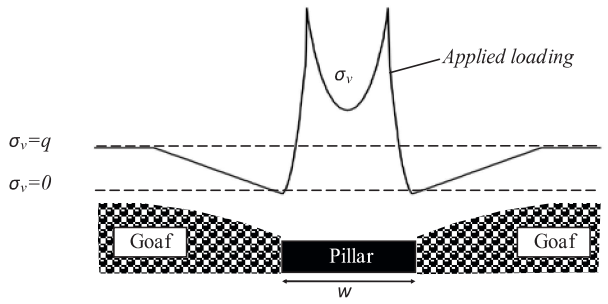

Figure 5. Problem definition, where q is equal to overburden stress.

strata was 0.025 MN/m^3, the mined seam height was 3 m, the lateral restraint applied at the rib-edge was zero, and the in-plane and out of plane elastic parameters were equal (i.e., $E'=E$ and $\nu'=\nu$).

SOLUTION METHODS

The changes to the in situ vertical stresses in coal seams underlying a seam being mined using the longwall technique were predicted using the finite element software ABAQUS. Only the strata beneath the first seam mined were included in the spatial model. A plain strain rectangle with appropriate in situ stresses was meshed (Figure 6) and an elastic analysis conducted. The rectangular section of rock analyzed was 500 m wide and 200 m high with a fixed boundary condition on the bottom and roller supports along the sides of the model. Wilson's equations for the vertical stress changes corresponding to the first mined seam were applied to the top surface of the finite element model. A very fine mesh was used in the vicinity of the elastic/yield boundary in the pillar in order to model the stress discontinuity in Wilson's equations. Values of the independent shear modulus (G') ranging from 0.1 to 1 times the isotropic shear modulus (G_{iso}) in the plane of the strata and a Poisson's ratio (ν¢) of 0.25 were considered in the study reported here. Table 1 presents the input parameters considered in the model and adopted in Wilson's equations.

Table 1. Material properties used in the model.

Variable	Definition	Values used in the general case
H	Depth to top seam	150 m
M	Mined seam height	3 m
φ	Friction angle of coal	32 degrees
σ_0	Strength of coal at zero confinement	10 MPa
σ_0'	Strength of failed material at zero confinement	0.25 MPa
p	Lateral restraint at the rib-edge	0 MPa
β	Abutment angle	21 degrees
w	Pillar width	30 m
IB	Interburden thickness	OB/IB = 6, (25 m)

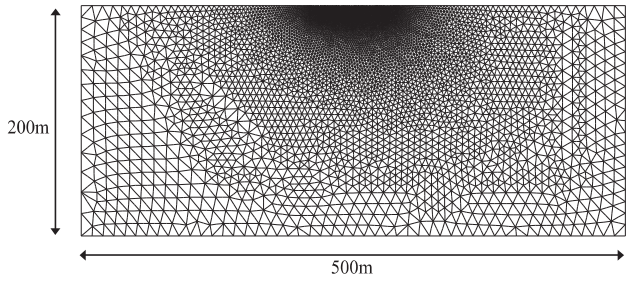

Figure 6. Finite element mesh used for the elastic analysis in ABAQUS for this study.

RESULTS

Figure 7 shows the predicted vertical stress at the level of the first-mined seam determined from Wilson's equations for the general case of a 30-m-wide pillar, at a depth of 150 m with an abutment angle of 21 degrees and all other variables with values as presented in Table 1. An isotropic shear modulus is assumed for the general case. The absolute values of E and G used in the analysis have not been reported as they are independent of the solution for a homogeneous isotropic medium. The distribution of the induced vertical stress in the underlying stratum as a result of this general case of pillar and goaf loading is presented in Figure 8. This figure shows that the changes in vertical stress to the original in situ vertical stresses occur as two lobes under the maximum peak pillar loadings. The major zones of primary influence extend about one pillar width down into the underlying strata. The vertical stress changes towards the edges of the model are approximately equal to zero. Therefore, at these locations the in situ vertical stress values would be equal to the original in situ stress field before any mining would have taken place in the overlying stratum. This is to be expected, as the vertical stress transmitted through the goaf, towards the edges of the model, is the same as the full overburden stress. The predicted stress distribution for the general case appears to be similar to that imposed by a rigid footing (Poulos and Davis, 1974). Figure 7 would differ from what would be predicted for by a rigid footing because Wilson's approach considers yielding in the first mined coal seam, and thus the maximum vertical stress does not align with the rib-edge (Figure 7). Instead, the peak stresses occur at the boundary separating the yielded and elastic zones.

Values of the stresses in the rock strata beneath the first-mined seam can be compared easily by reviewing the predicted final stress magnitudes at various depths in the strata. The stresses at various depths below the top of the model are presented relative to their ratio OB/IB (Figure 9), where OB is the thickness of the overburden for the first mined seam and IB is the thickness of the interburden (the vertical distance between the first and second mined seam). The maximum value of the ratio OB/IB considered here is 12, because values greater than this will necessarily correspond to very small interburden thickness. Mining under very small interburden is often referred to as ultra-close seam mining, which usually presents unique instability problems (Haycocks and Zhou, 1990, Seedsman, 2003). Because the values of stress change dissipate with depth through the strata, a minimum value of the ratio OB/IB of 4 has been considered.

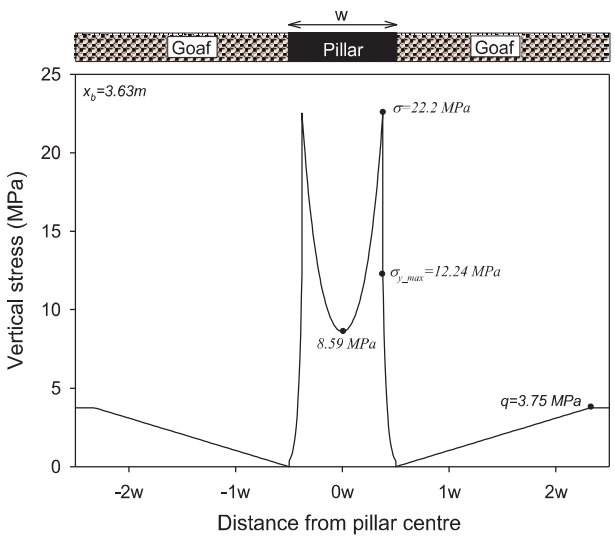

Figure 7. Vertical stress distribution calculated using Wilson's equation for yield in seam only for the general case.

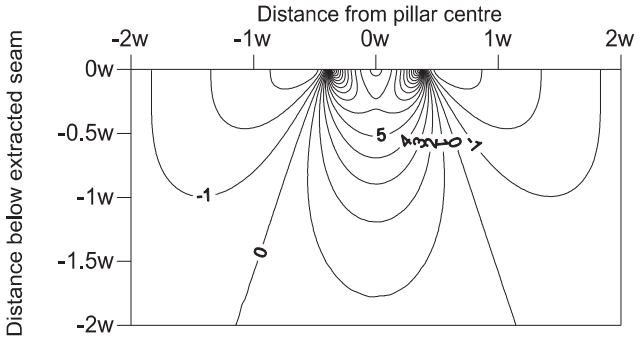

Figure 8. For the general case considered in this study, the final change in vertical stress distribution in MPa, and where w is the pillar width.

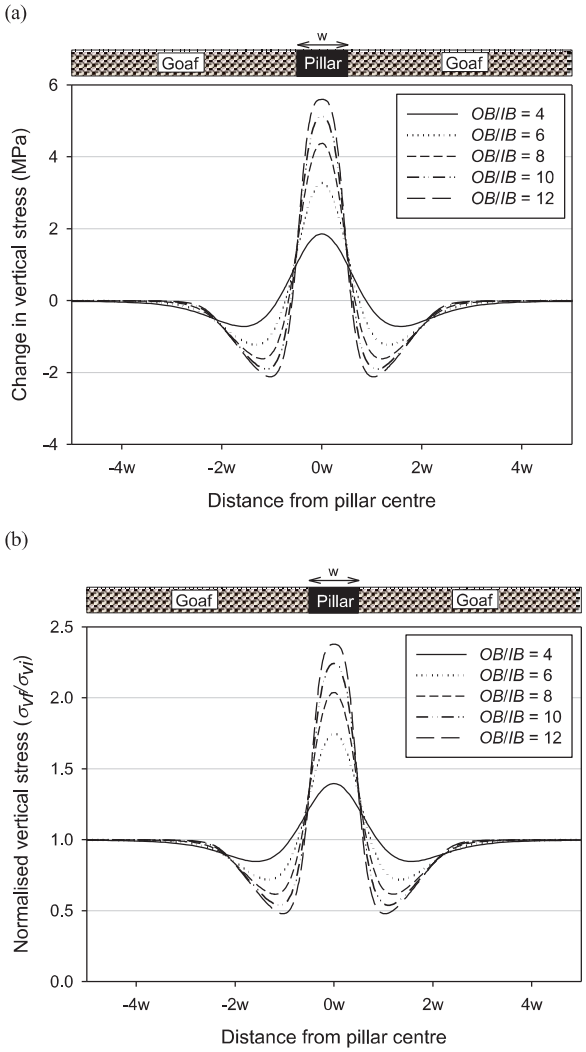

Figure 9. Vertical stress distributions at various depths below the first seam: (a) change in vertical stress values, and (b) vertical stress normalized by the initial vertical stress at the particular depth.

Figure 9(a) shows the predicted change in vertical stresses for various values of the ratio *OB/IB*. These results have been extracted from the plots shown in Figure 8, and are the values of change in final vertical stress predicted by the analysis. The shapes of the vertical stress change distributions for each depth all contain a similar inflection point located under the rib-edge, and differ only in the relative stress magnitudes. For large values of the ratio *OB/IB*, higher magnitudes of vertical stress change can be expected under the pillar, with a very sharp decrease in magnitude to less than the original in situ stress elsewhere. The changes in vertical stresses then rise to zero at a greater distance from the pillar. Figure 9(b) presents the final vertical stress after mining of the first seam (σ_{vf}) normalized by the initial vertical stress for the appropriate depth (σ_{vi}). For a value of the ratio *OB*/*IB* of 12, the maximum change in vertical stress corresponds to approximately 2.3 times the initial vertical stress. It is noted that at the mined seam, the maximum change in stress was approximately five times the in situ stress, so that for *OB*/*IB* = 12, the maximum vertical stress has attenuated by a factor of more than 2.

Transverse Isotropy Effects

Figure 10 shows the vertical stress variation for a range of independent shear modulus values and a ratio *OB*/*IB* of 6. The independent shear modulus has been normalized by the isotropic shear modulus (G_{iso}), such that the results for an isotropic material are plotted as G'/G_{iso} of 1. As the ratio of G'/G_{iso} decreases, the transversely isotropic behavior of the material increases, as discussed previously. Decreasing the independent shear modulus has the effect of transferring vertical stresses deeper into the strata. By reducing the independent shear modulus to a value of one-tenth of the value for isotropic conditions, the change in maximum vertical stress increased from 1.79 times the original in situ stress to 2.32 times the original in situ stress. This increase in vertical stress is 67% higher than the isotropic case. This increase in maximum stress appears to arise because transversely isotropic strata transfers the core pillar vertical stress deeper into the underlying stratum. As a result of stress balance a larger vertical stress relief under the

goaf is observed in transversely isotropic materials than for the isotropic cases.

Figure 10 also shows that if isotropic conditions are present, the maximum vertical stress of 1.79 times the original in situ stress occurs locally at the center of the overlying pillar. However, as the independent shear modulus is reduced, the maximum vertical stress no longer occurs at a single point. In extremely transversely isotropic strata it is predicted that two localized maximum vertical stress peaks would occur, which are located approximately under the edge of the yield/elastic boundaries. This localization of vertical stresses would be expected in extremely transversely isotropic materials such as coal measure strata as their redistribution of vertical stress in the horizontal direction via Poisson's effect is limited by the shear stress capacity of the bedding planes.

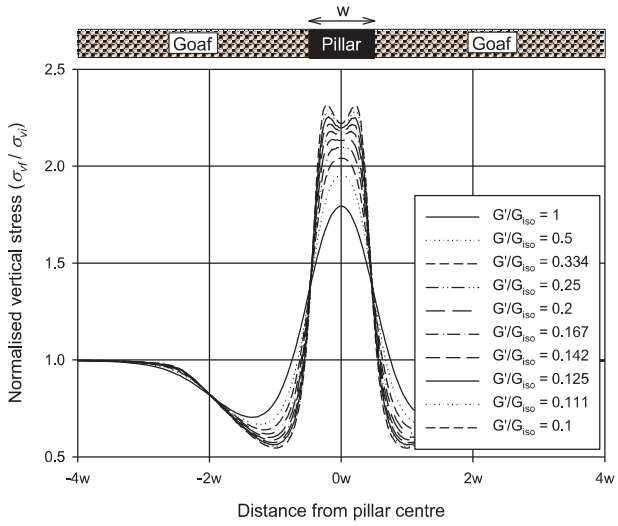

Figure 10. Vertical stress variation for a range of independent shear modulus values for a ratio OB/IB of 6.

To further understand the relative effect of transverse isotropic behavior, the maximum vertical stresses predicted for each of the ratios of G'/G_{iso} is presented in Figure 11. Results are presented for several ratios of *OB*/*IB*. At any given depth the relationship between the maximum predicted vertical stress and the ratio of the independent shear modulus to the isotropic shear modulus (G'/G_{iso}) is not linear. It was not possible to find a common relationship between the maximum vertical stress and the independent shear modulus that could describe each of the curves corresponding to different values of *OB*/*IB*. The nonlinear relationship shown in Figure 11 indicates that the vertical stress changes are most pronounced in the more highly anisotropic materials, i.e., low values of the modulus ratio, G'/G_{iso}.

DISCUSSION

It has been observed that transversely isotropic behavior in a stratum increases the maximum vertical stress induced at any given depth beneath a mined coal seam, relative to that which would be observed in an isotropic medium. Previous publications have documented that field measurements often record higher than expected vertical stresses (Lightfoot and Liu, 2010) as a

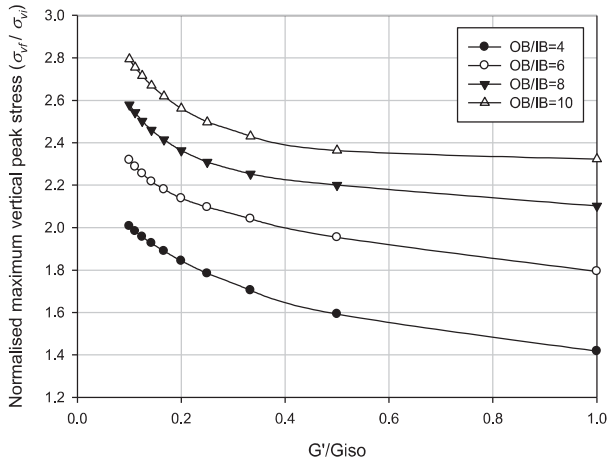

Figure 11. Variation of the maximum vertical stress with respect to independent shear modulus normalized by the isotropic shear modulus. (a) (b).

result of coal seam extraction. In this particular case, the expected vertical stresses were obtained from computer analyses conducted assuming that the coal measure strata could be approximated as an isotropic material. Lightfoot and Liu's main conclusion was the need for numerical modeling programs that could model effectively and efficiently laminated strata for underground coal measure stability analyses. The present study has shown how transverse isotropic effects, arising due to stratification in sedimentary rocks, can be considered implicitly by including an independent shear modulus in the stress-strain relationship of the rock strata.

The results from this study also show that if an analysis does not consider the effects of jointing in laminated rock strata (either implicitly or explicitly) the analysis is likely to underestimate the vertical stresses in a second seam underlying an extracted supercritical longwall panel. It is imperative when mining to be able to predict the expected vertical stresses in the lower seam. The predicted vertical stresses in conjunction with the expected horizontal stresses will govern any ground control instability issues for which an effective management plan should be devised. A 2D model was used for simplicity and further work using 3D models will be conducted by the authors in the future. The 3D modeling would be needed to evaluate the stresses around the longwall face and therefore the stresses below any upper mine.

Transversely isotropic rocks cause more rapid variation of vertical stress with horizontal distance relative to isotropic strata. The consequences for sudden changes in vertical stress could be more rapid changes in rock mass behavior, including its deformation response. The implication for multi-seam mining practice is that changes to mining conditions would occur more rapidly along the lower seam than would be predicted by an analysis assuming isotropic material behavior. The potential for rapid (or even gradual) changes in rock mass behavior would need to be acknowledged in the development of an effective risk management plan. The mine site may need to be prepared with resources to implement different ground control measures for sudden (or gradual) changes in stress conditions. The inability to deal with sudden changes in stress conditions could increase the

potential for failures to occur with consequent safety implications and reduction in productivity.

Including transverse isotropy in the elastic analyses results in a very strong "columnisation" of the vertical stresses, which are not observed in isotropic elastic analyses. This columnisation can provide explanations for many of the rock mass behaviors observed when undermining. For example, floor heave and poor rib conditions when under the goaf/solid boundary or chain pillars over overlying workings (Oram and Ponder, 1997, Lightfoot and Liu, 2010), interactions at greater depth (Dunham and Stace, 1978, Mark, Chase and Pappas, 2007), and also the onset of tensile roof stresses (Seedsman, 2003).

A limitation in effectively using the independent shear modulus for implicit modeling of stratified rock is the limited field measurements that are available to calculate its value and variability. As an initial estimate, it would be useful to collate vertical stress field measurements in the lower seam and use them to back-analyze the independent shear modulus of the stratum. Therefore, the results from this analysis could potentially be compared to field stress measurements from undermining of supercritical longwall panels in order to estimate the degree of anisotropy of coal measure rocks.

CONCLUSIONS

The bedding in coal measure stratigraphy inhibits lateral spread of stress, and the rock mass should not be assumed to behave like an isotropic material. The effects of bedding need to be considered either implicitly or explicitly when conducting computer modeling of the effects of proposed mine operations. The modeling described in this study has included transverse isotropy implicitly by adopting an independent shear modulus in the elastic constitutive equations of the rock mass. The effect of the independent shear modulus on the change in vertical stress in the strata underneath a supercritical longwall panel was assessed.

For the most severe case of transverse isotropy considered in this study, the change in vertical stresses observed in the lower seam was predicted to be up to 67% higher when compared to the isotropic case. The rapid variation of vertical stress with horizontal distance that is evident in transversely isotropic rocks is likely to be reflected in more rapid changes in rock mass response. These effects will have implications on the ground support design of lower seam pillars and roadways. The larger vertical stresses would need to be considered in light of the horizontal stresses to assess overall stability. The results for transversely isotropic rock also indicate that changes to mining conditions are likely to be more sudden, so mine sites should be prepared for gradual and perhaps even rapid changes in ground control support measures.

The nonlinear relationship between the change in maximum vertical stress and the independent shear modulus indicates that small variations in the independent shear modulus for highly anisotropic materials results in relatively large changes in the vertical stress in a rock mass that is strongly anisotropic. Therefore, there is a need to collect more information on realistic values of the independent shear modulus of coal measure strata.

ACKNOWLEDGEMENTS

The authors would like to acknowledge Ross Seedsman for his contribution to this study by sharing his experience in multi-seam mining projects.

REFERENCES

Gale, W. J. (Ed.) (2004a) Multi seam layout guidelines and feasibility of partial chain pillar removal Australian Coal Association Research Program report. C11032.

Howarth, R. & Monger, N. R. (2009) Chapter 16: Multi-seam working. in Australian Coal Mining Practice - Monograph 12 - Third Edition. AusIMM.

Haycocks, C., Karmis, M. & Ehgartner, B. (1982) Multiple seam mine design. In Proceedings of the International Symposium on Ground Control in Longwall Coal Mining and Mine Subsidence, pp. 59-65.

Chase, F. E., Worley, P. & Mark, C. (2005) Multiple seam mining interactions: Case histories from the Harris No.1 mine. In Proceedings of the 24th International Conference on Ground Control, Morgantown, WV, pp. 79-86.

Salamon, M. D. G. & Oravecz, K. I. (Eds.) (1976) Rock mechanics in coal mining, Chamber of Mines of South Africa report. Johannesburg, South Africa.

Salamon, M. D. G. (1990) Mechanism of caving in longwall coal mining. In Proceedings of the 31st U.S. Symposium on Rock Mechanics titled 'Rock Mechanics Contributions and Challenges', Hustrulid, W. A. & Johnson, G. A. (Eds.), A.A. Balkema, pp. 161-168.

Chekan, G. J. & Listak, J. M. (Eds.) (1993) Design practices for multiple-seam longwall mines: Information Circular 9360, United States Department of the Interior: Department of Mines report. Washington D.C.

Gale, W. J. (2004b) Rock fracture, caving and interaction of face supports under different geological gnvironments. Experience from Australian coal mine. In Proceedings of th 23rd International Conference on Ground Control in Mining, Morgantown, WV, pp. 11-19.

Morsy, K., Yassien, A. & Peng, S. S. (2006) Multiple seam mining interactions - A case study. In Proceedings of the 25th International Conference on Ground Control in Mining, Morgantown, WV, pp. 308-314.

Zipf, J. R. K. (2006) Numerical modeling procedures for practical coal mine design. In The 41st US Symposium on Rock Mechanics (USRMS), Golden, CO, pp.

Wittles, D. N., Reddish, D. J. & Lowndes, I. S. (2007) The development of a coal measure classification (CMC) and its use for prediction of geomechanical parameters. International Journal of Rock Mechanics and Mining Sciences, 44, pp. 496-513.

Esterbuizen, E., Mark, C. & Murphy, M. M. (2010) Numerical model calibration for simulating coal pillars, gob and overburden response. In Proceedings of the 29th International Conference on Ground Control in Mining, pp. 46-57.

Hsiung, S. M. & Peng, S. S. (1987a) Design guidelines for multiple seam mining, Part I. Coal Mining, 24(9), pp. 42-46.

Hsiung, S. M. & Peng, S. S. (1987b) Design guidelines for multiple-seam mining, Part ll. Coal Mining, 24(10), pp. 48-50.

Haycocks, C. & Zhou, Y. (1990) Multiple-seam mining - A state-of-the-art review. In Proceedings of the 9th International Conference on Ground Control in Mining, Morgantown, WV, pp. 1-11.

Hill, R. W. (1995) Multi-seam Mining on South African Collieries. In Proceedings of the 14th International Conference on Ground Control in Mining, Morgantown, WV, pp. 305-311.

Gerrard, C. M. & Pande, G. N. (1985) Numerical modelling of reinforced jointed rock masses, (I) Theory. Computer and Geotechnics, 1, pp. 293-318.

Morsy, K. & Peng, S. S. (2002) Numerical modelling of the gob loading mechanism in longwall coal mines. In Proceedings of the 21st International Conference on Ground Control in Mining, Morgantown, WV, pp. 58-67.

Badr, S., Ozbay, U., Kieffer, S. & Salamon, M. (2003) Three-dimensional strain softening modeling of deep longwall coal mine layouts. In FLAC and numerical modelling in geomechanics: Proceedings of the 3rd International FLAC Symposium, Brummer, R., Andrieux, P., Detournay, C. & Hart, R. (Eds.), Ontario, A.A. Balkema Publishers, pp. 233-239.

Su, D. W. H. (1991) Finite element modelling of subsidence induced by underground coal mining: The influence of material nonlinearity and shearing along existing planes of weakness. In Proceedings of the 10th International Conference of Ground Control in Mining, Morgantown, WV, pp. 287-300.

Seedsman, R. W. (2011) Application of the brittle failure criterion to the design of roof support in the soft rocks of coal mines. In Proceedings of the 11th Underground Coal Operators' Conference, University of Wollongong, Wollongong, Australia, pp. 60-72.

Suchowerska, A. M., Merifield, R. S. & Carter, J. P. (2012) Effect of abutment angle on stress distribution under supercritical longwall panels. In Proceedings of the 11th Australia-New Zealand Conference on Geomechanics, Melbourne, Australia, pp.

Whittaker, B. N. (1974) An appraisal of strata control practice. The Mining Engineer, 134, pp. 9-24.

Wilson, A. H. & Ashwin, D. P. (1972) Research into the determination of pillar size. The Mining Engineer, 141, pp. 409-417.

Wilson, A. H. (1983) The stability of underground workings in the soft rocks of the coal measures. International Journal of Mining Engineering, 1, pp. 91-187.

Choi, D. S. & McCain, D. I. (1980) Design of longwall systems. Transactions of the Society of Mining Engineers, AIME, 268, pp. 1761-1764.

Hsiung, S. M. & Peng, S. S. (1985) Chain pillar design for U.S. longwall panels. Mining Science and Technology, 2, pp. 279-305.

Mark, C. (Ed.) (1990) Pillar design methods for longwall mining U.S. Bureau of Mines report. IC 9247. Pittsburgh, PA.

King, H. J. & Whittaker, B. N. (1971) A review of current knowledge on roadway behaviour. In Proceedings of the symposium on roadway strata control, pp. 73-87.

Salamon, M. D. G. (1992) Strength and stability of coal pillars. In Proceedings of the Workshop on Coal Pillar Mechanics and Design, pp. 94-121.

Colwell, M. G. (Ed.) (1998) Chain Pillar Design (Calibration of ALPS) C6036, Australian Coal Association Research Program report.

Lightfoot, N. & Liu, N. (2010) The prediction of pillar interaction effects for deep multi-seam mining. In Proceedings of the 29th International Conference on Ground Control in Mining, Morgantown, WV, pp.

Gerrard, C. M. (1977) Background to mathematical modelling in geomechanics: The role of fabric and stress history. in Finite Elements in Geomechanics. Gudehus, G. (Ed.). John Wiley & Sons.

Seedsman, R. W. (2009) An update of conditions in the Donkin-Morien tunnels. In ROCKENG09 - Proceedings of the 3rd CANUS Rock Mechanics Symposium, Diederich, M. & Grasselli, G. (Eds.), Toronto, Canada, pp.

Goodman, R. E. & Duncan, J. M. (1969) The role of structures and soil mechanics in the design of surface and underground excavations in rock, . In Proceedings of Civil Engineering Materials Conference titled 'Structure Solid Mechanics and Design', Terini, M. (Ed.), Southampton, pp.

3Alehossien, H. & Carter, J. P. (1990) On the implicit and explicit inclusion of joints in the analysis of rock masses. In Mechanics of Jointed and Faulted Rock: Proceedings of the International Conference on Mechanics of Jointed and Faulted Rock, Rossmanith, H. P. (Ed.), Institute of Mechanics, Technical University of Vienna, A.A. Balkema, pp. 487-494.

Bandis, S. C., Lumsden, A. C. & Barton, N. R. (1983) Fundamentals of rock joint deformation. International Journal of Rock Mechanics and Mining Sciences & Geomechanics Abstracts, 20, pp. 249-268.

Poulos, H. G. & Davis, E. H. (1974) Elastic solutions for soil and rock mechanics, New York, Wiley.

Seedsman, R. W. (2003) Roof support in gateroads in multiple seam longwalls - lessons from ultraclose mining at Gibsons Colliery. In Proceedings of the 4th Underground Coal Operators' Conference, pp.

Oram, J. S. & Ponder, C. G. (1997) Measurement of effects of interaction and influence on mine layout design at Maltby Colliery. In Proceedings of 16th International Conference on Ground Control in Mining, August ed, Morgantown, WV, pp. 16-24.

Dunham, R. K. & Stace, R. L. (1978) Interaction problems in multiseam mining. In Proceedings of the 19th U.S. Symposium on Rock Mechanics, Stateline, NV, pp. 171-187.

Mark, C., Chase, F. E. & Pappas, D. M. (2007) Analysis of multiple seam stability. In Proceedings of the 26th International Conference on Ground Control Mining pp. 5-18.

Large Scale Ground Instability Caused By Failure of Underlying Pillars: a Case Study of Dynamic Multiple Seam Interaction

Christopher Mark, Principal Roof Control Specialist
Coal Mine Safety and Health MSHA
Pittsburgh, PA

Lee Barker, Roof Control Specialist
MSHA
Mt. Hope, WV

ABSTRACT

Severe dynamic multiple seam interactions can occur when active mine workings are subsided by underlying mining activity. The most dramatic events are usually caused by longwall mining or pillar recovery beneath open, overlying entries. But pillars in abandoned workings can also fail and cause subsidence and damage an overlying mine.

This paper describes a case history in which an apparent "pillar squeeze" in the abandoned workings of a lower seam was initiated during retreat mining in an upper seam. The event subsequently extended more than 1,500 ft and ultimately closed the upper seam mine. Analysis indicated that the pillars in the lower mine were adequately sized for the lower seam mining and were not affected by the initial development above them. When retreat mining in the upper seam had progressed several hundred feet, however, the pillars located directly beneath the pillar line were overloaded, and an extensive squeeze initiated in the underlying workings. The squeeze, in turn, subsided the overlying workings, causing widespread rib falls and roof instability.

Previous examples of dynamic multiple seam interactions resulting from delayed subsidence of underlying workings have been reported in the literature. This is, apparently, the first recorded incident in which pillar recovery in an active mine triggered pillar failure in an underlying mine, which then triggered a dynamic interaction that impacted the active overlying seam.

BACKGROUND

Multiple seam mining is very common in the mature coalfields of Central Appalachia. The incident described in this paper occurred in August 2011 in an area where mining has been conducted for decades. The Coalburg seam, the active seam in this case study, is at least the fourth seam in the area to be mined.

Figure 1 shows a portion of the geologic section of the area. The uppermost seam, the Kittanning, was mined before 1960. Due to the light cover above the Kittanning, workings in it are unlikely to have affected mining in the Coalburg. A longwall mine was later active in the Powellton seam, which is approximately 400 ft below the Coalburg seam, but the nearest longwall workings are approximately 1,500 ft to the south of the squeeze area.

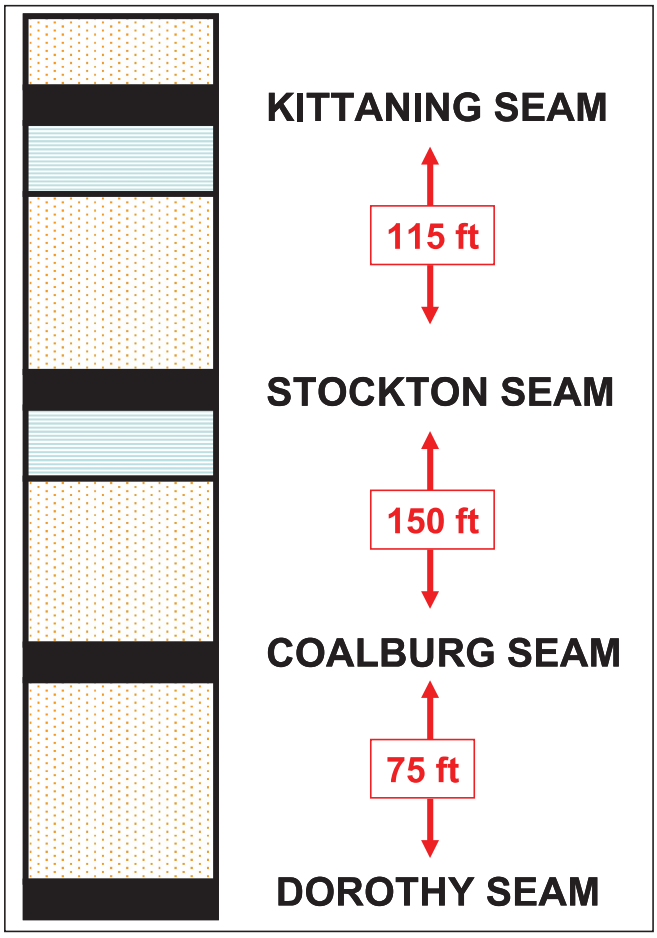

Figure 1. Upper portion of the geologic section in the vicinity of the Coalburg mine, with approximate interburden distances.

The most significant past mining was conducted in the Dorothy seam, approximately 75 ft below the Coalburg. The Dorothy Mine, which was opened in 1977, extracted about 3 million tons between

1983 and its final closure in 1991. Figure 2 shows the significant features of the Dorothy seam mining in the area of the incident, including the following:

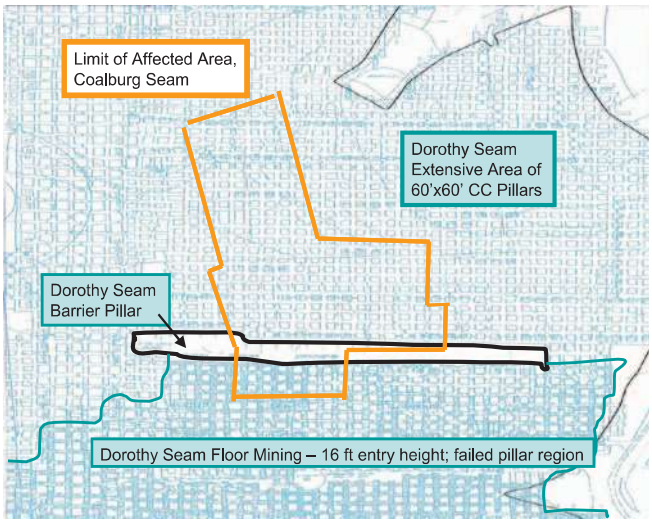

Figure 2. Map of Dorothy seam mining (showing the outline of the area in the Coalburg seam that was affected by the event).

- A large area of 60 x 60 ft (centers) pillars, which underlies most of the 2 Section and the Mains. No second mining was conducted in this area.
- An area where the floor was extracted, resulting in 16 ft mining heights.

The two areas are separated by a 140-ft-wide barrier. In the 60 x 60 ft area, the mining height was reportedly about 10 ft. In the area where the floor was extracted, miners familiar with the Dorothy Mine reported that the ground caved and the pillars presumably crushed.

The Coalburg Mine opened in 2005 and extracted approximately 500,000 clean tons of coal annually with 70 miners on two production units. Since the Coalburg seam is located near the top of the geologic section, the cover was relatively light. Above 2 Section, the maximum depth of cover was about 440 ft, and the minimum was only 100 ft. The original mining height in this part of the mine averaged about 11 ft.

In the area of 2 Section and the Mains, the pillars were developed on 70 x 100 ft centers (Figure 3). Where the Mains crossed the Dorothy barrier pillar, the pillar size was increased to 120 x 120 ft centers.

Conditions in the Coalburg seam Mains, 2 Section, and 1 Left off 2 Section were reported to have been excellent after development. Retreat mining was completed in 1 Left without incident beneath a maximum cover depth of 400 ft. Two rows of pillars were left in place at the mouth of 1 Left to isolate 2 Section from the abutment load.

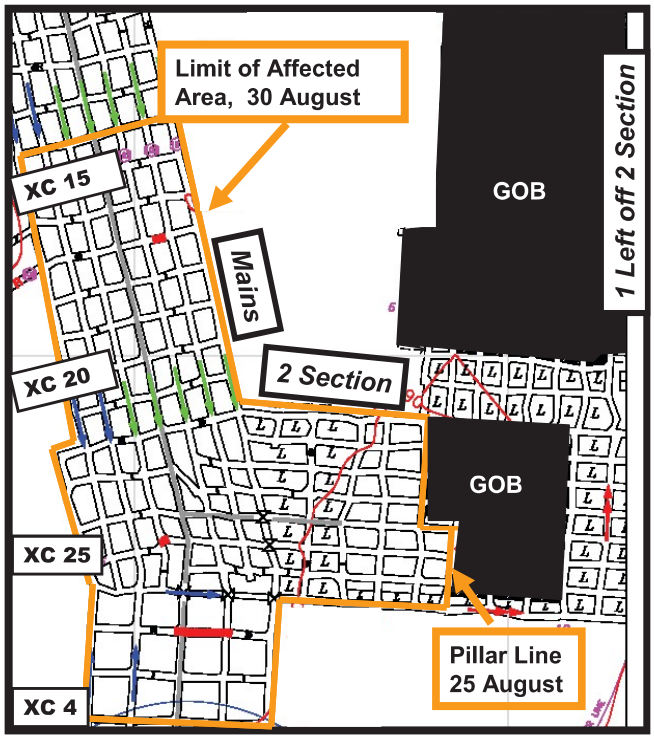

Figure 3. Map of Coalburg seam mining, illustrating the sequence of events.

EVENTS DURING THE INSTABILITY

Retreat mining was then initiated in 2 Section after leaving two rows of pillars near the outcrop to establish a bleeder. Four rows of pillars were extracted, and the pillar line was beneath the maximum depth of cover of 440 ft. At this point, (Figure 3. Pillar Line Aug 25), the rib conditions near the pillar line were so poor that the section was abandoned, and the equipment was removed to the mouth of the panel. Over the course of next two days, the squeeze rode out about 800 ft from the pillar line into the mains, causing pillar conditions to deteriorate and the operator to withdraw all miners from the area. Ventilation controls were crushed out, and the main water sump for collection of water went dry suddenly. In the following days, the squeeze continued to spread in both directions up and down the Mains.

Subsequent mapping (Figure 3) indicated that the worst conditions in the Mains were located directly over the Dorothy Seam barrier pillar, from approximately crosscut 24 in the small pillar area to crosscut 2 in the large pillar area (see the photos in Figures 4 and 5). The area from crosscut 18 to 24 was also severely damaged, with long radial tension cracks in the mine roof that ran parallel with the center of the entry. These cracks had intermittent crossing cracks, which further weakened the roof. The fact that no falls occurred in these areas was a testimony to the strength of the sandstone roof. There were also intermittent areas of slight bottom heaving. Virtually every rib had shed large pieces of broken coal and rock. Further damage was noted to crosscut 14 in the north and crosscut 4 in the south.

Figure 4. Floor heaving and rib roll has completely covered a belt drive located above the Dorothy barrier pillar.

Figure 5. Coalburg entry above the Dorothy barrier pillar almost filled with broken coal, leaving only a 14-ft-wide by 6-ft-high triangular opening.

ANALYSIS

A global instability of this magnitude almost always means that pillars have failed. In this instance, there are two sets of pillars that may be responsible, the ones in the Coalburg and the others in the Dorothy. To make things more complicated, activities in one seam can also affect the other (in other words, there can be interactions). The rock mechanics analysis presented in the next section will attempt to unravel the sequence of events.

The analysis was conducted using the NIOSH pillar design software packages Analysis of Retreat Mining Pillar Stability (ARMPS) and Analysis of Multiple Seam Stability (AMSS). The analysis begins with the original development of the 60x60 ft pillars in the Dorothy seam. For the maximum depth of cover [1] of 465 ft and an assumed 10 ft mining height, the ARMPS SF=1.59. Since this value exceeds the NIOSH suggested value of SF=1.5 (Mark 2010), it seems likely that these pillars were intact before mining commenced in the Coalburg seam. Note also that the floor mining in the Dorothy seam has very little effect on the 60x60-ft blocks because the analysis indicates that the 140-ft barrier shields them from the abutment load.

Next, we begin the evaluation of the Coalburg workings with the 2 Section. Because the underlying pillars in the Dorothy can initially be assumed to be intact, and 2 Section does not cross the Dorothy barrier, it seems appropriate to conduct a single-seam ARMPS analysis (rather than an AMSS analysis). For the same location analyzed above, the Coalburg depth of cover is 390 ft, and the calculated ARMPS SF = 3.03. Even if some side abutment load from the floor mining area is added (by adjusting the input parameters to include a side gob and a reduced barrier pillar width of 30 ft), the SF drops to just 2.82. These SF values are well above the NIOSH criteria, so the pillars would have been expected to be stable.

The development mining in the Coalburg seam is also unlikely to affect the stability of the Dorothy pillars. Therefore, with adequate pillar SF values for both seams, the analysis predicts the good conditions that were actually encountered in 2 East before pillar extraction commenced.

The next step is to conduct a single-seam analysis of the effect of pillar recovery in the Coalburg seam. The pillaring increases the load on the Coalburg seam pillars but only reduces the SF to 1.96 (or 1.85 if the effect of the side gob is considered). Again, since these values still exceed the NIOSH recommendation of 1.5, the pillars should have been stable *if there were no multiple seam effects*.

MULTIPLE SEAM INTERACTION

However, pillaring in the Coalburg seam did have additional affects on the Dorothy seam. The Dorothy pillars directly beneath the Coalburg pillar line now lie beneath a “gob-solid boundary” in a high stress abutment zone (Figure 6). This situation was modeled in AMSS by making the Dorothy the “active seam,” and subjecting it to the effects of overmining in the Coalburg seam. The AMSS analysis indicated that, under these conditions, the SF of the Dorothy pillars in the abutment zone is reduced to just 0.97 (assuming an 8 ft mining height). Therefore, it seems likely that pillar recovery triggered a pillar failure in the Dorothy seam. Once the process began, the failed pillars in the Dorothy shed load onto the adjacent intact pillars, which caused them to fail in turn. In this manner, the failure in the Dorothy could have propagated for some distance because there were no barriers or other large pillars to arrest it.

Failure of the Dorothy pillars beneath the open Coalburg workings created what is called a “dynamic multiple seam interaction” (Mark, 2007). The best example of a dynamic interaction is when a lower seam is longwalled beneath open overlying workings, causing them to subside. Dynamic

1 Note that the depth of cover used in an ARMPS or AMSS analysis is *not* the absolute maximum depth of cover. Rather, it is an *approximate average* of the depth of cover above the “Active Mining Zone” that is being analyzed. See Mark , 2010 for more details.

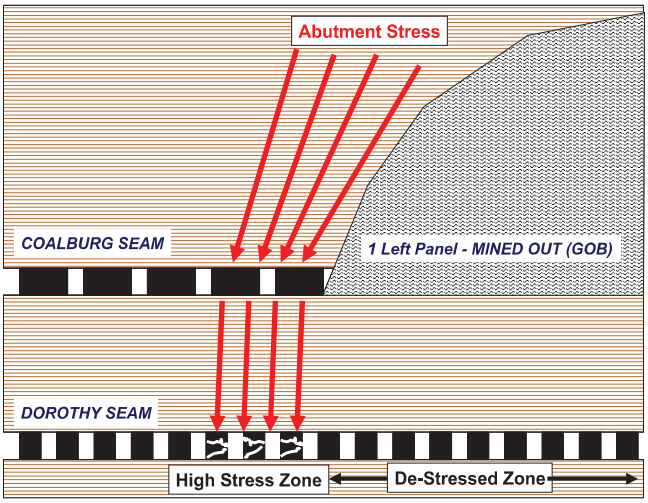

Figure 6. Cross-section sketch illustrating the creation of the high stress abutment zone, which initiated the failure of the Dorothy seam pillars.

interactions cause far more damage than typical multiple seam interactions. Most can be avoided by careful mine planning, but there have been instances in which delayed subsidence of underlying works has had the same destructive effect on overlying entries as active mining. In one published instance, a set of mains at a Kentucky mine was developed 180 ft above pillared works, and conditions were excellent for two years. Then the roof began to deteriorate dramatically, and heavy supplemental support was required to prevent major roof collapses. Apparently, the ground had not fully subsided until the two years had passed.

The current case may be the first recorded example of pillar recovery in an active mine triggering a pillar failure in an abandoned mine, which in turn triggered a dynamic multiple seam interaction that affected the active mine.

As the pillar failure progressed in the Dorothy seam, the interburden subsided, and the effects were obvious in the Coalburg seam. In addition, the squeeze in the Dorothy seam had the effect of throwing extra load onto the Dorothy barrier, turning it into an "isolated remnant pillar." An AMSS analysis shows that the SF of 70x100-ft pillars above the barrier would be reduced to 1.10, meaning it is likely that they would be highly distressed. The 120x120-ft pillars on the south side of the barrier would fare better, with an SF of 1.99, but the predicted entry conditions are still "red" even with an assumed strong roof (CMRR=65). Again, the analysis seems to align with the underground observations of the most severe conditions in the vicinity of the barrier.

Over the subsequent days, the squeeze continued up the Mains, finally coming to rest approximately 700 ft from the mouth of 2 Section. The depth of cover at this location is approximately 320 ft. Treating the failed area as an active gob, an ARMPS analysis yields an SF of 1.51 for a 10-ft mining height.

CONCLUSIONS

Coal mining in Central Appalachia will continue to be conducted in complex multiple seam situations. In this instance, pillar recovery in an active mine had unforeseen consequences on underlying abandoned workings. The back analysis presented in this paper indicates that the consequences could have been avoided if they had been predicted in advance. The case history underlines the necessity for careful mine planning to consider all the potential modes of failure.

REFERENCES

Mark, C. (2007). "Multiple seam mining in the US—background." In: *Proceedings of the Workshop on New Technology for Ground Control in Multiple Seam Mining*. Pittsburgh, PA: NIOSH IC 9495, pp. 3–14.

Mark, C. (2010). "Pillar design for deep cover retreat mining: ARMPS version 6." In: C. Mark and G. S. Esterhuizen, eds. *Proceedings of the Third International Workshop on Coal Pillar Mechanics and Design*. Morgantown, WV, pp. 106–121. (Available in the ARMPS Help/Resources files).

Investigating Abutment Load

Ihsan Berk Tulu, Graduate Research Assistant
Keith A. Heasley, Professor
West Virginia University
Morgantown, WV

ABSTRACT

In the Analysis of Retreat Mining Pillar Stability (ARMPS) program, the magnitude of the abutment loading adjacent to a gob area is calculated using an "abutment angle" concept. The extent of the abutment loading is determined solely as a function of depth from an empirically derived equation. In the recommended calibration method for LaModel, it was believed that the empirical equations for calculating the magnitude and extent of the abutment load, as used in ARMPS, were the best available methods for determining these critical overburden loading values. Therefore, similar calculations were implemented in the LaModel calibration method. However, the latest in situ stress measurements of abutment loading performed in the United States and Australia have shown that there can be significant deviations in the measured abutment magnitude and extent as compared to the predicted values from the empirical formulas used in ARMPS and LaModel. It seems reasonable that the overburden geology, depth, extraction panel width, and mining height should have a significant effect on the extent and magnitude of the abutment load. However, the current empirical formulas do not incorporate many of these significant parameters into determining the abutment load on the pillars. In this paper, stress measurements from US and Australian mines were back-analyzed by using analytical and numerical methods to investigate the measured abutment extent and loading.

Ultimately, it was determined that the original empirical abutment extent formula in conjunction with the original ALPS square-decay stress distribution function was supported by the case histories in this paper. Also, for depths less than 900 ft, the average 21° abutment angle was supported by the case histories; however, at depths greater than 900 ft, the abutment angle was found to be significantly less than 21° and should be calculated with a new proposed equation.

INTRODUCTION

The Analysis of Longwall Pillar Stability (ALPS) program has generally been accepted as the most comprehensive chain pillars design tool since it was first introduced to the US coal mining industry in the early 1990s by Mark (1990). ALPS was also recognized by the Australian mining industry, after Colwell, Frith, and Mark (1999) calibrated the ALPS program to Australian conditions. The success of ALPS led NIOSH to subsequently develop the Analysis of Retreat Mining Pillar Stability (ARMPS) program for designing retreat mining pillars (Mark and Chase, 1997). The main strength of the ALPS and ARMPS programs is not derived from the accuracy of their calculations, but rather the large databases that are used to calibrate them (Mark, 2009). However, following the Crandall Canyon Mine collapse in 2007, the National Institute for Occupational Safety and Health (NIOSH) revisited the issue of pillar design for deep-cover retreat mining (Mark, 2010). As a result of this work, it was found that the ARMPS overburden load prediction algorithm could be improved to more accurately predict the loading of narrow and deep panels. This new loading model recognizes the inherently greater stability of narrow and deep panels.

After the Crandall Canyon Mine collapse, Heasley et al. (2010) emphasized the importance of calibrating a numerical model. In fact, it was stated that the success and accuracy of a numerical analysis depends entirely on the accuracy of the input parameters. LaModel does provide default properties for most of the input parameters that were developed to give "reasonable" output for "average" mining conditions. However, these default parameters should not be considered the best set of parameters for a specific site. After the Crandall Canyon Mine collapse, the LaModel program was improved by implementation of a new calibration methodology for deep-cover retreat mining operations. Using the new calibration method, the first approximation of the overburden loads are calibrated to mirror those used in ALPS and ARMPS; however, the flexure of the laminated overburden and the relative stiffness/strength of the seam elements ultimately determine the final distribution of the overburden loads. Using the LaModel calibration method with a relatively small deep-cover database, the LaModel program was shown to classify the case histories slightly better than ARMPS (Tulu, Heasley, and Mark, 2010).

ABUTMENT LOADING IN ALPS AND ARMPS

In the ALPS and ARMPS programs, the magnitude of the abutment loading adjacent to a gob area is calculated using an "abutment angle" concept (Figure 1), and the extent of the abutment loading is determined solely as a function of depth from an empirically derived equation. In the recommended calibration method for LaModel, it was believed that the empirical equations

for calculating the magnitude and extent of the abutment load, as used in ALPS and ARMPS, were the best available methods for determining these critical overburden loading values. Therefore, similar calculations were implemented in the LaModel calibration method.

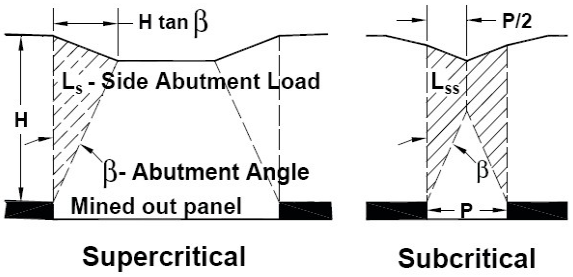

Figure 1. Abutment angle concept.

The in situ stress measurement studies used to develop the empirical abutment extent equation (Peng and Chiang, 1984) contain eight case histories where mining took place before 1984. Similarly, the average abutment angle (21°) used by Mark (1992) was developed from six case histories pre-1990. Certainly, current mines have significantly different panel dimensions than the mines where stress measurements were collected and used to derive the original empirical abutment extent formula and the average 21° abutment angle. In addition, the latest in situ stress measurements of abutment loading performed in Australia (Colwell, Frith, and Mark, 1999) and in the United States (Vandergrift and Conover, 2010) showed that there can be significant deviations in the measured abutment magnitude and extent as compared to the predicted values from the empirical formulas used in ALPS, ARMPS, and LaModel. It seems likely that the variation observed in the data is due to differences in the site-specific overburden geology, seam thickness, depth of cover, and/or extraction panel width, but the effect of these parameters has never been studied in a systematic fashion.

Abutment Angle Concept

Mark (1992) evaluated the three different methods, originally proposed by Wilson (1982), King and Whittaker (1971), and Choi and McCain (1980), to predict the side abutment loads, and he summarized that all three were very similar in application using an "abutment angle" approach. However, Mark indicated that all three methods calculated different values of the abutment angles because of different case histories. Further, Mark (1987) explained that the abutment angle should not be considered a physical reality but an approximation which defines the magnitude of the side abutment loading.

In 1992, Mark analyzed the abutment stress measurements from 5 US mines to infer the magnitude of the abutment loads and associated abutment angle in the US. In this study, vibrating wire stress meters (VWS) were used for all of the field studies. Mark (1987, 1992) calculated the measured side abutment load by multiplying the load-bearing area of the pillars by the average pillar stresses determined from the array of stress cells inside each pillar. In these studies, stress meters were not installed inside the solid coal of the next panel. Therefore, during the calculation of the measured side abutment loads, the load on the adjacent solid coal was ignored. A summary of the panel widths and depths from the case histories that were used by Mark (1992) to back-calculate abutment angles are shown in Table 1. Mark concluded that an average abutment angle of 21° would yield a conservative estimate of the side abutment load, but there was a wide range (10.7° to 25.2°) in the measured values, as seen in Table 1.

Abutment Extent Concept

Peng and Chiang (1984) summarized the abutment stress measurement studies performed prior to the mid-1980s, and they developed the well-known equation for calculating the extent of the abutment load (D) as a function of the depth (H).

$$D(m) = 5.13\sqrt{H} \quad D(m) = 5.13\sqrt{H}$$

$$D(ft) = 9.3\sqrt{H} \quad D(ft) = 9.3\sqrt{H} \quad D = 9.3\sqrt{H}$$

$$D = 9.3\sqrt{H} \tag{1}$$

Equation 1 was derived from 8 sets of stress measurement collected from six different mines. The depths at the eight stress measurement sites ranged from 450 ft to 875 ft, with an average of 585 ft. The extraction thicknesses at the case study sites went from a low of 4 ft to a high of 7.5 ft with an average of 5.61 ft. The panel widths ranged from 150 ft to 490 ft with an average of 321 ft. Table 2 summarizes the panel geometric parameters from the eight stress measurement sites used by Peng and Chiang (1984) to develop equation 1.

Abutment Stress Distribution

From the stress measurements at the five mines, Mark (1992) derived a function for the abutment stress distribution that had a square decay with distance (x) from the edge of the panel (Equation 2). He also calculated from the abutment stress distribution that the fraction "R" of the total side abutment load carried by the chain pillars may be determined by Equation 3.

$$\sigma_a(x) = \frac{3L_s}{D^3}(D - x)^2 \tag{2}$$

$$R = 1 - \left[\frac{D - x}{D}\right]^3 \tag{3}$$

where:

σ_a = the abutment stress level

x = the distance from the panel edge

L_s = the total side abutment load

D = the extent of the abutment stress

Table 1. Summary of the stress measurement sites used by Mark (1992).

Case	Seam	Panel Depth (ft)	Panel Width (ft)	Abutment Angle (deg.)
Mine A: 2	Pittsburgh	520	470	21.8
Mine B: 2	Pittsburgh	650	600	25.2
Mine B: 3	Pittsburgh	600	600	10.7
Mine B: 4	Pittsburgh	455	600	17.3
Mine D: 1	Lower Kittanning	760	1000	18.5
Mine E: 3	Harlan	630	500	20.3
	Average	603	628	18.97

Table 2. Summary of the stress measurement sites used by Peng and Chiang (1984).

Mine	Mining Height (ft)	Panel Depth (ft)	Panel Width (ft)	Panel Length (ft)	Seam
Valley Camp No.3	5.25	875	150	2655	Pittsburgh
Hendrix No. 22	5.00	450	150	2000	Elkhorn #3
Old Ben No. 24	7.50	620	462	1735	Herrin #6
Olga No.1	4.00	630	360	4200	Pocahontas #4
Quarto No. 4	6.50	500	-	-	Pittsburgh
Capco	6.00	570	484	3100	Pittsburgh

RE-ANALYSIS OF ABUTMENT EXTENT AND ABUTMENT ANGLE

The field stress measurement studies used to derive the default 21° abutment angle and the empirical abutment extent formula (Equation 1) highlighted some important facts. First of all, current mines have significantly different panel dimensions than the mines where these previous stress measurements were collected and used to derive the original empirical abutment formulas. However, in the intervening years, there has not been any updated or better approach proposed to predict the abutment extent or the abutment angle. In this paper, these traditional values for abutment extent and abutment loading are re-examined using more recent in situ stress measurements.

In order to measure the full abutment extent under deep cover, stress cells have to be placed relatively far into the adjacent panel, which is often not practical and seldom done. However, front abutment loads can be more easily used to provide an idea of the extent of the side abutment loading. Front abutment extents observed from some of the Western US mines (Haramy and Kneisley, 1989; Lu, 1982) showed a longer extent than the abutment extent predicted by Equation 1. Goodrich et al. (1999) also indicated that in the Deep Creek Mine in Utah, under the 2,000 ft depth of cover, an abutment extent distance of greater than 750 ft was observed. This distance was considerably higher than the one predicted by the empirical abutment extent formula (Equation 1). Goodrich et al. (1999) indicated that the massive and strong Castlegate sandstone in the overburden strata possibly caused this long abutment extent. In regard to the recommended abutment angle, it can be seen from Table 1 that there were not any stress measurements from a panel deeper than 760 ft, and most panels were 600 ft wide or less when the average 21° abutment angle was determined.

Stress Measurements Database

As part of this research to better define the abutment extent and the abutment angle, a database of stress measurements case histories was developed. In the database, there are 6 stress measurement case histories where multiple stress changes were monitored during the panel retreat (Colwell, Frith, and Mark, 1999). There are another 6 case histories where only the final full side-abutment stress change profiles were provided. In addition, there are 18 supplementary cases where only the total side abutment load was known. Twenty two of the 30 case histories come from Australian longwall mines and the remaining 8 cases are from US longwall mines. Table 3 shows the summary statistics for the 30 case histories used in this paper.

Calibration of the Stress Cells

In analyzing the stress cell pressures, it is not necessarily important which stress cell calibration method is used as long as the method is consistent from site to site (Mark, 1992; Colwell, Frith, and Mark, 1999). The stress measurement cases used in this paper include three types of stress cells: Vibrating Wire Stress cells (VWS); Hydraulic Stress Cells (HSC), which are used in Australia; and Borehole Platened Flatjacks (BPF), which are used in the US. Each type of cell was calibrated according to the most accepted calibration procedure recommended for that device to try and

Table 3. Summary statistics of the present stress measurement database.

	Panel Depth (ft)	Panel Width (ft)	Depth/ Width	Mining Height (ft)
Average	941	641	1.56	9
Standard Deviation	495	148	0.91	3
Minimum	410	344	0.45	5
Maximum	2,050	1,000	3.43	12

calculate a true stress change in the coal pillar. However, it is known that the different types of cells with the recommended calibration techniques show different responses.

Using 36 different pillar stress profiles measured in 6 different mines, Mark and Iannacchione (1992) derived individual pillar strength formulas for each of the stress measuring devices (VWS, Borehole Pressure Cells (BPC), and BPF) as a function of pillar width (w) and pillar height (h). Figure 2 shows a comparison of the pillar strength formulas derived from the different stress meters and the Bieniawski pillar strength formula. In this figure, note that the VWS and Bieniawski formulas match fairly well and the BPF cells show distinctly higher stress/strength.

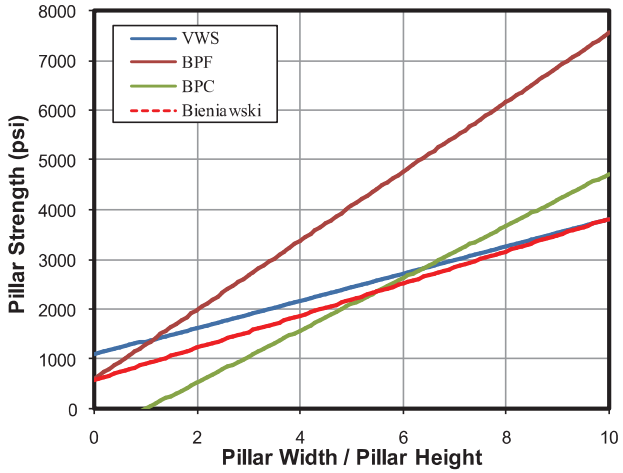

Figure 2. Comparison of the in-situ strength measurements with the Bieniawski formula.

In order to investigate the effect of stress meter calibration technique during the analysis of the stress measurements presented in this paper, the stress cells at each site were identically calibrated by using an expected Bieniawski pillar stress gradient. To do this calibration, the stress measured by the cells located in the yielded pillar edge were first determined from the loading history of the cells and the stress profiles. For instance, Figure 3 shows the loading history of the stress cells from one case study. In this figure, some of the stress cells (4, 5, 6, and 7) measured a peak cell pressure change and then the cell pressure decreased. It is assumed that this behavior indicated that the coal around the cell has reached peak stress and that the coal had started to yield. After the cells within the yield zones were determined, the initial development load was estimated using tributary area loading. The estimated development load was added to the maximum stress change measured at the cell location to calculate the peak coal strength measured by the cell. Next, the expected Bieniawski pillar stress at the cell location was calculated from the stress gradient function derived by Mark (1992):

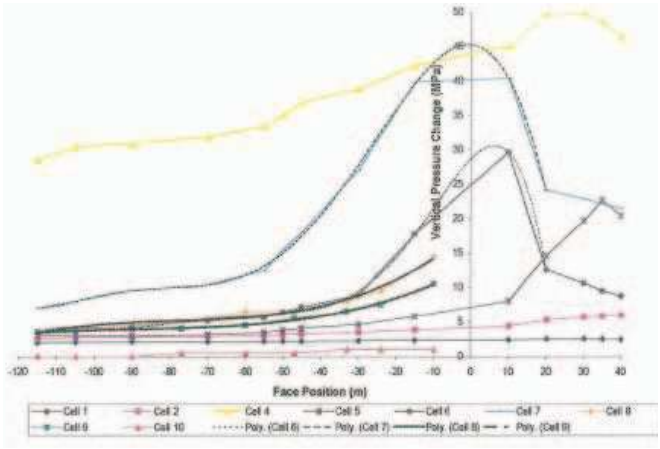

Figure 3. Loading history of the stress cells (after Colwell, Frith, and Mark, 1999).

$$\sigma_v(x) = 6.2 \times \left(0.64 + 2.16\frac{x}{h}\right) \quad (4)$$

where:

σ_v = the coal strength

x = the distance from the pillar rib

h = the height of the pillar

Then the expected coal strength versus the measured coal strength ratio at the cell location was calculated for each cell in the yield zone, and the average ratio of the all of the yielding cells was calculated. This average stress ratio was then used to adjust the measured stresses for all of the cells in that pillar.

Comparison of the Calibration Methods

In order to investigate the various stress meter calibration methods, six Australian stress measurement cases were used to compare the stress reduction factors used in Australia to calibrate HSC stress cells with the stress reduction factors derived according to expected Bieniawski stress gradient as described above.

The HSC cells were developed by Mincad Systems (Colwell, Frith, and Mark, 1999). Mincad Systems proposed two calibration procedures for the HSC cells. In this paper, the calibration procedure followed by Colwell, Frith, and Mark (1999) is used to compare the HSC cell results with the stress reduction factors found from the expected Bieniawski strength method. HSC cell

Table 4. Comparison of the calibration methods.

Case	Average Load Reduction Factor		Abutment Load/Total Load		Abutment Angle	
	Mincad	*WVU*	*Mincad*	WVU	*Mincad*	*WVU*
AU-1	0.81	0.73	0.61	0.54	25	22
AU-2	1.00	1.00	0.17	0.17	21	21
AU-3	0.90	0.81	0.22	0.20	19	17
AU-4	0.81	1.00	0.39	0.48	16	19
AU-5	0.79	1.00	0.26	0.33	8	9
AU-6	0.88	0.87	0.35	0.31	11	10

calibration formula proposed by Mincad Systems and used by Colwell, Frith, and Mark (1999) employs a calibration factor K=1 for a stress increase up to 715 psi and K=1.3 for that portion of the stress increase above 715 psi.

Table 4 shows the comparison of the calibration methods proposed by Mincad and WVU. In this table, the average load reduction factor is calculated by averaging the load reduction factors applied to the raw stress cell data. The abutment load/ total load ratio and abutment angles were calculated by using the laminated overburden load distribution method detailed in the next section.

A matched pair t-test (Dowdy, Weardon, and Chilko, 2004) was used to compare if the abutment angles calculated by the Mincad and WVU calibration methods are statistically different. In order to perform the test, first the difference between the calculated abutment angles using the two different calibration procedure (Mincad and WVU) for each case history was determined. Then, one sample t-test was performed to test if the mean of the differences was equal to zero. The statistical test result showed that, for the six cases, there was not any significant difference in abutment angles calculated by the two methods at a significant level of 0.05 (95% confidence level). This result implies that either the Mincad or the stress gradient calibration methods give essentially similar results.

Abutment Extent and Abutment Angle Calculation

After the calibrated stress profiles were determined using the calibration approach, the "measured" abutment extents and abutment angles were determined. Since none of the case histories physically measured to the extent of the abutment load, some type of abutment stress distribution had to be assumed, and then this stress distribution was used to extrapolate the stress measurements to determine the "measured" abutment extent. For this determination of the abutment extent from the stress measurements, two different potential stress distributions were analyzed: 1) the laminated overburden stress distribution and 2) the square-decay stress distribution.

Figure 4 shows typical stress change data collected from a two entry longwall mine. The area LA represents the abutment load on the gateroad pillar, and the area LB represents the abutment load on the adjacent solid coal. After the "calibration" of the stress cells, as explained in the previous section, the areas LA and LB were numerically calculated by integrating the load under the curve (Simpsons rule). Then the LA / (LA+LB) ratio was calculated.

For the laminated overburden stress distribution approach, Equation 5 gives the abutment stress magnitude (σ_1) as a function of the distance from the panel rib (x).

$$\sigma_1(x) = mq\frac{P}{2}\sqrt{\frac{2E_s}{E\lambda h}}e^{-\sqrt{\frac{2E_s}{E\lambda h}}x} \quad (5)$$

where:

m = the abutment load/total panel load ratio

q = the in situ stress

P = the width of the panel

E_s = the elastic modulus of the seam

E = the elastic modulus of the overburden

λ = a parameter of the laminated model

h = the seam thickness

In this equation, the laminated model parameter (λ) is defined as:

$$\lambda = \frac{t}{\sqrt{12(1-v^2)}} \quad (6)$$

where:

t = the lamination thickness

v = Poisson's ratio of the rock mass

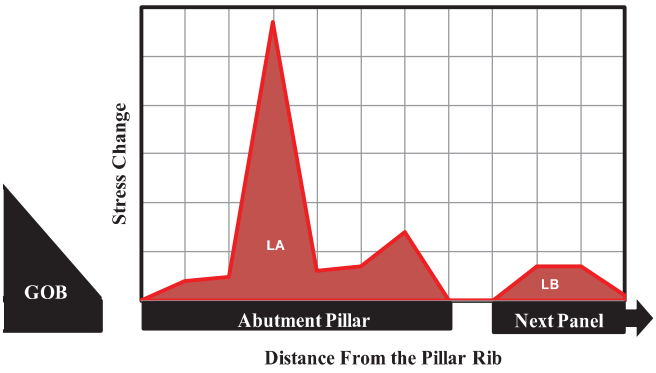

Figure 4. Typical stress change data from a two entry mine.

The percentage of the total measured load on the abutment pillar (n) for the two entry gate road in Figure 3 is calculated from the stress measurements as:

$$n = \frac{L_A}{L_A + L_B} \tag{7}$$

To determine the lamination thickness, which gives the same load percentage (n) of the side abutment load as measured in the field, first, the stress defined by the Equation 5 is integrated over the x1 distance to calculate the load on abutment pillar (see Figure 4).

$$L_A = \int_0^{x_1} \sigma_1(x)dx = -mq\frac{p}{2}\left(e^{-\sqrt{\frac{2E_s}{E\lambda h}}x_1} - 1\right) \tag{8}$$

Second, Equation 5 is also integrated over the x2 distance to calculate the total abutment load on the abutment pillar and solid coal (Figure 5).

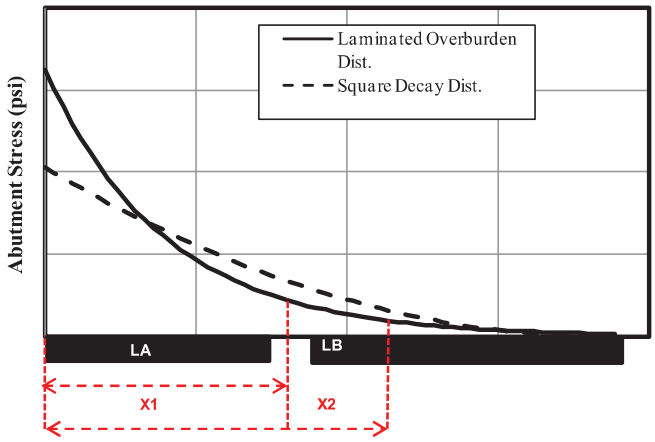

Figure 5. Analytical stress distribution functions.

$$L_A + L_B = \int_0^{x_2} \sigma_1(x)dx = -mq\frac{p}{2}\left(e^{-\sqrt{\frac{2E_s}{E\lambda h}}x_2} - 1\right) \tag{9}$$

Then the percentage of the abutment load on the abutment pillar can be determined by dividing Equation 8 by Equation 9 as:

$$n = \frac{-mq\frac{p}{2}\left(e^{-\sqrt{\frac{2E_s}{E\lambda h}}x_1} - 1\right)}{-mq\frac{p}{2}\left(e^{-\sqrt{\frac{2E_s}{E\lambda h}}x_2} - 1\right)} \tag{10}$$

Simplifying, and substituting back in for λ, we get:

$$0 = ne^{-\sqrt{\frac{2E_s\sqrt{12(1-\nu^2)}}{Eht}}x_2} - e^{-\sqrt{\frac{2E_s\sqrt{12(1-\nu^2)}}{Eht}}x_1} - n + 1 \tag{11}$$

Equation 11 can then be solved numerically for the lamination thickness which gives a loading percentage that matches the "n" value determined by field measurements. The resultant lamination thickness is then used in Equation 12, derived by Heasley et al. (2010), to calculate the extent of the abutment distance (D).

$$D_n = -\ln(1-n)\sqrt{\frac{Eht}{2E_s\sqrt{12(1-\nu^2)}}} \tag{12}$$

In order to back-calculate the abutment angle, the ratio of the total abutment load over the total panel load (qp/2) needs to be known. This ratio can be estimated by looking at the measured load on pillar A (LA) versus the amount of load on pillar A without any gob loading (see Equation 13).

$$m = -\frac{L_A}{q\frac{p}{2}\left(e^{-\sqrt{\frac{2E_s}{E\lambda h}}x_1} - 1\right)} \tag{13}$$

Finally, the value of the abutment angle can be back-calculated from the ratio "m" according to the subcritical or supercritical panel formulas.

For the square-decay stress distribution approach, Equation 2 gives the abutment stress distribution (σ_a) as a function of the full abutment extent (D) and the distance (x) from the panel rib. The calculated load on the abutment pillar for the two entry gate road system can be determined by integrating Equation 2 over the distance x_1 from the panel edge (see Figure 5).

$$L_A = \int_0^{x_1} \sigma_a(x)dx = \frac{3L_s}{D^3\left(D^2x_1 - Dx_1^2 + \frac{x_1^3}{3}\right)} \quad (14)$$

Likewise, Equation 2 is integrated over the distance x_2 from the panel rib to calculate the total load on the abutment pillar and solid coal.

$$L_A + L_B = \int_0^{x_2} \sigma_a(x)dx = \frac{3L_s}{D^3\left(D^2x_2 - Dx_2^2 + \frac{x_2^3}{3}\right)} \quad (15)$$

Then the percentage of the abutment load on the abutment pillar can be determined by dividing Equation 14 by Equation 15 as:

$$n = \frac{\frac{3L_s}{D^3\left(D^2x_1 - Dx_1^2 + \frac{x_1^3}{3}\right)}}{\frac{3L_s}{D^3\left(D^2x_2 - Dx_2^2 + \frac{x_2^3}{3}\right)}} \quad (16)$$

Finally, Equation 17 is solved numerically for the full abutment extent (D).

$$0 = n - \frac{D^2x_1 - Dx_1^2 + \frac{x_1^3}{3}}{D^2x_2 - Dx_2^2 + \frac{x_2^3}{3}} \quad (17)$$

After the calculation of the inverse squared abutment extent, the total abutment load (L_s) can be calculated by using the measured abutment load for pillar A and solving Equation 14 for the associated side abutment load.

$$L_s = \frac{L_A D^3}{3\left(D^2x_1 - Dx_1^2 + \frac{x_1^3}{3}\right)} \quad (18)$$

Finally, the abutment angle can be back-calculated from the values of "L_S" according to the appropriate subcritical or supercritical panel formulas.

RESULTS OF THE ANALYSIS

Re-Analysis of the Abutment Extent

The first parameter to be examined in this study was the extent of the abutment load. Figure 6 shows a comparison of the back-calculated abutment extents (for 90% of the total abutment load) for 13 of the case histories. The red, green, and black colors represent the abutment extents calculated by ARMPS, the square-decay fit to the field data, and the laminated model fit to the field data, respectively. Both ARMPS and the square-decay methods use the same stress distribution function and give fairly similar results. The difference between them is that ARMPS uses the full abutment extent (D) calculated by Equation 1, while the square-decay method calculates the full abutment extent for the individual stress measurement.

All three methods showed very similar trends. The laminated model gave the largest abutment extents, and the square-decay formula gave the smallest abutment extents. The ARMPS method calculated the abutment extent slightly larger than square-decay method and considerably lower than the laminated model. For low panel depths, the square-decay method calculated abutment extent less than the ARMPS method. However, as the panel depth increased, the square-decay method calculated the abutment extent similar to the ARMPS method.

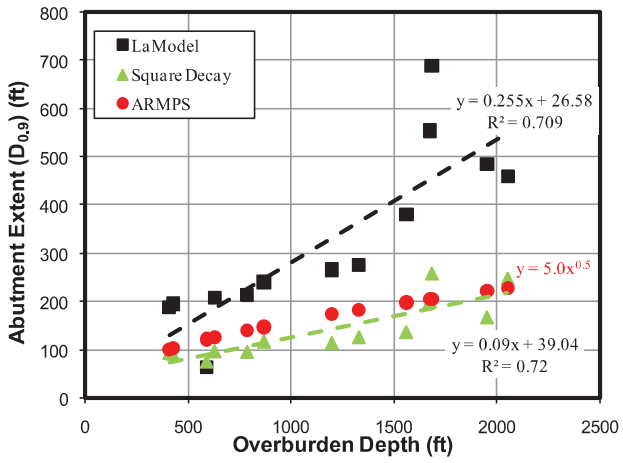

Figure 6. Extent of the abutment zone containing 90% of the abutment load.

Figure 7 shows just the comparison between the square-decay fit to the field data and the ARMPS method from Figure 6. The green points represent the field data, and the solid black line represents the linear least-square best-fit line to the field data. The upper and lower limits of the 95% confidence interval of the best fit line are shown by the dotted black lines. The red line represents the ARMPS abutment extent (D0.9) prediction equation. ARMPS predicts the abutment extent very close to the upper limit of the confidence interval from the square-decay field data. For depths less than 600 ft and higher than 1,500 ft, ARMPS prediction is inside the confidence interval.

As a result of this abutment extent analysis of the in situ stress measurement, it appears that traditional abutment extent formula given in Equation 1 very closely matches the square-decay fit to the field data used in this analysis. Stated another way, the field data in this analysis appear to support the abutment extent, as traditionally calculated by Equation 1.

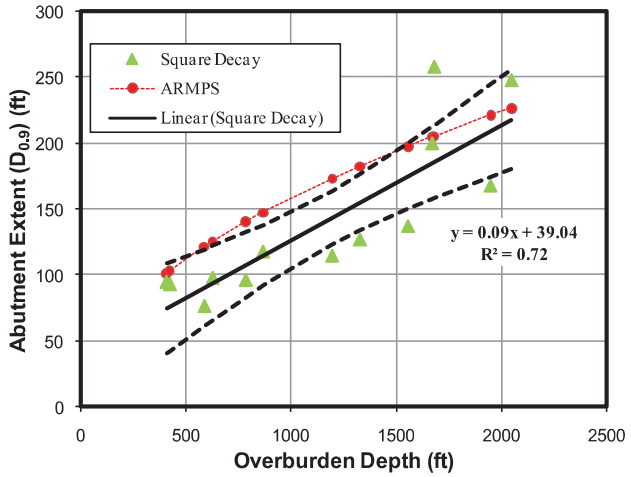

Figure 7. Comparison of the $D_{0.9}$ extent of the abutment zone back-calculated from square-decay method with original ARMPS method.

Re-Analysis of the Abutment Angle

In order to compare the effect of the different load distribution curves on the total abutment load magnitude, the abutment angles back-calculated from the laminated model, and the square-decay stress distribution functions were compared (see Table 5). In general, it was found that the laminated model calculated the abutment angles slightly higher than the square-decay method. A matched pair t-test (Dowdy, Weardon, and Chilko, 2004) was used to see if the abutment angles back-calculated by the laminated model and the square-decay curves were statistically different. The differences between the abutment angles calculations were statistically different at a significant level of 0.05 (95% confidence level).

Although the abutment angles calculated by the square-decay function and the laminated model are statistically different, the average difference is only 1.6°. This 1.6° difference only changes the magnitude of the total abutment load very slightly, and, for most practical purposes, the two methods essentially calculate the same abutment load.

Although it has been shown that the square-decay function and the laminated overburden function calculate similar abutment angles for the field data, the results of these calculations for deeper mines do not match the average 21° abutment angle used in ALPS and ARMPS. Figure 8 shows the results for the abutment angles back-calculated from the square-decay stress distribution curve. For the mines deeper than about 900 ft, it can be seen that the abutment angle values are all lower than 21° and distributed fairly evenly between the maximum value of 18° and minimum value of 6°, with the mean of 10°. For the mines with overburden depth less than 900 ft, the scatter is much larger, but the abutment angles are evenly distributed with a mean of 21°.

Based on the field data analyzed in this paper, the proposed abutment angle determination is shown as the red line in Figure 8 (Table 6). When the overburden depth is less than 900 ft, a constant abutment angle of 21° is proposed. Between 900 ft and 2050 ft, an abutment angle (β) that decreases with a continuous nonlinear power function of the depth (H) from 21° is proposed.

$$\beta = 21° \left(\frac{H}{900}\right)^{-1.59} \tag{19}$$

This equation was derived by fixing the starting point at 900 ft deep and 21°, and then performing a least-square error fit to the measured abutment angles above 900 ft deep.

Table 5. Comparison of the back-calculated abutment angles with different methods.

Case	Abutment Angles (Deg.)			OB Depth (ft)	Panel Width (ft)
	LaModel	Square Decay	LaModel Difference		
AU-1	25	22	+3	869	656
AU-2	21	19	+2	410	902
AU-3	19	17	+2	427	656
AU-4	16	16	0	591	427
AU-5	8	8	0	1558	656
AU-6	11	9	+2	787	476
AU-7	14	12	+2	1329	820
AU-8	15	11	+4	1683	745
AU-9	11	10	+1	1198	820
AU-10	11	10	+1	1673	778
US-1	10	8	+2	1950	640
US-2	8	8	0	2050	600
		Average	1.58	1210	681

SUMMARY AND CONCLUSIONS

In reviewing the ALPS and ARMPS pillar design methods, it was seen that the present calculations for abutment loading (both abutment extent and abutment angle) were derived from a limited number of field studies in the mid 1980s and 1990s (Mark, 1992 ; Peng and Chiang, 1984). These initial field studies had panel depths and widths that are significantly different from modern mine designs. In this paper, these traditional calculations for the abutment extent and abutment loading are re-examined using a current database of recent in situ stress measurements from 13 case studies with an additional 17 supplementary case studies.

The re-analysis of the extent of the abutment zone in this paper showed that the laminated overburden model calculated much larger abutment extents than the original ALPS equation and that the square-decay function calculated smaller abutment extents but close to the original equation. The large difference between the calculated abutment extents stems from the natural shape of the analytical load distribution curves that were used. As a result of the abutment extent analysis of the case histories in this paper, it was determined that the original empirical abutment extent formula in conjunction with the original ALPS square-decay stress distribution

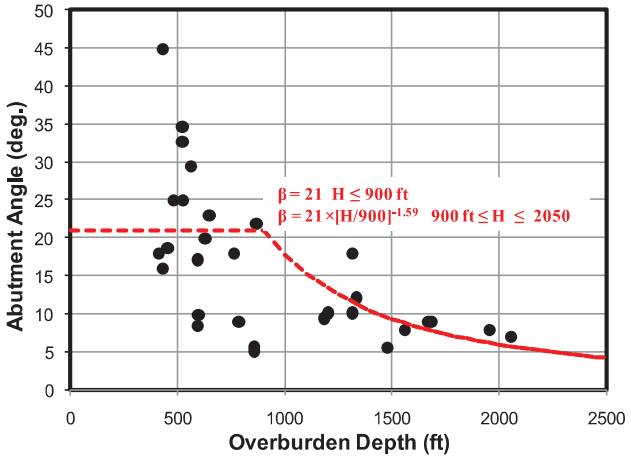

Figure 8. Abutment angles calculated using the square-decay model.

Table. 6 Proposed abutment angle concepts.

Overburden Depth (H)	Abutment Angle (deg.)
H ≤ 900 ft	21
900 ft ≤ H ≤ 2050 ft	$21 \times \left[\frac{H}{900}\right]^{-1.59}$

function sufficiently matched the field data. However, it should be noted that, in the database, there are not any case histories from the deep Western US mines. It is known that much longer abutment extents than predicted by the original abutment extent formula (Equation 1) have been observed in the some of the Western US mines (Haramy and Kneisley, 1989; Lu, 1982; Goodrich et al., 1999).

The re-analysis of the magnitude of the abutment load (as represented by the abutment angle) performed in this paper showed that, for higher overburden depths, the re-analyzed abutment angle appears to be much less than the 21° average traditionally used. Based on the field data analyzed in this paper, a new abutment angle calculation with depth is proposed (see Table 6). When the overburden depth is less than 900 ft, the 21° abutment angle proposed by Mark (1992) should be used. It is known from the ARMPS analysis that the 21° abutment angle works fine for the shallow cover cases (Mark, 2010). However, between depths of 900 to 2,050 ft, the abutment angle should be calculated with the nonlinear power function in Equation 19.

The effect of the panel width, overburden geology, and mining height on the abutment extent and abutment angle values was not found to be significant with the current data cases. However, it is believed by the authors of this paper that, certainly, the panel width and the geology of the overburden have an important effect on these two values. However, in the database of stress measurement used in this paper, the panel widths and geologies may not have varied enough to establish a significant difference.

In the future, it is desired to test the validity of the newly derived abutment angle calculation. One possible method to do this validation would be to re-analyze the large ARMPS database using the new abutment angle calculation to see if there is a better classification of successes and failures.

REFERENCES

Choi, D. S. and McCain, D. L. (1980). “Design of longwall systems.” *AIME Transactions 258*: 1761–1764.

Colwell, M., Frith R., and Mark, C. (1999). “Analysis of longwall tailgate serviceability (ALTS): a chain pillar design methodology for Australian conditions.” In: *Proceedings of the Second International Workshop on Coal Pillar Mechanics and Design*. Pittsburgh, PA: NIOSH, IC 9448, pp. 33–48.

Dowdy, S., Weardon, S., and Chilko, D. (2004). *Statistics for research*. 3rd ed. Hoboken, New Jersey: John Wiley & Sons, pp. 640.

Haramy, K. Y. and Kneisley, R. O. (1989). “Comparative study of western US longwall panel entry systems.” In: *Proceedings of the 30th US Symposium on Rock Mechanics*. Morgantown, WV: West Virginia University: pp. 125–132

Heasley, K. A., Sears, M. M., Tulu, I. B., Calderon-Arteaga, C. H., and Jimison II, L. W. (2010). “Calibrating the LaModel program for deep cover pillar retreat coal mining.” In: *Proceedings of the 3rd International Workshop on Coal Pillar Mechanics and Design*. Morgantown WV: West Virginia University, pp. 47–57.

Goodrich, R. R., Agapito, J. F. T., Pollastro, C., LaFrentz, L., and Fleck, K. (1999). “Long load transfer distances at the Deer Creek Mine.” In: *Proceedings of the Rock Mechanics for Industry, 37th U.S. Symposium*. Rotterdam, The Netherlands: Balkema, pp. 517–523.

King, H. J. and Whittaker, B.N. (1971). “A review of current knowledge on roadway behaviour.” In: *Proceedings of the Symposium on Roadway Strata Control*. London, UK: IMM, pp. 73–87.

Lu, P. H. (1982). “Rock mechanics instrumentation and monitoring for ground control around longwall panels.” In: *Proceedings of the International Symposium on State-of-the-Art of Ground Control in Longwall Mining and Mining Subsidence*. New York, New York: AIME Society of Mining Engineers, pp.1–8

Mark, C. (1987). *Analysis of longwall pillar stability*. Doctoral Thesis: The Pennsylvania State University, December.

Mark, C. (1990). *Pillar design methods for longwall mining*. Washington, D. C.: US Department of the Interior, US Bureau of Mines, IC 9247, pp. 53.

Mark, C. (1992).” Analysis of longwall pillar stability (ALPS): an update.” In: *Proceedings of the Workshop on Coal Pillar Mechanics and Design*. Washington, D. C.: US Department of the Interior, US Bureau of Mines, IC 9315, pp. 238–249.

Mark, C. and Iannacchione, A. T. (1992). “Coal pillar mechanics: theoretical models and field measurements compared.” In: *Proceedings of the International Workshop on Coal Pillar Design and Mechanics*. Washington, D. C.: US Department of the Interior, US Bureau of Mines, IC 9315, pp. 78-93

Mark, C. and Chase, F. E. (1997). “Analysis of retreat mining pillar stability (ARMPS).” In: *Proceedings of the New Technology for Ground Control in Retreat Mining*. Pittsburgh, PA: NIOSH, IC 9446, pp. 17–34.

Mark, C. (2009). “Deep cover pillar recovery in the US.” In: *Proceedings of the 28th International Conference on Ground Control in Mining*. Morgantown, WV: West Virginia University, pp. 1–9.

Mark, C. (2010). “Pillar design for deep cover retreat mining: ARMPS version 6.” In: *Proceedings of the Second International Workshop on Coal Pillar Mechanics and Design*. Pittsburgh, PA: NIOSH, pp. 106–122.

Peng, S. S. and Chiang, H. S. (1984). *Longwall mining*. 1st ed. Hoboken, New Jersey: John Wiley & Sons, pp. 720.

Tulu, I. B., Heasley, K. A., and Mark, C. (2010). “A comparison of the overburden loading in ARMPS and LaModel.” In: *Proceedings of the 29th International Conference on Ground Control in Mining*. Morgantown WV: West Virginia University, pp. 28–37.

Vandergrift, T., and Conover, D. (2010). “Assessment of gate road loading under deep western US conditions.” In: *Proceedings of the 3rd International Workshop on Coal Pillar Mechanics and Design*. Morgantown WV: West Virginia University, pp. 38–46.

Wilson, A. H. (1982). “The stability in longwall mining.” In: *Proceedings of the State of the Art in Ground Control in Longwall Mining and Mining Subsidence*. New York, New York: Society of Mining Engineers of the American Institute of Mining, Metallurgical, and Petroleum Engineers, pp. 89–95.

Massive Pillar Collapse: A Room–and–Pillar Marble Mine Case Study

Sandin E. Phillipson, Geologist
Roof Control Division MSHA
Pittsburgh, PA

ABSTRACT

The Mine Safety and Health Administration's Roof Control Division responded to a massive ground failure at an underground marble mine in northern Georgia. The ground failure occurred in a benched area that had been abandoned in the early 1990s. It involved the failure of an estimated 19 pillars, in conjunction with a massive roof fall of an undetermined extent that was at least 60 ft high. Pillars in the benched area had been mined nominally 40 x 40 feet to a height of 50 feet ft, with 40-ft mining widths, although it seems likely from measurements and accounts from mining personnel that pillars were even smaller than intended. Average overburden depth was 500 ft, and the rock mass was characterized by three sets of intersecting geological discontinuities that not only defined very blocky conditions that were conducive to pillar spalling and volume loss, but they were also adversely oriented in such a way as to cut diagonally through pillars at a high angle.

The recently released S-Pillar software from NIOSH was used to determine pillar safety factors in the failure area and indicated that pillars were undersized for the conditions. S-Pillar was used to assess pillar stability in active areas to evaluate the likelihood of experiencing similar collapses in the future. S-Pillar correctly identified the pillars in the bench area as having been at risk for instability, in light of their ultimate failure. A two-dimensional finite element model was used to evaluate the possible stages of failure and to assess the likelihood of continued failure in the benched area that might affect more distal mine openings. Although stone mines are generally characterized as having more forgiving conditions than those found in softer sedimentary rocks, the failure shares some characteristics with domino-style massive pillar collapses experienced in coal and trona mines. First, the minimum dimension of the benched area approached 350 ft; second, the pillars defined by benching had small width-to-height ratios (0.8), and; third, the pillar failure area was slightly greater than 4 acres.

The massive pillar collapse and associated roof fall illustrate the importance of incorporating pillars that have been properly sized for depth and for the final bench height. Furthermore, the designed dimensions must be adhered to during the actual mining process. Finally, the importance of understanding the geological conditions and their effect on the rock mass is critical.

INTRODUCTION

On September 21, 2011 at 3:45 a.m., employees on the surface at an underground marble mine located in northern Georgia felt what they thought was a shot being fired underground. Shortly thereafter, it was found that a portable toilet inside the mine and a tag-in board outside the portal had been knocked over by an apparent air blast. Further investigation revealed that a massive roof fall had occurred in the benched area of a portion of the mine that had been abandoned in the early 1990s. Fortunately, the massive collapse resulted in no injuries. Following notification of the Mine Safety and Health Administration (MSHA), personnel from the Southeastern Metal and Nonmetal Safety and Health District conducted a traverse around the perimeter of the failure area and determined that up to 19 pillars had collapsed amidst a massive roof fall. Although such domino-style pillar collapses have happened in coalmines (Mark, Chase, and Zipf, 1997) and trona mines (Swanson and Boler, 1995), the extent of failure that occurred at the study mine is almost without precedent in stone mines (Dismuke, Forsyth, and Stewart, 1994), which are commonly characterized by relatively forgiving environments due to high rock strengths. The height of the roof fall was later confirmed by drilling from an upper level to be at least 60 ft, although the maximum height and extent of the roof fall is unknown. The pillar failure encompassed a rectangular area 300 ft in width by 600 ft in length. The width may be considered to be larger if an additional row of pillars that is exhibiting signs of failure is included.

Because of the large pillar failure area, the possibility that failure might continue to propagate into active portions of the mine and the possibility that similar failure might be encountered in newer areas of the mine that had been planned to incorporate benching, MSHA Technical Support conducted an evaluation of the failure mechanism and ground conditions in various parts of the mine. Measurements of dimensions, strata orientation, and structural discontinuities were obtained for incorporation into the NIOSH S-Pillar software program (NIOSH 2011), as well as a staged finite element model using Phase^2 (Rocscience, Inc. 2011). These models were used to assess the mechanism and progression of the failure, evaluate pillar stability in old and new workings, and evaluate the likelihood of continued failure in old and new areas. This case study validates the use of S-Pillar to evaluate stability in underground stone mines, highlights the importance

of understanding the effects of structural discontinuities on pillar stability, and reinforces the need to adhere to the designed pillar dimensions to maintain stability.

BACKGROUND

The subject mine is one of several underground room-and-pillar mines that extract marble in an area approximately 50 miles north of Atlanta, Georgia (Figure 1). The mines are developed in the Cambrian-aged Murphy Marble, a formation within the Murphy Belt, which predominantly contains marble and schist with lesser amounts of quartzite and meta-conglomerate. These metasediments were originally deposited in a stable region as conglomerate, sandstone, shale, and calcic and dolomitic limestone (Graham 1969). Following deposition in the Cambrian, deformation occurred near the end of the Ordovician (as a result of the Taconic Orogeny) and again at the end of the Pennsylvanian (as a result of the Alleghanian Orogeny) (Graham 1969). The Murphy Belt, representing a tightly folded, overturned syncline, trends northeast from northern Georgia into southwestern North Carolina and includes, from oldest to youngest, the Nantahala, Brass town, Murphy, Marble Hill Hornblende Schist, and Andrews Formations (Fairley 1969). Later interpretations of the stratigraphy differ by including quartzite units (Tusquitee Quartzite and Nottely Quartzite) of formation rank in the sequence (Power and Forrest 1973; Groszos 1986). Although the sequence of lithologic units is agreed upon by previous studies, the assignation of those units to formal formations has been confusing and inconsistent (Power 1976). The Murphy Marble is interpreted by Power and Reade (1973) and Groszos (1986) to represent a carbonate bank. Near the study mine, Fairley (1969) and Power (1976) interpreted the Murphy belt to have been folded into an overturned syncline, and the marble interlaces with and passes laterally into the schist of the Andrews and Brass town Formations (Power and Reade 1973).

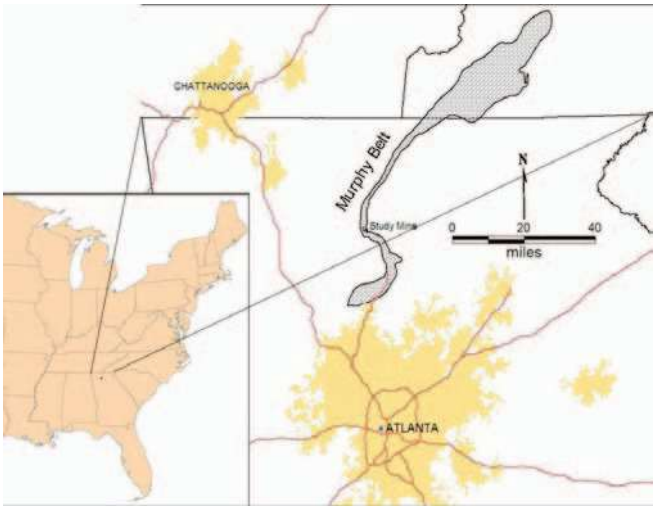

Figure 1. Location map showing position of study mine relative to the extent of the Murphy Marble in northern Georgia and southwestern North Carolina.

The subject mine is located in the informally named Whitestone Belt, one of three discontinuous pockets of marble that occur within the Murphy Belt (Power 1976). The Whitestone Belt is overlain by the quartz-biotite schist of the Brass town Formation, substantiating interpretations that the marble occurs on the overturned limb of a syncline (Power 1976). The marble is divided into an upper (actually lower in the stratigraphic sequence because of overturning), medium- to fine-grained dolomitic marble and a lower, coarse-grained calcite marble. The dolomitic marble is in contact with the overlying quartz-biotite schist, which hosts many thin layers of talc-phlogopite schist (Power 1976). The main body of the unit is massive, fine-grained dolomite marble that is 500–600 ft thick but may have been repeated due to faulting. Along the two-mile outcrop of the Whitestone Belt, eight random room-and-pillar mines had been developed by 1976, using lateral mining dimensions of 38–64 ft (Power 1976). Bench heights in older workings reached 150 ft, but, by 1976, ultimate mining heights had been reduced to 65 ft (Power 1976).

The strike and dip of the formation in the northern Georgia marble mining district is variable, but marble banding along the Whitestone Belt generally trends N 05° W and dips toward the east from as little as less than 10° to as much as 30°. This local northerly trend is significantly different from neighboring legs of the Murphy Belt, which trend northeast and southeast, respectively. Where the marble bands dip less than 10°, mine workings appear very similar to a standard limestone mine that would be characterized by a relatively horizontal roof horizon. Where the dip increases, mining levels at this and other northern Georgia marble mines are arranged in a series of horizontal stair-steps that may partially overlap as the levels follow the formation to depth. In these examples, although mining levels remain horizontal, the roof horizon is commonly characterized by a saw-toothed profile, defined by intersecting partings and joints that define hanging wedges. Because of the propensity for these wedges to drop out of the roof despite scaling, at least one area marble mine performs routine pattern bolting to ensure that the wedges are supported. Bolting is not, however, performed at the study mine.

The mine extracts marble for its calcium carbonate content by the regular room-and-pillar mining method on multiple levels, generally stepping gently downward toward the east. The mine is characterized by a prominent “dog leg” where the marble formation changes strike and dip, associated with a change in ground conditions and mining layout (Figure 2). Initial mining, characterized broadly as random room-and-pillar, was conducted on the 1,070-ft level, which represents the elevation above sea level at outcrop in the valley. In the northern half of the mine (that area north of the hinge point in the dog leg), regular room-and-pillar mining was conducted on the 920-ft level and the 880-ft level, stepping down toward the east with the dip of the marble. This area had been abandoned in the early 1990s, although ramps are being developed to the 720-ft level to continue to follow the formation down-dip. In the southern half of the mine, regular room-and-pillar mining was conducted on the 890-ft and 820-ft levels, which are superimposed because of the very low dip angle of the formation, representing the current active mining horizons. The collapse occurred in the 920-ft level, which had been mined in the 1980s and subsequently benched in the central area in the late 1980s to early 1990s. The original mining height was planned for 25 ft, and the ultimate benched height was 50 ft. Mining dimensions are defined by pillars designed 40 x 40 ft with 40-ft mining widths. Actual mining widths were generally measured as 42–43 ft.

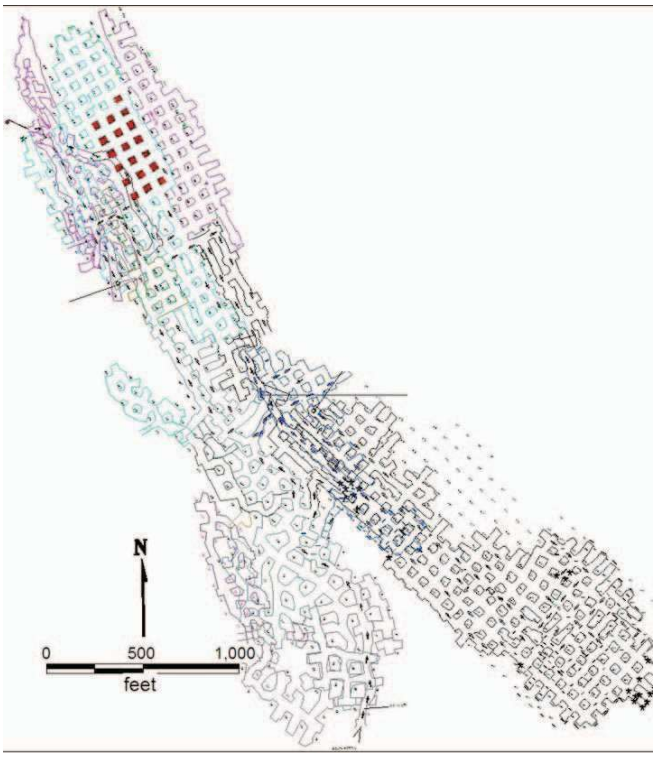

Figure 2. General mine map, showing extent of pillar failure area (red) in relation to the rest of the mine. Prominent "dog leg" represents change in strike and dip of the marble deposit, and coincides with a change in ground conditions.

METHODOLOGY

Measurements of the strike and dip of structural discontinuities, as well as their spacing, were collected in different parts of the mine using a standard Brunton hand transit and tape measure. Measurements of mining dimensions were obtained in the mine using a laser range meter and compared to planned dimensions portrayed on digital mine maps. Observations were conducted at the margin of the collapse area and in the active mining area. The condition of the roof and pillars was assessed in various parts of the mine. These values were used for performing evaluations of pillar stability with the NIOSH S-Pillar program (Table 1) and used for input parameters in the Phase^2 (Rocscience, Inc. 2011) finite element modeling program (Tables 2 and 3). Fifteen thousand psi represents the default value for unconfined compressive strength in S-Pillar, a program based on case studies of limestone mines. A marble mine in the same formation, within approximately five miles of the study mine, reported that core samples of the deposit exhibited UCS values of 12,000 psi, considered low for the marble as a whole. Thus, the 15,000-psi value is considered reasonable and may, perhaps, even be generous. Input values in Phase^2 are based on published values for a range of samples since actual geotechnical data were not available for this specific mine.

Pillar safety factors were determined with S-Pillar for the collapse area and compared to the current active mining area. The sequence of mining, benching, and pillar collapse was represented in Phase^2 in a series of staged excavations. Pillars were removed in the model to simulate their failure. The eastern-most pillar was removed first, based on recollections of mine personnel who stated that those pillars exhibited sloughing shortly after benching and on their portrayal on mine maps as being noticeably undersized compared to the neighboring pillars.

Table 1. Input values used to assess pillar stability in the collapse area with S-Pillar at the study mine.

Parameter	Value
Pillars	Square
Heading Centers	80 ft
Heading Width	40 ft
Crosscut Width	40 ft
Development Height	25 ft
Benched Height	50 ft
Maximum Cover Depth	500 ft
Unconfined Compressive Strength	15,000 psi
Large Discontinuities?	Yes, spaced 30 ft, dip 60°

OBSERVATIONS

Observations in the collapse area were conducted at the southern and western margin of the benched area (Figure 3). At the southwestern margin of the benched area, the west sides of the pillars are 25 ft high where benching ceased but are 50 ft high on the east side, where they have been exposed by benching or where a ramp had been driven onto the 920-ft level (Figure 4). The roof of the drift, even at the margin of the collapse area, was extensively damaged with what appeared to be recent small falls of rock, accompanied by pillar sloughing, based on the bright, fresh surfaces exposed in contrast to the dark soot coloration on areas that had remained intact for a long period of time. In this area, the contorted marble beds strike approximately N 05° W and dip up to 20° E. Prominent, iron-stained joints strike parallel to the marble but dip perpendicularly to marble banding (N 10° W, 63° W). A second, less prominent joint set strikes N 65° W and is oriented vertically.

The roof fall material consisted of very large, angular blocks and slabs (6-10 feet long) that were piled up above the 50-ft high roof line, obscuring any pillars that might have remained in the interior of the fall rubble (Figure 5). The lip of a very large fall cavity was visible in the roof, although the top and inside surfaces could not be discerned because of condensation in the air that obscured long-distance vision. The large blocks were jagged-edged and did not generally exhibit flat surfaces that would be indicative of unraveling along joints. Instead, the blocks' jagged edges were suggestive of failure by bending stress.

Farther west from the fall, on the unbenched portion of the 920-ft level, pillars were observed to respond to additional abutment loading resulting from the massive collapse. All pillars in these rows over a distance of eight crosscuts were characterized by prominent, dipping joints that strike parallel to marble banding but dip diagonally through the pillars from corner to corner (Figures 6 and 7). The pillars exhibited freshly spalled surfaces along the joint traces, and the joints exhibited open apertures even in the center of the pillar. Some joints appeared to have a milled, rubble-like appearance that is suggestive of shearing. The damage observed in the 25-ft-high pillars is suggestive of additional abutment loading resulting from the adjacent, massive collapse.

Table 2. Input values for rock properties used to assess collapse area with Phase2 at the study mine.

Parameter	Value
Initial Element Loading	Field stress and body force; 1:1 ratio of horizontal to vertical stress
Poisson's Ratio	0.3
Young's Modulus	432,000,000 psf
Failure Criterion	Mohr Coulomb
Material Type	Plastic
Tensile Strength	345,000 psf
Peak Friction Angle	35°
Peak Cohesion	400,000 psf
Dilation Angle	10°
Residual Friction Angle	30°
Residual Cohesion	40,000 psf
Residual Tensile Strength	28,800 psf
Unit Weight	165 pcf

Table 3. Input values to describe geological discontinuities affecting the rock mass for evaluating collapse area with Phase2 at the study mine.

Parameter	Value
Marble Banding Partings	
Slip Criterion	Mohr Coulomb
Tensile Strength	0 psf
Peak Cohesion	23,000 psf
Peak Friction Angle	30°
Normal Stiffness	600,000 psf/ft
Shear Stiffness	600,000 psf/ft
N 05° W, 65° W Joints	
Slip Criterion	Mohr Coulomb
Tensile Strength	0 psf
Peak Cohesion	15,000 psf
Peak Friction Angle	28°
Normal Stiffness	400,000 psf
Shear Stiffness	400,000 psf
N 05° W, 90° Joints	
Slip Criterion	Mohr Coulomb
Tensile Strength	0 psf
Peak Cohesion	23,000 psf
Peak Friction Angle	30°
Normal Stiffness	600,000 psf/ft
Shear Stiffness	600,000 psf/ft

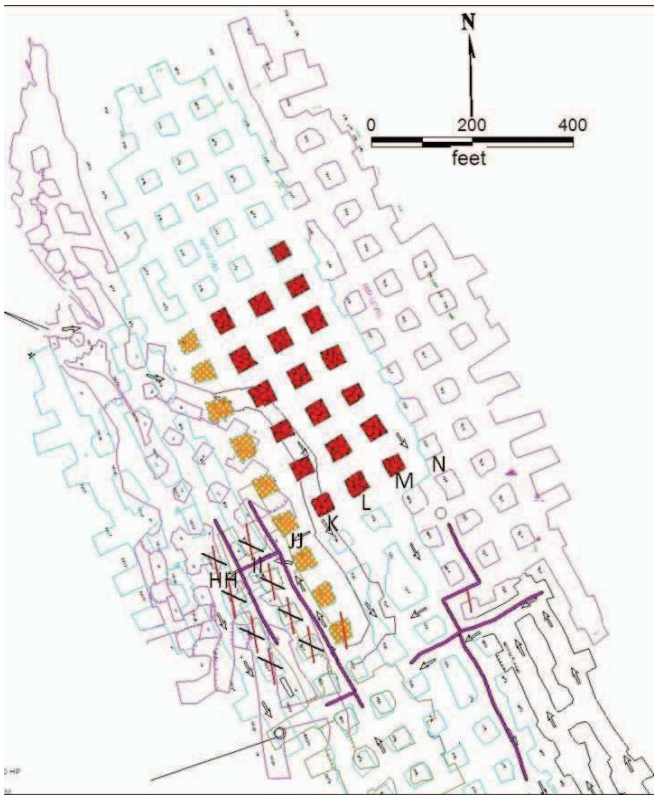

Figure 3. Map of collapse area, showing observation traverse (heavy purple line) and damaged pillars (red = believed to have failed; orange = taking weight, exhibiting degradation). Red lines represent prominent, iron-stained joints; black lines represent joints. Collapse was localized to the benched area of the 920-ft level, shown in light blue.

Figure 4. The row of pillars at the margin of the benched area is characterized by extreme degradation, with the eastern portions (facing the benched side) 50 ft tall and exhibiting failure along pre-existing geological structures.

Figure 5. Roof fall debris is composed of very large blocks. The photo vantage point is approximately 40 ft from the rubble.

Figure 6. Open-aperture joint, which strikes N 10° W and dips 63° W, is located in the center of pillar II28. This orientation of joints typically runs diagonally from corner to corner in the JJ, II, and HH pillars. White outline represents close-up shown in Figure 7.

Further assessment was performed in adjacent areas of the 920-ft level where active haulage ways were defined and in the southern area of the mine where active mining was being conducted, in order to ascertain whether widespread collapse should be a prevailing concern in this mine. Observations in those areas indicated that the quality of the ground was much better than in the collapse area. There appear to be two main reasons for this, both of which are reflections of the geological conditions. First, the set of joints that strikes N 05° W and dips approximately 65° W, thereby dissecting pillars diagonally, is not present south of the collapse area. Therefore, it appears that this joint set exerts a particularly deleterious effect on ground stability when present. This diagonally crosscutting joint set is not only in the most unfavorable orientation for pillar stability but is also generally characterized by

Figure 7. Close-up of Figure 6, showing open aperture along joint that penetrates deeply into the pillar. This feature contrasts with the irregular, localized nature of small fractures that represent blast damage on the pillar skin.

heavy iron staining, indicating open apertures that easily transmit water and offer little to no cohesion between opposing blocks of rock. Second, a change in dip, from up to 20° in the collapse area to less than 10° in the southern, active area results in a more stable roof horizon that is not characterized by a sawtooth profile of intersecting joints. It is interpreted that the sawtooth profile makes it easier for progressive raveling to occur, especially since the mine does not install rock bolts. Although the southern area hosts abundant, closely spaced (10–24 in.) vertical joints that strike N 65° W, they do not exhibit open apertures, and pillars exhibited virtually no evidence of spalling (Figure 8).

Figure 8. Typical condition of pillars on the 820-ft and 890-ft levels, showing an absence of open-aperture joints or evidence of raveling.

DISCUSSION AND ANALYSIS

S-Pillar

The 920-ft level collapse area shares several similarities with the circumstances of domino-style cascading collapses in coalmines. These types of collapses are commonly characterized by wide panels (350 ft) that encompass more than 4 acres. (The study mine's collapse area encompassed 4.1 acres.) In these collapses, tall, slender pillars (those with a small width-to-height ratio) had been developed (Mark, Chase, and Zipf 1997). It is interpreted that those were finely balanced systems and that the failure of only a single pillar was enough to shed load onto surrounding pillars, precipitating a cascading, rapid failure. Research performed by NIOSH on stone mine pillar performance identified two main factors in predicting pillar instability: 1) width-to-height ratio of 0.8 or less and 2) safety factors of 1.8 or less (Esterhuizen, Dolinar, and Ellenberger 2008; Esterhuizen, Dolinar, and Ellenberger 2011; Esterhuizen, Dolinar, Ellenberger, and Prosser 2011) (Figure 9). Pillar stability was further influenced by the spacing and orientation of planar geologic discontinuities. Pillars in the failed 920-ft level were 50 ft high and 40 x 40 ft, defining a width-to-height ratio of 0.8, cut by high-angle joints that further degraded the strength of pillars that only had a safety factor of 1.1 as calculated by S-Pillar.

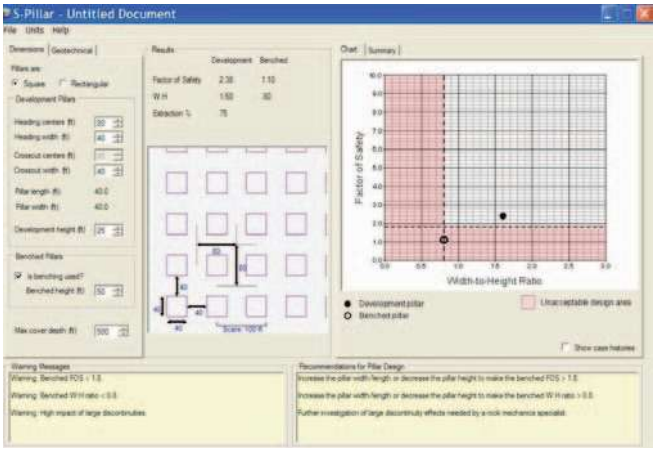

Figure 9. Analysis of pillar design on the 920-ft level using NIOSH S-Pillar software for limestone mines. Benched pillars on 920-ft level are solidly outside the acceptable design category, with a safety factor calculated by S-Pillar of only 1.1.

Mine personnel stated that the M row of pillars in the benched area had exhibited signs of degradation shortly after benching, prompting the abandonment of the area in the late 1980s or early 1990s. Other mine personnel suggested that the back horizon may have encroached upon or even reached the contact with the overlying quartz-biotite schist which, especially in combination with the previously reported talc layers, could have represented a large potential delamination plane. The mine map portrays the M pillars as smaller than the nominal 40 x 40 ft dimensions, which results in an even lower width-to-height ratio and lower safety factors. It is, therefore, interpreted that failure initiated in the M row and that, as those pillars failed, their loads were transferred onto the adjacent, meta-stable benched pillars, which failed in succession. Because the area had been abandoned for many years, the relative timing of pillar failure and roof failure is unknown. Measurements in adjacent areas indicated that mining widths were generally several feet larger than the nominally planned 40 ft, resulting in corresponding pillar dimensions several feet smaller than 40 x 40 ft. Thus, the pillars are likely to have actual width-to-height ratios and safety factors that are even smaller than would be indicated for the planned dimensions.

Conditions in the southern, active mining areas appear much better than in the collapse area. The marble exhibits a very low-angle dip so that it is nearly horizontal, greatly reducing the occurrence of wedges in the back. Further, the N 10° W, 65°W joints that represent planes of preferential weakness and negatively influence pillar stability in the north are absent. The 890-ft level is not intended to ever be benched because of the 43-ft sill thickness to the underlying 820-ft level. NIOSH S-Pillar software indicates that for the current 25-ft development height, pillars should display acceptable width-to-height ratio (1.5) and safety factor (2.39) values. The lower, 820-ft level, is intended to be benched. Even though ground conditions appeared good during the underground evaluation, the S-Pillar analysis indicates that, when benching is performed, the resulting pillars will be on the margin of acceptable design (Figure 10). The S-Pillar software illustrates the importance of pillar dimensions used in the pillar strength calculations to determine the pillar safety factor. The software indicates that a 40 x 40 x 50-ft pillar is on the margin of acceptable stability, and the mine must recognize the importance of adhering to the designed dimensions. Despite the intention to mine pillars 40 x 40 ft, with 40-ft mining widths, the widths measured were generally 42–43 ft. The S-Pillar analysis indicates that this loss of pillar volume would be sufficient to transition the resulting benched pillars out of the acceptable design field, as the pillar safety factor is reduced from 1.87 to 1.62.

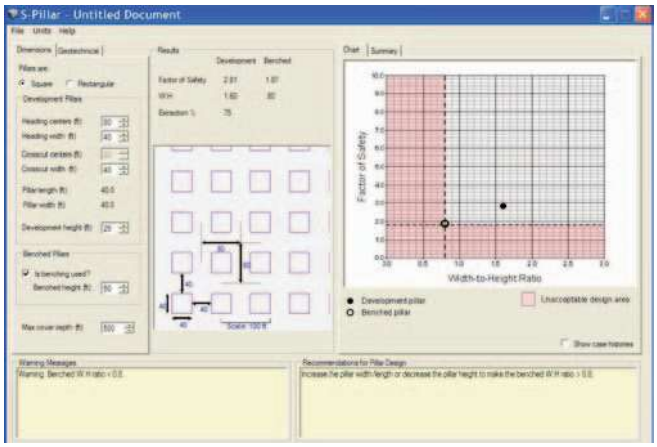

Figure 10. NIOSH S-Pillar analysis results for benching on the 820-ft level, showing marginal but still acceptable stability.

Finite Element

Observations suggest that the JJ, II, and HH pillars (labeled in the following diagrams) are being subjected to excessive loading. The JJ pillars, which are adjacent to the 50-ft benched area, could fail. Thus, large-scale collapses could continue in the northern area as remaining pillars are, in effect, removed. A finite element modeling program was used to assess the possible progression of failure, and the possible consequences of continued failure (Figures

11a-f). The two-dimensional model, which treats square pillars as strip pillars, incorporated major geologic discontinuities, including partings along dipping marble beds (inclined 20°), vertical joints, and 65° dipping joints that dissected pillars as ubiquitous joints. In the model, strength factors (equivalent to a safety factor for model elements but calculated differently from the safety factors discussed in terms of S-Pillar) for elements in the K, M, and N pillars were reduced to less than 1 immediately upon benching the 920-ft level (Figure 11b). It should be recognized that the model results should be interpreted only as stability trends, rather than absolute values. At this stage, the model suggests that both the M and K pillars are affected by elements with safety factors less than 1.

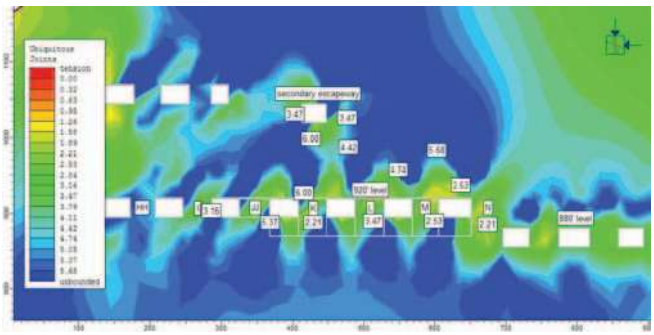

Figure 11a. Distribution of safety factors with development only on the 880-ft and 920-ft levels. Pillar rows are annotated as referred to in the text. Box in upper right portrays orientations of geologic discontinuities incorporated in the model, based on field observations.

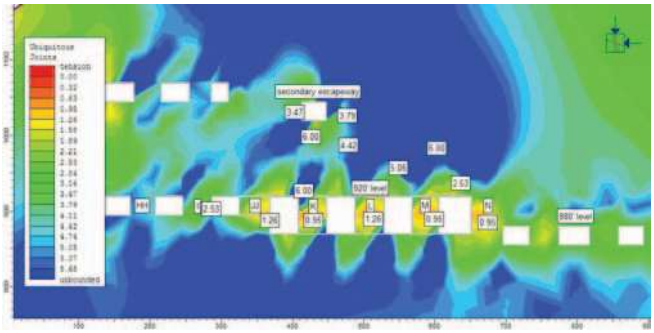

Figure 11b. Distribution of safety factors following benching of the 920-ft level to 50-ft height. Note the significant reduction of element safety factors in benched pillars compared to Figure 11a.

However, the M pillar was chosen as the first pillar row to fail based on smaller-than-planned dimensions on the mine map, and statements from mine personnel indicating that the M pillars had been subject to constant raveling, interpreted as a sign of taking weight, possibly from cantilevering beneath the quartz-biotite schist delamination horizon. Following the loss of the M pillar, interpreted as the most likely to have failed in the benched area, elements in the L pillar also exhibited safety factors of less than 1, and safety factors began to exhibit a marked decrease in the roof of the resulting unsupported area (Figure 11c). With the loss of the L pillar, safety factors in the K pillar were drastically reduced, and safety factor values less than 1 propagated high into the roof, indicating the onset of the large roof fall that occurred (Figure 11d). As failure progressed to include the loss of the K pillar, safety factor values in the JJ pillar were reduced to less than 1, and two arcs of low-value safety factors were shown developing high into the roof, similar to a pair of closing pincers (Figure 11e). Figure 11e represents the observed state of the ground at the time of the investigation, with a large roof fall having developed above the failed pillar area, the JJ (and likely also the N) row of pillars taking weight, and a large reduction in safety factor values for elements in the II pillars. The model results tend to be substantiated by the presence of open joints and freshly spalled surfaces observed on the JJ, II, and HH pillars. It should be recognized that pillars need not have toppled over or collapsed completely in order to represent a state of failure. Instead, it is more likely that the pillars would have gradually crushed out, deforming after a style of strain-softening as incremental movement occurred along numerous joint planes. Most of the pillars likely retained some low level of residual strength and could even exist as remnants among the roof fall debris. However, the pillars are considered to have failed when that residual strength was no longer equal to the axial stress imparted from the weight of the overlying rock mass. With the expected continued destabilization and eventual failure of the JJ pillar, the model indicates the potential for an enlargement of the ground collapse area in the roof so that, even a secondary escape way, prudently abandoned, would be encompassed by safety factor values less than 1, despite being located 100 ft above the roof of the collapse area (Figure 11f).

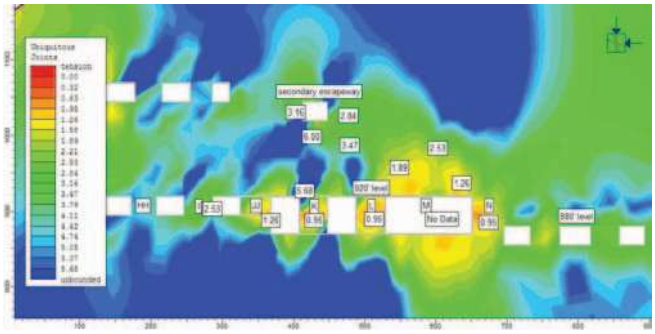

Figure 11c. Distribution of safety factors following the loss of the M pillar, interpreted to have been the first to fail based on mine personnel accounts.

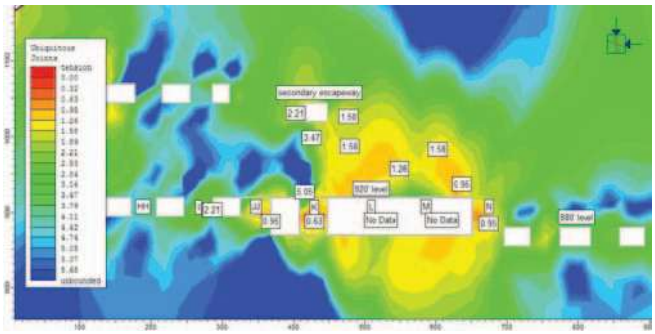

Figure 11d. Distribution of safety factors following the loss of the L pillar.

CONCLUSIONS

The MSHA Technical Support, Roof Control Division conducted an assessment of ground conditions at the study mine in order to better understand the causes of a massive collapse in an abandoned area and to determine whether the active mining levels might be subject to the same potential for collapse. Underground observations indicate the geological conditions are different in

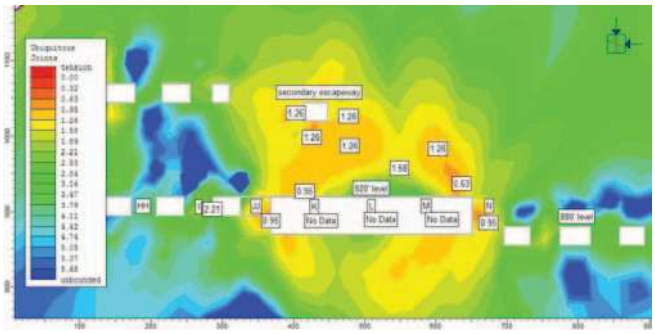

Figure 11e. Distribution of safety factors following the loss of the K pillar. The distribution of low-value safety factors generally mirrors the shape of the large roof fall cavity that was observed during the underground investigation. Note the low safety factors affecting the JJ pillar, which is substantiated by field observations as indicated in Figure 4.

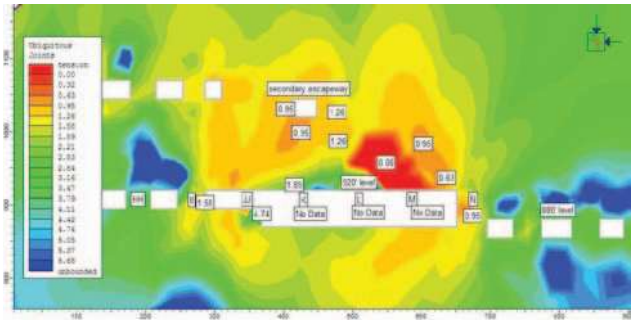

Figure 11f. Distribution of safety factors following potential, but likely, loss of the JJ pillar. With the loss of the JJ pillar, the potential ground collapse area expands to encompass the former secondary escapeway, located approximately 100 ft above the 920-ft level. Safety factor values in the II pillar have been greatly reduced, as substantiated by field observations as indicated in Figures 6 and 7.

the abandoned, collapsed area compared to the active areas. At this time, the potential for pillar failure in the active portions of the mine, on the 820-ft and 890-ft levels is low. This is mainly because of more favorable geological conditions characterized by an absence of the N 05° W, 65° W joints and a moderation of the marble dip to less than 10° that resulted in elimination of the heavily jointed, sawtooth roof profile.

Analysis of the collapse and active areas appears to validate the effectiveness of the NIOSH recently released S-Pillar software for evaluating pillar stability in stone mines. Although the case study database is based on limestone mines, the marble in this instance appears to have similar enough properties that actual failures occurred as would have been indicated by very low S-Pillar safety factors. Because S-Pillar has essentially been calibrated to the site-specific conditions at this mine by being able to back-analyze an actual collapse, S-Pillar results should be carefully considered when designing bench heights in future mining areas.

It must also be noted that actual mined dimensions should be the same as designed dimensions. Mining widths of 43 ft, resulting from blasting over break of 1.5 ft on each of the four pillar sides, translates into a pillar that is 37 x 37 ft rather than 40 x 40 ft. This is 14% smaller than intended. If pillars are already designed to meet only the minimum stability value, to allow maximum recovery, this 14% could represent the difference between stability and failure when combined with other unexpected circumstances that may adversely affect pillar quality. In addition to adhering to designed dimensions, the effect of depth and associated axial load must also be recognized when following a dipping horizon. A traditional design that has been used for many years could be found to be inadequate at greater depths.

Finally, the importance of understanding the effect of geological discontinuities cannot be overstated. Rock strength may mean little when the rock mass is characterized by several intersecting sets of closely spaced joints, particularly when joints are arrayed to cut diagonally through pillars.

REFERENCES

Dismuke, S. R., Forsyth, W. W., and Stewart, S. B. V. (1994). "The evolution of mining strategy following the collapse of the window area at the Magmont mine, Missouri." In: *Proceedings of the CIM Annual General Meeting, District 6, Metal Mining*. Vancouver, BC, Canada: Canadian Institute of Mining, p. 3–8.

Esterhuizen, G. S., Dolinar, D. R., and Ellenberger, J. L. (2008). "Pillar strength and design methodology for stone mines." In: *Proceedings of the 27th International Conference on Ground Control in Mining*. Morgantown, WV: West Virginia University, pp. 241–253.

Esterhuizen, G. S., Dolinar, D. R., and Ellenberger, J. L. (2011). "Pillar strength in underground stone mines in the United States." *International Journal of Rock Mechanics and Mining Sciences 48*(1); 42–50.

Esterhuizen, G. S., Dolinar, D. R., Ellenberger, J. L., and Prosser, L. J. (2011). "Pillar and roof span design guidelines for underground stone mines." Pittsburgh, PA: NIOSH IC9526, pp. 1–64.

Fairley, W. M. (1969). "Stratigraphy and structure of the Murphy marble belt in parts of northern Georgia." *Georgia Geological Survey Bulletin 80*: 89–120.

Graham, R. S. (1969). "Stratigraphy and structure of the Murphy marble belt between Whitestone and East Ellijay, Georgia." *Geological Society of America, Special Paper*: pp. 398.

Groszos, M. S. (1986). "The stratigraphy of the Murphy Group in the Murphy syncline of northern Georgia." *Geological Society of America, Abstracts with Programs*: pp. 224.

Mark, C., Chase, F. E., and Zipf, R. K. (1997). "Preventing massive pillar collapses in coal mines." In: Mark, C. and Tuchman, R. J., eds. *Proceedings of the New Technology for Ground Control in Retreat Mining*. Pittsburgh, PA: NIOSH IC9446, pp. 35–48.

NIOSH. (2011). *S-Pillar—Software for stone mine pillar design*. http://www.cdc.gov/niosh/mining/products/product187.htm

Power, W. R. and Forrest, J. T. (1973). "Stratigraphy and paleogeography in the Murphy marble belt." *American Journal of Science 273*: 698–711.

Power, W. R. (1976). "Economic geology of the Georgia marble district." In: Proceedings of the Twelfth Forum on the Geology of Industrial Minerals. Atlanta, Georgia: State of Georgia, Department of Natural Resources, Environmental Protection Division, Georgia Geologic Survey, pp. 59–68.

Rocscience, Inc. (2011). *Phase^2 software, v. 8.004*. http://www.rocscience.com/products/3/updates/25

Swanson, P. L. and Boler, F. (1995). "The magnitude 5.3 seismic event and collapse of the Solvay trona mine: analysis of pillar/floor failure stability." *U.S. Bureau of Mines Open File Report 86-95*: 82.

The Extraction of Main Heading Pillars with a Longwall at Nre Wongawilli Colliery

Ry Stone, Geotechnical Engineer
Strata Engineering (Australia) Pty Ltd
Charlestown, Australia

ABSTRACT

To maintain longwall continuity, NRE Wongawilli Colliery extracted the approximately 20-year-old Thompson Mains and in doing so, 20 roadways were holed into during longwall retreat. The orientation of these roadways with regard to the longwall face varied between (i) a parallel alignment where the entire roadway was simultaneously subjected to a significant increase in vertical stress on holing and (ii) a more favorable high angle of alignment, meaning that only a portion of the roadway was subjected to an increase in vertical stress on holing. In addition, the longwall holed into and was recovered in one of the existing roadways.

The geotechnical environment presented several additional challenges during longwall retreat. The orientation of the stress field resulted in a major horizontal stress notch on the maingate and an elevation in the major horizontal stress in front of the longwall face during the retreat up to an adjacent goaf edge. The presence of geological structure zones also resulted in both swings in the major horizontal stress direction and increased levels of roof deformation.

The gate road support designs were based on commonly accepted strata management techniques and principles. The support designs in the hole-through roadways were based on empirical design models generated from (i) aconceptual geomechanical model of pre-driven hole-throughand recovery roads and (ii) a worldwide database on pre-driven hole-throughand recovery roads.

Imperative to the success of extracting the panel was a site-specific strata management process. In this regard, consideration was given to the following: roof displacement monitoring in the gate roads (in particular, Longwall (LW) Acceleration Position), roof-to-floor convergence monitoring in the hole-through roadways, the ability of the mine to limit downtime prior to and during holing by utilizing an Authority to Mine (ATM) type process, and the use of Trigger Action Response Plans (TARP).

INTRODUCTION

NRE Wongawilli Colliery is located in the Southern Coalfield, approximately 100 km south of Sydney in New South Wales, Australia. The longwall operation extracts the lower portion of the 8 to 9 m thick Wongawilli Seam at depths between 280 and 370 m. To date, the mine has successfully extracted 14 longwalls ranging from 75 to 175 m in width and 350 m to 3 km in length.

To maintain longwall continuity, the mine extracted the existing Thompson Mains as part of LW 19 (see Figure 1). The NW-SE trending panel was developed with continuous miners approximately 20 years ago. To limit the number of roadways holed into during longwall retreat, B and C Headings were used for the maingate and tailgate respectively,resulting in a 75 m wide longwall face. The longwall commenced retreat in 25C/T and was recovered in 4 C/T. As a result, 20 roadways were successfully holed into during longwall retreat.

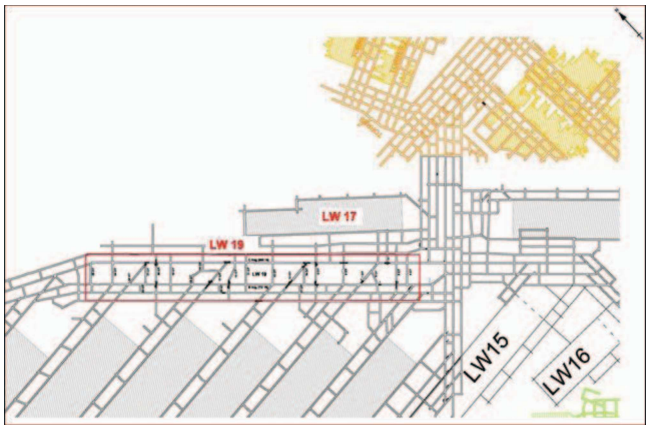

Figure 1. Copy of Mine Plan showing the location of LW 19.

GEOTECHNICAL ENVIRONMENT

The geotechnical considerations used to determinethe adequate support requirements for the extraction of LW 19 include the orientation of the hole-through roadways with respect to the longwall face, the structural competency of the roof, the in situ stress regime, and the presence of geological structure. The impact of these factors with regard to ground support was assessed using local and worldwide databases.

Panel Layout

During the extraction of LW 19, 20 roadways with various alignments to the longwall face were holed into. In regard to the orientation of these roadways with respect to the longwall face, 13 were aligned parallel to the face and in thesecases, the entire roadway was simultaneously subjected to a significant increase in vertical stress on holing.Seven were aligned at a more favorable high angle, meaning that only a portion of the roadwayat any one timewas subjected to an increase in vertical stress on holing.

Figure 2a illustrates that on holing into the roadways aligned parallel with the longwall face, the width of the fender is reduced incrementally and as such, the fender and roadway are subjected to a large increase in stress along the entire face as the cantilever in the roof rotates onto the longwall face and powered supports.In the second scenario, Figure 2b shows that on holing into roadways aligned at a reasonably high angle to thelongwall face, the wedge shaped fender restricts both the rotation of the cantilever and the width of the roof span at the intersection with the face. Becauseof the roadway's high angle of intersection with the longwall face, it is also of note that the magnitude of vertical stress reduces away from the intersection.

Consideration was also given to the impact of the adjacent goafs and the consequent re-distribution of stress in the form of pre-existing abutment loading. The extent of the existing abutment loading from adjacent goaf areas is a function of the depth and width of the surrounding pillars. Critically, the vertical stress concentration decays in a parabolic fashion away from the goaf edge. As shown in Figure 1, as LW 19 was separated from the LW 17 goaf by approximately 100 m of coal and from several longwalls to the west by 100 to250 m of coal, it was deemed that the panel was not subjected to any significant abutment loading effects from these goafs. This is confirmed by calculating the maximum extent of the side abutment loading using the following equation:

$$D = 5.13 * \sqrt{H} \quad \text{(Peng and Chiang, 1984)} \qquad (1)$$

Where:

D = extent of side abutment load (m)

H = Depth of Cover (m)

The results indicate that for the maximum Depth of Cover in the panel, any side abutment loading would extend a maximumof 96m from the adjacent goaf.

Roof Lithology and Structural Competency

Exploration boreholes and roof borescopes at the mine were used to assess the composition of the immediate roof in the Wongawilli Seam. The data indicates that the lithology of the immediate roof generally remains consistent throughout the mine including LW 19. The mine typically extracts the first 3 to 3.5 m of the approximately 8 to 9 m thick coal seam.

In terms of the immediate roof, Figure 3 indicates that the first 5 to 6 m is dominated by interbedded units of coal and mudstone, and the approximately 1 m thick tuffaceousWongawilli Sandstone.

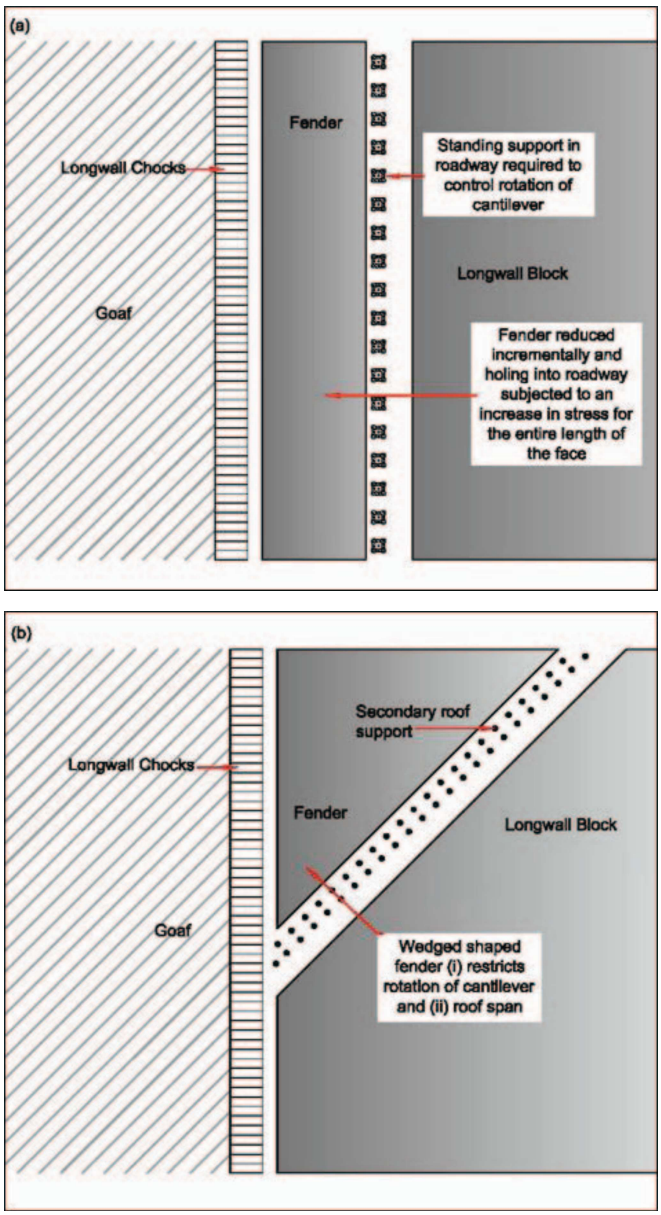

Figure 2. Schematic showing longwall holing into (i) roadways aligned parallel with the longwall face and (ii) roadways aligned at a reasonable high angle to the longwall face.

Overlying the coal and mudstone is a variable and interbedded sequence of sandstones, siltstones, and carbonaceous shales. The base of the Wongawilli Sandstone is typically located between 2.5 to 2.7 m into the roof and, in comparison to the surrounding coal and mudstone, is very stiff. As a result, it is especially susceptible to horizontal stress driven buckling.

The Coal Mine Roof Rating (CMRR) generally ranges between 30 and 40, which suggests a roof of weak or limited competency. As a means of comparison, it is generally accepted that any roof which has a CMRR of <35 is classed as very weak, 35 to 45 as weak, 45 to 55 as moderate and >55 as strong.

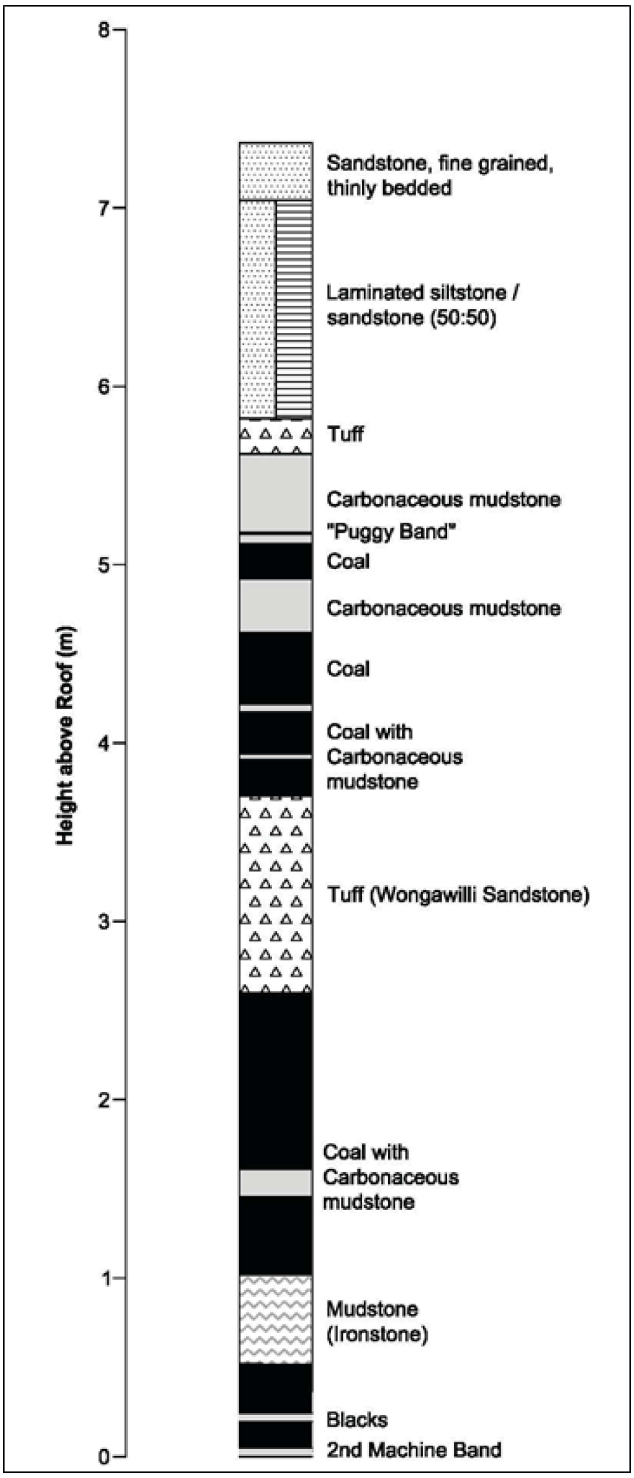

Figure 3. Typical roof lithology logged in the immediate roof.

In Situ Stress Regime

The Thompson Mains are located at a depth of between 320 and 350 m.In the context of current coal mining experience in Australia, this is indicative of a moderate Depth of Cover. At these depths, horizontal stress is a major consideration in the strata management at the mine. In view of Australia's proximity to a number of active plate tectonic margins, the ratio between the major and minor horizontal stress typically varies between 1.5 and 3:1 and as such, can have a significant directional impact on roof behavior during both development and longwall retreat.

Generally at the mine, the major horizontal stress is aligned in a regional NE-SW direction (see Figure 4). It is however of note that local variations in this trend have been mapped and measured around geological structures at the mine.

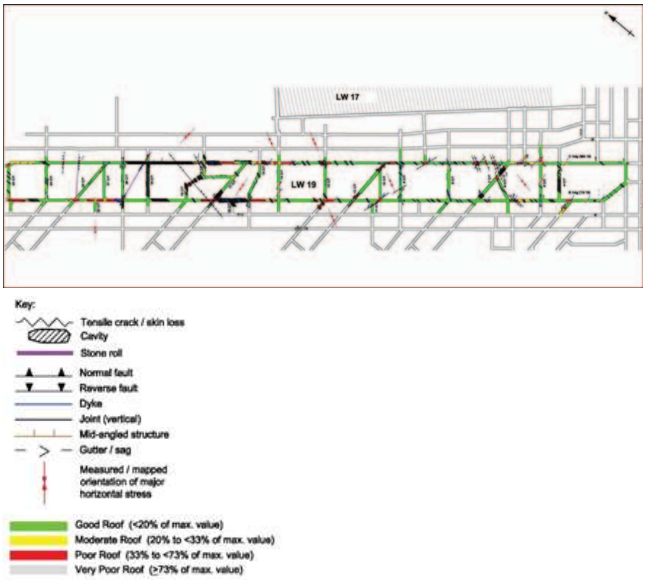

Figure 4. Copy of mine plan showing the (i) roof condition mapping and (ii) major horizontal stress direction.

As shown in Figure 4, roof condition mapping undertaken in the roadways indicated thatin areas, the major horizontal stress re-orientates to a more WNW-ESE direction. This rotation of the stress field was located in and around a zone of geological structure encountered in the inby end of the panel.

Geological Structure

In terms of geological structure, several zones of minor faulting were encountered in the panel (see Figure 4). Two of these zones located between 5 and 8 C/Ts and 15 and 20 C/Ts comprised of NNW-SSE trending normal faults and persistent jointing. The measured throw on these faults indicated an offset of no more than 100mm. In addition, two NE-SW trending reverse faults were encountered between 23 and 24 C/Ts. These faults were associated with stone rolls protruding intothe base of the coal seam. Elsewhere in the panel, the stone rolls trended in a WNW-ESE direction and were not accompanied with the aforementioned thrust faulting.

GATE ROAD SECONDARY SUPPORT

As a result of the high horizontal stress magnitudes found in Australian coalmines, horizontal stress driven roof buckling during longwall retreat is a common occurrence in gate roads. The resulting elevation in horizontal stress ahead of the retreating longwall face can induce significant surges in roof displacement.

The required level of roof support in gate roads during longwall retreat relies heavily on identifying areas susceptible to large surges in roof displacement. The main factor to consider in addition to the Depth of Cover is the orientation of the major horizontal stress with regard to the longwall gate roads.

During roadway development, Gale and Blackwood (1987) demonstrated that the "percentage of good roof" reaches its maximum if the roadway's angle of intersection with the major horizontal stress is less than 35º and its minimum if the angle of intersection is greater than 55º (see Figure 5). This work also demonstrated that if the roadway intersects the major horizontal stress at a reasonably high angle, the majority of the roof deformation will concentrate on the side of the roadway that first intersects the major horizontal stress during roadway development. As longwall extraction is essentially a large-scale version of roadway development, the same concept can be applied in this case. Of particular significance in this regard is however whether the major or minor horizontal stress concentrations around the maingate or tailgate end of the face (see Figure 6).

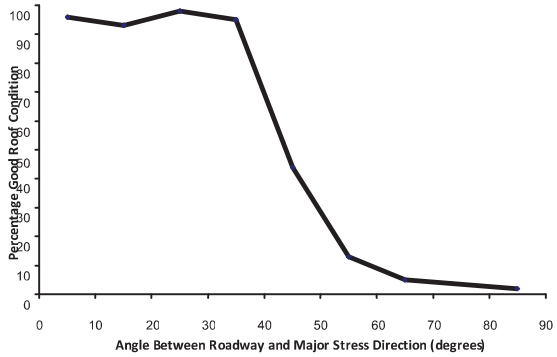

Figure 5. Impact of Angle of intersection with major horizontal stress and roof conditions during roadways development.

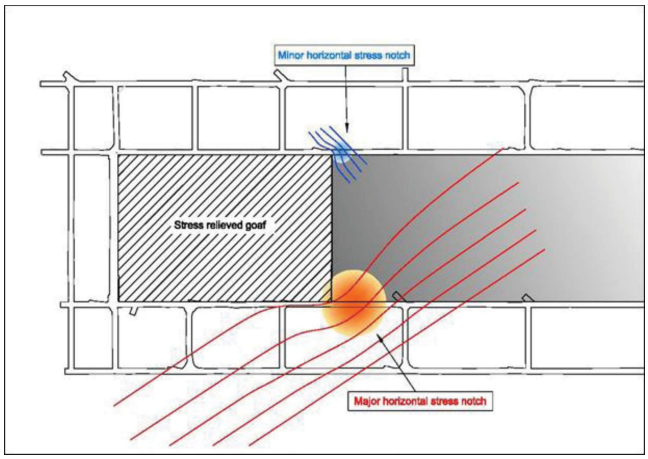

Figure 6. Schematic illustration showing the major and minor horizontal stress notching on the gate roads during longwall retreat.

Another factor to consider with regard to the gate road support is the location of cut-throughs. During longwall retreat, the magnitude of horizontal stress concentrations in the gate roads will increase on the inby side of a cut-through and reduce on the outby side of a cut-through. This phenomenon is described by Thomas and Wagner (2006), whereby "the tendency for the horizontal stress to concentrate between the longwallgoaf and the cut-through and the subsequent ability of the cut-through to relieve the horizontal stress about the gate road when the face retreats outby of the cut-through". Shown in Figure 7, this is calleda "pinch-point" and typically extends for a distance of 34m inby of the cut-throughcenter-line. Conversely, the stress relief typically extends around 20m outby of the cut-through center-line.

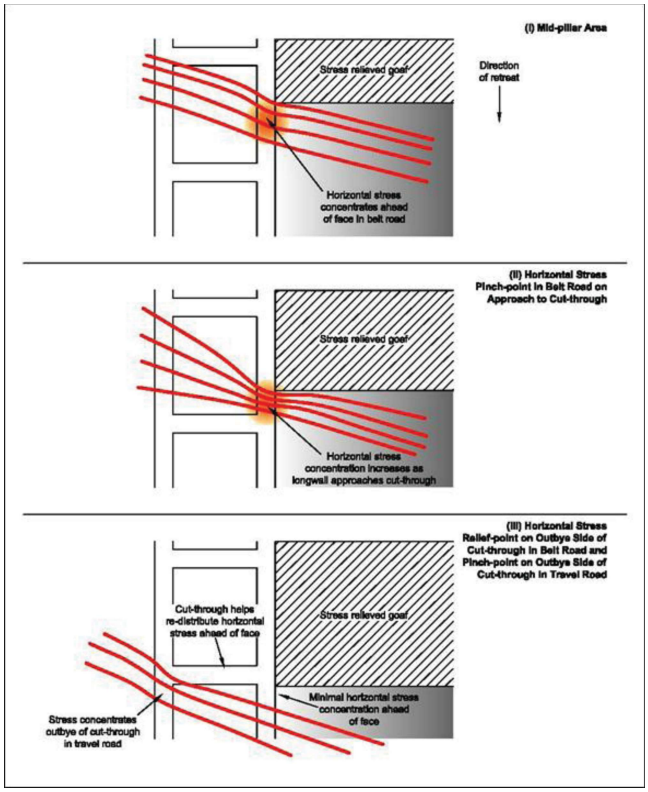

Figure 7. Schematic illustration of stress pinching.

Maingate Secondary Support

Considering the regional orientation of the major horizontal stress, the roadway was subjected to a major horizontal stress notch during longwall retreat (see Figure 4). In addition, this stress notch was elevated between 13 and 17 cut-throughs, where the horizontal stress concentrated between the two converging goafs as the longwall retreated up to the LW 17 goaf edge (see Figure 4). However, it is of note that as a result of the surrounding goafs, a significant amount of horizontal stress relief was encountered, especially on the outby side of LW 17 where the longwall was surrounded by goaf on both sides (see Figure 1).

On development, the majority of the maingate roof was originally supported with mesh and 6 x 2.7 m long X-grade bolts every 1m. In regard to secondary support in the maingate, the

design of the support system focused onmaximizing the thickness and, hence, the load-bearing capacity of any beam action present in the roof. To maximize the reinforcing ability of the support system, 8 m long, pre-tensioned 60-tonne capacity cables were used.Where appropriate, to utilize the mechanical advantage inherent within a buckling roof beam, the cables were biased to the axis of buckling.

Inby of the LW 17 pinch-point, the following secondary roof support was installed: (i) 2 x 8 m long cables every 1m in the intersections and pinch-points, (ii) 3 x 8 m long cables every 2 m in the mid-pillar areas and, (iii) 1 x 8 m long cable every 1m in the stressed relieved side of the cut-throughs. To cater for the elevation in horizontal stress associated withthe LW 17 pinch-point, the roof was supported with 2.5 to 3 x 8 m long cables every 1m. Outby of the LW 17 pinch-point, the following secondary roof support was installed: (i) 3 x 8 m-long cables every 2 m in the intersections and pinch-points, (ii) 2 x 8 m long cables every 2 m in the mid-pillar areas, and (iii) 1 x 8 m long cable every 2 m in the stressed relieved side of the cut-throughs. The only exceptions to the above were in already deformed roof or in and around geological structure where additional support was installed depending on the mapped roof conditions.

In terms of the rib support, the ribs were originally supported with mesh and 2 x 1.8 m long mild-steel bolts every 1 m. Where appropriate, the steel mesh and bolts were stripped from the blockside ribs to limit the amount of steel cut-out by the shearer. These ribs were re-supported with plastic mesh and 2 x 1.8 m long fibre-glass bolts every 1 m.

Tailgate Secondary Support

Compared to the maingate, it is of note thatduring longwall retreat,the tailgate was subjected to a more favorable minor horizontal stress notch and located next to a goaf along its entire length.As such, a significantdegree of horizontal stress relief was experienced. Although to a lesser magnitude thanthe maingate, the minor horizontal stress also increased as the longwall retreated up to the cut-throughs.

The standing support plan was an empirical design based primarily on proven successful cases at the mine. The mine site standard for tailgate standing support is 900 and 1,200 mm Link–N-Locks,which have a proven support capacity of approximately 225 and 300 tonnes respectively at 300mm of convergence.To maximize aerial coverage, the standing support was installed as close as practically possible to the roadway center-line and out of reach of the shearer.

Maintaining a minimum distance of 50 m outby the retreating longwall face, 900 mm Link–N-Locks were installed (i) on 2 to 3 m centers in the intersections and pinch-points, which equates to a standing support density of between 75 and 112 tonnes/m, (ii) on 3 to 4 m centers in the mid-pillar areas, which equates to a standing support density of around 56 to 75 tonnes/m and (iii) on 4m centers in the stressed relieved side of the cut-throughs, which equates to a standing support density of 75 tonnes/m. The only exception to this wasthe area in and around the zone of geological structure located in the inby end of the panel where,as a result of the adverse roof conditions, the roadway was supported with 1,200 mm Link–N-Locks on 3 m centers and as such, a standing support density of 100 tonnes/m.

LONGWALL HOLING GEOMECHANICAL MODEL

The proposed geomechanical model is based on monitoring data and anecdotal information collected from previous longwall holings. The model is illustrated in Figure 8 and can be summarized as follows (Thomas, 2010):

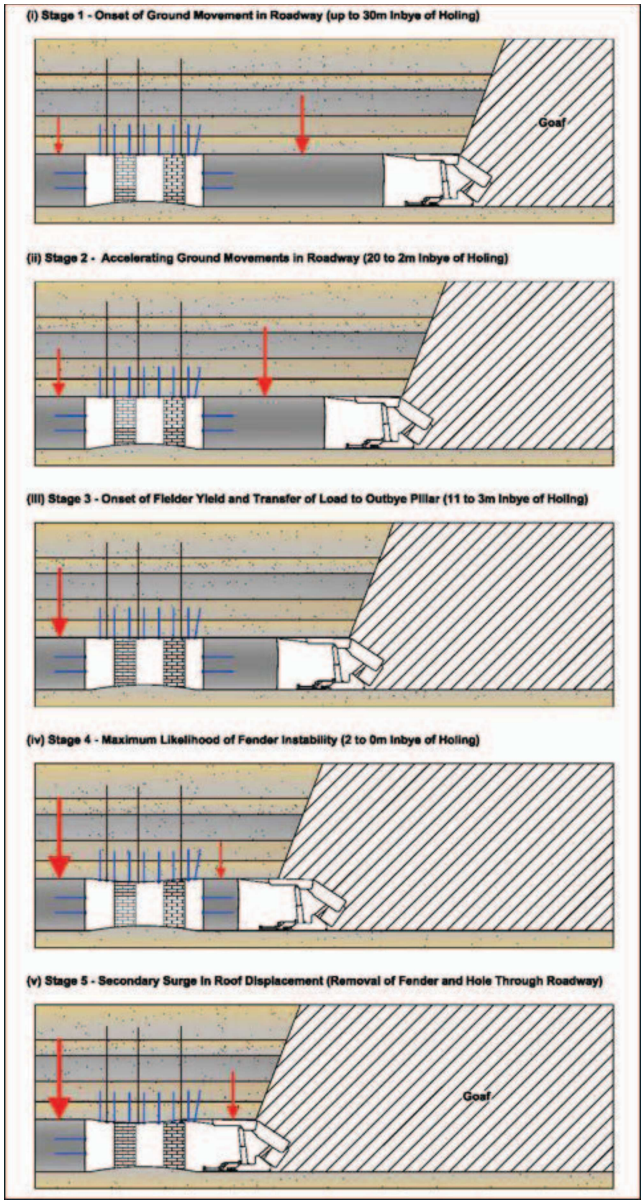

Figure 8. Proposed geomechanical model for longwall holing.

Stage 1: Onset of Roadway Closure—Up to 30m Inby of Holing

This initial stage represents the first time that the build-up in abutment load ahead of the longwall face has a measurable influence on ground conditions in the roadway (see Figure 8a).

At this point, the vertical abutment load acting on the fender would be expected to be higher than that acting on the solid pillar located on the outby side of the roadway.

Stage 2: Accelerating Ground Movements—20 to 2m Inby of Holing

During Stage 2, the rate of roof-to-floor and rib-to-rib convergence in the roadway and the rate of poweredsupport loading starttoaccelerate (see Figure 8b). This stage is also associated with a notable increase in audible fracturing in the fender.

This increase in deformation relates to the rotation of the upper roof as a cantilever (or series of cantilevers) onto the fender, the increasing build-up in vertical stress on the fender, and floor heave as the fender punches into the floor.

Stage 3: Transition to a Yielding Fender—11 to 3m Prior to Holing

During this stage, despite the reducing width of the fender, the general rate of convergence in the roadway, the rate of poweredsupport loading, and the amount of audible fracturing reduces (see Figure 8c).

This radical change in behavior is related to the softening of the fender and the ability of the overburden to redistribute load on to the neighboring blocks of wider and stiffer coal (see Figure 9). All indications are that this is a stiff loading system and, by implication, a displacement-driven loading environment.

Stage 4: Maximum Likelihood of Fender Instability—2 to 0m Prior to Holding

As a result of the reducing width-to-height ratio of the fender, at this stage in the holing, the likelihood of a fender or a weighting-type failure increases (see Figure 8d). Of the weighting failures contained within the worldwide database, the width-to-height ratio of the fender typically ranged between 0.7 and 1.3.

The likelihood of failure is controlled by (i) the stiffness of the overburden and hence, the consequent ability of the roof to redistribute load away from the fender, (ii) the ability of the standing supports to control roof-to-floor convergenceand in doing so, protect the fender, and (iii) the density of support installed in the fender (inby rib).

Stage 5: Secondary Surge in Roof Displacement—Holing into the Roadway

At the point of holing, when the last of the fender is cut out, the rate of roof displacement in the roadway accelerates and the magnitude of load on the powered supports increases (see Figure 8e).

This behavior is related to the increase in roof span ahead of the powered supports and the location of the powered supports several meters back from the coal face (now equatingto the outbyribline of the roadway).

At this point in the holing process, it is desirable to retreat the longwallthrough the roadway as quickly as possible. It also demonstrates the critical importance of the fender, even when it is only 1m or so thick, and the standing support.

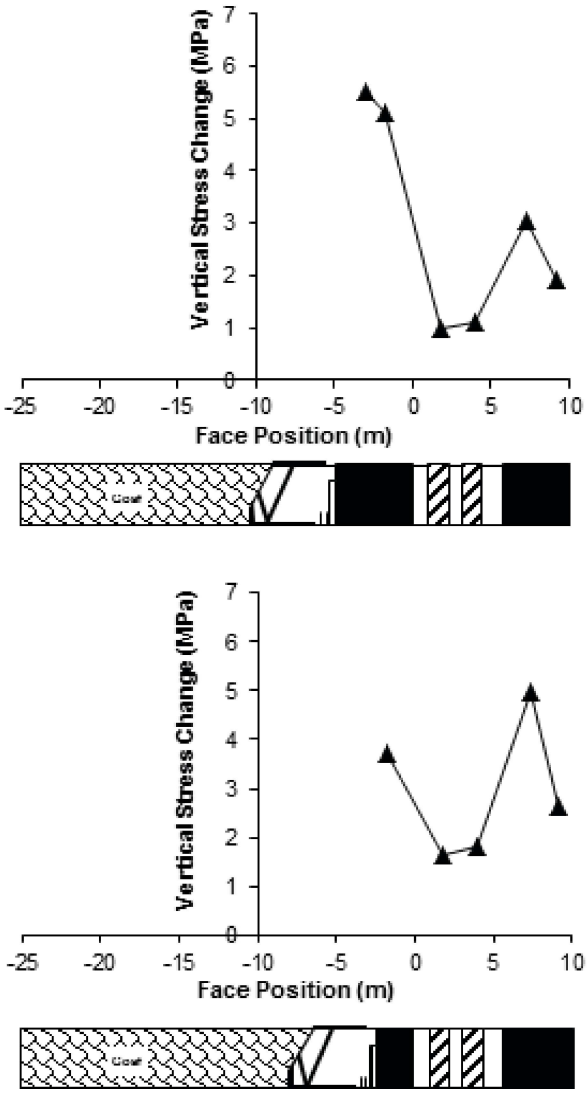

Figure 9. Measured transfer in vertical stress on holing in a US mine.

SECONDARY SUPPORTINTHE HOLE-THROUGHROADWAYS

In addition to the geomechanical model previously presented, the support designs required for holing into existing roadways with a longwallare also based on an empirical model. In this case, the database for the empirical model comprises138 case histories from 26 mines from the US, Australia, South Africa, and the UK. This worldwide longwall holing database includes examples where the longwall holed into and was recovered in the roadway and examples where the longwall holed into and mined through the roadway (Thomas, 2010).

Considering the results of thegeomechanical and empirical models, the ground support design standards utilized for the hole-thru roadways can be summarised as follows:

- As a minimum standard, the density of standing support must be greater than 1.2 MPa and the density of roof reinforcement less than 0.9 MN/m (see Thomas, 2010 for details).
- To arrive at the final density of support, consideration should be given to the Depth of Cover. As the onset of fender yield is controlled by depth (see Figure 11), the greater the Depth of Cover, the more the fender and roadway will deform on holing and hence, the greater the density of support required to control the fender and the associated roof deformation.

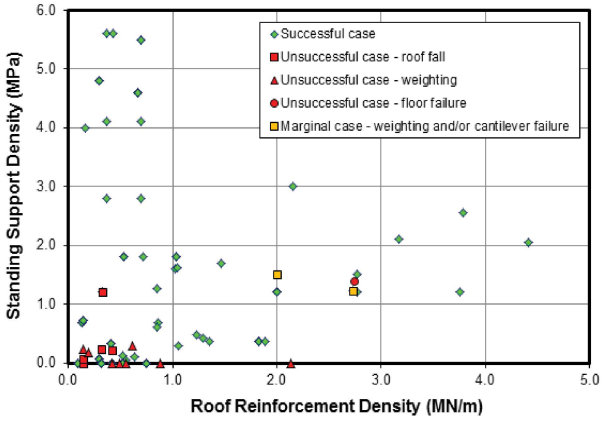

Figure 10. Longwall holing database showing relationship between roof reinforcement and standing support density, and the incidence of failure.

- Case histories in Australia have proven that a lower density of standing support can be installed if the inby rib (fender) is supported with high reinforcement densities (between 0.5 to 2 MN/m), which helps maximise the likelihood that the fender will remain fully load bearing through to holing.
- Although there does not appear to be any clear relationship between the incidence of failure and CMRR, generally, as the CMRR reduces, higher densities of standing support and roof reinforcement are installed (see Figures 12 and 13).

Considering each of the above, the following support densities were used for LW 19: (i) a minimum standing support density of 1.2 MPa in the mid-face area and nil to 0.5 MPa in the protected ends, (ii) a minimum RDI of 2 MN/m in the roof in the mid-face area and 3 MN/m in the protected ends, and (iii) a minimum RDI of 1 MN/m in the inby rib.

The protected end effects are a result of the large neighbouring pillarsand the consequent likelihood that the maingate and tailgate ends of the face are protected from the near-seam weighting process. Previous shield monitoring data at the mine indicates that the protected end effects extend approximately 30 m in from the gate ends (see Figure 14). Critically in regard to the protected ends was the decision to install a higher density of roof reinforcement on the basis that this would allow the mine to reduce the density of standing support in these areas.

The exception to the above was in the angled cut-troughs where as a result of the roadway's high angle of intersection with the longwall face and the high density of secondary support installed

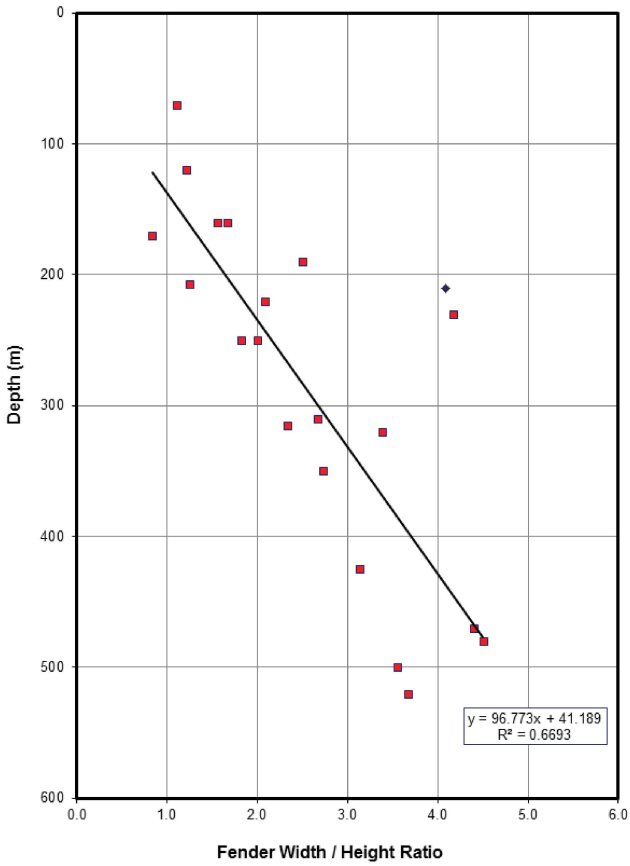

Figure 11. Measured relationship between the onset of fender yield and depth of cover.

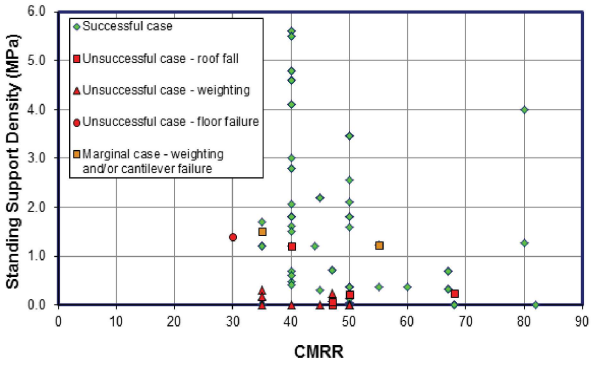

Figure 12. Longwall holing database showing relationship between CMRR and standing support density.

in the roof and ribs (3 MN/m in the roof and 1.3 MN/m in the ribs), no standing support was installed.

In terms of the support hardware utilized, the standing support consisted of 5 by 3780 tonne-capacity concrete-fibre-cribs, 8 m long 60 tonne-capacity cables installed into the roof; and

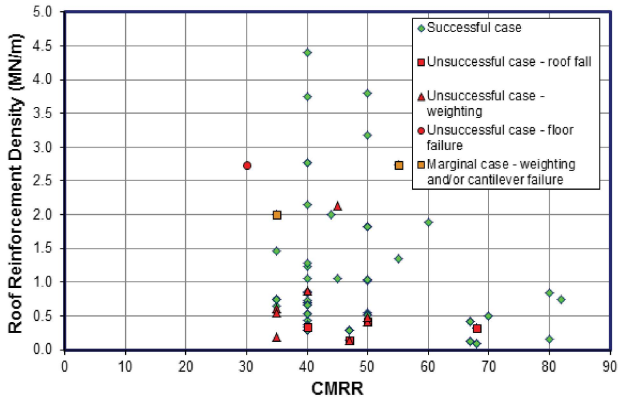

Figure 13. Longwall holing database showing relationship between CMRR and roof reinforcement density.

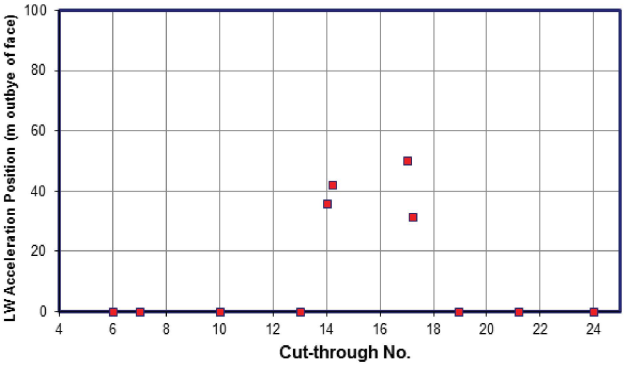

Figure 14. Longwall Acceleration Positions measured in MG 19 during longwall retreat.

3 m long 43-tonnecapacity post grouted fibre-glass dowels installed in the ribs.

In regard to the standing support, it is important to recognize that in a displacement driven environment such as this, the roof and floor will converge and that the main aim of the standing support is to control (and not stop) the resulting closure and share some of the superimposed load with the fender. Accepting this, the standing support should be capable of tolerating the anticipated magnitude of roof-to-floor closure and as such, a total of at least 500 mm of softwood packing was installed in the base and on top of the cribs. Previous monitoring work undertaken at the mine suggests that the standing support must be capable of tolerating at least 250 mm of roof-to-floor closure. Laboratory tests undertaken previously by Strata Engineering demonstrated that the load/deformation characteristics of softwood enable in excess of 50% strain to occur before the standing support reach their maximum load bearing capacity (Strata Engineering, 2004).

In regard to location, the standing support was biased toward the inbyriblinesothat it was better able to utilize the mechanical advantage inherent in the rotating cantilever(s) in the roof. Prior to and during holing, the roof above and in front of the longwall face rotates as a cantilever onto the goaf and as such, the fulcrum point is located on the oubyribline. As a result, the mechanical advantage that is inherent in the roof increases toward the inbyeribline.

In addition, the standing support considered needed to be cuttable and capable of tolerating out-of-plane movement. The points considered in this regard included the slenderness of the standing support and the need to ensure that the long axis of the supports was installed perpendicular to the longwall face.

In terms of the cables installed into the roof, the pattern of secondary roof support considered (i) the mechanical advantage inherent in the roof and hence, (as above) the need to bias the cables toward the inby rib, (ii) the need to maintain some form of beam behavior in the roof so that during holing, the roof is able to span and redistribute load away from the fender, and (iii) in the case of recovering the powered supports, the need to control the goaf edge and the roof ahead of the canopy tips.

STRATA MANAGEMENT

Imperative to the success of extracting LW 19 and most notably, holing into the pre-driven roadways was strata management. Strata management is a procedure that formalizes the decision making process when developing and accessing ground support designs. The key concept is that the ground support designs and mining methods are tailored to the anticipated and encountered geotechnical environment in a controlled manner. As for LW 19, consideration was given to the following:roof displacement monitoring in the gate roads (in particular, LW Acceleration Position (Thomas and Wagner, 2006), roof-to-floor convergence monitoring in the hole-through roadways, the ability of the mine to limit downtime prior to and during holing by utilizing an Authority-to-Mine-type system (ATM), and the use of Trigger Action Response Plans (TARP).

LW Acceleration Position

One of the essential concepts used to characterize the behavior of coal measure roof strata during longwall retreat is LW Acceleration. The LW Acceleration Position relates to the position outby of the face where the roof displacement rate first exceeds a rate of 10mm per week. Basically, this concept means that for any given condition, the earlier the roof starts to respond to the approaching abutment load, the more the roof will deform around the gate end of the longwall face and hence, the greater the density of support required to control the roof.

LW Acceleration can therefore be used to both back-analyze the success of a support design and/or the adequacy of a support design during longwall retreat (ie, as part of a strata management process) and can effectively be interpreted as a “measure of success”.

In regard to the LW Acceleration Positions measured in MG 19, the following are of note:

- Between 14 and 18 C/Ts (in LW 17 pinch-point), the roof accelerated between 32 and 50 m outby of the face.
- In this area, between 40 and 60 mm of roof displacement was measured.
- Inby of 18 C/T and outby of 14 C/T, no appreciable accelerations were measured (see Figure 15).

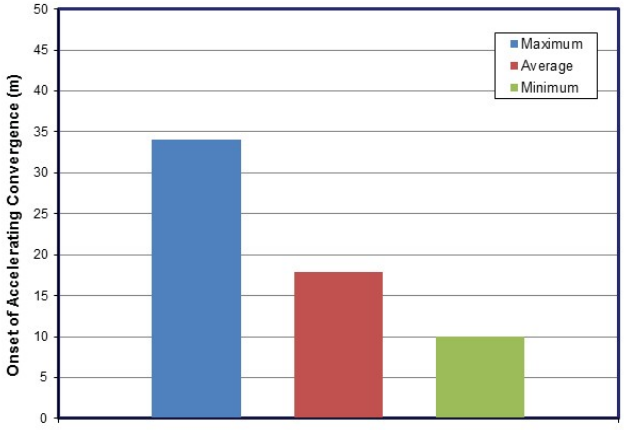

Figure 15. On-set of roof-to-floor convergence measured in the roadways in LW 19.

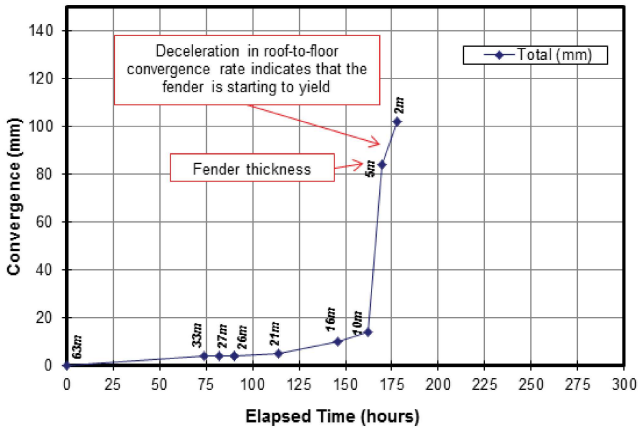

Figure 16. Example of the fender starting to yield prior to holing into the roadway.

Generally, in roof that has been supported with between 2.5 and 3 x cables every 1 m (as in this case) any acceleration positions of <30 m outbye of the face indicate that the roof has been over-supported, 30 to 60 m outby of the face, adequately supported and to >60 m outby of the face, under-supported. On the basis of the above, these results were therefore viewed as favorable and as such, indicate that the maingate was supported to an adequate level.

Roof-to-Floor Convergence Monitoring

In terms of the longwallgeomechanical holing model previously presented, the roof-to-floor convergence data measured in LW 19 indicates the following:

- The rate of convergence started to accelerate when the longwall face was located between 34 and 10m from holing (see Figure 16).

- On average, the longwallface was located 18 m from holing during the on-set of convergence.
- The slight deceleration in convergence rate measured when the longwall face was located between 9 and 2 m from holing indicates that the fender was starting to yield and as such, redistribute the overburden load onto the surrounding blocks of coal (see Figure 17).

- More specifically, the data indicated that during the majority of the holings, the fender started to yield between 5 and 2 m from holing.
- On holing, the total convergence measured ranged between 11 and 183 mm and an average of 54 mm (see Figure 18).

In regard to the onset of fender yield, the above data indicates that the width to height ratio of the fenders ranged between 0.7 and 3. Figure 19 shows that this range plots near or below the anticipated onset of yield. The lower than expected values most likely are a result of the narrow panel width and the likelihood that the longwall panel was not subjected to the full abutment loading.

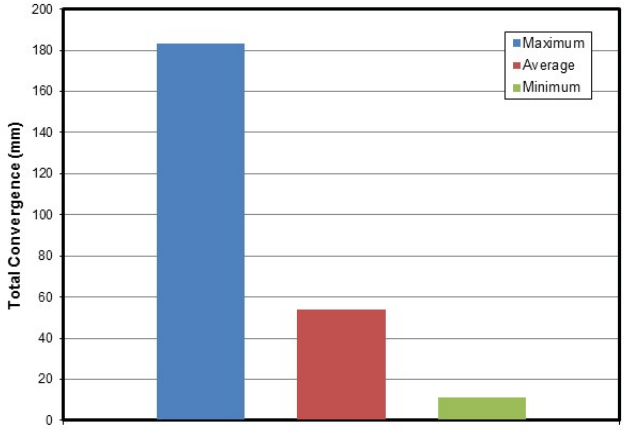

Figure 17. Total roof-to-floor convergence measured on holing into the roadways in LW 19.

As stated previously, the fibre-cribs were constructed with enough softwood to withstand 500 mm of roof-to-floor convergence. The maximum measured convergence of 183 mm was well within this design standard. It is however of note that on average, a slightly higher amount of roof-to-floor convergence (i.e., 65 mm) was measured in the protected ends than that measured at or near the mid-face (i.e., 41 mm). This is almost certainly a result of the lower densities of standing support installed in the protected ends compared to the mid-face areas.

The roof-to-floor convergence monitoringtherefore reasonably reflects those conditions anticipated by the longwallgeomechanical modeland indicates that the design standard used for the support regime was adequate. The data also indicates that the thickness of softwood used in the construction of the fibre-cribs was adequate for the amount of roadway closure encountered during longwall holing.

Authority to Mine (ATM)

The Authority-to-Mine (ATM) concept aims to ensure that the operators are forewarned of any anticipated changes in ground conditions and secondly, that the operators understand what actions are required as a result of any pending changes in ground conditions.

Critical to the success of LW 19 was the adoption of a management plan to ensure that the condition of the longwall face and the hole-through roadways were assessed on a regular basis, and no stoppages were planned on the lead up to holing. On this basis, the panel was divided up into five zones and in each zone, the anticipated geotechnical and mining hazards during longwall retreat were identified.

The geotechnical hazards specified (i) the presence of geological structure and holing into overwide roadways as a moderate riskand (ii) a no-stopping zone once the entire longwall face was located within 15 m of holing into a sub-parallel roadway as a high risk. In addition, each zone contained a geotechnical checklist that determined whether the recommended secondary support and monitoring had been installed to standard and whether additional support might be required.

The mining hazards identified in the panel included changes inroof horizons in both the gate roads and hole-through roadways, areas where concrete bases from old driveheads had been left in the floor, and the existence of false roofsin old overcast that had been removed. An operational check list also ensured that all maintenancerelated activities were performed when the longwall was in a safe stopping zone and that a flight plan was issued to deal with any anticipated changes in cutting horizon.

Trigger Action Response Plans (TARPs)

The main concept of a TARP system is to empower the operators to assess for themselves the actions required with respect to changing ground conditions. In order to be effective, the TARP must be readily understood by a cross section of the workforce, must focus on the recognition of the key geotechnical drivers, and be supported with training to equip the operators in the identification of changing ground conditions.

For the purpose of LW 19, two TARPs were utilized:a longwall retreat TARP and a longwall holing TARP. In both cases, it was imperative that any activation of triggers that required remedial action were communicated to mine management.

The longwall retreat TARP identified actions for deteriorating roof and rib conditions in the maingate and tailgate, roof clearanceabove the BSL, the location of the goaf edge in the tailgate, and deteriorating roof conditions on the longwall face.

The longwall holing TARP was initiated once the longwall entered the no-stoppage zones. At this point, the operators ceased using the longwall retreat TARP until the roadway was holed. The longwall holing TARP identified actions for deterioratingroof conditions on the face, the tip-to-face distance before the face is cut by the shearer, deterioration of roof and rib conditions in the roadway, andthe condition of the standing support (see Figure 20).

CONCLUSION

Wongawilli Colliery successfully extractedthe existing Thompson Mains without any significant strata control problems. The average roof-to-floor convergence measured in the hole-through roadways was approximately 54 mm, and the maximum measured was 183 mm. These results were within the range of assumptions used for the input into the design and as such, indicate that the support regime utilized in these roadways was adequate. In terms of the LW Acceleration Positions measured in the maingate, positions of between 32 and 50 m were measured as the longwall mined up to the adjacent goaf, and no appreciable accelerations were measured elsewhere in the gate road. These results are viewed as favorable and again, indicate that the maingate was supported to an adequate level.

The success of this panel demonstrated that with the correct support regime and strata management, a longwall can mine through and be recovered in pre-driven roadways. As a result of this achievement, the mine plans to extract other main heading pillars with the longwall.

REFERENCES

Bauer, E., Listak, J., Berdine, M., Bookshar, W., Raab, D., and Mucho, T. (1988).“Longwallrecovery utilizing the open entry method and various cement-concrete supports.” In: *Proceedings of the 7th InternationalConferenceonGround Control in Mining*.Morgantown, WV: West Virginia University,pp. 30–42.

Gale W. J. and Blackwood R. L. Stress Distributions and Rock Failure Around Coal MineRoadways. *Int. Journal of Rock Mech. Min. Sci&Geomech. Abstract. Vol 24 No. 3,* pp. 165-173, 1987.

Peng, S.S. and Chiang, H.S. (1984).*Longwallmining*.Hoboken, NJ: Wiley& Sons, pp. 708.

Strata Engineering (2004). Use of Wood Packing to Reduce Stiffness of Fibre Reinforced Cribs in LW 9 Pre-Driven Recovery Road. Report to Elouera Colliery, June 2004.

Thomas, R (2010). “Recent developments in pre-driven recovery road design.” In: *Proceedings of the 27th International Conference on Ground Control in Mining*. Morgantown, WV: West Virginia University, pp. 197–205.

Thomas, R. and Wagner, C (2006).“Maingateroof support design and management during longwallretreat in the Australian coal industry.”In: *Proceedings of the 25th International Conference on Ground Control in Mining*. Morgantown, WV: West Virginia University, pp. 191–197.

Think Like a Roof Bolt – Then Make It Scream –

Greg Smith, President
EMS Mining
Lebanon, OH

ABSTRACT

This paper documents the use of bench testing equipment developed to enhance the understanding of, and improve upon, common roof bolt support systems. Most roof bolt systems consist of components that are covered within the scope of ASTM (American Society for Testing and Materials) standards. However, ASTM does not specify testing methods or performance standards for complete roof bolt "systems". It only designates testing methods and minimum performance standards for roof bolt "components". Improved understanding and continuous improvement of these systems is essential given the enormous impact that they have on the safety and profitability of underground mining operations. Bench testing equipment has been developed that effectively measures and records multiple points of deformation in a rock bolt support system while load is being applied. With this testing capability, an improved understanding of component and system stress distribution can be obtained and devices and methods for visual load indication can be developed. This paper is formatted as case studies where testing was performed to demonstrate load versus deformation profiles and to develop system improvement products.

INTRODUCTION

No standardized tests or specifications exist for roof bolt *systems*. 30 CFR Parts 57 and 75 both reference the American Society for Testing and Materials (ASTM) standard F432 for performance and testing standards. ASTM F432 is titled "Standard Specification for Roof and Rock Bolts and Accessories," i.e., *components*. How these components work together as a *system* is only briefly referenced within the annex and appendix. Components will behave differently in an actual system as compared to how they perform in the standardized ASTM tests. It is imperative to understand how the components behave within the system and conditions that they are operating in. Mine operators need to make sure that their *system* is designed, installed, and managing the ground properly. It is the responsibility of the manufacturer only to meet the minimum standards and specifications for the *components* they make. If no other tests or specifications are agreed upon between customer and supplier, the standard ASTM component tests and minimum specifications apply.

Figure 1 is a sketch of a simple point anchor, mechanical roof bolt system. This system must distribute the force "F" generated from an unstable rock mass through all the components and contact points to a supporting stable rock mass. The visible portion of an installed roof bolt system includes the bolt, flange, head or nut, washer, plate, and roof rock. This is the Immediate Roof Reaction Zone (IRRZ). This area of the system is critical because it is in contact with the unstable rock and the components undergo significant point loading, bending, and shear. The IRRZ can be a weak point in the support system. It is also important because it can provide insight and visual indication of the forces acting on the system. Bench test equipment was developed to study the IRRZ of roof bolt systems. Figure 2 is a concept sketch of the bench testing equipment (patent pending). It is portable for easy transportation, set up, and on-site testing. It is capable of performing standard ASTM tests on components, but more importantly, it tests complete full-length *systems*. The following case studies detail the use of this test equipment while being used to study *system* performance and while developing visual load indicating methods and devices.

CASE STUDY #1

The goal of testing in this study was to evaluate a mine's support system. The system consisted of a #6 grade 60 headed rebar bolt, a grade 2 dome plate and an engineered washer. The mine wanted to understand how the bolt, plate, and washer performed as a system and what signs of loading were exhibited at the IRRZ.

Bolts and plates were first tested in accordance with ASTM F432 to obtain benchmark load vs. deformation relationships. The systems were then tested with platens simulating different roof conditions. One test simulated a flat roof with no voids. The other test simulated a 10 degree angled roof with a 4 inch diameter by 1 inch deep void centered under the plate. During system tests, load and deformation data of the bolt, plate/washer, and total system were simultaneously collected.

Figure 3 shows the ASTM test result for a #6 grade 60 headed rebar bolt of the type used for a subsequent system test. Note the non-linear response during initial loading up to 7,500 lbf caused by the bending of the bolt body. This is typical for most headed and torque / tension bolts tested. The bolt yielded at 27,500 lbf, failed at

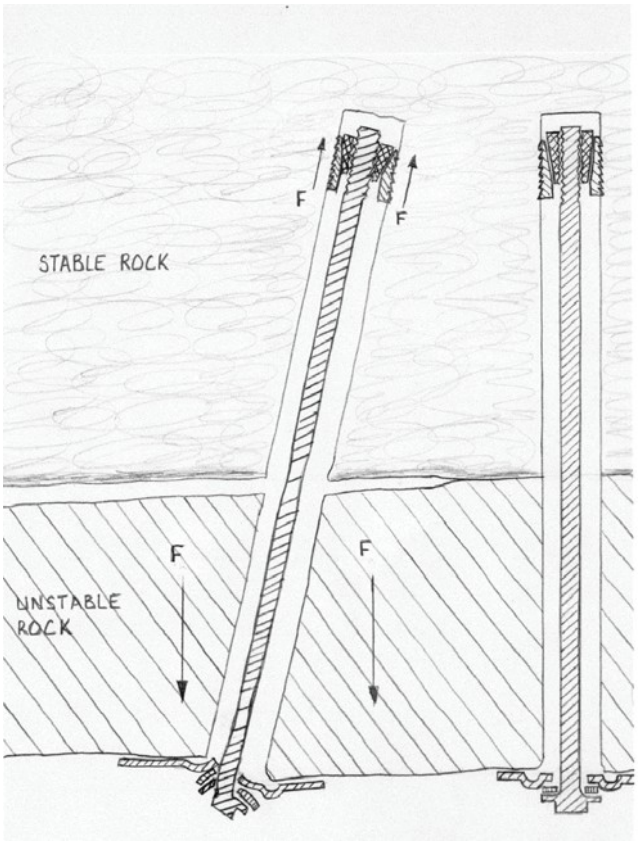

Figure 1. Mechanical rock bolt system.

45,000 lbf, and deformed roughly 1.8 inches before breaking. For future comparison and correlation with the system test, note that at 40,000 lb, the bolt had deformed roughly 0.75 inches.

Figure 4 is the test result of this same bolt in a system with the plate and washer. The platen simulates a 10 degree angled installation with a 4 inch diameter by 1 inch deep void centered under the plate. The red line represents the bolt; the blue line is the plate and washer; and the green line is the total system. Flattening of the plate and washer occurs at 25,000 lbf, and the bolt yields at 27,500 lbf. As the system continues to load between 25,000 lbf and 27,500 lbf, the plate and washer deform at a greater rate than the bolt and the system maintains a load just below the bolt yield point. The plate and washer continue to deform by flattening out as the bolt yields and starts into its plastic strain hardening range. At 30,000 lbf, the plate gets pulled into the void and the bolt relaxes along its elastic stress-strain curve. The plate contacts the bottom of the void after the system has deformed a total of approximately 1.6 inches. After the plate bottoms out, the bolt deforms at a greater rate than the plate and washer. The test was stopped at the minimum ultimate strength of the bolt (39,600 lbf.). For the purpose of correlation to the ASTM test of the bolt, note the same bolt yield point of 27,500 lbf and bolt deformation of 0.75 inches at 40,000 lbf.

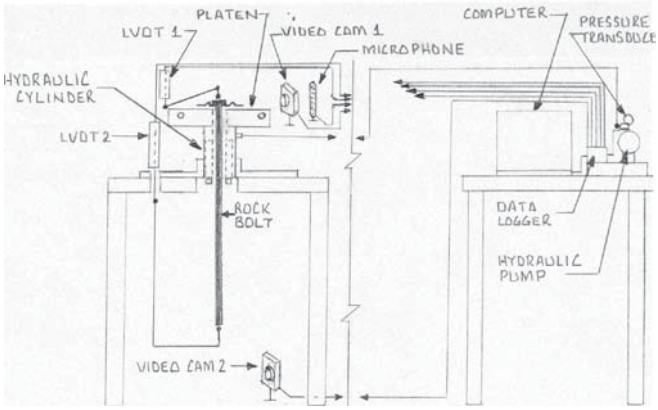

Figure 2. Schematic of Rock Bolt Testing Equipment.

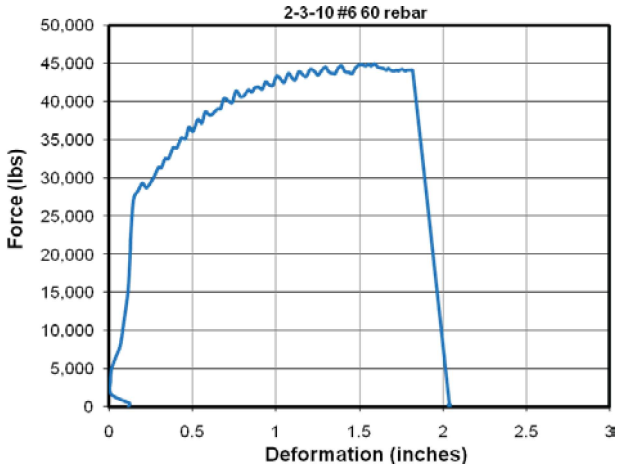

Figure 3. Case Study #1 - ASTM F432 Rock Bolt Test.

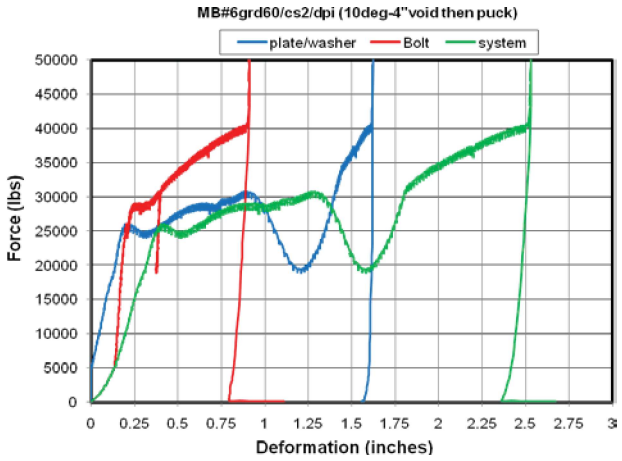

Figure 4. Case Study #1 - System Test (1).

Figure 5 shows the result for a different system test. The platen simulates a flat roof (i.e. 0 degree) with no void. In this test, a number 6 grade 60 headed rebar bolt from a different manufacturer was used. Flattening of the plate and washer begins around 25,000 lbf. This bolt yields at 30,000 lbf. At 32,000 lbf, the plate and washer begin to pull into the borehole and then become very stiff. The bolt then continues to deform plastically, reaching an ultimate load of 45,000 lbf before breaking.

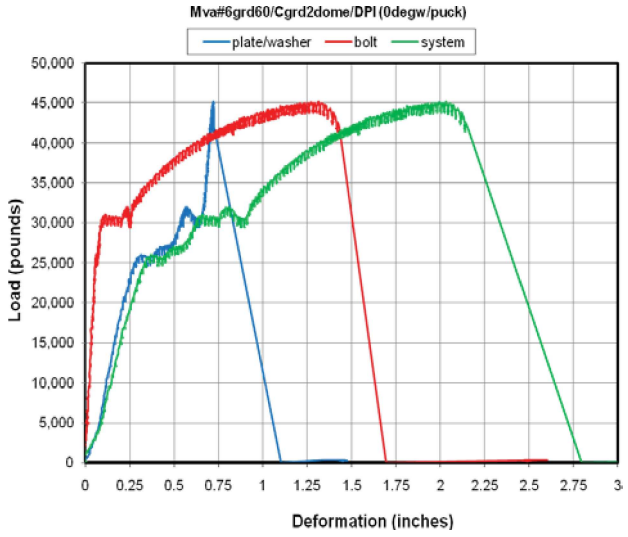

Figure 5. Case Study #1 - System Test (2).

These tests were used to show the mine what their system was actually providing in terms of support profile and visual indication. If miners see the plate and washer begin to flatten and if all the components in the system are held to a tight tolerance, they know that the bolt is at or near yield point. When they see the plate and washer start to pull into the drill hole, the bolt is in plastic deformation. However, buyers beware. The support profile of the components in this system can change significantly and still meet ASTM standards. This could result in a completely different system response which might not show any significant signs of loading. For instance, the grade 2 plate might be manufactured such that the ASTM test was 0.251 in deformation at a load of 29,000 lbf. The ASTM plate test is performed by inducing load with a flat 1-3/4" diameter surface. The engineered washer used in this system loads the plate with a "circular line" contact zone at a diameter of 3 inches. This greatly increases the strength of the system and could result in little to no discernible deformation of the plate until the bolt is well into plastic deformation. Additionally, the supplier is not obligated to inform the customer of changes that effect the product unless it no longer meets ASTM standards. They could ship the customer a 21,000 lbf ASTM plate or a 29,000 lbf ASTM plate. The supplier is only responsible to make sure that the components are within their respective ASTM standards.

CASE STUDY #2

Testing was performed to assist in the transfer and adaptation of visual tension indicating technology for use in mine roof bolts. SmartBolts® are direct tension indicating bolts used in industrial applications where proper tension is critical for safety and production. They directly monitor bolt tension and indicate its value through a color change of an indicator installed into the bolt head. When the bolt has zero load, the indicator is red. As the bolt is loaded, it progressively turns from red, to maroon, to purple, to black. If the bolt is loosened, the color reverses. The color will correlate to a specific tension load on the bolt in real time. The load/color relationship is designed to the customer's requirements. The color indicator is a retro-reflective material similar to that used on new street signs and is capable of being seen from a distance when a cap lamp is directed onto it. Figure 6 shows the principle of operation.

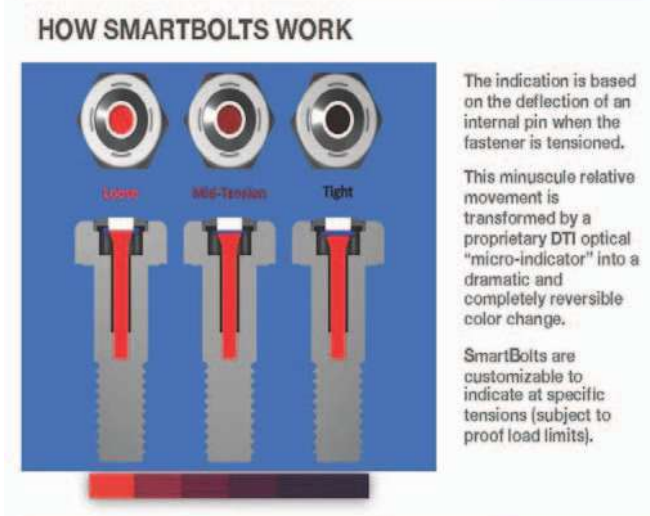

Figure 6. Case Study #2 - SmartBolts® principle of operation.

SmartBolts® operate within the elastic range of a material. As such, the specific characteristics of the elastic range of the target roof bolts are critical in the design of the indicator for the application. For this test, a standard headed roof bolt was installed such that the load was transferred uniformly under the bolt head. The bolt was loaded to its yield point and the load versus deformation profile was evaluated to determine the bolt's true elasticity.

Figure 7 is a plot of the data stream for a 0.804-in grade 75 headed rebar bolt. Each dot represents a data point reading. The graph details the elastic range from a "pre-set" load of 3,000 lbf to the yield point of around 45,000 lbf. Note the non-linearity caused by flattening of flash under the bolt head for the first 10,000 lbf (or 0.040 inches of displacement). Then observe the non-linear stress/strain from 10,000 lbf to about 17,000 lbf. The stress/strain becomes linear from 17,000 lbf to 35,000 lbf and then begins to curve again until the yield point of 45,000 lbf. When the load is released, the bolt relaxes along what should be the true stress/strain curve for the material. This implies that the imperfect bolt isn't completely elastic and, even at loads well below the yield point, it will undergo some permanent deformation.

Figure 8 is the color card developed for a 0.804-inch-diameter SRD grade 75, 72-inch-long resin-assisted SmartBolt®. The indicator was designed to verify proper installed tension and monitor increasing load. The bench test equipment was used to develop the load / deformation relationship and correlate it to color change

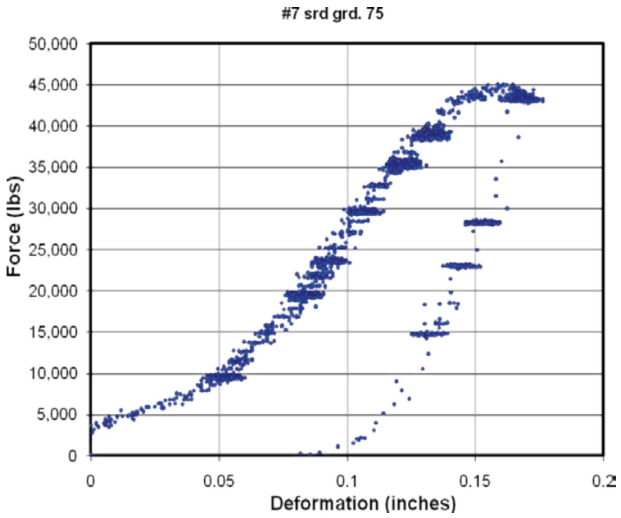

Figure 7. Case Study #2 - Elastic Stress/Strain in a Rock Bolt.

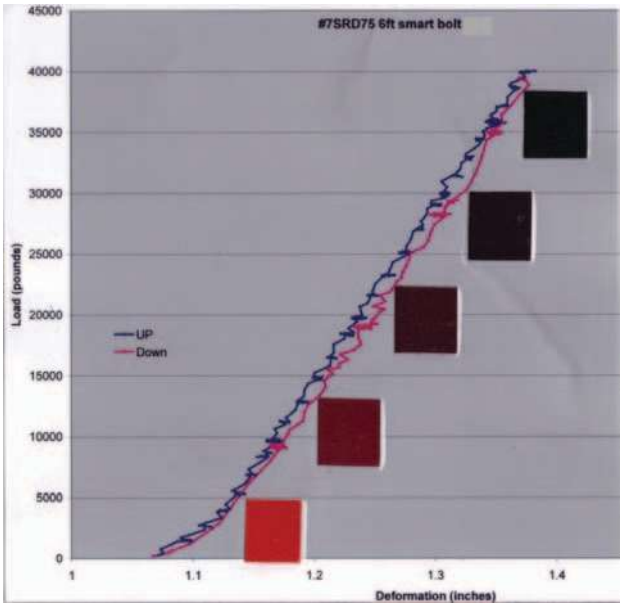

Figure 8. Case Study #2 - Color Key for .804"/ grade75/ 72" SmartBolts®.

Figure 9 is a screen shot taken from the test video for a mine SmartBolt. The manufacturer of this bolt is different than the bolt shown in Figure 7. It is a 0.804-inch-diameter grade 75, 72-inches-long headed rebar bolt. It is fitted with a SmartBolt® indicator. Again, the non-linear stress/strain curve is apparent (although improved over the bolt in Figure 7). The dark purple SmartBolt indicator communicates that the bolt is within 75% of its yield point (roughly 34,000 lbf).

Figure 10 is another screen shot taken at the end of the same test. The bolt had been cycled several times during the test as evidenced by the multiple lines on the graph. After the first load / unload cycle, the stress/strain became linear and tracked consistently. The indicator's red color indicates 0 lbf (i.e. "loose").

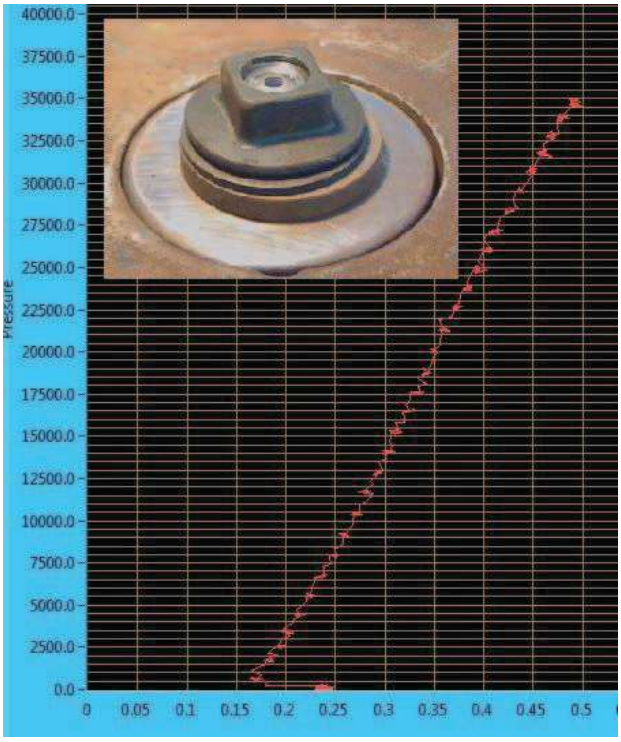

Figure 9. Case Study #2 -Mine Roof SmartBolts®at 35,000 lbf tension.

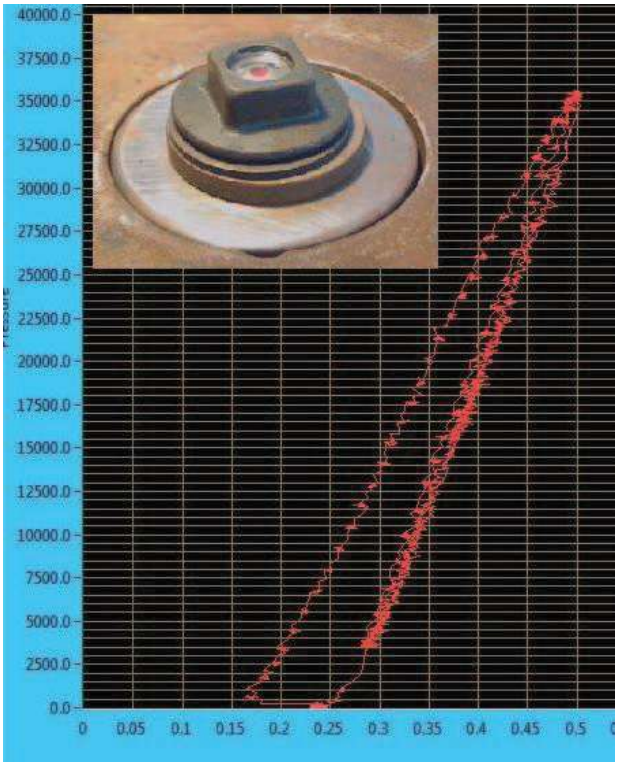

Figure 10. Case Study #2 - Mine Roof SmartBolts®at 0 lbf tension.

Figure 11 shows this type of mine SmartBolts® bolt after installation underground at its targeted pre-load of around 20,000 lbf.

Figure 11. Case Study #2 - Mechanical/Resin Bolt Installed with 20,000 lbf.

CASE STUDY #3

As part of a continuous improvement project, a patented extruded "soft" washer was evaluated as a possible improvement to a system. The system, shown in Figure 12, included a #7 grade 60 headed rebar bolt, a patented grade 3 extruded plate, and the extruded washer. It was tested with a platen simulating a flat roof, 1⅜ inch diameter borehole, with a 4 inch diameter by 1 inch deep void centered under the plate. The test was conducted by loading the system to the rated ultimate strength of the bolt.

Figures 12, 13, and 14 are screen shots taken from the test video. Figure 12 shows the system ready to test with 1,500 lbf pre-load. The green line is the bolt; the white line is the plate and washer; and the red line represents the total system. Figure 13 shows the system indicating load with the plate (white line) dog-earing between 32,000 and 35,000 lbf. When the plate dog-ears, the bolt relaxes and then reloads along its elastic stress/strain curve (green line) Figure 14 shows the system near failure at 57,000 lbf which is above the 54,000 lbf minimum ultimate load specification for the bolt.

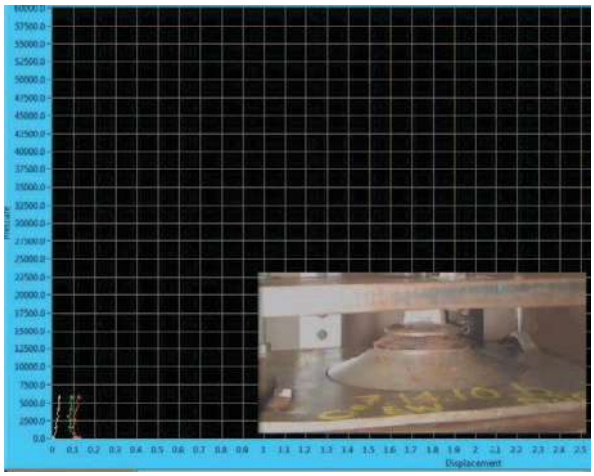

Figure 12. Case Study #3 - System test at pre-load.

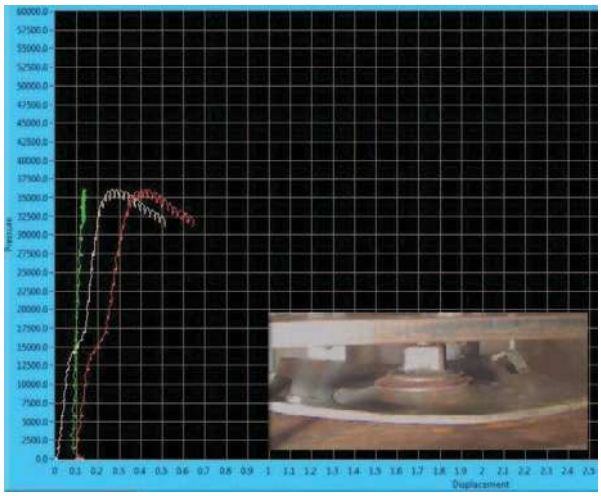

Figure 13. Case Study #3 - System test at 32,000 lbf.

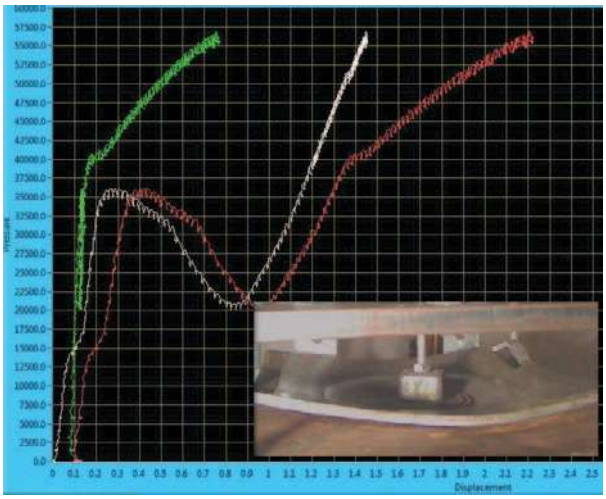

Figure 14. Case Study #3 - System test at 57,000 lbf.

Figure 15 is a picture of a grade 3 extruded plate in a system with a number 7 grade 60 headed rebar bolt taking load underground. This plate is held to a tighter tolerance than the minimum standard outlined in ASTM F432-10. Instead of just meeting the ASTM specification (less than 0.250 inch deflection at a load greater than 30,000 lbf), this plate is held by the manufacturer to less than 0.250 inch deflection at a load greater than 30,000 lbf AND greater than 0.250 inch deflection at a load greater than 34,000 lbf. With the assurance provided by the tighter specification, and from the bench testing described above, the mine knows the bolt is now in plastic deformation. Note the channel in the background of the picture. The channel was installed because miners observed the system indicating that the bolt was at or beyond yield point and they acted to provide the necessary additional support

Figure 15. Case Study #3 - Extruded Bearing Plate indicating bolt beyond yield point.

CASE STUDY #4

A study of the load deformation profile of the IRRZ of a roof bolt system was conducted as part of an overall system evaluation. The mine wanted to know what the system looked like when it was loading. The system consisted of a 0.694-inch-diameter, grade 75 headed mechanical bolt with 3/4-10 threads, a grade 3 conventional dome plate, a cast spherical washer, and the anchor wedge.

The test parameters included a 1⅜ inch diameter hole, 10 degree roof angle, and a 4 inch diameter by 1 inch deep void centered under the plate. The test utilized the full length mechanical bolt with load being applied through the anchor wedge.

Figures 16, 17, and 18 are screen shots from the test video. Figure 16 shows the system with 3,500 lbf pre-load. The green line is the bolt; the white line is the plate and washer; and the red line is the total system. Figure 17 shows the system after reaching the yield point of the bolt and deforming the plate. Note the locations (at 19,000 lbf and 30,000 lbf) where the bolt head suddenly moves sideways as evidenced by the white line's sudden shift. The reason for this is that the spherical washer is acting as an inclined plane and is pushing the side of the bolt into the side of the plate. Figure 18 shows the system after the test was reset to take it to failure. Again, the bright white area is indicating horizontal forces (i.e. "shear") being induced by the washer. The physical samples showed an elongated hole in the plate and witness marks on the side of the bolt and washer where the shear occurred.

In this test, load vs. deformation was measured and monitored for a bolt system from the anchor through the bolt threads, bolt body, bolt head, washer, and plate. In this system, every bolt is essentially "proof tested" for proper installed tension by observing the spherical washer as it begins to dimple into the plate. When any miner observes dog-eared plates, they can take immediate safeguarding action such as posting no entry and notifying others in the area. However, as noted in the previous examples, simply meeting the requirements of ASTM F432 is not enough to ensure the reliability of this system. The mine operator must work with the supplier to ensure that the component specifications are robust and will provide the desired system results

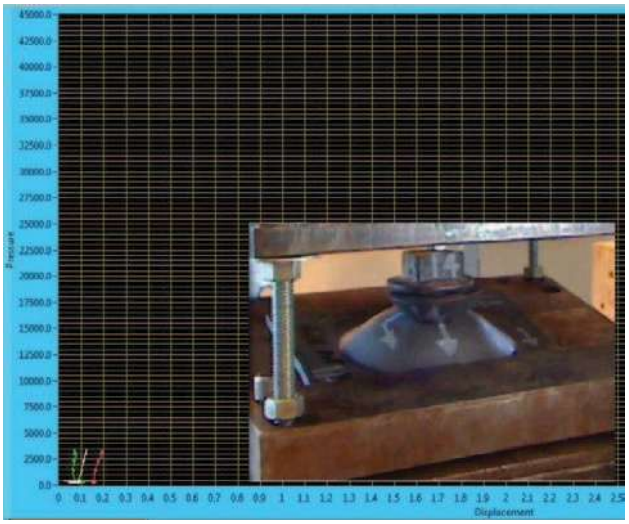

Figure 16. Case Study #4 - System test at 3,500 lbf pre-load.

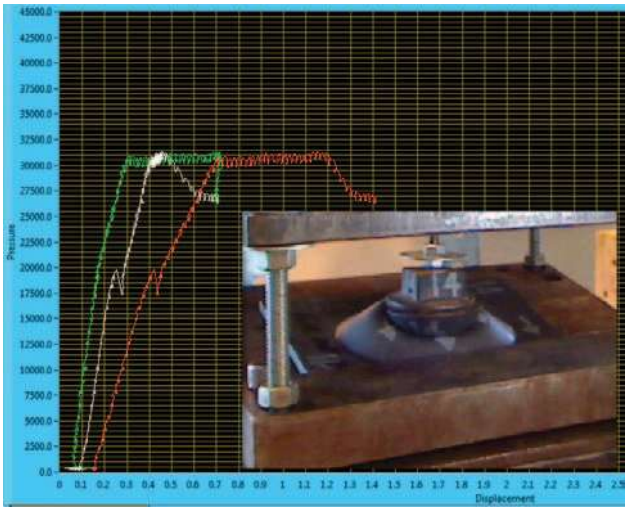

Figure 17. Case Study #4 - System test at 26,000 lbf.

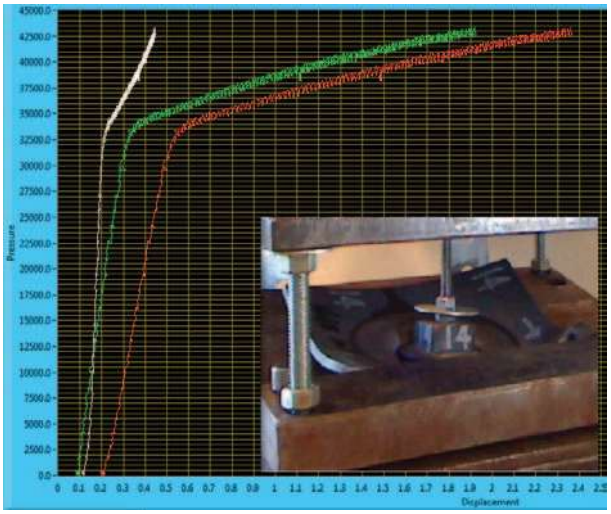

Figure 18. Case Study #4 - System test at 43,000 lbf.

FUTURE TESTING AND SYSTEM IMPROVEMENTS

When possible, testing should include the mine's roof rock as the platen surface. Roof rock is another variable that will affect the overall support profile. Where appropriate, future testing should also include loading the bolt by tensioning it through torque. Torque can then be added to the data set to improve our understanding of torque/tension relationships. Score marks from spinning the bolt on the sharp edges of the plate center hole and other physical observations will become apparent when incorporating these variables into the bench tests.

Additional testing is also required to evaluate the anchorage profile of support systems. In-mine testing, such as encapsulated pull tests, should be performed and the graphs plotted alongside the bench test results. This additional data will provide for a greater understanding of the many variables associated with the anchor components and installation process. This is necessary for improvements in consistency and reliability.

Because ASTM only addresses components, mine operators need to test systems to ensure that they consistently and reliably perform as intended. Components must work together and provide the desired system results even when each component is allowed to vary within the allowable tolerances. For example, does the support system perform differently when the grade 3 plate being supplied yields at 41,000 lb instead of 31,000 lb? Answers to questions like this will affect how components and systems are specified.

Finally, mine operators should develop a culture of continuous improvement as it concerns their ground support systems. Problems exist and are often observed. These problems include bolts broken at couplers, bolt anchor failures, bent and broken heads, torque/tension bolts broken at threads, and bolts pulled through plates just to name a few. Too often, roof falls are associated with these and other types of system weaknesses. Indeed, there are many opportunities for improvements. The cost and impact of bolting operations to the total mine enterprise is enormous. To improve it starts with an understanding of what is really happening and then asking, "is there a better way?". A culture of continuous improvement in roof bolting will provide tremendous returns for the investment.

CONCLUSIONS

There is a lot to be observed, simulated, understood, and improved upon in roof bolt support systems. A flexible bench testing device to simulate and monitor these systems has been developed for studying the IRRZ (Immediate Roof Reaction Zone), which includes the roof, plate, washer, and the head or termination area of rock bolt support systems.

The testing device simulates installed conditions and simultaneously monitors multiple points of rock bolt systems while taking on load. This type of testing is necessary for improving the understanding and performance of support systems. Physical testing provides benefits, including visualization and physical samples, that offer additional clues, (such as witness marks) to help understand system and component behavior. Testing will help educate miners and provide them with a better understanding of their support systems. It will provide a baseline from which mines can perform audit testing and evaluate potential improvements.

REFERENCES

ASTM F432-10. Standard Specification for Roof and Rock Bolts and Accessories. ASTM International, 100 Barr Harbor Drive, PO Box C700, West Conshohocken, PA 19428.

A Stability Factor for Supported Mine Entries Based on Numerical Model Analysis

Gabriel S. Esterhuizen, Principal Research Engineer
Office of Mine Safety and Health Research
National Institute For Occupational Safety and Health
Pittsburgh, PA

ABSTRACT

This paper addresses the need for a method to compare the effectiveness of different support systems when designing ground support in coal mines. At present, support design methods include empirical methods based on observations of past performance of installed support systems, analytical methods where the roof is typically simulated by elastic beams and numerical model analysis. The approach presented in this paper estimates the relative stability of a support design through geotechnical evaluation of the rock mass and numerical model analysis of the interaction between the rock mass and the support system. Models are used first to simulate the design performance at the expected rock conditions. The rock strength is then reduced until collapse is indicated in the model. The stability factor is then calculated as the ratio of the expected rock mass strength to the rock mass strength at the onset of collapse, and is similar to the well-known factor of safety used in engineering practice. The stability factor can be used to assist in developing a final support design by comparing the effectiveness of various support systems and the stability of excavations under various geological and loading conditions. Examples of the method's application in three different geological settings are presented.

INTRODUCTION

Large unplanned falls of ground in the active workings of coal mines are reported to the Mine Safety and Health Administration (MSHA) if the fall extends at or above the supported horizon, if ventilation is interrupted, if it results in an injury or it impedes men and material access. More than 1,200 such large falls of ground are reported in United States underground coal mines annually (Mine Safety and Health Administration, 2011). Each fall represents a safety hazard and can be considered to be a failure of the ground support system. The problem of large roof falls is being addressed at the National Institute for Occupational Safety and Health (NIOSH), where research is being conducted to develop improved support design methods to better match support systems to coal mines' prevailing ground conditions.

Although 1,200 large roof falls represent a significant safety hazard, when viewed from the perspective of support system success rate, these roof falls represent the failure of a very small percentage of installed support systems. For example, NIOSH researchers investigated a number of mines with a high incidence of roof falls and found that between 0.2% and 2.0% of the total exposed roof fell in reportable roof falls (Klemetti, 2012). In these mines, the support systems can be said to be 98.0% to 99.8% successful against large roof falls. The success rate is no surprise given that roof support systems have seen continuous improvement, resulting in a tenfold reduction in US ground fall fatality rates since the 1930's (Pappas et al. 2000). However, the potentially fatal consequences of a single large-scale roof fall remains unacceptable, and every effort should be made to eliminate these hazardous events.

This paper presents an approach that NIOSH engineers are using to estimate the stability of supported coal mine excavations against large-scale collapse. The method provides relative results, allowing the designer to compare alternative support scenarios under varying ground conditions. The focus of the method is on stress-driven roof falls that are the result of failure of the surrounding rock material. Falls related to individual geological structures, such as large slips or faults, are not included. Smaller skin falls that occur between supports are also excluded from this study.

Success and Failure Considerations

When designing a supported excavation, it is necessary to consider the strength variability of the surrounding rocks and loading conditions. An adequate margin of safety must be included in the design so that the excavation will remain stable under an unfavorable combination of strength and loading conditions. The classic factor of safety used in engineering design is one way of accounting for the variability. The appropriate value of the safety factor is usually determined through experience or can be determined based on failure probability considerations (Harr, 1987).

The factor of safety is usually calculated by comparing the strength, also known as the capacity, of a structure to the expected load. Unlike many engineering structures, the stability of an underground excavation cannot readily be determined by comparing the "load" to the "capacity" and calculating a classic factor of safety. First, the loads or stresses are redistributed in the relatively boundless rock mass around the excavation; thus, it

is not clear which loads should be considered. Also, the system's capacity is not easily defined because the support system is usually integrated within the rock mass being supported, and there is no clear distinction between capacity of the installed supports and the enhanced capacity of the reinforced rock to resist collapse.

The problem is somewhat simplified when the type of failure being evaluated is clearly defined. Mining engineers are interested in the functional success of mine excavations. The excavation must fulfill its function of providing safe access to the working face. The excavation is considered a failure if it no longer fulfills this function. Functional failure should not be confused with failure of the rock material around the opening. In many cases, damaged or failed rock material can exist around an excavation, yet the support system maintains stable conditions and the excavation is functionally successful. In the case of the large reportable roof falls under consideration, "failure" can be defined as the occurrence of a large roof fall that extends up to or above the bolted horizon. Conversely, "success" is defined as the avoidance of a large roof fall.

Since the loading and support capacity of underground mine excavations are not clearly defined, using the term *safety factor* may result in confusion. For example, unsupported excavations can be adequately stable, but the factor of safety would be zero if calculated as the ratio of support capacity to rock load. An alternative approach is presented in this paper where the excavation stability is expressed as a *stability factor*, which attempts to express the degree of safety of an excavation in similar terms as the classic factor of safety.

METHOD FOR CALCULATING THE STABILITY FACTOR

The proposed stability factor is calculated as a ratio of the average rock mass strength (the capacity) to the required rock mass strength to prevent collapse from occurring (the demand). Numerical models are used to simulate the excavation, loading conditions and support system and determine the rock strength that is required to prevent collapse from occurring. This is achieved by using the strength reduction modeling technique (Zienkiewicz, et al., 1975; Lorig and Varona, 2000) in which the modeled rock strength is gradually reduced until collapse is indicated by the inability of the model to reach a state of equilibrium. Laboratory test results, supplemented by rock classification data and field stress measurements, are used to provide inputs for the numerical models.

Numerical Models

Numerical modeling was selected as the most appropriate method for assessing the stability of an excavation for given rock mass, support and stress conditions. Empirical methods and analytical solutions are also available for evaluating the stability of the rock around coal mine excavations (Panek, 1962; Mark, 2000; Canbulat and van der Merwe, 2009; Frith and Colwell, 2010). While these solutions are useful in design decision-making, they seldom capture the complexity of the interaction between a support system and the failing rock mass. Numerical models have the capability of simulating rock failure development, post failure response and ultimate collapse of the surrounding rock while tracking the interaction of the support system with the failing rock mass. The FLAC3D finite difference software (Anon, 2011) was selected to conduct the model analyses.

It is recognized that in most mining situations, data on the rock strength, deformability and loading conditions are limited. In such data limited situations numerical models provide a method of understanding the mechanisms that affect the behavior of a system (Starfield and Cundall, 1988). Ultimately, the model results should only be used as a tool to assist in developing a final design.

Strength Reduction Technique

The strength reduction technique has a long history in numerical model analysis (Zienkiewicz, Humpheson and Lewis, 1975) and has often been applied in rock slope stability engineering to determine the safety factor of rock slopes (Lorig and Varona, 2000), but has not been widely used for underground excavation analyses. The technique is applied by first conducting a stability analysis using average rock strength properties. Depending on the outcome, the analysis is repeated using either a decreased or increased rock mass strength until the point of collapse is satisfactorily bracketed. Strength adjustments are achieved by simultaneously reducing or increasing the cohesion, tensile strength and the coefficient of friction of the rock matrix and the bedding planes. The stability factor is simply calculated as the inverse of the strength adjustment factor at the point of collapse of the modeled excavation. For example, if collapse occurs when the strength is reduced by a factor of 0.8, the stability factor would be 1.25.

The occurrence of collapse is indicated by the inability of the model to reach a state of equilibrium after an extended number of solution cycles. Usually, this means that a roof collapsed at a constant velocity and equilibrium could not be reached. When applying the technique to underground coal mine excavations, it was found that floor heave was sometimes the mode of ultimate instability. This occurred because the floor rocks were weaker than the roof rocks. All analyses were therefore conducted by only reducing the rock mass strength above the roof of the excavation while leaving the coal and floor rocks unadjusted.

NUMERICAL MODEL DEVELOPMENT

The general approach for selecting model inputs and model analysis followed the procedures developed at NIOSH (Zipf, 2006). The modeling approach closely resembles the "synthetic rock mass" concept (Pierce et al., 2007) in which the rock matrix and the discontinuities are modeled separately. This approach is necessary to capture both rock matrix failure and bedding-related slip in the sedimentary coal measure rocks. One significant addition to the approach outlined by Zipf is that strength anisotropy of the rock matrix was included in the models.

The strain-softening ubiquitous joint constitutive model in FLAC3D was used to simulate the bedded coal measure rocks. The models were run in the small-strain mode to alleviate the formation of unrealistic kink-bands in the ubiquitous joint materials. Support units were modeled using the built-in finite element structural components available in FLAC3D. Interfaces were modeled between the different rock units, allowing joint opening and closing to be simulated. The built-in programming language in FLAC3D was used to incorporate the strength anisotropy of the models' bedded rock.

Inputs for the numerical models were obtained from laboratory strength testing, field monitoring and rock mass classification data

where available. Unavailable data were based on best estimates from published and other sources.

Anisotropic Rock Strength

The inclusion of anisotropic rock strength in the model analyses resulted in improved agreement with monitored field performance of excavations. The strength of bedded rocks can be highly anisotropic, and this phenomenon has an especially important impact on roof stability when subject to the high horizontal stress found in many coal mines. Field tests on rock core using the point load index apparatus have shown that strength anisotropy can vary from a ratio of approximately 1.0 down to a ratio of less than 0.2 for highly laminated shale (Molinda and Mark, 1996). A review of strength anisotropy data obtained by standard uniaxial compression testing and point load testing seems to indicate that the point load method underestimates the compressive strength in the direction parallel to the bedding. This is not unexpected, since the point load apparatus essentially tests the tensile strength of the rock. However, the point load strength in the direction parallel to the bedding has been found to be an excellent indicator of bedding strength and is used in the determination of the Coal Mine Roof Rating (Molinda, Mark and Barton, 2002). For modeling the compressive strength of bedded rocks parallel to the bedding, the strength reduction indicated by the point load test was halved. For example, if the point load tests indicated that the strength parallel to the bedding was 50% of the perpendicular strength, then the strength was reduced by 25% in the models.

Where data on the point load strength parallel to the bedding were not available, the discontinuity intensity rating (DIR) used in the Coal Mine Roof Rating (CMRR) was used to obtain an initial estimate of the strength anisotropy. The DIR varies from a rating of 9 for closely spaced persistent beds to 35 for widely spaced discontinuous beds. The strength anisotropy ratio was calculated as:

$$R = 0.28\, e^{0.04 \times DIR} \quad (1)$$

The value of R varies from 1.0 for massive rocks to 0.4 for strongly bedded rocks with a DIR value of 9. This relationship was found to result in realistic roof performance in models simulating high horizontal stress conditions.

The implementation of anisotropic rock strength in the numerical models was achieved by creating a user-defined function that reduced the rock strength to the bedding-parallel strength when the angle between the major principal stress and the bedding surface was less than 15 degrees.

Model Layout

The models presented here were set up to simulate cross-sections through coal mine entries in various geological settings encountered in the United States. More elaborate models of entries and cross-cuts can be created if desired. The model boundaries were located at least three entry widths away from the edges of the entry and extended about 20 meters (65 feet) above and 10m (33 ft) below the entries. The outer boundaries of the models were fixed against normal displacement, while allowing displacement to take place along the boundary surface (roller boundaries). The models were typically 1.2 m thick in the direction perpendicular to the section, which represents the typical slice of rock supported by a single row of bolts. The element (zone) sizes in the vicinity of the entry were between 0.25 and 0.35 m (10 to 14 in). The element width was increased up to about 1.2 m (4 ft) at the excavation's remote locations where rock failure was not expected to occur. In relatively thin geologic beds, the element height was constrained to the thickness of the bed.

Rock bolt supports were modeled across the entry roof, located in the center of the slice. The boundary conditions caused the model to effectively simulate a long entry excavation with repeating rows of supports.

The stress within the models was initialized based on field stress measurements, where available, or using the best published data available for the geological region. When field stress measurements were not available, the horizontal stress was based on the relationships published by Mark and Gadde (2008) in which the horizontal stress is affected by the modulus of elasticity of each rock layer.

Model Calibration

The response of numerical models is highly dependent on the strength and loading parameters used as input. The accuracy of input parameters used in numerical models are affected by the uncertainties associated with projecting laboratory scale rock strength to the field scale, the post failure properties of the broken rock and the natural variability of rock properties and stresses in the field.

A model based on average properties and stress conditions is therefore unlikely to match the rock mass response at a particular experimental location in a mine, and it is necessary to adjust some of the model parameters to better match the specific site response. As more experience is gained converting laboratory tests to field scale properties, the amount of calibration required is likely to decrease. In the case studies presented below, the most common adjustment was the large scale cohesion of the rock mass. In some instances, it was necessary to also adjust the strength of the rock parallel to the bedding to match cutter-type failure initiation. However, all adjustments were maintained within realistic limits.

In each case presented below, the calibrated model response was required to qualitatively match the observed field conditions, such as roof damage, coal rib spalling and bolt loading. Where available, the model response was also required to reasonably match the field measured displacements within the rock mass.

CASE STUDY APPLICATIONS

Three examples are presented where the stability factor approach has been used to evaluate entry stability in wide-ranging geological and stress settings. For each case, the model response is discussed for the observed conditions and then the strength reduction technique is applied to determine the stability factor of the excavation.

Pittsburgh Seam Case Study

An excavation in the Pittsburgh seam monitored in great detail was selected as a modeling case study. The entry was selected for detailed stress and deformation monitoring because it was anticipated the entry would be subject to significant horizontal stresses as a second longwall face approached and passed it (Oyler et al., 2004). The entry was located at a depth of 180 m (600 ft) and was 4.8 m (16 ft) wide by approximately 2.1 m (7 ft) high.

The immediate roof may be subdivided into three units: the lower 2.7 m (9 ft) consisted of weak carbonaceous shale and coal, a slightly stronger claystone sequence from 2.7 to 5.4 m (9 to 18 ft) and a significantly stronger limestone above 5.4 m. The initial horizontal stress was estimated based on published equations for the eastern United States (Mark and Gadde, 2008). The initial vertical stress was 5 MPa (725 psi) and the horizontal stress within the stiffer upper shale unit was 9 MPa (1,300 psi) with the stress in other layers being higher or lower, depending on their elastic modulus. The excavation was supported using 22mm (7/8 in) diameter 2.4 m (8 ft) long grouted combination bolts which had 1.2 m (4 ft) of resin grout and 3.6 m (12 ft) long cable bolts with 1.2 m (4 ft) of resin grout. Initial conditions were good in the entry, but some roof cutters were observed in the vicinity. As the longwall approached, conditions deteriorated but the entry did not collapse during the entire monitoring period; that period ended when the longwall face passed the entry. Stress change monitoring results indicated that the horizontal stress increased by up to 10 MPa (1,450 psi) as the longwall approached.

A model of the entry and installed supports was created using rock strength and stress data from the detailed monitoring experiment. Table 1 summarizes the main rock units and the strength parameters used in the final calibrated model. The model was subject to increasing loads to simulate the effects of the approaching longwall, and displacements within the rock mass were determined and compared to field monitoring results. Figure 1 shows the central detailed part of the model in which the bolt and cable locations can be seen. The figure also displays the extent of rock mass damage around the excavation when the horizontal stress had increased by 7 MPa (1,015 psi).

Figure 2 shows the field measured and model determined displacements in the roof as the stress was increased to simulate the approach of the longwall; the model results closely resemble the monitored results. The detailed shape and magnitude of the displacements depend on selection of strength properties for the roof beds in the model. Small changes can be made to the model to match a specific set of field data. The model also provided satisfactory qualitative results. It indicated stability of the overall roof with minor spalling or cutter formation at the corners during the development stage. It also indicated that the entry would remain open, but with considerable rock damage and support yield at the final loading stage when the longwall face would be at its closest location relative to the entry. The rock damage at this elevated stress conditions formed a dome-shaped zone in the roof, which is typically observed when roof collapses occur.

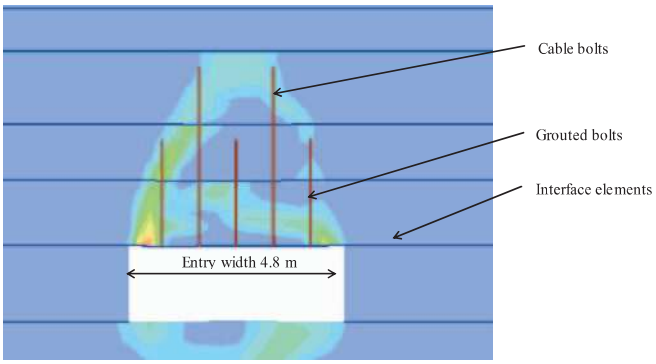

Figure 1. Pittsburgh seam case study showing rock damage contours when the vertical stress had increased to 7 MPa by approaching longwall. Warmer colors indicate increasing damage (plastic strain).

The stability factor of the supported entry was first determined for development conditions. Collapse occurred in the model after the rock strength had been reduced by a factor of 0.34 resulting in a stability factor of 2.94. Considering that the excavation was supported to survive elevated loading conditions induced by the approaching longwall, the relatively high stability factor under development conditions was expected.

Additional scenarios were evaluated where the stability factor was determined for the entry supported by bolts alone, without

Table 1. Key rock properties for modeling the Pittsburgh seam case study.

Rock type	Thick-ness (m)	UCS Lab (MPa)	Elastic modulus (GPa)	Friction angle (deg)	Cohesion (MPa)	Tensile strength (MPa)	Bedding Cohesion (MPa)	Bedding friction (deg)
Shale	18	40	15	28	6.97	2.32	1.98	23.0
Limestone	6	100	35	42	12.91	4.30	11.26	39.1
Gray shale	1	70	20	30	11.72	3.91	3.91	25.0
Gray shale	1.7	40	15	28	6.97	2.32	1.98	23.0
Black shale	1.3	25	10	28	4.36	1.45	0.88	23.00
Shale/coal	1.5	20	8	25	3.70	1.23	0.51	20.00
Coal bed	1.8	16	3	35	2.42	0.81	1.09	30.45
Shale	3	15	15	28	6.97	2.32	1.98	23.00
Shale	16	15	15	28	10.45	3.48	2.97	23.00

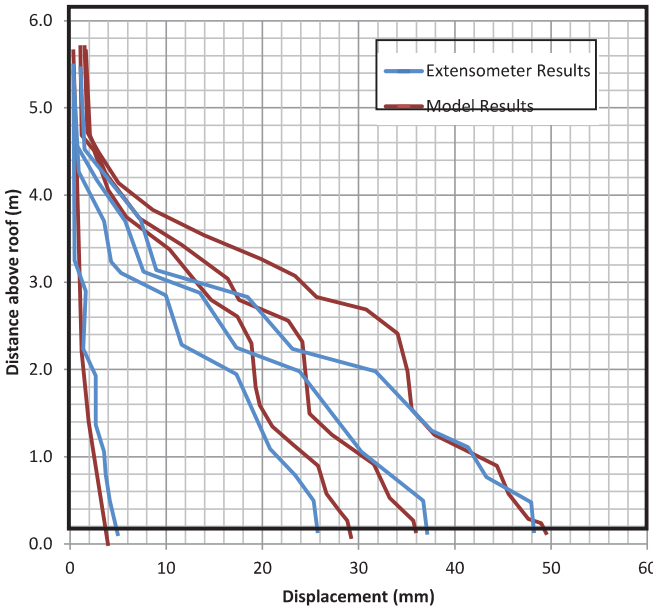

Figure 2. Graph showing comparison of model and field monitoring results of displacements in the roof as loading was increased by an approaching longwall for the Pittsburgh seam case study.

cable bolts. The stability factor reduced to 2.54. A final evaluation was made where the entry was modeled with no support, under initial development conditions. For this case, the stability factor was found to be 1.31. The result was not surprising, as the entries are able to remain stable for one or two shifts with only side bolt support, before the center bolt is installed. A stability factor of 1.31 seems to indicate that temporary stability is possible with limited support.

Thick-Weak Strata Case Study

The second case study is a room and pillar mine in the Illinois Basin where a bolt performance experiment was conducted (Spearing et al., 2011). This case was selected to test the modeling method and the derived stability factor in thick-weak strata. The mine is located in the Danville No. 7 coal bed with 6.1 m (20 ft) wide entries and 24.4 m by 24.4 m (80 ft by 80 ft) center-to-center pillars at a depth of about 100 m (330 ft) in the test area. The seam thickness was approximately 1.5 m (5 ft) in the test area and approximately 0.8 m (2.6 ft) of roof shale was extracted to provide adequate clearance for installing instrumentation.

The immediate roof consists of medium gray, silty shale with a total thickness of approximately 1.5 m (5 ft). This is overlain by a medium gray to dark gray shale unit with gradational contact between the two units. The shale was generally featureless with some lighter gray and possible sandier zones. Stress measurements were conducted at the site and found that the major horizontal stress was aligned nearly parallel to the development direction. For modeling purposes, the vertical stress was 2.4 MPa (350 psi) and the horizontal stress in the plane of the model was 4.5 MPa (650 psi).

The rock properties used in the model are summarized in Table 2. Note the low modulus of elasticity of the shale rocks determined by laboratory tests. Various support types were tested in the experiment. The model simulated full column resin grouted bolts 19mm (3/4in) in diameter and 1.8 m (6 ft) long, with five bolts in a row across the entry width spaced 1.2 m (4 ft) apart. During the test the supports were subject only to the stress changes normally encountered during room and pillar mine development. This implies that the average vertical stress in the surrounding coal increased from the initial cover load of 2.4 MPa to 4.3 MPa, based on the extraction ratio of 43.7%. The ground conditions during support installation were good, with minor cutters formed along the entry edges. During the course of the experiment, the ground conditions remained good and no significant instability was reported.

A model was created of the test entry with supports installed under the initial stress conditions. The model demonstrates that some bedding slip occurs in the immediate roof and limited shear failure near the corners. This agrees well with observed conditions of minor cutters near the entry corners. The vertical loading in the model was increased to 4.3 MPa to simulate the full development of the room and pillar workings, and this additional loading resulted in 2-3mm (1/4 in) of additional roof displacement and an increase in the loading of the supports near the center of the entry from about 20 kN to 40 kN (2 t to 4 t). This agrees well with monitoring results. The supports near the edges of the entry encountered loads of up to 80 kN (8 t), which appears to have been caused by additional damage at the corners. The model indicated minimal changes to the overall stability conditions with the increase in stress.

The stability factor was calculated for the entry under development conditions, and it was found to collapse when the strength was reduced by a factor of 0.51, resulting in a stability factor of 1.98. At the collapse point of the excavation, a chimney-type zone of failure started to form, as shown in Figure 3. This chimney type collapse is typical of bedded materials.

Deep Cover Mine Case Study

The studied mine is a longwall operation where the response of the gateroads and pillars was monitored as part of a NIOSH research effort (Lawson, Zahl and Whyatt, 2012). The depth of cover in the study area varied from 450m to 700 m (1500 to 2300 ft). The roof consists of gray shale overlain by fine-grain sandstone with inter-bedded shale streaks. Coal bands may appear in the shale unit at various locations. The study location is referred to as the 2 North Outby Instrumentation Site. At the study location, a 15 cm (6 in) coal stringer was located at approximately 2.7 m (9 ft) above the entry roof. The sandstone is overlain by further shale beds and coal beds. Table 3 shows the layer thicknesses and rock properties used in the model analyses. The support system consisted of 1.8m fully-grouted rock bolts supplemented by 3.6 m (12 ft) grouted cable bolts. Steel straps and screen were used to provide additional area support.

The horizontal stress in the region is known to be highly anisotropic, with the major horizontal stress being approximately equal to the vertical stress and the minor stress being about one-third of the vertical stress (Maleki, Stewart and Stone, 2007). The major horizontal stress was aligned approximately parallel

Table 2. Key rock properties for modeling the Illinois basin case study.

Rock type	Thick-ness (m)	UCS Lab (MPa)	Elastic modulus (GPa)	Friction angle (deg)	Cohesion (MPa)	Tensile strength (MPa)	Bedding Cohesion (MPa)	Bedding friction (deg)	Bedding tensile strength (MPa)
Shale	15.0	40	3.5	28	6.97	2.32	1.98	23.0	0.10
Shale	4.6	30	3.5	28	5.23	1.74	1.05	23.0	0.05
Shale	0.8	30	3.5	28	5.23	1.74	1.05	23.0	0.05
Shale	1.5	25	3	28	4.36	1.45	0.60	23.0	0.05
Coal bed	1.8	16	3	35	2.42	0.81	1.09	30.45	0.10
Shale	5.2	30	3	25	5.54	1.85	0.50	20.00	0.05
Shale	1.8	30	3	25	5.54	1.85	0.50	20.00	0.05
Shale	5.0	30	3	25	5.54	1.85	0.50	20.00	0.05

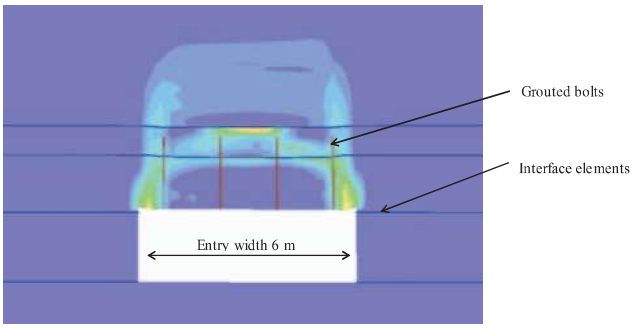

Figure 3. Thick shale case study showing rock damage contours at point of collapse. Warmer colors indicate increasing damage (plastic strain).

to the gate roads. Detailed observations were made of the ground conditions prior to the approach of the longwall and during longwall advance. Initially the roof of the gate roads was undamaged, while the coal ribs showed minor deterioration with less than 50 cm (1.5 ft) of spalling. Conditions deteriorated considerably as the longwall approached, with floor heave and increased rib spalling occurring. However, the roof only showed minor damage with the appearance of tension cracks. Roof displacement monitoring using multiple borehole extensometers showed very limited extension of the roof, less than 5 mm (0.2 in), possibly indicating that the roof rocks did not experience significant stress change.

The numerical model used to simulate this case study is shown in Figure 4, which also shows the principal stress orientation and

Table 3. Key rock properties for modeling the western coal mine case study.

Rock type	Thick-ness (m)	UCS Lab (MPa)	Elastic modulus (GPa)	Friction angle (deg)	Cohesion (MPa)	Tensile strength (MPa)	Bedding Cohesion (MPa)	Bedding friction (deg)	Bedding tensile strength (MPa)
Shale	3.0	70	20	30	11.72	3.91	3.9	25.0	0.10
Coal	1.2	30	3	35	4.53	1.51	2.0	30.4	0.10
Shale	0.9	60	15	28	10.45	3.48	2.9	23.0	0.10
Sandstone	4.8	150	40	42	19.37	6.46	19.3	40.8	6.46
Shale	0.6	36	10	28	6.27	2.09	1.2	23.0	0.05
Coal	0.3	30	3	35	4.53	1.51	2.0	30.4	0.10
Shale	2.8	55	15	28	9.58	3.19	2.7	23.0	0.10
Coal-Mined	2.4	30	3	35	4.53	1.51	2.0	30.4	0.10
Shale	3.0	100	25	32	16.07	5.36	6.2	27.1	0.10
Sandstone	1.2	130	40	42	16.79	5.60	16.7	40.8	5.60
Coal	0.6	30	3	35	4.53	1.51	2.04	30.4	0.10
Shale	10.0	80	25	32	12.86	4.29	5.0	27.1	0.10

the colors indicate the magnitude of the minor principal stress at the initial development loading stage. The figure shows that tensile stress exists in the immediate roof of the excavation, which can result in tensile failure of the roof shale. Although tensile failure was not observed under the initial loading conditions, the first sign of deterioration of rock conditions was typically the formation of tensile cracks in the roof. Tensile fracturing at these depths of cover might be considered to be unusual, but considering that the horizontal stress in the model's plane is about one-third of the vertical stress, such large tensile stresses are not unexpected in the immediate roof of the square excavation. The laboratory scale coal strength was adjusted to 30 MPa (4,350 psi), giving an in-situ coal strength of 17.4 MPa (2,500 psi) in the model, to match the observed minor spalling of the coal ribs.

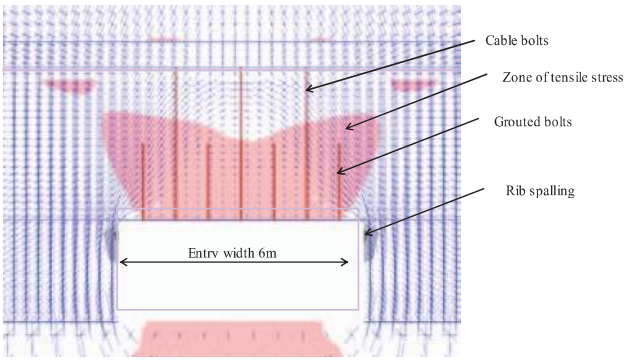

Figure 4. Principal stress plot for the deep western mine case study showing tensile stress zones in the roof and floor of the excavation under development conditions. Tensile stress zones shown in red, rib spalling in gray.

The calibrated model was loaded by an additional 7 MPa (1,015 psi) vertical stress to simulate increased loading caused by the approaching longwall. This stress state caused the model to respond with significant failure of the rib coal, which increased the effective excavation span and induced further tension in the roof. Floor damage was indicated, also in the form of tensile cracking. This model behavior agrees well with the observed deterioration

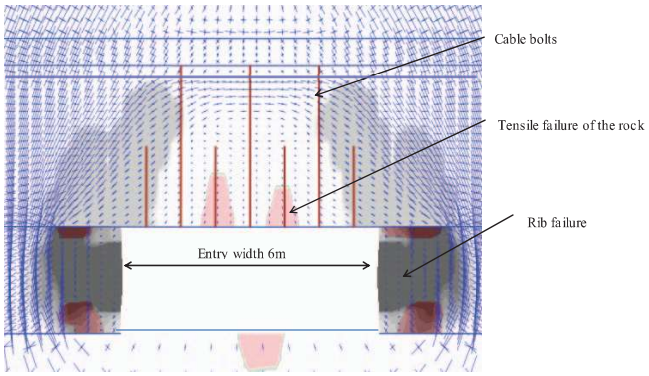

Figure 5. Zones of tensile failure (red zones), rock damage (gray shading) and stress trajectories (blue) for the deep western mine case study under increased vertical loading.

of the entry. Although the additional tensile stress caused vertical fractures to develop in the models up to approximately mid-height of the grouted supports, the grouted bolts and cable bolts did not experience a significant increase in loading. Inspection of the model results showed that the cable bolts extended by no more than 4mm (0.15 in), which concurs with the monitoring results. Figure 5 shows the failure state of the rock around the entry. The stress trajectories indicate that an arch has formed over the entry and the bolts are contained within this arch.

The model results discussed above seem to indicate that the roof of the excavation was in a state of tension, which increased as the longwall abutment loading increased. The roof, therefore, did not experience any direct load increase from the added vertical loading. The function of the support system is to hold the fractured rock in place, which it achieved admirably with the screen and straps attached to the bolts. One would expect the stability factor to be relatively high because the support system is not directly loaded by the surrounding rock mass; stability factor values of 1.63 were calculated for the development loading condition.

At the elevated stress condition, the stability factor of the roof was found to be also 1.63, which at first was surprising. However, it was clear that the roof over the excavation was only affected by increased tension, which caused additional tensile fracturing. This did not cause any significant additional loading of the supports.

Ultimate collapse occurs in the model when the rock strength is reduced to such a state that a circular shear surface forms through the coal ribs and the roof moves downwards as a unit with the cable bolts and grouted supports embedded within, as shown in Figure 6. This collapse mode was identical to the mode of collapse of the roof under development loading conditions, hence the same stability factor.

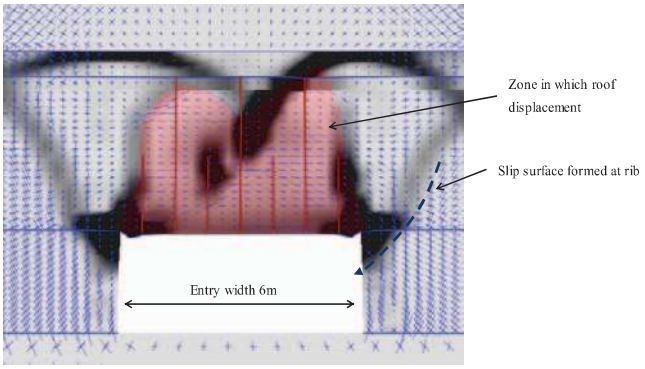

Figure 6. Rock damage (gray-black shading), roof displacement (red shaded area) and stress trajectories (blue) at the point of ultimate collapse of the roof in the deep western case. The red contour indicates displacement of greater than 50mm (2in).

CONCLUSIONS

The method of determining the stability factor through the strength reduction method is not novel, and has been used in other branches of geotechnical engineering. This study showed that the approach can be used as a tool to assist in support design by estimating the relative stability of excavations in various ground

conditions, stress conditions and with various support systems. The success of the method depends on developing numerical models that capture the essential failure mechanics of the rock surrounding the excavation and the response of the support system to these changes. The reliability of the models can be improved through a process of calibration against actual observations, as demonstrated in this paper.

Stability indices for the case studies examined were relatively high, which concurs with observations that only a small proportion of mine entries actually collapse during their operational life. The method can sometimes produce unexpected results when a high stability factor value is indicated, but local instability issues, such as unraveling of failed rocks between support units, may exist. It is necessary to clearly separate local stability issues from large-scale collapse evaluations.

The application of numerical models in the design of structures in rock is highly dependent on the quality of the input parameters, as in any engineering design. When designing in variable rock masses, the input values are not fully known and models should be used as a tool to better understand the system under consideration. The determination of a stability factor for supported entries is a step in this direction.

DISCLAIMER

The findings and conclusions in this paper are those of the authors and do not necessarily represent the views of the National Institute for Occupational Safety and Health. Mentioning any company name, product or software does not constitute endorsement by NIOSH.

REFERENCES

Anon. (2011). FLAC3D Fast Lagrangian Analysis of Continua in 3 Dimensions, Itasca Consulting Group, Minneapolis, MN.

Canbulat I., van der Merwe, J. N. (2009). "Design of optimum roof support systems in South African collieries using a probabilistic design approach." Journal of the South African Institute of Mining and Metallurgy, Vol. 108. 71-89.

Frith, R., Colwell, M. G. (2010). "AMCMRR – An Analytical Model for Coal Mine Roof Reinforcement." In: *Proceedings, 29th International Conference on Ground Control in Mining, West Virginia University, Morgantown, West Virginia*. July 27-29. 38-45.

Harr, M. E. (1987). *Reliability Based Design in Civil Engineering*. New York: McGraw-Hill, 290 pp.

Klemetti, T. (2012). Personal Communications, Pittsburgh, February 2012.

Lawson, H., Zahl, E., Whyatt, J. (2012). "Ground Condition Mapping: A Case Study." In: *2012 SME Annual Meeting, Seattle, Washington: Society for Mining, Metallurgy, and Exploration, Inc., Preprint*. 9.

Lorig, L., Varona, P. (2000). "Practical Slope Stability Analysis using Finite-Difference Codes." In: *Slope Stability in Surface Mining, eds. Hustrulid W.A., Mc Carter M.K. and van Zyl D.J.A. Society for Mining Metallurgy and Exploration, Littleton, Colorado*. 115-124.

Maleki, H., Stewart, C. Stone, R. (2007). "Three-Seam Stress Analyses at Bowie Mines, Colorado." In: *Proceedings, 26th International Conference on Ground Control in Mining, West Virginia University, Morgantown, West Virginia, July 27-29*. 29-35.Mark, C., Molinda, G. M., Barton, T. M. (2002). "New Developments with the Coal Mine Roof Rating." In: *Proceedings, 21st International Conference on Ground Control in Mining, West Virginia University, Morgantown, West Virginia, August 6-8*. 294-301.

Mark, C. (2000). "Design of Roof Bolt Systems." *In: Mark, C., Dolinar, D.R., Tuchman, R., eds. New Technology for Coal Mine Roof Support, Proceedings, NIOSH Open Industry Briefing, NIOSH IC 9453, 2000*. 111-132.

Mark, C., Gadde, M. (2008). "Global Trends in Coal Mine Horizontal Stress Measurements." In: *Proceedings of the 27th International Conference on Ground Control in Mining, West Virginia University, Morgantown, West Virginia*. 319-331.

Mine Safety & Health Administration. (2011). Web page: http://www.msha.gov/stats/statinfo.htm.

Molinda G. M., Mark C. (1994). "Coal Mine Roof Rating (CMRR): A Practical Rock Mass Rating for Coal Mines." Pittsburgh, PA: U.S. Department of the Interior, Bureau of Mines. *IC 9387*. 83.

Molinda, G. M., Mark, C. (1996). "Rating the Strength of Coal Mine Roof Rocks." Pittsburgh, PA: U.S. Department of the Interior, Bureau of Mines. *IC 9444*. 36.

Oyler, D. C., Mark, C., Gale, W. J., Chen, J. (2004). "Performance of Roof Support Under High Stress in a U.S. Coal Mine." *SME preprint 04-135. Littleton, Colorado, Society for Mining, Metallurgy, and Exploration, Inc*. 7.

Panek, L. A. (1962). "The Effect of Suspension in Bolting Bedded Mine Roof." US Department of the Interior, Bureau of Mines. *Report of Investigations 6183*. 59.

Pappas DM, Bauer ER, and Mark C (2000). "Roof and Rib Fall Incidents and Statistics: A Recent Profile." *In: Mark, C., Dolinar, D.R., Tuchman, R., eds. New Technology for Coal Mine Roof Support, Proceedings, NIOSH Open Industry Briefing, NIOSH IC 9453, 2000*. 3-21.

Pierce, M., Mas Ivars, D., Cundall, P., Potyondy, D. (2007). "A synthetic rock mass model for jointed rock." In: E Eberhardt (Ed.) et al., *Proceedings of the 1st Canada-US Rock Mechanics Symposium.* Vancouver, Taylor & Francis, London (2007). 341-349.

Spearing, A. J .S., Gadde, M. (2011). "Improving underground safety by understanding the interaction between primary rock bolts and the immediate roof strata." *Final Report (October 2011). NIOSH Contract No. 200-2009-32518 (2009)*. 283.

Starfield, A. M., and Cundall P.A. (1988). "Towards a Methodology for Rock Mechanics Modelling." International Journal of Rock Mechanics and Mining Sciences and Geomechanics Abstracts, 25(3). 99-106.

Zienkiewicz, O. C., Humpheson, C., Lewis, R. W. (1975). "Associated and Non-Associated Visco-Plasticity and Plasticity in Soil Mechanics", *Geotechnique*, 25. 617-689.

Zipf, R. K. (2006). "Numerical modeling procedures for practical coal mine design (2006). In: *Proceedings of the 41st U.S. Rock Mechanics Symposium, Golden, Colorado, June 17-21, 2006*. Alexandria, Virginia: American Rock Mechanics Association, 2006. Jun: 1-11.

Load Transfer Distance Calibration of a Coal Panel Scale Model: a Case Study

Mark K. Larson, Mining Engineer
Jeffrey K. Whyatt, Mining Engineer Omshr
NIOSH - Spokane Research Laboratory
Spokane, WA

ABSTRACT

Calibration of LaModel for deep coal mines begins with adjustment of overburden stiffness for load transfer distance. This calibration determines whether mining induced stresses are concentrated in the immediate abutment of the gob, or spread over a wider area. In the absence of site information, an empirically-based estimate is often used. Where data is available, a recommended calibration procedure can be followed, as is done in this case study at a deep western longwall mine, with minor modifications and extensions. In this case, data sources included borehole pressure cells, flatjacks installed in series with support Cans, and observed changes in ground conditions. Calibration was based on the first detection of mining-induced stress from the advancing longwall. Detection was found to depend on the type and sensitivity of measurement. Borehole pressure cell data with a 20-psi-increase detection threshold were chosen as the standard, in accord with data used in deriving empirical relationships. Application of this standard produced a load transfer distance estimate roughly four times the empirical relationship developed by Peng and Chiang (1984). This is a significant deviation with important implications for panel design at this site. Data from flatjacks, ground condition observations, and borehole pressure cells with higher threshold values, were tightly clustered and show load transfer distances from two to four times empirical guidance. Ratios between various measurements can be used to adjust measurements to the standard (although they may depend on mine geology). Once established, ratios can be used to adjust estimates, say from support flatjacks or ground observations, to the standard, where borehole pressure cell data is not available.

INTRODUCTION

Ground stress models are assuming a greater role in the design of deep mines, particularly deep coal mines (deep or deep cover in this paper refers to those mines where the first panel of a district is subcritical). Their use was addressed by the Mine Safety and Health Administration (MSHA) in Program Information Bulletin P09-03 (Skiles and Stricklin, 2009). This PIB joins a large body of literature addressing the proper verification and calibration of ground stress models. This body includes use and review of ground stress models in the course of MSHA accident investigations (e.g., Gates, et al., 2008). The Office of Mine Safety and Health Research (OMSHR), within the National Institute for Occupational Safety and Health (NIOSH), has recognized these trends and their importance to mining of coal under deep cover (National Institute for Occupational Safety and Health, 2010). This paper was motivated by that recognition, and is part of OMSHR's effort to improve methods for deep coal mine design. The paper addresses use of measurements and observations of load-transfer distance to calibrate a LaModel simulation of ground response to mining. Such calibration is recommended by Heasley (2008, 2009) and Heasley et al. (2010), but published guidance on executing the calibration process in a deep coal mine is sparse. Moreover, there is little information on the relative utility and sensitivity of various measurements and observations that might be used in model calibration. This paper was developed to address these deficiencies and provides a case study of model calibration to load-transfer distance, as indicated by a variety of measurements and observations from a longwall coal mine operating under deep cover.

CALIBRATION METHOD—LOAD-TRANSFER DISTANCE

A calibration process that tunes LaModel to more accurately model the vertical stress distribution for a specific coal panel has been presented (Heasley, 2008, 2009; Heasley, et al., 2010). This process calibrates three critical model parameters (rock mass stiffness, gob stiffness and coal strength) in precise order. The first, rock mass stiffness, is calibrated to produce a realistic extent of the abutment zone at the edge of critical gob areas (Heasley, 2008). This paper addresses that process, leaving subsequent steps for future examination.

Finite Load-Transfer Distance (Peng & Chiang and Mark Equations)

Vertical stress concentration on the seam decays in some manner (e.g., in a parabolic trend) as distance from the gob increases. Load-transfer distance is often thought of as a specific distance at which the effects of a gob are evident in existing or future openings. Such disturbances usually extend furthest from the side of a gob in the middle of long panel (i.e. a two-dimensional cross section). Strictly speaking, this side-abutment extent defines the load-transfer distance (e.g., Peng, 2006), and is reported as a finite value.

Peng and Chiang (1984) reviewed a number of studies that included borehole-pressure-cell (BPC) and vibrating wire stress cell (VWS) measurements of load-transfer distance (e.g., Peng and Park, 1977; Peng, 1977; Wade and Conroy, 1980). Mark (1990) characterizes the criteria in these studies as the distance from the panel edge that abutment stress increases could be detected. Peng and Chiang plotted distances found in these studies against the depth of overburden (Figure 1), and established the following empirical relationship between the two:

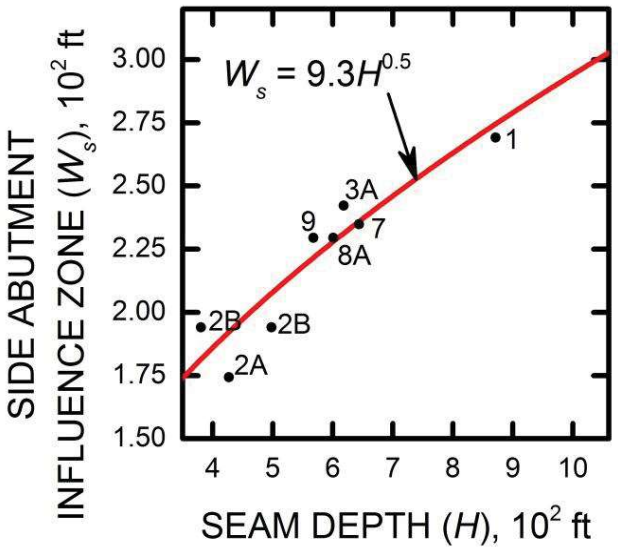

Figure 1. Extent of side-abutment-influence zone and seam depth (after Peng and Chiang, 1984, Figure 2. 3.9).

$$D_{1.0} = 9.3\sqrt{H}, \quad (1)$$

where

$D_{1.0}$= distance into the side abutment at which the stress resulting from mining is no longer detected, and

H = depth of cover in ft.

Mark (1990) plotted the magnitude of stresses measured by VWSs at various distances from an abutment in other studies (Figure 2). He found that the stress decay in an abutment with distance (D) could be described by a simple function.

$$\Delta\sigma = \left(\frac{3L_s}{D_{1.0}^3}\right)(D_{1.0} - x)^2, \quad (2)$$

where

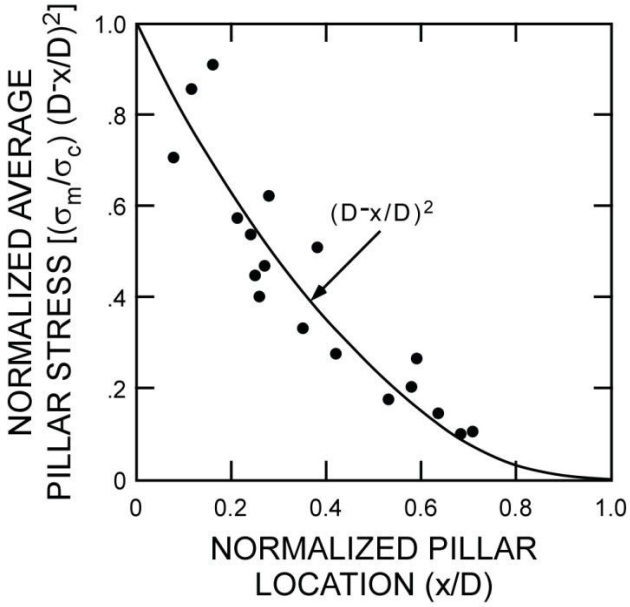

Figure 2. Stress decay with distance in a gob abutment(after Mark, 1990, Figure 10.).

$\Delta\sigma$ = increase of stress on the side abutment resulting from mining of the panel,

L_s = total load transferred to the abutment, and

x = distance into the side abutment from the gob.

Mark (1990) showed how his observation could be coupled with knowledge of the load-transfer distance (or its estimation with Peng and Chiang's equation) to estimate loading of pillars (Figure 3).

The stress function is easily integrated to find pillar loads. It can also be integrated to estimate the extent of a zone carrying 90% of the load transferred from the gob, which results in equation 3.

$$D_{0.9} = 5\sqrt{H}, \quad (3)$$

where

$D_{0.9}$= distance (ft) into the side abutment within which 90% of the load increase resulting from mining is applied, and

H = depth of cover in ft.

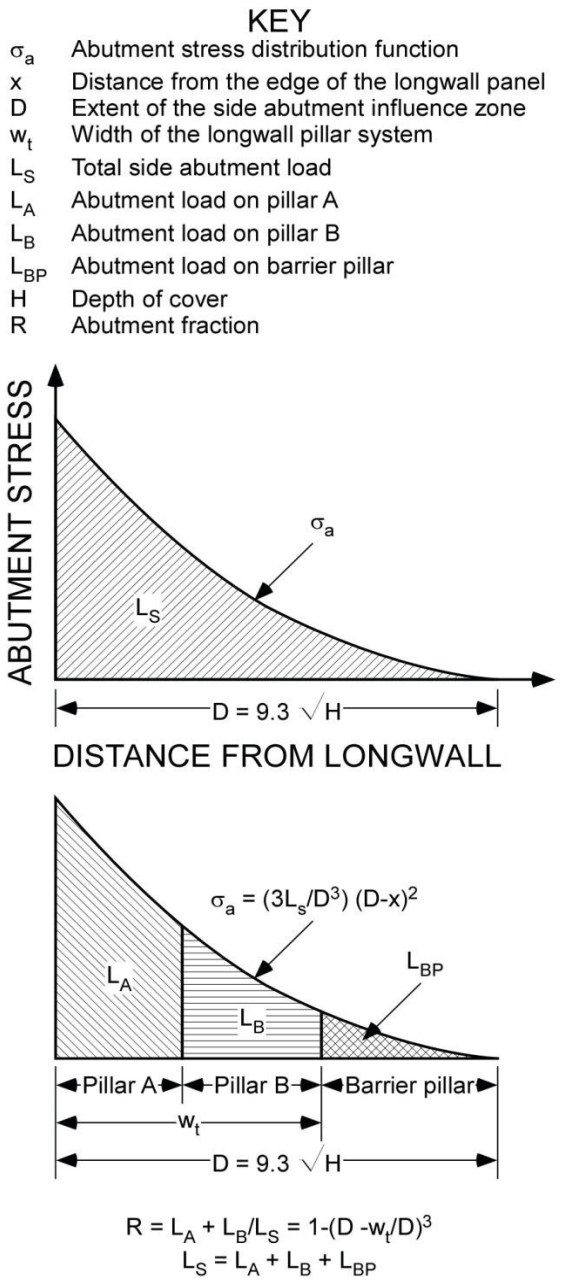

Figure 3. Estimation of side-abutment pillar loading in ALPS (after Mark, 1990, Figure 9.).

Infinite Load Transfer (LaModel and Overburden Parameters)

Load-transfer distance is a more difficult concept when numerical models based upon elastic theory or elastic bending laws are used. These theories indicate that every disturbance will decay to an infinitesimal disturbance at infinity. Where this is true, the distance at which transferred loads are first evident may depend on the observation type and sensitivity. It's not surprising, then, that they also deviate from the empirical stress decay equation proposed by Mark. Heasley et al. (2010) demonstrated this by plotting the Mark and LaModel stress decay curves for one particular case (Figure 4).

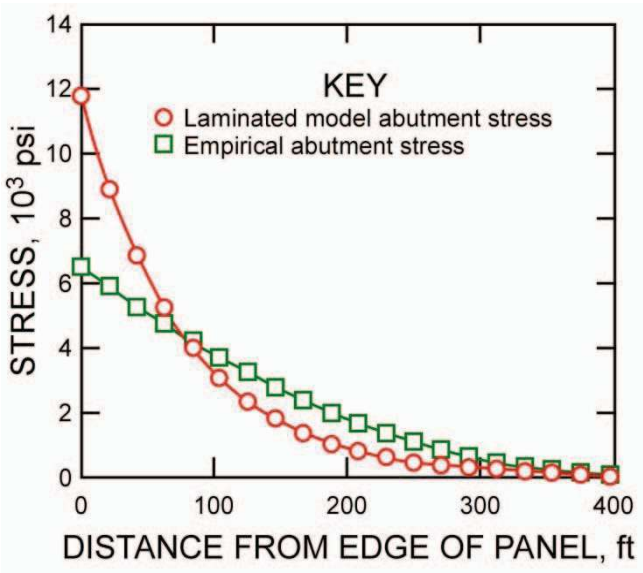

Figure 4. A comparison of stress distribution estimates in the abutment developed by LaModel and the empirical method of Mark and Chase for a particular case (after Heasley, et al., 2010, Figure 1).

Heasley Recommended Calibration Method

In the first step of his recommended calibration process, Heasley uses load-transfer distance to calibrate overburden stiffness. The issue of finite versus infinite load transfer is not part of Heasley's analysis in that it focuses on the region that carries 90% of the abutment load, thus neglecting the tails of the load distribution. He requires that the boundary of this region be identical for the two methods, allowing him to derive an equation that defines overburden thickness:

$$t = \frac{2E_s\sqrt{12\left(1-\upsilon^2\right)}}{Eh}\left(\frac{5\sqrt{H}-d}{\ln(0.1)}\right)^2 \quad (4)$$

where

E = elastic modulus of overburden,

υ = Poisson's Ratio of overburden,

E_s = elastic modulus of the seam,

h = seam thickness,

d = extent of the coal yielding at the edge of the gob, and

H = seam depth.

Heasley incorporates this calculation for t in the lamination-thickness wizard that is part of LamPre v. 3.0.

Overburden elastic modulus is simply a weighted average of moduli of overlying layers. Recall that the $\sqrt[5]{H}$ term Longwall is the empirical width of the abutment zone carrying 90% of the abutment load. Thus, calibration to the empirical expectation of load-transfer distance is very simple. Heasley and Sears (2009) affirmed that specific field measurements give the best estimate of the abutment zone, but that measurements are not always available. They counseled that visual observations may be used when measurements are lacking, but they provided no guidance on a method of obtaining or using those observations. However, they recognized that sensitive instruments will likely detect load transfers well before loads rise sufficiently to impact ground conditions in mine entries.

Heasley Recommended Calibration Method Modifications

The recommended calibration strategy was applied to this case study with two small adjustments and refinements. First, the single seam solution is invariant with the product of overburden modulus and lamination thickness (Et), making this product the actual overburden stiffness property (Larson and Whyatt, 2009a, 2009b). This minor change is accommodated by a simple re-ordering of the calibration equation to read:

$$Et = \frac{2E_s\sqrt{12\left(1-\upsilon^2\right)}}{h}\left(\frac{5\sqrt{H}-d}{\ln(0.1)}\right)^2 \quad (5)$$

A second modification simplifies the introduction of load-transfer distance into this equation. While it is relatively easy to note the first instance of pressure, displacement, or change in ground conditions, it is not at all clear how to locate the $D_{0.9}$ boundary. Indeed, Peng and Chiang's original equation was derived from observations of the first indication of loading. One way around this difficulty is to find an "effective" value of H from observations of the extent of loading. That is, re-order equation 1 so that observations and measurements of $D_{1.0}$ can be used to find an "effective" H. Then, substitute this value, rather than the actual overburden depth, into the calibration equation. This substitution implicitly assumes that the empirical relationship for stress decay with distance (equation 2) is valid for all load-transfer distances.

IMPLEMENTATION – CASE STUDY

The remaining challenge in execution of the calibration procedure is estimation of the distance at which the influence of mining is first detected ($D_{1.0}$) This step is somewhat site specific, as options for instrumentation, and the utility of observations, will depend on local characteristics of the ground response to mining. As such, implementation is explored in the context of a case study at a deep western coal mine. Roof members consisted of interbedded mudstone, siltstone, shale, and sandstone with coal stringers. The floor consisted of an interburden overlying a lower split of the coal seam. Limited observations showed the interburden ranged from 1 to 15 ft. Thinner portions consisted of mudstone, while thicker portions were roughly equal intervals of mudstone overlying sandstone. A ground monitoring program at the mine included BPCs installed in gate-road pillars (Figure 5 and Figure 6), flatjack pressure cells installed with supplemental support Cans in gate-road entries, roof extensometers, and observations of roof, rib and floor deformation. Of these, roof extensometers failed to provide any consistent, useful information indicating the first arrival of mining-induced stress. Entry closure and entry closure rate measurements were not considered because of the infrequent nature of those manual measurements. $D_{1.0}$ was estimated for each of the other methods.

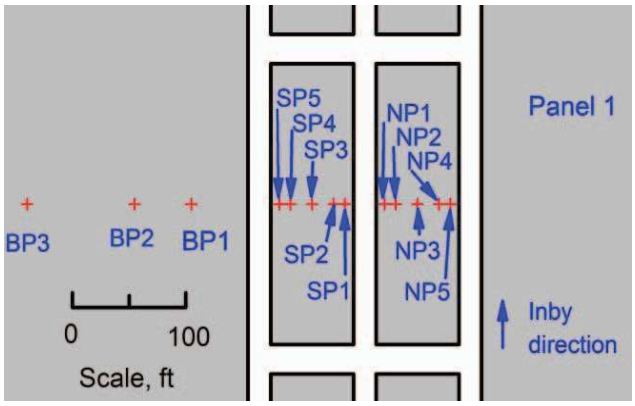

Figure 5. Layout in plan view of borehole pressure cells at the 1 North Outby instrumentation site (tailgate of Panel 1). Average depth of cover = 2,238.6 ft.

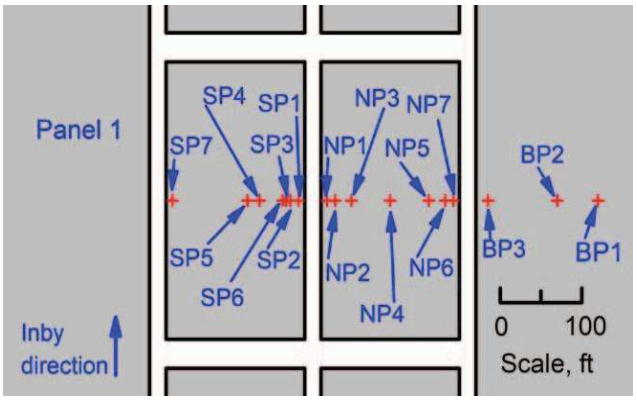

Figure 6. Layout in plan view of borehole pressure cells at the 2 North Outby instrumentation site (headgate of Panel 1). Average depth of cover = 2,268.4 ft.

Borehole Pressure Cells

Interpretation of BPC measurements involves two factors. The first is evaluating whether a particular cell is performing properly. That is, is it properly seating and pressurized? The second is to discriminate first loading from measurement noise and, potentially, influences other than mining that can induce a cell response. Since empirical relationships are part of the calibration process, it is also desirable that the threshold for detection be comparable to other studies.

The following criteria were used to eliminate specific BPCs from the analysis:

1. Erratic readings;
2. A pressure bleed-off, even if minor, as it muddles determination of stress arrival;
3. Installation notes indicating BPCs may have been damaged during installation; and
4. Significant inconsistencies with adjacent instruments (this screens local effects as well as poorly performing cells).

Pressure cell transducer resolution in this study was about 2 psi, and cells were monitored hourly with a 14-bit datalogger. A 9-point running average (i.e., the average of the current measurement and four measurements before and after it) was used to mask noise while picking the first arrival of pressure. Cell pressures are not ground pressures, and various adjustments have been proposed. Vandergrift and Conover (2010) found that the ratio of ground pressure to cell pressure varies from about 0.8 to 1.1 for similar conditions and low cell pressures, depending on assumptions and the method chosen. Given this modest adjustment, this analysis will assume parity between cell and ground pressure changes with regard to detection of the first arrival of loading.

The arrival of loading was defined by a threshold pressure increase above equilibrium loading. Load-transfer distances for pressure increase thresholds of 10, 20, 30, 50 and 100 psi were identified for each cell that passed the reliability screen. Figure 7 is typical, showing the increase in raw pressure plotted against face location (i.e., linear gate-road travel distance between face and instrumentation line). Figure 7 also demonstrates that the load-transfer distance depends heavily on the choice of pressure threshold.

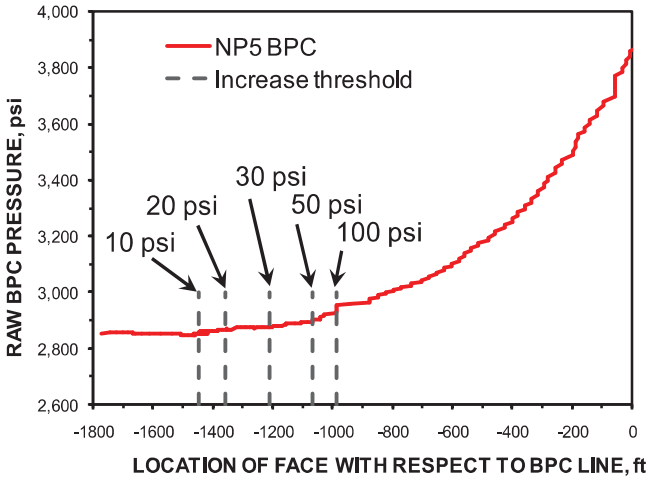

Figure 7. Typical raw BPC pressure versus location of longwall face with respect to the BPC instrument line. A negative location means the face inby the BPC line. Also shown re the locations of various thresholds of increase in pressure.

The 20-psi threshold was chosen for this study. This choice is somewhat arbitrary, but provided solid, consistent results. It appeared to avoid some of the noise and local influences that affected very small thresholds. The threshold also appeared to be consistent with the historical studies used by Peng and Chiang in developing equation 1 (e.g., Peng and Park, 1977; Peng, 1977; Wade and Conroy, 1980). 20-psi results are listed in Table 1 along with the computed true direct distance to the gob corner (end of the longwall face).

Support Can Loads

Loads on four 30-in-diameter yieldable standing support Cans located in a headgate gate-road intersection were measured with flatjacks (Figure 8). The data were treated in a fashion similar to BPCs to find load arrival distances (Table 2). Load resolution was 5.4 to 5.8 lb, depending on the flatjack diameter used (28 to 30 in). As before, a 9-point running average and an arbitrary load threshold that seemed to be above the noise and local effects (0.03 ton or 60 lb) were used. Given installation timing, there was much less opportunity to establish an equilibrium baseline before pressures began increasing. Still, load arrivals were judged to occur after 300 ft or more of face advance.

Ground Condition Mapping

Ground condition mapping is an attractive alternative to instrumentation, but can't be implemented with the precision or data frequency of instruments. However, it has the distinct advantage of being easy to conduct in any accessible mine entry. In this case, only those observations taken in the vicinity of the instrumentation sites are examined, and the inspection frequency was limited to when investigators were able to visit the mine site (Lawson, Zahl and Whyatt, 2012). The ratings range from 0 to 5, with 0 representing no deterioration and 5 representing complete failure, which implies that the entry has been rendered impassable. The rating system used is described more in the Appendix. The onset of loading was judged to occur when the ground condition rating of any of the roof, ribs, or floor exceeded an increase of 0.5. Given the paucity of inspections, a specific distance was not estimated. Rather, the interval "bracketing" this distance is reported (Table 3). Figure 9 and Figure 10 are plots of ground condition rating at the 1 North Outby and 2 North Outby instrument sites (see Figure 5 and Figure 6) with distance to the face. These also show while the floor appears unaffected by loading in 1 North, it is the roof that appears untouched by loading in 2 North. The bracketed distances at each site barely miss overlapping, as the minimum distance from the 1 North Outby site is only 10 ft larger than the maximum from the 2 North Outby site.

Adjusting to Equivalent Side-Abutment Load-Transfer Distance

The distance to an increment of mining induced stress increase depends on the location relative to the panel. This is illustrated in Figure 11 for the case study panel geometry, modeled without gate roads using LaModel. The base LaModel case used a thickness-weighted average rock modulus and lamination-thickness-wizard-determined lamination thickness of 443.3 ft, and provides pre-mining stresses according to distance from seam to surface. As noted earlier, the largest load-transfer distance for any contour is the side-abutment distance. Distances in all other directions are

Table 1. Distance from gob of first indication of load transfer at BPCs — method of 20-psi increase. 1 North was the tailgate and 2 North was the headgate.

1 North Outby site				2 North Outby site			
Instrument	**Lateral distance, ft**	**Distance along panel, ft**	**Net distance to gob corner, ft**	**Instrument**	**Lateral distance, ft**	**Distance along panel, ft**	**Net distance to gob corner, ft**
BP2	286	1430	1428.3	NP3	227.5	1469.5	1457.0
BP3	381	1599	1613.8	NP4	275	1451	1446.8
NP1	65.5	1556	1527.4	NP5	322.5	1362	1369.7
NP2	55.5	1599	1570.0	NP6	342.5	1451	1460.9
NP3	36.5	1533	1503.4	NP7	352.5	1387	1401.1
NP4	17.5	1533	1503.1				
NP5	7.5	1580.25	1550.3				
SP1	100.5	1448.75	1422.2				
SP2	110.5	1507	1481.0				
SP3	129.5	1500.75	1476.3				
SP4	148.5	1599	1575.9				
SP5	158.5	1556	1534.1				
		Average	**1515.5**			**Average**	**1427.1**
		St. Dev.	**58.2**			**St. Dev.**	**40.0**
		Average of both sites		**1471.3 ft**			

Depth of yield (*d* in equations 4 and 5), of 30 ft, was subtracted to obtain the net stress decay distance.

Table 2. Distance from gob of first indication of load transfer at support cans.

0.03-ton increase method			
Instrument	**Lateral distance, ft**	**Distance along panel, ft**	**Net distance to gob corner, ft**
I	364.3	846.5	891.6
H	374.0	961	1001.2
G	364.3	979.5	1015.1
J	374.0	953	993.8
		Average	**975.4**
		St. Dev.	**56.6**

Yield distance, which was subtracted to obtain the net distance, was 30ft.

Table 3. Distance from gob of first indication of ground condition deterioration at BPC line.

1 North Outby instrument site			2 North Outby instrument site		
Min/Max	**Distance along panel, ft**	**Net distance, ft**	**Min/Max**	**Distance along panel, ft**	**Net distance, ft**
Minimum	868	838	Minimum	128	98
Maximum	955	925	Maximum	858	828

Yield distance, which was subtracted to obtain the net distance, was 30ft.

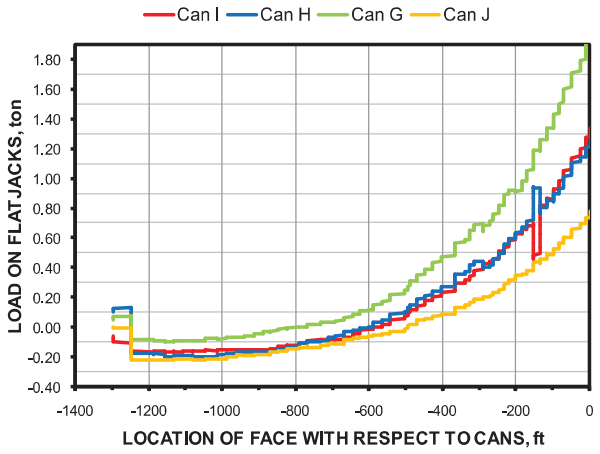

Figure 8. Load on support-Can flatjacks with distance of face to each individual Can. A negative location means the longwall face is inby the Can.

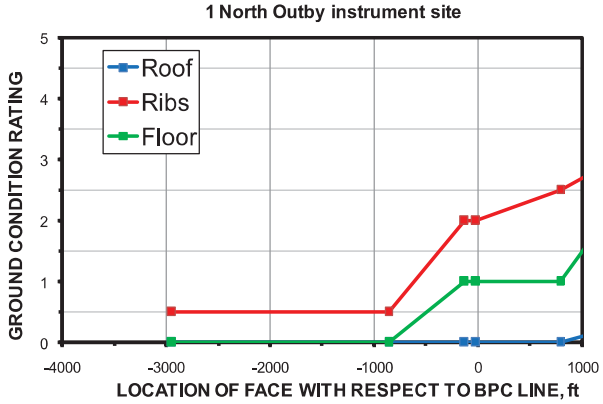

Figure 9. Ground condition of the roof, ribs, and floor at the 1 North Outby line of BPCs [after Lawson, Zahl, and Whyatt(2012), figure 5]. A negative location means the face is inby the observation location.

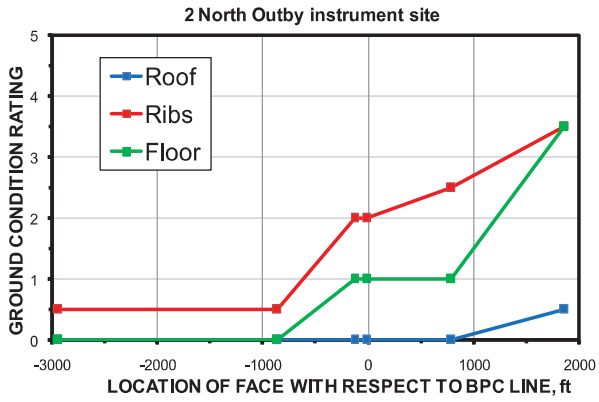

Figure 10. Ground condition of the roof, ribs, and floor at the 2 North Outby line of BPCs [after Lawson, Zahl, and Whyatt(2012), figure 6]. A negative location means the face is inby the observation location.

a fraction of this length. These fractions were determined for a threshold of 10 psi, which was then under consideration as the load transfer distance threshold, but the proportions are approximately equivalent for any threshold. As such, distances in these directions can be adjusted to equivalent side-abutment distances simply by dividing by this fraction. It was assumed that changes in overburden properties would proportionately affect all distances.

Figure 12 is a plot of these ratios with the angle from the corner for both the headgate and tailgate. The differences between the headgate and tailgate may arise from slight changes in overburden thickness, nearby variable topography, or some differences in roof lithology. However, the differences are not much. A 5th order polynomial function was fit to each set of data to easily relate net load-transfer distance for whatever angle is positioned an instrument to side-abutment load-transfer distance. Tables 4, 5, and 6 show the net distances, angles, and side-abutment distances calculated in this manner for distances determined with BPCs, those determined with instrumented support Cans, and those determined from ground condition mapping, respectively. Given the infrequent ground condition mapping that took place and looking at the results of both sites, a good estimate for side-abutment distance would be a range of 900 to 1000 ft, and a nominal value of about 960 ft.

CASE STUDY RESULTS

The case study provides three different estimates of load-transfer distance, determined by three different methods—BPC's (with three different stress-increase thresholds), support Can flatjacks and ground condition mapping. These estimates are summarized in Table 7 and can be compared to the default distance of 441.5 ft, derived with equation 1. The low standard deviations listed earlier (Tables 4 and 5) and a plot of the relative first response to transferred load, show that these estimates are independent, most likely illustrating significant differences between methods in sensitivity to transferred loads. These contrasts in sensitivity may be influenced by local features. For example, flatjack sensitivity is likely to vary with immediate roof structure and primary and secondary support. Still, the distance ratio, 20-psi BPC : flatjack : observation, of roughly 1.0 : 0.71 : 0.55 suggests how flatjack data and observation data might be adjusted to estimate transfer distances likely to be measured by BPCs.

However obtained, the BPC-load-transfer distances are clearly established as the reference measurements used in development of the calibration method. Thus, once a BPC measurement —or measurement estimate—is established, an effective value of H can be determined and inserted into the calibration equation (as outlined at the beginning of this paper). This procedure modifies the value of overburden stiffness, Et, by a calibration factor, also listed in Table 7. Distances obtained for support Cans and ground condition observations should be adjusted, as noted above, to provide similar results to BPCs.

Results for properties derived from the actual depth, H, and the calibrated or effective H, are illustrated in Figure 13 and Figure 14, along with measured load-transfer distances. In Figure 13, with member-thickness-weighted average of rock mass stiffness and wizard-determined lamination thickness, the 20-psi contour in the side abutment is found 565 ft from the edge of the yield zone in the next panel to be mined. This result is somewhat longer than

the empirical estimate of 441.5 ft, but it falls short of that distance determined with BPC measurements. Obviously, a drastic change in rock mass stiffness is required to bring the load transfer distance to the vicinity of the load-transfer distance measured with the BPCs. Calibration succeeded in moving the 20-psi contour in line with measurements (Figure 14). The minor shortfall likely reflects the fact that the calibration procedure neglects load transferred through the gob. As Heasley (2008, 2009; Heasley, et al., 2010) notes, rock mass stiffness calibration is only the first step in the calibration process, followed by gob stiffness and coal strength. Moreover, calibration may be conducted in an iterative fashion, depending on the precision desired.

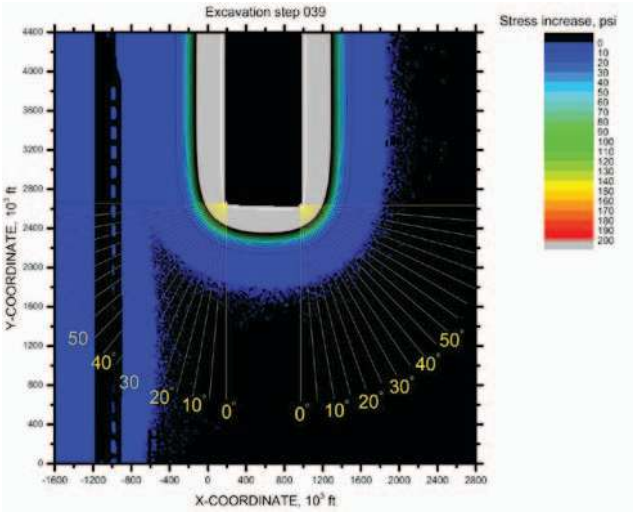

Figure 11. Color contours of increase in stress resulting from mining of panel. Lines at various angles from the corner of the gob (yellow) and edge of yield zones (white) are superimposed. This permitted easy measuring of load-transfer-distance factors.

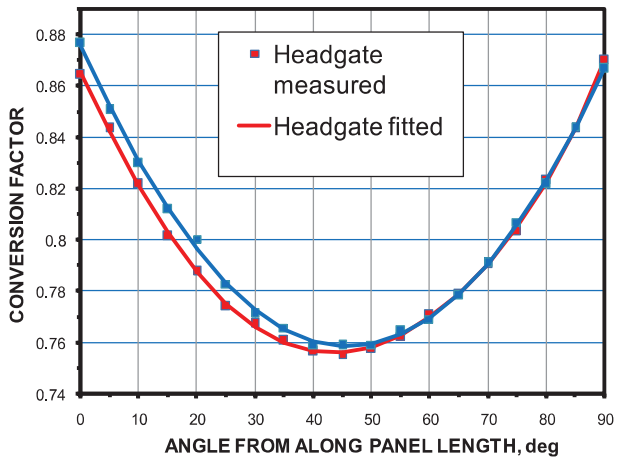

Figure 12. Ratio of load-transfer distance at various angles from gob corner to side-abutment load-transfer distance.

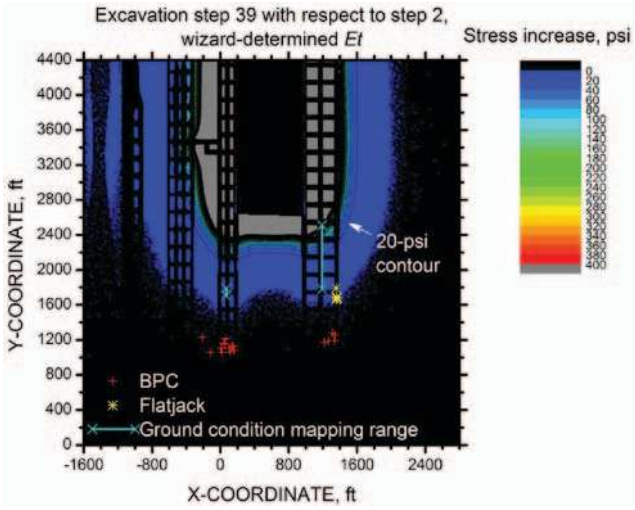

Figure 13. Contours of stress increase over pre-panel-mining stress for case of wizard-determined Et. Locations of first arrival of stress of BPCs, flatjacks on support Cans, and the ranges determined from ground condition mapping are shown.

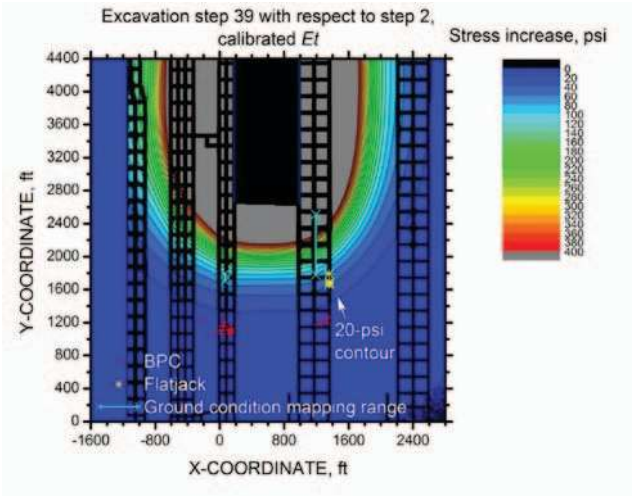

Figure 14. Contours of stress increase over pre-panel-mining stress for case of a calibrated Et. Locations of first arrival of stress of BPCs, flatjacks on support Cans, and the ranges determined from ground condition mapping are shown.

CONCLUSIONS AND DISCUSSIONS

A method for calibrating LaModel overburden stiffness using instruments and observations has been demonstrated with minor enhancements and extensions. The chief innovation to the method was to use an "effective" value for overburden depth (H) in empirical equations, allowing the first arrival of longwall stress to be integrated into Heasley's calibration equation. This method minimizes issues with interpreting borehole pressure cell data while allowing incorporation of other data types, including support Can loads and ground condition observations, in this case.

Table 4. Parameters calculated to obtain equivalent side-abutment load-transfer distance and effective H from BPC measurements using method of 10psi increase.

1 North Outby instrument site					2 North Outby instrument site				
Instrument	**Angle, ft**	**Factor**	**Equivalent side-abutment load- transfer distance, ft**	**Effective H, ft**	**Instrument**	**Angle, ft**	**Factor**	**Equivalent side-abutment load-transfer distance, ft**	**Effective H, ft**
BP2	13.40	0.818	1972.9	45004.8	NP3	8.80	0.826	1763.5	35958.1
BP3	2.41	0.864	1767.8	36134.1	NP4	10.73	0.819	1767.6	36124.6
NP1	1.99	0.866	1812.9	37999.4	NP5	13.32	0.809	1693.3	33151.6
NP2	1.36	0.869	1730.0	34605.9	NP6	13.28	0.809	1805.8	37700.8
NP3	0.65	0.872	1722.8	34315.6	NP7	14.26	0.806	1739.3	34976.8
NP4	0.27	0.874	1773.0	36345.3					
NP5	3.97	0.857	1660.1	31865.2					
SP1	4.19	0.856	1730.9	34638.7					
SP2	4.93	0.852	1732.1	34689.2					
SP3	5.31	0.851	1852.6	39681.2					
SP4	5.82	0.848	1808.2	37803.4					
SP5	11.31	0.826	1729.7	34593.7					
		Ave.	**1774.4**	**36404.1**			**Ave.**	**1753.9**	**35566.5**
		St. Dev.	**80.7**				**St. Dev.**	**41.4**	
Ave. equivalent side-abutment Load-transfer distance, ft					**1764.2**				
Average effective H, ft					**35984.1**				
NC = Not calculated									

Table 5. Parameters calculated to obtain equivalent side-abutment load-transfer distance and effective H from support can load measurements using method of 0.03-ton increase.

0.03-ton increase method				
Instrument	**Angle, ft**	**Factor**	**Equivalent side-abutment load-transfer distance, ft**	**Effective H, ft**
I	23.29	0.779	1144.5	15143.7
H	21.26	0.784	1276.9	18851.2
G	20.40	0.786	1290.7	19262.6
J	21.43	0.784	1268.1	18591.9
		Average	**1245.0**	**17922.6**
		St. Dev.	**67.7**	

This case study defined a 20-psi raw BPC pressure increase as a standard for calibration as it appeared to most resemble the resolution used in development of popular empirical relationships. However, this is a matter open to some debate and the choice of threshold pressure does have a significant impact on results. Distances were also computed for higher thresholds and other types of data (Can pressures and ground conditions observations). These distances ranged from two to four times the empirical standard, demonstrating the importance of method sensitivity and emphasizing that the load-transfer mechanics at the mine studied deviate significantly from the empirical standard. The relative distances produced by various methods are of particular interest. Results show a ratio of 1.0 : 0.71 : 0.55 (20-psi BPC : Can load : ground condition observation) between distance estimates by method. This ratio can be used to estimate the equivalent distance for our BPC standard from other measurements and observations. The ratio can also be used to plan instrument placement. For instance, ground observations might be used to determine how far ahead of the face support Can flatjacks need to be installed. In this case, the flatjacks appeared to be installed just in time, or possibly a bit later than ideal. However, further work is needed to determine how sensitive these ratios are to local conditions.

Calibration of the model was accomplished by adjusting the overburden stiffness (*Et*: elastic modulus times lamination

Table 6. Parameters calculated to obtain equivalent side-abutment load-transfer distance and effective H from ground condition mapping.

1 North Outby instrument site					2 North Outby instrument site				
Instru-ment	Angle, ft	Factor	Equivalent side-abutment load-transfer distance, ft	Effec-tive H, ft	Instru-ment	Angle, ft	Factor	Equivalent side-abutment load-transfer distance, ft	Effec-tive H, ft
Min	0	0.865	968.6	10847.5	Min	0	0.865	113.3	148.4
Max	0	0.865	1069.2	13216.8	Max	0	0.865	957.0	10590.2

Table 7. Listing of equivalent side-abutment load-transfer distance, their ranges, average calibration factors and average new rock modulus.

Instrument/Method	Equivalent $D_{1.0}$ load-transfer distance, ft			Calibration factor of average	*Et* with new rock modulus, psi•ft
	Average	Minimum	Maximum		
BPC, 20-psi increase	1764.2	1660.1	1972.9	15.969	1.66072E+10
BPC, 50-psi increase	1467.2	1295.0	1669.1	11.045	1.14869E+10
BPC, 100-psi increase	1216.3	796.5	1408.8	7.591	7.89396E+09
Support can, 0.03-ton increase	1245.0	1144.5	1290.7	7.887	8.20255E+09
Ground condition mapping	962.8	113.3	1069.2	4.717	4.90549E+09

thickness) in accord with a slightly revised version of Heasley's calibration equation. This calibration succeeded in bringing mining-induced stress estimates, in this case the 20-psi-increase contour, into close alignment with BPC measurements (Figure 14). There was a slight shortfall in the calibrated model distances, likely due to shifting of stress to gob areas which is not accounted for in the calibration equation.

The most significant result of this calibrated model is that load transfer distance estimates are significantly longer than that calculated with equation 1, (the empirical standard) at this deep western coal mine. The preferred 20-psi threshold for BPCs indicated a load-transfer distance roughly four times the empirical standard. Alternative thresholds and types of data indicated a range of distances, all between two and four times the standard. That is, all data and threshold definitions considered here indicate significantly larger load-transfer distances relative to the empirical standard. This will significantly impact pillar load calculations, suggesting that specific engineering design would be appropriate at this site.

Calibration by load transfer distance does not specifically address the shape of the load curve close to the gob. While knowledge of the load curve near the gob is highly desirable for purposes of mine layout design, that curve is highly affected by gob stiffness and seam strength, which are the next steps in the calibration process as outlined by Heasley (2008, 2009) and Heasley et al. (2010).

ACKNOWLEDGMENTS

The authors gratefully acknowledge the cooperation of Oxbow Mining Company and its engineering staff in this study. This work would not have been possible without the hard work of co-worker Eric Zahl and Oxbow employee Justin Evans in keeping the instruments and dataloggers operational. The expertise of Agapito Associates personnel in drilling and BPC installing the BPCs is gratefully acknowledged. The work of coworkers located in Pittsburgh installed and monitored support Can flatjack pressures and made this data available to us. The ground condition mapping was conducted by co-workers Heather Lawson and Eric Zahl; the authors gratefully appreciate their good work and providing that data.

APPENDIX — GROUND CONDITION RATING SYSTEM

The ground condition rating system used by Lawson et al. (2012) is reproduced here for convenience of the reader. Tables 8, 9, and 10 contain the descriptions of the rib, roof, and floor conditions rating criteria, respectively.

The findings and conclusions in this paper are those of the authors and do not necessarily represent the views of the National Institute for Occupational Safety and Health. Mentioning any company name, product or software does not constitute endorsement by NIOSH.

REFERENCES

Gates, R. A., Gauna, M., Morley, T. A., O'Donnell, J. R., Jr., Smith, G. E., Watkins, T. R., Weaver, C. A., and Zelanko, J. C. (2008). "Report of Investigation - Fatal Underground Coal Burst Accidents, August 6 and 16, 2007, Crandall Canyon Mine, Genwal Resources Inc, Huntington, Emery County, Utah." ID No. 42-01715, 2008, Department of Labor, Mine Safety and Health Administration, 472 pp.

Heasley, K., Sears, M. M., Tulu, I. B., Calderon-Arteaga, C., and Jimison, L. (2010). "Calibrating the LaModel Program for Deep Cover Pillar Retreat Coal Mining." In: *Proceedings: 3rd International Workshop on Coal Pillar Mechanics and Design*. Mark, C.,Barczak, T., and Esterhuizen, G. S. eds. (Morgantown, WV: July 26, 2010) Morgantown, WV: West Virginia University, pp. 47-57.

Heasley, K. A. (2008). "Some Thoughts on Calibrating LaModel." In: *Proceedings: 27th International Conference on Ground Control in Mining*. Peng, S. S., et al. eds. (Morgantown, WV: July 29-31, 2008) Morgantown, WV: West Virginia University, pp. 7-13.

Heasley, K. A. (2009). "An Overview of Calibrating and Using the LaModel Program for Coal Mine Design." In: *Proceedings of the International Workshop on Numerical Modeling for Underground Mine Excavation Design*. Esterhuizen, G. S., et al. eds. NIOSH Information Circular 9512, (Asheville, NC: June 28, 2009) Pittsburgh, PA: U.S. Department of Health and Human Services, pp. 63-74.

Heasley, K. A., and Sears, M. M. (2009). "Implementing Energy Release Rate Calculations into the LaModel Program." October 7, 2009, West Virginia University, Morgantown, WV, 50 pp.

Larson, M. K., and Whyatt, J. K. (2009a). "Critical Review of Numerical Stress Analysis Tools for Deep Coal Longwall Panels Under Strong Strata." In: *Preprints 2009: 2009 SME*

Annual Meeting & Exhibit and Colorado Mining Association's 111th National Western Mining Conference. Miller, H., et al. eds. (Denver, CO: February 22-25, 2009) Denver, CO: Society for Mining, Metallurgy, and Exploration, Inc., Preprint 09-011, 012 pp.

Larson, M. K., and Whyatt, J. K. (2009b). "Deep Coal Longwall Panel Design for Strong Strata: The Influence of Software Choice on Results." In: *Proceedings of the International Workshop on Numerical Modeling for Underground Mine Excavation Design*. Esterhuizen, G. S., et al. eds. NIOSH Information Circular 9512, (Asheville, NC: June 28, 2009) Pittsburgh, PA: U.S. Department of Health and Human Services, pp. 75-87.

Lawson, H., Zahl, E., and Whyatt, J. (2012). "Ground Condition Mapping: A Case Study." In: *2012 SME Annual Meeting, "Mine to Market: Now It's Global"* (Seattle, WA: Feb 19-22, 2012) Englewood, CO: Society for Mining, Metallurgy, and Exploration, Inc., Preprint, 9 pp.

Mark, C. (1990). "Pillar Design Methods for Longwall Mining." U.S. Bureau of Mines Information Circular 9247, 1990, 55 pp.

National Institute for Occupational Safety and Health (2010). "Research Report on the Coal Pillar Recovery under Deep Cover." Congressional Report. National Institute for Occupational Safety and Health, Pittsburgh, PA, 82 pp.

Peng, S. S. (1977). "Roof Control Studies at Olga No. 1 Coal Mine, Coalwood, WV." In: *Engergy Resouces and Excvation Technology: Proceedings, 18th U.S. Symposium on Rock Mechanics*. Wang, F.-D., and Clark, G. B. eds. (Keystone, CO: June 22-24, 1977) Golden, CO: Colorado School of Mines Press, pp. 1C3-1 to 1C3-6.

Peng, S. S. (2006). *Longwall Mining*. 2nd edn (Morgantown: West Virginia University), 635 pp.

Peng, S. S., and Chiang, H. S. (1984). *Longwall Mining* (New York: John Wiley & Sons), 720 pp.

Peng, S. S., and Park, D.-W. (1977). "Rock Mechanics Study for the Shortwall Mining at the Valley Camp No. 3 Coal Mine, Triadelphia, WV." U.S. Department of the Interior, Bureau of Mines Contract No. J0155125, West Virginia University, Morgantown, WV, 104 pp.

Skiles, M. E., and Stricklin, K. G. (2009). "General Guidelines for the Use of Numerical Modeling to Evaluate Ground Control Aspects of Proposed Coal Mining Plans." Mine Safety and Health Administration Program Information Bulletin No. P09-03, March 16, 2009, U.S. Department of Labor, 7 pp.

Vandergrift, T., and Conover, D. (2010). "Assessment of Gate Road Loading under Deep Western U.S. Conditions." In: *Proceedings: 3rd International Conference on Coal Pillar Mechanics and Design*. Mark, C.,Barczak, T., and Esterhuizen, G. S. eds. (Morgantown, WV: July 26, 2010) Morgantown, WV: West Virginia University, pp. 38-46.

Wade, L. V., and Conroy, P. J. (1980). "Rock Mechanics Study of a Longwall Panel." *Mining Engineering,* Vol. 32, (No. 12): pp. 1728-1735.

Pillar Design Considering the Plastic Behavior of the Coal Seam

Andre Zingano, Senior Lecturer
Depart. of Mining Engineering
University Federal of Rio Grande Do Sul
Porto Alegre, Brazil

ABSTRACT

The variation in pillar behavior at underground coal mines working in the Bonito coal seam is observed in both research and mining company case studies. There is no consistency in pillar behavior, as it varies from mine to mine. In some cases, it is possible to find rib yields for both excavation modes and pillar sizes. This paper's objective is to investigate pillar behavior for different load conditions and pillar sizes. Three-dimensional numerical simulation models considering these factors were built. A matrix was then assembled to compare pillar behavior between loading conditions, as well as between different pillar sizes with the same loading condition. The results showed some pillar rib plasticity due to vertical loading and stress relief independent of the pillar size and load. For the same load conditions, the yielding thickness is the same for different pillar sizes.

INTRODUCTION

Coal pillar design can be determined via two different approaches: analytical/empirical models, or 2D and 3D numerical models. For analytical and empirical models, the pillar design procedure takes into account the coal seam strength and overburden load (Salamon and Munro, 1963; Bieniawski, 1968 and 1974). The empirical methods assume that the strength of the pillar is constant for whole pillar. Wilson's analytical approach (1982) considered the host rock (roof and floor) interactions to determine the final pillar strength. Pillar rib yielding is not considered in empirical models, but it influences the final (or global) pillar strength. Salamon (1992) developed an analytical model based on plastic deformation of the pillar. These last two authors consider that the stress and strength are not the same for the whole pillar. The plastic behavior has been studied by many researchers (Peng, 2008; Morsy, 2003; Zingano et al., 2005), and all of these studies explained the rib plasticity and yielding behavior by numerical modeling, and they also suggested some pillar design. Zingano (2006) studied the effect of pillar rib reinforcement and shoed that the rib bolting has just a skin support.

Yielding or plastic behavior of a pillar rib is caused by one of three factors: (i) stress relief at the rib due to entry excavation; (ii) vertical stress concentrations at the pillar rib; and (iii) effect of the type of excavation (blasting or mechanical). The strain softening plastic portion around the pillar rib can reduce the global pillar strength and stress distribution. If the pillar fails or collapses, the plastic portion is more significant than the elastic portion. If the pillar has a small amount of plastic perimeter, it cannot be considered yielded or failed; it is only a skin effect that is caused by the issues listed above.

When faced with this kind of problem, some engineers normally increase the pillar width to try to reduce the plastic thickness at the pillar rib. They believe that the high vertical stress concentration was the cause of the pillar rib plasticity, due to the size of the pillar. However, increasing pillar size can reduce the plastic thickness around the pillar but will not eliminate this problem; this is because the stress relief will occur on any pillar size.

The coal pillar design for the Bonito seam has been studied since the 1990's (Zingano, 2002; Gonzatti, 2007), but some pillar failures and accidents during the last 15 years have exhibited pillar behavior (Zingano et al., 2004 and 2005). There are discontinuities in the coal seam including are cleats and two set of joints with dip ranging from 45 to 50°. These discontinuities in the pillar form blocks that slip during, or after, excavation. However, this process of block slippage is independent of the excavation mode. The ribs of the pillar exhibit plastic behavior with some spalling caused by the joints and blasting excavation. Similar behavior is observed with mechanical excavation however, with a lower intensity. Rib support with bolts and mesh is applied to avoid rock block slippage. Also, joints and cleats are responsible for the heterogeneity and the low strength of the coal seam (Zingano et al., 2010; Stein et al., 2011).

The stability of the entry is affected by the method of extraction in addition to the geomechanical properties of the coal measures. The method of excavation—blasting or mechanical—also has some influence on rib behavior, as indicated earlier. One more factor that will affect the rib yielding is the stress redistribution due to excavation.

The vertical stress will be concentrated, and horizontal stresses will be relieved at the pillar ribs. These redistributions will cause displacement of the pillar ribs. This displacement will cause some cracks around the pillar ribs. Figure 1 shows the cracks near the pillar rib; in this case, the cracks were caused by stress and

Figure 1. Cracks formed around the pillar rib due to blasting and stress concentration.

blasting. Therefore, the question is: how much does the stress contribute to plastic behavior and crack formations?

A matrix considering the pillar size and coal seam depth was created, and 3D numerical models were built for each matrix intersection (Table 1). The percentage of plastic behavior was estimated to determine if the pillar was (i) elastic, (ii) elastic/plastic or (iii) in plastic failure. The same matrix was created for the empirical pillar design model so the approaches could be compared.

The numerical models are a 3D intersection of two entries, where it is expected to have more plastic behavior at the pillar corners.

The decision whether the pillar fails or not is determined by the relative size of the on between plastic and elastic portions in the pillar. The pillar is considered failed if more than 20% of the pillar area exhibits plastic behavior. This criterion is considered for all pillar sizes, even for larger width-to-high ratio.

Table 1. Numerical models that were built, considering the pillar width and seam depth.

Pillar width (m)	Depth (m)								
	50	70	100	150	200	250	300	400	500
7	XX	XX	XX	XX	XX				
9	XX	XX	XX	XX	XX	XX			
12	XX	XX	XX	XX	XX	XX	XX		
17		XX	XX	XX	XX	XX	XX	XX	
20		XX	XX	XX	XX	XX	XX	XX	XX
23		XX	XX	XX	XX	XX	XX	XX	XX
30			XX	XX	XX	XX	XX	XX	XX
40				XX	XX	XX	XX	XX	XX

For the empirical approach matrix, the Salamon-Munro (1967), Bieniawski (1981) and ARMPS approaches were used. The minimum factor of safety of 1.5 was considered for pillar failure.

The material properties applied to both approaches are presented in Table 2. For the empirical approach, the coal strength was considered the same when comparing the results with the numerical model.

Table 2. Material properties for the rock mass for each layer.

Rock Type	Rock mass Young's Modulus (MPa)	Rock Mass Compressive Strength (MPa)	Cohesion (MPa)	Friction Angle (degree)
Arenito maciço	24,709.89	22.1	5.5	37
Arenito laminado	9,753.87	16.6	4.5	33
Carvão	2,241.38	5.2	2.0	20
Siltito da camada	1,241.38	5.2	2.0	15
Siltito do piso	17,837.51	10.18	3.0	29

Empirical Approach

The objective of this empirical matrix was to use the numerical modeling approach to show failure limits.

The pillar design considered the relation between its strength and load, represented by the tributary area (Peng, 2008). For pillar design in Brazil, the formula most often used is the Salamon-Munro (1967) approach, and the Obert-Duvall formula is also applied (Zorzi et al., 1993).

Three pillar design methods (i) Salamon-Munro, (ii) Bieniawski, and (iii) ARMPS – Analysis of Retreat Mining Pillar Stability was used for the analysis. Version 6 of the ARMPS program was used. The coal strength used was 5.2 MPa. The safety factor considered to be pillar failure was 1.5, as is recommended by most pillar empirical formula methods including ARMPS.

Table 3 shows the results for the three methods. The Salamon-Munro method is very conservative, and the ARMPS and Bieniawski methods gave quite the same safety factor. This is because 95% of cases were predicted to be successful with a SF>1.3 with the Salamon-Munro formula.

Numerical Model

To simulate pillar behavior for different widths and seam depths, 3D models were developed to simulate the pillar behavior in an entries intersection. The entries width was 6 m and the pillar height was 4 m. The pillar width used for each model only simulated one-fourth of the pillars (Figure 2). The numerical models consider the elastic-plastic materials based on the Mohr-Coulomb failure criteria.

Table 3. Factor of safety for the three empirical methods considered in this study: (i) ARMPS, (ii) Bieniawski and (iii) Salamon-Munro.

Pillar width (m)	Depth (m)								
	50	70	100	150	200	250	300	400	500
7	1.5/1.5/1.2	1.1/1.1/0.9	0.7/0.8/0.6	0.5/0.5/0.4					
9	2.1/2.2/1.7	1.5/1.5/1.2	1.1/1.1/0.8	0.7/0.7/0.6					
12	3.1/3.1/2.3	2.2/2.2/1.7	1.5/1.6/1.2	1.1/1.0/0.8	0.9/0.8/0.6				
17		3.4/3.5/2.4	2.4/2.4/1.7	1.6/1.6/1.1	1.2/1.2/0.8	1.1/1.0/0.7	1.0/0.8/0.6	0.9/0.6/0.4	
20		4.1/4.2/2.8	2.9/3.0/2.0	1.9/2.0/1.3	1.5/1.5/1.0	1.3/1.2/0.8	1.2/1.0/0.7	1.0/0.7/0.5	0.9/0.6/0.4
23		4.9/5.0/3.2	3.4/3.5/2.2	2.3/2.3/1.5	1.7/1.8/1.1	1.4/1.4/0.9	1.3/1.2/0.7	1.1/0.9/0.6	1.0/0.7/0.4
30			4.7/4.8/2.8	3.1/3.2/1.9	2.3/2.4/1.4	1.9/1.9/1.1	1.8/1.6/0.9	1.4/1.2/0.7	1.2/1.0/0.6
40				4.3/4.4/2.3	3.2/3.3/1.7	2.6/2.6/1.4	2.1/2.2/1.2	1.8/1.7/0.9	1.6/1.3/0.7

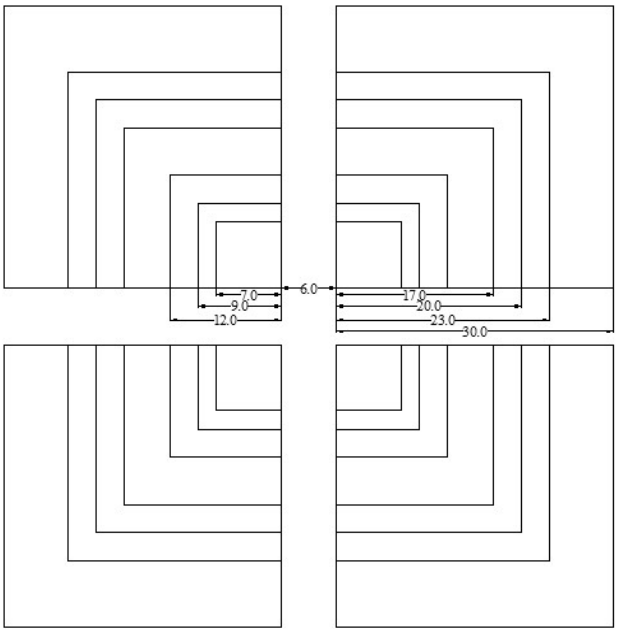

Figure 2. Geometry of the model for each pillar width.

The objective of these simulations by numerical models was to analyze the pillar stability based on the amount of plastic mode elements compared with the amount of elastic mode elements. The pillar is considered failed if the number of plastic state elements is greater than the elastic state elements.

The plastic elements are located at the pillar ribs and make a certain thickness around the pillar. If the plastic thickness is more than 20% of the pillar area, then the pillar is considered failed. The element size for all of the models was 0.5m. It is easy, then, to calculate the plastic thickness around the pillar and calculate the ratio between the plastic and elastic areas. In these models, the blasting effect was not considered, meaning that the excavation of the entries was assumed to be by mechanical methods.

The models were built considering the geologic sequence for the coal seam formation, including the floor and roof rocks. The floor is a siltstone layer and the immediate roof is a thin layer of laminated sandstone, overlaid by another layer of laminated sandstone and massive sandstone. Some interfaces were inserted between the coal seam and immediate roof, and also between the laminated sandstones layers. The initial load used a ratio between horizontal and vertical stress equal to one.

The excavation sequence was considered in the model. The first entry was completely excavated, after which the two crosscuts were excavated (Figure 3).

Table 3 shows the ratio and percentage between the plastic and elastic elements. It can be noted that there is a limit line between the stable and failure zone, and an interface between them (elastic-plastic zone) for pillar widths greater than17 m. The stable zones between Table 3 and 4 can be compared, and the limit lines for both matrixes are in almost the same position.

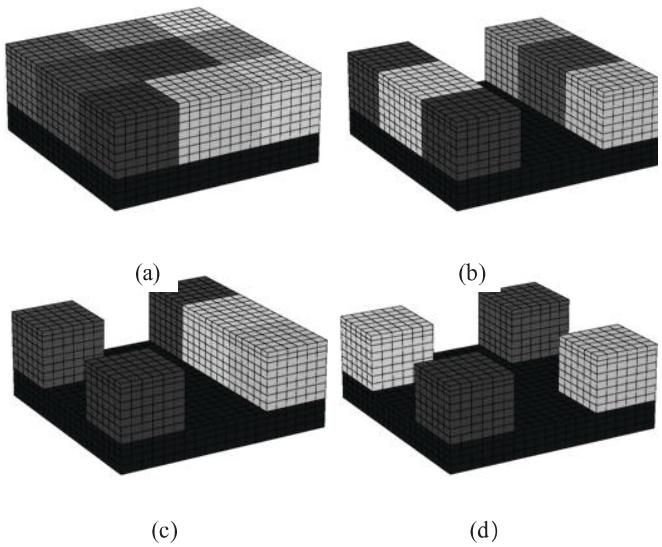

Figure 3. Excavation sequence for the model (a) before excavation – loading step; (b) excavation of the entry; (c) excavation of the left entry; and (d) excavation of the right entry.

Figure 4 shows the failure evolution of a 17 m wide pillar with increasing coal seam depth. It can be seen that the plastic zone thickness increases with the seam depth. This kind of behavior is expected because the vertical load on the pillar increases with depth.

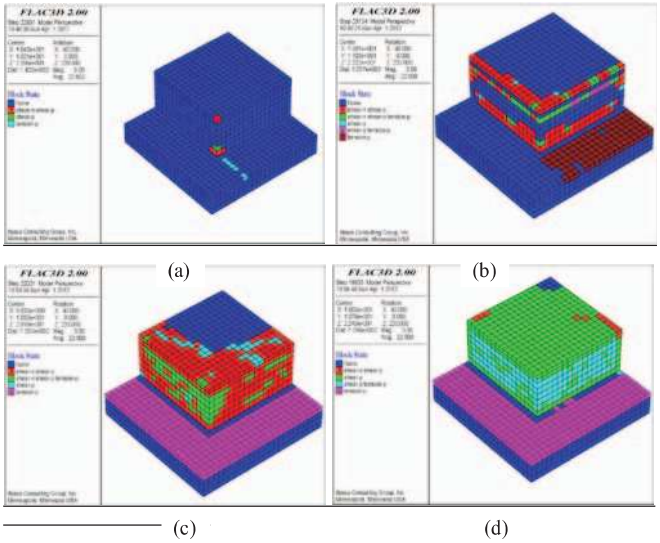

Figure 4. Plastic behavior evolution with increasing depth for 17m pillar width at (a) 70m, (b) 100m, (c) 150m and (d) 250m.

If the depth is held constant, one can see that the plastic zone around the pillar reduces a little bit as the pillar size increases. It reduces one or two elements, and also reduces that plastic percentage (see Figure 5). This behavior implies that the cause of the plastic behavior is stress distribution in the pillar and the stress relief due to excavation. For the 17 m pillar width, the plastic zone thickness is 3 m around the pillar corner. The plastic zone thickness reduces to 2.5 m for a 20 m pillar width, and to 1.5m for a 23 m pillar width. After that, the plastic zone thickness remains fairly constant.

Therefore, there is no reason to increase pillar size to reduce the plastic zone around it, but it is necessary to avoid rib spalling and block slipping from the rib and rib displacement.

CONCLUSIONS

This work met its objective because the numerical models showed that there is a plastic zone around the pillar, and this plastic zone thickness will depend to the load applied to the pillar.

At both matrixes, the areas are coincident. One can see that the yield area around the pillar does not decrease with increasing pillar width, which means that the plastic behavior is caused by the overburden load and by stress relief.

Before increasing pillar size to reduce the plastic zone, it is necessary to use some rib support or reinforcement to reduce rib displacement and avoid rib falling and block slipping.

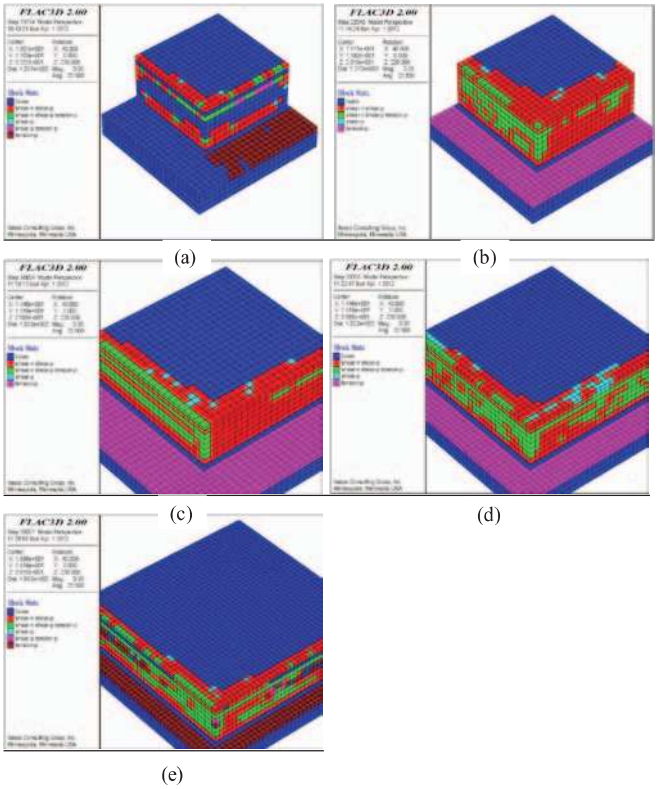

Figure 5. Plastic behavior evolution for the same depth (150m) and pillar size increase at (a) 17m, (b) 20m, (c) 23m, (d) 30m and (e) 40m.

REFERENCES

Koppe, J.C., Munaretti, E., Zingano, A.C. (2010).“Comparison between excavation methods for coal underground mining in Santa Catarina State” (in Portuguese). Internal Report.

Paludo, C., Dalmina, L., Martins, C., Zingano, A. C. (2008). “Blasting and vibration effect on the coal pillar ribs” (in Portuguese).*V Brazilian Underground Mining Conference, Belo Horizonte, setembro de 2008*.

Peng, S.S. (2008). *Coal Mining Ground Control*. Morgantown Printer, Morgantown, West Virginia, USA.600.

Salamon, M.D.G., Munro, A.H.A. (1967).*A study of the strength of coal pillar*s. J. S. African Institute of Mining and Metallurgy. 68. Johannesburg, África do Sul.55-67.

Stein, M., Guazzelli, S., Zingano, A.C., Koppe, J.C.(2011).“Study of mechanical behavior for Bonito Coal Seam” (in Portuguese). *III Brazilian Coal Conference*. Gramado, RS.

Zingano, A.C., Koppe, J.C., Costa, J.F. “Violent pillar collapse – a case study.” *23st International Conference on Ground Control in Mining*. Peng, Mark, Khair and Heasley, Eds. Morgantown, West Virginia, USA. August, 2004.

Zingano, A., Stein, M., Karas, R. (2010).“Methodology for mechanical behavior estimative to the roof-seam-floor layer in underground coal mining” (in Portuguese).*VI Brazilian Underground Mining Conference*. Belo Horizonte, september2010.

Zingano, A.C., Koppe, J. C., Costa, J. F. (2007). “Modeling barrier-pillar between coal mine sections” (in Portuguese). REM – Revista da Escola de Minas. 60:2, 219-226. Univ. Fed. Ouro Preto – MG, 2007.

Zingano, A. C., Koppe, J. C., Costa, J. F.(2006). “Pillar Reinforcement or Rib Support.”25thInternational Conference on Ground Control in Mining. Peng, Mark, Khair and Heasley, Eds. Morgantown, West Virginia, USA.347-353.

Zingano, A. C., Koppe, J. C., Costa, J. F. (2005). “Modeling the arc-effect of a coal mine roof.”24thInternational Conference on Ground Control in Mining. Peng, Mark, Khair and Heasley, Eds. Morgantown, West Virginia, USA.155-161.

Zingano, A.C. (2002). “Geomechanical characterization for coal pillar design” (in Portuguese). PhD dissertation. PPGEM – Univ. Fed. Do Rio Grande do Sul. Porto Alegre, Brazil. 220.

Zorzi, L., Agostini, I. M., Gonzatti, C.(1993). Suggested method for coal pillar design, Technical Bulletin n°23, CIENTEC, Porto Alegre, Brazil.

ARMPS (2010).Version 6.Centers for Disease Control-National Institute for Occupational Safety and Health, http://www.cdc.gov/niosh/mining/products/#Software

Gonzatti, C. (2007). “Proposta para a estimative da resistência a compressão uniaxial in situ de camadas de carvão com a utilização de geofísica” (in Portuguese). PhD dissertation. Universidade de São Paulo – São Carlos, 274.

Salamon, M. D. G. (1992). “Strength and stability of coal pillar”. In; *Proceedings of the Workshop on Coal Pillar Mechanics and Design, US Bureau of Mines, IC-9315.*94-121.

Bieniawski, Z.T. (1981).“Improved design of coal pillars for U.S. mining conditions.”*First Conference on Ground Control in Mining*. Peng, S., Ed. Morgantown, West Virginia, USA.13-22.

Bieniawski, Z. T. (1974) “Estimating the strength of rock materials”. *J. S. Afr. Inst. Min. Metall.*, **74**(8):312fr. I

Bieniawski, Z.T., 1968, ***The effect of specimen size on strength of coal***, Int. J. of Rock Mech. and Mining Sci., vol.5, pp.325-335

A Mine Evaluation Protocol Using Applied Rock Mechanics Techniques

Gary B. Petersen, Owner
Rock Mechanics Assist
Ishpeming, MI

Jay R. Nopola, Staff Engineer
Mining & Energy Engineering
RESPEC Consulting & Services
Rapid City, SD

ABSTRACT

The author has developed a seven-step process called the Applied Rock Mechanics (ARM) Protocol that the author has used to solve numerous roof stability problems in mines throughout North America since 1975. It is a practical evaluation process using trained observation, innovative data collection instrumentation, video borehole cameras, analytical processes, and controlled testing methods that have become highly effective in solving ground control problems in every type of underground mine. This paper will describe each of the steps of the protocol and how the rock mechanics engineer applies them to resolve a typical ground control problem.

INTRODUCTION

Every roof fall that takes a life is a tragedy. Perhaps the greater tragedy is that these events can be predicted, and therefore, loss of life or serious injury can be avoided. With proper application of the Applied Rock Mechanics (ARM) Mine Evaluation Protocol, ground control problems can be diagnosed and either resolved through support systems or an alteration to the mine design, or they can be allowed to fail in a safe and nondestructive manner. The ARM protocol can be a key aide to safe, productive, and profitable mining operations by eliminating unexpected roof falls like the one shown in Figure 1.

Applied Rock Mechanics, which has also been referred to in the industry as Practical Rock Mechanics, is a real-world approach to understanding rock behavior in mines. A well-trained applied rock mechanics engineer can be very effective in solving a wide spectrum of ground problem issue by using the ARM protocol presented here.

The applied approach to rock mechanics differs from, but is complementary to, the computational and numerical modeling approach. Significant advancements have been made to numerical modeling capabilities over the past decade. Nevertheless, modeling requires that certain assumptions of field conditions are made and remain consistent within the parameters of the computer model. As everyone in the mining industry is aware, however, field conditions are anything but consistent. Fractures, faults, inclusions, changes in crystalline structure, planes of weakness, water intrusion, and

Figure 1. Unexpected Roof Fall in a Limestone Mine.

any of a large number of other anomalies exist in the real world. Incorporation of all of these geological features within a numerical model is often impossible. Consequently, an accurate model needs to account for these features by making certain assumptions and allowances. Modeling can be helpful for generalized analysis of the problem but can be ineffective in dealing with the actual conditions in the mine.

As helpful as modeling is for a big-picture analysis, the applied approach finds its best application in the real world of actual mine conditions. For this reason, there is a fundamental difference between the two approaches. In the modeling approach, the analyst typically brings a set of rock specimens into the laboratory for the analysis of the material's properties, such as compressive strength, shear strength, creep, and stiffness. The results of those laboratory tests are used to infer rock properties that are then used in computer modeling calculations. A limited number of specimens are tested under ideal laboratory conditions. Even a well-developed testing program cannot account for all the possible variations of the actual rock in the field. In contrast to this, the applied approach is to treat the mine itself as the "laboratory." In this way, every observable parameter can be taken into consideration in the analysis under actual, not ideal or approximated, conditions. To put it another way, whereas the modeling based approach is beneficial in analyzing the

mine before its construction, the applied approach is the necessary in assessing conditions in the mine once mining has begun. If used correctly the two approaches can be complimentary to each other.

Functioning from this paradigm of viewing the mine as the laboratory, the applied rock mechanics engineer spends most of his time in the mine rather than in the laboratory or office. The engineer carefully observes the mine's geometry and geology and uses relevant instruments to measure rock deformation and to locate possible failure epicenters. For example, to determine the performance or stability of a questionable site in the mine, extensometers may be installed in the roof and pillars, and roof-to-floor closure stations may be installed in the rooms. The data collected from these instruments not only provide total deformation, but also the rate of deformation. A study of the plots of these data will indicate whether the roof and/or pillars are in a stable state or if they are headed toward failure.

Once the evidence is collected and the data is analyzed, the applied rock mechanics engineer then determines what the various problems may be. This analysis may involve additional numerical modeling that incorporates the field data. This information allows the mine management and the appropriate production personnel to make informed decisions on possible corrective actions based on real mine-generated data. Options may include installing a support system, removing the failing rock, or abandoning and barricading the affected area. Following a thorough discussion and review by all involved parties, an agreement is reached on a course of action.

As often occurs, if the plan involves a mine design change, a test site is chosen in a safe location and the recommended design change is implemented. Suitable instrumentation is installed to perform ongoing observations and measurements so that the results can be compared with the previous design to ascertain if the revised design sufficiently resolves the problems. The applied rock mechanics engineer observes and monitors on an ongoing basis so he can learn from the results and make continual improvements.

DESCRIPTION OF THE 7-STEP APPLIED ROCK MECHANICS (ARM) PROTOCOL

Having discussed the benefits of the ARM approach and the overview of how the applied rock mechanics engineer accomplishes the tasks, the entire protocol is presented here step-by-step.

1. Making Observations

A trained rock mechanics engineer can learn much by walking around the mine making observations. When assessing ground conditions, it is a matter of the good, the bad, and the ugly. It is important to look at the good conditions, the bad conditions, as well as the ugliest locations in the mine to see what is revealed about the geomechanics. In almost every case, the clues to bad ground conditions are observable in the mine. It is a matter of looking in the right places. The trained rock mechanics engineer will observe why the ground is so good in one place in the mine and so bad in another. The answer to this question is a key part to the solution, and the primary method of determination is through specific, trained observation.

2. Mapping Ground Conditions

Next, the observations are put on a mine map to reveal patterns or trends. Failure patterns are important pieces of information that directly shed light on the potential solution. There are two categories the rock mechanics engineer is looking for: geological features and rock failures.

Mapping geological features, such as joints, faults, discontinuities, anomalies, rock types, and bedding, are critically important to the rock mechanics engineer, especially those features that appear to have an effect on ground conditions. For example, vertical jointing may not be as detrimental to ground conditions as non-vertical jointing. That being the case, the non-vertical jointing should be highlighted in the mapping process. Using the room-and-pillar grid for placement, linear features are mapped. Magnetic north and map north are noted. In addition, photographs can be effective for estimating the approximate dip as exact surveys, and dip measurements may not be needed.

Mapping rock failure is crucial in determining the failure mechanism. The failure mechanism is a composite of all the factors (geological and stress) that contribute to the failure and some factors are more problematic than others. On the map, all factors are identified and assessed from most problematic to least. Rock failure types that should be mapped are roof falls, roof shears, cutters, guttering, buckling of the roof or floor, tension fractures, offsets in roof holes, crushing or rock flour, and roof potting. These features should be mapped as accurately as possible, showing both direction and magnitude. For example, in a roof fall, the shape of the fall, height of the fall, and any predominant direction of the fall are shown. Mapping several roof falls in an area will begin to show commonality among the falls, as shown in Figure 2. Although not normally necessary during the initial mapping phase, highly accurate three-dimensional (3D) surveys of the falls are possible using various technologies such as LIDAR (Light Detection and Ranging).

The goal of the mapping is to give the rock mechanics engineer a sense of the predominant damaging stress component(s) and whether it may be vertical overburden stress or horizontal tectonic stress. The tendency of most mining personnel is to think that rock failure is primarily caused by vertical overburden loading; however, in our experience, high horizontal stress is frequently the problem. Some signs of high horizontal stress issues are roof shears, cutters, guttering, buckling of the roof or heaving of the floor, offsets in roof hole, crushing or rock flour, roof potting, and elliptical-shaped roof falls, to name the most frequently observed [1]. Other things to map are mining geometry such as large intersections, entry orientation, extraction, pillar dimensions, room heights, as well as things like the type of support systems installed and where the support is taking load. The rock mechanics engineer should map all of the pertinent data to begin formulating a picture of the stresses involved, as shown in Figure 3.

3. Borescoping Roof Holes

With the introduction of high-resolution, close-focus mini-cameras over the last decade, borehole video cameras, like the one shown in Figure 4, have become an indispensable tool in the rock mechanics engineer's information-gathering process. This technology allows the rock mechanics engineer to visually observe

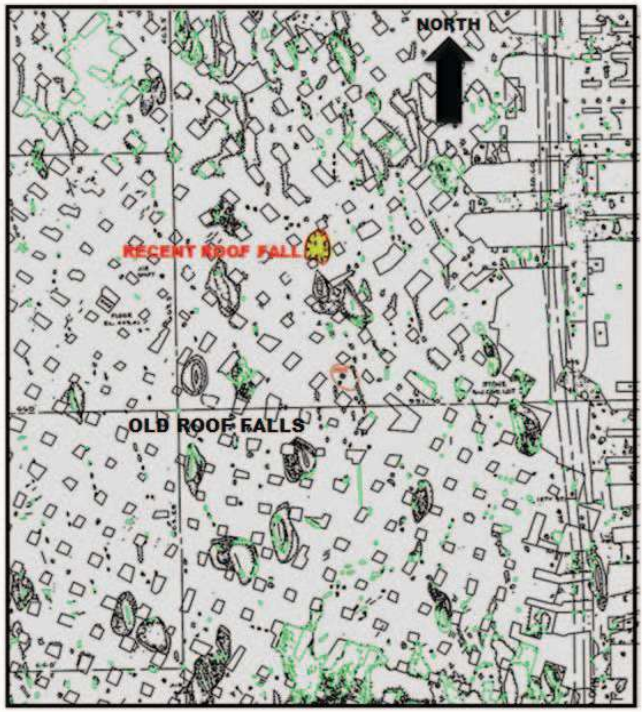

Figure 2. Example of Mapped Roof Falls Exhibiting a Pattern of Elliptical-Shaped Falls With the Long Axis in the North/South Orientation, Indicating the Principal Horizontal Stress Direction is East/West.

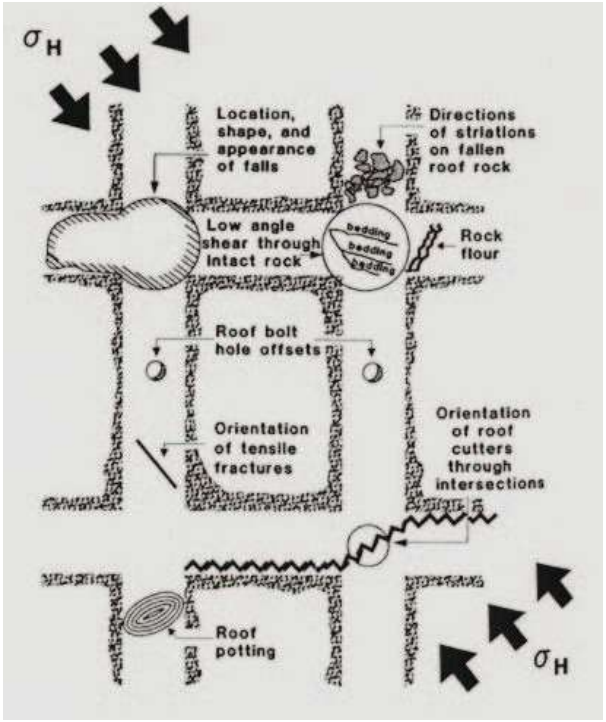

Figure 3. Stress Mapping Features [Mucho and Mark, 1994].

in real time the integrity of the rock in the roof beam, as shown in Figure 5. Roof holes are drilled and cleaned with water or brushes and the camera head is inserted in the hole using an insertion rod with distance marks. The camera can scope holes tens of meters long but are most commonly used in holes about 3 to 7 meters above the roof.

The camera head is designed to enable a 360-degree view at the wall of the roof hole. The image is displayed on a monitor screen and can be recorded with narration and viewed later on a computer or other video device. The files are also archived for future reference. The engineer makes notes and observations on a scaled template of the roof hole during the scoping process.

In addition to using the borescope to gather data for the long-term analysis of ground stability, the rock mechanics engineer can also use the camera to evaluate the geology and potential for stressfailures at the mining face. By scoping roof holes near the mining face, the engineer can gather data to determine whether or not the roof rock is favorable or unfavorable geology. In many cases, when a mine experiences an unexpected roof fall, it is because the geology in the roof changes as the face advances and the miners have been unaware of the change. The camera allows the engineer to immediately recognize weaker geology in the roof rocks and appropriate corrective action can be taken; for example, adjusting the roof support system to accommodate for the new conditions.

Figure 4. Borehole VideoCamera Used in Scoping Roof Holes.

Figure 5. Scoping Roof Holes in a Salt Mine.

The borescope allows the engineer to efficiently view how the roof beam reacts to mine-induced stresses by scoping holes back from the advancing face where the pillars and roof beam come under full loading conditions. The camera shows the engineer if separations or fractures, as shown in Figures 6 and 7, have developed in the roof beam along with their locations. If the engineer finds fractures or separations close to the mine roof, this is a cause for immediate concern and action, especially if the roof is not mechanically supported. Fractures or separations found higher up the borehole are especially a concern if they are above the bolt anchorage. Logging these locations, as shown in Figure 8, is highly effective in assessing roof performance and stability and, therefore, in predicting and preventing roof falls.

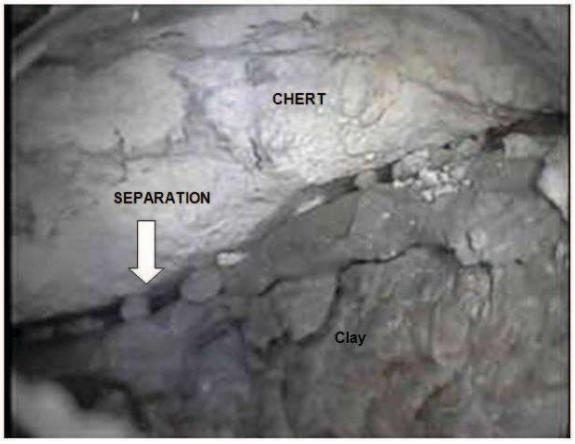

Figure 6. A View From the Borehole Camera Showing a Separation Associated With a Change in Roof Geology.

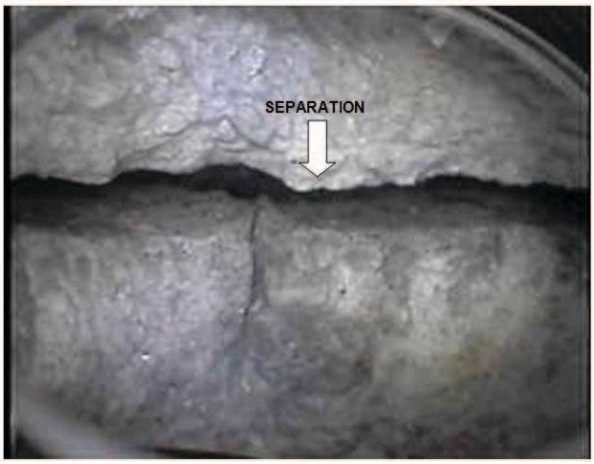

Figure 7. A View From the Borehole Camera Showing aSeparation in the Roof Rock.

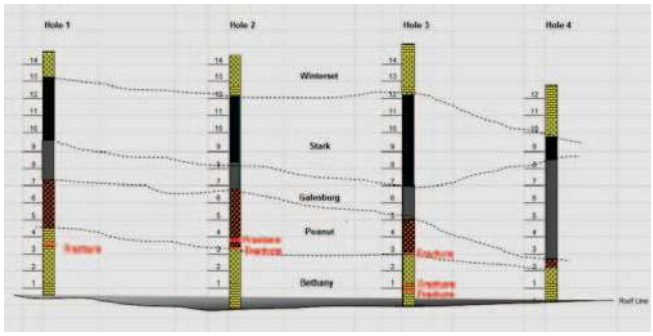

Figure 8. An Example of a BoreholeLog Showing Information Obtained by the Borehole Camera. The log shows changes in geology and roof fractures.

The borehole camera, when properly used, is a valuable tool in numerous ways because it allows the rock mechanics engineer to see into the rock of the roof or pillar. The information allows the engineer to assess the geological conditions and stress failures in the roof rock as a significant part of evaluating the stability of the roof. This is a valuable tool for examining the roof rock in areas of higher exposure to mining personnel in locations such as underground shops, warehouses, offices, lunchrooms, other gathering places, and travelways. If the camera results indicate possible issues with the roof beam, roof monitors can be installed to measure the stability.

4. Installing and Monitoring Instruments

Following initial observations, mapping, and bore scoping, the applied rock mechanics engineer will determine the types of the instruments and placement locations best suited to reveal the additional information needed to properly diagnose the particular mine's roof stability issues. For example, imagine the engineer examines the borescoping data and sees some fracturing

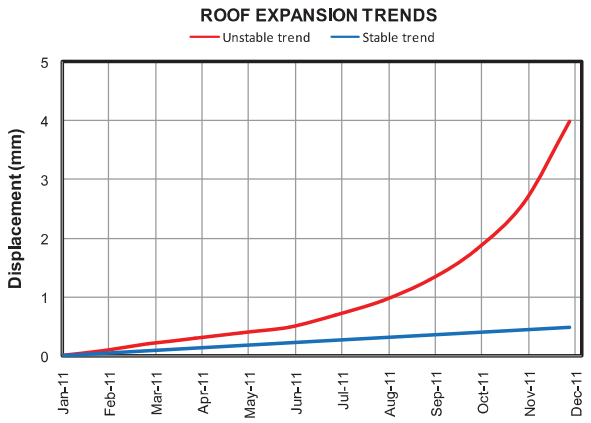

Figure 9. An Example of a Stable and Unstable Trend Based on Roof Extensometer Readings.

occurring in the roof beam. Roof extensometers are then installed for continuous monitoring of the sag of the roof, and the data are plotted on a graph similar to Figure 9. Examining the graph over time, the engineer can determine if the roof is in a stable or unstable condition, in addition to how fast the instability is progressing.

Roof-to-floor closure measurements are typically performed by installing anchor points in the roof and floor and measuring the distance between the points with a portable closure rod. The convergence rod method results in much higher accuracy and consistent data tracking over time than the easier laser distance-measuring devices used by some technicians. In less traveled areas where an instrument can be left in place, roof-to-floor measurements can be made using relatively inexpensive telescoping rods and a dial gage, as shown in Figures 10 and 11.

In accumulating the needed data for analysis, an applied rock mechanics engineer who is intimately familiar with a mine site can take a more effective approach to the instrumentation of his "laboratory". For example, the field engineer is more likely to make many simple, less expensive measurements rather than a few more complicated, expensive measurements. Additionally, he is likely to leave his instruments installed over a long period of time to track the changes over time. The rock mechanics engineer is also likely to measure strain rather than stress because it is much easier and more reliable, and the rate of strain or deformation is a good predictor for instability and rock failure. The most commonly used instruments are roof and pillar extensometers and roof-to-floor closure meters. In addition, some of the roof extensometers include a safety-warning flag feature that drops a reflectorized rod which is suspended from the roof if excessive roof expansion occurs. This simple feature has alerted miners that the roof is moving and evacuation of the area is necessary, saving a number of lives.

5. Compiling and Analyzing Results

Step 5 is when the rock mechanics engineer compiles the information and data to define the root causes of the problems and identifies the failure mechanisms. The mapped observations, photographs, borescope logs, and data from the instruments are

Figure 10. Roof-to-Floor Closure Station Left in Place in a Remote Area of a Salt Mine.

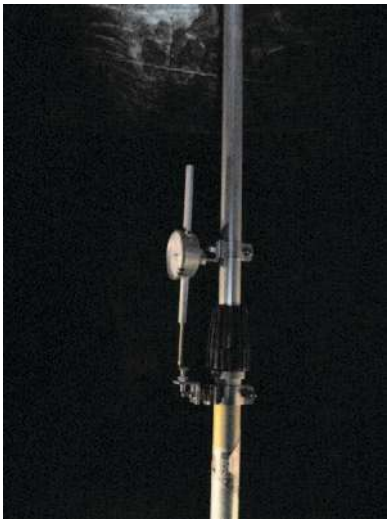

Figure 11. A Dial Gauge and Telescoping Rods Are a Simple Way to Get Very Accurate Closure Measurements. .

analyzed and conclusions are drawn about the possible causes. Many factors are considered, including the effects of mining direction, blasting procedures, water, weak geology, room width, pillar size, and horizontal stress, to name a few. Occasionally, this step raises new questions and identifies additional data needed. If necessary, the engineer may repeat some of the first four steps of the ARM protocol. The data and preliminary conclusions are then prepared for presentation to the key stakeholders.

6. Implementing the Solution

Once the root causes of the problems are well defined, the process of defining and implementing the solution occurs. The engineer then begins the process of communicating with the key stakeholders in the organization to keep everyone fully informed. The group examines the problems and failure mechanisms involved and a solution is agreed upon. This process may include members

of mine management, production personnel, and safety people. If the problem is major enough, the engineer may recommend that a team of outside experts be assembled to help develop the solution.

Once a solution is agreed upon, if applicable a test site can be chosen for testing the intended solution and to determine whether the recommended changes will yield the intended result. If the recommended change is significant enough, then the test could be run in an appropriate area of the mine so that if the test does not work as planned, the mining process will not be disrupted. For example, it is not recommended that a significant mine design change be implemented over a large area of the mine without first testing it in a designated test location.

7. Follow-up Assessment of the Implemented Changes

Once the change has been implemented in a controlled setting, the results will be measured and compared to the results before the change. Steps 1 through 5 of the ARM protocol are implemented in the test area to determine the success of the proposed solution. Questions such as "Did the new design solve the problem?" and "Can it be improved on?" are asked throughout the test period. The tested result is then implemented throughout the affected areas in the mine followed by ongoing monitoring and then repeating whichever steps of the protocol are indicated to test and verify that the solution is indeed solving the problem.

TYPICAL IMPLEMENTATION OF THE PROTOCOL

Now that steps 1 through 7 have been described, the following discussion is a typical approach an applied rock mechanics engineer might take in response to a request to evaluate a section of the mine for potential roof falls. The engineer would first go into the mine and observe how the ground is behaving while speculating about potential failure mechanisms. The engineer views the pillars as the rock specimens and the overburden pressure on the pillars as the load frame. The rock specimens (pillars) are all sizes and shapes with their natural flaws. The engineer starts by measuring pillar heights and widths. It is noted that the mine plan calls for 12-meter-wide pillars, but after blasting and scaling, the pillars are closer to 11 meters wide. This means the room widths are wider than specified, which is confirmed by taking measurements. The engineer also notes what effect that extra room width might have on the integrity of the roof beam.

The engineer then borescopes some roof holes, which reveal that the roof beam is sagging and bed separations are developing. To determine how much the roof beam is deforming, the engineer installs roof extensometers and roof-to-floor stations, taking and recording a baseline measurement. Continuing his observations, the engineer notices some peculiar geological features and starts sketching them on a mine map. The engineer then communicates with the miners familiar with that location to learn that the ground has been occasionally making snapping noises in several locations and the pillars are scaling more than usual in that section. This information tells the engineer more about the problem that needs to be identified and adds that information to his mine map.

After analyzing the collected data, it is determined that although the likelihood of an immediate failure is remote, the instrumentation shows more movement is occurring than historical levels, and continuous monitoring is needed to determine the long-term stability of the area. The appropriate people are notified.

CLOSING REMARKS

Mine roof collapse can be predicted by using a proper application of the Applied Rock Mechanics (ARM) Mine Evaluation Protocol. The ground control problems that cause these collapses can be diagnosed and avoided either by appropriately designed roof support systems; an alteration to the mine design; or, if necessary, they can be either allowed or forced to fail in a controlled and safe manner. The benefits of the ARM protocol to the industry in miner safety and in preventing economic loss are numerous and significant.

Unfortunately, the practice of Applied Rock Mechanics appears to be becoming increasingly rare. The mining industry is facing a clear shortage of professional mining people because of a deficit between newly trained entrants to the industry and the older generation headed toward retirement [2]. This trend is compounded when it comes to applied rock mechanics engineers as the focus in both academia and in the industry over the last couple of decades has been on the development of the computational/modeling approach to rock mechanics.

Most of the mining engineers who are currently being trained are only learning the modeling approach. As a result, the underground mining industry is rapidly losing the science, and in some ways, the "art" of Applied Rock Mechanics. Although the modeling approach is valuable, both are needed. Only the applied approach can accomplish the in situ real-world analysis necessary to predict and prevent roof falls and other types of rock failure to a high degree of success. Furthermore, the incorporation of the field observations of the applied rock mechanics into numerical modeling will increase the effectiveness of these models. Unless there is a change in this trend, the industry will lose a very effective method in solving ground control problems.

CONCLUSION

The Applied Rock Mechanics (ARM) protocol is an effective method to evaluate ground conditions in an underground mine, identify the root cause(s) or potential problems, and develop an effective solution. It is a direct and practical approach to understanding and solving ground control problems, making these problems more predictable and avoidable by proper application of support systems, altering the mine design, or allowing failure in a safe manner. The ARM protocol and similar approaches are needed in industry for safe, productive, and profitable mining operations. The industry would do well to engage the principles of Applied Rock Mechanics to work with common modeling practices, bringing together the best of both worlds to benefit all underground mining operations.

REFERENCES

Mucho, T.P. and C. Mark. 1994. Determining horizontal stress direction using the stress mapping technique. 13th Conference on Ground Control in Mining 1994.280–281.

Hill, L. 2011. Skills crunch looms again as mining firms vie for talent. Mining Weekly.com June.

Post–Collapse Seismicity of the Crandall Canyon Mine Using Double Difference Relocations

Tex M. Kubacki, Ground Motion Analyst
University of Utah Seismograph Stations
University of Utah
Salt Lake City, UT

Michael K. McCarter, Professor
Mining Engineering
University of Utah
Salt Lake City, UT

Kristine L. Pankow, Research Assistant Professor and Assistant Director
University of Utah Seismograph Stations
University of Utah
Salt Lake City, UT

ABSTRACT

In 2007, the University of Utah Seismograph Stations (UUSS) temporarily expanded its seismic monitoring network in Emery County, Utah, in response to the August 6 Crandall Canyon mine collapse that trapped six workers. In spite of this additional coverage, no seismic events were located in the area during a six-day period (gap) from August 8 to August 13. The Mine Safety and Health Administration (MSHA) "Command Center Log Books" however, contain references to 16 instances of underground "bumping" and "bouncing" that occurred during the gap. When ground truth information provided by the log books is compared to the raw seismic data recorded by the UUSS network, the correlation offers insight into the chronology of mining-induced seismicity (MIS) in the aftermath of the collapse. The new research focuses on identifying and locating seismic events that occurred during the six-day gap using double-difference relocation techniques and correlating them with log book ground truth. Ten seismic events were identified in the vicinity of the mine during the six-day gap, ranging in magnitude from coda magnitude (M_C) 0.5 to 1.4. Three of these events were amenable to location by double-difference techniques. The location of one of these events is directly confirmed by ground truth information from the log books. As a result of this new research, the accuracy of Crandall Canyon double-difference locations has been improved, and the number of events correlated with ground truth information has increased. The seismic events occurring in and around the collapsed area appear in two distinct sections of the mine—east and west of the center of collapse. It was originally reported that the post-collapse events occurred in episodic clusters. The first two episodes occurred to the east, followed in time by a cluster on the west, and then by a third episode on the east. With the addition of new events to the data set, this pattern is no longer as clear, although the events still occur in clusters. Only one MIS cluster was found to occur within the bounds of the minimum estimated collapse area (Pechmann et al., 2008).

INTRODUCTION

At 2:48 AM MDT on August 6, 2007, a 4.5 coda magnitude (M_C), 3.9 local magnitude (M_L), mining-induced seismic event accompanied a collapse (Pechmann et al., 2008) that trapped six mine workers 2,000 ft underground (MSHA, 2007) at the Crandall Canyon bituminous coal mine located in Emery County, Utah. Shock waves from this event and others occurring in the same area and time-period were recorded by the seismic monitoring system of the University of Utah Seismograph Stations (UUSS). In response to the M_C 4.5 mainshock, UUSS installed a temporary network of five portable surface stations from August 7 to August 9 in close proximity to the mine (as shown in Figure 1) to increase seismic network coverage and achieve better locations. By August 13, data from three of the temporary, short-period, vertical component stations were integrated into the UUSS automatic detection system (Pechmann et al., 2008). In spite of this increased effort at seismic monitoring, no events above the calculated minimum magnitude of completeness (M_C 1.6) were located by the UUSS via routine data processing during a nearly six-day period (gap) from August 8 until August 13 (Pechmann et al., 2008; Warner et al., 2009).

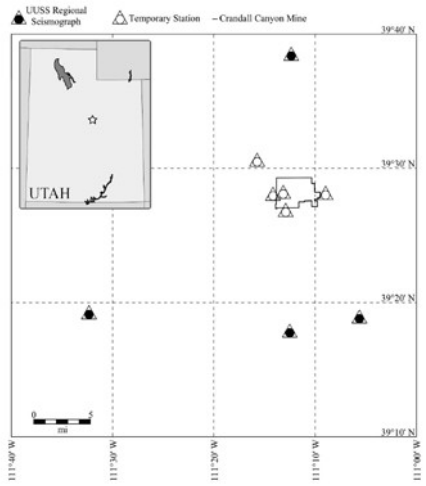

Figure 1. Map of UUSS regional and temporary monitoring network in relation to the Crandall Canyon mine as of August 2007.

During the ten days following the collapse, a continuous miner was deployed to clear the entries in an attempt to reach the suspected location of the trapped workers. At 6:38 PM MDT

on August 16, an M_C 2.0 (M_L 1.6) rib-burst at Entry 1, Crosscut 127, fatally injured three rescue workers and put an end to any further attempts at recovering the six trapped mine workers (MSHA, 2007).

The research presented here offers a revised and more complete study of the MIS that occurred at the Crandall Canyon mine during August 2007. Seismic data have been used to locate MIS that occurred during the six-day gap, providing a better understanding of the chronology of mining-induced seismicity (MIS).

PREVIOUSLY LOCATED EVENTS

To better understand the nature of the MIS at Crandall Canyon, a catalog of 189 events located within a 1.9-mi radius of the mine and dating from August 2, 2005, to August 27, 2007, was compiled. This catalog was limited to those events that had been located according to the routine earthquake location procedures of the UUSS (Pechmann et al., 2008).

In order to refine the automatically calculated locations of the previously defined catalog, the events were first relocated using a Master Event method in which arrival times were adjusted by station delays calculated from the three largest events that occurred after the temporary network was installed. The station delays correct for errors in the velocity model (Pechmann et al., 2008). To further refine the results, the events were relocated a second time using a double-difference method (hypoDD) (Waldhauser and Ellsworth, 2000). This method involved using travel time differences for paired events recorded at the same station to invert for relative locations (Pechmann et al., 2008; Pankow et al., 2008). These relative locations were then shifted by a fixed distance such that the location of the fatal August 16 rib-burst coincided exactly with its known ground truth location (39.4670°N, 111.2170°W) (Pechmann et al., 2008; MSHA, 2007). Due to a feature of the double-difference software that removes events from the inversion if in any iteration the depth becomes less than zero, only 150 of the 189 events could be relocated (MSHA, 2007; Waldhauser and Ellsworth, 2000).

In addition to the events included in the master event catalog, a subsequent study (Warner et al., 2009) led to the identification of 35 seismic events below the minimum magnitude of completeness that occurred in the area of interest during the six-day gap. These events, ranging from M_L 0.1 to 1.4, could not be precisely located via automated procedures because of their low magnitudes; however, relative east/west locations were determined in relation to 111.2179°W, the estimated center of collapse (Pechmann et al., 2008; Warner et al., 2009).

DATA SET

Station Data

Station data for events previously located and reported by the UUSS have been processed according to routine earthquake location procedures. Figure 1 shows the locations of several of the seismic recording stations in closest proximity to the mine. Continuous seismic waveforms from these and other nearby stations were requested from the Incorporated Research Institutions for Seismology (IRIS) Data Management Center for times corresponding to 16 events reported in the MSHA "Command Center Log Books," as well as for the larger (M_L > 0.9) events identified by Warner et al., 2009. The waveforms were examined and P- and S-wave arrival times and coda magnitude durations were determined using UUSS routine data analysis software.

Ground Truth

Crandall Canyon's management kept several log books during the routine mining operations that took place before the collapse. These log books include the "Production Report" and the "Shift Foreman's Report" (MSHA, 2007). An additional set of MSHA "Command Center Log Books" detailing the rescue attempt were also kept (MSHA, 2007). Entries in these log books provided researchers with ten ground truth locations for various "bumps" and "bounces" (colloquial terms referring to seismicity experienced in underground coal mines) (MSHA, 2007) that could be directly correlated to seismic events relocated via double-difference method in the original analysis (Pechmann et al., 2008).

As reported by MSHA, the average error between the ground truth locations reported in the log books and the double-difference locations calculated from the master event catalog was approximately 450 ft (MSHA, 2007). This average does not include the fatal event used to shift the locations by a fixed distance, as the error for that event is forced to zero (MSHA, 2007).

In addition to the ten ground truth locations used in previous studies, further review of the "Command Center Log Books" kept during the six-day gap uncovered references to 16 cases of bumps and bounces, resulting in seismic events that were not automatically located by the UUSS. These cases represent 16 ground truth instances that have gone previously unexamined. They indicate that the six-day gap was not truly void of seismic activity.

NEW EVENTS

Location

Close study of the seismic waveforms recorded during the gap yielded ten events with enough confidence to properly locate. These ten events were located using the station delays determined from the Master Event analysis in the original study. Once located, the ten events were added to the master event catalog, which now consists of 199 events. A plot of the coda magnitudes of all events occurring within a 1.9-mi radius of the Crandall Canyon mine during August 2007 is included in Figure 2.

Double-Difference Relocation

The 199 events of the new master event catalog were relocated using a double-difference method. HypoDD (Waldhauser and Ellsworth, 2000) calculated meaningful locations for 157 of the 199 events, increasing the previous number of refined locations by seven. The 157 relocated events were then shifted as before based on the known location of the fatal August 16 rib-burst. The additional seven events do not provide much useful information on their own; however, if they can be coupled with ground truth information, they can be used to better verify the locations of the remainder of the catalog.

Of the newly-added events that were able to be relocated using hypoDD, one could be directly confirmed by ground truth

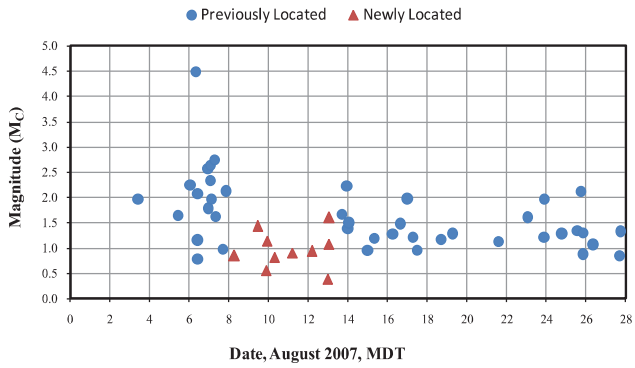

Figure 2. Coda magnitudes of all located events occurring within a 3-km radius of the Crandall Canyon mine during August 2007. Events shown as triangles occurred during the gap.

information from the log books. The event was reported as follows: "Had a bump at 19:40 north corner of entry" ("Command Center Log Book," 2007). At that time, the continuous miner used in the rescue efforts had reached 75 ft inby (west, toward the working face) of Entry 1, Crosscut 124 ("Command Center Log Book," 2007). This can be assumed to be the true hypocentral location of the event. HypoDD relocated this event approximately 300 ft due east, between Crosscuts 122 and 123.

Figure 3 shows a map of the mine-workings surrounding the collapsed area that compares the revised double-difference locations to the ground truth locations taken from the log books. Discounting the fatal August 16 event used for shifting the locations, the average error between the double-difference locations and the ground truth locations has been improved from approximately 450 ft to 340 ft.

events, this pattern is not as clear, though two clusters remain obvious (Figure 4). Between August 6 and August 9, a total of nine events occurred to the east of the minimum estimated collapse area. These nine events are mostly M_C 2.0 or greater. Between August 13 and August 15, a cluster of five M_C 1.0–2.0 events occurred to the west of the collapse, though they are occasionally interrupted by larger events to the east. The period following August 16 is marked by a seemingly random distribution of smaller events, beginning slightly more heavily on the east and terminating slightly more heavily on the west. Notably, very few events occur directly within the minimum estimated collapse area.

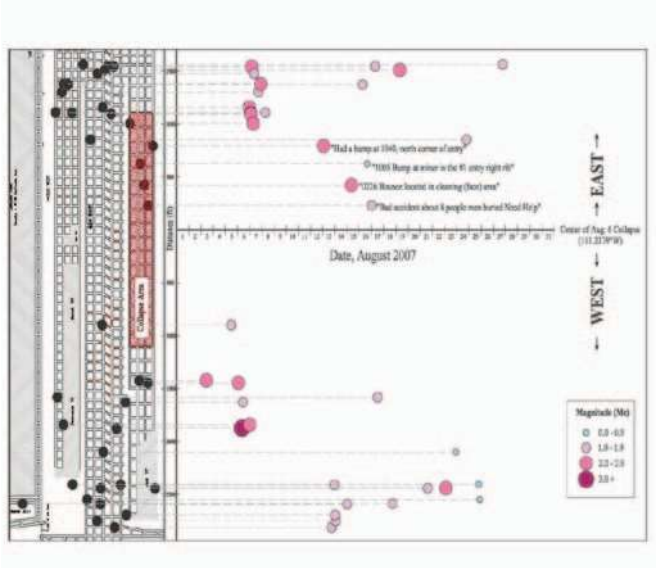

Figure 4. Chronology of double-difference events by location relative to the center of collapse during the month of August 2007.

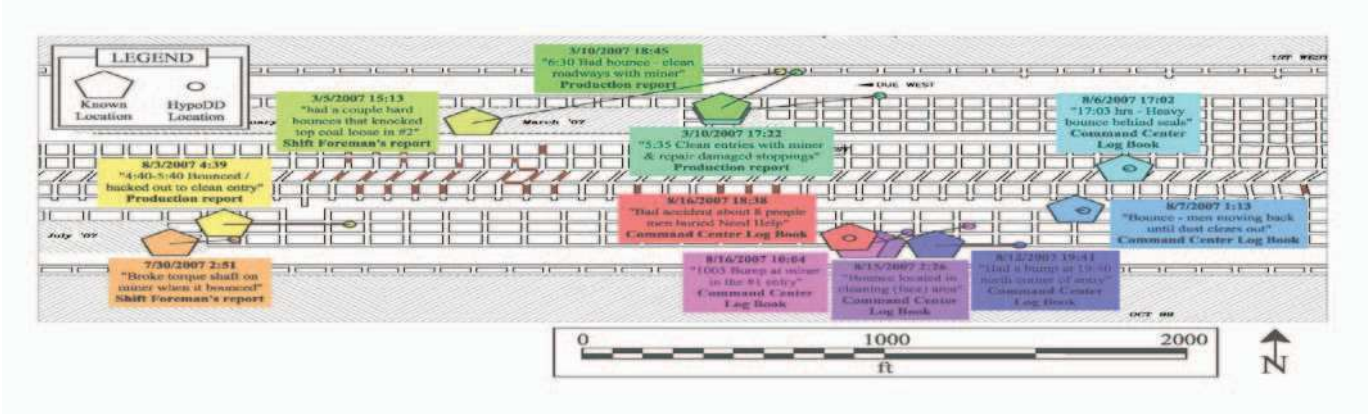

Figure 3. Map of Crandall Canyon mine workings comparing revised double-difference locations (circles) to ground truth locations taken from the log books (pentagons).

CHRONOLOGY OF SEISMICITY

Past studies report that the events following the mainshock tend to cluster in episodic bursts (Warner et al., 2009). Furthermore, it was reported that these bursts begin heavily to the east of the collapse, shift briefly to the west on August 13 and 14, and then return to the east (Warner et al., 2009). With the addition of new

It is yet unknown whether the overall pattern of episodic bursts was caused by the changing of stress patterns attributable to the rescue efforts of the continuous miner crew, or simply by natural pressure changes occurring in the wake of the mainshock. The pattern of seismicity indicates that at least one small grouping of four events on the east side of the collapse is closely related to the activities of the rescue crew. These four events, marked with

ground truth information in Figure 4, occur in close proximity to the continuous miner's location during the rescue attempt and culminate with the fatal August 16 rib-burst. These events occur several hundred feet to the southwest of the nearest, larger cluster of events to the east of the collapse. They are the only events to occur within the minimum estimated collapse area reported by Pechmann et al. 2008 and shown in Figure 4.

CONCLUDING REMARKS

The ten new events located in this study serve as a testament to the importance of ground truth information in seismic monitoring. The six-day gap in reported events was filled using approximate times and locations taken directly from the log books, which helped to pinpoint P-wave arrivals more easily. The procedures described in this paper have been used to compile a more complete seismic catalog of Crandall Canyon and ultimately provide a better understanding of MIS in the wake of a serious mine collapse.

Making full use of any available ground truth information is important for both mines and researchers alike. Well-kept log books may be the best indicators of true hypocentral locations in mines lacking dense seismometer arrays. In an emergency response situation where accurate event locations can be achieved, it is important to do so quickly in the hopes of immediately identifying high-stress areas of the mine. Achieving accurate locations could prove useful in helping rescue workers avoid areas marked by heavy clusters of MIS, should collapses similar to Crandall Canyon occur in the future.

In addition to creating a more complete picture of MIS at the Crandall Canyon mine, the addition of new events to the catalog has significantly improved the average accuracy of the double-difference locations of all the events, so far as that accuracy can be tested against ground truth. The improvement seen in location accuracy for events occurring after the installation of the temporary seismic array suggests the importance of denser spacing of monitoring devices than are typically seen in central Utah.

ACKNOWLEDGEMENTS

The authors of this paper can do nothing more than offer our most sincere and heartfelt condolences to the families and friends of Kerry Allred, Dale Black, Don Erickson, Luis Hernandez, Gary Jensen, Brandon Kimber, Carlos Payan, Brandon Phillips, and Manny Sanchez. Best wishes are also extended to those injured in the rescue attempt.

We would like to offer special thanks to Mark Hale, Paul Roberson, Katherine Whidden, Jim Pechmann, Meagan Boltz, Marcela Torres, and Bill Blycker for all their technical support on this project. We would also like to thank Rachel Anderson, Sam Margulies, Julie Bare, Matt Stern, Justine Cammisa, and Greg Lytle for their guidance along the way. This research was made possible through funding and support from NIOSH and the State of Utah.

The views and conclusions contained in this document are those of the authors and should not be interpreted as representing the opinions or policies of NIOSH or other sponsors of this research.

REFERENCES

"Command center log book." (2007). Mine ID: 42-01715, Log Book, Bk. 1 of 2. Mine Safety and Health Administration.

MSHA. (2007). "Coal mine safety and health report of investigation, underground coal mine, fatal underground coal burst accidents August 6 and 16, 2007, Crandall Canyon Mine, Genwal Resources Inc." Mine Safety and Health Administration. CAI-2007-15-17.

Pankow, K.L., McCarter, M.K., Arabasz, W.J., Burlacu R.L. (2008). "Coal-mining-induced seismicity in Utah—improving spatial resolution using double-difference relocations." In: *Proceedings of the 27th International Conference on Ground Control in Mining*. pp. 91–97. [http://icgcm.conferenceacademy.com/papers/detail.aspx?subdomain=icgcm&iid=347].

Pechmann, J.C., Arabasz, W.J., Pankow, K.L., Burlacu, R.L., McCarter, M.K. (2008). "Seismological report on the 6 August 2007 Crandall Canyon mine collapse in Utah." *Seismological Research Letters*. *79*(5):620–636.

Waldhauser, F., Ellsworth, W.L. (2000). "A double-difference earthquake location algorithm: method and application to the northern Haywood fault." *Bulletin of the Seismological Society of America*. *90*:1353–1368.

Warner, J.M, Phipps, P.J., McCarter, M.K., Pankow, K.L. (2009). "Monitoring post-collapse seismicity—an analysis of Crandall Canyon events." Presented at the SME Annual Meeting. Denver, Colorado.

The Estimation of Ground Control Risk By Real–Time Quantitative Visual Assessments

Alexander Garcia, Dr
Golder Associates (UK) Ltd.
Burton-on-Trent, United Kingdom

Peter Altounyan, Dr
Arkadiusz Rostocki, Mr
Golder Associates. (UK) Ltd
Burton-on-Trent, United Kingdom

ABSTRACT

Roof and rib falls are the basic ground control hazards associated with underground roadways during development, stand up and, if applicable, retreat. Falls of ground can happen following the deterioration of supports or rock conditions over time, and particularly as a consequence of continuing rock deformation and/or failure to install adequate support. Once developed, the risk of a failure is increased due to the effects of time as well as to front abutment stresses through retreat mining. The measurement of strata displacement using monitoring equipment is a form of ground control risk assessment. These monitoring systems are active, or "live", in a sense that risk is assessed real-time. However, there are circumstances in which falls of ground can occur without the prior recording of excessive movement. In addition, monitoring equipment is typically placed at set intervals, and strata conditions could vary between these points. Consequently, a visual assessment of other factors contributing to the risk of a fall should be made in order to complete a ground control risk assessment. Such surveys are usually one-off, thus capturing roadway conditions at one particular point in time. Ongoing deterioration is not documented through such one-time surveys, and there is a requirement for real-time or live assessment where a system is in place so that observation data can be updated on an ongoing basis, and a useful summary of prevailing roadway states produced on demand. To address the shortfalls of one-time assessments, a 'live' computer-based quantitative ground control risk assessment process has been developed. It combines visual observations processed in a quantitative manner with existing monitoring data into an interpretable output which indicates zones of roadway where there is an increased risk of a fall of ground from the roof or sides, so that remedial action can be carried out to mitigate that risk. Through improved procedures, it is now possible to generate a ground control risk assessment for each roadway, and one which can be updated frequently. This paper aims to outline and describe the assessment process.

INTRODUCTION

Preventing falls of ground is essential in single-entry mine roadways, as these serve multiple functions: a ventilation route, coal or materials transport, a travel way and an escape route. This is why emphasis is put on systematic roof movement monitoring in UK mines. Even if no personnel are injured, the financial cost of falls – in terms of lost production alone – justifies the use of considerable resources to ensure that they are eliminated. Falls of ground after a roadway has been supported can happen as a consequence of continuing rock deformation and/or a failure to install adequate support. The risk of a failure can also increase later due to time-related deterioration in rock or support conditions, or due to stress changes including the imposition of front abutment stresses through retreat mining.

Ground control risk assessments have previously been undertaken in UK longwall coal mines by performing visual surveys prior to face retreat. These capture roadway conditions at a particular point in time but do not document ongoing deterioration or front abutment effects.

Ideally, ground control risk assessment surveys should be both *quantitative* and *live:* quantitative so that observations are converted to numerical values related to the level of risk, and live, meaning that the ground control risk is frequently re-assessed. This requires data to be updated on an ongoing basis so that a summary of the current roadway state can be produced on demand. This paper describes the origins and development of a live quantitative ground control risk assessment scheme recently developed by Golder Associates.

GROUND CONTROL IN UK COAL MINES

The introduction of rock bolt supports over the period between 1985 and 1994, together with a simultaneous switch from advancing to retreat longwall mining, represented a major change in working methods in British coal mines (Hindmarsh, 1995). The remaining UK deep coal mines work a single 250m to 350m longwall panel at depths between 800m and 1050m. Longwall panels are separated by stable "finger" pillars typically wider than one-tenth depth of cover. Parallel gateroads are driven as rectangular single entries, without crosscuts, by a full-width bolter miner. Gateroad support typically includes 2.4m fully resin-encapsulated rock bolts at 0.6m to 1.0m spacings, supplemented with caged cable bolts or flexible rock bolts where necessary. "Link-n-lock" type cribs are generally used as additional tailgate support ahead of the retreating longwall.

To ensure safe conditions when rock bolts were introduced in single-entry roadways, roof movement action levels were adopted as indicators of the need for any additional support. These action levels are the maximum roof movements allowed, either within or above the rock-bolted height, before additional support must be installed. The roof movement is indicated by dual-height telltales installed every 20m in rock-bolted roadways (Bigby, 1995).

The telltales are simple dual-height wire extensometers used to monitor ground movement and to differentiate between movement occurring within the bolted horizon and movement occurring above the bolts. They are installed at regular intervals along the roadway (usually every 20m) and can be read to the nearest millimetre (Figure 1). They also serve as safety devices, giving continuous visual indication of the level of movement that has occurred since installation to persons travelling the roadway (Kent et al., 1999). These simple safety devices were probably the most significant single factor in the success of rock bolting in UK ground conditions, and their installation remains standard practice in all UK bolted roadways. Dual-height telltales, or their modern electronic equivalent, are now also in regular use in many other mines worldwide (Bigby et al., 2010).

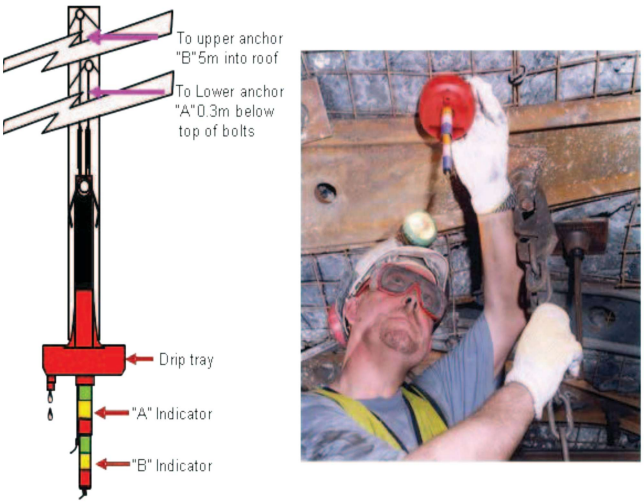

Figure 1. Dual-height telltale and inspection by mine official.

ASSESSING GROUND CONTROL RISKS

Changes to UK mining legislation in the 1990s placed much greater support design responsibility on the mine manager, compared with the earlier proscriptive rules enforced by mines inspectors. New legislation also introduced a risk assessment approach to evaluate potential hazards.

Roof and rib falls are the basic ground control hazards associated with coal mine roadways. The systematic measurement of roof strata displacement is a form of ground control risk assessment, based on the assumption that the risk of a roof fall is directly related to the level of movement occurring, and initially this requirement for risk assessment was considered to be met in rock-bolted roadways by the roof movement monitoring and by the statutory district inspections undertaken every shift by safety officials. There are, however, circumstances in which falls of ground can occur without excessive movement being first recorded on monitoring devices. In addition, local features between monitoring points can sometimes cause falls of ground. Rib movement is not generally measured in the same way as roof movement, so monitoring does not provide information on the rib fall risk.

The need for an improved system for visually assessing ground control risk in rock-bolted roadways in the UK was emphasised by falls of ground at Welbeck and Thoresby Collieries in the North Nottinghamshire coalfield in 1995 and 1996, respectively (Cartwright and Bowler, 1999). Investigations revealed that lateral shearing of the roof beds had occurred along a discrete bedding horizon as a result of increased abutment stress associated with a longwall retreat face. In addition, highly corrosive strata water, which was present at the same horizon, corroded the rock bolts and thereby reduced the reinforcement capacity. The falls occurred between the locations of the routine strata deformation monitoring devices and the incipient failures were not detected by roadway inspections.

These incidents highlighted one of the circumstances in which falls of ground could occur without excessive roof movement being first recorded. In addition, local geological features between monitoring points can sometimes cause falls of ground, and it is also possible that the roof monitoring devices have been incorrectly installed, or have become trapped by roof shear and are not functioning properly. Rib movement is not generally measured in the same way as roof movement, so monitoring does not provide information on the rib fall risk. Consequently, it was concluded that an assessment of all factors contributing to the risk of a fall of ground was needed to complete a ground control risk assessment. The practice of making a systematic visual survey of roadway conditions following development in British coal mines was then introduced.

APPLICATION TO UK MINES

The first ground control roadway risk assessment system was developed for Thoresby and Welbeck Collieries in 1996 in response to the falls of ground (Cartwright and Bowler, 1999). The system was developed specifically to identify roadway zones where rock bolts might fail on face retreat, and risk factors included an uneven roof profile, local changes in immediate roof geology and the presence of high-saline water leading to bolt corrosion pitting. Areas identified as high risk were re-supported prior to coming under the face-front abutment influence.

Subsequently, risk assessments were developed by specialist engineers to address specific ground control problems, including junction stability in room and pillar workings and rib failures in gateroads, as well as more general roadway risk assessments with a wider scope and a greater number of variables. These roadway risk assessments were later widely applied in gateroads prior to retreat in order to prioritise the installation of additional support to high-risk areas. The assessment was based upon a combination of a visual survey of roof, rib and support conditions, assessment of roof monitoring data and an examination of mining plans. The survey was split into 20m roadway sections centred on roof telltale positions. The system was tailored to fit the seam and roadway characteristics at the mine involved, based on a standard methodology and analysis logic.

The system of visual assessment of ground control risk was effectively operated in parallel with the normal roof movement monitoring scheme, with the greater of the two risk levels assumed to apply. Figure 2 illustrates the general logic applied. Computer spreadsheets were developed to reduce processing time and improve accuracy and consistency throughout the assessment.

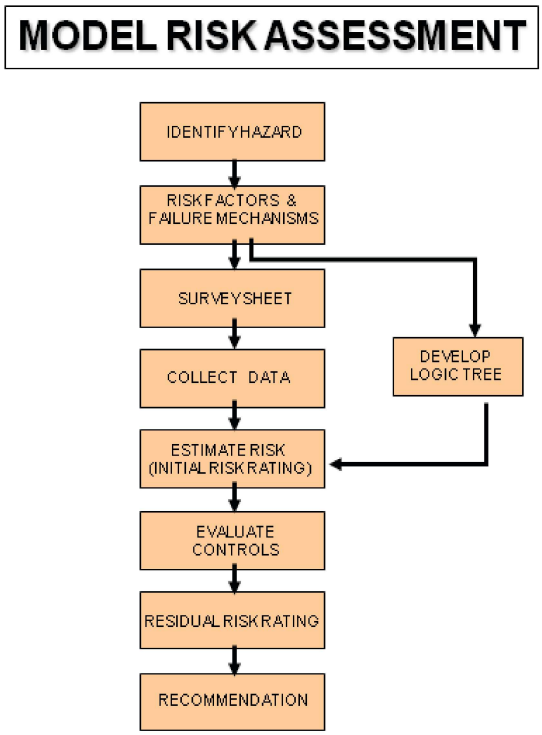

Figure 2. Model Risk Assessment methodology.

For the roadway roof, the surveyed roadway zones were identified as high-, medium- or low-risk based on the visual survey or measured roof movements. Roof movements beyond action levels, by definition, denote high risk. Movements on development exceeding 50% of action levels were taken to denote medium risk. The visual assessment data could also result in a low-, medium- or high-risk rating depending on the severity of risk factors, including overall roof profile, cavities, visible roof shearing, fracturing or guttering, roof water, overloaded or broken bolts, mesh and strap deformation.

The two ribs were evaluated separately from the roof, based purely on the visual assessment of rib and support conditions. In each case, existing risk controls in the form of any installed remedial support were assessed to determine the residual risk ratings. The basic output from the risk assessment was a table containing the initial risk ratings, residual risk ratings and recommendations on additional remedial support or other actions required. The aim was to reduce all high or medium risk zones to low risk by installing appropriate additional support well before any influence was felt from the retreating face. An assessment was also made of likely behaviour on retreat, based on previous experience, and taking into account the position of known structural or geological features and measured and visible deformation on development. Zones predicted to become high risk on retreat could then be proactively targeted for installation of substantial extra supports, such as cable bolts.

Although this risk assessment system is still used, it does have some shortcomings. These are now being addressed by the development of the live risk assessment system described below.

THE DEVELOPMENT OF A LIVE RISK ASSESSMENT METHOD

The need for an improved ground control risk assessment system

The safety record of rock-bolted single entries in the UK is good; a significant reduction in falls of ground accidents followed the replacement of steel arches by rock bolts (Arthur et al., 1998; Bigby et al, 2006), but isolated incidents still occur. Comprehensive and systematic management of roadway and support conditions is needed if all falls of ground are to be eliminated; the use of ground control risk assessment is an essential part of this management process. All relevant factors should, therefore, be taken into account when assessing roadway and support conditions, and visual inspection is just as important as telltale monitoring in providing information to allow ground control risk to be assessed.

However, any safety system incorporating visual inspection relies on the human element, and this is a potential weakness – our judgments are subjective, we make mistakes and we are affected by “habituation”. We become used to the conditions we see regularly, and may not recognise gradual but significant changes. It is, therefore, important that a system of this kind avoids these problems by simple, clear procedures, minimising any requirement for qualitative judgment.

Previous ground control risk assessments as described previously have been “one-off” surveys, typically of gateroads prior to face retreat. Resources are then focused on high-risk areas before and during the subsequent retreat. Risk ratings determined following development have been assumed to remain valid during retreat, but this has not always proved to be the case. Not all factors which influence face retreat are visible on roadway inspection or known in advance. Conditions can deteriorate significantly under the influence of the front abutment loading from the approaching face, and this may include roadway zones classified after development as low risk. Therefore, the risk assessment should be updated as the face retreats to take account of changing conditions and, ideally, updating should be so frequent that the assessment effectively becomes “real time” or “live.” These frequent reassessments should only be required in sections of roadway subject to changing conditions; that is, areas potentially influenced by nearby mining activity. Resources can, therefore, be concentrated on these active mining zones.

System Requirements

A comprehensive ground control risk assessment survey requires a trained specialist engineer. In practice, full re-assessments can only be undertaken periodically, depending on engineer workload. However, not all surveyed parameters are subject to change (faulting, initial roadway size and support pattern, for example), so once an initial detailed survey has been established suitably trained assistants can carry out weekly (or even daily) inspections of active mining zones to look systematically for

changes in relevant parameters including deteriorating roof or ribs, the deformation of support plates, etc. This can be achieved with a simpler visual classification and reporting procedure, which could be operated by less skilled but trained personnel. Through improved procedures, it could therefore be possible to generate a ground control risk assessment for each roadway updated for active mining zones each day (a "live" risk assessment), with associated reporting. This information would be up to date, more accurate and easier to interpret. Ideally, observations should also be converted to numerical data using a clear and repeatable process to allow risk calculations to be made. To fully develop such a system, the following steps are needed:

1. Identify a site's potential failure mechanisms, associated risk factors and their relative importance.
2. Establish and test the initial risk assessment logic, including a simple, clear and reliable method of quantifying visual observations.
3. Incorporate the completed risk assessment logic in a suitable computer program with associated data handling and reporting capabilities.
4. Develop simple inspection report sheets for use by personnel, undertaking weekly or daily inspections.
5. Develop a system for inputting this data accurately and rapidly to the risk assessment database, computing the resulting risk levels and reporting results to relevant personnel.
6. Undertake an initial risk assessment survey to collect all base data.
7. Undertake associated training to ensure all personnel involved are competent in their roles.

The target areas for the live risk assessment process (active mining zones) also need to be defined. For retreat gateroads, these are the sections of gate roadway influenced by front abutment loading from the approaching face. In typical UK conditions, this influence can be seen for up to 200m or more, and the appropriate length needs to be identified for each site. A similar live assessment process could, in principle, be applied to other active mining zones where conditions are changing, such as development headings and roadway repair sites where major dinting or "ribbing off" is being undertaken.

System Description

It is intended that the live risk assessment is operated in addition to the normal roof movement monitoring system. Either system can indicate the need for the installation of additional supports. The process addresses overall roadway ground control risk, with separate assessments of ground control risks made for the roof and left- and right-hand rib sides.

The live risk assessment logic and the associated software system have been developed for the mines by Golder Associates. The system makes use of tailored Excel spreadsheets to store, manipulate and process data. In order to design, refine and calibrate the software, preliminary risk assessment surveys are undertaken by Golder Associates in a section of roadway with the survey reporting on conditions within each 10m length of roadway. Subsequent inspections are, however, undertaken by mine staff using guided observation booking sheets listing possible categories for each factor to be visually assessed, so that the most appropriate description can be circled (i.e. a "tick box" process). Factors to be assessed separately for the roof and each rib side during repeat surveys include:

- Overall and structural condition, cut profile, bulking, guttering, etc.
- Installed support and condition, corrosion, plate loading, broken bolts, mesh and strap conditions.

The survey data is input into the Excel spreadsheets, which converts the observations into numerical values. At present this is done through drop-down fixed list boxes in Excel, which duplicate options given on the underground booking sheets (Figure 3). The observations are processed to give two summary parameters used to characterise the visual conditions in each 10m zone. These are roof (or rib) integrity and support condition, which are both expressed as percentages in order to make them readily understandable (Figure 4). The roof or rib integrity starts at 100%, though as conditions deteriorate this percentage will reduce. The corresponding support condition parameter is also expressed as a percentage; an initial value of 100% is generated if the support is correctly installed to the specified design. This percentage falls as visual support conditions deteriorate. However, if appropriate remedial support is installed in response to these visual conditions, or in response to monitored roof movement, then this percentage increases. Unlike the roadway condition parameter, the support condition can go above 100% if the remedial support installed is considered to be more than necessary to maintain effective roadway support. The aim is to maintain the support condition parameter at 100% or more. For each zone, a risk rating is derived based on the conditions and support ratings, this being Lower, Moderate or Higher. The risk scale is initially calibrated so that an area which is of clear concern is rated higher by the program, and areas that are of no concern are rated lower. Therefore, the ratings are relative to the roadway being surveyed (rather than absolute). As the system is live, there is scope to track trends in risk. Areas which are deteriorating from one survey to the next can be identified by a negative trend depicted in the summary output by a downward red arrow, even though the overall risk rating may remain unchanged. Equally, areas which have been improved through remedial work will report a positive trend, depicted by a green upward arrow.

Current Status

The system status at the time of writing is now being operated in retreat roadways at sites in the UK. It is too early to report the impact on ground control safety, but the system is proving to be relatively easy to operate, with mine staff able to update the risk assessment spreadsheets following retreat roadway inspections and issue recommendations to mine management staff based on current conditions. The systematic and quantitative approach encouraged by the scheme procedures, together with very simple data entry procedures, helps to minimise any requirement for subjective judgement and associated human error. Currently, the survey and inspection data are gathered using paper report sheets. However, it may be possible in the future to directly input data to the software database as easier input options and new hardware systems (tablet PCs) are developed. The fundamental aim with ongoing software development is to produce a program that is user friendly, simple and gives reliable assessment results.

Location			Visual Observati						
ZONE Metre Mark Start	ZONE Metre Mark End	Survey Area	Active General Assessed Condition	Active Geology	Active Roof Fractures	Active Fault / Slip	Active Water	Active Water Location	Active Straps OB Water Mark
0	5	Yes	Standard	Coal	LHS	Yes	Damp	Cen	2
0	10	Yes	Excelent	Mudstone	None	No	None	N/ A	None
10	20	Yes	Good	Mudstone	None	No	None	N/ A	None
20	30	Yes	Good	Mudstone	None	No	None	N/ A	None
30	40	Yes	Excelent Good Fair Poor V' Poor Uneven Fall	Mudstone	None	No	None	N/ A	None
40	50	Yes		Mudstone	None	No	Has Been	RHS	5
50	60	Yes		Mudstone	None	Possible	Has Been	RHS	None
60	70	Yes	Fair	Mudstone	None	No	Has Been	RHS	3
70	80	Yes	Good	Mudstone	None	Possible	Damp	RHS	None
80	90	Yes	Fair	Mudstone	RHS	Possible	None	LHS	1
90	100	Yes	Fall	Mudstone	LHS	No	None	N/ A	None
100	110	Yes	Good	Mudstone	None	No	None	N/ A	None

Figure 3. Example of part of a visual data input spreadsheet with rating options, showing selection by drop-down menu.

Maingate Roof				WK 2			
09 January 2012 TO 15 January 2012							
ZONE		Roof Movement	Integrity (Observations)	Support	Highest Level of Support	Current Risk Rating	Trending
FROM	TO	Roof Monitoring					
0	10		100.0%	100.0%	Development	Lower	
10	20	1 No Action	100.0%	100.0%	Development	Lower	
20	30		100.0%	100.0%	Development	Lower	
30	40	2 No Action	100.0%	100.0%	Development	Lower	
40	50		91.6%	86.5%	Development	Lower	
50	60	3 No Action	78.2%	86.5%	Development	Moderate	
60	70		95.0%	86.5%	Development	Lower	
70	80	4 Action	63.2%	96.5%	Extra 2 SB	Moderate	
80	90		50.1%	100.9%	2 FB/CB	Moderate	
90	100	5 No Action	86.6%	120.0%	2 FB/CB	Lower	
100	110		100.0%	112.1%	2 FB/CB	Lower	
110	120		100.0%	120.0%	2 FB/CB	Lower	
120	130	6 No Action	86.6%	114.4%	2 FB/CB	Lower	
130	140		59.8%	200.1%	Full Row SB	Lower	
140	150		Goaf	Goaf	Goaf	Goaf	
150	160		Goaf	Goaf	Goaf	Goaf	
160	170		Goaf	Goaf	Goaf	Goaf	

Figure 4. Examples of Excel spreadsheet outputs showing risk ratings.

CONCLUSIONS

A quantitative ground control risk assessment scheme has been developed to consider the roof and rib visual conditions together with the integrity of the installed support and local geological factors on a live, rather than one-off, basis. The ground control risk assessment scheme is intended to continuously assess the conditions of coal mine roadways, and is able to produce an objective risk rating for defined intervals along roadways. It is currently being used at coal mines in the UK.

Live risk ground control assessment systems can help to ensure that developing roadway deformation and support problems are identified early. The visual information is up-to-date, more accurate and easier to interpret, allowing better management of ground control risks. Consequently, resources can be effectively deployed through targeted remedial action to rectify problems well before they can result in falls of ground.

REFERENCES

Arthur J., Waite K., Altounyan P. (1998). "Guidance on the Use of Rockbolts to Support Roadways in Coal Mines – A UK Code of Practice." *Symposium of Rock Mechanics and Productivity and the Implementation of Codes of Practice*. West Rand, South Africa.

Bigby, D. (1995). "Rock Mechanics Design for Rockbolted Roadways in British Coal Mines." In: *Proc. Int. Mining Tech' 95 Symp*. Beijing, CCMRI China. 258-268.

Bigby, D. N., Altounyan, P.F.R.,Cassie, J. (2006). "Coal Mine Ground Control in Western Europe: Past, Present and Future." In: *25th International Conference on Ground Control in Mining*. Morgantown, West Virginia, USA.

Bigby, D., MacAndrew, K., Hurt, K. (2010). "Innovations in Mine Roadway Stability Monitoring Using Dual Height and Remote Reading Electronic 'Telltales'." Aziz, N., Ed. In: *10th Underground Coal Operators' Conference*. University of Wollongong and the Australasian Institute of Mining and Metallurgy.

Cartwright, P., Bowler, J. (1999). "The Development and Use of Risk Assessment Techniques to Assess Roadway stability in the Parkgate Seam at Thoresby Colliery." In: *18th International Conference on Ground Control in Mining*. Morgantown, West Virginia. 72-81.

Hindmarsh, W. E. (1995). "The Management of Rockbolting Within British Coal." In: *2nd International Conference Of Roof Control In Mining*. RWTH Aachen.

Kent, L., Cartwright, P., Bigby, D. (1999). "Tunnel Deformation Monitoring Action Levels in Coal Mines for Support/ Reinforcement Design." In: *18th International Conference on Ground Control in Mining*. Morgantown, West Virginia. 98-107.

A Management System to Develop Occupational Health & Safety in Ground Control Operations of Underground Mines

Kazem Oraee, Professor
Stirling University
Stirling, United Kingdom

Nikzad Oraee-Mirzamani
Imperial College London Business School
London, United Kingdom

Arash Goodarzi
Occupational Safety
Ministry of Labor and Social Affairs
Tehran, Iran

ABSTRACT

Falls of ground have historically been the main cause for fatalities in underground mines. Although recent advances in technology have reduced the number of such accidents, when failures occur they usually result in severe consequences. Risks of rock falls, use of heavy machinery and electrical apparatus, entry to confined spaces, working in noisy and dusty environments, and working on unstable platforms are some of the hazards in ground control operations. Managing these risks requires a management regime involving strict adherence to operational codes of practice and an enshrined culture of safety. These should be subsequently reinforced through active participation of management, systematic training, and stringent internal and third party auditing.

Accident reports show that the major contributing factor in most rock fall accidents is the failure to adequately manage known risks due to the lack of a systematic process. OHSAS 18001 (Occupational Health and Safety Assessment Series) is an international occupational health and safety management standard specification to develop occupational health and safety at the workplace.

This standard is intended to help mine operators control occupational health and safety risks. Addressing the requirements of OHSAS 18001 can be a complex and demanding task. A comprehensive guide for efficient and accurate implementation of this standard is provided in this paper. The discipline can be used to establish an accountable management system foreground control activities in underground coal mines. The paper also provides guidelines for preparing necessary documents, devising safety policies, procedures, performing risk assessment, and handling instructions. Finally, the paper concludes by providing a sound analytical basis in terms of the creation of a robust safety management system foreground control operations in underground mines. Full benefits of implementing an effective and systematic operational health and safety management system are illustrated. The procedure adopted and prescribed in this paper can be used in all underground coal mines where lack of appropriate ground control practices can create deficiencies in both safety and productivity.

INTRODUCTION

Mining can be a dangerous occupation with many potential health hazards: more than 104,000 miners have died in mining accidents in the United Stated since 1900 (Sherard, 2011). Approximately 631,000 U.S. soldiers and other Americans were killed in wars during the same period (Fischer, 2007). It is therefore conceivable to think that a silent war has been taking place in mines during the last century. Most of these fatalities occurred from 1900 to 1978 when laws and control system were ineffective (Sherard, 2011).

Coal provides 30% of primary energy needs, and over 7 million people are employed in this sector globally. Some of the worst human disasters have occurred in this industry, and even to date, mining is performed in very dangerous conditions in some countries. Most of the mining fatalities nowadays occur in developing countries where occupational health and safety rules are neglected.

Continuous technological advances and a highly skilled workforce have allowed the coal mining industry to provide a safer workplace in developed countries. Since 1970, coal production has increased nearly 75%, and fatal injuries have decreased by approximately 93% in the United States (MSHA, 2010). Nevertheless, underground mining still has one of the highest fatal injury rates of any U.S. industry—more than five times the national average compared to other industries (NIOSH, 2011).

Historically, roof and rib falls have been the greatest cause of fatalities in underground coal mines, and they remain the greatest safety problem in underground coal mining to date. Between 1999 and 2008, nearly 40% of all underground fatalities were attributed to roof, rib, and face falls (NIOSH, 2011). Poor roof and rib conditions lead operators in many mines to use roof support systems to prevent accidents. Although recent advances in technology have reduced the total number of such accidents drastically, when failures occur, they usually result in severe consequences. Risks of rock falls, use of heavy machinery and electrical apparatus, entry to confined spaces, working in noisy and dusty environments, and working on unstable platforms are only some of the hazards associated with ground control operations. Ground control operators are arguably the hardest working persons

in the mine (Compton, 2007). They are constantly lifting, bending, pulling and carrying materials that they need to control the roof of the mine. Adding support installation to this already labor-intensive job increases the risk of stress and strain injury to the operators.

Managing these risks requires a management regime that includes strict adherence to operational codes of practice and an enshrined culture of safety. Accident reports show that the major contributing factor in most rock fall accidents is the failure to adequately manage known risks due to the lack of a systematic process. Occupational Health and Safety Assessment Series 18001 (OHSAS) is an international occupational health and safety management standard specification to develop occupational health and safety at the workplace.

OHSAS 18001

OHSAS 18001 is an assessment model for the management of health and safety in systems that were developed to promote effective health and safety management. It is intended to help an organization control occupational health and safety risks. OHSAS 18001 has been developed to be compatible with the ISO 9001:2000 (Quality) and ISO 14001:2004 (Environmental) management systems standards so that it facilitates the integration of quality, environmental, and occupational health and safety management systems by organizations. OHSAS complies with applicable legal requirements, though compliance with this Standard does not confer immunity from legal obligations. It was developed by a selection of leading trade bodies and international standards and certification bodies to address a gap where no third-party certifiable international standard exists.

Occupational health and safety (OHS) measures take into account all conditions and factors that affect, or could affect, the health and safety of employees or other workers (including temporary workers and contractor personnel), visitors, or any other person in the workplace. An OHS management system is part of the overall organization's management. A management system is a set of inter-related elements used to establish objectives, and a policy to achieve those objectives. A management system includes an organizational structure, planning activities (for example, risk assessment and the setting of objectives), responsibilities, practices, procedures, processes, and resources. The OHSAS Standard is based on the methodology known as Plan-Do-Check-Act (PDCA). The basis of the approach is shown in Figure 1.

The main elements of OHSAS 18001 are given in Table 1.

Scope and Objectives

The scope of the OHS management system defines the objectives and its boundaries (such as physical boundaries). It does not state specific health and safety performance criteria, nor does it give detailed specifications for the design of a management system. The scope has been prepared to ensure that the mine operator at an underground mine has provided adequate consideration of all ground control aspects relevant to the safe design and operation of the mine they are responsible for.

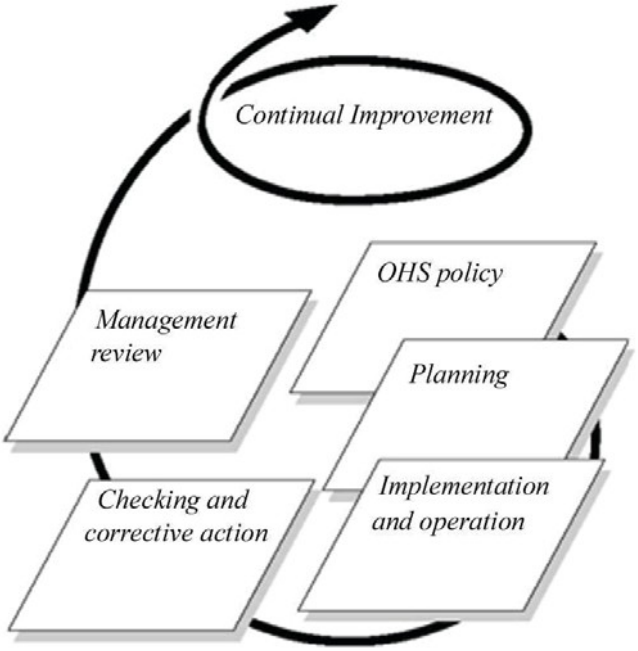

Figure 1. Operational heath and safety management system model for the OHSAS Standard.

POLICY

The ultimate goal and direction operating to an entity's OHS performance is set out in the OHS policy, which is formally expressed by top management. The OHS policy provides an appropriate framework, within the defined scope, for the nature and scale of the OHS risks to all persons working under the control of the organization. The framework also helps with setting tasks, action, and setting OHS objectives. The objectives should be consistent with the OHS policy and be specific, measurable, achievable, reasonable, and time bounded.

PLANNING

Planning is the organizational process of creating and maintaining a plan regarding the activities required to create the OHS objectives. The procedures for the ongoing hazard identification, risk assessment, and determination of necessary controls are the most important aspects of planning (see Figure 2).

An OHS Risk Assessment is the structured and systematic identification and analysis of workplace hazards, with the aim of reducing the risks of exposure to hazards. The OHS Risk Assessment is a decision making process that involves considering the consequences of accidents combined with the probability of exposure to risks. Furthermore, it includes analyzing and comparing alternative methods and to select among activities that may be less harmful. Various risk assessment techniques are available. Operators utilize many different risk assessment techniques such as what if, fault tree analysis, failure mode, and effects analysis.

Table 1. The main elements of OHSAS 18001.

Clause	Description	Clause	Description	Clause	Description
—	Introduction	4.4	Implementation and operation (title only)	4.5.3	Incident investigation, nonconformity, corrective action and preventive action (title only)
1	Scope	4.4.1	Resources, roles, responsibility, accountability and authority	4.5.3.1	Incident investigation
2	Normative references	4.4.2	Competence, training and awareness	4.5.3.2	Nonconformity, corrective and preventive action
3	Terms and definitions	4.4.3	Communication, participation and consultation	4.5.4	Control of records
4	OHS management system elements (title only)	4.4.4	Documentation	4.5.5	Internal audit
4.1	General requirements	4.4.5	Control of documents	4.6	Management review
4.2	OHS policy	4.4.6	Operational control		
4.3	Planning (title only)	4.4.7	Emergency preparedness and response		
4.3.1	Hazard identification, risk assessment and determining controls	4.5	Checking (title only)		
4.3.2	Legal and other requirements	4.5.1	Performance measurement and monitoring		
4.3.3	Objectives and programme(s)	4.5.2	Evaluation of compliance		

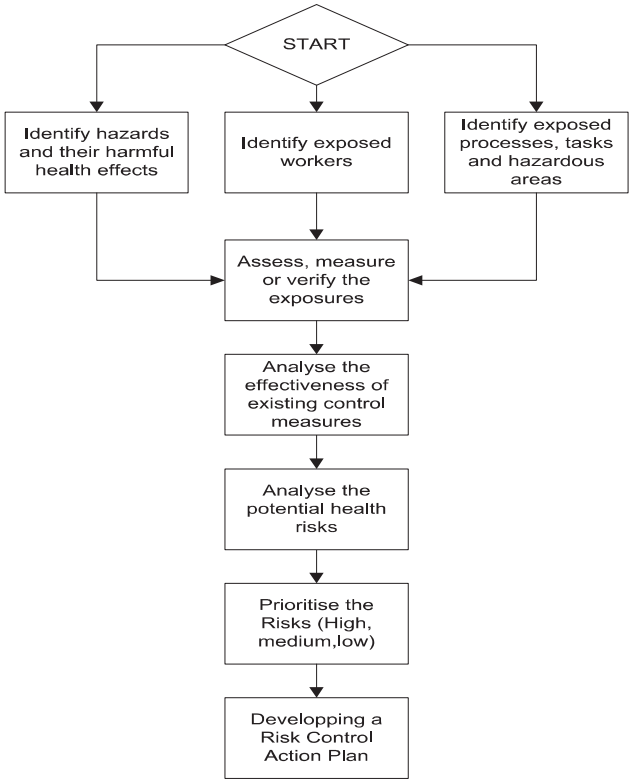

Figure 2. Risk management flowchart.

Mines are complex workplaces and the range of hazards and potential exposures to hazards are extensive. Identifying health hazards is the first step in an OHS risk assessment process. Compiling incident reports, audit reports, occupational illness and injury reports, fault reports of equipment, and Material Safety Data Sheets (MSDS) may be useful for documenting such risks.

It is suggested that conducting a survey of the workplaces will help harmonize, consolidate, and finalize the identification of health hazards. Some key aspects to be considered are as follows:(suggest including topics directly associated with 'ground control' rather noise, vibration, radiation, heat, cold, mist, gases, fibers etc.)

- Physical potential hazards (noise, vibration, lighting, radiation, heat, and cold)
- Chemical potential hazards (dusts, fumes, vapors, mists, liquids, gases, and fibers)
- Safety issues (rock fall, electrical shock, machinery accident, fire and explosion, working at height, and accident involving hydraulic pressure).

Assessing exposure levels is the next step after identifying health hazards in an OHS risk assessment process. It characterizes exposures in terms of their intensity and duration for processes, tasks, and areas. Exposures can be estimated qualitatively or quantified by measurement. A risk assessment worksheet provides the necessary tools to assess risk and therefore avoid it, or to reduce the possibility and percentage of accidents and other risk related incidents. A worksheet for identifying potential hazards and assessment of the risks is provided in Table 2.

Table 2. Checklist for identifying potential hazards and assessing the risks.

Potential Hazard	Likely to be found Yes/No/Not Sure	Details of specific hazard	Likely harmful effects	Acute/Long latency	Hazard rating	Where located (area/process/task)
Rock fall	Yes	falls of small rocks from the mine roof	Injury or dead	Acute	100	between roof bolts
High pressure of hydraulics fluid	Yes	The rupture of the high pressure hose	Injury or dead	Acute	100	Near power support systems

Risk rating is calculated based on the potential health consequence of each identified health hazard with the likely levels of exposures to it, and by the likelihood of the hazard occurring or being present. With a predefined numerical ranking, these risks can be quantified by using the following formula:

$$Risk rating = Consequence \times Probability of exposure \times Period of exposure \times Uncertainty$$

The numeric values for each function of the equation can be found in Tables 3,4,5,6, and 7.

Table 3. Consequence and numerical rating.

Consequence	Numerical Rating
Exposure at this level is unlikely to lead to harm.	1
Non-life threatening reversible health effects.	15
Adverse health effects that are permanent but do not significantly affect quality of life or longevity.	50
Adverse health effects that are generally permanent and could lead to a significant reduction in quality of life and/or longevity.	100

Table 4. Probability of exposure.

Probability of exposure	Numerical Rating
Low	3
Medium	6
High	10

Table 5. Period of exposure.

Period of exposure	Numerical Rating
Rare (Once per year)	0.5
Unusual (a few times year)	1
Short periods of time (a few times per month)	2
Continuous for between 2 and 4 hours per shift	6
Continuous for 8 hours shift	10

Upon completion of hazard identification and risk assessment, it should be ensured that risks are eliminated or minimized; an ounce of prevention is better than a pound of cure. There are several levels of control to deal with adverse exposures. In order of reliability, effectiveness, and likelihood of reducing exposures they are as follow: elimination, substitution, engineering (including isolation), administration (including education and training), and personal protective equipment.

Mines of all kinds are increasingly concerned with achieving and demonstrating sound occupational health and safety performance, but the range of potential exposures is extensive in mining ground control operations. The OHS management system includes all such risks and determined control. Due to the lack of a systematic management, operators cannot adequately prioritize and address the risks that lead to most accidents. OHSAS provides easy to use guidance and a proven method that will assist in developing a systematic approach to managing hazards that cause accidents. The operator should document and keep the results of identification of hazards, risk assessments, and determined controls up-to-date.

Some determined controls of ground control operations are:

Contact With Live Electrical Conductors or Energized Machine Parts

Electric shocks are a serious problem in the mining environment. Electrical accidents are not restricted to some activities but cover the entire spectrum of mining such as ground control operations. Many ground control machines such as modern bolting rigs, scaling machines, and T.B.M are often powered by electricity. They

work at the harsh environment and any fault or unsafe electrical condition may make fatal accidents.

- Inspect all cables for damage including nearby cables. Test all circuits to ensure that they have been de-energized before beginning work.
- Take electrical measurements to identify any stray electrical currents.
- Conduct repair work at a safe distance from any energized cables.
- Familiarize workers with the work area, and be aware of any hazards.

Table 6. Uncertainty in extent of hazard.

Uncertainty in extent of hazard	Numerical Rating
Certain	1
Uncertain	2
Very Uncertain	3

Table 7. Calculated risk rating, classification of risk, and action.

Calculated risk rating	Classification of risk	Action
400 and above	Intolerable risk	Requires immediate discontinuation/shutdown
200–399	Very high risk	Requires immediate mitigation action with a program to develop a permanent solution
70–199	High risk	Requires mitigation action as soon as possible
20–69	Potential risk	Requires mitigation action and/or monitoring
Under 20	Tolerable risk	Requires monitoring

Potential Accidents Involving the High Pressure of Hydraulics

Hydraulic systems are popular on many types of ground control equipment such as power support systems and hydraulic jacks. Hydraulic systems must store fluid under high pressure more than thousands pounds per square inch. The fluid, under tremendous pressure is hot.

The rupture of the high pressure hose or the residual hydraulic fluid while the hose releases from circuit may spray into the miners' eyes and lead to chemical injuries or strikes to body.

- Disconnect the high pressure circuit on each shield with high pressure valves and electro-hydraulic isolation control buttons.
- Work on a circuit after the pressure is turned off and any locked in pressures have been released.
- Work on a shield component after it is blocked against inadvertent motion.
- Look for damaged hoses or controls.
- Do not place high pressure hoses in travel ways or in areas where miners would be regularly exposed to them.
- Educate miners that certain cylinders contain high pressure after shutting off the valves.
- Check valves keep the pressure in the cylinders to keep the roof supported.

Rock Fall

The result of the hazard of a loose rock falling from a roof or sidewall and striking someone can be fatal if direct physical contact is made.

- The design and installation of ground support and reinforcement systems must be capable of withstanding static and dynamic loads.
- Identify and remove loose roof material from a safe position.
- Always conduct a thorough visual examination of the roof, face, and ribs immediately before work is performed and thereafter as conditions dictate.
- Always stay alert for changing conditions in the work area.
- Release and remove roof support jacks remotely.
- Install breaker post from the outby side of the remaining pillar block toward the pillared out areas.
- Prevent of bounce/outburst on the active longwall face.
- Keep the boom of a scaling machine to a minimum angle to reduce the risk of a rock bouncing into the cab.
- Scale any loose or hazardous roof material using proper equipment and scale from a safe location.
- Know and follow the approved roof control plan including the approved pillaring procedures.
- Be alert to any change of roof conditions.
- Mine personnel not essential to the specific activity should remain outside the work zone.
- Never travel inby supported areas.
- Use roof screen to prevent falls of small pieces of rock from between roof bolts.
- Check roof bolting machines for proper torque settings. Abnormally high torque may also add to the problem of distorted expansion shells.
- Re-instruct roof bolting machine operators as to proper installation procedures, such as proper drill hole depth, resin cartridge length, and installed torque.
- Install and examine test holes regularly for changes in roof strata.
- Use "hands off" drilling method while rock bolt installation operations.
- Assess the suitability of ground controls in variable ground conditions (e.g., expansion shell bolts are generally ineffective in soft rock, as are friction bolts where the correct hole diameter cannot be maintained).
- Be sure that the correct hole length is drilled and holes are flushed clean of all drilling sludge.
- Ensure that the orientation of the hole is appropriate for the excavation geometry and expected block movement. Axial tensile loading of the steel elements installed in the rock is generally preferred; shear loading should be avoided.
- Drill hole nearly perpendicular to the rock surface; use of hemispherical ball and domed plates may be required where this cannot be achieved.

- Appropriately match the load capacity of the anchorage method, bar, or tendon and surface restraint fittings to prevent the premature failure of any one component.
- Ensure that all steel and other components designed to be encapsulated in resin or cement grout are clean of all oil, grease, fill, loose or flaking rust, and any other materials deleterious to the grout.
- Where full grout encapsulation of the steel elements is required, the method of grouting should show a grout return at the collar of the hole; other methods that can demonstrate complete hole filling may also be appropriate.
- Use correct tensioning or loading procedures for the various rock support and reinforcement systems.
- Ensure that plates and/or straps against the rock surface have the required thickness to prevent nuts or barrel and wedge anchors from being pulled through the plate and/or strap at the ultimate tensile strength of the tendon when loaded against the rock surrounding the bore hole.
- Recognize and remedy corrosion issues.
- Check that blast vibrations have not loosened threaded reinforcement systems.
- Regularly carry out load tests on point anchored rock bolts and friction anchored rock bolts.
- Check fully grouted reinforcement systems on a regular basis to ensure that the grout strength and encapsulated length of the bar or tendon is adequate.
- Implement an action plan when it is found that the load capacity of the installed support or reinforcement system, grout strength, and/or encapsulated length does not meet specifications.
- Store resin grouts at the temperature range recommended by manufacturer.
- Use resin grouts before their “use by” date, or within a specified period of time.
- Mix resin grouts for the recommended time and at the recommended speed; these should not be exceeded.
- Mix cement grout at the recommended water cement ratio and at the recommended angular speed in the specified equipment for the required time.
- Ensure that water used for cement grout mixing is of the required quality or the cement used should be able to develop the required uniaxial compressive strength with the run of mine water supply.
- Ensure that any additives (e.g. retarders, accelerators, fluidizers, etc.) to the cement grout mix are added in the recommended amounts and at the specified time in the mixing and pumping process.
- Clean and maintain all grout mixing and pumping equipment on a regular basis.
- Regularly maintain any pumping equipment used to pressurize rock support and reinforcement and operate it at the recommended pressure.
- In shotcrete mix specifications, state the slump of the mix, the uniaxial compressive strength, and a measure of the toughness of the product at specified time intervals prior to or following mine application, as appropriate.
- Collect samples of the mine shotcrete mix at specified intervals, under normal mine operating conditions, and test the mix by a registered concrete testing laboratory for compliance with the shotcrete design specifications.
- Test shotcrete thickness regularly during placement to ensure that the specified thickness has been applied; a means of permanently marking the shotcrete surface with a depth gauge probe may be appropriate.

Working at Height

Rock reinforcement is included in some activities such as scaling, bolting and screening. These activities involve generally working at height.

Steps, platforms, walkways, handrails, handholds, and guardrails must be designed to provide safe entry to, and exit from, a machine operating station and areas where maintenance is performed.

- Use proper fall protection equipment such as the full body harness.
- Make sure ladders, steps, and platforms are securely anchored and well maintained.
- Make sure boarding ladders and travel ways are well illuminated and unobstructed.
- Make positive contact with the machine operator before mounting or dismounting equipment.

Measures for risk management should reflect the principle of the elimination of hazards where practicable, followed in turn by risk reduction (either by reducing the likelihood of occurrence or the potential severity of injury or damage), with the adoption of personal protective equipment (PPE) as a last resort. The legal and other OHS applicable requirements relevant to ground control are taken into account in the OHS management system.

IMPLEMENTATION AND OPERATION

Resources, Roles, Responsibility, Accountability, and Authority

Top management shall take ultimate responsibility for the OHS management system. Management commits to providing resources including human resources and specialized skills, organizational infrastructure, and technology and financial resources, as well as defining roles, allocating responsibilities, and delegating authorities to facilitate effective OHS management in accordance with this OHSAS Standard.

Competence, Training, and Awareness

Each person who has an impact on OHS is competent on the basis of appropriate education, training, or experience. The operator shall provide training to meet the training needs of personnel, which should take into account differing levels of responsibility, ability, language skills, and literacy. The effectiveness of the training should be evaluated thereafter. Safety subjects relevant to ground conditions and control must be included in training programs and the training required must be provided to miners before they begin work at a mine, or before they receive new work tasks or assignments. Each worker must have a sound understanding of identifying hazardous ground conditions and safe mining practices to keep them safe.

The people who are working under an operator’s control should be aware of the actual or potential consequences of OHS to their work activities and their roles and responsibilities in OHS management system.

OHSAS requires mine operators to provide information to miners concerning hazards. It is based on two safety and health principles: (1) miners have a right to know about the hazards where they work, and (2) miners have the responsibility to know about hazards at workplace.

Communication, Participation, and Consultation

Safety begins with teamwork; therefore, communication among various levels, participation from workers, and consultation are essential to implement the OHS management system. An example of the minimum contribution by workers to reduce ground control accidents is the examination of the roof in the work area prior to commencing work and being alert of changing roof conditions.

Documentation

Documentation provides evidence. Documentation is proportional to the level of complexity, hazards, and risks concerned and is kept to the minimum required for effectiveness and efficiency. The basis of the documentation is shown in Figure 3.

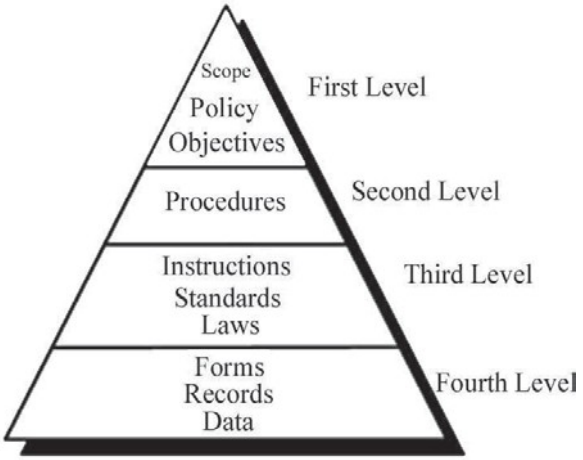

Figure 3. Documentation pyramid for OHSAS Standard.

All aspects of ground control are included in the ground control plan. It outlines the system used to manage ground control. All supporting documentation shall be readily available and reviewed regularly.

Control of Documents

Documents required by the OHSAS Standard shall be controlled. The producers of control of documents shall provide approval of documents for adequacy prior to being issued, and revise them if necessary. A competent authority is generally authorized to control the ground control plan.

Operational Control

The operator shall apply operational controls over the identified hazards to manage the OHS risks. Operational control includes controls related to purchased goods, equipment, services, contractors, and other visitors to the workplace.

Emergency Preparedness and Response

The operator shall establish that the producers identify the potential for emergency situations and response to such emergency situations to prevent or mitigate associated adverse health and safety consequences.

Being prepared for emergencies means ensuring that the necessary equipment and supplies are readily available and that all employees know what to do when an unplanned event occurs, such as a roof collapse. These procedures should be in writing, and employees should have the opportunity to practice their emergency response skills regularly. An emergency plan should include the needs of relevant interested parties, for instance, those of emergency services and neighbors.

CHECKING

Performance Measurement and Monitoring

OHSAS 18001 requires that OHS performance be monitored on a regular basis. The monitoring mechanism shall control both qualitative and quantitative proactive and reactive measures of performance (conformity with the OHS programs, operational criteria, and incidents) and the effectiveness of prevention methods.

Ground support and monitoring of ground control issues used must be implemented in a suitable manner in relation to the particular mining environment at any location in a mine. The monitoring data needs to be systematically recorded to build up a good understanding of how the mine is performing with time. Monitoring data also needs to be conveyed to the employees in a timely and clear method, explaining the risks and actions required to be taken.

Evaluation of Compliance

OHSAS 18001 requires that compliance with applicable legal and other requirements is monitored and records maintained.

Governments authorize the formulation of the code of regulations for mine safety, and parliaments legislate laws relevant to mining. International organizations such as International Labor Organization and the World Health Organization have offered OHS recommendations. Governments employ many inspectors to ensure that operators observe the national and international laws. The establishment of OHSAS 18001 satisfies governments on operators' adherence to OHS codes.

Incident Investigation, Nonconformity, Corrective Action, and Preventive Action

OHSAS 18001 requires incident investigation, nonconformity, corrective action, and preventive action. The wording of this requirement has been enhanced to ensure that incidents are investigated and that results are recorded and analyzed.

Nowhere is this more evident than in effective incident investigation, where prejudices, preconceptions, and value judgments predominate, along with limiting beliefs such as "most accidents are caused by human error/unsafe acts." Such models

subconsciously restrict the flow of information and result in many relevant factors in an incident being overlooked.

Control of Records

OHSAS 18001 requires an operator to ensure that the mine develops a procedure for identifying, maintaining, and disposing of safety-related records. The procedure for the control of records should require that records be legible, protected, and readily retrievable. Records are essential to demonstrate the satisfactory operation of the safety management system.

Internal Audit

An organization confirms through internal audit that their OHS management system complies with intentions and with the requirements of OHSAS 18001.

Rock mass characteristics change during the process of mining; consequently, it is necessary during operation that the operator undertakes regular audits of ground control systems to ensure continued validity of all components within the system and formally modify the process as indicated by the audit.

MANAGEMENT REVIEW

Top management shall review the organization's OHS management system at planned intervals to ensure its continuing suitability, adequacy, and effectiveness. Reviews shall include assessing opportunities for improvement and the need for changes to the OHS management system, including the OHS policy and OHS objectives.

CONCLUSION

The goal of all mine safety professionals is to make mines a safer place to work. Nearly every mine eventually encounters poor roof conditions and the need to control ground at some point. Reducing the number of rock falls and other hazards during ground control operation injuries by establishing an OHS management system will help. It has been appreciated for many years that effective management of occupational health and safety can significantly reduce risk exposure and potentially improve an organization's profitability and sustainability. Leading studies have recognized that implementing a formal occupational health and safety management system based on OHSAS 18001 is an excellent means of achieving this business aim.

The OHSAS specification is applicable to any mining operator from small-scale mine to mining multinational consortium. All of De Beers Group's diamond mining operations and Rio Tinto's sites acquired prior to 2005 are certified to OHSAS 18001 standard.

REFERENCES

British Standard, (2007). "Occupational health and safety management system-requirements."British Standard Institution.

[http://shop.bsigroup.com/en/ProductDetail/?pid=000000000030148086].

Brady, B.H.G., Brown, E.T.(2006).*Rock mechanics for underground mining*. India: Springer.

Brauer, R.L. (2006). *Safety and health for engineers*. New Jersey: John Wiley &Sons, Inc.

Compton, C., Gallagher, S., Molinda, G., Mark, C., (2007), "Roof screening for underground coal mines: recent developments." 26th International Conference on Ground Control in Mining.

Cahill, J., Lee, M. (2006)."Ground control at Leinster nickel operations."*Journal of the South African Institute of Mining and Metallurgy*.*106* (July): 471–478.

Fischer, H., Klarman, K., Oboroceanu, M.J. (2007). "American war and military operations casualties: lists and statistics." Congressional Service Research.

Goetsch, D.L. (2008). *Occupational safety and health for technologists & engineers and managers*. New Jersey: Pearson Education, Inc.

MacNeill, P. (2008). International mining fatality database: project report. Overview of the project undertaken at the New South Wales department of primary industries. In: Minerals and Petroleum, New South Wales Government. [http://www.dpi.nsw.gov.au/minerals/safety/publications/statistical-publications/international-mining-fatality-review].

Mark, C., Pappas, D.M., Barczak, T.M. (2009). "Current trends in reducing ground fall accidents in US coal mines*." SME Annual Meeting and Exhibit*. Littleton, CO:Society for Mining, Metallurgy, and Exploration, Inc.

MSHA(2008)."Coal miner's handbook for roof and rib control." U.S. Department of Labor, Mine Safety and Health Administration.

Oraee, K. (2005). *Support in mines*. Tehran, Iran: Amirkabir University Press.

Safe work Australia, Inc. (2011). *Code of practice. Ground control for underground mines*.Safe work Australia.

Sherard, G.E. (2011). "Pennsylvania mine accidents 1869–1972." Genealogical society of Pennsylvania.

http://www.cdc.gov/niosh/mining/topics/topicpage20.htm

http://www.msha.gov/stats/centurystats/coalstats.asp

http://www.riotintoalcan.com/ENG/ourapproach/34_safety.asp

http://www.debeersgroup.com/Sustainability/Employees/Safety/

Subsidence and Uplift Prediction in German and Polish Hard Coal Mining

Axel Preusse, Director
Heinz-Jürgen Kateloe, Assistant Professor
Institute of Mine Surveying & Mining Subsidence Engineering
Rwth Aachen University
Aachen, Germany

Anton Sroka, Director
Institute of Mine Surveying & Geodesy
Freiberg University of Mining & Technology
Freiberg, Germany

ABSTRACT

For the last 150 years, subsidence damage to the surface has been an unavoidable phenomenon associated with underground coal mining. In particular, the mechanization of mining methods in multiple seam mining and the concentration of mining activities in densely populated European metropolitan areas (e.g., Ruhr, Upper Silesian industrial region) have led to mining having a very strong influence on the earth's surface. In both these regions, surface subsidence of more than 20m has been reported up to now in comparison to the original state. Underground coal mining in these regions strongly impairs all kinds of surface use, such as urban and industrial development, infrastructure (roads, waterways, and railways) and pipelines—without restricting the functionality of those objects to a greater extent.

Demanding and, in some cases, globally unique engineering solutions have been developed and implemented for this purpose. The previously mentioned mining and industrial regions are still very strongly characterized by the (increasingly declining) coal industry and will remain dependent to a large extent and for an indefinite period on artificial drainage measures because subsidence that has already occurred is irreversible.

This paper will primarily discuss the prediction of subsidence that is caused by intensive multiple seam mining and its influence on surface objects (e.g., underground pipelines). However, an approach for predicting ground uplifts due to rising mine water as a consequence of mine closures will also be described.

INTRODUCTION

In order to maintain the viability of infrastructures at the ground surface during mining activities, prediction methods that accurately estimate land subsidence have always been of great significance. These methods have been constantly improved over the past few decades so that computerized and highly accurate ground movement models are now available. In Germany and Poland, these models have been expanded in order to be able to also predict wide-ranging surface uplifts, which, in the long run, might occur due to rising mine water in abandoned mine sites. In order to accurately calibrate this model for predicting uplifts due to rising mine water, even more specific data is required that will be comprehensively available in the future due to the inclusion of remote sensing data. In this context, an international research project has recently started that will be discussed in this paper.

The first methods developed for subsidence prediction in German and Polish hard coal mining have the goal of proportionally attributing the surface damage costs caused by mining activities in numerous mines to the subsidence caused by individual mines.

However, these methods have formed the mathematical basis for the surface-damage-reducing planning of mining activities for approximately 60 years. The aim is to design the panel geometry and the temporal mining process in such a way that the expected surface damage is minimized. The minimization or prevention of surface damage can also be achieved through plausible qualitative and quantitative predictions of future mining-induced impact and the special protection of endangered structures and buildings.

SUBSIDENCE PREDICTION IN GERMAN AND POLISH HARD COAL MINING, ESPECIALLY WITH REGARD TO MULTIPLE SEAM MINING

The geometric integration method that has been used in Eastern Europe and German-speaking countries for predicting ground and surface movement for approximately 50–60 years is based on the assumption that the so-called "influence function" (Figure 1) is a corresponding parametric Gaussian function (Knothe 1957; Ehrhardt and Sauer 1961). According to the Knothe theory, the subsidence of the ground surface that is located above a "mining element" can be calculated using the following formula:

$$s(r,t) = s_e(r) \cdot f(t)$$

with $$s_e(r) = \frac{a \cdot V}{R_K^2} \cdot \exp\left(-\pi \frac{r^2}{R_K^2}\right)$$

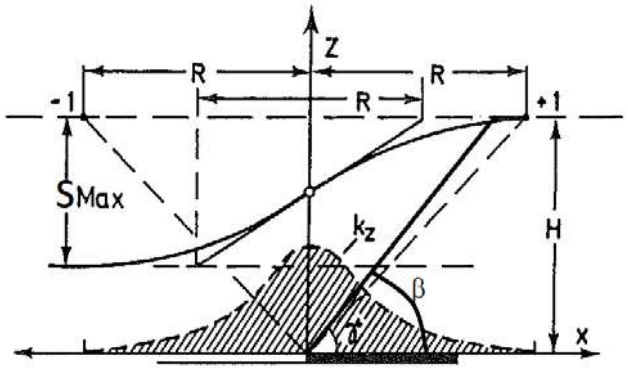

Figure 1. Subsidence curve above the panel edge and the influence function k_z (mining depth H, angle of draw γ, angle of main influence β, radius of main influence R, maximum subsidence s_{Max}) (Kratzsch 1997, Knothe 1957).

$$f(t) = 1 - \exp(-c \cdot (t - t_0))$$

$$V = \Delta x^2 \cdot g$$

whereby, the mathematical symbols used have the following meanings:

s(r,t) – Subsidence of a point within the elementary trough at a point in time t

$s_e(r)$ – Final subsidence of this point on the ground surface (for $t=\infty$)

r – Horizontal distance of this calculation point from the mining element

f(t) – Time function

a – Subsidence factor

V – Volume of the mining element

c – Time coefficient $\left(\frac{1}{\text{day}}, \frac{1}{\text{month}}, \frac{1}{\text{year}}\right)$

t_0 – Point in time of mining this element

R_K – Radius of main influence $(R_K = H \cdot \cot\beta)$

β – Angle of main influence

H – Mining depth

Δx – Edge length of the area of the mining element

g – Seam thickness

In the Knothe method, the angle of main influence describes the zone in which there is a strong probability that surface damage can occur and not the margins of the subsidence trough. The key values *a*, β, and *c* are generally determined based on in-situ measurements. In practice, predicted and measured subsidence profiles are iteratively compared in order to find the best matching key values.

The so-called "RAG subsidence prediction method" has been used in Germany for approximately 50 years. There is a mathematical equivalence between the Knothe theory and the RAG subsidence prediction method that results from the different definitions of the bordering angle of the mining impact. There is a dependency between the angle of main influence β from the Knothe theory and the angle of draw γ from the RAG subsidence prediction method that can be described by the following formula, β being around 10% steeper than γ:

$$\pi \cdot \tan^2\beta = k \cdot \tan^2\gamma$$

with $k = -\ln 0.01$

When this equation is applied, the results of the prediction using both of these methods, meaning the Knothe theory and the RAG subsidence prediction method, are identical.

The use of these methods faces ever-greater difficulties with increasing mining concentrations and the intensive effect on the ground surface resulting from the mining of multiple seams. These difficulties result from the fact that these progressive mining activities strongly affect and, therefore, change the original material characteristics or the original material behavior of the rock strata above the mine. This phenomenon is described in German specialist literature as "multiple seam mining."

Anomalies in the Subsidence Trough as a Result of Increased Multiple Seam Mining and the Associated Change to the Material Characteristics of the Rock Strata

The anomalies found in practice and described in specialist literature for the measured subsidence troughs, in comparison to the traditional method of subsidence prediction, generally focus on four characteristic features. These are

1. Maximum subsidence
2. Maximum tilt
3. Subsidence deficits within the range of the trough slopes
4. Almost even trough margins

These characteristic features are illustrated in Figure 2 and are shown in comparison to a traditional subsidence trough. The traditional solution is based on the RAG subsidence prediction method and the assumption, at least until 1984, that the angle of draw γ was by definition constant. It stood at 54° for a flat formation (Pfläging 1984).

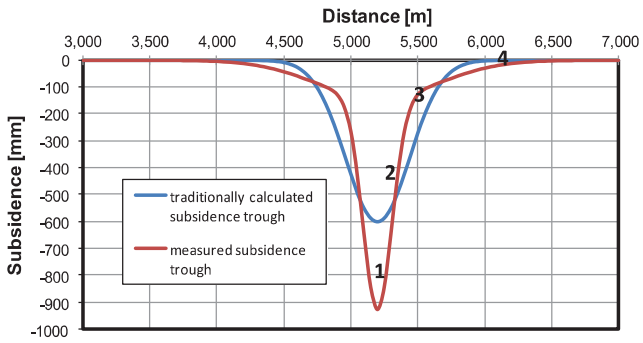

Figure 2. Comparison of the classically calculated subsidence trough with a mutated subsidence trough due to increased multiple seam mining (Sroka & Hößelbarth 2010).

As an example, the investigations carried out by Dżegniuk und Niedojadło will be presented here. The authors (Dżegniuk and Niedojadło 1981) presented the results of their investigations into multiple seam mining on the basis of subsidence measurements that covered a mining period of five seams. The results were published in graphical form and are represented in Figures 3, 4, and 5.

The figures clearly show that the value for the subsidence factor *a* (Figure 3), the angle of main influence β (Figure 4), and the time coefficient *c* (Figure 5) get larger in line with the increasing number of seams mined, meaning with increased multiple seam mining. In practice, this means that the trough becomes deeper and deeper, the trough slopes increasingly steeper, and the surface movements ever faster. These qualitative characteristics correspond fully to the phenomenon observed in the Ruhr region.

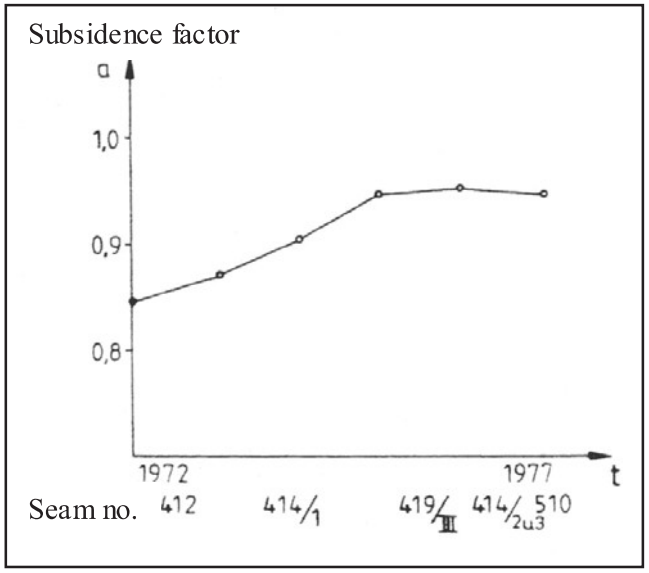

Figure 3. Temporal change of subsidence factor a due to multiple seam mining (Dżegniuk & Niedojadło 1981).

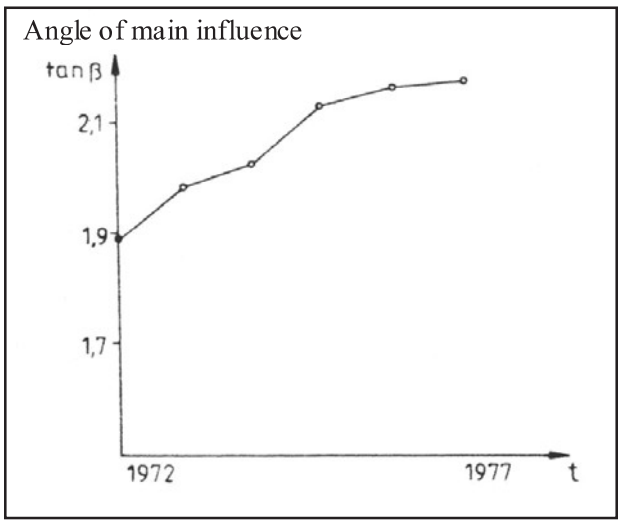

Figure 4. Temporal change of angle of main influence β due to multiple seam mining (Dżegniuk & Niedojadło 1981).

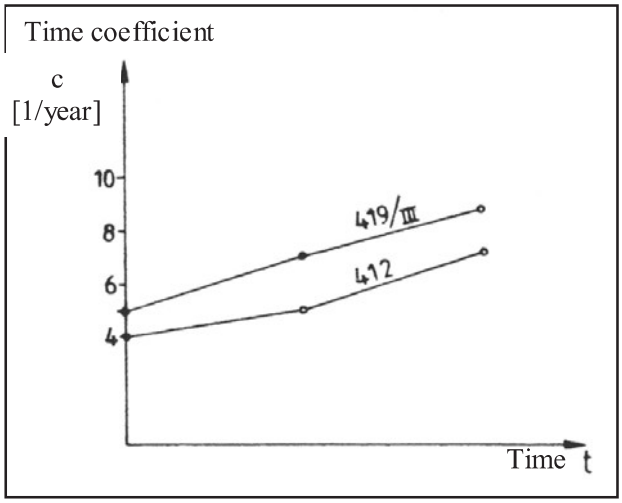

Figure 5. Temporal change of time factor c due to multiple seam mining (Dżegniuk & Niedojadło 1981).

However, in view of the different geological and tectonic conditions and the medium mining depth, the question must be asked as to whether a qualitative transfer of the multiple seam mining coefficient—characteristic of the Upper Silesian coal field—to the Ruhr region is possible. In addition, it is noticeable that the special angles of draw for multiple seam mining describe the steepness of the trough slopes and the maximum subsidence very well but do not explain the much too even trough margin. This has resulted in many scientists being of the opinion that the whole trough profile should not, therefore, be calculated using only the angle of draw (Smolarski 1967; Sauer 1973, 1975; Sroka and Schober 1985; Białek 2003; Hößelbarth and Sroka 2006).

Sroka and Schober (1985) have suggested that, as a result of the very high level of multiple seam mining, changes in the behavior of materials should be described using different functions, similar to the area of classical mechanics where elastic, plastic, and viscous behavior are each described using different mathematical approaches.

Subsidence Prediction Approaches for Areas of Multiple Seam Mining

As far back as the beginning of the 1950s and 1960s, in areas of intense multiple seam mining, significant deviations were observed between the subsidence predictions calculated with the aid of Gaussian influence functions and the actual subsidence measured in-situ. This was one of the reasons why Smolarski (1956, 1967) proposed describing the subsidence resulting from a mining element using two Gaussian functions in order to determine both the mid-section of the subsidence trough and the trough margin (Figure 6):

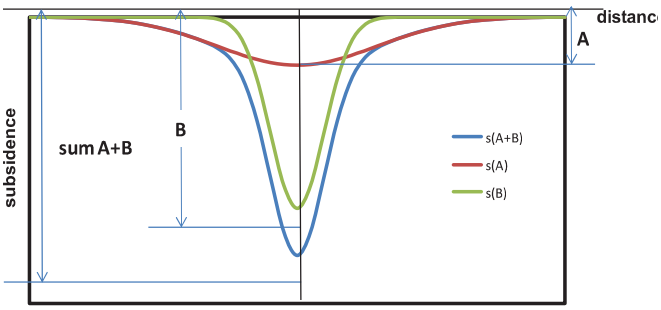

Figure 6. Graphical illustration of the proposed solution of Smolarski (1967).

$$s(x) = A \cdot \exp\left(-\frac{x^2}{\alpha}\right) + B \cdot \exp\left(-\frac{x^2}{\beta}\right)$$

The variables used have the following meanings:

α,β – Variance function that describes the horizontal spread of both of the individual subsidence troughs

A,B – Proportion of the maximum subsidence s_{max} for the mining element (s_{max} = A+B)

In Germany, there have been numerous reports published about the effects of intense multiple seam mining since 1969 (Lautsch 1971, 1974; Sauer 1973, 1975). According to Sauer (1975), there have been occurrences of trough formations with steeper slopes and, therefore, increased tilts—which is a significant change in comparison to earlier observations.

In German literature for this period, a number of possibilities for taking into account the changes resulting from intense multiple seam mining and mining concentrations were proposed for the prediction of surface movements (Sauer 1973, 1975; Pfläging 1984).

In his published work from 1973, Sauer wrote, amongst other things, that "an adjustment above the calculation is currently only possible to a limited extent through the distribution of compensation zones and using calculative angles of draw of approximately 63°. If necessary, it requires working with two angles of draw for flat formations." He continued: "It is necessary to observe here that the calculated angle of draw must not be perceived as the angle to the border of the mining influence range but rather as a factor that when changed allows for an adjustment of the shape of the subsidence trough."

In his published work from 1975, he introduced the term "ground-specific angle of the trough center" instead of the calculative angle of draw. Unlike the angle of draw, the ground-specific angle of the trough center is not defined to the border of the subsidence trough. It serves only to adjust the inner form of the trough. According to Sauer, this requires a ground-specific angle of the trough center of between 63° and 67.5°.

It must be taken into account that the panel edge zone will also have an effect on the form of the calculated subsidence trough. If this zone of partial convergence is considered within the calculation, then less subsidence is calculated at the sides of the subsidence trough than when not applying the panel edge zone in the calculation. In addition, increasing the subsidence factor (according to Sauer for caving "a" = 1.0) results in a deepening of the subsidence trough. This has the most powerful effect on the deepest part of the trough and the least effect on the trough margins. However, these measures do not lead to any improvement in describing the subsidence on the even trough margins (Figure 7).

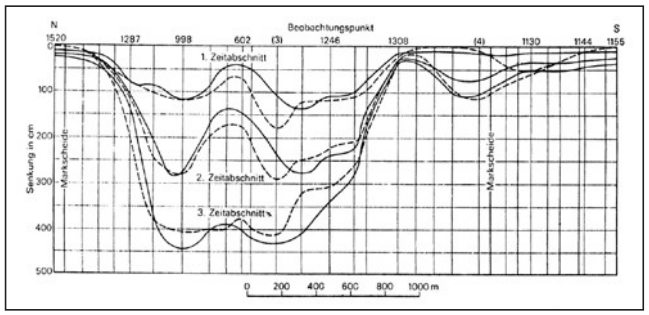

Figure 7. Measured (solid curves) and calculated subsidence values (dashed curves, γ = 70 gon) along a monitoring line (Sauer 1975).

In the opinion of Sauer, a possible solution for describing the impact phenomena of multiple seam mining is the superposition of two subsidence curves, meaning a subsidence curve with an even ground-specific angle of draw is superposed onto a curve with a steep ground-specific angle of the trough center. However, this solution has not been implemented in the German hard coal mining industry up to now. In contrast, it has been widely used in Poland for approximately 10 years as the standard process for predicting subsidence (Białek 2003).

According to this method, the subsidence of a point can be calculated using the following formula:

$$s(a;\lambda_1,\beta_1;\lambda_2,\beta_2) = \lambda_1 \cdot s(a,\beta_1) + \lambda_2 \cdot s(a,\beta_2)$$

with: $\beta_1 < \beta_2$ and

$\lambda_1 + \lambda_2 = 1.0$

The variables used in the formula have the following meanings:

a – Subsidence factor (for caving a = 0.9)

β_1 – Specific angle of draw for describing the trough margin

β_2 – Specific angle of draw for describing the trough center

λ_1, λ_2 – Proportional volume of the individual troughs for generating the total sum subsidence trough

The two angles β_1 and β_2 are combined into one angle for technical reasons, which assumes the role of the official angle of main influence β:

$$\beta = \arctan\left[\lambda_1 \cdot \tan\beta_1 + (1-\lambda_1) \cdot \tan\beta_2\right]$$

The angle defined by Białek β corresponds to the ground-specific angle of the trough center from Sauer or the special angle of draw for multiple seam mining from Pfläging. According to Sauer, a special angle of draw for multiple seam mining of at least 63° should be introduced for areas with heavy mining concentrations and those with high levels of multiple seam mining.

Case Study 1: Prediction of Ground Movements Due to Multiple Seam Mining

In Figure 8, the differences between the subsidence troughs for virgin ground and intensely exploited ground are illustrated using a mining panel. The input data is as follows:

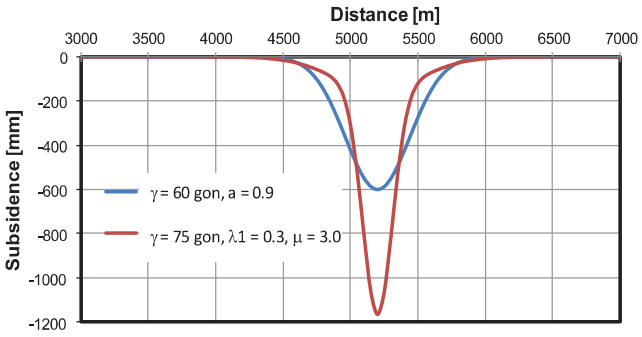

Figure 8. Comparison of calculated subsidence troughs using the default parameters (a = 0.9, γ = 60 gon) and the proposed solution, respectively (Sroka & Hößelbarth 2010).

- Virgin ground: a= 0.9, γ = 60gon,
- Intensely exploited ground: a = 1.0, γ = 75 gon, λ_1= 0.3

$$\mu = 3.0 = \frac{\tan\beta_2}{\tan\beta_1}$$

- Panel data: d = 300 m, H = 1000 m, M = 2.0m,

paneledgezone = 50 m

However, experience to date has clearly shown that a realistic adjustment of the calculated values is only possible when taking into account the panel edge zone (Sauer 1975). The width of an unweighted panel edge zone is determined in specialist literature using different formulas. These formulas show the dependency of the width of the panel edge zone to the mining depth *H* or the radius of main influence *R*:

- According to Szpetkowski (in Białek 2003):

$$b = 1.2 \cdot \sqrt{H} \quad [m]$$

- According to Białek (2003): b = 0.07·H

$$b = (0.12 \text{ to } 0.18) \cdot R$$

- According to Sroka: b = (0.10 to 0.15)· R

$$b = \sqrt{H}$$

with:

R = H · cotγ and

γ – Special angle of draw for multiple seam mining

Taking the panel edge zone into account calls for a change to the calculation method. In a calculation made without the panel edge zone, the subsidence calculation is achieved through the separate calculation of the subsidence caused by individual panels and the use of linear superposition (meaning summation). In the case illustrated in Figure 9, the total sum value for the subsidence of a point has been calculated using the following formula:

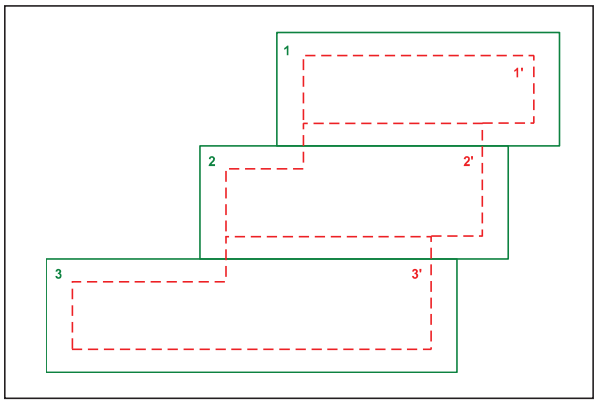

Figure 9. Illustration on subsidence prediction with regard to an edge zone (Sroka & Hößelbarth 2010).

$$s(1+2+3)=s(1)+s(2)+s(3)$$

This means every mining panel can be calculated separately.

This is not the case when the panel edge zone is taken into account. The subsidence that is caused by mining the third panel can only be calculated as the difference between the whole subsidence, meaning the subsidence caused by panels 1, 2, and 3, and the subsidence that was caused by the first two panels:

$$s(3')=s(1'+2'+3')-s(1'+2')$$

The solution presented here using two Gaussian functions is comparatively easy to implement. The prediction must only be carried out twice with different pairs of parameters (α_i , γ_i — *for* i = 1,2), and the calculated subsidence values are then added together. An identical process is valid for the calculation of other components of surface movement.

Case Study 2: Protection of Underground Pipelines

In the Ruhr district, public and private infrastructure pipelines are made of cast iron, steel, plastics, or asbestos cement. The legal framework, technical regulations, and normative standards define which pipeline materials may be used for the transmission of which type of medium. Thus, it is only permitted to transport ground water endangering substances, as well as inflammable or explosive products, in steel pipelines. Ground movements, due to underground mining, are transmitted via the soil to the pipeline and cause extra strain within the steel pipeline (see Figure 10). In extreme cases, durable deformations can occur that are characterized by an oval form or a fold in the pipeline. To avoid or minimize damage, balancing elements are installed into the relevant pipeline, reducing the ground movements that might otherwise cause damage.

Figure 10. Mining-induced leakiness of a stuffing box expander.

The distance between the balancing elements is not determined by random but by using a calculation method developed in the scope of a PhD thesis (Spielberg 1999) that represents the currently available standard in science and technology. This calculation method takes into account all relevant variables that impact on the movement behavior of steel pipelines in mining areas, such as technical data for the pipeline design (e.g., steel grade, wall thickness, weld seam quality), soil conditions (e.g., friction), laying depths of the pipelines, operational impact (working pressure, corrosion), and mining impact. Mining has not caused any damage to steel pipelines protected by this calculation method to date, which is described in detail by Preusse et al. (2004).

The following example shows the protection provided to a municipal gas pipeline network (see Figure 11). Four gas pipelines of size DN 200 PN 4 were laid in steel pipes in four streets. Different mining panels will affect these pipelines in the coming years. In this example, only the influence of one single panel was assumed for protection purposes.

The following is the mining data for the panel:

Mining depth: H = 800 m

Long wall face width: b = 360 m

Panel length: l = 1000 m

Seam thickness: M = 2.0 m

The ground movements were predicted using the following characteristic values:

Subsidence factor: a = 0.95

Angle of draw: g = 60 gon

Time factor: z = 1

Radius of critical area: R = H × cot g = 581 m

The following pipeline data was considered:

Steel grade: St 37.0

Yield strength: s = 235 N/mm²

Welding seam factor: S_N = 1

Pipe external diameter: d = 219.1 mm

Pipe wall thickness: s = 4.5 mm

Wall thickness tolerance: Δs = 0.35 mm

Corrosion flux: k = 0.0 mm

Safety factor: S_F = 1.5

Expander resistance: w = 25 N/mm² (compensator expander)

Expander path: ΔL = ± 200 mm (on centric adjustment)

Operational influences:

Operating pressure: Po = 4 bar = 0.4 N/mm²

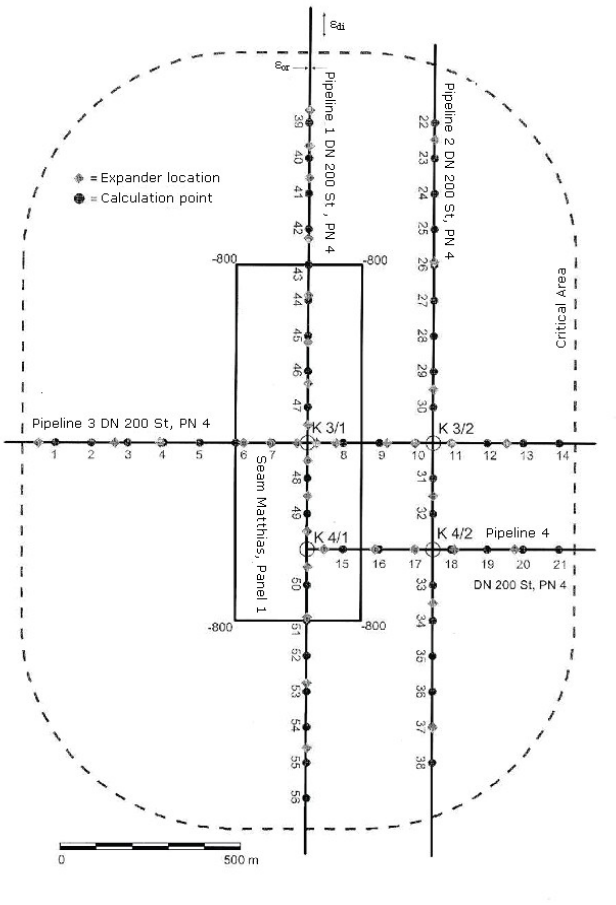

Figure 11. Illustration of the calculated expander distances for the pipelines 1, 2, 3, and 4.

The pipeline operator provided the following details concerning the soil conditions and laying data:

Moist volume weight: $\gamma = 18\ kN/m^3$

Friction coefficient: $m = 0.25$

Transfer coefficient: $h = 1.0$

Laying depth: $t = 1.0\ m$

The calculation point distance was set to about 10 % of the radius of the critical area (50m) for the prediction. In Figure 11, only every second calculation point is displayed. Particular attention was given to junctions and crossovers because these points act like anchor points in the soil. Due to their influence as anchor points, these have to be uncoupled, if necessary, from the rest of the pipeline via a balancing element to prevent future mining-induced damage to the pipeline.

Via the shape-modification-energy-hypothesis which considers the influence of multi-axial states of strain, the following pipeline strains and, subsequently, the linear changes in the soil were calculated:

for the extension area:

$$\sigma_{T,perm.} = 161\ N/mm^2$$
$$\varepsilon^{+}_{P/S,perm.} = 0.77\ mm/m$$

for the compression area:

$$\sigma_{C,perm.} = 152\ N/mm^2$$
$$\varepsilon^{-}_{P/S,perm.} = 0.72\ mm/m$$

The permissible linear changes were exceeded by the results of the prediction so that the pipeline had to be protected. In this case, the transmission behavior of the soil onto the embedded pipeline is approximately the same as the movement dispersion within the soil (transfer coefficient h = 1, 0).

When looking at the protection, it is important that the most unfavorable results are always considered (e.g., a critical compression maximum). Otherwise, critical intermediate states might remain unrecognized, which can no longer be identified on an overall view of several panels due to the overlapping of different areas of extension or compression.

Figure 11 shows the results of protecting the gas pipeline. The expander distances of pipeline 1 turn out to be clearly lower compared to the parallel running pipeline 2. The influence of compression in the area of pipeline 1 clamps this pipeline more strongly than in the area of pipeline 2, where impact by compression is lower.

For junctions and crossovers, expander distances were limited to about 50 % of the permissible length to uncouple these anchor points from the rest of the pipeline network due to the expected impacts of later mine activity.

AN APPROACH FOR PREDICTING GROUND UPLIFTS DUE TO RISING MINE WATER

In addition to continuous movement sequences from deep hard coal extraction, in particular in the case of increased mining activities in the rock, it is also possible for discontinuous movements to occur at the surface within the area of the so-called “discontinuity zones.” As a prerequisite, uniform troughs require a “healthy” (little-worked) rock that is largely free from geological faults with a thick, low-bending covering rock, which largely compensates for the discontinuous movements of the basic rock (Kratzsch 1997). If these preconditions are not met, the subsidence trough will deviate from its ideal form or show locally limited anomalies, such as ground cracks or ground steps. Such anomalous trough forms may have tectonic, extraction, or hydrological and/or hydro-geological causes.

With regard to the consideration of possible long-term damage as a consequence of underground extraction, such discontinuity areas may also play an important role in connection with the renewed increase in mine water levels in areas where mines have been shutdown. Thus, following a renewed increase in mine water levels, the reverse process to subsidence, namely an uplift process, can occur at the surface. Ground movements in the form of uplifts at the ground surface have only been dealt with more specifically by specialist literature in recent years. Although

these uplift phenomena at the ground surface are not completely new, the building damage associated with them (Figure 12) was identified for the first time from about the year 2000 in the location of Wassenberg (Rhineland, Germany) following the closure of the former hard coal mine Sophia Jacoba and the abandonment of mine water drainage (Baglikow 2003). The uplift phenomena observed so far have been within the low decimeter range, the general control of which does not represent any technical problems. However, the uplift differences on this side and beyond a discontinuity zone cropping out at the ground surface, with buildings on top of it, do represent a problem (Figure 13).

In theory, these effects may also occur in other hard coal areas if conditions of this type exist (i.e., uplifts, caused by an increase in mine water level, within the area of discontinuity zones while simultaneously making intensive use of the ground surface).

Figure 12. Uplift damages to the old city hall in Wassenberg, Germany.

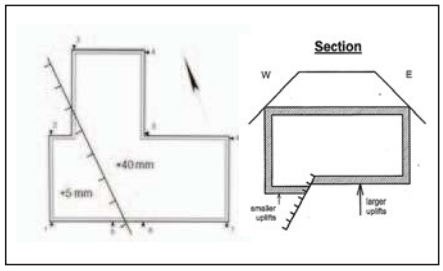

Figure 13. Uplift difference at a tectonic fault.

Using suitable data material, RWTH Aachen University, Freiberg University of Mining and Technology, and Clausthal University of Technology have carried out joint research into the fundamentals, interrelationships, and dependencies for the spatial and temporal occurrence of mine-related lifting phenomena (Figure 14). Furthermore, existing uplift prediction methods will be investigated as to their usability and modified in accordance with the principles derived from this analysis (Holzheim, Preusse, and Sroka 2006). One of these methods (Fenk 2000) is based on the assumption that a mine flooding would lead to an expansion of rock strata which were shattered by the mining activities. Employing the elastic approach of Hooke, surface uplifts can be calculated by the following equation:

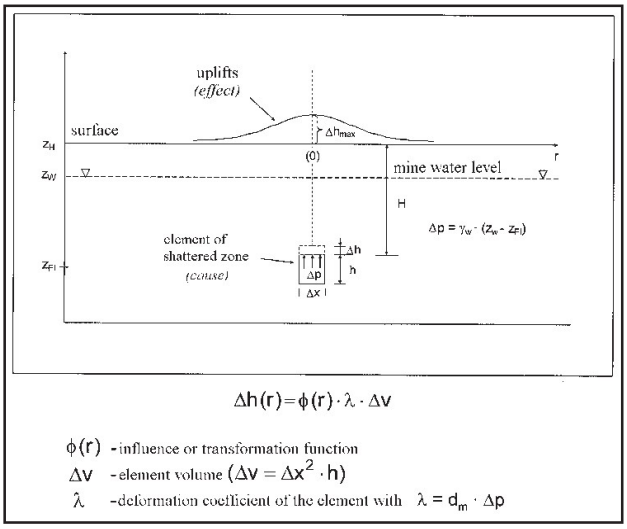

Figure 14. Sroka's uplift prediction model.

$$h = d_m \cdot \gamma_w \cdot \left[\frac{E_s}{H \cdot \gamma_G} - 1 \right] \cdot W \cdot s_E$$

with:

h – final surface uplift after cessation of mine flooding

d_m – strain coefficient of the shattered rock strata

γ_w – specific water weight

E_s – stiffness coefficient of the shattered rock strata

γ_G – specific ground weight

W – water rise within the ground

H – depth of the deepest mining horizon

s_E – mining-induced final subsidence of the surface

GMES4MINING – MONITORING OF GROUND MOVEMENTS AND OTHER PHENOMENA

Spatial information is not only needed for an accurate calibration of ground movement prediction methods, but for all phases of the mining life cycle. The main issues are the economical prospecting and exploration of deposits, as well as environmentally friendly and safe mining activities from mine planning, mine development, and mineral extraction through to closure and reclamation. A recent research and development project, named GMES4Mining and funded by the Federal State of North Rhine-Westphalia, Germany, and the European Union, European Regional Development Fund, aims to develop multi-sensorial analytical methods, as well as geographic information technologies (Benecke et al. 2012). In particular, high-resolution hyper spectral and multispectral data, as well as radar data, will be tested in combination with innovative in-situ measures (e.g., latest geophysical exploration methods,

ground-based radar, and geoinformation technologies. All methods used will be bundled as cross-technology geoservices and optimized in line with the actual requirements in the industry within pilot studies in selected mining areas in Germany and abroad. The final objective is to strengthen the support for all processes in prospection, exploration, and monitoring for the purposes of environmental protection and operational safety in mining.

In order to achieve the optimal adaptation of the GMES4Mining technologies and procedures with regards to both technical and economic aspects, a user survey has been started to gather the geoinformation needs associated with any mining activities. Therefore, the GMES4Mining project team asks mining companies all over the world to support GMES4Mining by taking part in this user survey, which is being carried out by RWTH Aachen University. A questionnaire was compiled and designed to be answered on a PC (Kateloe 2012). This questionnaire relates to surface mining, underground mining, well mining, and storage mining, especially in the context of the prospecting and exploration of mineral deposits, ecological monitoring and ground movement monitoring.

The questionnaire includes

- General questions about a company's mining activities
- General questions about remote sensing within mining projects
- General questions about data processing within mining projects
- Questions about the requirements for prospecting and exploration of mineral deposits
- Questions about the requirements for ecological monitoring
- Questions about the requirements for monitoring of ground movements, even with regard to calibrating ground movement prediction methods

The project partners would be very pleased if mining companies worldwide are willing to answer the GMES4Mining questionnaire. Please download the questionnaire from the following website: http://www.gmes4mining.de/, section "User survey".

Once completed, the user survey will be concluded with a workshop in which the general survey results will be presented and discussed with representatives from mining companies and other institutions.

CONCLUSIONS

The geometric integration method that has been used in Eastern Europe and German-speaking countries for predicting ground and surface movement for approximately 50–60 years is based on the assumption that the so-called "influence function" is a corresponding parametric Gaussian function. The anomalies found in practice and described in specialist literature for the measured subsidence troughs that arise from intense multiple seam mining of the ground, in comparison to the traditional prediction calculations, indicate, in particular, a subsidence deficit in the trough slopes and largely even trough margins.

The method presented here for the prediction calculations based on the superposition of two Gaussian functions can lead to significantly better results than the traditional Knothe or RAG subsidence prediction methods. The experience gained from the Upper Silesian coalfield and the Ruhr region has been very promising. A better prediction calculation method enables more effective planning of the mining activities in terms of surface damage minimization.

As shown in this paper, it is possible based on these Gaussian functions to plan protection measures for underground pipelines and to successfully carry out predictions for surface uplifts that result from the abandoning of mine dewatering activities.

Long-term experience in the field of subsidence prediction in German hard coal mining can be of great significance for mining regions abroad. As papers that have been presented at the International Conference for Ground Control in Mining in the past have reported, mining-induced subsidence is an increasingly important factor in the approval of mine plans. While transferring these prediction methods that have been developed to operational maturity in European coal districts into the international coal industry, some adjustments regarding the different mining conditions (e.g., applied mining methods) could be necessary. Essential adjustments shall be discussed in dialogue with international experts present at the ICGCM. If applicable, some joint international research projects relating to this increasingly important field may be initiated.

In terms of achieving an accurate calibration of the model designed to predict uplifts due to rising mine water, even more specific data is required, which will be comprehensively available in future due to the inclusion of remote sensing data. In this context, the international research project GMES4Mining has been recently started, and mining companies worldwide are invited to support the process of developing cutting-edge geo services for mining projects by taking part in a user survey on the geo information needs associated with mining activities.

REFERENCES

Baglikow, V. (2003). "Subsidence damages after cessation of mine dewatering in deep mining." (German). *J. Markscheidewesen 2*, pp. 45–49.

Benecke, N., Zimmermann, K., Müterthies, A., Pakzad, K., Stephan, S., Kateloe, H.-J., Preusse, A., Pebesma, E., and Prinz, T. (2012). "GMES4Mining—Innovative Geoservices for Exploration and Monitoring of Mining Areas." In: *Proceedings of the AIMS 2012, Seventh International Symposium Rockbolting and Rock Mechanics in Mining*. Aachen, Germany.

Białek, J. (2003). "Algorytmy i programy komputerowe do prognozowania deformacji terenu górniczego." *Monografia, Wydawnictwo Politechniki Śląskiej*. Gliwice, Poland.

Dżegniuk, B. and Niedojadło, Z. (1981). "Zmienność parametrów teorii S. Knothego w trakcie eksploatacji kolejnych pokładów węgla." *J. Geodezja 29, 1981, Polska Akademia Nauk, Kraków*, Poland: pp. 3–10.

Ehrhardt, W. and Sauer, A. (1961). "Die Vorausberechnung von Senkung, Schieflage und Krümmung über dem Abbau in flacher Lagerung." *J. Bergbauwissenschaften 8*(18): Germany.

Fenk, J. (2000). „An analytic approach to the calculation of surface uplifts due to the flooding of underground mines" (German). *J. Markscheidewesen 2*, pp. 420–422.

Holzheim, M., Preusse, A., and Sroka, A. (2006). "Impacts of the mine water rise on the ground surface—State of the scientific knowledge." (German). In: *Proceedings of the 8th Aachen Abandoned Site and Mining Subsidence Conference*. RWTH Aachen University.

Hößelbarth D. and Sroka, A. (2006). "Ein Beitrag zur Vorausberechnung abbaubedingter vertikaler Bodenbewegungen." In: *Proceedings of the 7. Geokinematischer Tag, Vol. 2006-1*. Essen, Germany: VGE Verlag, pp. 308–318.

Kateloe H.-J. (2012). "GMES4Mining – Work package 2000 user survey." (German). Interim report 2011 (unpublished) for the joint R&D project "GMES4Mining—GMES-based geoservices for mining to support prospection and exploration as well as the integrated monitoring for environmental protection and operational security." Supported by the European Union, European Regional Development Fund, and the Federal State of North Rhine-Westphalia. RWTH Aachen University, Germany.

Knothe, S. (1957). "Observations of surface movements under influence of mining and their theoretical interpretation." In: *Proceedings of the European Congress on Ground Movements*. Leeds, West Yorkshire, UK.

Kratzsch, H. (1997). "Mining subsidence engineering." (German). 3rd ed. Bochum, Germany: Deutscher Markscheider-Verein.

Lautsch, H. (1971). "Über die Kinematik der Bodenbewegungen beim Abbau mehrerer flacher Flöze innerhalb eines tektonischen Bereichs." In: *Proceedings of the Lagerstättenerfassung und -darstellung, Bodenbewegungen und Bergschäden, Ingenieurvermessung, Kolloquium Ingenieurmäßige Lagerstättenbearbeitung. Vol. 1*. Clausthal-Zellerfeld, Germany, pp. 121–145.

Lautsch, H. (1974). "Die erweiterte Trogtheorie zur Deutung bergbaulich bedingter Bodenbewegungen." *J. Glückauf-Forschungshefte 1974*(5): 167–173, Germany.

Pfläging, K. (1984). "Die Quantifizierung des Durchbauungsgrades." *J. Das Markscheidewesen 1984*(2): 359–367, Germany.

Preusse, A., Sroka, A., Spielberg, P., Kateloe, H.-J., and Clemens, D. (2004). "A method to determine expander spacing for steel pipelines in mining districts." In: *Proceedings of the 23rd International Conference on Ground Control in Mining*. Morgatown, WV: West Virginia University, pp. 165–172.

Sauer, A. (1973). "Vergleich von Messungsergebnissen an Beobachtungslinien und Ergebnissen von Vorausberechnungen von Bodenbewegungen." In: *Proceedings of the Lagerstättenerfassung und -darstellung, Bodenbewegungen und Bergschäden, Ingenieurvermessung, Kolloquium Bodenbewegungen und Bergschäden. vol. 4/1973*. Berlin, Germany, pp. 311–327.

Sauer, A. (1975). "Die Einflüsse von Durchbauungsgrad, Abbaukonzentration und Abbaugeschwindigkeit auf die Vorausberechnung von Bodenbewegungen." J. Glückauf-Forschungshefte 1975(1): 16–26, Germany.

Smolarski, A. (1967). "On some applications of linear mathematical models to the strata mechanics." *Prace Komisji Nauk Technicznych, Polska Akademia Nauk, Mechanika 3*. Kraków, Poland.

Spielberg, P. (1999). "Pipelines under impact of underground mining. A contribution to the prevention of damages." (German). Doctoral Thesis, TU Bergakademie Freiberg.

Sroka, A. and Schober, F. (1985). "Ein Beitrag zur Erfassung der Durchbauung." In: *Proceedings of the VIth International Congress International Society for Mine Surveying*. Rotterdam, The Netherlands: A.A. Balkema, pp. 634–644.

Sroka, A. and Hößelbarth, D. (2010). "Studie über Möglichkeiten zur Vorausberechnung von Senkungen in stark durchbautem Gebirge." Bericht zum RAG-Forschungsvorhaben 4183172/B59/DE, TU Bergakademie Freiberg. Germany 12/2008–09/2010, unpublished.

Knowledge Is Power: Introducing the MIDAS, a New Permissible Datalogging System for Use in Mines

Tristan H. Jones, Associate Service Fellow
NIOSH-Pittsburgh Resarch Lab
Pittsburgh, PA

ABSTRACT

Beginning in 1987, miniature dataloggers approved by the Mine Safety and Health Administration (MSHA) were publicly available for sale. The principal among these was the model CR21XQM, manufactured by Campbell Scientific, Inc. These dataloggers had been tested and were deemed permissible by MSHA and thus could be installed in the return air of an underground coal mine. In 1996, production of all permissible Campbell Scientific dataloggers ceased due to lack of sales. Data collection with these dataloggers has been a staple of ground control research in the United States for decades, and, without them, or a replacement, the capability to monitor ground behavior is severely impacted. Since that time, any party requiring a permissible datalogger has needed to borrow one that was purchased during the production years. In order to fill this technology gap and ensure its own data-gathering capabilities, the National Institute for Occupational Safety and Health (NIOSH) has developed and refined its own miniature data acquisition system (MIDAS). On February 16, 2010, MSHA deemed the MIDAS to be permissible and approved it for use in the return air of an underground coal mine.

The MIDAS is an intrinsically safe, 16- or 24-bit datalogger, compatible with a wide range of resistive, single-ended, and differential-type instrumentation. It contains enough data storage memory to operate for over a year with typical data rates and is efficient enough to do this on a single C-sized alkaline battery for that entire period. It is menu-driven and requires no programming knowledge to operate. It supports wireless or hardwired communication for datalogger setup and data download.

This paper describes the design, field and laboratory testing, and capabilities of the MIDAS datalogger. While not as fully -functioned as the CR21XQM, it is the only new permissible datalogger available, and there is intent to make it available to the mining industry for purchase.

INTRODUCTION

In many mine research studies, users require the ability to collect large amounts of raw data in an automated fashion. Mine operational decisions also frequently hinge on the collection of data concerning mine conditions and status. Mine safety decisions are also increasingly becoming dependent upon automated data collection and display systems.

The most fundamental and useful data collection and storage systems are miniature dataloggers. They offer simplicity that is not available with large, mine-wide data collection systems. They allow for the collection of large amounts of data from a wide variety of instrumentation. They are small and inexpensive enough to deploy quickly on an as-needed basis, yet robust enough to withstand long-term installations where they are exposed to the hazardous environment of an underground mine for extended periods. The primary limitation of these devices lies in the fact that most of those available do not meet MSHA regulations regarding permissibility. MSHA requires that all electrical equipment installed in the return air of an underground coal mine meet strict standards with regard to prevention of the ignition of hazardous methane or coal dust accumulations that can pose a threat to miner safety.

The critical aspect of permissibility must be considered when contemplating any data collection installation in underground coal mines. In order to prevent the datalogger from acting as an ignition source for accumulated methane or coal dust, it must be specially designed and undergo thorough investigation and testing by MSHA before being granted permissibility. Coal miner safety is protected by the fact that any electrical devices, including dataloggers installed in return air, have been tested to ensure that an electrical fault cannot ignite the atmosphere.

Due to the time, expense, and extra work involved in achieving a permissibility certification, few companies have been willing to undergo the process with their products. The potential market for a permissible datalogger is also small. It has proven difficult for a commercial enterprise to justify expending the resources necessary to achieve certification for a suitable datalogger.

Historically, only four dataloggers have achieved MSHA permissibility certification, including the CR21XQM (21X) and CR10XQM dataloggers made and designed by [1]Campbell Scientific, Inc. (CSI), the Omnidata Polycorder from Omnidata

[1] Mention of specific products and manufacturers does not imply endorsement by the National Institute for Occupational Safety and Health.

International, Inc., and the MB-6TL Vibrating Wire Datalogger produced by RocTest, Inc. Of the four dataloggers, the CR21XQM is by far the most robust in its application and has received the most use by underground mine researchers and mines requiring datalogger installation in return air.

The 21X datalogger has operated safely and reliably for almost 25 years, having been given MSHA approval on March 7, 1988 (Mine Safety and Health Administration, 2012). Its companion, the CR10XQM, was approved on June 15, 1990, but received a low level of interest from the industry. Both dataloggers ceased production in 1996, and while the 21X is still supported by the manufacturer, support will only be continued as long as the original parts can still be replaced with identical components, a requirement of the permissibility certification (Conner, 2010; Campbell Scientific, Inc., 2012). The CR10XQM and the Omnidata Polycorder are no longer serviced by the manufacturer, rendering them obsolete. While the MB-6TL is still available, it is only compatible with Vibrating Wire Instrumentation, limiting its usefulness.

This obsolete status is a major disadvantage to using the 21X. If any of these dataloggers were to be destroyed or severely damaged, they could not be replaced. Even repair of these dataloggers is expensive, given the costs of shipping to and from the manufacturer, the materials, and the lost time. This is partially because the repair must usually be completed by the manufacturer in order to ensure permissibility compliance.

In order to resolve some of the issues with using the available outdated dataloggers and ensure a permissible device, NIOSH developed the MIDAS datalogger. The current version of the MIDAS is actually the fourth version. The previous versions have been used and tested since 2002, and the design of the system began in 1999. It has been built to operate the type of sensors frequently utilized in ground control research. This datalogger has been designed to meet the needs and requirements for use in underground coal mines, making it an extremely robust and useful addition to the engineer's toolkit (Figure 1).

DESIGN CRITERIA

As the 21X datalogger continued to age, it became increasingly more apparent that a replacement datalogging solution needed to be found. A new general purpose datalogger for use in underground coal mines needed to meet the current and future needs of a variety of potential stakeholders, including government, academic, and industrial researchers, as well as be suitable for use in a mine operational capacity, or even as a component in a future hazard warning system. Any datalogger designed to replace the 21X needed to be a full-functioned device capable of being used in a wide array of capacities. Therefore, design of the MIDAS datalogger was completed with certain requirements in mind, listed below, in order to ensure maximum utility.

Design of a new system offers the opportunity to upgrade decades-old equipment and minimizes the chance that monitoring could be halted or prevented by a lack or failure of equipment suitable for use in return air. A new system design also ensures the functionality of the system to meet specific requirements for a datalogger in mining, underground coal mining in particular. Additionally, electronics and computer miniaturization have

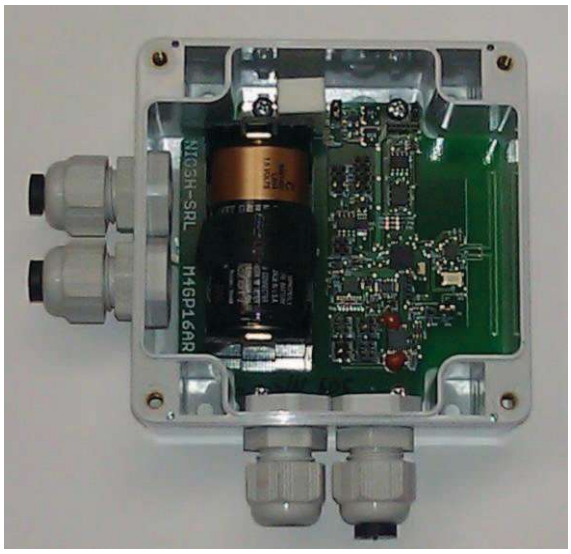

Figure 1. MIDAS datalogger without lid.

advanced significantly in the quarter-century since the 21X was released. The use of modern data-gathering equipment and software has the potential to significantly expand research capabilities while reducing costs for equipment maintenance.

After considering past research needs and techniques, current and upcoming technology, and potential future research directions, some key features were identified as desirable in a new datalogging solution:

- **Ability to interface with key types of instrumentation**: Two types of data-gathering instrumentation are used in ground control research. The first is fully resistive in nature and configured in either single-ended or differential forms. The second is vibrating wire. An MSHA-approved vibrating wire datalogger is already currently available, and options exist to utilize CR21XQM dataloggers with vibrating wire instruments as well. For these reasons the MIDAS will not be designed to be vibrating wire compatible.
- **MSHA permissibility**: A new datalogger must be intrinsically safe and be granted a permissible certification by MSHA. This will allow installation in the return air entries of an underground coal mine and will eliminate the need for electrical and flame barriers such as explosion-proof enclosures.
- **Capability of wireless data download**: A new datalogger should offer the option to download data wirelessly to a handheld device. This would eliminate some of the reliance on wires and cables running to a safe location—wires that frequently get cut during normal mining activities. This also would allow the datalogger to be located in areas that may become inaccessible in the future and still allow data to be collected as long as the unit survived.
- **Inexpensive and expendable**: The datalogger must be inexpensive. Ideally, a datalogger should be inexpensive enough to be considered "throw-away." This would allow great flexibility in installation location.
- **Automated operation and data storage**: It is necessary that the datalogger be capable of operating independently

of a separate controlling computer attached via wire or data cable. The unit should be capable of automatically collecting and storing data in a digital format until the data can be downloaded.

- **Utilization of programmable sample times**: The datalogger must provide the excitation voltage for instruments connected to it at programmable times in intervals ranging from seconds to days. Ideally, it would be possible to set varying sampling time programs for individual instruments on the same datalogger; however, an inexpensive datalogger would allow for the use of multiple dataloggers for this purpose.
- **Single-point download capability**: It should be possible to install the datalogger so that it can retrieve data from multiple locations. An example of this would be to gather data from many positions along a single entry such as a tailgate. This may involve wiring instruments from these multiple locations to a single datalogger or installing a series of dataloggers in different locations and directing all the signals to a common point. The purpose of this is to allow for a single point of contact for data download.
- **Small size and easy portability**: A new datalogger should be more portable than currently available dataloggers. The CR21XQM is typically housed in an enclosure measuring 13.4" x 15.5" x 7.7", and the total package weighs more than 20 pounds, not including instrumentation or wiring. Given the state of modern electronic miniaturization, a significant reduction of this size and weight would be ideal.
- **Improved battery life and data storage capacity**: The datalogger should offer a battery life and storage capacity better than that found on the 21X, given identical sensor suites.
- **Sufficient accuracy and resolution for current and future needs**: The 21X contains a 14-bit analog-to-digital (A/D) converter. In most cases, this has proven to be sufficient for the needs of NIOSH research. However, given the decreases in cost for similar components and the possibility that the MIDAS might be offered to the public, an increased resolution should be utilized.

MIDAS SYSTEM FUNCTIONALITY

Component Overview

The MIDAS datalogging system consists of multiple components working together to achieve maximum utility. The system was granted MSHA permissibility on February 16, 2010. The primary component is the MP4GP16A General Purpose Datalogger. This is the motherboard for the system and handles all of the communication, excitation, and data storage.

The MIDAS has been designed to meet all of the design criteria outlined in the previous section. The datalogger consists of a 16-bit A/D converter, which accepts ratiometric return voltages from fully- resistive instrumentation. Powered by a single C-sized alkaline battery, it is capable of operating with a full load of eight connected instruments for over a year. This is the maximum number of instruments the datalogger can support without added components, as eight is the total number of input channels on the main board.

The datalogger is small compared to the 21X, measuring only 4.3in square and 2in tall. The datalogger housing meets the National Electrical Manufacturers Association standard for protection against dirt and moisture penetration (NEMA 4) and uses cable glands for cable passage into the unit. The unit has also been tested against total submersion in water to depths of less than one foot for up to one week without moisture penetration (though the housing is not specifically rated for submersion).

The datalogger includes four 2.5-V excitation channels, four interconnected ground channels, and eight single-ended input channels. The A/D converter provides a resolution of 1 part in 65,536 units. Neither the excitation voltage nor the resolution can be changed by the user. The datalogger also includes 16MB of solid state memory, which allows it to store over 5 million scans of one single-ended instrument. This memory is enough to run for over 3 years with a one-minute sampling interval, without filling the memory to capacity. The memory is not erased if the unit loses power, and recording stops if the memory reaches capacity.

Additional components, including an instrumentation amplifier (IA) or strain gage digitizer (SGD), can be connected to the main datalogger. The IA allows four of the single-ended instruments on the main datalogger to be replaced with four differential instruments, such as strain gage bridge pressure transducers. In place of the IA, the SGD allows an additional 22 "three-wire connected" strain gages or seven full bridge sensors. In both cases, all sensors receive their excitation power from the main datalogger power supply. While the IA remains a 16-bit interface, the SGD actually increases the resolution of the connected instrumentation to 24 bits. This data resolution is important when the datalogger is connected to strain gauges in instruments, such as strain-gauged roof bolts.

Datalogger Communication

The system also includes a component designed for interfacing with the datalogger called the Datalogger User Interface (DUI, Figure 2).The DUI communicates with the datalogger via wireless signal and operates in the 2.4-GHz radio frequency band, using a proprietary communications protocol differing from the standard 802.11 protocol often occupying the same band. A low-power radio chip was chosen to minimize power drain.

The wireless communication range of the datalogger and DUI is limited primarily by line-of-sight. In above-ground tests, the datalogger has been successful in communicating at ranges exceeding 2,000 ft; in underground tests, ranges in excess of 1,400 ft have been recorded (limited by entry length). Even though the communication is limited to line-of-sight, the system has been shown to be capable of transmitting through small apertures or between obstacles and reaching the receiver on the other side.

The DUI is the primary method of communication with the datalogger for both programming and data retrieval. It is an MSHA-approved permissible device that gives the user access to all of the datalogger's settings and includes a MicroSD flash memory card upon which it stores downloaded data. It operates on two AA batteries and is capable of communicating with up to 256 individual dataloggers over a wireless connection.

The DUI is also available with an optional hard-wired interface. This interface can be used to communicate with up to 64 dataloggers at one time, all wired in a daisy-chain fashion along a

Figure 2. The Datalogger User Interface (DUI).

4-wire RS485-type network cable. This method of connection to the dataloggers allows all 64 dataloggers to be downloaded from a single location and is not line-of-sight dependent. The maximum allowed cable length for communication in this method is 10,000 ft, allowing the user to download data from the dataloggers from nearly 2 miles away.

LABORATORY TRIALS

A number of laboratory trials were completed during the development phases of the MIDAS. These were designed to test the reaction of the system to variables such as temperature change and transmission distance.

As part of the design process, the MIDAS datalogger was subjected to a series of controlled temperature tests. This served to identify how the unit responded to changes in temperature, as well as to check the response of different types of precision resistors.

Temperature Evaluation

The datalogger motherboard accepts up to eight single-ended resistive sensors. To test the datalogger temperature response, the motherboard was fitted with eight ultra-precision voltage divider resistors and then run through a temperature swing in an environmental chamber. Figure 3shows the response of the motherboard in terms of the deviation of the analog-to-digital converter (ADC) count over a -40 to +60 degree C (-40 to +140°F) temperature range. As can be seen, the temperature effect of the datalogger motherboard itself is negligible compared with what might be expected from actual sensors.

In addition to the motherboard test, the IA module was also tested. In this case, the gain of the amplifier was set to 300 for a full-scale span of 8.3mV.The instrumentation amplifier board was

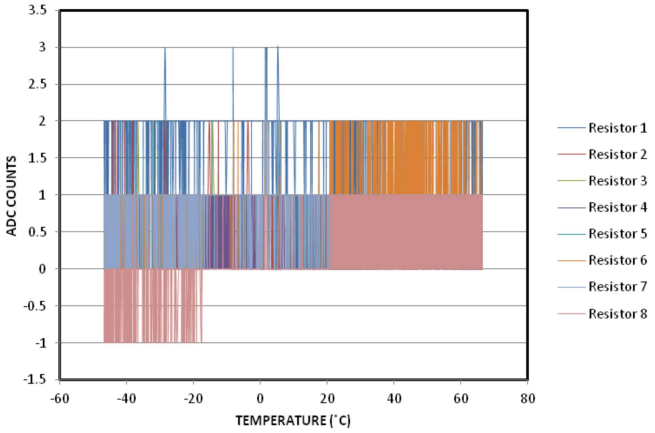

Figure 3. Temperature response of the MIDAS datalogger when fitted with known, ultra-precision resistors, over a 100-degree Celsius range(-40 to +140°F).

fitted with four ultra-precision full-bridge connected resistors. The temperature was again varied from -40 to +60degrees C (-40 to +140°F).This time more variation in the response was seen. This variation was principally caused by the imprecision of the resistor temperature coefficient, not the IA itself (Figure 4).

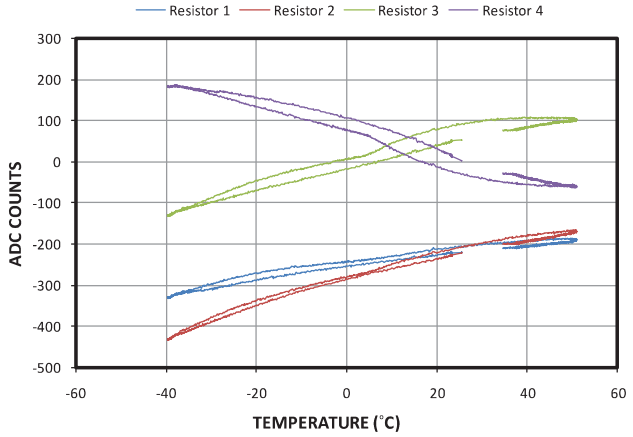

Figure 4. Temperature response of the MIDAS datalogger while using an instrumentation amplifier fitted with known, ultra-precision resistors, over a 100-degree Celsius range(-40 to +140 °F).

Transmission Evaluation

Transmission distance was tested underground at the NIOSH Safety Research Coal Mine, Pittsburgh, PA, and on the surface at the same facility. Straight-line testing was completed in the longest entry in the mine, at 1,400 ft. The MIDAS was hung from the roof of an entry with a height of approximately 6.5 ft. The DUI was used to test for communication ability by conducting data communication checks every 100 ft as the DUI was moved away from the MIDAS. Along that straight, unobstructed line, communication was successful the entire length of the entry.

While previous transmission testing proved that communication is nearly impossible around corners, further evaluation showed that successful communication could be achieved with general obstructions between the devices. For this test, obstructions in the signal line-of-sight were varied and included man-doors and material piles (Figure 5.) They were arranged as follows:

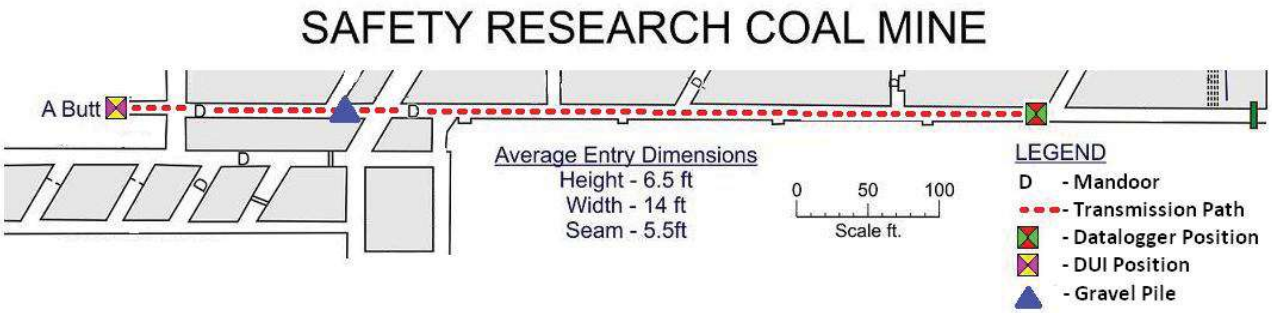

Figure 5. Plan view of the Pittsburgh Safety Research Coal Mine MIDAS transmission test.

- 431 ft from the datalogger was an open man-door, approximately 60in by 34in
- 44 ft beyond the door was a pile of gravel and stopping material, approximately 42in tall
- 116 ft beyond the gravel pile was an open 30in by 24in man-door
- 63 ft past the man-door was the end of the entry, which was the location of the DUI

Underground test results showed that the MIDAS and DUI were able to reliably communicate over a straight-line distance of 654 ft, even with significant obstructions in the line-of-sight, and that the MIDAS should not be expected to communicate around corners. Surface tests at the NIOSH Safety Research Coal Mine made up the remainder of the transmission distance testing. In these tests, the MIDAS and the DUI were able to communicate successfully over a distance of approximately 2,150 ft.

FIELD TRIALS

MIDAS dataloggers were installed in the tailgate of an operating longwall mine along with a 21X datalogger. The goal of the test was to evaluate the operation of the MIDAS in actual mining conditions, as well as to compare the results provided by the MIDAS to those collected by the 21X.

The instrumentation included a suite of rotary potentiometers mounted directly to wood cribs or to the roof in order to monitor the crib and roof-to-floor convergence. The entire dataset collected by the 21X included seven crib and seven roof-to-floor convergence stations. One of the crib/roof-to-floor pairs of sensors was chosen, and identical secondary sensors were installed immediately adjacent to the primary sensors. The primary sensors were connected to the 21X, while the secondary sensors were connected to a MIDAS datalogger. The secondary sensors were placed close to and were anchored (as much as possible) identically to the primary sensors.

The 21X was installed approximately 500 ft away from the instrumented cribs, about 10 ft into a crosscut, to keep it sheltered from mining activities. In order to maintain line-of-sight communications down the entry, the MIDAS datalogger was strapped to the roof screen in the top corner of the entry, 200 ft away from the sensors. Apart from this difference in datalogger placement within the entry, there were no other significant differences in the way the two systems were installed. Mining progressed along the panel and as it neared the dataloggers, both were removed from the mine.

The resulting datasets were combined to allow the performances of the dataloggers to be compared (Figure 6). Over the span of the 180-day evaluation period, the results showed very good agreement between the two dataloggers. The sensors installed on the crib showed nearly identical readings from each of the dataloggers, with the difference between their readings averaging only 0.01in over the first 140 days of the test. Following that, there is an obvious drop in the readings from the 21X before the two units returned to nearly identical readings at around day 175. It should be noted that this type of unexplained shift in data is actually a common occurrence with the 21X and is one of the reasons that a replacement is necessary.

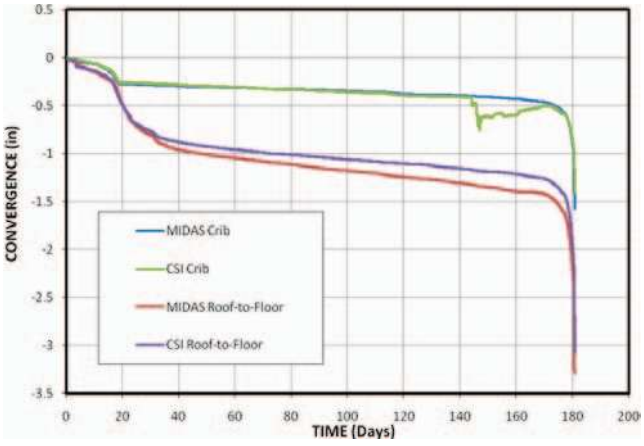

Figure 6. Performance comparison between the MIDAS and Campbell Scientific dataloggers with mine convergence data.

The roof-to-floor convergence sensors are much more dissimilar than those installed directly on the crib. A very large part of this is attributed to the location—being installed on the roof—which certainly provides a much less stable and less uniform installation surface than the wooden crib. That said, at their worst the two sensors only differ by a maximum of 0.24in and have an average difference of 0.14in over the entire period.

The field trial showed that the MIDAS was highly capable of functioning over a long period of time in the mine. No damage occurred to the units, and they withstood the moist and dusty environment without difficulty. The data collected by the MIDAS were very similar to and, in some cases, better than that returned by the 21X, which has been the standard for coal mine data collection for decades. Finally, it is important to note that other successful in-mine field experience has been gathered using the MIDAS and its predecessors but not all of those results are available for publication at this time. Interested readers should consult the following publications for more information: Sunder man et al., 2003; Signer & Sunder man, 2003; Signer et al., 2004.

SUMMARY

The MIDAS system has been designed as a replacement for the Campbell Scientific CR21XQM and CR10QM dataloggers for primary usage in mines. As an MSHA-permissible datalogger, the MIDAS is acceptable for use in underground coal mines, an environment in which it has been particularly difficult to identify other acceptable data recording options.

As designed, the MIDAS meets all of the criteria set forth for a permissible mine datalogger. It has performed successfully during all field and laboratory trials and has exceeded expectations in many regards. It has been shown to return similar or better results when compared with previous datalogging technologies. Transmission distance tests returned results that exceeded expectations with regard to both distance and the ability to transmit through limited obstruction. The datalogger has also performed exceptionally well with regard to having an extensive data storage capacity and battery life.

Currently, NIOSH is in negotiations with external organizations so that they may assume production and sales of this new technology. The hope is that in the very near future the MIDAS will be commercially available to the mining industry. This will fill a critical need for datalogger technology to help ensure mine worker safety.

Disclaimer: The findings and conclusions in this report are those of the authors and do not necessarily represent the views of the National Institute for Occupational Safety and Health.

REFERENCES

Campbell Scientific, Inc. (2012). “Company history.”www.campbellsci.com/history

Conner, K. (2010). Campbell Scientific, Inc. northeast sales engineer. Personal communication.(T. Jones, interviewer).

Mine Safety and Health Administration.(2012). “Approval and Certification Center, Part 18 Instrument Approvals.” http://www.msha.gov/TECHSUPP/ACC/lists/18instrm.pdf.

Signer, S. P. and Sunderman, C. (2003).“New tools for roof support evaluation and design.” In: S. S. Peng, C. Mark, A. Wahab Khair, and K. Heasley, eds. *Proceedings of the 22nd International Conference on Ground Control in Mining*. Morgantown, WV: West Virginia University, pp. 114–118.

Signer, S. P., Pile, J., and Bessinger, S. (2004). “Bolt load changes during initial face advance and cross-cut breakthrough.” In: S. S. Peng, C. Mark, S. Finfinger, S. Tadolini, A. Wahab Khair, and K. Heasley, eds. *Proceedings of the 23rd International Conference on Ground Control in Mining*. Morgantown, WV: West Virginia University, pp. 250–257.

Sunderman, C. B., Signer, S. P., and Johnson, J. C. (2003).“A miniature data acquisition system with LED warning lights.” In: R. K. Singhal, K. Fytak, and C. Chiwetelu, eds. *Proceedings of the Fourth International Conference on Computer Applications in the Minerals Industries (CAMI 2003)*. Calgary, AB: Computer Applications in the Minerals Industries, p. 7.

New Monitoring Technologies for Measuring the In-situ Performance of Rock Bolts

Hani Mitri, Professor
Mining Engineering
McGill University
Montreal, Canada

Andrew Hyett, President
Yiledpoint Inc.
Kingston, Canada

D. Raju Guntumadugu, Ph. D. Student
Mining Engineering
McGill University
Montreal, Canada

ABSTRACT

Understanding the interaction between rock bolts and underground rock movement is critical for safe and cost effective underground excavation design. Although early research on this subject involved a balance of theoretical analysis and field measurement, recent work has been heavily focused on analytical and numerical studies. This paper describes technologies that have the potential to redress the balance through instrumentation of rock bolts deployed under routine operating conditions in underground mines. Two new products are presented in this paper. Firstly the U-cell coupler is a load cell device that can be routinely coupled to the threaded end of a bolt prior to installation. It measures the "series" load at the head of the bolt. Secondly, the d-REBAR involves an array of small-diameter, long-base length displacement sensors recessed into grooves along the entire length of the bolt. Both new instruments are interfaced with on-board digital signal conditioning and telemetry. Methodologies for the deployment of the new instrumentation and guidelines are presented for the interpretation of results based on data obtained from field trials. Successful field installations demonstrate the viability and practicality of these new technologies and, moreover, provide important insight in to rock bolt/rock mass interaction.

INTRODUCTION

Early researchers combined theoretical and experimental research (Freeman, 1978) and (Farmer, 1975). In recent years, the research emphasis has become progressively biased towards analytical and numerical investigations. The advantage of combining the experimental with the theoretical research component is that a support design feedback loop can be established for which predictions from the theoretical and numerical models can be compared against in situ measurements to calibrate the modeling input parameters. Such a feedback loop is more likely to engage practicing engineers and operational decision-makers who may dismiss theoretical or numerical studies alone.

AXIAL ROCK BOLT BEHAVIOR IN A CONTINUUM ROCK MASS

The concepts associated with end-anchored and partially grouted rock bolts are generally well understood. Along the free length of the bolt, the load is constant and equal to the resisting force developed by either a mechanical anchor or a partial section of resin grout.

The case for fully grouted rock bolts is more complex, which probably explains why the majority of recent theoretical studies have been focused on the axial deformation of fully grouted rock bolts in response to a continuous distribution of rock mass convergence. A conceptual model was presented by Freeman (1978). If the bolt is installed with a rigid plate at the bolt head and the excavation surface displaces equally, the neutral point occurs at the excavation surface (Figure 1). The point of maximum axial load along the bolt is referred to as the neutral point and is defined as the point at which the rock mass and the bolt displace equally so that the shear stress within the resin annulus is zero.

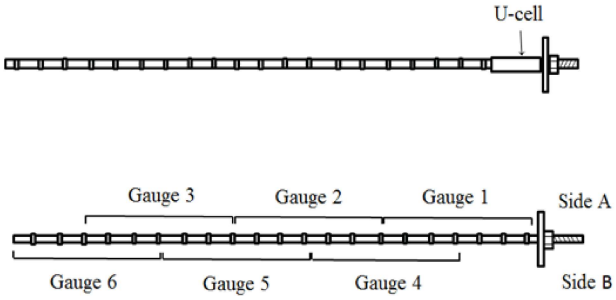

Figure 1. Load distribution along the rock bolt for face plate, attached at the excavation surface, a) no face plate , and b) face plate attached at the excavation surface (Freeman.T.J, 1978).

Many variations of analytical and numerical models have been developed (Mitri and Rajaie, 1990; Tang and Mitri, 2000; Tadolini and Mitri, 2002; Li C, 2009; Martin, Tijani, and Hadj-Hassen, 2011; Deb and Das, 2010; Hyett, Moosavi, and Bawden, 1996). These variations have provided progressively more sophisticated

predictions of how the axial load distribution will change along the bolt and, more importantly, how the bolt will interact with the rock mass to restrain ground movement. For a specific rock mass behavior, the rock bolt performance depends on factors such as the following: (i) the mechanical properties of the bolt and faceplate, (ii) installation characteristics, such as whether the rock bolt is pre-tensioned, (iii) the bond interface properties between the bolt and the resin grout, (iv) the bond properties between the resin grout and the rock, and (v) the timing of bolt installation after excavation.

AXIAL ROCK BOLT BEHAVIOR IN A DISCONTINUOUS ROCK MASS

In a discontinuous rock mass, the load distribution along the bolt will be dominated by discrete rock mass displacements on a limited number of discontinuities (Li, 2009). A closed form solution to this problem was developed by Hyett, Moosavi, and Bawden (1996) for cable bolts. Numerical models demonstrated that, especially for longer bolts such as fully grouted cable bolts, several peaks in load may occur along the bolt length. Such an effect was observed experimentally by Bjornfot and Stephansson (1984) for long rock bolts in hard, blocky rock at the Kiruna Mine in Sweden.

LATERAL ROCK BOLT BEHAVIOUR IN A DISCONTINUOUS ROCK MASS

A dowel effect occurs when a rock bolt transects a rock discontinuity that is undergoing shear behaviour. If the rock bolt is aligned perpendicular to the discontinuity, then the deformation may be almost perfect shear, although, in general, a combination of shear and axial deformation will occur. Experimental evidence shows that dowel effect is often localized within a 200 mm section (Ferrero, 1995). Numerous instances have been reported for failed bolts that display permanent shearing following exposure after a fall of ground (Li, 2009). McHugh and Signer (1999) stated that shear loading can significantly contribute to the failure of bolts used for rock reinforcement in coal mines. However, research on the shear deformation of rock bolts is far less extensive than that of axial deformation because the complex loading mechanism is difficult to monitor, and the uncertainties of determining just where loading is taking place make it difficult to accurately determine shear loads (McHugh and Signer, 1999).

PREVIOUS IN SITU MONITORING OF ROCK BOLTS

An extensive body of experimental research and development has been conducted in the US over a 30-year period, principally by NIOSH and its predecessor, the United States Bureau of Mines (Signer and Jones, 1990; Signer, Mark, Franklin, and Hendon, 1993; Signer, Cox, and Johnson, 1997). Signer and Jones (1990) tested fully grouted roof bolts with strain gauge instrumentation.

NEW MONITORING TECHNOLOGIES

The two new monitoring technologies, the U-Cell and dREBAR, presented in this paper for evaluating rock bolt performance is shown in Figure 2.

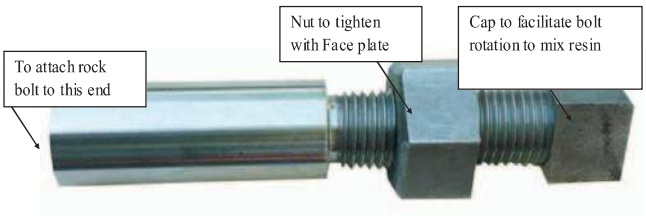

Figure 2. Two new technologies, U-Cell and d-REBAR.

The U-Cell: Point Load Measurement at the Head of the Rock Bolt

The U-cell (Figure 3) is a steel coupler attached to a rock bolt prior to installation that can measure the axial load at the head of the bolt (Mitri, 2011; Mitri, 2012). If the axial strain (ε) in the U-cell is known, it is possible to calculate the axial load, F as follows:

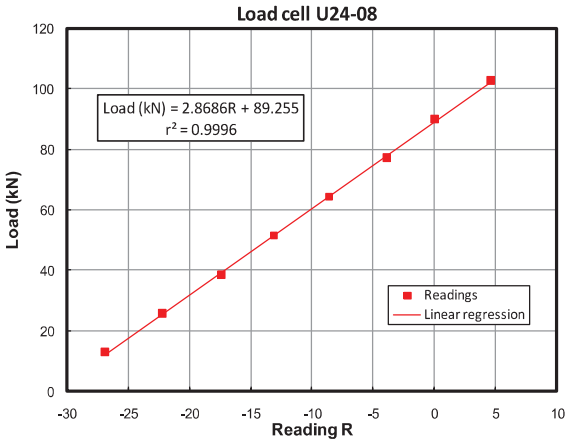

Figure 3. The U-cell, typical diameter 31mm for 16mm or 19mm rock bolts, and 35mm diameter for 22mm rock bolts.

$$F = \varepsilon.E.A \quad (1)$$

Where ε is the axial strain measured by the strain gauge embedded in the U-cell, A is the cross-sectional area of the U-cell where the strain gauge is located, and E is the modulus of elasticity of the steel from which the U-cell is manufactured. The underlying concept of the U-cell technology is to monitor the axial load, F, at the head of the bolt. In practice, the U-cell strain readings (R) must be referenced to an initial unloaded state (R_0), usually measured immediately prior to installation:

$$\varepsilon = f(R - R_0) \quad (2)$$

Referring to Equations (1) and (2), the axial load, F can be written as

$$F = f((R - R_0), A, E) \quad (3)$$

Since equation (3) depends on E, it is valid only in the linear elastic range of the U-cell material. Thus, when the U-cell

is designed for a specific rock bolt, its cross sectional area is engineered to ensure that the stress at the sensor location remains below the yield strength of the high-strength steel from which it is fabricated. It should be noted however that the U-Cell elastic limit load is designed to exceed the ultimate strength of the bolt to which it is coupled. The purpose of load cell calibration is to determine k in the following equation:

$$F = k\,(R-R_0) \tag{4}$$

To do this, the instrument is loaded in a test frame to at least 50% of its intended capacity, which often represents 80 to 90% of the bolt capacity.

U-cell readings need to be corrected for temperature changes; otherwise, an increase in temperature in the mine would lead to over estimation of the rock bolt load and vice versa. If T_0 is the temperature during the initial reading (R_0), and the ambient temperature of the mine changes during the monitoring period to T_1, then the thermal strain ε_T induced in the U-cell will be the following:

$$\varepsilon_T = a\,.\,(T_1-T_0) \tag{5}$$

where a is the coefficient of thermal expansion of the steel material (typically in the range of 12 to 14 x 10^{-6} m/m/C). The apparent change in load caused by this strain component, which must be eliminated from the load calculation, is given by

$$DF = a\,.\,EA\,(T_1-T_0) \tag{6}$$

or simply

$$DF = G.\,\Delta T \tag{7}$$

where G is determined from laboratory tests conducted over an industrial temperature range.

An on-board digital interface unit for the U-cell has been developed to perform the following three tasks:

i. zeroing the reading prior to installation by saving the offset into memory (Equation 2)
ii. applying the calibration coefficient k (Equation 4)
iii. applying the temperature compensation (Equation 7)

As a result, an accurate load reading can be directly displayed to personnel working in the vicinity of the instrumented rock bolt.

D-REBAR: Distributed Strain Measurement Along The Length of Rock Bolt

A distributed instrumentation scheme for rock bolts involves a compromise between the number of gauges (i.e., cost) and the accuracy with which the strain profile along the bolt is resolved. Instrument cost is important because a percentage of instrumented bolts will be lost due to operational-related attrition. At first, this is because the installation process involves spinning the grouted bolt in the resin and, thereafter because, at the production face, the proximity of mobile heavy machinery presents an on-going hazard. The accuracy with which the load distribution along the bolt is measured using a discrete number of gauges depends on (i) the number of gauges, (ii) the base-length of the gauges, and (iii) the intrinsic accuracy and resolution of the gauges. Short base-length measurements will very accurately measure the load at specific locations but could be unrepresentative of the intervening bolt length, especially if load concentrations occur at discontinuities. Long base-length measurements will capture localized deformation due to any discrete points of loading. However, due to an averaging effect, they will underestimate the extreme values, especially if the strain profile varies dramatically.

Displacement Sensor Approach

The displacement sensor approach has been proposed (Hyett and Mitri, 2012; Spearing et al., 2011) based on an array (i=1 to N) of sub-micron resolution displacement sensors that measure the change in displacement or stretch (u^i) of the bolt. The end-points of the displacement sensor are attached to the bolt to define a base-length (L), typically in the range of 200–500 mm, in other words, more than an order of magnitude longer than for a resistive foil strain gauge.

The corresponding strain (e^i) for the i^{th} sensor is determined from the following:

$$e^i = u^i/L \tag{8}$$

The derivation of axial load, bending load, and displacement along the bolt, based on the individual strain gauge outputs, has been described elsewhere (Spearing, et al., 2011; Hyett and Mitri, 2012). One highly significant advantage of the d-REBAR technology is its ability to monitor very large magnitudes of strain. Two different configurations, termed stacked and staggered, have been used (see Hyett and Mitri, 2012 for details).

CALIBRATION

The U-Cell

The U-cell is first calibrated under axial loads ranging up to 90% of the elastic limit of the target rock anchor for which it is designed. The calibration chart provides a linear relationship between the axial load (in the desired units) and the bridge output in millivolts. The typical calibration of the U-cell is presented in Figure 4. This type of calibration allows the U-cell to be connected to existing data loggers for d-REBAR or MPBX in the mines. Possible options for load monitoring include a) portable strain gauge reader, b) data logger, c) TCP/IP-enable data logger, and d) wireless transmission of data that are based on WiFi transmission waves (Mitri, 2011). When a portable strain gauge reader is used, the calibration chart is provided in units of load versus microstrain. The use of portable units is simple and practical in areas that do not require continuous load monitoring.

D-REBAR

Calibration of the instrumented rock bolts involves axial loading of the bolt to determine the relationship between applied and measured strain. Results from a typical axial calibration test are shown in Table 1. Calibration data is typically collected on the third loading cycle.

Table 1. Axial calibration of d6 REBAR.

Applied Strain(ue)	Meas. Strain 1(ue)	Meas. Strain 2(ue)	Meas. Strain 3(ue)	Meas. Strain 4(ue)	Meas. Strain 5(ue)	Meas. Strain 6(ue)
-0.3	+ 0	+ 0	+ 0	+ 0	+ 0	+ 0
165.8	+ 164	+ 166	+ 167	+ 166	+ 165	+ 163
328.6	+ 323	+ 327	+ 328	+ 326	+ 325	+ 324
668.6	+ 678	+ 678	+ 680	+ 677	+ 677	+ 673
992.0	+ 990	+ 994	+ 997	+ 993	+ 994	+ 990
1323.0	+ 1315	+ 1319	+ 1323	+ 1319	+ 1320	+ 1317
1652.6	+ 1649	+ 1653	+ 1654	+ 1651	+ 1653	+ 1649
Cal Slope	0.9973	0.9992	1.0017	0.9985	1.0001	0.998
Cal Offset	0.3247	1.5109	1.8226	1.3188	0.4321	0.6371

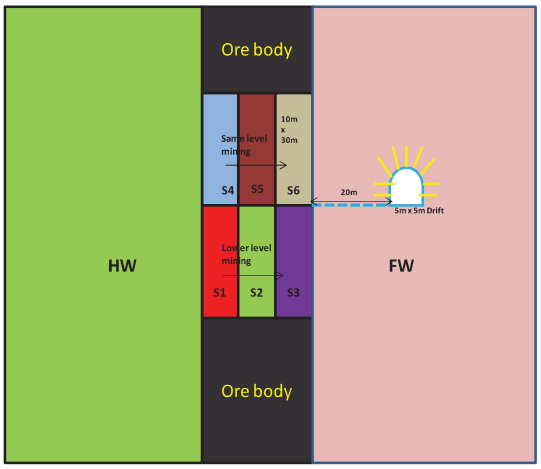

Figure 4. Typical calibration of U-Cell.

CASE STUDIES

The U-cell

The U-cell technique is applicable to virtually any type of rock anchor, such as mechanical rock bolt, cone bolt, grouted rebar, and forged head bolt.

Twenty U-cells were installed in a deep hard-rock mine to monitor the axial load on the rock bolts in response to the nearby mining. The U-cells were installed both on fully grouted rebars and on modified cone bolts (MCB). All these U-cells were installed in a footwall drift walls, and the back and the axial loads were observed as the nearby mining progressed. The initial loads on the bolt head measured immediately after installation is presented in Table 2.

Since the monitoring program is still underway, it will be some time before mining-induced loads are recorded. Alternatively, numerical modeling was performed to simulate the mining sequence and evaluate the rock bolt performance. In this analysis, the aim was to examine the location of the maximum load concentration along the fully grouted rock bolt.

Table 2. Initial loads on U-Cells installed in fully grouted rebars.

U-Cell ID	Level	Location	Load (kN)
2	4900	Wall	9.1
4	4900	Wall	16.2
14	4900	Wall	18.0
19	4900	Wall	19.9
3	4900	Back	9.6
22	4900	Back	23.95
5	5000	Wall	14
6	5000	Wall	26
12	5000	Wall	17
7	5000	Back	18.4
10	5000	Back	9.0
11	5000	Back	21.0
16	5100	Wall	7.88
23	5100	Back	36.13
24	5100	Back	56.40

NUMERICAL MODELING OF THE CASE STUDY

In an effort to examine the location of the maximum load concentration along the fully grouted rock bolt, numerical modeling of the case study was performed using the finite difference modeling software FLAC of Itasca. A multi-stage simulation of mine-and-fill sequence in the vicinity of the haulage drift was conducted to examine the performance of the fully grouted rock bolts. Mining sequences are simulated in two directions: from lower to upper levels and from hanging wall to footwall in retreat. FLAC was chosen as the numerical analysis tool because it has the capability of modeling the interaction between the rock support elements and the rock mass. The model geometry is shown in Figure 5.

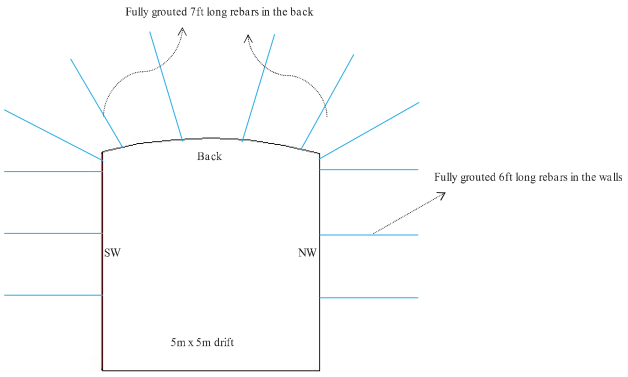

Figure 5. Model geometry.

The standard drift primary support pattern, as adopted in the mine, was used in the modeling and is shown in Figure 6. The mechanical properties of the rock mass material that comprise the model, as well as those of the mine backfill, are presented in Table 3. All rocks are treated as Mohr-Coulomb elasto-plastic materials.

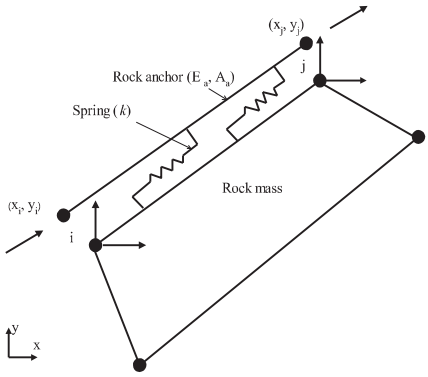

Figure 6. Drift primary support pattern. The bolts in the back are 7 ft long, those in the walls are 6 ft long.

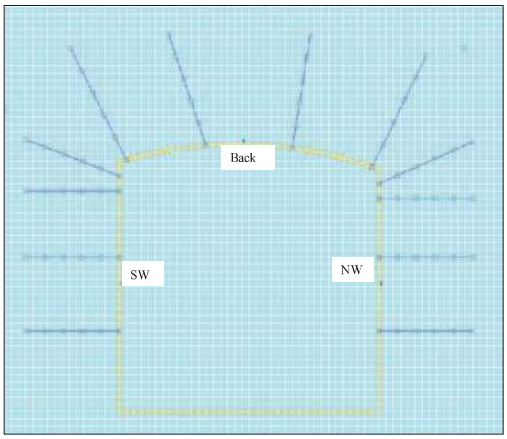

Figure 7. Basic model of rock bolt element (Tang, Mitri, and Bouteldja, 2000).

The modeling technique of rock support elements is based on the assumption that the rock support is attached to the rock mass through a set of continuous shear springs representing the shear bond stiffness of the rock-grout interface, the grout shear stiffness, and the grout-bolt interface shown in Figure 7. In order to model the grouted rebar more accurately, each rebar is divided into six elements, which are linked to the rock mass with shear springs.

Primary support with fully grouted rebars is installed during the haulage drift development, and the sequencing of the nearby mining commenced subsequently. Rebar mechanical properties are presented in Table 4. As mining activities continue with primary support in place, the mining-induced axial loads in the rebars continue to increase. Figure 8 shows the layout of simulated rebars on the drift section.

Axial loads along the distance of the rock bolts were examined during the analysis. Figure 9 shows the axial loads along the distance of the rock bolt from both walls and the back of the drift. It can be clearly observed that the maximum concentration of the load is at the bolt head in these locations. It is obvious that the U-cell, with the point load measuring capability at the head of the bolt, is the appropriate instrument to monitor the maximum axial loads in the rock bolt.

The d⁶ REBAR

Case Study 1: Rock Bolt Behavior in a Coal Mine (Spearing et al., 2011;Hyett and Mitri, 2012)

Four instrumented (stacked gauges) rock bolts were installed across a heading in a coalmine. Bolts #73 and #74 were installed at the center of the excavation and #71 and #75 at the wall. The response of the individual strain gauges for #73 is shown in Figure 10. Lengthwise, profiles of axial strain (e_{axial}) and axial displacement (u_{axial}) was plotted in Figure 11 for all four bolts. 2,000 mm of axial displacement was measured by the rock bolts at the center of the span (#73 and #74), which is approximately twice what was measured by the bolts adjacent to the wall (#71 and #75). Figure 12 shows the location of the four rock bolts superimposed with contour plots of bolt displacement (in microns) and bolt strain (in microstrain—153 mε being equivalent to 1 tonne).

Case Study 2: Yielding Rock Bolt Behavior in a Deep Hard Rock Mine (Punkkinnen and Hyett, 2012).

Figure 13 shows the field result for a fully grouted resin rebar presented by Punkinnen and Hyett (2012). The response of the six strain gauges with time is shown in Figure 13a. The noticeable jump in strain is associated with a major blast followed by a mN 1.9 micro-seismic event. The corresponding distribution of axial strain along the length of the bolt is shown in Figure 13b. Below the elastic limit, 153mε corresponds to a load of 10kN. It can clearly be observed that the 1m section of the rock bolt nearest the head has exceeded its elastic limit following the event on December 1st. The corresponding elongation of the rebar (Figure 13c) jumps from around 0.5 mm to 3.5 mm.

Table 3. Rock mass properties used in the model.

Property	Hanging wall	Ore	Foot wall	Backfill
Density (Kg/m^3)	2,782	4,531	2,916	2,000
E (GPa)	25	20	65	0.1
Poisson's ratio	0.24	0.22	0.23	0.3
Cohesion (MPa)	4.8	10.2	5.7	1.0
Tensile strength(MPa)	0.11	0.31	0.51	0.01
Friction angle(^{0})	38	43	54.9	30

Table 4. Rock bolt mechanical properties used in model.

Property	Value
E (GPa)	200
Diameter (mm)	19
Yield (kN)	125
Perimeter (m)	0.059
Tensile strain	0.09

DISCUSSION AND CONCLUSIONS

Two new technologies, the U-cell and d-REBAR, offer significant potential for the accurate monitoring of rock bolt performance. Both technologies have been interfaced with digital signal processing technology to provide actionable output data at the immediate underground location.

The U-cell technology is shown to be simple, practical, and efficient. The technology is universal in the sense that it can be adapted to any type of rock bolt. Also, the numerical modeling case study shows that the maximum axial load is concentrated at the head of the bolt. Data from case studies using the d-REBAR, presented in this paper and elsewhere (Hyett and Mitri, 2012; Spearing et al., 2011), indicate that this new instrument can provide a solution for the determination of axial loading of rock bolts. The design, which uses long base length strain gauges to monitor separate sections of the bolt, has two distinct advantages:

i. It is able to accurately monitor both the strain and displacement of the bolt, which can be compared with numerical and analytical models.
ii. The long base length tends to cancel out any local perturbations, especially those related to localized lateral shearing movements that can complicate the analysis.

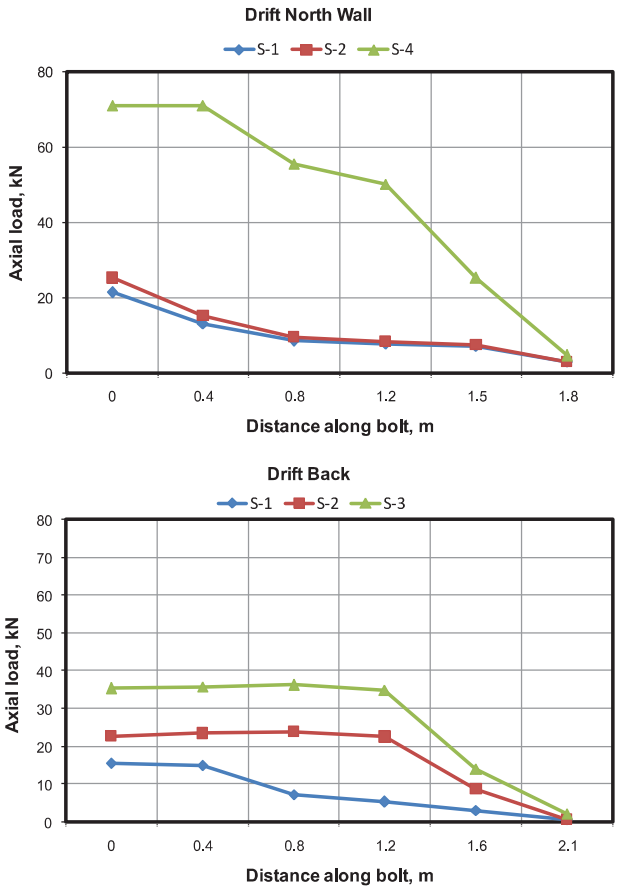

Figure 8. Drift section in FLAC grid showing primary support installed.

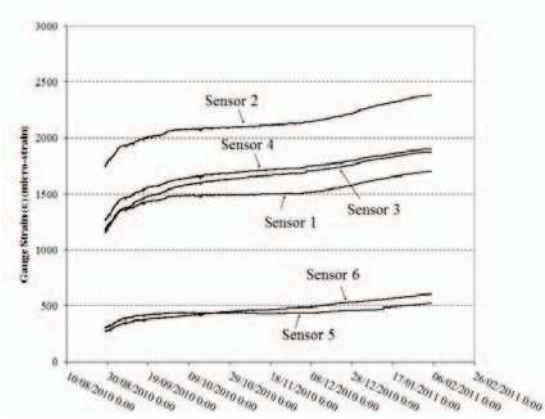

Figure 9. Axial load along the distance of rock bolt after the lower level mining.

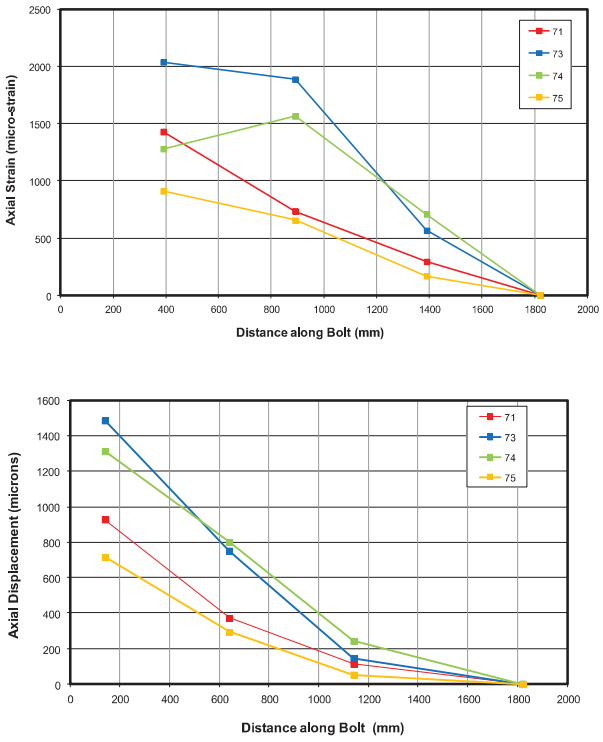

Figure 10. Typical strain gauge results for a single rock bolt (#73) with stacked gauges. The three displacement sensor pairs are arranged as follows: 1 and 2 are the stacked pair nearest the head, 3 and 4 in the center of the bolt and 5 and 6 at the toe end.

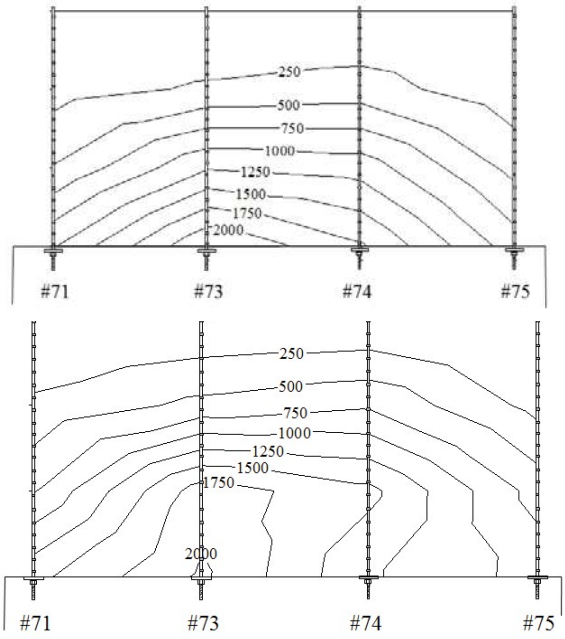

Figure 11. (Top) Axial stretch or displacement along the bolt length and (bottom) strain distribution along the bolt length (153mε/tonne).

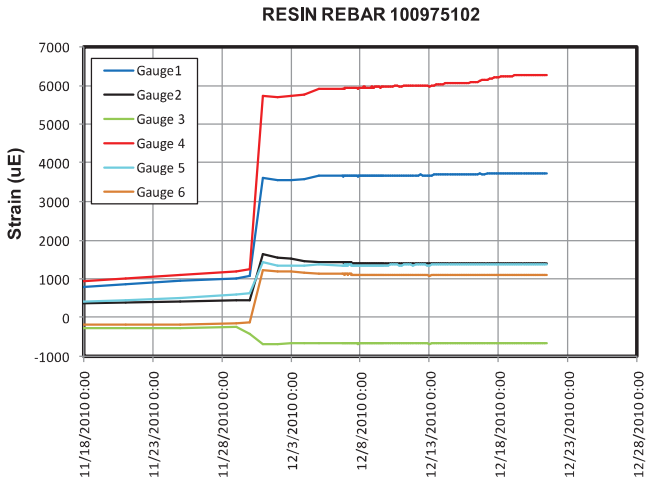

Figure 12. Spatial contoured plots of the axial displacement (upper plot) and axial strain (lower plot). In the lower plot, 153mε is equivalent to 1 tonne, so the maximum load on bolt #73 is around 13 tonnes.

The case studies conducted to this point have yielded consistent results that have enabled techniques, such as spatial contouring, to be applied. This analysis technique provides a powerful visual rendition of the data that enhances data presentation at the operational level. Furthermore, the plots can be directly overlaid on results from numerical models, thus, facilitating back-analysis.

Like any other new technology, there are a number of limitations, and hence there is room for further improvement. Work is currently underway on MSHA permissibility and is expected to be established within the next six months. Another limitation is the ability of the D-rebar to capture shear and bending behavior. A generalized measurement of bending would require 3 grooves so that the direction and magnitude of the bending vector can be resolved. The only case where 2 grooves can achieve this is when the direction of bending is known *a priori* and the bolt is aligned accordingly. This is difficult from both a theoretical and practical point of view.

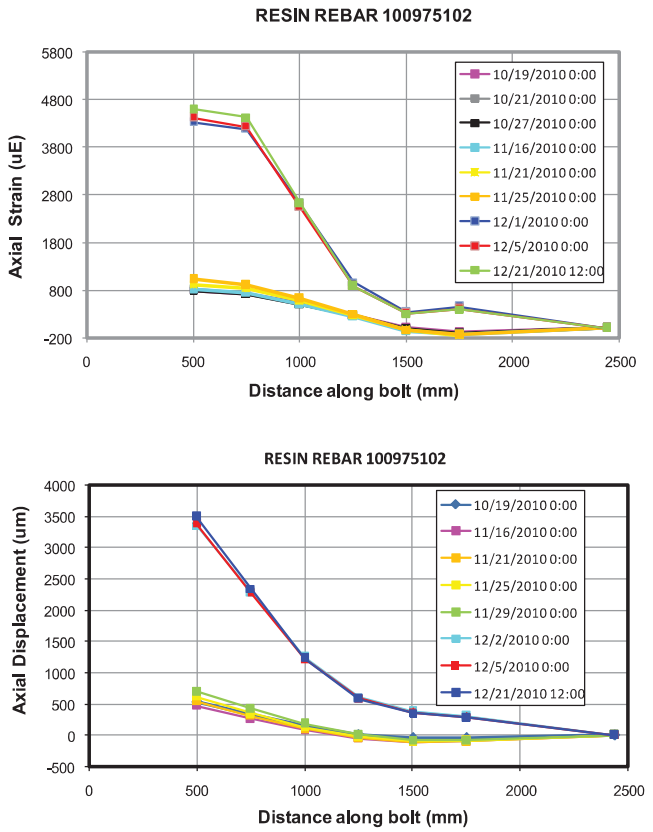

Figure 13. The response of a fully grouted d[6] REBAR during mining. a: the response of the individual strain gauges. b: the strain distribution along the rock-bolt length (153 mε = 10kN) c: the corresponding elongation versus length (a) (b).

REFERENCES

Bjornfot, F. and Stephansson, O.(1984). "Interaction of grouted rock bolts and hard rock masses at variable loading in a test drift of the Kiirunavaara Mine, Sweden." In: O.Stephansson, ed. *Proceedings of the International Symposium on Rock Bolting*. Rotterdam, The Netherlands: Balkema: pp. 377–395.

Deb, D. and Das, C.D. (2010). "Bolt-grout interactions in elasto-plastic rockmass using coupled FEM-FDM techniques."*Advances in Civil Engineering 2010*(Article ID 149810): 1–13.

Farmer, I. W. (1975). "Stress distribution along a resin grouted rock anchor."*International Journal of Rock Mechanics and Mining Sciences and Geomechanics Abstracts 12*(11): 347–351.

Ferrero, A.M. (1995). "The shear strength of reinforced rock joints." International Journal of Rock Mechanics and Mining Sciences and Geomechanics Abstracts 32(6): 595–605.

Freeman, T.J. (1978). "The behaviour of fully grouted bolts in the Kielder experimental tunnel." *Tunnels and Tunnelling 10*: 37–40.

Hyett, A.J. and Mitri, H. (2012)."Two new technologies for measuring the in situ performance of rock bolts."In: *Abstract Volume of Proceedings of the Seventh International Symposium on Rock Bolting and Rock Mechanics in Mining*. Aachen, Germany: AIMS, abstract number -036.

Hyett, A.J., Moosavi, M., and Bawden, W.F. (1996). "Load distribution along fully grouted bolts, with emphasis on cable bolt reinforcement."*International Journal for Numerical and Analytical Methods in Geomechanics 20*(7): 517–544.

Li, C. (2010). "Field observations of rock bolts in high stress rock masses."*Rock Mechanics and Rock Engineering 43*(4): 491–496.

Martin, L. B., Tijani, M., and Hadj-Hassen, F. (2011). "A new analytical solution to the mechanical behaviour of fully grouted rock bolts subjected to pull-out tests."*Construction and Building Materials 25*(2): 749–755.

McHugh, E. and Signer, S. P. (1990)."Roof bolt response to shear stress: laboratory analysis."In: *Proceedings of the18th International Conference on Ground Control in Mining*. Morgantown, WV: West Virginia University, pp. 232–238.

Mitri, H.S. (2011)."Evaluation of rock support performance through instrumentation and monitoring of bolt axial load."In: *Proceedings of Coal Operators' Conference*. Wollongong, NSW, Australia: University of Wollongong, pp. 136–140.

Mitri, H.S. (2012). "Instrumented coupler load cell for rock anchors." US Provisional Patent Application: January.

Mitri, H.S. and Rajaie, H. (1991). "Shear bond stresses along cable bolts."In: *Proceedings of the 10th International Conference on Ground Control in Mining*. Morgantown, WV: West Virginia University, 90–96.

Signer, S.D., Cox, D., and Johnson, J. (1997). "A method for the selection of rock support based on loading measurements." In: *Proceedings of the 16th International Conference on Ground Control in Mining*. Morgantown, WV: West Virginia University, pp. 183–190.

Signer, S. P. and Jones, S. D. (1990). "A case study of grouted roof bolt loading in a two-entry gate road."In: *Proceedings of the 9th International Conference on Ground Control in Mining*. Morgantown, WV: West Virginia University, pp. 35–41.

Signer, S.P., Mark, C., Franklin, G., and Hendon, G. (1993). "Comparisons of active versus passive bolts in a bedded mine roof." In: *Proceedings of the 12th International Conference on Ground Control in Mining*. Morgantown, WV: West Virginia University, pp. 16–23.

Spearing, A., Gadde, M., Lee, S., and Ray, A.(2011). "The initial performance of commonly used primary support on US coalmines." In: *Proceedings of the 30th International Conference on Ground Control in Mining*. Morgantown, WV: West Virginia University, pp. 183–190.

Tadolini, S. and Mitri, H.S. (2002). "Field and numerical analysis of resin-grouted cable bolts used for coal mine longwall roof support."In: Hammah, Bawden, Curran and Telesnicki, eds. *Proceedings of the North American Rock Mechanics Symposium*. Toronto, ON, Canada: University of Toronto, pp. 713–719.

Tang, B., Mitri, H.S., and Bouteldja, M. (2000). "Finite element modeling of rock anchors."*Proceedings of the ICE—Ground Improvement 4*(2):65–71.

Is Mining Coal at a 900M Below Surface at the Xuandong Coal Mine in China Challenging or Just Interesting Rock Mechanics?

Wouter Hartman, Mr
Mining Geotechnical
Geohart Consultants
Melbourne, Australia

Mark Everson, Mr Simtars
Brisbane, Australia

Ben Pang, Mr
Sarra Hayes, Mrs
Mining Geotechnical
Geohart Consultants
Melbourne, Australia

ABSTRACT

Xuandong Coal Mine is mining coal in one of the most challenging underground environments in the world. This work has found that it is not only challenging but it also has the composition for some interesting rock mechanics and ground control conditions. The paper highlights the extreme mining and rock mass behavior conditions encountered when mining coal at 900 m below surface. It was found that the ground control environment associated with geological weakness, low coal material strength and stiffness, was reasonably well controlled; however, the chain pillar geometry and design did not take these geological weaknesses into consideration. Some of the chain pillars employed were quite large, which resulted in floor punching and secondary floor heave, which causes extreme difficulty for production. No barrier pillar has been employed except for the center 164-m-wide main headings pillar with a w/h ratio in excess of 40.

After assessing the location and geometry of a 200-m-thick dolerite sill overlaying the coal measures, we found the probability of it breaking up into to smaller fragments and producing a larger goaf to be low. Therefore, the influence of the dolerite sill on chain pillar loading is considered small compared to the low coal, immediate floor and roof rockmass strength.

It is further recognized that horizontal stresses could be locked up within the dolerite sill, which would likely result in regional bending that would be distributed through the chain pillars. This has, to some extent, already occurred, and the effects have been seen and felt through excessive floor heave, pillar punching, and coal bumps (seismicity). We've also found that there was a need to employ basic rock mechanics principals in assessing the stability of future multiple seam mining layouts.

INTRODUCTION

In January 2006, the Asia-Pacific Partnership (APP) on Clean Development and Climate was established, bringing together Australia, China, India, Japan, the Republic of Korea, and the United States to address the challenges of climate change, energy security, and air pollution in a way that encourages economic development and reduces poverty. In October 2007, Canada was also welcomed as an official member. The APP represents approximately half of the world's emissions, energy use, GDP, and population, and it was an important initiative that engaged, for the first time, the key greenhouse gas emitting, coal producing, and coal consuming countries in the Asia-Pacific region. The project is administered through the Australian Department of Resources, Energy and Tourism (RET) and the Coal Division of the Chinese government's State Administration of Work Safety (SAWS). A steering committee consisting of representatives from Australia and China was established to oversee progress of the project. After inspecting numerous mines, it was agreed to base the project at the Xuandong No. 2 coal mine in Xuanhua County (Hebei Province), approximately 150 km northwest of Beijing (Figure 1). Xuandong mine is part of the Zhangjiakou Mine Group, which in turn is owned by the JiZhong Energy Group Co., Ltd.

The key objectives of the project were to

1. Improve safety at the Xuandong No. 2 Mine
2. Provide a model for achieving mine safety and health improvements at other Chinese coal mines
3. To strengthen cooperation between Australia and China on coal mine safety issues.

In 2009 project managers were appointed by both countries:

- Queensland's Safety in Mines Testing and Research Station (Simtars) was appointed as the Australian project manager
- Xuandong mine appointed its senior management team as their project manager.

The work began with a mine site study/safety audit to establish a general understanding of the mine, its current work practices, and geological conditions. The mine study was divided into key areas: strata control, gas management, equipment and operations emergency response, and emergency preparedness.

This study was followed with a broad-brush risk assessment (BBRA), which identified major hazards and ranked them in accordance with the likelihood of the event occurring and the consequences if they did occur. Following the BBRA, in order to address the identified hazards it was agreed to carry out a number of key activities:

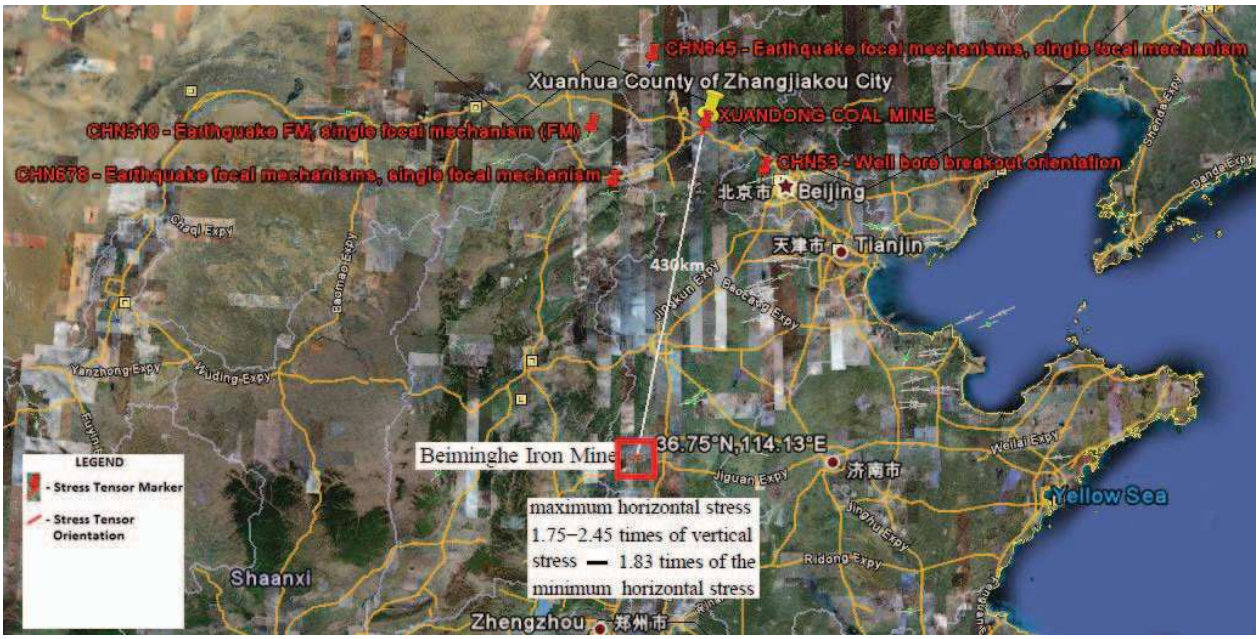

Figure 1. Location of Xuandong No. 2 Coal Mine.

(1) Safety Health Management System, (2) Regional strata control review, (3) Directional drilling trial, (4) Ventilation modeling, (5) Gas monitoring system, (6) Energy isolation and lock out systems, (7) Stone dusting, (8) Localized strata control, (9) Training, (10) Mine safety internal awareness campaign, (11) Mine safety training base, (12) Gas basic parameter lab, (13) Mine nitrogen injection for fire control, (14) V2 coal seam ground floor confined water hydro-geological condition supplemental survey, and (15) Underground emergency rescue stations.

These activities were conducted within the larger framework of the Safety Health Management System developed by mine management, a framework based on the principles of formalized risk assessments, the development of Principal Hazard Management Plans (PHMP), and Trigger Actions Response Plans (TARPS).

Other key initiatives included mine safety training programs for all levels of management and mine workers, as well as the introduction of specific technologies to assist in improving mine safety. These technologies include mine ventilation modeling software, a new tube bundle gas monitoring system and mine gas analysis software, energy isolation hardware, and systems and the trialing of limestone stone dusting at the mine. Limestone dust is widely used in Australian mines to stop methane gas explosions from propagating into a more powerful and deadly coal dust explosion.

To address concerns of gas outburst and strata control, an in-seam directional drilling trial was conducted, as well as a separate drilling activity to conduct a stress measurement test of the large overlying dolerite sill. From the result of this stress test a stress model was developed as well as a 3D model of the mine and a Strata Principle Hazard Management Plan. The majority of the 17 activities have now been completed and the Project official end was in November 2011, with a small number of activities still being finalized in 2012. These being the installation of a tube bundle gas monitoring system and gas analysis software, completion of a strata management plan to improve safety for the IV coal seam which is 14m below the III_3 coal seam.

The Australia-China Coal Mine Safety Demonstration Project has sought to share knowledge between Australian and Chinese coal miners to improve safety for all coal miners. The focus of the paper discusses some of the issues that emerged from work done by Geohart Consultants in their contribution to activities 2 and 8: regional strata control review and localized strata control.

XUANDONG COAL MINE BACKGROUND

Xuandong Coal Mine No. 2 of Zhangjiakou Mining Group Co., Ltd, is located 10 km to the southeast of Xuanhua County of Zhangjiakou City. The coal is mined from the No. III_3 Coal Seam, which varies in thickness from 2.1 m (panels 102/103) in the Northwest to 4.26 m (panel 206) in the Southeast. The III_3 coal seam is mined between 869.68 m and 936.7 m below the surface.

The general dip of the coal seam is in a southeastern direction at a nominal 5 degrees. Seam No. IV_1, which is located approximately 14 m below the No. III_3, seam is currently being prepared for full-scale mining. A longwall mining method is employed on the No. III_3 seam, and the general mining direction is in a southeast–northwest direction. The longwall panels vary in width from a 100 m (pillar to pillar, 105 panel) to 162 m (pillar to pillar, panel 207). At the time of the regional strata control review, two longwall panels were actively being mined: III_3 Panel 208 and III_3 Panel 2011. Panel 209 was being prepared (i.e., main-gate roadway and cut through development) for the next stage mining (See Figure 3).

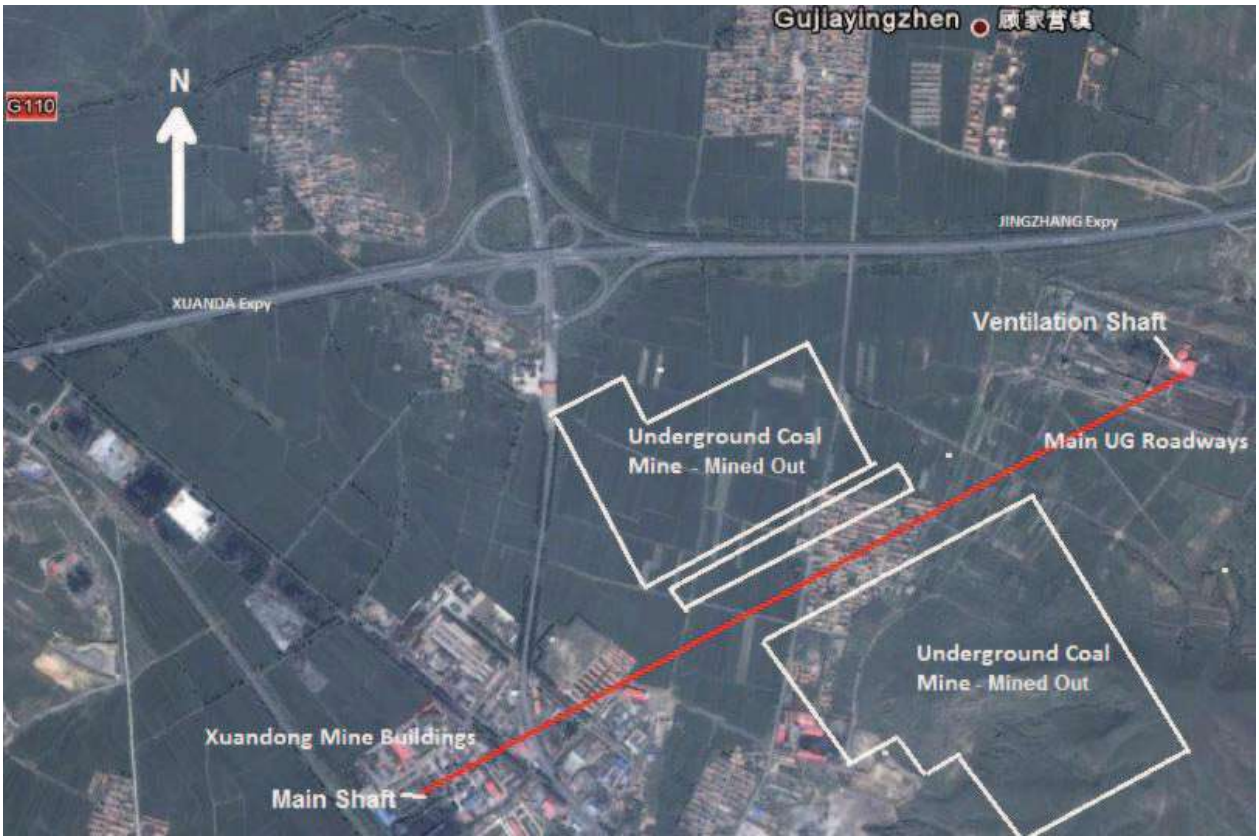

Figure 2. Close-up location and extent of Xuandong No. 2 Coal Mine no. III_3 seam.

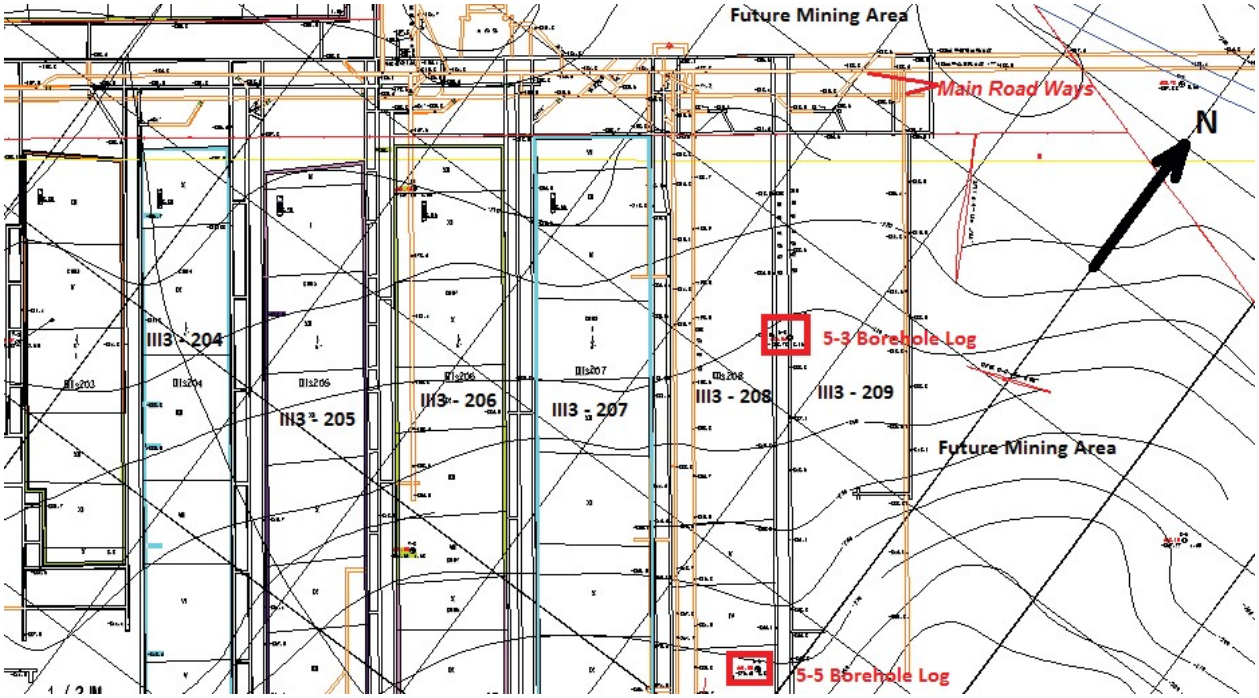

Figure 3. Borehole location detailing overlaying strata.

GEOLOGY

A generalized geological sequence is presented in Table 1. The No. III_3 coal seam is described as the main mineable seam. The coal seams extracted by at the No. 2 mine are complicated with a number of interbedded gangue layers (i.e. interburden waste rock). The coal seam in III_3 201 longwall district is described as unstable with more interbedded layers. Apparently there were only one or two interbedded gangue layers while driving III_3 203 longwall for a distance of 100 m, and then the interbedded gangue layers gradually increased to three or four layers after 400 m. In another case, which has been verified during the underground visits, the interbedded gangue appeared intermittent while driving the III_3 209 maingate for about a 100 m and then increased from two to four layers after 400 m. It would appear that one of these layers, when exposed to moisture/groundwater, transforms into a soft clayey coal that behaves in a plastic manner. This behaviour is quite likely because of the medium ash content of the coal. The thickness of the interbedded layers generally varies from 0.1 m to 0.5 m but occasionally reaches a thickness of 1.0 m to 1.2 m.

Table 1. Local overburden strata units.

Strata Unit	Cumulative Thickness
Alluvium	80m
Loess	165m
Andesitic Laval	330m
Andesitic / Interclastic Breccia	490m
Silty sandstone / water laid tuff	687m
Andesitic Volcanics Breccia	744m
Tuff	789m
Breccia / Sandstone	880m
III_3 Coal Seam	885m

The thickness of the No. III_3 coal seam varies across the Xuandong No. 2 Mine property. This issue is of extreme importance because this dictates the geometry of the chain pillars where the floor of the No. III_3 coal seam is used as the marker during roadway development (Figure 3). The pillar height will thus change throughout the longwall, rendering various strengths due to the height variability. This changing of seam height was verified during our underground visit to III_3 209, where the maingate roadway height changes along its entire length. The generalized overburden strata of the Xuandong No. 2 Mine (Table 1) does not provide full detail surrounding the overlying strata for future planned longwall panels (III_3 209 panel); therefore, a detailed look at the borehole logging information representative of the future longwall mining area was required. Two boreholes were selected for logging information review: boreholes 5-3 and 5-5 (Figure 3).

The two boreholes revealed the presence of a dolerite sill overlaying the No. III_3 coal seam:

- Borehole 5-3 (Collar at 635.96 m): Dolerite sill detected from a depth of 607.03 m to 835 m with a thickness of around 228 m. No. III_3 coal seam intercepted at 865.86 m to 869.68 m (3.82 m thick).
- Borehole 5-5 (Collar at 661.09 m): Dolerite sill detected from a depth of 413 m to 421.38 m (8.35 m thick); 630.36 m to 659 m (28.64 m thick); and 695.2 m to 888.4 m (193.2 m thick). No. III_3 coal seam intercepted at 931.9 m to 936.7 m (4.8 m thick).

The horizontal distance between the two bores was measured to be 430 m with a vertical surface elevation difference of 25.13 m. The No. III_3 coal seam has a gentle dip of 5.4 degrees towards the south-southeast. Borehole No. 5-5 shows the same dolerite sill that occurs in Borehole No. 5-3. The dolerite sill is, however, 35 m thinner in Borehole No. 5-5. Borehole No. 5-5 is showing a presence of two additional layers of dolerite material above the major dolerite sill (see Figure 5, east-west cross section). The geometry (thickness) of the large dolerite sill appears to be slightly different in a north-south direction to the east-west cross section and limited to the northern part of the mine (Panel III_3 203). Figure 6 shows the dolerite sill in a west/southwest – east/northeast section reproduced from a longitudinal section (Boreholes 1-3, 10-1, 9-3, and 3-4).

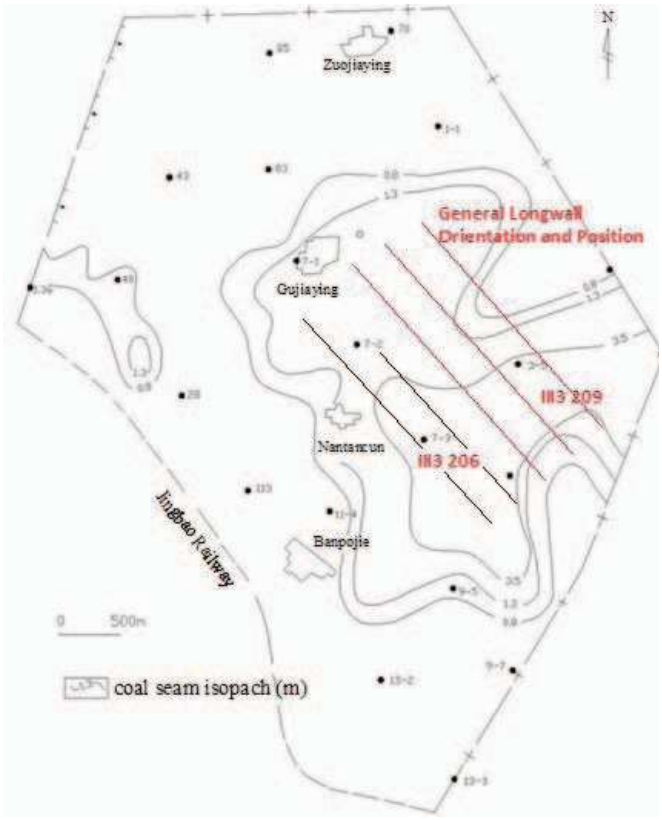

Figure 4. Isopach contours of No. III_3 Coal Seam.

Table 2 details the immediate roof and floor sedimentary rock layers that influence the local strata control around longwall panels III_3 208 and III_3 209. The geological layer information was obtained from borehole logs 5-3 and 5-5.

During our review we visited both the No. III_3 coal seam and the No. IV_1 coal seam and roadway development areas. From detailed investigation we found that the No. IV_1 coal seam was only around 14 m below the No. III_3 coal seam. The IV_1 coal seam does not appear to exist or is uneconomical (total thickness too small) below the No. III_3 coal seam around panels III_3 208 and III_3 209 (See Table 2 for detail).

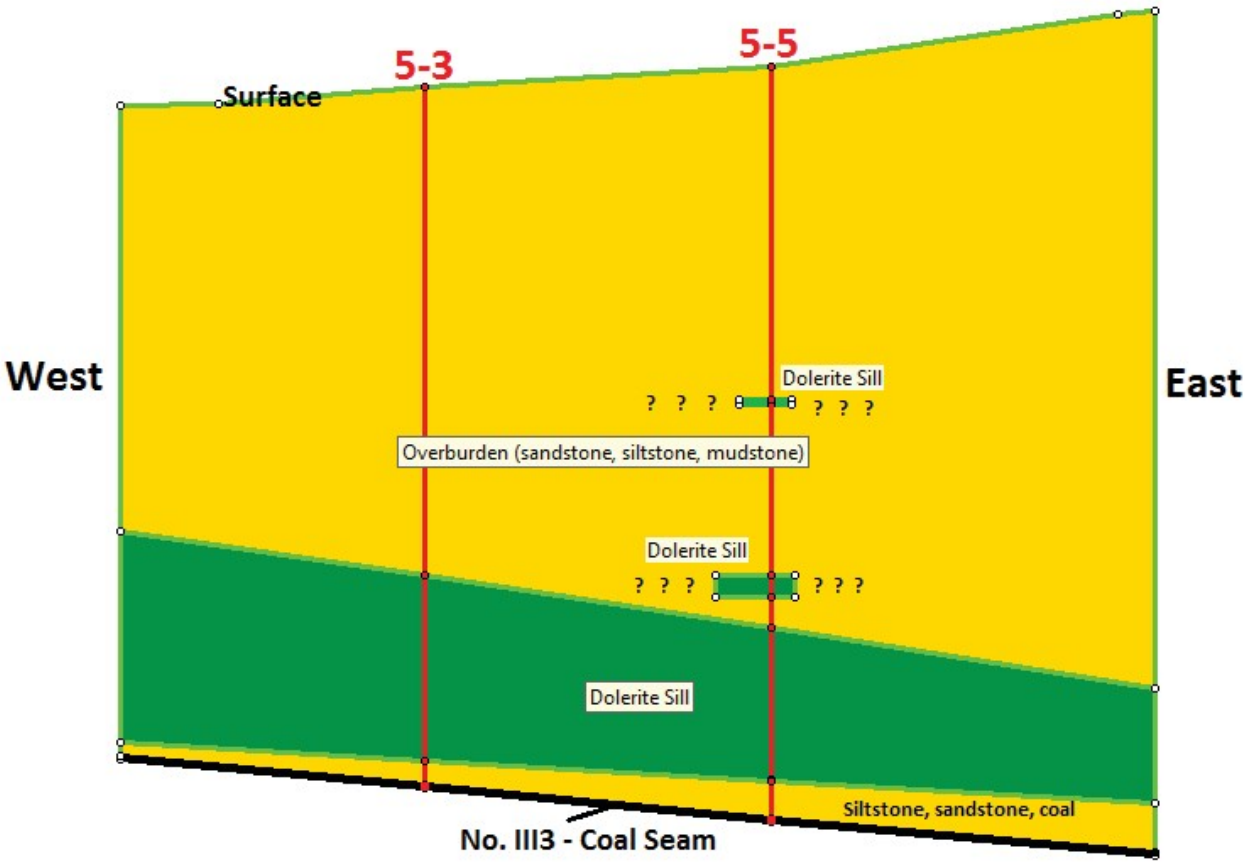

Figure 5. Southeast–northwest section showing overlaying strata above the III_3 coal seam portraying the dolerite sill and other discontinuous dolerite material using the 5-3 and 5-5 borehole data.

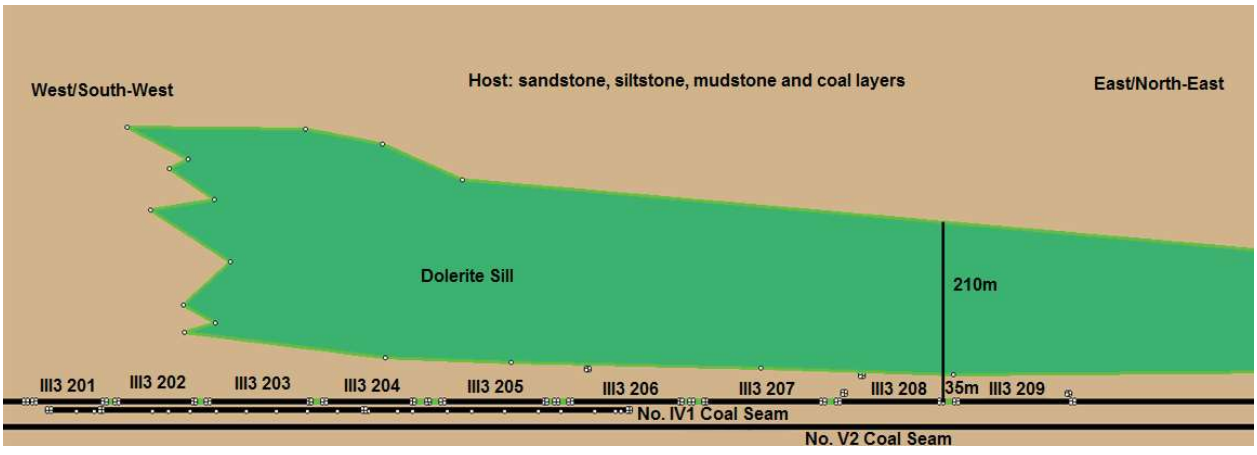

Figure 6. West-southwest–east-northeast section showing overlaying strata above the III_3 coal seam portraying the dolerite sill limited to the northern part of the mine (No. 4 Longitudinal Section).

Table 2. Immediate roof and floor of III3 Coal Seam – BH 5-3 and 5-5.

Borehole Number	5-3	Collar elevation	635.96	Borehole Number	5-5	Collar elevation	661.09
Rock Type	Borehole Depth below surface (m)	Collar elevation & drill hole depth markers	Layer Thickness	Rock Type	Borehole Depth below surface (m)	Collar elevation & drill hole depth markers	Layer Thickness
		Total Roof	21.8			Total Roof	27.11
Bottom Mudstone	844.05	-208.09		Bottom Siltstone	904.8	-243.71	
Bottom Coal	**844.95**	-208.99	**0.9**	Bottom Coal	905.1	-244.01	0.3
Bottom Siltstone	856.9	-220.94	11.95	Bottom Siltstone	917.5	-256.41	12.4
Bottom Fine Sandstone (fossil plant interlayer)	858.2	-222.24	1.3	Bottom Medium Grained Clastic Sandstone (coal seam inter layer)	927.7	-266.61	10.2
Immediate Roof - Bottom Siltstone (0.3m Fine sandstone interlayer)	**865.85**	**-229.89**	**7.65**	**Immediate Roof - Bottom Siltstone (0.3m fine sandstone interlayer)**	**931.91**	**-270.82**	**4.21**
Bottom of III3 Coal Seam	**869.68**	**-233.72**	**3.83**	**Bottom of III3 Coal Seam**	**936.7**	**-275.61**	**4.79**
Immediate Floor - Bottom of Mudstone	**870.2**	**-234.24**	**0.52**	**Bottom of Mudstone & Silstone**	**939.7**	**-278.61**	**3**
Bottom of Mudstone	875	-239.04	4.8	Bottom of Medium grained sandstone	940.44	-279.35	0.74
Bottom of siltstone	878.14	-242.18	3.14	Bottom of Coal	940.76	-279.67	0.32
Coal	878.44	-242.48	0.3	Medium grained clastic sandstone	942.39	-281.3	1.63
Siltstone	879	-243.04	0.56	Coal	942.87	-281.78	0.48
coal	879.45	-243.49	0.45	Siltstone	947.88	-286.79	5.01
Siltstone	882.51	-246.55	3.06	Medium grained clastic sandstone	949.76	-288.67	1.88
Coal	883.06	-247.1	0.55	Coal	950.46	-289.37	0.7
??	885.84	-249.88	2.78	Fine Sandstone	952	-290.91	1.54
Bottom of Coal Seam	886.27	-250.31	0.43	Pelitic Sandstone	953.54	-292.45	1.54
		Total Floor	16.59			Total Floor	16.84

The floor is of equal importance because it represents the foundation for the chain pillars. The immediate floor (Mudstone / Siltstone) of the No. III_3 Coal Seam appears to vary in material and in thickness for this particular area (Borehole 5-3 (0.52m) and 5-5 (3m) representing longwall panel III 208 and III 209).

The most dominant geological feature of the deposit is the consistent presence of what is reported to be a typically 200 m thick "dolerite" sill (described as "volcano rock") that is located from 200 m to only 35 to 40 m above the III3 Seam in the area of 207 and 208 Panel. This is a very significant stratum in the overburden apart from the thick conglomerate unit and it is extremely rare (although not without precedent) to find a sill unit of such thickness in coal measures sequence.

GEOTECHNICAL INFORMATION

Local Mine Stress

During the regional strata control review process, we found no stress measurement data for the Xuandong No.2 underground coal mine. However, information regarding regional stresses (Ouyang et al, 2009) suggests the maximum principal stress orientation is in east-northeast/west-southwest (Figure 1). We made recommendations regarding the need for stress measurement results in order to fully understand the regional and local strata behavior. However, there was also a need to determine material strength for the sandstone and dolerite sill. Consequently, stress measurements were completed in two locations:

- Sandstone material in an area north of the main roadways and a reasonable distance away from the mined out areas.
- Dolerite sill material in an area close to the main ventilation shaft at the base of the dolerite sill (we anticipated some interference due to boundary effects).

This was seen as a major step towards incorporating sound strata control principles for safe coal mining practice in China. The results from the stress measurements (Table 3 and 4) revealed that the difference between the maximum principal stress and the intermediate principal stress for both the sandstone and the dolerite sill are quite similar. What was quite interesting is that the principal stress orientation for the dolerite sill and the sandstone appear to have swapped. The close proximity of the stress measurement within the dolerite sill to the rockmass boundary may have had an effect. Hence we would have to assume that the maximum stress orientation would be around 230 degrees, close to being horizontal.

Strata Strength

The roof of the III_3 coal seam mainly consists of siltstone and fine sandstone, and partially medium grained sandstone with larger quarts mineral inclusions, sandy mudstone, and mudstone. Their characteristics are calcareous binding, compact, and stiff, which compares well with the information in Boreholes 5-3 and 5-5. The immediate roof also exhibits the appearance of a false roof in some areas and is described as a carbonaceous mudstone, and its thickness ranges between 0.1 m and 0.3 m. The compressive strength of the immediate roof, as per supplied documentation, varies between 35.51 MPa and 190.98 MPa (See Table 4b), which would generally be considered as a strong roof.

The III_3 coal seam is described as a complicated coal seam. The complication is represented by several interburden mudstone/ siltstone layers, 0.1 m to 0.3 m in thickness, distributed throughout the coal mass. The coal strength, as supplied by Xuandong Coal Mine, is 8.9 MPa. It is understood that this is the strength of a coal block, which does not include any interburden layers. This means that the coal strength, as presented, is an overestimation of the coal seam strength. Coal, in general, is considered weak if its uniaxial compressive strength (UCS) is less than 10 MPa (Peng, Tsang, and Hsiung, 1989).

Table 3. Stress measurement test results.

	Max. principal stress σ_1			Intermediate principal stress σ_2			Min. principal stress σ_3		
Measure point	Value	Direction	Dip angle	Value	Direction	Dip angle	Value	Direction	Dip angle
	(MPa)	(°)	(°)	(MPa)	(°)	(°)	(MPa)	(°)	(°)
Diabase 1	66.55	336.7	-27.0	59.76	243.3	-6.6	20.77	140.8	-62.1
Diabase 2	64.93	335.6	-26.6	53.55	243.3	-4.5	24.79	144.3	-62.9
Diabase 3	73.61	207.7	10.5	64.48	113.8	19.6	24.60	144.2	-67.5
Sandstone 1	66.92	232.9	1.0	51.98	323.0	4.2	19.95	309.4	-85.7
Sandstone 2	69.51	227.7	0.5	55.44	317.7	9.5	19.90	314.8	-80.5

Table 4a. The results of the uniaxial compression tests.

Rocks group	**Test number**	**Diameter (mm)**	**Height (mm)**	**Failure load (kN)**	**Uniaxial compressive strength σc /MPa**	**Modulus of elasticity E/GPa**	**Poisson's ratio**
Diabase / Dolerite	A1	49.44	99.21	135.00	70.32	114.3	0.282
	A2	49.28	98.94	84.22	44.16	*	*
	A3	49.50	98.66	163.50	84.96	32.9	0.231
	A4	49.81	101.58	193.00	99.05	47.10	0.303
	A5	49.13	98.73	161.00	84.93	44.6	0.364
	A6	49.25	100.50	132.40	69.50	57.2	0.285
	average	49.40	99.60	144.85	75.49	59.22	0.293
Sand-stone	B1	49.20	100.21	156.40	82.27	37.39	0.278
	B2	49.41	99.67	104.50	54.50	27.35	0.249
	B3	49.22	99.95	93.03	48.89	37.6	0.248
	B4	49.33	99.56	92.57	48.43	34.00	0.226
	B5	49.20	99.78	101.20	53.23	18.19	0.183
	B6	49.32	99.82	134.70	70.51	17.80	0.250
	average	49.28	99.83	113.73	59.64	28.72	0.239

The floor of the III_3 coal seam is mainly composed of siltstone and finestone, and partially medium sandstone and sandy mudstone. Their characters are argillaceous binding. The compressive strength of the immediate floor varies between 80.8 MPa and 95.89 MPa (See Table 4b), which is generally considered to be a strong floor. It was not known which strata unit was tested. We suspect it could have been one of the siltstone or fine sandstone units. Underground observation of primary and secondary floor heave however suggests a weaker immediate floor.

The behavior (i.e., controlled or uncontrolled breaking) of the dolerite sill is critical to the regional stability of the Xuandong. No. 2 Mine. The section below highlights longwall panel geometries that will have an effect (e.g., sudden energy release) on the behavior of the dolerite sill. The UCS of dolerite has been tested and varies between 99 MPa and 44 MPa (see Table 4a) with an elastic modulus range between 114.3 GPa and 32.9 GPa (see Table 4b). This is in excess of the values usually encountered for the other sedimentary rock types in the overburden (i.e., predominantly siltstone/mudstones, fine sandstone, conglomerate, etc.), which have a UCS around 35.51 MPa and elastic moduli between 6 GPa and 30 GPa. The dolerite would also be much denser than the surrounding rock, in the region of 3000 kg/m^3. However, the mass behavior of the sill is more likely to be controlled by the mechanical properties (i.e., cohesion and friction coefficient) of the joints in the sill than the properties of the intact material (Van der Merwe, 1995). Van der Merwe (1995) suggests that cohesion of 500 kPa to 100 kPa and frictional angle of 30° to 40° would be reasonable. One of the exploration sites to the northeast of Xuandong Mine exhibits dolerite core, which is believed to be similar to the dolerite sill overlying the Xuandong No. 2 Mine longwall panels (Figure 7).

Table 4b. The mechanical properties of the roof and floor of mineable coal seams.

Coal seam No.		III_3		IV_1		IV_2		V_2		Gateway Surrounding rock
		roof	floor	roof	floor	roof	floor	roof	floor	(J2j1)
lithology		siltstone, finestone, gritstone	siltstone, mudstone	siltstone, sandstone, sandy mudstone	siltstone, finestone, medium sandstone, gritstone	siltstone, finestone, medium sandstone, gritstone	siltstone, finestone, medium sandstone, gritstone	siltstone, finestone, mudstone	siltstone finestone mudstone siderite stone	sandy conglomerate
Compressive Strength (MPa)	Drying condition	104.80	127.5	127.5	125.8	140.41		103.07	28.71	115.70
	Water-absorbing condition	41.29-131.0	90.48	90.48	82.56	40.59-133.93	77.67	47.56		78.80
	Natural condition	35.51-190.24	80.80-95.89	13.30-63.20	33.80-59.00	33.80-152.66	33.90-89.00	16.10-107.77	18.40	
Tensile strength (MPa)		1.69-2.98	1.49-11.81	0.70-11.81	2.0-8.19	1.02-8.83	1.90-9.29	0.90-4.21	1.10-3.32	
Shear strength	Internal friction angle(°)	32°42′-36°59′	28 °6′	28°6′-37°23′	24°0′-38°5′	21°6′-39°47′	30°39′-39°47′	33°30′-39°49′	42°0′	41°3′
	Cohesive affinity (MPa)	17.80-25.2	9.7	8.92-10.02	8.78-29.50	6.72-18.80	6.56-28.61	7.66-13.37	10.63	11.30
Firmness coefficient (f)		$\frac{4.73}{3.3\sim6.77}$	$\frac{4.34}{1.98\sim9.23}$	$\frac{4.12}{2.28\sim9023}$	$\frac{5.12}{3.35\sim8.42}$	$\frac{5.25}{2.92\sim13.66}$	$\frac{4.48}{3.03\sim7.92}$	$\frac{3.30}{2.33\sim4.48}$	$\frac{3.25}{2.07\sim4.85}$	8.04

MINE DESIGN

A review of the historical panel widths (max. 156 m and min.72 m), seam heights (max. 4.53 m and min.1.15 m), and pillar widths (max. 32 m to 164 m and min. 12 m) provided an overall view of historical and current mine design (See Table 5). The pillar w/h ratios vary between 14.8 and 2.6 (excluding the main roadway pillar). A review of the coal seam thickness highlights the inconsistency in seam height and panel widths (face lengths) throughout Xuandong No. 2 Mine.

The w/h ratio is the main geometrical consideration in determining a pillar's strength and stability, not simply its width, as is all too often the case. Width/height ratios in excess of 10 are generally regarded as indestructible pillars, although Xuandong Mine's coal properties, interburden layers, surrounding strata, and loading environment were carefully examined. It is worth noting that for a given pillar height, as the width is progressively reduced, the pillar core which reduces in width first, while the yield zones on either side of the core remain roughly constant in width. There comes a point where the core becomes too narrow to sustain the load, and eventually for narrower pillars, the core disappears altogether and the two yield zones intersect, resulting in a full yielding pillar. However, the design philosophy is for stable coal pillars (i.e. current depth in excess of 900 m below surface) as the purpose of these pillars as per current design methodology suggests that these pillars should be employed to protect the main access roadways for operating longwall's. Significant deformation, however, was observed in the III_3 208 and 209 longwall panels. This could either be the result of lower width:height ratios (See Table 6) for these two longwall panels, unfavourable pillar behaviour, unfavourable floor behaviour, and/or rib support ineffectiveness; we suspect a combination from all of the above.

GROUND BEHAVIOR

During our second underground visit to the III_3 208 longwall tailgate, III_3 208 main conveyor heading, and III_3 209 maingate, we experienced a coal bump, or a low energy seismic event, which was quite likely related to energy being released from the overlying dolerite sill. This is hypothetical, because the ground motion felt as if energy had been released from above compared to a floor bump or seismic source generated from below. The author experienced many of these seismic events at other mines and is quite familiar with seismic event ground motion direction. However, without multiple sensors location it would be impossible to accurately locate the seismic event.

Underground inspections to various workplaces were conducted over a period of five days. The following areas were targeted to reveal specific information for the assessment of regional strata control behaviour (Figure 8):

- III_3 209 maingate roadway
- III_3 208 tailgate, coal face, and maingate, III_3 209 maingate roadways
- Main ventilation adit, incline, and No. IV coal seam roadways located 14 m below the III_3 coal seam
- III_3 2014 mining district

III_3 209 Maingate Roadway

Investigation for this area took place on Friday, June 4, 2010. We observed that the 209 maingate roadway had deformed/squeezed to 2.3 m high and 3.4 m wide from its original developed 3.5-m height and 4-m width. The deformation occurred over a period of approximately 18 months since initial development. A large part of this deformation originates from the floor (consisting of mudstone and siltstone) and the III_3 208 coal rib (inclusive of mudstone interburden layers). In addition, groundwater was found to seep through the roof at one location. It was here where we first noted

that the coal structure changed due to the exposure to water and that it had a clayey appearance.

deformation and damage in the sidewalls (ribs), which indicated that the local stress orientation was vertical. It was here that it

Table 5. Historical review of panel length, seam height, and pillar widths.

Longwall Number	Panel Width (m)	Coal Seam Height (m)	Pillar	Width	Width:Height Ratio (w/h)		Comments Borehole Numbers
			Main Gate (m)	Tail Gate (m)	Main Gate (MG)	Tail Gate (TG)	
III3 101	72	1.15	164 (main roadway stability pillar?)	14	142	12.1	BH 9-2
III3 102	140	2.02	N/A	30		14.8	BH 62
III3 103	116	2.08	30	12	14.8	5.76	BH 80
III3 104	120	1.65	12	16 & 10	7.3	9.7 & 6.1	BH 9-1
III3 105	108 (NW) 92 (SE)	1.65	16 &10	12 & 12	9.7 & 6.1	7.3 & 7.3	BH 9-1
III3 106	102	2.34	12 & 12	14	5.1 & 5.1	5.9	BH 7-2
III3 201	92	1.95	Abutment	12	-	6.2	BH 10-1
III3 202	100 (NW) 54 (SE)	2.58	12	16	4.6	6.2	BH 9-3
III3 203	134 (NW) 112 (SE)	2.58	16	16	6.2	6.2	BH 9-3
III3 204	116	2.58	16	16 & 16	6.2	6.2 & 6.2	BH 9-3
III3 205	140	3.95	16 & 16	12 & 16	4.0 & 4.0	3.0 & 4.0	BH 51
III3 206	152	3.95 4.53	12 & 16	12 & 16	3.0 + 4.0 2.6 + 3.5	3.0 & 4.0 2.6 & 3.5	BH 51 BH 7-3
III3 207	156	3.95 4.53	12 & 16	16	3.0 & 4.0	4.0	BH51 BH 7-3
III3 208	136	3.15 3.87	16	16	5.1 4.1	5.1 4.1	BH 5-3 BH 5-5
III3 209	156	3.15 3.87	16	N/A	5.1 4.1	N/A	BH 5-3 BH 5-5
Max	156	4.53	164	32			
Min	72	1.15	12	12			
Ave	125	2.92	32.3	20.3			

III_3 208 Tailgate, Coal Face and Maingate and III_3 209 Maingate Roadways

Investigation for this area took place on Saturday, June 5, 2010. We again observed significant floor heave and rib bulging in the III_3 208 tailgate. Longwall panel III_3 208 mining face showed distinct mudstone layers within the coal seam. During our visit we experienced a bump (low energy seismic event) that was likely located further up in the overburden strata (dolerite sill).

Main Ventilation Adit, Incline and No. IV_1 Coal Seam Roadways

The investigation for this area took place on Saturday, June 5, 2010, where classical rock mechanics ground behaviour was observed. The main ventilation adit showed signs of severe

became all too clear that the ground support efficiency is not adequate to manage ground deformation. When we reached the IV_1 coal seam development 14 m below the III_3 coal seam longwall high extraction area, classic roadway deformation was observed due to the chain pillars punching into floor. During our visit we experienced a significant bump (medium energy seismic event) that was directly underneath the chain pillar on the III_3 coal seam.

III_3 2014 Mining District

The investigation for this area took place on Tuesday, June 8, 2010. This area has showed some of the worst deformation from what we have observed around the mine. One of Xuandong Coal Mine's senior officials indicated that the roof sagging and floor

Figure 7. Exploration site northeast of Xuandong No. 2 Mine, exhibiting dolerite core.

$$\sigma_p = 7.2 \times \frac{w^{0.46}}{h^{0.66}} \quad (1)$$

Where, h is pillar height; w is pillar width; and σ_p is pillar strength in MPa.

The formula above formed the basis for the generic squat pillar strength formulation (Madden, 1991). It has been found that the majority of the pillars at the Xuandong No.2 Mine have a w/h ratio in excess of 5, hence the appropriateness to use the formulation as part of a prelimanary strength evaluation.

Table 6. Pillar Strength for a number of chain pillars for a width to height ratio in excess of 5.

Longwall Number	Panel Width (m)	Coal Seam Height (m)	Pillar Width		Width:Height Ratio (w/h)		Comments Borehole Numbers	Pillar Strength (MPa)
			Main Gate (m)	Tail Gate (m)	Main Gate (MG)	Tail Gate (TG)		
III_3 103	116	2.08	30	12	14.8	5.76	BH 80	24.36
III_3 104	120	1.65	12	16 & 10	7.3	9.7 & 6.1	BH 9-1	
III_3 105	108 (NW) 92 (SE)	1.65	16 &10	12 & 12	9.7 & 6.1	7.3 & 7.3	BH 9-1	20.86
III_3 106	102	2.34	12 & 12	14	5.1 & 5.1	5.9	BH 7-2	
III_3 203	134 (NW) 112 (SE)	2.58	16	16	6.2	6.2	BH 9-3	27.34
III_3 204	116	2.58	16	16 & 16	6.2	6.2 & 6.2	BH 9-3	
III_3 208	136	3.15 3.87	16	16	5.1 4.1	5.1 4.1	BH 5-3 BH 5-5	19.38
III_3 209	156	3.15 3.87	16	N/A	5.1 4.1	N/A	BH 5-3 BH 5-5	

heave (deformation) had occurred over a long period of time and was not related to one significant event. Therefore, dynamic displacement could be ruled out in this case. It must be noted that a significant reverse fault has been indicated on the mine plans and could be related to the severe ground behaviour in this specific area. It has also being noted that the coal mass strength is significantly lower than the immediate roof and floor.

COAL PILLAR ANALYSIS FOR REGIONAL STABILITY

We had a look at the chain pillars' strength to compare with other similar cases. There are several variations of formulae for pillar strength and one of the most popular formulas is the Salamon-Munro Coal Pillar Strength Formula (Van der Merwe, 1995).

$$Squat_Pillar_Strength = k * \frac{R_o^{\ b}}{V^a}\left\{\frac{b}{\varepsilon}\left[\left(\frac{R}{R_o}\right)^{\varepsilon} - 1\right] + 1\right\} \quad (2)$$

Simplified to

$$Squat_Pillar_Strength = \frac{0.0786}{V^{0.0667}}\left\{R^{2.5} + 181.6\right\} \quad (3)$$

Where,

V is pillar volume

R is pillar w/h ratio (note *w* is equivalent width for rectangular pillars – W_e)

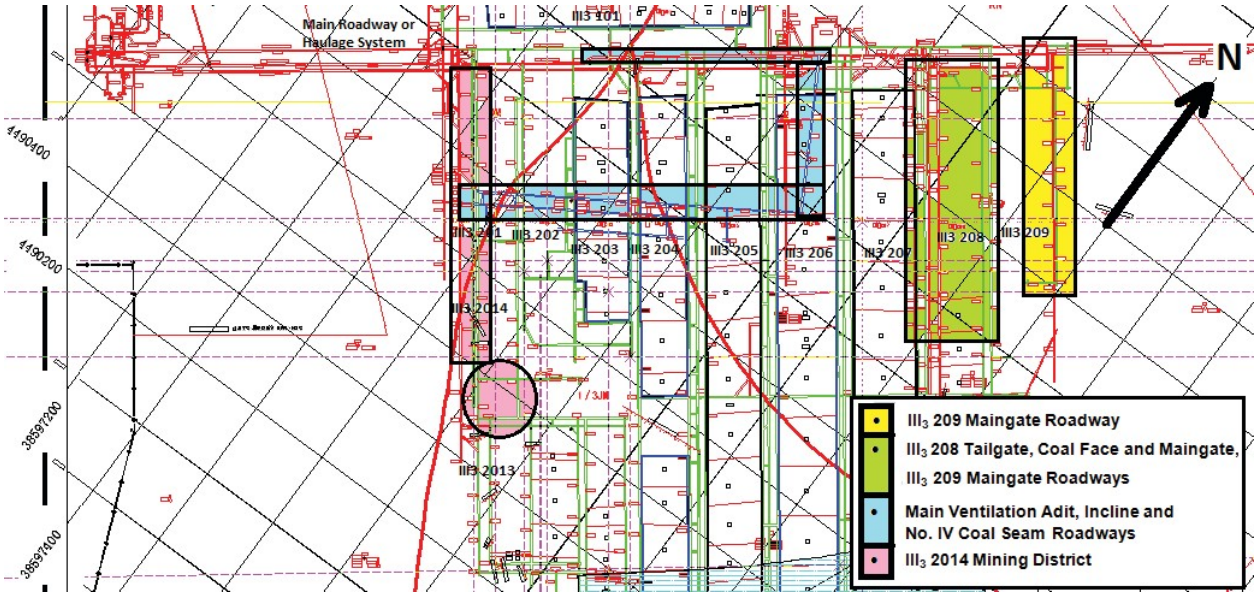

Figure 8. Location of workplaces inspected.

Table 7. Qualitative yield pillar performance with back calculation of pillar loads (Schissler, 2002).

Mine & Panel	Mining Height(ft)	Cover Depth x Panel Width (ft)	# of Entries	Size of Pillar(s) (ftxft)	Pillar Strength MPa, (psi)	Pillar Width: Height Ratio	Development Stability Factor	% Load Transferred	Successful or Unsuccessful	Remarks from Literature
Castle Gate No. 3[1]	7.2	1164 x500	2	30x 80	13.3 (1926)	4.2	0.71	93%	U	Strong coal, inhibited yielding
Cimarron Mine[2]	7.9	500 x500	2	30x 80	12.5 (1806)	3.8	1.54	82%	U	Weak roof
Cottonwood Mine[3]	7.9	1800 x550	2	30x 80	12.5 (1806)	3.8	0.43	96%	S	Strong roof
Wilberg Mine[4]	7	1600 x550	2	30x 80	13.6 (1965)	4.3	0.52	95%	S	Strong roof
Wilberg Mine[5]	7	1600 x550	2	30x 80	13.6 (1965)	4.3	0.52	95%	S	Strong roof
Sunnyside (SS) A3 9L, 1961+	5	1000 x550	2	30x100	17.4 (2520)	6.0	1.12	83%	S	Good stability
SS A4 4N 1968-1972[7]	6	1550 x500	2	25x95	13.3 (1926)	4.2	0.51	95%	S	Reduced TG bumps
SS A4 5N 1968-1972[8]	6	1800 x500	2	35x95	17.0 (2466)	6.0	0.64	91%	S	Good conditions
SS A4 3N 1968-1972[9]	6	750 x500	2	30x90	15.1 (2196)	5.0	1.28	83%	S	Reduced bumps
SS A4 3N 1968-1972[10]	6	1350 x500	2	45x85	20.7 (3006)	7.5	1.11	80%	U	Bumps in tailgate
SS A5 2S 1972-1974[11]	5.5	1100 x750	2	25x85	14.1 (2049)	4.5	0.74	92%	S	"Best mining to date"
SS A6 11L 1969-1980[12]	6	2000 x450	2	25x110	13.3 (1926)	4.2	0.40	96%	S	No trouble
SS A7 10L 1978-1981[13]	6	2200 x450	2	80x180	33.8 (4896)	13.3	1.42	43%	U	Massive bump
SS A8 #3 1974[14]	5	1800 x700	2	30x95	17.4 (2520)	6.0	0.62	91%	S	No trouble
SS A9 16R	6	2200	2	75x90	31.9	12.5	1.21	70%	U	Bumps

To further justify the use of the squat pillar formulation for prelimanary analysis, Watson (2003) did some comparison studies for a w/h ratio range between 3 and 9 and found that pillar strength predicted by numerical analysis agrees reasonably well with that given by Salamon's formula or the squat pillar formula. There is however limitation in using the empirical formulation in isolation and not comparing it with a 2D elasto plastic numerical analysis that incorporates weak layers within coal pillars.

Table 6 provides some indication of the variance in pillar strength throughout the Xuandong No. 2 mine for w/h ratios in excess of 5. This variance in pillar strength is a function of the w/h ratio and the length of the pillar. In order to look into the factor of safety for each of the pillars, a numerical model would be appropriate to determine the average stress within some of the pillars. (This is currently the subject of investigation following the stress measurement results.)

However, a preliminary two-dimensional finite element model was developed for a section across the southeastern longwalls (III_3 201 through III_3 309). This section incorporates the 210 m thick dolerite sill which spans above longwalls III_3 203 through to III_3 209. *Phase*[2] version number 7.0 was used for this preliminary analysis; it is a powerful 2D elasto-plastic finite element stress analysis program for underground or surface excavations in rock or soil. It can be used for a wide range of engineering projects and includes support design and tabular mining. We assessed various scenarios in terms of model building and resultant outcomes:

- Pillar with no interburden layers
- Pillars with interburden layers
- Pillars simulated with weak layer in the floor

Initially the model did not provide similar lateral displacements that have been observed in the III_3 209 maingate roadway, as this was the only real measurement that could be used for some kind of back analysis. The field stress state had been assumed as gravity incorporating an in-plane k-ratio of 2.45 and an out of plane minor stress k-ratio of 1.83 (assumed preliminary stresses prior to stress measurement results). This will need verification through our next investigation phase. A very fine mesh was used around the pillar and roadways to allow for multiple iterations of nodes (see Figure 9). The observed coal rib deformation could not be achieved through normal boundary conditions; hence boundary conditions between the coal and mudstone interburden layers have been artificially introduced via the introduction of a thin layer with weak material properties, to simulate the observed behaviour. A back analysis for the purpose of reproducing underground chain pillar behaviour using various material properties were conducted for 0.515m of displacement similar to what we've observed and confirmed by senior officials at the mine (see Figure 10). Figure 11 shows the maximum principal stress distribution throughout the chain pillar indicating the expected trend with zero stresses on the surface boundary with two peaks a few metres away from the ribs.

DEEP COAL MINE REGIONAL STRATA CONTROL COMPARISON

It was considered appropriate to investigate and provide some background on yield pillars, because the potential for a yield pillar system for the Xuandong Coal Mine is eminent due to their experience with coal bumps and our own experience with seismicity. Yield pillars have been used in coal mines for a long time, especially in deep coal mines to manage aggressive ground behavior.

A mine pillar becomes a yield pillar or a yielding pillar as a result of progressive loading and subsequent post-peak performance. As a result of mining in the vicinity of the pillar, the pillar load, or average vertical stress acting on a pillar, gradually increases from the initial virgin value towards the maximum load bearing capacity, or pillar strength. In this stage of loading, both the pillar load and the mean pillar deformation (or average vertical convergence) increases simultaneously, that is, the pillar's load deformation curve is in its ascending branch. This ascending portion of the pressure deformation curve is defined as Zone I (see Figure 12). The pillar load is at its maximum when its value reaches the pillar strength. If the pillar were to deform beyond this point, its load bearing capacity will diminish; that is, the load-deformation curve of the pillar would move into its descending branch or Zone II. If a pillar is in the descending branch of its load-deformation curve, it is regarded as a yield or yielding pillar. The turning point separating the ascending and descending branches of the load-deformation curve defines the pillar convergence corresponding to the maximum pillar strength, or maximum load bearing capacity.

Zones II and III are the strain softening portion of the load-deformation curve of a yield pillar. Zone II is the area where strain energy can be dissipated rapidly and sometimes violently, as in the case of a bump. Other than numerical modeling, virtually no in-mine observation exists as to the shape of Zone III. Schissler (2002) presented case histories of yield pillars used in the past 40 years and compared them with respect to qualitative parameters and certain calculated values in Table 7. The table contains the mining height, depth of cover, longwall panel width, number of entries in the gateroad system, size of the pillar of width by length, pillar(s) strength, w/h ratio, development load stability factor, and percent load transferred of the yield pillar.

Reference is made in particular to the mining depth of 854 m below surface (SS 23L Site 3) for a seam height of 1.828 m, and panel width 213.4 m. A pillar w/h ratio of 5.8 had been employed successfully (see Table 7 for other comparisons). Schissler further suggests that yield pillars should only be used in coal mines where the roof and floor rock have a CMRR[1] rating of 50 or better. In lower quality rock, the roof may be incapable of transferring the load that the yield pillars try to shed to adjacent abutment areas.

CONCLUSION

In conclusion the regional strata control is to some extent, by default (geological weakness) reasonably well controlled. The current chain pillar geometry is designed for stability; however, no geological weakness is taken into consideration during this process, which could affect the strength of the chain pillars. Some of the chain pillars are possibly within the critical w/h ratio and not large enough to redistribute stresses). Therefore, this resulted in secondary floor punching and resultant floor heave, which

1 *CMRR (Coal Mine Roof Rating) – system developed by the U.S. Bureau of Mines in the early 1990s. The system is aimed at characterizing roofs of coal mines. The CMRR is a rock mass classification system that rates the structural competence of mine roof on a 0 to 100 scale. The final rating is dependent on field characteristics of jointing, shears, and water entrainment and dependent on strength characteristics such as compressive strength.*

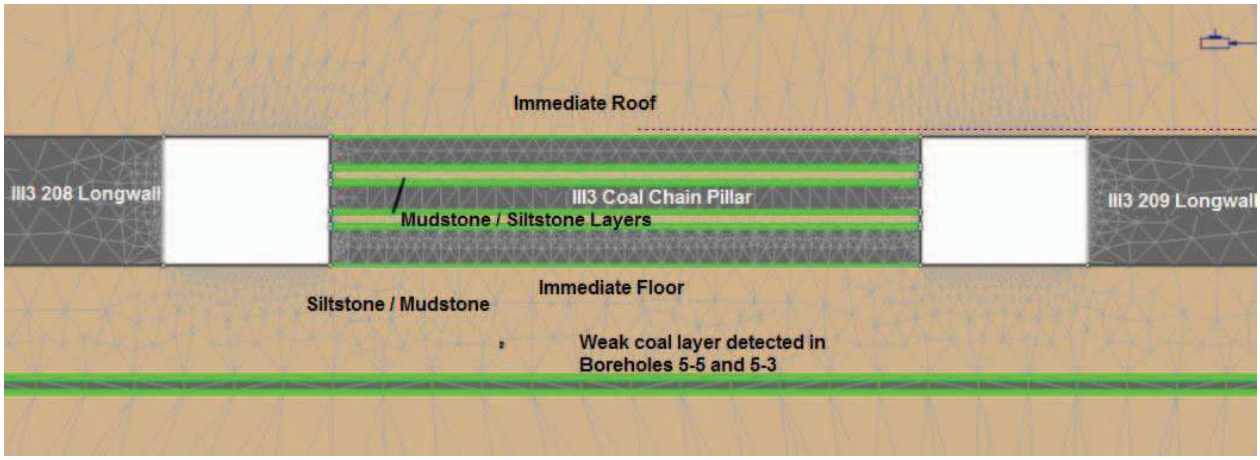

Figure 9. Chain pillar model showing fine mesh used to allow for more refined simulation between III_3 208 and III_3 209 longwalls.

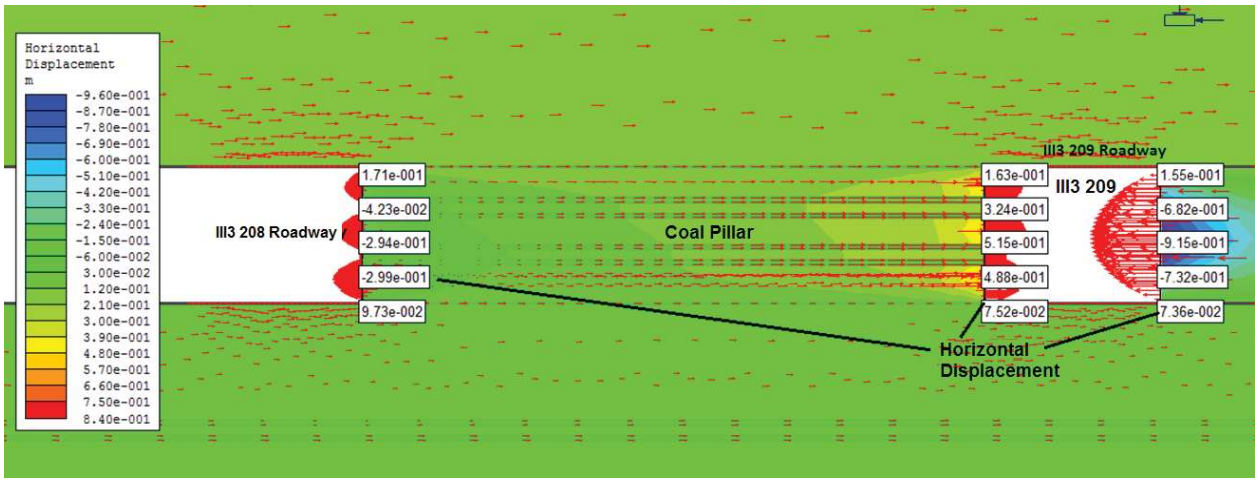

Figure 10. Chain pillar behavior between III_3 208 and III_3 209 longwalls.

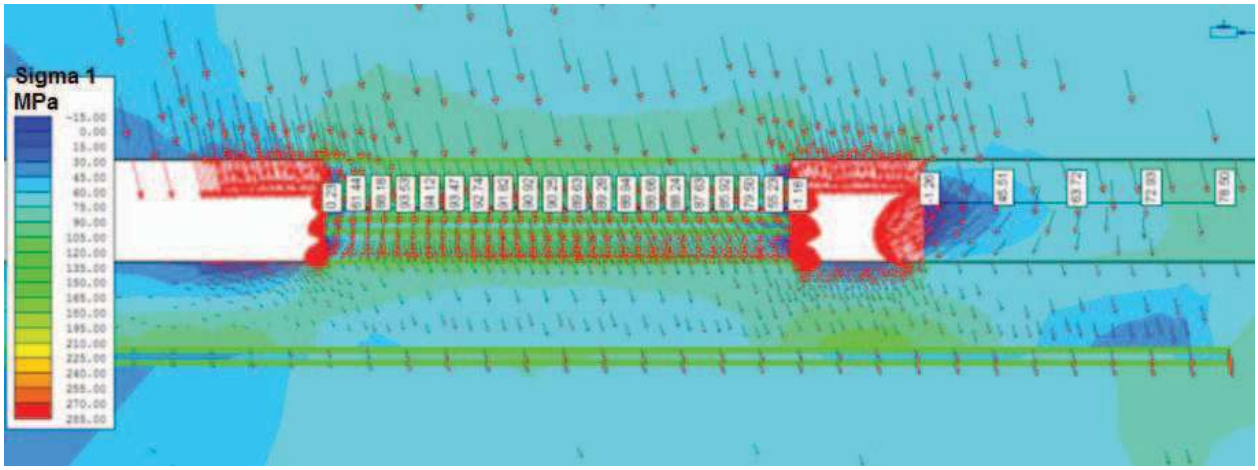

Figure 11. Graph showing trend of maximum principal stress distribution through the III_3 208 and III_3 209 longwall chain pillar.

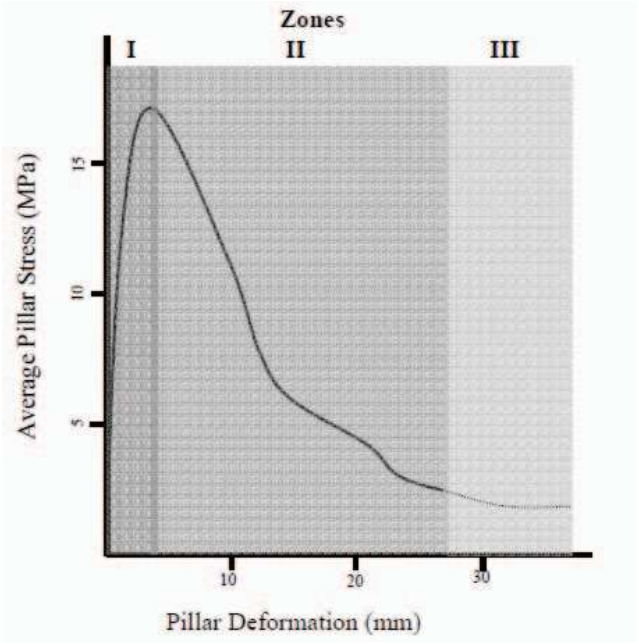

Figure 12. Pillar stress compression curve for a coal pillar (Schissler, 2002).

causes extreme difficulty to drive the longwall mining and thus production. No barrier pillar as such has been employed except for the centre 164-m-wide main headings pillar with a w/h ratio in excess of 40. This in itself would be considered a regional stability pillar because it separates the two mining regions and intends to provide protection for the main headings (main roadways and main ventilation return airway), which is currently showing signs of severe deformation. The ground support installed in these headings is quite in-effective in managing the effects of the ground movement.

Having assessed the location of the dolerite sill and its geometry, the probability of it breaking up in smaller fragments and producing a larger goaf is low. It thus is anticipated that a gap may appear below the base of the dolerite sill. It is further recognized that horizontal stresses could be locked up within the dolerite sill, which is likely to result in regional bending that will likely be distributed through the chain pillars. This has to some extent already occurred and the effects have been seen and felt through excessive floor heave, pillar punching, and coal bumps (seismicity).

It was thus a consideration that a yielding chain pillar design is appropriate for the Xuandong No. 2 Mine to effectively manage the regional strata control. This will minimize aggressive and excessive secondary floor heave problems. It will also prevent the possibility of dynamic pillar failures and injury to personnel.

In consideration of this and availability of required information to implement this strategy the following points need to be considered:

No proper process in place to finalize chain pillar dimensions due to geological consideration. To be more explicit, every longwall would require a detailed investigation of immediate roof and floor condition (i.e., CMRR would be required—current and future core drill hole information to be used). The investigation into immediate floor condition would evaluate for possible weak floor in considering potential foundation failure that could result in severe floor heave, which we have seen in many instances.

In implementing this strategy, no additional barrier pillars would be required other than the central stability pillar to protect access to and from longwall panels. In combination of the above strategy there would be a need to upgrade the current ineffective rib support. As with a yielding pillar design, effective rib spall control needs to be in place to effectively manage or confine the yield zone. During the investigation it was found that the support system employed was ineffective in controlling rib spall.

It was further found that the single development without a second escapeway under the III_3 coal seam pillars has the potential for entrapment during potential dynamic ground motion (e.g., pillar punching).

ACKNOWLEDGEMENTS

The authors would like to thank the Australian Federal Government, the Chinese Federal Government, Xuandong Coal Mine, and SIMTARS for their valued contribution during the investigation process. We also would like to thank Xuandong Coal Mine's senior management team for their cooperation during the investigation process.

REFERENCES

Madden, B.J. (1991). "A re-assessment of coal-pillar design". J.S. Afr. Inst. Min. Metall., vol. 91, no.1. Jan. 1991. pp27-37.

Peng, S.S., Tsang, P., Hsiung, S.M. (1989). "Yield pillar application under strong roof and strong floor condition—a case study. *Rock Mechanics as a Guide for Efficient Utilization of Natural Resources*. Rotterdam, Netherlands: A.A. Balkema.

Schissler, A. (2002). "Yield pillar design for coal mines based on critical review of case histories" [Thesis]. Department of Mining Engineering, Colorado School of Mines.

Van der Merwe, J.N. (1995). "Prediction of dolerite sill failure." In: *Proceedings of the 8th Congress of the International Society for Rock Mechanics*. A.A.Balkema.

Ouyang, Z., LI, C., XU, W., LI, H. (2009). "Measurements of in situ stress and mining-induced stress in Beiminghe Iron Mine of China." *Journal of Central South University of Technology*. 16(1):0085−0090.

Watson, J. (2003). "The strength of coal pillars." In: *Proceedings of the 1st Australasian Ground Control Conference*. Sydney, Australia: UNSW Press.

Applications of Microseismic Monitoring in China's Underground Coal Mines

Xiangxi Wu, Geophysical Analyst
Mining and Geo-Tech
ESG Solutions
Kingston, Canada

Chao Liu, Associate Professor
School of Energy Engineering
Xi'an University of Science and Technology
Xi'an, China

Zara Hosseini, Sales Manager
Cezar Trifu, Executive Vice President
ESG Solutions
Kingston, Canada

ABSTRACT

Longwall and continuous mining are prevalent methods employed by Chinese underground coal operations. The main ground control challenges include roof skin deformation, roof collapse, and outbursts of coal, gas, and water. Microseismic monitoring provides valuable information on rockmass behavior and fracture propagation caused by stress redistribution, active geological structures, or gas build up within the coal strata and the surrounding rockmass. Collecting and assessing seismic data has proven to be an instructive tool for engineers to better assess ground conditions and mitigate seismic hazards associated with mining. The development of intrinsically safe and explosion proof certified seismic monitoring equipment has revolutionized China's underground coal mines. The use of this technology allows for the optimization of gas drainage at an increased rate of two at a 50% higher purity without any increase in drilling costs. Microseismic monitoring can also be used in identifying seismically active faults and shear zones. This information can be used to assess and revise mining strategies to improve safety and ground stability.

INTRODUCTION

Microseismic monitoring has been employed routinely in hard rock mines for more than 40 years (Alexander and Trifu, 2005). The technology has also been applied in research studies carried out in coal mines (e.g., Luo et al., 1998; Gale et al., 2001; Westman et al., 2001). However, the difficulties associated with the maintenance of seismic sensor arrays in a rapidly advancing longwall mining environment have delayed its implementation in this environment.

In the United States, rock mechanics is called upon to improve safety by addressing any potential design deficiencies (Heasley, 2011). While microseismic monitoring has been part of the ongoing research, the transfer of this technology to the industry remains largely undeveloped. In China, on the other hand, the need for enhanced work safety through a better understanding of the rockmass conditions under a fast mining extraction rate has led the Chinese mining industry to fast track the use of microseismic monitoring over the past few years. This study reports on the use of this technology in China's deep coal mines, outlining some applications as well as the results obtained.

INTRINSICALLY SAFE AND EXPLOSION PROOF SEISMIC SYSTEM CONFIGURATION

The general configuration of a microseismic monitoring system operating in a coal mine is similar to that of a system employed by any hard rock mine. The principal system components are as follows:

- Seismic sensors, which record the ground motions generated by the stress released during the fracturing process. Seismic sensors can be geophones, which record ground velocity, or accelerometers, which record acceleration. The 2D layout of the coal operations makes it very difficult to install seismic sensors in a 3D array configuration.
- Recorders, which convert the seismic signal from analog to digital.
- Time synchronization equipment, including a central or master time server and time receivers that provide time stamping of the acquired data.
- Data communication equipment, consisting of twisted copper cables from sensors to the recorders, and fiber optics from recorders to the central acquisition workstation.
- Seismic acquisition and processing workstation, which acquires and processes the seismic data in continuous and/or triggered mode. Seismic processing software can provide automatic and manual results, subsequently allowing for their interpretation, visualization, and reporting.

Deep coal mines require a sensor array that can effectively record and determine small fracturing corresponding to moment magnitude below zero ($M_w < 0$). The potential presence of methane imposes major restrictions on the installation and operation of underground systems. Most of the coal mines in the United States can deploy recording and acquisition equipment in ventilated areas containing fresh air, leaving only the sensors placed in methane exposed areas. Sensors, therefore, must be Intrinsically Safe (IS) and connected to the recorders through IS barriers.

In China, however, there are often no certified fresh air areas in deep coal mines. This is why recorders must also satisfy explosion proof requirements. As such, in addition to the IS barriers, the junction boxes containing seismic recorders are also explosion

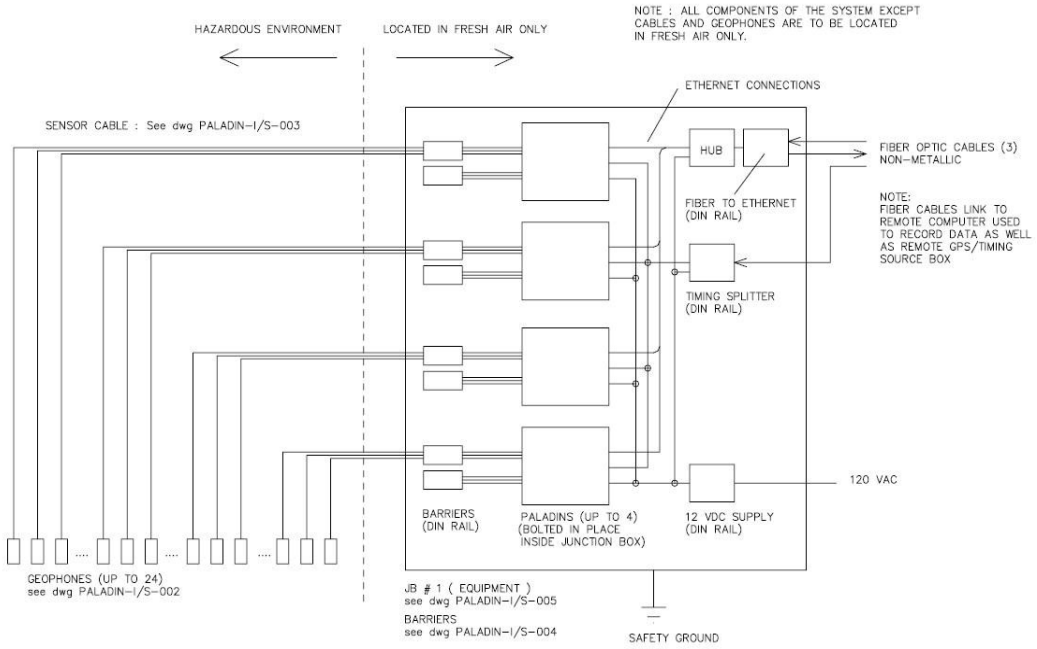

Figure 1. Intrinsically safe MSHA-certified seismic system configuration; seismic recorders must be located in ventilated, fresh air areas.

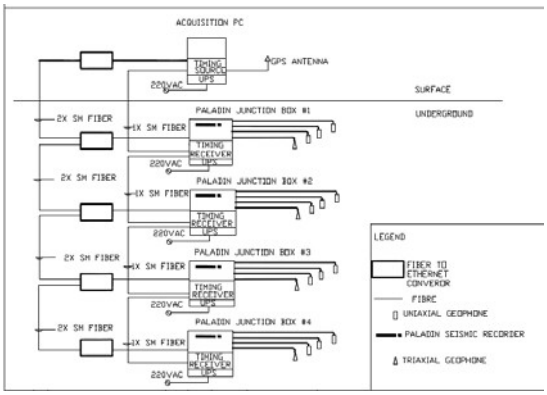

Figure 2. Intrinsically safe and explosion proof MA-certified seismic system configuration; the IS barriers are installed inside explosion proof junction boxes, which allow seismic recorders to be located in non-ventilated areas.

proof and specially designed to withstand the accidental release of energy stored inside these recorders.

Figure 1 shows a system configuration provided by ESG Solutions with IS sensors, as certified by the U.S. Mine Safety and Health Administration (MSHA). Figure 2 presents a configuration also offered by ESG Solutions, with IS sensors and explosion proof recording hardware certified by China's Mining Products Safety Approval and Certification Center (MA). Worth noting, the MSHA certification is not directly transferable to China. Regardless of the similarity between some of the technical specifications, the MA certification demands independent testing carried out at one of the MA Centers.

While the MSHA certification does not require expensive explosion proof junction boxes for the underground equipment, the MA certification offers the possibility of installing this equipment closer to the sensor array. This has the direct effect of reducing the cable cost, electrical interference, signal attenuation, and various maintenance problems associated with running long twisted copper cables, thus allowing an improved signal quality.

SEISMIC ARRAY DESIGN IN UNDERGROUND COAL ENVIRONMENTS

The type and sensitivity of seismic sensors as well as the array configuration are essential in the performance of a microseismic system in coal mines. One issue to consider when designing a microseismic monitoring system in coal is the rockmass characteristics. Coal is a soft rockmass characterized by a relatively lower quality factor (Q) and slower P- and S-wave velocities compared to the hard rockmass encountered in metal mines. These characteristics lead to a significantly higher attenuation of the high frequency waveform in coal strata, even when recorded at a short distance from the seismic source. Accelerometers are generally more sensitive for detecting higher frequencies, characteristic to weak, lower magnitude seismic events, while geophones are more suitable for the recording of the lower frequency range, appropriate for relatively stronger, higher magnitude seismicity (Alexander and Trifu, 2005). In soft rockmass environments, however, high sensitivity geophones are preferred over accelerometers in underground sensor arrays because of the significantly higher attenuation of the acceleration with distance.

Figure 3 presents an example of the geophone array installed by ESG Solutions at Wudong coal mine, a longwall coal mine in Xinjiang Province, China. Geophones are installed in the south roadway of the 620#43 longwall panel (20 m width) and north roadway of 655#45 longwall panel (25 m width). The inter-sensor distance along both roadways is about 150 m. These sensors provide a frequency bandwidth from 6 to 1,000 Hz, with

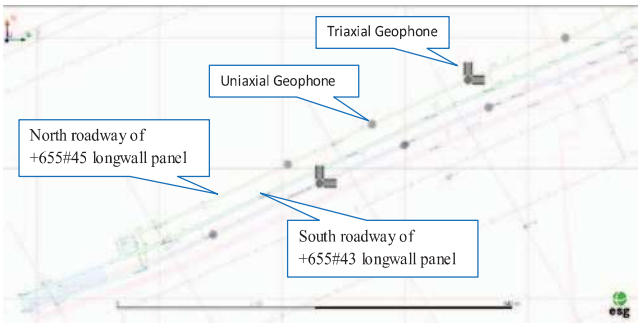

Figure 3. Geophone array at Wudong coal mine.

a sensitivity of 51 V/m/s (undamped). Such an array can monitor seismic events between M_w -1.5 to 2.

Another challenge in the installation of seismic sensors in underground coal mines is that most of these mines have only one working level that follows the quasi-horizontal coal seam. Consequently, underground sensors can be installed only in accessible areas around the coal panels, which results in a planar sensor array. In case of a planar sensor array, event location errors in the depth coordinate will be higher than those in the horizontal coordinates. Moreover, event locations based on first P- and S-wave arrivals at uniaxial sensors cannot resolve the intrinsic symmetry that comes with a planar array. Figure 4 shows the expected event location errors at Wudong coal mine for a uniaxial geophone array. As seen in the right hand side of this figure, such an array will not be able to resolve whether seismic events occur above or below the array. It is strongly recommended to add triaxial geophones, because they can provide additional information through wave polarization analysis, which can resolve the above uncertainty. Alternatively, a three-dimensional array can be installed but this will increase the drilling costs. A preliminary array design will evaluate the array performance in terms of sensitivity and event location accuracy, based on the number and type of sensors, as well as their position with respect to the monitoring area. The results depend on the quality of the geological and rockmass information available.

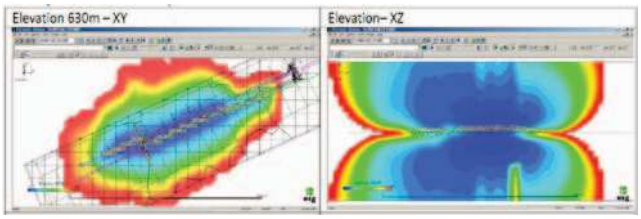

Figure 4. Simulation results estimate seismic event location errors at Wudong coal mine between 15 m (blue) and 200 m (red).

SEISMIC DATA PROCESSING AND INTERPRETATION

Data processing includes seismic event identification and location, along with the evaluation of its magnitude and other source parameters. A seismic waveform analyzer (WaveVis™) allows the users to view the seismic waveforms, pick the P-and S-wave arrival times, perform event location, spectral analysis, etc. Typical waveforms and amplitude spectra are shown in Figure 5 using the WaveVis™ software for a seismic event with M_w -0.3 that occurred at Wudong coal mine on September, 19, 2011, at 13:45:20 local time. Amplitude spectra indicate that frequencies above 100 Hz are heavily attenuated.

Figure 5. (a) Typical waveforms and (b) amplitude spectra for a M_w -0.3 seismic event that occurred at Wudong coal mine. The vertical line on the amplitude spectra marks 100 Hz.

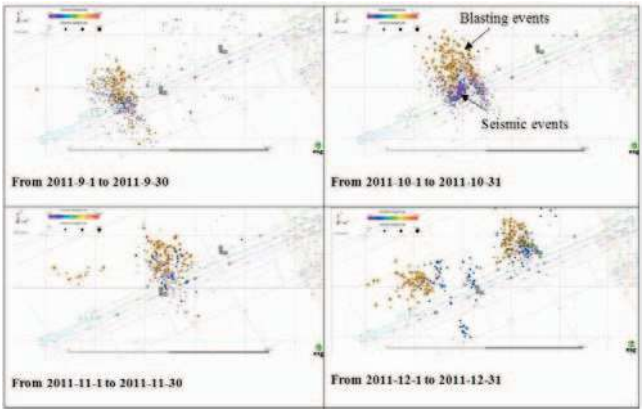

Figure 6. Plan view of monthly seismic (blue) and blasting (yellow) activity at Wudong coal mine from September to December 2011.

The seismic visualizer (SeisVis™) provides an interactive, three-dimensional display of event locations, magnitudes, and other source parameters with respect to the site geometry. Figure 6 presents an example of the SeisVis™ plan view option, which illustrates the monthly seismic and blasting events at Wudong coal mine from September to December 2011. This function can assist the ground control engineer to record blasting and create images of the roof subsidence process following the support retreat sequence. Unexpected clusters of microseismicity and the occurrences of large seismic events indicate potential ground hazards in certain areas.

CASE STUDY #1—GAS DRAINAGE OPTIMIZATION

Xinzhuangzi is a gassy, longwall coal mine in central China. In order to prevent coal and gas outbursts, and control gas emissions during mining, it is required to partially drain the gas from the coal seam. The main challenge of gas drainage is to first identify the areas of high gas concentration in order to improve gas extraction efficiency. Based on research work carried out at Huainan coal mine, Yuan and Liu (2003) proposed a model in which gas accumulates in a cavity above the roof. A microseismic monitoring system was installed at Xinzhuangzi mine to monitor the facture development in the roof strata.

Following a three-month monitoring period, from April to July 2009, the clustering of microseismicity allowed the identification of a circular shaped fracture region in the mine roof, as shown in Figure 7a (Chao, 2011). This result closely matches the cylindrical circular model (Figure 7b) that characterizes the roof cavity collecting gas that has migrated from the coal seam through the surrounding fractures. Subsequently, an optimized coal gas drainage procedure was designed to extract coal gas from the respective cavity.

Figure 8 plots the gas extraction rate and purity after the optimization of the gas drainage scheme. Compared to the previously used conventional gas drainage procedure, the optimized scheme improved the gas extraction rate from 3-8 m^3/min to 5-15 m^3/min. Also, the optimized procedure raised the gas purity by approximately 50%, all without any increase in drilling costs (Chao, 2011).

CASE STUDY #2 —FAULT IDENTIFICATION AT XINZHUANGZI COAL MINE

Seismic monitoring is a very reliable tool in identifying seismically active, indefinite geological features within the mining zone or a better characterization of already mapped structures. A seismically active shear zone or fault can result in a cluster of microseismicity and occasional large magnitude events. Any seismic event associated with a geological structure can be further analyzed and used in conjunction with other available geological data to identify and characterize seismically active structures, aiming to improve mining strategies around these zones of potential instability and hazardous conditions.

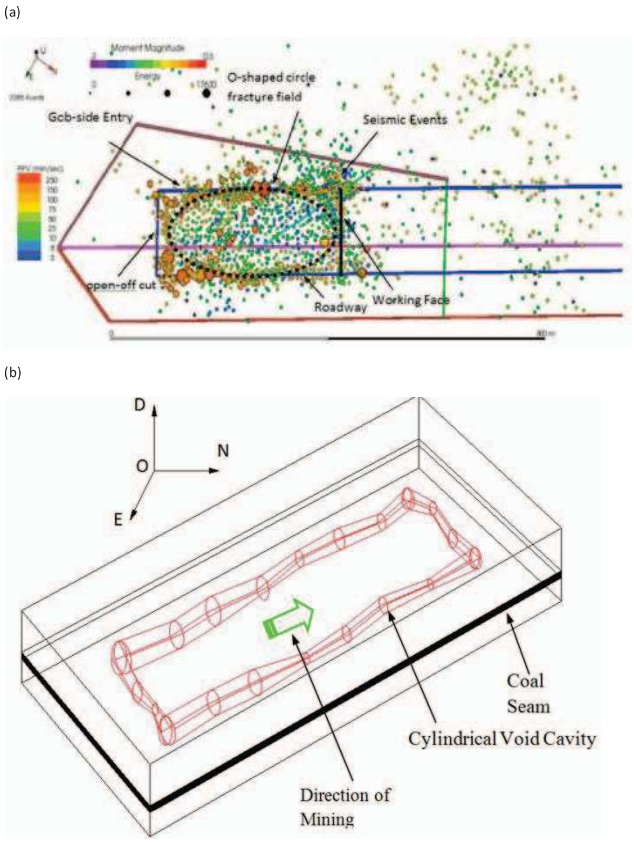

Figure 7. (a) A seismic clustering pattern identifies a circular shaped fracture zone in the roof of Xinzhuangzi coal mine, matching the (b) model of a gas cavity.

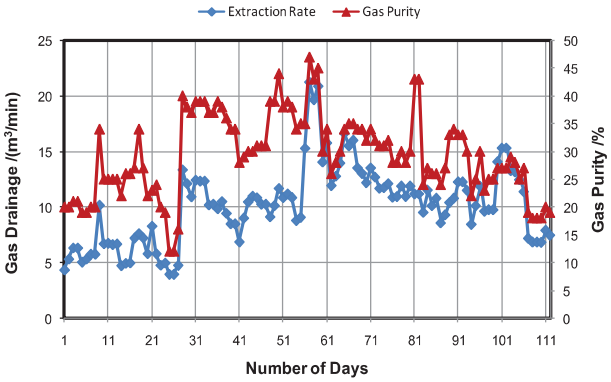

Figure 8. Gas drainage rate and purity after optimization.

Figure 9 presents the result of a two-dimensional active seismic study carried out by Anhui University of Science and Technology, in which two faults were explored: F10-5(10) and Fa. The seismic moment density, calculated from passive microseismic source parameters is shown in Figure 10, underlining the areas of the Fa and F10-5(10) faults (Chao, 2011).

The comparison of Figures 9 and 10 proves that passive and active seismic monitoring results are consistent with each other. It is worth noting, however, that only passive monitoring can identify active faulting through the presence of induced seismicity on pre-existing geological features. Additionally, passive monitoring provides continuous, real-time imaging of active fault zones, while active seismic monitoring offers static results, only from time to time. As such, the objective of passive monitoring is the identification of new, unknown faults and the characterization of active faulting. This allows an evaluation of the impact of faulting onto mining, thus enabling ground control personnel to suggest more effective support solutions.

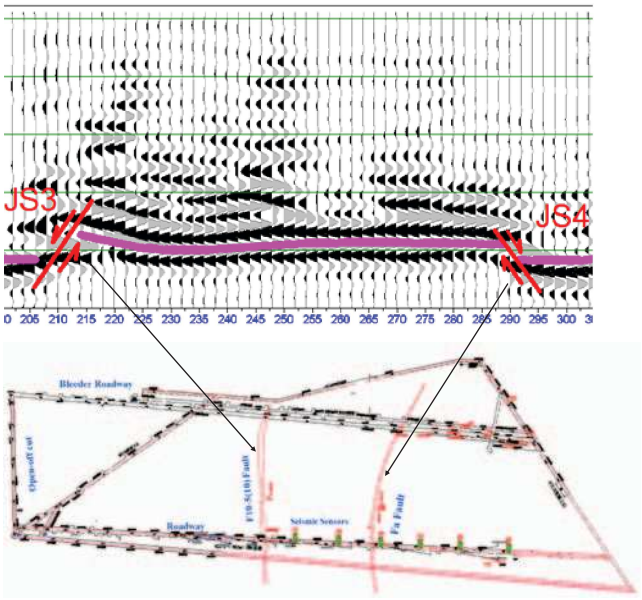

Figure 9. A two-dimensional active seismic survey indicates the presence of two faults at Wudong coal mine, JS3, or F10-5(10), (bottom left), and JS4, or Fa, (bottom right).

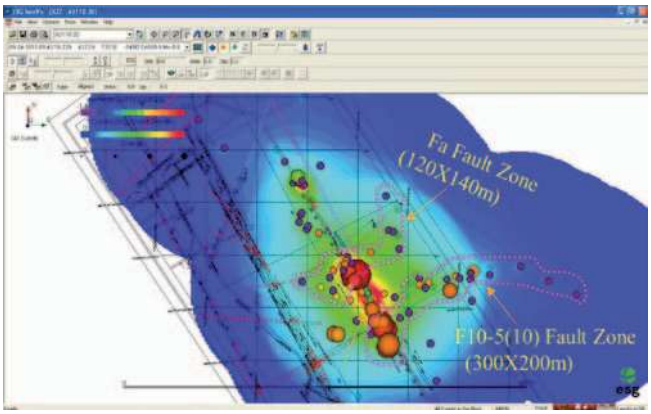

Figure 10. Seismic moment density evaluated from microseismic source parameters for events in the areas of the Fa and F10-5(10) faults at Wudong coal mine. (a) (b) (a) (b).

CONCLUSIONS

This overview documents several applications of microseismic monitoring technology in underground coal mines. The presence of methane and unventilated areas require IS and explosion proof equipment. Ideally, the sensors are installed in close proximity to the advancing coal face. However, the relocation of seismic monitoring hardware is not trivial, reason for which the redeployment of the sensor array needs to be carefully planned. Geophone arrays are recommended due to reduced attenuation of ground velocities compared to accelerations, even for small source-sensor distances. While uniaxial geophones offer the best return on cost vs. performance, the planar layout, due to the presence of only one mining level, requires the use of at least a few triaxial geophones in order to eliminate the intrinsic symmetry in seismic event location. The use of microseismic monitoring allows the identification of the effects of stress redistribution within the coal seam. In particular, the technology is presently used in Chinese coal mines for the optimization of gas drainage, identification of new faults and shear zones, as well as characterization of active faulting. Simplex ray tracing and migration algorithms are currently under development to improve the depth accuracy of event locations carried out using planar sensor array geometry.

REFERENCES

Alexander, J., Trifu, C-I. (2005). “Monitoring mine seismicity in Canada.” In: Potvin, Y., Hudyma, M., eds. *Controlling Seismic Risk*. Perth, Australia: Australian Centre for Geomechanics, pp. 353–358.

Chao, L. (2011). “Research on hazard mechanism and microseismic warning method for gas dynamic disasters of mining coal-rock” [Dissertation]. Dalian University of Technology.

Gale, W.J., Heasley, K.A., Iannacchione, A.T., Swanson, P.L., Hatherly, P., King, A. (2001). “Rock damage characterization from microseismic monitoring.” In: *Proceedings of the 38th U.S. Symposium of Rock Mechanics*. Taylor & Francis.

Heasley, K.A. (2011). Rock mechanics— a key to eliminating mine disasters.” Keynote lecture, 45th U.S. Symposium on Rock Mechanics. San Francisco, CA: June 26–29.

Luo, X., Hatherly, P., Gladwin, M. (1998). “Application of microseismic monitoring to longwall geomechanics and safety in Australia.” In: *Proceedings of the 17th International Conference on Ground Control in Mining*.

Westman, E.C., Heasley, K.A., Swanson, P. L., Peterson, S. (2001). “A correlation between seismic tomography, seismic events and support pressure.” In: *Proceedings of the 38th U.S. Symposium of Rock Mechanics*.Taylor & Francis.

Yuan, L., Liu, Z. (2003). “Study on the technique of roof gas drainage from mine coal seam in Huainan mine area.” *Journal of Coal Society*. *28*:149–152.

Track Entry Deformation Subjected to Longwall Mining in the Overlying Seam: a Case Study

Wenbing Xie, Professor
Shengguo Jing, Lecturer
China University of Mining & Tech.
Xuzhou, China

Yuexian Guo, Senior Engineer
Shanxi Coking Coal Group International Development Co., Ltd.
Taiyuan, China

ABSTRACT

At Renlou Coal Mine, Huaibei Mine Area, the track entry deformed significantly after longwall mining in an overlying multiple seams. The supporting characteristics of primary roof bolts and shotcrete with wire mesh are closely related to the movement of the mine's surrounding strata. A case study of a track entry deformation was monitored during the longwall mining of a selected overlying panel. The measured data showed the unique entry deformation pattern during the longwall mining in the overlying seam. Underground extensometer measurement showed that entry stability was mainly affected by the periodic roof weighting of longwall mining in the overlying seam. The displacement of the deeper strata occurred a head of the immediate vicinity of the entry. Thereafter, deformation of the roof and floor strata was in the form of shearing of the shallower strata. Due to the use of heavy-duty roof bolting with wire-mesh, the roof-to-floor and rib-to-rib convergences were small, but the floor heave was large, greater than 80% of the roof-to-floor convergence. The measured displacement from extensometers varied with the position of the monitored cross-sections and depth into the roof. There were several deformation patterns, such as shearing movement, compression, and expansion, and the variations between compression and expansion. Strata compression at the entry surface was always accompanied with shearing movement at the deeper strata. During the longwall mining, the whole surrounding strata of the entry moved toward the opening.

Underground practical experience indicated that prior to mining, the entry was supported very well in excellent conditions. After mining, however, it deformed greatly. The current entry support technology was not effectively control the severe deformation incurred in entries driven in soft strata due to the following reasons: (1) little is known about the entry deformation behavior of the strata surrounding the opening and (2) the degree of interactions between entry deformation and roof bolting with wire mesh is not well understood. Consequently, effective supporting systems cannot be properly selected to control its deformation and maintain a stable supported surrounding structure.

INTRODUCTION

An entry support stability in soft strata under the longwall panel II $7_2$14 was conducted at a mine in Huaibei mine area, China. Instrumentation was used to monitor the displacement around a cross-section of a track entry prior to longwall retreating in the overlying seam. The objective was to determine the entry deformation characteristic in order to select effective roof support methods and reduce large entry deformation due to the dynamic abutment pressure induced by longwall mining in the overlying seam.

The south track entry at level -720 m was located in weak strata below coal seams 7_2, 7_3, and 8_2. The average overburden depth was 750 m. The distance from coal seams 7_2 and 7_3 ranged from 43 to 70 m and was 20–50 m below the 8_2 seam. The relationship between the -720 m entry and longwall panel II $7_2$14 is shown in Fig. 1.

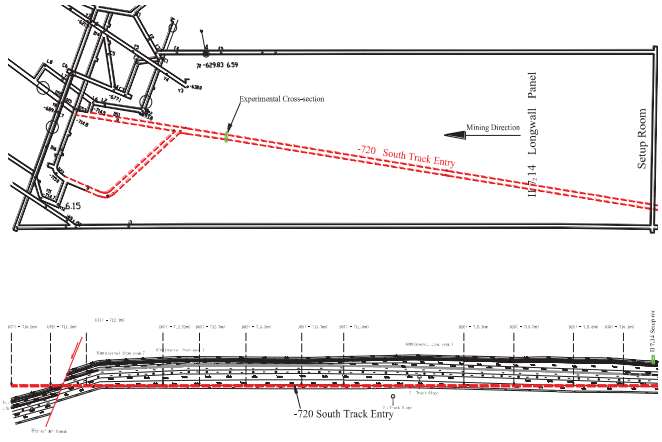

Figure 1. Plan and cross-sectional views of -720 south track entry and longwall panel II $7_2$14.

The track entry was supported with 3-m-long fully grouted bolts on development (800 × 800 mm in spacing), 6.5-m-long cable bolts, and 100 mm shotcrete with wire mesh. The roof of the track entry consists of fine sandstone, claystone, and claystone with aluminum. The floor consists of sandstone and claystone.

Those strata were classified as weak rocks because the uniaxial compressive strengths determined in the laboratory were low. Entry deformation was insignificant during development and prior to longwall approach. However, as the longwall approached, the entry would be subjected to severe deformation if the entry supports were not strengthened.

INSTRUMENTATION

Multiple-position extensometers instrumentation were used to monitor the roof strata displacement in the -720 south track entry during retreat mining of a panel II $7_2$14 in the overlying seam. The orientation of the entry was almost parallel to the longwall retreat direction. The entry had been supported with high strength steel bolts prior to the longwall mining because the entry would be affected by the front abutment pressure generated by the longwall mining in the overlying seam. Fig. 2 shows the instrumentation layout installed at the test site. Nine extensometers were deployed equal distance around the periphery of the entry. The extensometer was placed 6 m deep into the strata, and each extensometer consisted of 6 anchors spaced 1 m apart. Additional extensometer was installed with two anchor points to measure bed separations in the roof, close to 5# extensometer.

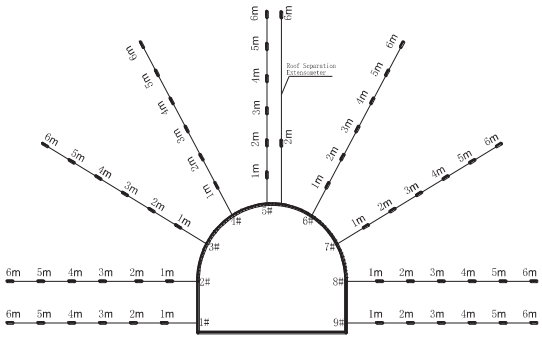

Figure 2. Instrumentation plan around the cross-section of the south track entry.

The instrument readings were collected, including displacement in the immediate vicinity of the openings and deeper strata. The extensometer with two anchors (2 m and 6 m deep) was installed at entry center was used to monitor bed separations in the roof.

Roof separation between the two anchors was determined by subtracting the reading of the No. 2 anchor (2 m deep) from that of No. 6 anchor (6 m deep) as shown in Eq (1).

$$S_{2,6} = S_6 - S_2 \quad (1)$$

where

$S_{2,6}$ = separation between strata at 2 m and 6 m deep,

S_2 = measured anchor movement at anchor 2 m deep, and

S_6 = measured anchor movement at anchor 6 m deep,

Multiple-position extensometers were used to monitor entry deformation surrounding the entry strata during the upper seam longwall mining. The relative displacement between the two anchors was calculated by Eq (2).

$$U_{n,n-1} = S_n - S_{n-1} \quad (2)$$

where:

$U_{n,n-1}$ = displacement between two adjacent anchors; n is the anchor number (1–6),

S_n = displacement at anchor n, mm, and

S_{n-1} =displacement at anchor n-1, mm.

DEFORMATION IN THE TRACK ENTRY

Surface deformation of the entry

The surface deformation around the track entry is a comprehensive index reflecting the entry stability. Figs 3 and 4 show the surface displacement and displacement velocity with respected to longwall face positions

The observation shows that the extent of front abutment zone was about 95 m outby the longwall face. The displacement was negligible before the upper seam longwall passed it, indicating that the instrumentation location of the -720 m track entry was not affected by the front abutment pressure of the upper seam longwall mining. When the entry was located below the gob after the longwall passed the instrumentation station, the entry had a large deformation, which goes against the common expectation that the entry would have a small deformation (Fig. 3 and Table 1).

Underground measurements showed that entry deformation increased after the upper seam longwall face passed the instrumentation station. The roof sags were 26 mm and 27 mm when the longwall face was 23 m and 92 m outby the instrumentation station, respectively. The magnitude of floor heave was determined by subtracting the roof sag from the roof-to-floor convergence. The floor heave was severe, which conformed to on-site observations. The floor heave accounted for about 80% of the total roof-to-floor convergence when the station was 92 m outby the longwall face.

Subsequent observations indicated that due to severe floor heave, the rib-to-rib and roof-to-floor convergences also increased. The rib-to-rib convergence was 28 mm; the roof sag was 34 mm; and the floor heave was 127 mm when the longwall face was 221 m outby the station. The results showed that under high-strength supports, the roof and the ribs were stable, while the floor was unstable. Therefore, it might need to reduce the floor heave in order to increase the entry stability.

Fig. 3 shows that the total amount of deformation continued to increase with the distance of face retreating; either the instrumentation station was subjected to the front abutment or the rear abutment pressures. However, the rate of deformation was not always increasing; it changed in a waveform, as shown in Fig. 4.

Table 1. Entry deformation vs. face position.

Stations distance from the mining face, m	4	23	34	49	70	81	92
Rib convergence, mm	11	8	14	13	13	15	11
Roof-to-floor convergence, mm	9	40	44	80	83	117	138

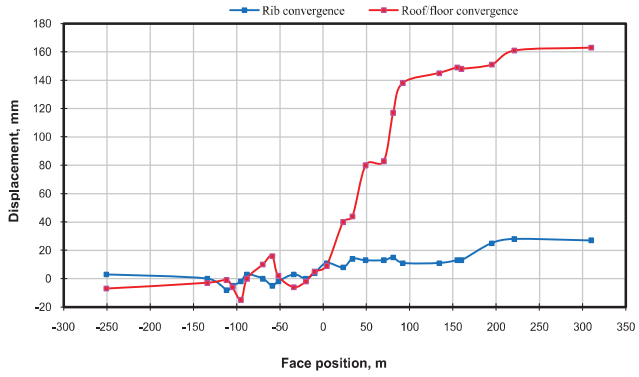

Figure 3. Surface movement profiles with respected to face position.

The wave variation of the rate of deformation occurred even when the face was inby the instrumentation station. This was closely related to the occurrence of mining induced pressures.

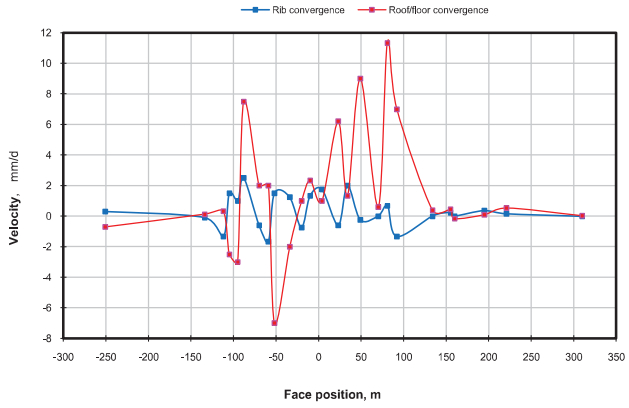

Figure 4. Displacement velocity profiles around the entry.

Underground measurements showed that the first caving interval of the immediate roof was 20 m; the first main roof weighting interval was 50 m; and the periodic main roof weighting interval ranged from 13.8 to 17.8 m, with an average of 15.4 m. Fig. 4 shows the rates of roof-to-floor and rib-to-rib convergences. Though they were not strictly correlated with the periodic weighting interval of the main roof, they were affected by the periodic roof weighting of the overlying longwall face retreating. The rates of roof-to-floor and rib-to-rib convergences also appeared in the waveforms, with the peaks (or valleys) of the rib-to-rib convergence corresponding to the valleys (or peaks) of those of the rate of floor heave. It shows that entry stability was more affected by the periodic roof weighting of the upper seam longwall retreating.

Although the wavelengths of the rates of roof-to-floor and rib-to-rib convergences differ, basically they coincided each other. The average wavelength was

$$(29 + 49 + 33 + 25 + 32)/5 = 33.6 \text{ m}.$$

The average wavelength of 33.6 m was about twice the periodic weighting interval of the main roof based on the monitored data. The measured data showed that roof and rib deformations were insignificant, and the entry was in good condition, while the floor hove in a waveform. It indicated that the main roof periodic weighting affected not only a specific cross-section of the entry, but also the entire entry within the extent of the abutment pressure. This was why the floor of the track entry hove periodically. The effect of the main roof periodic weighting on the ribs and roof differed from that on the floor.

Since the floor was not supported, the effect of main roof periodic weighting was much stronger, while the effects on the roof and ribs were much weaker. If no effective measures were taken immediately, the resulting severe floor heave could have caused the whole supported structure to become unstable. Further investigation indicated that if the floor heave continued to increase, the rib-to-rib and roof convergences tended to increase also. Therefore, immediate measures must be taken to control the severe floor heave.

It can be seen from Fig. 4 that when the face was 23–92 m outby the instrumentation station, the periodic roof weighting had the most influence on the stability of the entry around the instrumentation site. After the longwall face passed the instrumentation site, the entry was under the gob. However, when the face was 23 m outby the site, the effect and zone of influence of periodic caving on entry stability was far more than when it was under the front abutment pressure.

The measured rates of roof-to-floor and rib-to-rib convergences showed that when the longwall face was far outby the instrumentation station, the effect of main roof periodic caving was still conspicuous. This was because, after mining, the roof and floor at the face evolved from non-contact to contact each other, while the stress at the face changed from stress relief to gradually receiving load from the roof. At a location some distance inby the face, the roof load began to gradually recover. Due to the occurrence of broken cantilever beams with supports at both ends as a result of periodic caving in the roof, the roof and floor pressures recovered to the original or even exceeded the original position. Of course this interpretation needs to be confirmed by detailed follow-up analysis of the measured pressure changes. As the periodic caving continued, the influence zone became larger and larger. The measured rib-to-rib and roof-to-floor convergences show that the location of maximum influence was 81 m outby the face. The influence was greatly reduced when it was 134 m outby the face.

Fig. 5 shows the redistribution of floor vertical stresses during longwall mining. Three vertical stress zones were defined according to the floor reactions during the longwall mining. Zone IV was classified as the front abutment zone, zone V as the stress relief zone, and VI as the stress recovery zone.

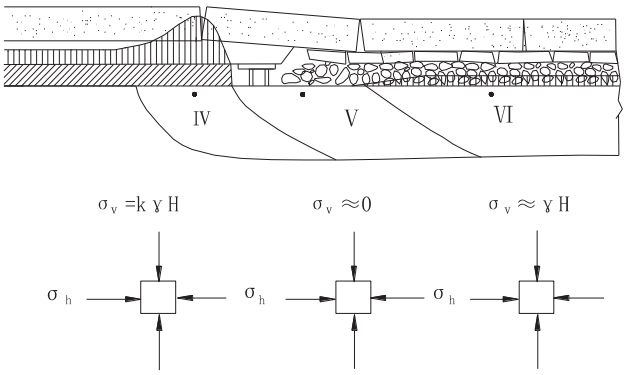

Figure 5. Redistribution of floor stresses during longwall mining.

Bed separation in the roof

The roof extensometer measures bed separations between strata within and outside the roof bolting horizons in order to evaluate the stability of entry subjected to longwall mining. Monitoring of bed separation was performed at the same time the rib-to-rib and roof-to-floor convergences were monitored. The monitoring stations and measured bed separations are shown in Fig. 6.

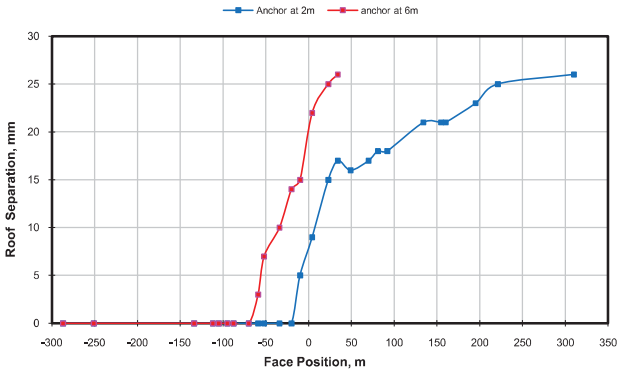

Figure 6. Roof separations vs. face distance.

The development of bed separations in the roof was similar to those of entry surface displacements. Fig. 6 shows that readings at the 6-m-deep anchor were first observed when the longwall was 70 m inby the instrumentation station and increased as the longwall face approached. During this period there was no reading at the 2-m-deep anchor position. The 2-m-deep anchor started to show the readings when the longwall face was 20 m inby the instrumentation station. This indicated that the strata between 2 m and 6 m deep exhibited shear deformation when the longwall face was 20–70 m inby the instrumentation station. The maximum roof separation was 14 mm. The strata at the 2-m-deep anchor did not exhibit shear deformation.

After longwall mining, the stresses around the opening redistributed, especially under the influence of the main roof periodic caving. The entry was subjected to the abutment pressure propagating downward from the floor of the longwall face to the surrounding strata of the entry, which caused shearing deformation in the entry roof.

As the longwall advanced, strata separations increased equally both within the 2-m and the 6-m-deep strata. During this period, bed separations occurred mainly within the 2-m-deep anchor locations in the form of shear deformation. Moreover, the shear deformation increased little between the 2-m and the 6-m-deep strata. When the longwall was 34 m outby the instrumentation station, the rate of increase of bed separations decreased greatly within the 2-m-deep strata. Thereafter, although bed separations within the 2 m horizon continued to increase, the amount of the changes was relatively small.

As observed from the development of bed separations within the 2-m-deep anchor, there was a close correlation between bed separations and main roof periodic weighting. The curve of development of bed separations also exhibited in a waveform. The development of bed separations stabilized when the roof strata stabilized.

Displacement at deep strata surrounding the entry

It was important to monitor and analyze the displacement in deep strata in order to understand its influence on the supporting performance of roof bolts and entry stability. Deep anchors were placed as shown in Fig. 2. Model KDW-1 deep anchors were installed on the ribs, while Model KDW-2 deep anchors were installed in the arch section. Measurements from the anchors installed around the entry showed that a self-supporting zone had been developed around the surface strata due to the application of high-strength support bolts technology. Bed separations in the deep strata around the cross-section of the instrumentation station were small. Bed separations measured by all the extensometers were less than 29 mm.

The measurements from all the extensometers around the entry cross-section showed that the three extensometers installed in the arch section better reflecting the movement of the surrounding strata. The displacement readings from the No. 4 extensometer conformed to those of extensometers at the same horizon, indicating that the displacement readings for the No. 4 extensometer were correct. As for the displacement readings for No. 5 and No. 6 extensometers, it was likely that some deep anchors failed. However, the monitored results can still show the strata displacement patterns.

Only selected readings were recorded from the No. 7 extensometer because the connecting cable was broken due to corrosion of extensometer wires. Therefore, the recorded data from the No. 7 extensometer were limited. The connecting cables for other anchors were seldom broken. The recorded readings of the anchors were collected and analyzed for the displacement of the surrounding strata.

No. 1 extensometer

Fig. 7 shows the No. 1 extensometer displacement profiles located at the left bottom corner of the monitored cross section. The measured displacement ranged from -11 mm to 4 mm. The positive values indicate that new cracks were developed or the relative movement along the existing fractures occurred, generating shear deformation. The negative values indicate that the existing fractures were closed due to compression. The profiles of Fig. 7(a) show that the displacement profile's curves were wavy due to the main roof periodic weighting, although the readings from each anchor were different. The extensometer readings were affected significantly when the longwall face was between 134 m inby and 155 m outby the monitored station.

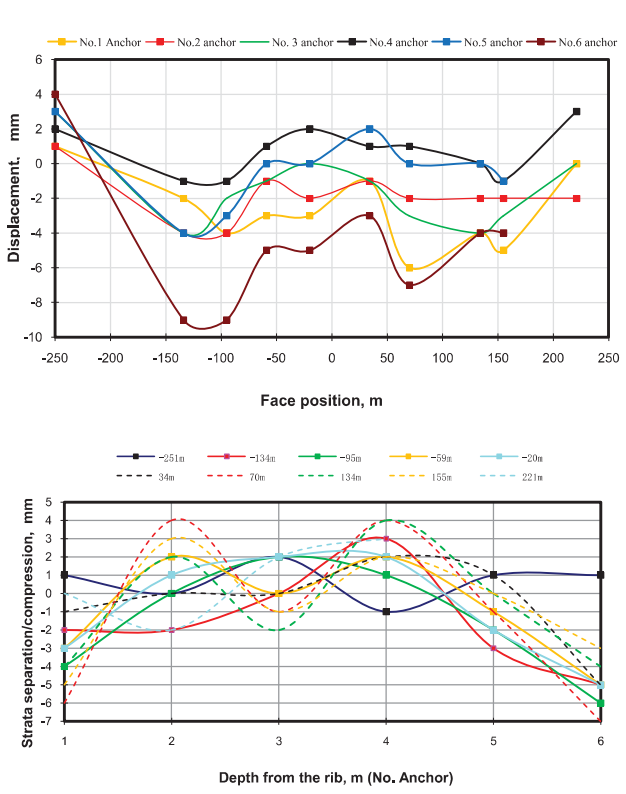

Figure 7. Measured displacement profiles for No. 1 extensometer (a) Measured displacements for each anchor (b) Measured displacement with respect to face position.

Measurements from No. 1 extensometer show that due to stress concentration, shear fractures occurred at the left bottom corner of the monitored cross section. Prior to the arrival of the influence of longwall mining, deformation within the 0–2-m-deep horizon involved closure of existing fractures. After the arrival of the influence of longwall mining, major deformation within the 0–1 m and 4–6 m deep horizons involved closure of existing fractures, which creates compression, while the major deformation within the 1–2 m and 3–4 m deep horizons was shearing as shown in Fig. 7(b).

No. 2 extensometer

Fig. 8 shows the displacement profiles for No. 2 extensometer that was located at the mid-height of the rib. Readings from its anchors showed that during the initial period of the influence of the abutment pressures, the major deformation occurring within the bolted horizon was closure of existing fractures. After the arrival of the influence of the abutment pressure, new fractures were generated, or existing factures slid along their fracture surfaces within the 1–3 m and 4–6 m deep horizons, creating shear deformation. On the other hand, the major deformation within the 0–3 m and 3–4 m deep horizons was closure of existing fractures, creating compression.

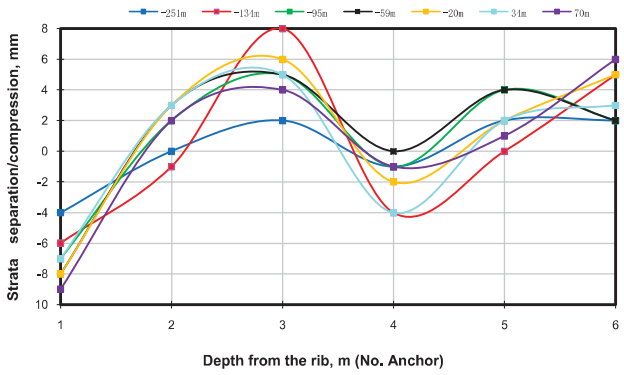

Figure 8. Strata separation profiles for No. 2 extensometer.

No. 3 extensometer

Fig. 9 shows the measured displacement profiles of the No. 3 extensometer that was located at the arch section of the left rib. The measured data show that either before or after the arrival of the influence of the abutment pressures, major deformation within the 0–1 m deep bolting horizon was closure of existing fractures, but within the 1–2 m deep horizon major deformation involved new fractures or shear deformation.

No. 4 extensometer

Fig. 10 shows the displacement profiles of the No. 4 extensometer located at the top of left rib. The measured data show that after the arrival of the influence of the abutment pressures, new fractures and shear deformation were generated within the 1–2 m, 3–4 m, and 5–6 m deep horizons. Within the 2–3 m and 4–5 m deep horizons, the major deformation was closure of existing fractures, creating compression.

It can be seen from the measured readings of the No. 4 extensometer that the variation trends of the deep anchor displacement coincided with entry surface deformation and bed separations in the roof. When the longwall face was 59 m inby, the displacements of anchors in the deep surrounding strata were small. As the face approached, the displacements increased. After the longwall face was 134 m outby the monitored station, the displacements of deep anchors stabilized.

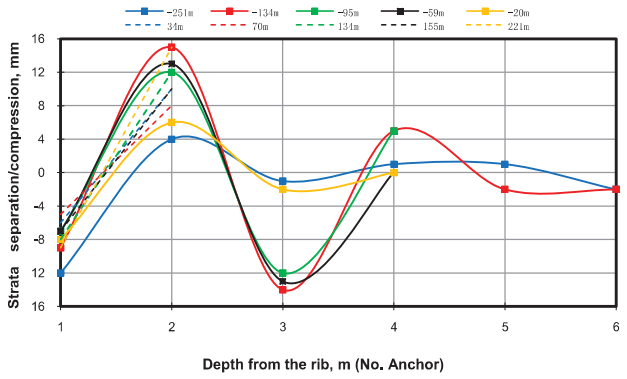

Figure 9. Strata separation profiles for No. 3 extensometer.

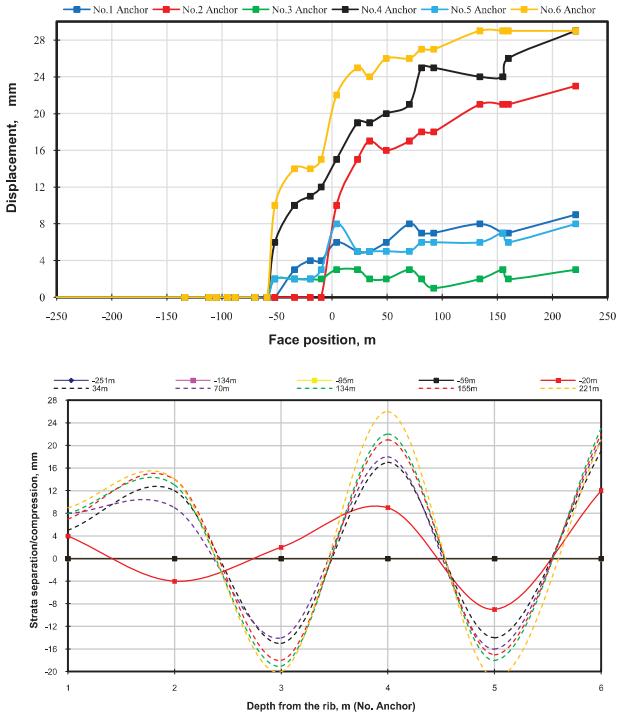

Figure 10. Measured anchor displacement profiles (a) Measured anchor displacement profiles (b) Strata separation profiles for No. 4 extensometer.

No. 5 extensometer

Fig. 11 shows the measured displacement profiles of the No. 5 extensometer located at the entry top center. The measured deformation ranged from 0 to 11 mm. The major deformation within the shallow 1-m-deep horizon was expansion due to broken strata.

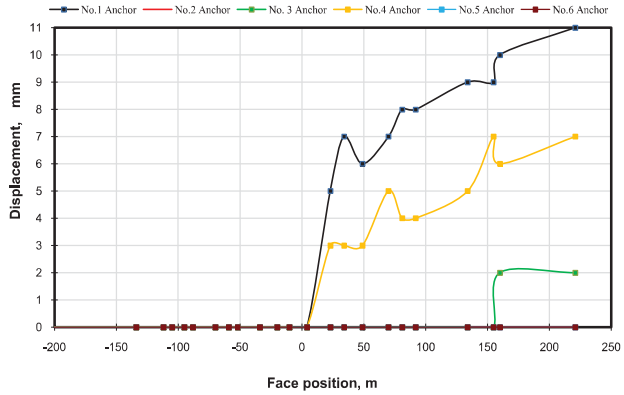

Figure 11. Measured anchor displacement profiles for No. 5 extensometer.

The measured displacements between deep anchor displacements and bed separations in the roof coincided well. As compared to the bed separation data, the displacements of the 2 m and 6 m anchors failed. However, the measured data for anchor No. 1 show that the displacement within the 1 m horizon increased rapidly when the longwall face passed the monitored station, which agreed with that measured by the 2-m-deep anchor of extensometer for bed separation measurement. Comparing the measured data between the anchor displacements of the No. 5 extensometer and bed separation roof extensometer, it can be seen that the shear deformation within the 2 m horizon was larger than that within the 1 m horizon, indicating that shear deformation also occurred within the 1–2 m deep horizon.

No. 6 extensometer

Fig. 12 shows the displacement profiles of No. 6 extensometer located in the top arch section of right rib. Extensometer No. 6 was symmetrical about the entry centerline with extensometer No. 4. After having been subjected to the influence of the abutment pressures, initially shear deformation occurred within the 4–5-m-deep horizon, followed by shear deformation within the 1–2 m deep horizon. After passage of the longwall face, the major deformation within the 1–2 m deep horizon was shear movement.

No. 7 extensometer

The data from No. 7 extensometer were limited due to many broken extensometer wires.

No. 8 extensometer

Fig. 13 shows the displacement profiles of No. 8 extensometer located at the right side rib. The measured data show that within the bolting horizon the major deformation was shearing, which occurs within the 0–1 m and 2–3 m deep horizons. As for the strata outside the bolted horizon, it was shearing within the 4–6 m deep horizon, and closure of existing fractures within the 3–4 m deep horizon occurred prior to passage of the longwall face.

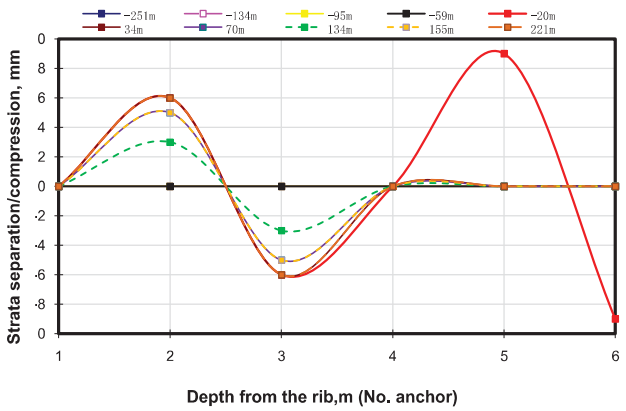

Figure 12. Strata separation profiles for No. 6 extensometer.

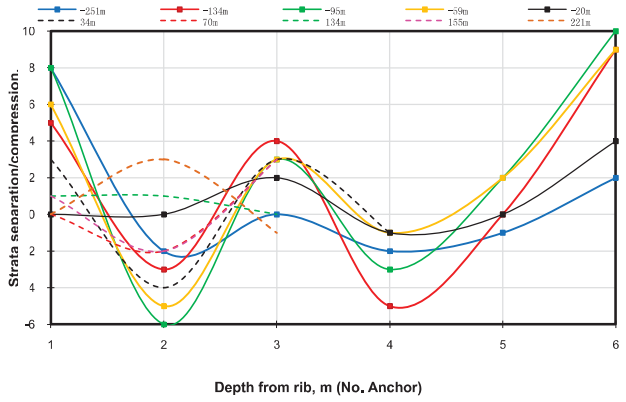

Figure 13. Strata separation profiles for No. 8 extensometer.

No. 9 extensometer

Fig. 14 shows the measured profiles of the No. 9 extensometer located at the right bottom corner. Just like that located at the left bottom corner, fractures were well developed due to stress concentration. During the initial period of the influence of the front abutment pressure, closure of existing fractures was the major deformation within the bolted horizon. After the entry was subjected to the dynamic abutment pressure, major deformation consisted of closure of existing fractures, generation of new fractures, and shearing within the bolted horizon. Within the 0–1 m deep horizon, however, there occurred more closure of existing fractures. As for the area outside the bolted horizon, during the initial period of the influence of the front abutment pressure, deformation consisted mainly of a generation of new fractures and shearing. After passage of the longwall face, major deformation consisted of closure of existing factures, generation of new fractures, and shearing.

SUMMARY

Based on the measured entry surface movement, deeper anchor displacement, and bed separations in the roof resulting from the influence of the abutment pressures from longwall mining in the overlying seam, the following conclusions can be made:

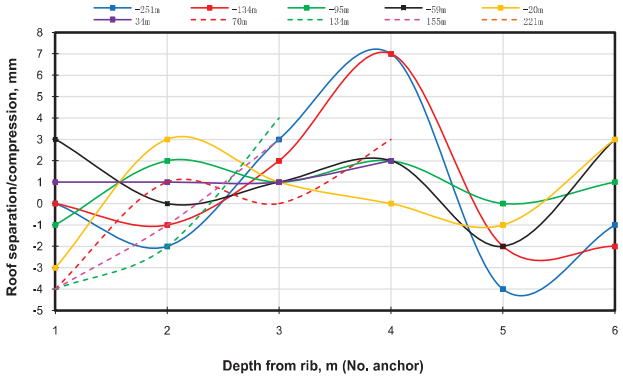

Figure 14. Strata separation profiles for No. 9 extensometer.

1. The extent of the influence zone of the abutment pressures on the instrumentation station ranged from 134 m outby to 155 m inby the longwall face. The major influence zone was from 59 m outby to 134 m inby the longwall face.
2. The rates of rib-to-rib and roof-to-floor convergences, although not strictly corresponding to the main roof periodic weighting, were affected by the periodic weighting, because their rates of convergences appeared as the waveforms. This indicated that the entry stability was greatly affected by the periodic weighting. This is a unique characteristic of how the longwall mining activities can affect the deformation of strata surrounding the track entry.
3. Although the displacement profiles of all deep anchors vary, they were all similar and appeared in waveforms under the influence of main roof periodic weighting. Some anchor displacements were positive, while others were negatives. A positive value indicates that new fractures were generated or the existing fractures slid along their surfaces, creating shearing deformation. A negative value indicates closure of existing fractures, creating compressive deformation.
4. The ribs and rib bottom corners are more sensitive to periodic weighting than the arch section. Shear fractures are well developed at the rib bottom corners due to stress concentration. Concurrent with the generation of new fractures and shear deformation, more existing fractures were closed. At the left bottom corner, the major deformation was the closure of existing fractures in strata within 0–1 m deep. At the right rib bottom corner, however, the major deformation was generation of new fractures and shearing in strata within 0–1 m deep.
5. Closure of existing fractures in the surrounding strata is in general accompanied by shear deformation in the deeper strata. Closure of existing fractures was the result of the deeper strata moving and squeezing toward the shallower strata. Simultaneously, during the process of closing existing fractures, the shallower strata probably move toward the entry.
6. The No. 4 extensometer displayed the largest displacement, and it was one of the mining pressure display points. However, considering the supported surrounding strata as an integrated structure, it was not the source point causing the deformation of the supported rock structure. From the characteristics of the measured deep anchor displacements, the inward movements of the left bottom corner and mid height of right side rib were the sources that caused the deformation of the supported structure. This conclusion can be clearly seen from the loading history of various roof and cable bolts.

7. The rates of rib-to-rib and roof-to-floor convergences show that the average distances or intervals between wave peaks and valleys were twice of those of the main roof periodic weighting. This coincided with the wavy floor heave.
8. The floor heave was large, while both the roof-to-floor and rib-to-rib convergences were relatively small. The magnitude of floor heave was more than 80% of the roof-to-floor convergence when the longwall face was 92 m past the instrumentation site.
9. When the longwall face was 160 m past the instrumentation site, both the rib-to-rib and roof-to-floor convergences increased due to large floor heave. Therefore, considering the supported surrounding strata as an integrated structure, it is necessary to control the floor heave.

REFERENCES

Jiang, J., Feng, Z., Han, J. (1999). "Classification of structural stability of surrounding rocks of roadway affected by overhead mining and decision making of support parameters." *Chinese Journal of Rock Mechanics and Engineering*. *18*(1):81–85.

Kang, H.,Wang, J., Lin, J. (2010). "Case studies of rock bolting in coal mine roadways." *Chinese Journal of Rock Mechanics and Engineering*. *29*(4):649–664.

Lu, S., Fu, G., Tang, L. (1999). "Regularity of deformation of rocks around roadway under mining influence and change of rock bolt resistance." *Journal of China University of Mining & Technolog*. *28*(3):201–203.

Liu, Q., Yang, M. (2002). "Analysis on deformation of surrounding rock masses of tunnel using bolt-grouting support and its mechanism. *Chinese Journal of Rock Mechanics and Engineering*. *21*(8):1158–1161.

Zeng, F. (2007). "The loss of stability and supporting method for the soft and dynamic tunnels." *Journal of China Coal Society*. *32*(6):573–576.

Li, S. (1983). "Field measurement and analysis of rock bolt strain." *Journal of China Coal Society*. (1):55–64.

Zhao, H., Ma, F., Ding, D., Zhang, Y. (2009). "Roadway deformation mechanism and failure model under the influence of mining." *Journal of China Coal Society*. *34*(5):599–604.

Jing, H., Fu, G., Guo, Z. (1999). "Measurement and analysis of influential factors of broken zone of deep roadways and study on its control technique." *Chinese Journal of Rock Mechanics and Engineering*. *18*(1):70–74.

Farmer, I.W., Robertson, J.T. (1975). "Effect of pack construction on roadway stability behind working faces." *Mining Engineer*. *134*(175):599–608.

Yang, J., Xia, J. (2005). "Test study on the complete deformation property of bolted stratified surrounding rockmasses." *Journal of China Coal Society*. *30*(4):414–417.

Zhang, X., Jing, HW. (2009). "Analysis of excavation damage in highly stressed surrounding rocks of roadways." *Journal of Mining and Safety Engineering*. *26*(1):45–49.

Wang F.H., Qian, Q.H, Zhang, B.H. (2008). "Zonal fracturing mechanism in deep crack-weakened rock masses." *Theoretical and Applied Fracture Mechanics*. *50*(1):57–65.

Zhang, X., Miao, X. (2002). "Numerical simulation on layer-crack and failure of laminated rock masses." *Chinese Journal of Rock Mechanics and Engineering*. *21*(11):1645–1650.

Sashurin, A.D., Berkutov, V.A. (1979). "Determination of boundaries of a fracture zone during underground working of deposits with hard surrounding rocks." *Journal of Mining Science*. *15*(1).

Zhou, X., Qian, Q. (2007). "Zonal fracturing mechanism in deep tunnel." *Chinese Journal of Rock Mechanics and Engineering*. *26*(5):877–885.

Application of Chain Conveyor Cutter (CCC) to Highwall Mininig System

Takashi Sasaoka, Assistant Professor
Dept. of Earth Resources Engineering
Kyushu University
Fukuoka, Japan

Hiroshi Takamoto, General Manager
Mmi Coal Tech Co. Ltd
Tokyo, Japan

Shizuo Ikuta, Doctor Course Student
Hideki Shimada, Associate Professor
Akihiro Hamanaka, Doctor Course Student
Kyushu University
Fukuoka, Japan

Kikuo Matsui, Professor
Kyushu University
Fukuoka, Japan

ABSTRACT

Chain Conveyor Cutter (CCC) is a chainsaw-type machine and originally developed for the construction of underground walls and/or ground improvements. CCC was developed from the accumulated technology of coal mining, combining the cutting technology of a shearer and the fuctions of chain conveyor. The CCC can cut harder soils and soft rocks, and vertically mixes the cut soils/rocks with cementing material selected through the discharging port installed at the bottom of the machine. In Indonesia, highwall mining trials have already been conducted in several coal mines. However, full-scale and regular operations have not been done yet due to the ground and machine control issues from their geological conditions. In order to overcome these problems, the application of CCC to highwall mining systems was proposed, and its applicability and technical issues to be solved were investigated in this research.

This paper discribes the characteristics of CCC system and discusses the application of CCC to highwall mining systems.

INTRODUCTION

Indonesia produces over 250 million clean tons of coal annually. It is also the second largest coal exporter to Japan, accounting for about 32Mt of coal every year. Over 99% of the coal produced in Indonesia comes from surface mines (Petromindo.Com, 2010). More open-cut mines will be developed and more coal will be mined in order to fill the great demand both in Indonesia and the rest of the world.

In open-cut mines in Indonesia, many mining operations have developed long highwalls which have been abandoned due to the current economy. Mines have transitioned to lower stripping ratio blocks of coal or overlying seams. In some cases, coal lies buried beneath spoil heaps or is covered with mud and water. There is a great deal of coal beneath abandoned and working highwalls. Considering these situations, it seems to be worth introducing highwall mining systems into Indonesian open-cut mines.

Final highwalls of open-cut mines can form the starting point for other mining methods, such as new highwalls or underground mining. In its basic application, highwall mining is a technique utilized after an open-cut portion of a reserve has been mined, sometimes prior to the introduction of underground mining (Seib, 1993). In this system, the coal seam is mined by remotely operated equipment, such as an auger machine or a modified continuous miner incorporated into a highwall mining system. Major issues of highwall mining systems include a lower coal recovery because pillars are left behind, and the instability of openings and highwalls due to the pillar and roof failures.

In Indonesia, highwall mining operation trials have been conducted at several surface coal mines. However, a full-scale or regular operation has still not yet been tested. The application of the highwall mining system is restricted by the conditions of coal seams such as their dip, thickness, roll, split of the seam, existence of faulting and folding, etc. Considering Indonesian coal seams possess conditions such as very weak strata and steep coal seams, the application of current highwall mining systems is very limited. In order to overcome these problems and apply highwall mining systems to the Indonesian coal mining industry more widely, the application of the CCC system to highwalls was investigated by our research group.

This paper describes the characteristics of the CCC system, and discusses its application to highwall mining and the technical issues to be solved.

APPLICATION OF HIGHWALL MINING SYSTEM IN INDONESIA

Highwall Mining System

Many coal seams that are presently uneconomical or technically unsuitable for conventional surface mining techniques can be recovered using highwall mining systems. Final highwalls of open cut coal mines can form the starting point for other mining methods, such as highwall or underground mining. In its basic application, highwall mining is a technique utilized after the open-cut portion of a reserve has been mined, sometimes prior to the introduction of underground mining (Seib, 1993).

In these mining systems, a continuous miner or an auger machine is primarily used to extract coal from the highwalls.

Recently, other systems such as Bucyrus Highwall Miners (formerly Superior Highwall Miners).

The major continuous miner system is the Addcar system. This system consists of a continuous miner, addcars (belt conveyor cars), a launch vehicle, a stacker conveyor and a loader as shown in Figure 1. The Addcar system can excavate rectangular holes over 350m long, and the size of the hole depends on the specifications of the continuous miner. Fully automated control of the system is achieved with the aid of advanced navigation technology, including a roof and floor passive gamma detector system, inclinometers, a ring laser gyroscope and programmable logic controller (PLC).

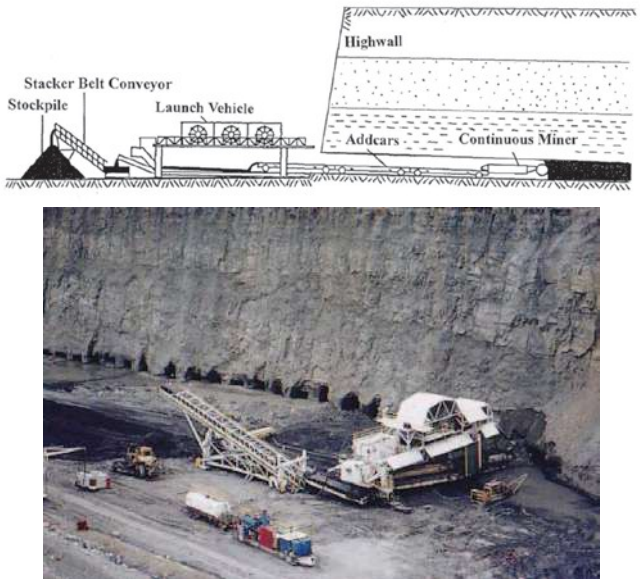

Figure 1. Addcar system.

The auger system, as shown in Figure 2, is very simple and can excavate holes over 100m long and 0.5m in diameter or greater into the coal seams in highwalls, depending on the application methods. This system is more maneuverable than the Addcar system, and can be applied when shorter lengths of highwall are presented.

One of the first true "highwall mining systems" to be demonstrated, the Metec miner system, was introduced in 1981 and featured in a number of trade exhibitions during the 1980s. As a successor of the Metec miner, the Bucyrus (formerly Superior) highwall mining (SHM) is now attracting significant attention in the world. This system consists of a continuous miner, double auger flights, a stacker conveyor and a front-end loader, as shown in Figure 3 (Davison, et al., 2006). This system can excavate rectangular holes over 300m long, has maneuverability along the bench which is important for the higher productivity, and the machine is equipped with four crawlers allowing for rapid positioning from hole to hole.

Highwall mining systems have been used extensively in the US and Australia due to their safety and economics. In Indonesia, only the auger system has been used at a few mines (Furukawa, et al., 2009).

Figure 2. Auger System.

Figure 3. Metec miner system.

Geotechnical and Operational Issues for Application of Highwall Mining Systems to Indonesia

Highwall mining systems have improved mining operations due to their safety and productivity. However, the application is restricted by coal seam conditions such as the dip, thickness, roll, split of the seam, existence of faulting and folding, etc.

Indonesian coal measure rocks are generally very weak (Sadisun, et al., 2004). Moreover, some coal measures rocks such as shale, mudstone, and siltstone show an excessive slaking behavior, leading to a severe deterioration of their mechanical properties. The weak immediate roof tends to fall easily and heavy equipment, such as continuous miners, also tend to sink into the softened floor or slip on the floor. Besides, the dip of coal seam in Indonesia is unpredictable and often very steep. It is difficult, or almost impossible, to apply the current highwall mining systems into steeper dipping coal seams, over 15 degrees.

Considering these conditions in Indonesian coal seams, the application of current highwall mining systems may be limited in Indonesia. Therefore, other techniques or systems have to be introduced in order to recover valuable coal resources effectively.

CHAIN CONVEYOR CUTTER SYSTEM

Background of Development of Chain Conveyor Cutter (CCC)

Mitsui Miike Coal Mine was the largest mine in Japan. Before closing in March 1997, the mine extracted coal beneath the inland

sea of Ariake for more than 100 years and developed advanced technology in the field of coal winning and tunneling. The Mitsui Miike High Power Plant (MHP) was opened in 1988 and realized an average daily capacity of 10,000 tons of coal. It contributed safely until mining ended (Ikuta, et al., 2010).

Based on the accumulated technology of coal mining in Miike, a new machine for constructing underground continuous wall-the Chain Conveyor Cutter (CCC) – was developed. The system, which was developed beginning in 2000, combines the cutting technology of a shearer with the functions of a chain conveyor. Its development was a new type of effective working method for civil engineering fields. The CCC already had applications in the construction work of underground continuous impermeable curtain (UCIC), and this construction work was a success.

CCC System

As shown in Figure 4, the CCC is installed on a pile driver and penetrated into the ground. It is very similar to a chain conveyor, but the cutting bits are attached on the scraper bars which connect the twin outboard chains. Its cutting depth is up to 20 m. The cross-section of cutting area is rectangular in shape, 0.75 m wide and 1.2 m long. The CCC consists of a driving unit, a middle section and a return unit from the top of the machine. The drive motor capacity is an 180 kW inverter drive. The middle section consists of a number of middle posts according to the ground depth to be improved, and the middle posts are connected with bolts and two parallel 50 A pipelines are installed inside the posts to pump cement slurry or other materials from the inlet port down to the discharge port on the return unit. The return unit is located at the bottom of the machine. The cutting bits mounted on the scraper bars cut the soil while running along the return unit. The faster the CCC is sunk and/or the harder the soil, the more severe the impact load on the return unit. The elements of the return unit were given sufficient strength and durability, and the sealing system was designed tightly enough against soil and cement slurry mixtures.

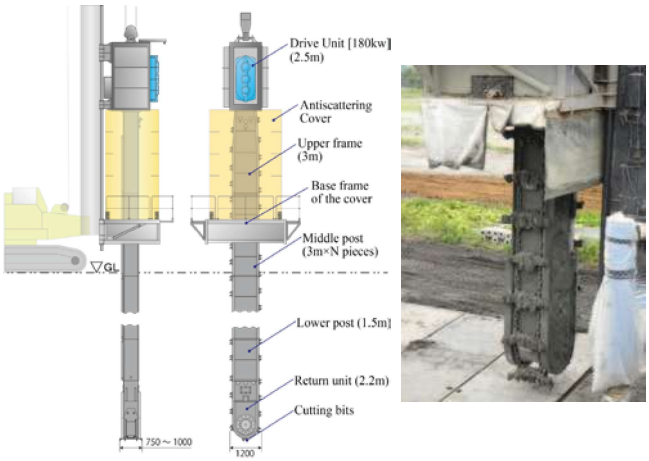

Figure 4. Conceptual diagram and Photos of CCC.

While the CCC is being sunk, the cutting bits run at maximum 60 m per minute with discharging cement slurry, as shown in Figure 5. The scraper bars attached to the twin outboard chains scrape up, agitate and mix the cut soil with cement slurry, named "conveyor effects". There exists only a small amount of room for the soil cement that "conveyor effects" works with, and the soil cement is raised up to the ground surface. Scraper bars running down to the return unit convey raised cement slurry down to the ground. Once the CCC reaches the predetermined depth, the unit is raised to the surface and the void is filled with the mixture of soil and cement. The CCC creates high quality and homogeneity improved wall in the ground

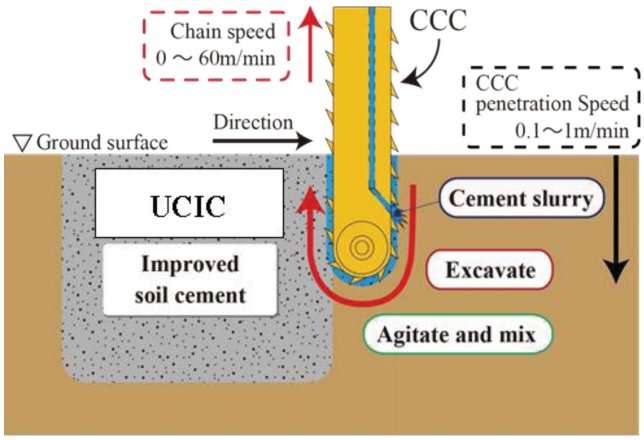

Figure 5. Conceptual diagram of CCC movement.

APPLICATION OF THE CCC TO HIGHWALL MINING SYSTEM

Basic Concept of the Application of CCC to Highwall Mining System

The CCC is able to handle various types of ground exceeding a 50 in N value (Ikuta, et al., 2011). This is because of the 180 kW water-cooled invertor drive and electric motor driving system. The variable chain speed and strong force enabled the CCC to cut coal and coal measure rocks. In addition to the strong force, the unit controls the cutting resistance by changing body penetration speed down to the ground and/or changing lapping distance between adjacent columns.

Figure 6 shows the schematics of a new highwall mining system using the CCC under different dips of coal seams. As shown in these figures, the rack and pinion drive system is used to control the direction of the cutter head along the dip when the seam is inclined. In the case of a horizontal coal seam, the rack & pinion or crawler drive system is used not only for direction control, but also to produce enough thrust for cutting coal and pushing the unit. When the CCC penetrates into the ground without discharging slurries, cut coal is lifted to the surface and creates a rectangular void. Applying the CCC system, any dip of coal seam was excavated downward, even in weak floor conditions. Moreover, the openings can be stowed effectively; a highwall mining with stowing can also be conducted by using the CCC system. After creating an opening, the CCC is raised and fills up with stowing materials, such as waste rock/soil if required, and a rotating chain unit works effectively for hauling the stow materials down to the opening (See Figure 7). As stowing occurs immediately after coal extraction, it could help diminish the movement of strata and pit slope. Making use of this function, physical properties of the stowing material are designed

and controlled by mixing waste rocks/soils, cement and additive materials. Therefore, the application of the CCC for highwall mining systems can not only extract steep and/or thin coal seams, but also maintain the stability of pillars and increase the coal recovery under weak geological conditions.

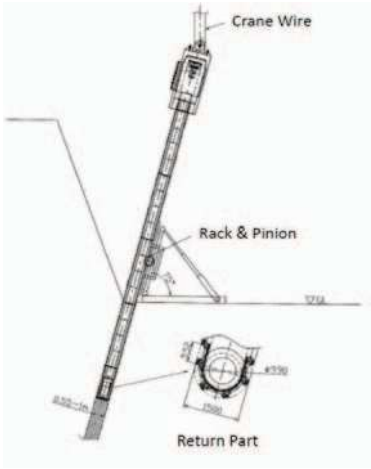

(a) Dip of coal seam = 75

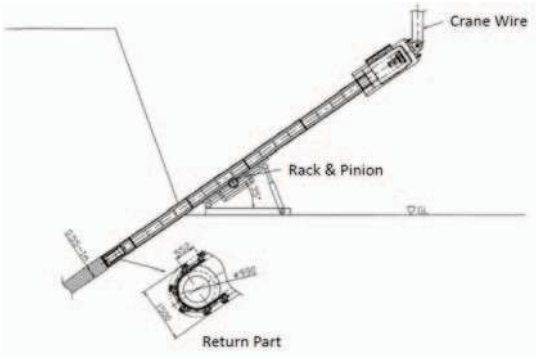

(b) Dip of coal seam = 35

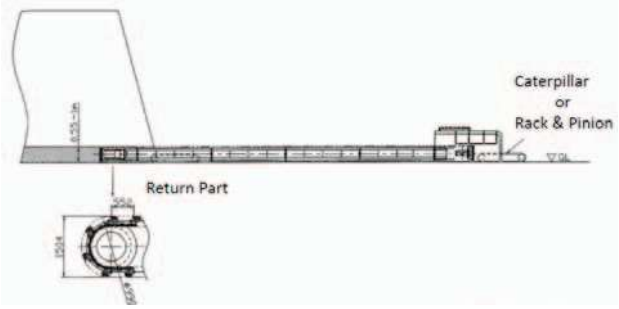

(c) Dip of coal seam = 0

Figure 6. Conceptual diagram of a highwall mining system using the CCC.

Numerical Analysis

In order to discuss the stability around the openings drivaged by the CCC system under weak geological conditions such as in Indonesia, finite element modeling was applied. Non-linear analysis was performed using the two-dimensional FEM cord

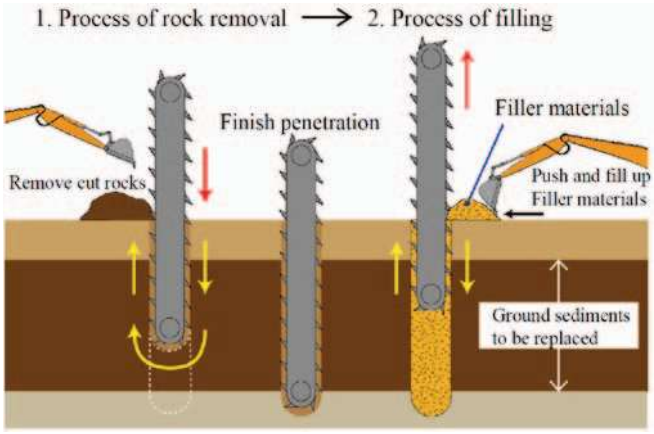

Figure 7. Cutting and backfilling system of CCC.

Phase[2] (Rocscience, 2009). For simplicity, a two-dimensional model was used in this analysis as shown in Figure 8. The coal seam thickness is 3m and the immediate roof and floor are mudstone. The initial vertical stress (P_v) was assumed to be the depth pressure ($P_v = \gamma h$, where γ = unit weight of overburden and h = cover depth or highwall height) and the initial horizontal stress (P_h) was variable. Five rectangular openings with the dimension of 1.2m in width and 1.0m in height were excavated, one after the other, in the coal seam. The pillar width (W_p) between the two openings was assumed to be 0.6m and 1.2m.

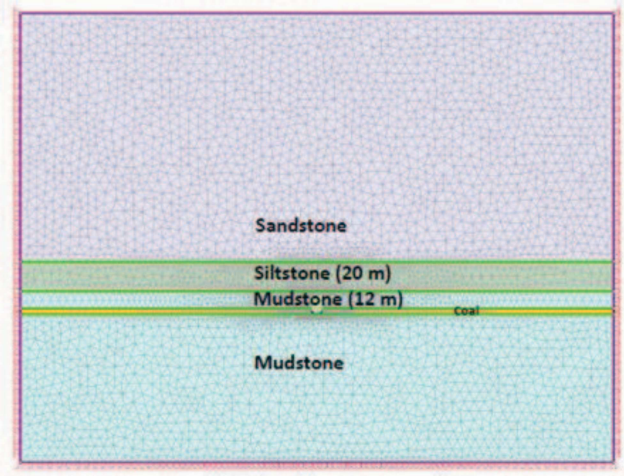

Figure 8. Finite element model.

The following well-known Hoek & Brown criterion was employed as a failure criterion;

$$\frac{\sigma_1}{\sigma_C} = \frac{\sigma_3}{\sigma_C} + \left(m\frac{\sigma_3}{\sigma_C} + s\right)^{\frac{1}{2}} \quad (1)$$

Where σ_1 = major principal stress at peak strength, σ_3 = minor principal stress, *m* and *s* = constants that depend on the properties

of the rock and the extent to which it had been broken before being subjected to the failure stresses, and σ_C = uniaxial compressive strength of the intact rock material.

The mechanical properties and parameters of the coal, rocks and stowing material are listed in Table 1. These values were obtained from rock samples collected in an Indonesian coal mine. Stowing material is assumed to be a waste rock with flyash and cement. Stowing material is fully injected into the opening and is assumed to behave in an elastic-plastic manner.

Table 1. Mechanical properties of rocks and stowing material used in this analysis..

Rock Type	**Sandstone**	**Siltstone**	**Mudstone**	**Coal**	**Stowing Material**
Unit weight (kgf/m^3)	2,205	2,486	2,071	1,300	1,700
Young's modulus (MPa)	1,404	1,478	533	1,000	500
Poisson's ratio	0.31	0.29	0.31	0.28	0.3
Tensile strength (MPa)	0.50	0.70	0.30	0.21	0.2
Friction angle (degree)	30	32	25	21.4	30
Cohesion (MPa)	0.50	0.25	0.30	0.21	0.30

Figure 9 shows the failure development around the openings/pillars at different depths. Here, the pillar widths and the ratio of P_h/P_v were 1.2m and 1/3, respectively. The pillars and ribs tend to fail with shear failure and the roof and floor with tensile failure with increasing mining depth or highwall height. Of course, these failure modes depend on the initial stress conditions.

Figure 10 shows the failure development around the openings with narrow pillars. The pillar width was 0.6 m. With the narrow pillar, the openings show the less stability and the pillars fail much more severely even though the cross section was relatively small compared with conventional highwall mining system. This situation will lead to unstable work conditions, and sometimes the CCC is caught in the opening and becomes impossible to withdraw.

In order to improve the stability of pillars/openings and the mechanism of CCC, the application of stowing system and its effect were investigated. Figure 11 shows the failure development around the openings filled with the backfilling materials that contains waste rock, flyash and cement. It assumed in this analysis that stowing is done while raising the CCC and, after the filling openings are consolidated, next opening is extracted. It is clear that backfilling helps the openings keep stable compared to the situation as shown Figure 10. However, at greater depth, backfilling is less effective. In such case, we have to consider the use of a wider pillar, a narrower opening and stronger backfilling material. Although, the backfilling function was not dealt with clearly in the analysis, it must be understood that the confinement by backfilling and the infiltration of backfilling slurry content into the failure zone improve mechanical properties of the broken pillars.

From the these numerical analyses, it can be concluded that the highwall system with stowing by using the CCC system is an effective mining system for extraction of coal seams where a conventional one cannot be applied, such as weak strata conditions and thin coal seam, etc.

CONCLUSIONS

This paper proposed the new highwall mining system using the Chain Conveyor Cutter (CCC) based on the characteristics of the unit and discussed its applicability by means of numerical analysis. From the results of numerical analyses, it can be concluded that this new highwall mining system has a great potential over a wide group of applications for various geological conditions where conventional systems cannot be applied, such as weak strata conditions and steep and/or thin-thick coal seams, etc.

However, highwall mining requires a depth of at least 300 meters to be competitive. So, the scaling up has to be considered from its structure and power points of view. Moreover, the cutting height of the CCC is not large – just 1.0m — so, in order to increase coal recovery and/or extract thick coal seams, the application of multi-lift mining should be discussed.

ACKNOWLEDGEMENTS

The authors would like to express sincere thanks to those who assisted us in the development and application of the CCC to the field works, and gave us future prospects of CCC applications. Also, a grateful thanks to Suseno Kramadibrata and Budi Sulistianto at the Institute Technology Bandung, Indonesia, for his assistance with this project.

REFERENCES

Freeman, B. (2006). "Highwall Systems," In: *Coal Magazine*, September/October. 7-12.

Furukawa, H., Matsui, K., Sasaoka, T., Shimada, H., Ichinose, M. (2009). "Applicable Underground Coal Mining System in Very Thick Seams," In: *Proceeding of the Mine Planning and the Equipment Selection 2009*. Banff, Canada. CD-ROM.

Ikuta, S., Matsui, K., Shimada, H., Sasaoka, T. (2010). "Development of Chain Conveyor Cutter," In: *Proceedings of International Symposium on Earth Science and Technology* Fukuoka, Japan. 61-64.

Ikuta, S., Matsui, K., Shimada, H., Sasaoka, T. (2011). "Study on the Application of Chain Conveyor Cutter to Environmental Protection and Disaster Prevention," In: *Proceedings of International Symposium on Earth Science and Technology*. Fukuoka Japan. 495-500.

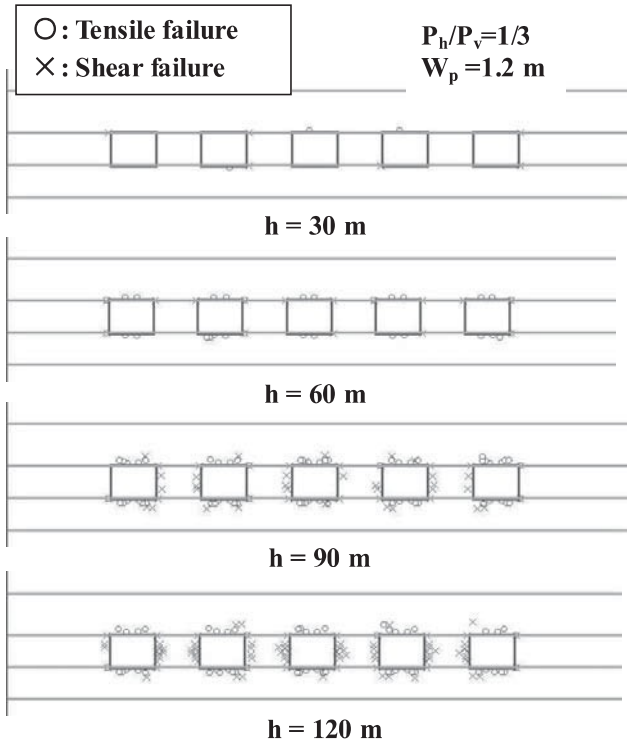

Figure 9. Failure development around the openings at different depths.

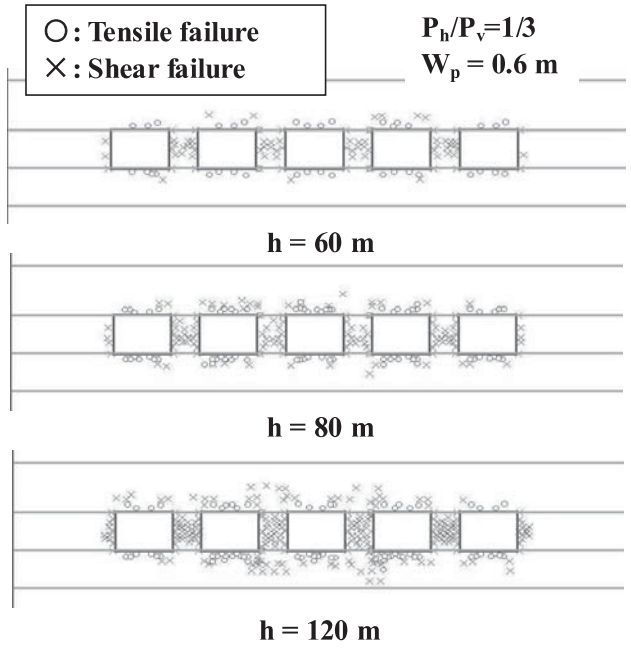

Figure 10. Failure development around the openings with narrow pillars.

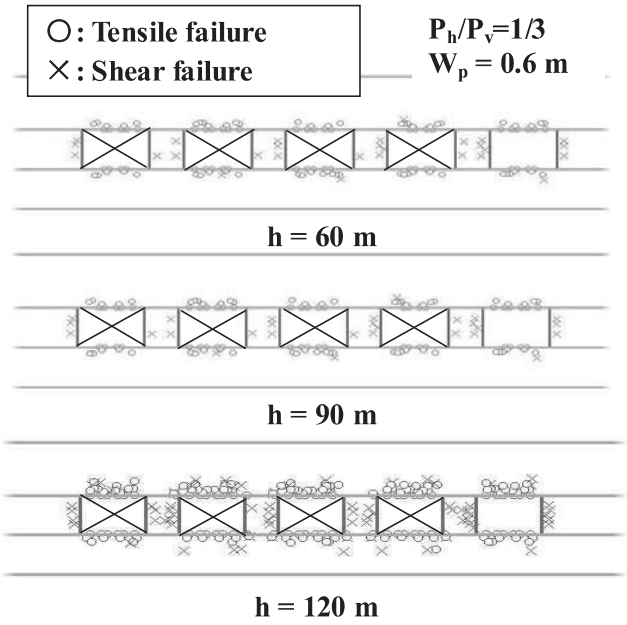

Figure 11. Failure development around the openings with backfilling.

Petromindo.Com. (2010). Indonesian Coal Book 2010/2011, 3-28.

Sadisun, I. A., Shimada, H., Ichinose, M., Matsui, K. (2004). "Petrograpical Properties and Index Properties of Sedimentary Argillaceous Rocks Vis-a-vis Slakeability." In: *Proc. of 2nd International Workshop on Earth Science and Technology*. Fukuoka, Japan, 495-502.

Seib, W. T. (1993). "Australian Coal mining Practice." A. J. Hargraves and C. H. Martin, eds. *The Australian Institute of Mining Metallurgy*. 238-242.

Rocscience Inc. (2006). "Application of the Finite Element Method to Slope Stability." In: http://www.grow.arizona.edu/GrowGetResource.php?url=http://www.rocscience.com/library/pdf/SlopeStabilityUsingPhase2.pdf&resourceid=1595.

The Evaluation of Empirical Coal Pillar Strength Formula Based on Uncertainty Criterion

Navid Hosseini, Phd
Islamic Azad University, South Tehran Branch
Tehran, Iran

Behdeen Oraee-Mirzamani, Phd Student
Centre For Environmental Policy, Imperial College London
London, United Kingdom

Kazem Oraee, Professor
University of Stirling
Stirling, United Kingdom

ABSTRACT

Several empirical equations to estimate coal pillar strength have been presented in academic studies. The development processes of these equations are similar and are usually obtained by fitting the mathematical function (curve) to field data. One of the best criteria to evaluate the quality of fitting for such equations is the correlation coefficient R^2, which has limited applicability. It is necessary to calculate the correlation coefficient access to the initial data for which the equation is presented; this is impossible for many coal pillar strength formulas. This paper presents a new approach based on the analysis of uncertainty amplitude to compare the coal pillar strength. This approach utilizes a combination of parameters such as Mean Squared Error (MSE), Root Mean Squared Error (RMSE), function type and degrees of freedom. The confidence level of constants is subsequently formed and the correlation coefficient becomes more comprehensive. Therefore, for an effective comparison, the efficiency and accuracy of coal pillar strength formula can be used.

Keywords: Coal Pillar Strength, Correlation Coefficient, MATLAB, Uncertainty Criterion

INTRODUCTION

The use of coal pillars for roof stability in underground coal mining is an old approach whereby roof stability depends on the bearing capacity of the coal pillar. If the applied load exceeds the coal pillar strength limit, the pillar fails and the possibility of roof collapse is increased (Brady and Brown, 2004). In addition, as the pillar dimensions increase, a reduction in mining recovery occurs because the quantity of coal remaining to be used as a pillar is increased (Oraee et al., 2008). The fluctuation of the pillar dimensions threatens the safety of mining and reduces the economic efficiency; therefore, the selection of an appropriate formula for coal pillar design plays a significant role in safety, economics and operational performance (Hosseini et al., 2010).

In recent years, significant research has been carried out on the determination of coal pillar strength, and various formulae have been introduced. The majority of these formulae is empirical and is based on shape, effective dimensions and the laboratory testing of cubic coal samples (Hosseini et al., 2010; Mark, 1990; Su and Hasenfus, 1999; Peng, 2006). While some limits persist, the experimental nature of these equations reduces their complexity. Determining the amplitude with accuracy is one of the most important of these limitations (Hosseini, 2007).

Based on the basic principles of statistical engineering, the correlation coefficient (R^2) is one of the best criteria for evaluation of such equations (Bird, 2003). Although the correlation coefficient is a well known statistical indicator that has many advantages, it also has some limitations. It is necessary to access the initial data in order to compare the equations of coal pillar design using the correlation coefficient. On many coal pillar strength formulae, however, such access is not possible. Therefore, due to this limitation and other similar cases, using the correlation coefficient on its own is inadequate and other mathematical and statistical criteria are needed for evaluating these equations.

COAL PILLAR STRENGTH FORMULA

Although the pillar-bearing capacity depends on various parameters, the width-to-height ratio (W/H), which acts as an indicator for pillar dimension, and the uniaxial compressive strength of intact coal play a significant role in pillar strength (Peng, 2008). Therefore, in many of the equations, the pillar strength is calculated based on these two critical parameters. Many equations that are used to estimate the coal pillar strength have been presented hitherto. Based on available field data in this research, Bunschinger (Equation 1), Bieniawski (Equation 2), Holland (Equation 3) and Oraee-Hosseini (Equation 4) are four well known equations that were selected for comparison and evaluation. The respective equations are given below (Hosseini, 2007; Peng, 2008; Oraee et al., 2009a):

$$\sigma_p = \sigma_1(0.778 + 0.222\frac{W}{H}) \quad (1)$$

$$\sigma_p = \sigma_1(0.64 + 0.36\frac{W}{H}) \quad (2)$$

$$\sigma_p = \sigma_1 \sqrt{\frac{W}{H}} \tag{3}$$

$$\sigma_p = \sigma_1 \exp(-0.43 + 0.668\sqrt{\frac{W}{H}}) \tag{4}$$

where σ_p is the pillar strength, σ_1 is the uniaxial compressive strength of a cubical specimen, W and H are width and height of pillar, respectively.

EVALUATION OF COAL PILLAR STRENGTH FORMULA

The equations of coal pillar strength are obtained based on field data. Therefore, the quality of these equations can be examined from the statistical engineering viewpoint. One of the most common statistical criteria for evaluation of these equations is the correlation coefficient (R^2), which is calculated through *Equation 5* (Bird, 2003):

$$R^2 = 1 - \frac{\sum[\sigma_{p_i} - f((\frac{W}{H})_i)]^2}{\sum(\sigma_{p_i})^2 - (\sum\sigma_{p_i})^2/n} \tag{5}$$

where σ_{pi} and $(W/H)_i$ are the pillar strength and width to height ratio of pillar of ith element in field data of n data pair.

In the correlation coefficient, the efficiency of each coal pillar strength formula is determined based on errors of regression related to both the type of function and quality of raw data. The correlation coefficient assumes that the coal pillar strength is only related to the width-to-height ratio and the uniaxial compressive strength of coal. While other parameters, such as roof and floor condition, and the geomechanical properties of coal have an important role in coal pillar bearing capacity disregarded in coal pillar strength formulae. Therefore, a more efficient criterion for the evaluation of coal pillar strength equations is required. In fact, with determination of certainty of amplitude, the risk of error and uncertainty are denoted.

Erroneous data can be obtained in the field due to measurement conditions (Hosseini, 2007). Thus, adjusting for the uncertainty, the effects of input data on the equation should be studied where the constants of each coal pillar strength equation are considered as a variable which may have different (diverse) values.

In fact, the amplitude of each constant should be determined in terms of their lower and upper bounds. On the other hand, if $(X_1,..., X_n)$ is a series of field data, the $R(X_1,..., X_n)$ as upper bound function, the $L(X_1,..., X_n)$ as lower bound function should be determined. The probability of a function placed between upper and lower bounds are calculated by *Equation 6* (Bird, 2003):

$$P[L(X_1,...,X_n) < f(\sigma_3) < R(X_1,...,X_n)] = 1-\alpha \tag{6}$$

where α is the percentage of allowable error of estimation and (1-α) is the confidence level. The uncertainty of the function (equation of coal pillar strength) by the distance of upper bound and lower bounds will be shown.

DETERMINATION OF UNCERTAINTY

A dataset for the evaluation of the coal pillar strength formula has been created using field data (Hosseini, 2007; Oraee et al., 2009b). Subsequently, uncertainty is studied by drawing the curve of the equation of each coal pillar strength formula using the *Curve Fitting* toolbox of MATLAB (MATLAB, 2010) and fitting this data. The fitting curves of coal pillar strength formula (Equations 1 to 4) on the data are shown in Figure 1. These curves are drawn using the coal pillar strength formula based on adjusting the constant coefficients.

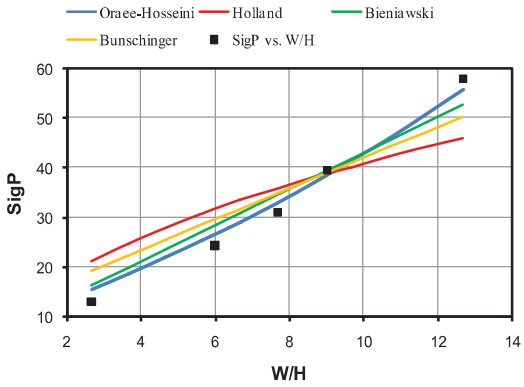

Figure 1. The curve fitting of coal pillar strength formula on the filed data. The vertical axis is, and the horizontal axis is.

In order to determine the uncertainty, the upper and lower prediction bounds of each coal pillar strength formula are drawn. Prediction bounds define the lower and upper values of the associated interval, and define the width of the interval. The prediction is based on an existing fit to the data. Additionally, the bounds can be simultaneous and measure the confidence for all predictor values, or they can be nonsimultaneous and measure the confidence only for a single predetermined predictor value. Simultaneous bounds measure the confidence that a new observation lies within the interval regardless of the predictor value. The nonsimultaneous prediction bounds for a new observation at the predictor value x are given by:

$$P_{n,o} = y \pm t\sqrt{s^2 + xSx^T} \tag{7}$$

where s^2 is the mean squared error, t depends on the confidence level, and is computed using the inverse of Student's t cumulative distribution function, and S is the covariance matrix of the coefficient estimates, $(X^T X)^{-1}S^2$. Note that x is defined as a row vector of the design matrix or Jacobian evaluated at a specified predictor value. The simultaneous prediction bounds for a new observation and for all predictor values are given by:

$$P_{s,o} = y \pm f\sqrt{s^2 + xSx^T} \tag{8}$$

where f depends on the confidence level, and is computed using the inverse of the F cumulative distribution function. The nonsimultaneous prediction bounds for the function at a single predictor value x are given by:

$$P_{n,f} = y \pm t\sqrt{xSx^T} \tag{9}$$

The simultaneous prediction bounds for the function and for all predictor values are given by:

$$P_{s,f} = y \pm f\sqrt{xSx^T} \tag{10}$$

Figures 2 to 5 show the uncertainty amplitude of each equation with 95% precision and field data of coal pillar strength.

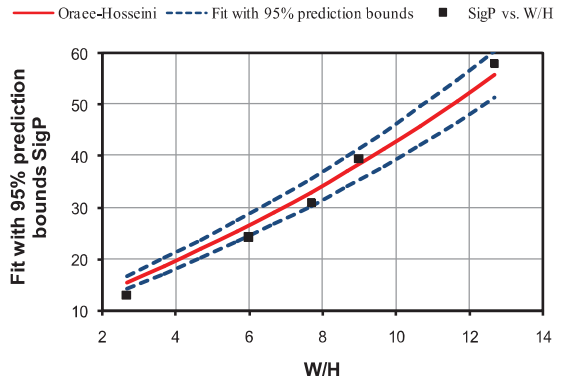

Figure 2. The curve of Oraee-Hosseini formula with 95% prediction bounds and field data.

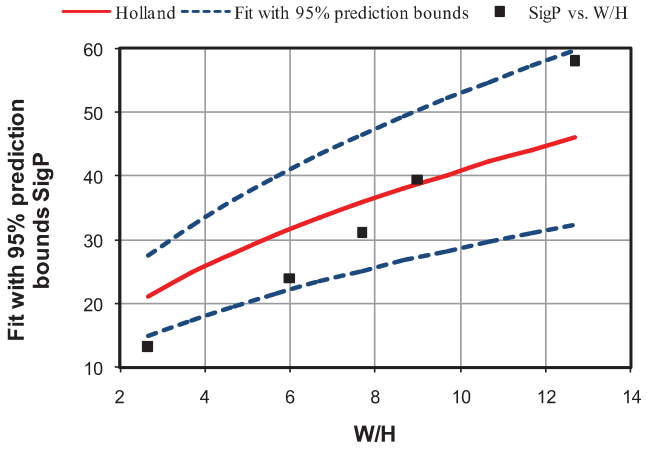

Figure 3. The curve of Holland formula with 95% prediction bounds and field data.

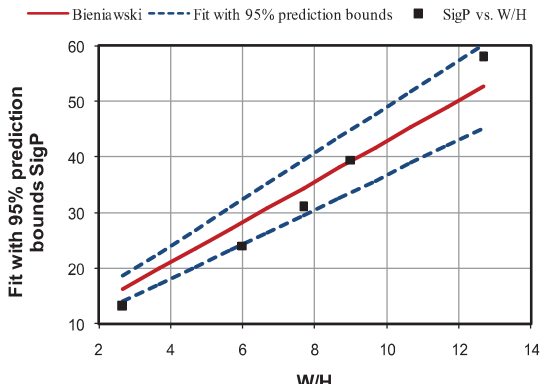

Figure 4. The curve of Bieniawski formula with 95% prediction bounds and field data.

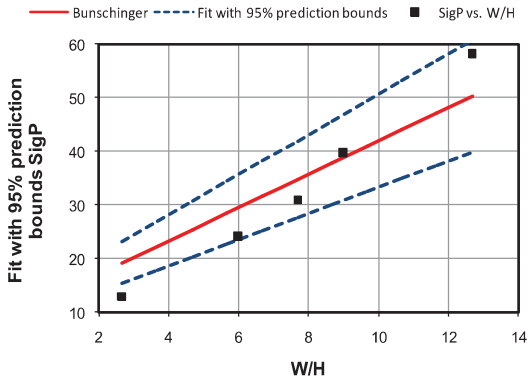

Figure 5. The curve of Bunschinger formula with 95% prediction bounds and field data.

RESULTS AND DISCUSSION

As shown above, the variation trend of the prediction bound for the various formulae are different. The Holland formula has the most uncertainty, while the Bunschinger formula has the second highest uncertainty. The Oraee-Hosseini formula, however, shows a lower uncertainty. The Holland and Oraee-Hosseini formulae have linear equations, whereas the equations of Bunschinger and Bieniawski formulae are nonlinear. With regards to the data utilized, certain advantages based on linear or nonlinear equations have not been accessed.

Overall, the uncertainty of each coal pillar strength formula is shown by the distance of the upper and lower bounds from the fitting curves. The closer the upper and lower bounds, the higher the confidence level of coal pillar strength formula will become, and vice-versa. To understand the uncertainty of each coal pillar strength formula more clearly, the trends of the distance between the upper and lower prediction bounds with 95% precision for various coal pillar strength formula are depicted in Figure 6.

As generally observed in all of the above formulae, uncertainty increases with the increasing width-to-height ratio of the pillar. Also, the increasing rates of uncertainty for all formulae are almost identical. Based on the uncertainty criterion, the Oraee-Hosseini formula is ranked first and Bieniawski, Bunschinger and Holland are ranked second to fourth, respectively. Of course, this would be

related to the nature and properties of the field data; most of the data that is used in this research was collected at the Tabas coal mine in Iran. It should be noted that the Oraee-Hosseini coal pillar strength formula is presented based on the Tabas field data.

CONCLUSION

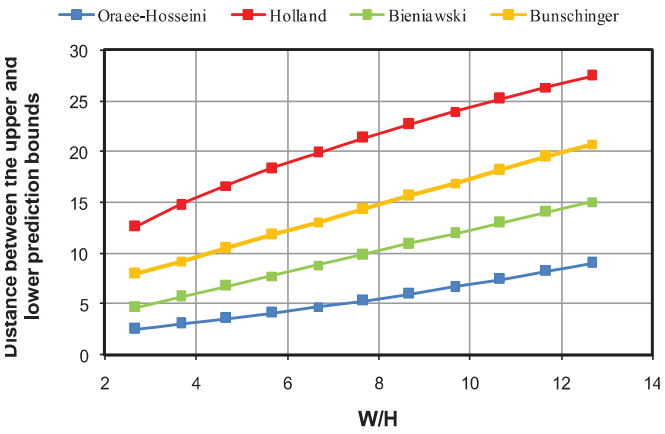

Figure 6. The trends of the distance between the upper and lower prediction bounds.

Some of coal pillar strength formulae in this paper are compared based on uncertainty. According to the results, whilst considering the limited field data of the coal pillar strength, the prediction of Oraee-Hosseini coal pillar formula is more suitable than other failure criteria. The prediction certainty and confidence of coal pillar formulae are decreased as the width-to-height ratio of the coal pillar is increased. Therefore, according to field characteristics, operational conditions and geomechanical properties, the appropriate coal pillar strength formula for each area, such as the equation with the highest certainty, can be selected. In short, the uncertainty can be used as a guide to select the appropriate coal pillar strength formula.

Using the correlation coefficient is the conventional method of evaluating equations fitted on data. However, the results of this study show that the use of uncertainty in the selection of the coal pillar strength formula as a new approach is a more applicable criterion. The calculation is usually impossible since the correlation coefficient requires the initial data, and that is complicated to obtain. The uncertainty criterion for each new data point can be used in a simple way, and the new approach that is presented in this paper is applicable to any underground coal mine.

REFERENCES

Bird, J. (2003). *Engineering Mathematics*, Elsevier Science, Newnes, London, UK 531.

Brady, B.H.G., Brown, E.T.. (2004). *Rock Mechanics for Underground Mining*. London, UK: George Allen & Unwin.. 628.

Hosseini, N. (2007). *Modelling of Pillars in Longwall Method Using Advanced Numerical Techniques*. *M.Sc. Thesis.* IAU, South of Tehran branch, 235.

Hosseini, N., Oraee, K., Gholinejad, M. (2010). *Optimization of Chain Pillars Design in Longwall Mining Method*. In: 29th International Conference on Ground Control in Mining (ICGCM). Morgantown, West Virginia, USA. 67-70.

Mark, C.. (1990). *Pillar Design Methods for Longwall Mining*. USBM Information Circular 9247. Washington, D.C. 1-53.

MATLAB version 7.11.0.584 (2010) Help and demos, for MATLAB reference, curve fitting toolbox.

Oraee, K., Hosseini, N., Gholinejad, M. (2008). *3D Strain Softening Modelling of Coal Pillars in a Deep Longwall Mine*. In: Proceedings of Seventeenth International Symposium on Mine Planning and Equipment Selection (MPES 2008). Beijing, China. 761-767.

Oraee, K., Hosseini, N., Gholinejad, M. (2009a). *Coal Pillar Strength Based on the Ground Reaction Curve – A New Approach*. In: Proceedings of the 28th International Conference on Ground Control in Mining. Morgantown, West Virginia, USA. 21-24.

Oraee, K., Hosseini, N., Gholinejad, M. (2009b). *Estimation of Coal Pillar Strength by Finite Difference Model*. In: Proceedings of the 2009 Coal Operators' Conference. Wollongong, Australia. 53-60.

Peng, S. S. (2006). *Longwall Mining, Second edition*. Society for Mining, Metallurgy, and Exploration, Inc. (SME), Department of Mining Engineering, West Virginia University, USA, 621.

Peng, S. S. (2008). *Coal Mine Ground Control, Third edition*. Society for Mining, Metallurgy, and Exploration, Inc. (SME), Department of Mining Engineering, West Virginia University, USA, 764.

Su, D. W. H., Hasenfus, G. (1999). *Coal Pillar Strength and Practical Coal Pillar Design Considerations*. In: Proceedings of the Second International Workshop on Coal Pillar Mechanics and Design. Pittsburgh, Pennsylvania, USA. Department of the Interior, Bureau of Mines. 155-163.

Prediction of First Weighting Distance in Longwall Coal Mining By 3D Numerical Modeling – A Case Study

Haile Manteqi, Master of Science
Department of Mining Engineering
Azad University of South of Tehran Branch
Tehran, Iran

Kourosh Shahriar, Professor
Amirkabir University, Tehran, Iran
Tehran, Iran

Rahman Torabi, Associate Prof
Shahrood University of Technology
Tehran, Iran

ABSTRACT

In longwall coal mines, estimation of roof strata condition, sequence of loading, and supporting requirements are of a high degree of importance, and they are directly related to production and safety. Also, a prediction of the initial caving distance is rather complicated to calculate, because there are many parameters that effect caving process—roof and floor strata conditions, thickness of immediate roof, depth of cover, excavation geometry, and magnitude, and direction of principal stresses. This paper presents the results of 3D numerical modeling of the initial caving mechanism using the finite difference code *FLAC*^{3D} at the E1 longwall panel of the Parvade 1 underground mine located in the Tabas area in the central part of Iran. The initial caving distance obtained was 10.4 m. Also, the results of numerical modeling have been compared to the analytical methods, such as Peng's method. The results show good agreement with each other.

INTRODUCTION

Longwall mining is an underground mining method that has a high rate of production capacity and mechanization ability. This mining method, which is appropriately applied for soft rock, flat lying, bedded ore bodies, gradually became a widespread mining method among European coal mines at the beginning of the 19th century. It was then applied in some U.S. coal mines with the development of self-advancing support mechanisms in early 1960s (Oraee, 2001).

Underground coal production around the world using the longwall mining method doubled during the 1990s (Oraee, and Bangian, 2010). The main reasons for this improvement include the following: the high level of mechanization, increased safety, adequate design of panels, and well-designed ventilation systems (Peng, 2006). Due to longwall mining, coal production has been increasing in recent years, mainly because of the highly mechanized procedure and safety of this method. For high safety, well-managed ground control and prediction of strata movements around the coal seam are two essential parameters.

Strata control in longwall mining has been a challenging area of research since its introduction in the underground coal mining industry worldwide. A reliable prediction of the caving behavior of strata and its interaction with the roof support helps in the selection of sustainable mining parameters and rational capacity of supports. It is a prerequisite for developing a reliable support selection tool, which is essential for successful planning of longwall working in a given mining condition.

Theoretical models for predicting initial caving and periodic caving distances are based on plate-beam theory and bending moment approach. A number of empirical models have been developed on the basis of either concept or some field experience to assess the caving behavior of strata. Some of these approaches suggest roof classifications for qualitative assessment of caving behavior. Some other models propose quantitative relation to predict the span of main fall. Similar relations have been proposed by various researchers to estimate the span of periodic caving. A few models give both the options of qualitative assessment of roof caving and the quantitative assessment of caving span (Singh and Singh, 2009).

Although application of numerical modeling technique for strata control in longwall workings is not a new topic of research, most studies with progressive face advance have not included an assessment of the strata-support interaction. Most of these studies have been done using elastic analysis where simulation of face advance bears no importance. This paper describes a numerical modeling technique to assess the acceptability of the model for predicting the caving behavior of strata in a given strata condition. the performance of the numerical model is compared with field observations at the E1 longwall panel of the Parvade 1 underground mine which is located in the Tabas area of the central part of Iran.

The Tabas coal region is one of the most comprehensive coal resources in Iran. A large volume of coal reserve and appropriate geometry of coal seams in Tabas have created the required conditions for using the longwall mining method. The most important coal seam in the Tabas region is the C1, which has an average thickness of 1.8 m. In this region longwall mining has been applied for just one section of the C1 seam. Development and opening of the ore body have been carried out through inclined openings. The width of the panels (length of the faces) is from 200 to 220 m, and the length of the panels is about 1,000 m. Longwall mining is carried out by the retreat method (Oraee, and Bangian, 2010).

TABAS UNDERGROUND MINE AND PRODUCTION METHOD

Tabas Underground Mine is a main mine of Iranian Coal Enterprises and is located in the Tabas District of Iran near Tabas city and Khorasan Province (see Figure 1). The Parvade Coalfield lies approximately 85 km south of the oasis town of Tabas in mid eastern Iran. It is 402 km from Birjand and 369 km from Yazd. The total probable anthracite reserve in the Parvade region is approximately 1.2 billion tons. The minable reserve suitable for underground production is 28 millions ton in the Parvade 1 only. The average calorific value of anthracite in Tabas District is 13500 BTU/lb, with average sulfur content of 1.5% (IRITEC, 2003).

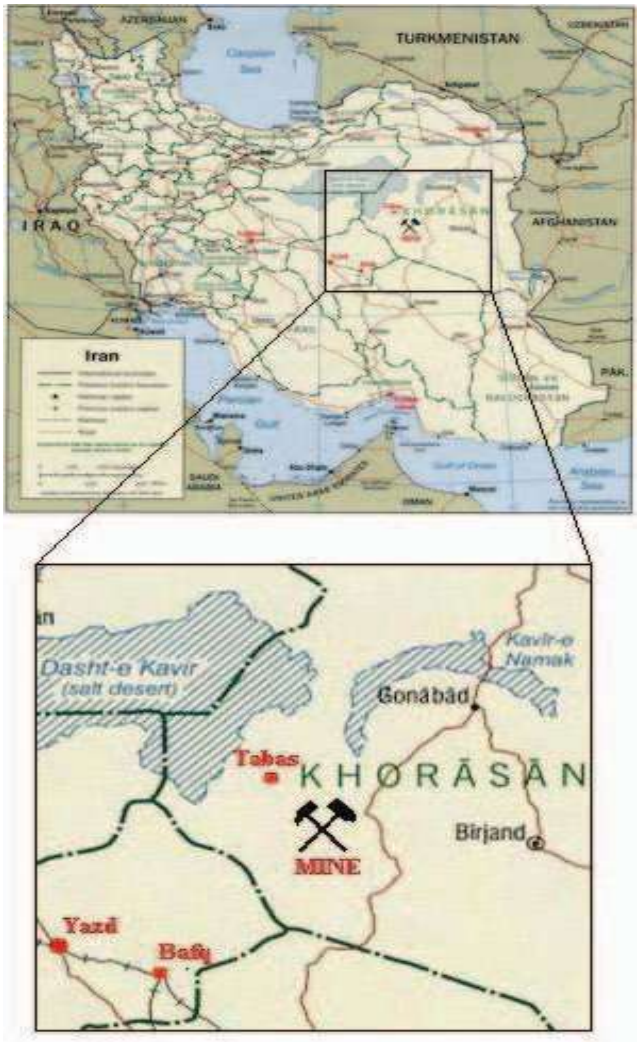

Figure 1. Map of Tabas region.

Production started at Parvade Underground Mine in 1995 by traditional methods. A conventional support system was used until 2002, and a fully mechanized face was established in 2006. The average depth below the surface is approximately 550 m, and the 1.8-m-thick coal seam has a slope, on average, of 10°. A generalized stratigraphic column showing the coal seam together with roof and floor strata is presented in Figure 2. Five main geological units—sandstone, mudstone, silty mudstone, sandy siltstone, and siltstone—are present in the mine area.

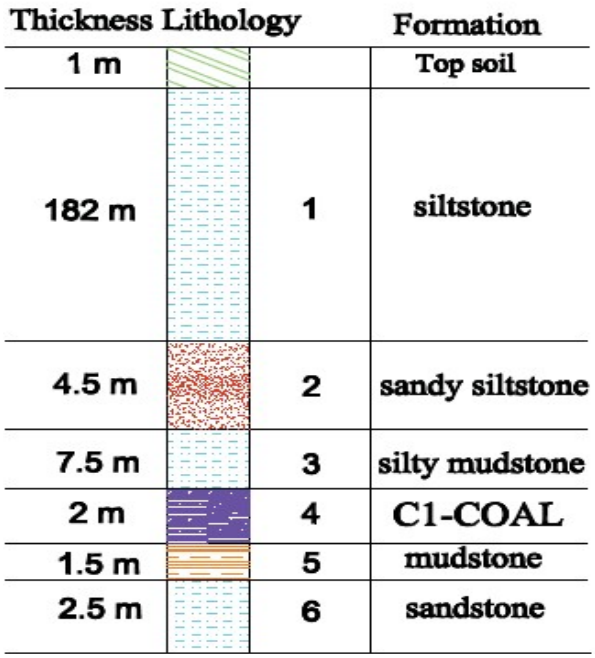

Figure 2. A generalized stratigraphic column at Parvade coal mine.

There is a 20–40 cm thick mudstone at the roof contact of the coal seam, which frequently creates instability problems due to its low strength and fractured characteristics. Therefore, it has been extracted with coal seam. There is a silty mudstone layer (layer 3 on Figure 2) just above the listric mudstone layer. The silty mudstone layer is stronger and thicker than listric mudstone and is 7.5 m thick. There is a mudstone layer (layer 5 on Figure 2) that has an average thickness of 1.5 m at the floor of the seam. The sandstone layer (layer 6) located at the floor is stronger than the sandy siltstone (layer 2) and siltstone (layer 1). The coal seam (layer 4) contains three mud bands—10, 40, and 10 cm thick from top to bottom. Physical and mechanical characteristics of the coal and surrounding rock are presented in Table 1.

As seen in Figure 3, 27 panels were planned for extraction by means of a fully mechanized face. At the time of this study, one adjacent longwall panel, E1, had been completed and the production was being carried out at the E2 panel. Coal has been produced by means of longwall retreat with the caving production method where a 2-m-high longwall face was operated at the floor of the coal seam (Figure 4).

CONVENTIONAL METHOD

Peng's Theoretical Method

When a longwall panel of sufficient width and length is excavated, the overburden roof strata are disturbed in order of severity from the immediate roof toward the surface. The

Table 1. Physical and mechanical properties of coal and surrounding rocks.

Formation	Definition code	relative density	Uniaxial compressive strength (MPa)	Tensile strength (MPa)	Internal Friction angle (φ)	Cohesion C (MPa)	Modulus of elasticity E (MPa)	Poisson's Ratio v	*RMR*	*GSI*
Siltstone	1	2.7	37	2.5	24	1.30	2838	0.26	24	19
Sandy siltstone	2	2.5	73	2.6	-	-	2987	0.25	28	23
Silty mudstone	3	2.6	18	0.3	-	-	2256	0.28	20	17
Coal	4	1.6	6	-	15-25	0.01	316	0.25	5	9
Mudstone	5	2.6	24	-	18	0.94	2838	0.31	22	18
Sandstone	6	2.7	72	6.3	31	8.69	5281	0.25	32	27

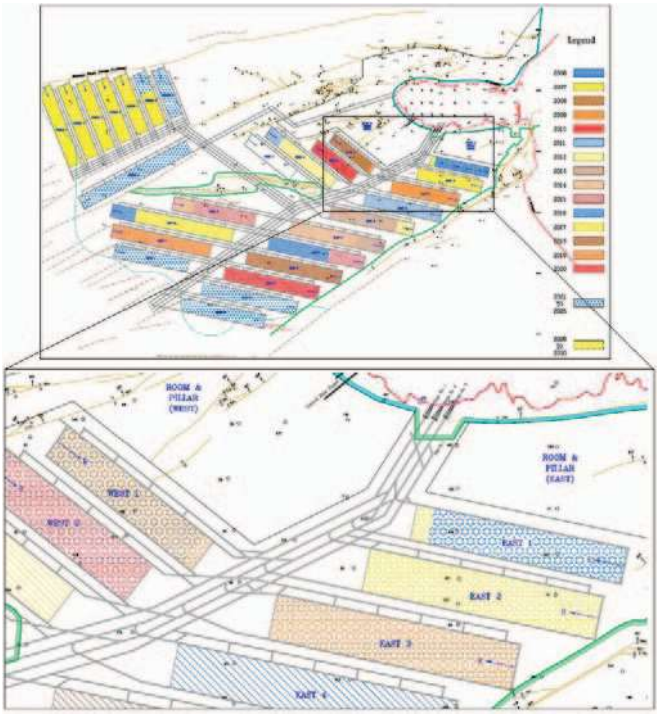

Figure 3. A plan view of Parvade underground mine.

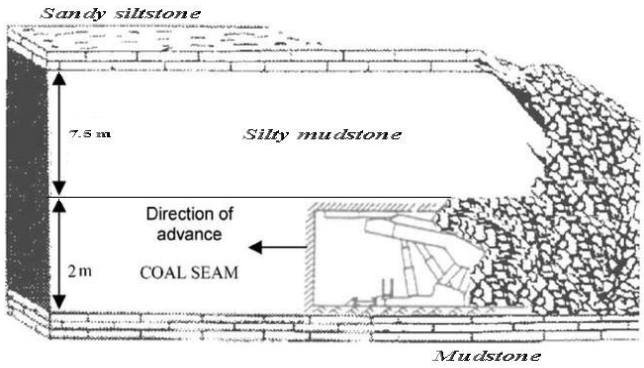

Figure 4. Longwall caving method as applied at Parvade underground mine.

overburden roof strata are divided in four zones shown in Figure 5: the caved zone, the fractured zone, the continuous deformation zone, and the soil zone (Peng, 2008). The caved zone is created as the mining face advances, and the immediate overburden falls and fills the void created by the extraction of the coal. The caved zone extends upwards and is 2 to 10 times the extraction thickness. The fractured zone is located above and around the caved zone and is characterized by near vertical fractures and bedding plane shearing caused by the passage of the longwall face. Bed separation can occur in this zone. The fractured zone can extend 15 to 60 times the extraction thickness. Above the fractured zone is the continuous deformation zone. On the surface, there is a soil zone of varying depth depending on the location. In this zone, cracks open and close as the longwall face comes and goes.

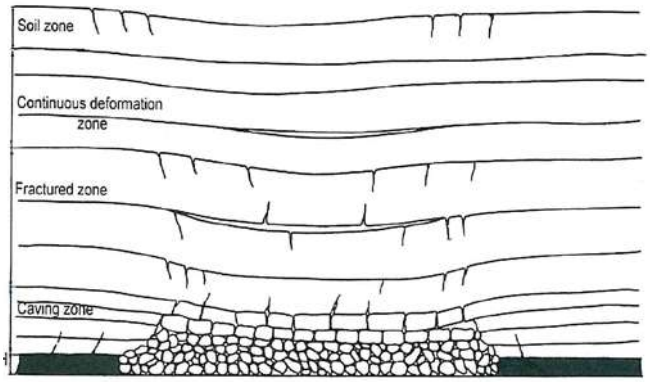

Figure 5. Overburden movement resulting from longwall mining.

Movement of the different zones has different degrees of effect on roof control at the longwall face. The effect decreases as the strata are located farther up from the roof line. Those strata, the movement of which will affect roof control at the long wall face, can be classified into two types: immediate and main roofs (Peng, 2006). The immediate roof is that portion of the overburden strata lying immediately above the coal seam top, with a height approximately 2 to 10 times that of the mining height. Above the immediate roof, the strata in the lower portion of the fractured zone are called the main roof (Figure 6).

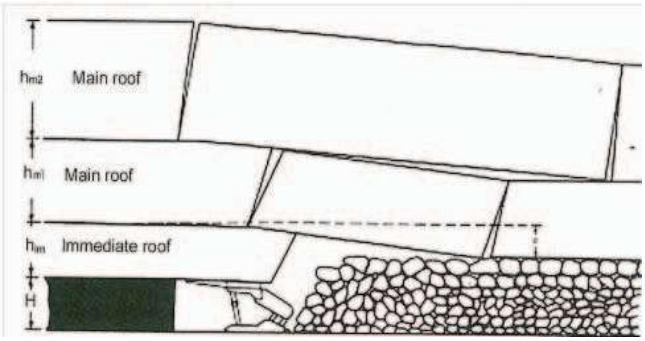

Figure 6. Immediate and main roofs.

Formulation of Caving Height or Thickness of The Immediate Roof

The thickness of the immediate roof is the basis for designing roof control techniques. Normally, caving initiates from the lowest strata in the immediate roof and propagates upward into the fractured zone. The process of caving in each stratum begins with the stratum sagging downward as soon as it is undermined. When the downward sagging of the stratum exceeds the maximum allowable limit, it breaks and falls. As it falls, its volume increases; therefore, the gap between the top of the rock piles and the sagged but uncaved stratum continues to decrease as the caving propagates upward. When the gap vanishes, the caving will be stopped. Thus the height of the caving must satisfy the following condition (Peng, 2006) (Figure 6):

$$H\text{-}d = h_{im}(K\text{-}1) \quad (1)$$

$$\text{And } d \le d_0 \quad (2)$$

where

H is the mining height,

d is the sagging of the lowest uncaved strata,

d_0 is the maximum allowable sagging (without breaking) of the lowest uncaved strata,

h_{im} is the thickness of the immediate roof or caving height, and

K is the bulking factor of the immediate roof.

Therefore, according to the Equation 1, the caving height can be determined by

$$h_{im} = (H\text{-}d)/(K\text{-}1) \quad (3)$$

It must be noted that if $d=d_0=H$, then $h_{im}=0$, which means no caving; that is, the roof sags gradually until it touches the floor. On the other hand, if $d=d_0=0$

$$h_{im} = H/(K\text{-}1) \quad (4)$$

Formulation of Initial Caving

There are many complexities in roof loading design in longwall coal mining when the strata above the coal seam has not moved yet and the first collapse is expected. Therefore, theoretical models must be used for predicting the initial caving. The distance is assessed based on beam theory with fixed ends and a beam bending moment approach. A beam fixed at both ends that is affected by uniformly distributed load is shown in Figure 7 (Beer and Johnston, 2005).

According to Figure 7, the reaction forces at both ends are shown in Figure 8.

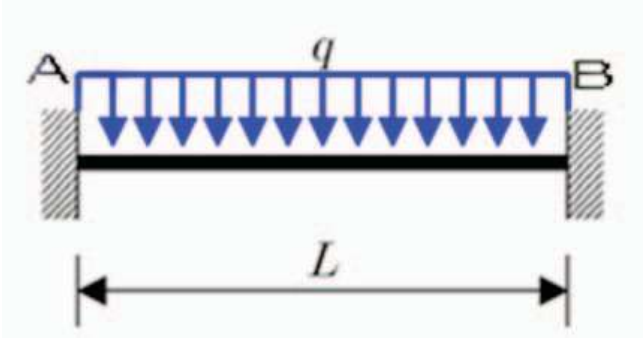

Figure 7. A beam fixed at both ends that is affected by a uniformly distributed load.

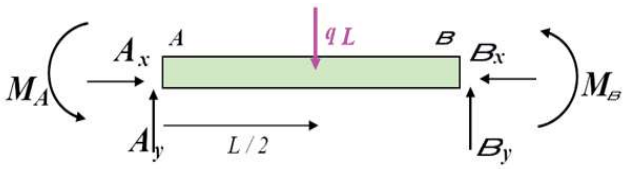

Figure 8. The reaction forces at beam supports.

Therefore, the equilibrium equations are as follows:

$$\sum F_x = 0 \quad (5)$$

$$\sum F_y = 0 \quad (6)$$

$$\circlearrowleft + \sum M = 0 \quad (7)$$

where

A_x and B_x are reaction forces in the x direction,

A_y and B_y are reaction forces in the y direction,

L is the length of beam,

q is the force per unit of beam length,

and M_A and M_B are bending moments at beam supports.

According to the equilibrium equations, the bending moments have been calculated by another method called super position method:

$$M_B = qL^2/12 \quad (8)$$

The maximum bending moment occurs at both ends of supports (Equation 9) and also the maximum of tensile stress that is sustainable for a beam fixed at both ends is as follows in Equation 10:

$$M_{max} = qL^2/12 \quad (9)$$

$$\sigma t_{max} = M_{max} C/I \quad (10)$$

where

σt_{max} is the maximum tensile stress,

C is the neutral axis distance of beam from neutral surface, and

I is the moment of inertia.

Additionally, C and I have been calculated in Equations 11 and 12 for a rectangular beam:

$$C = h/2 \quad (11)$$

$$I = bh^3/12 \quad (12)$$

where

h is the beam height and

b is the beam width.

Therefore, by means of Equations 9 through 12, knowing that is $q = \gamma b h$, where γ is the beam density, the maximum allowable length of the beam is estimated as follows:

$$L = \sqrt{\frac{2\sigma_t h}{\gamma}} \quad (13)$$

where L is the maximum allowable length of the beam or distance of the initial caving,

σ_t is the tensile strength of the immediate roof or the beam,

γ is the density of the immediate roof or the beam, and

h is the thickness of the immediate roof or the beam.

ROCK PROPERTIES

Assessment of Material Properties and Rock Mass Strength

Proper assessment of rock mass strength and modulus values is very important for a meaningful numerical modeling study of caving behavior and support requirements. Therefore, physical and mechanical properties of each geological unit must be properly determined. In general, intact rock properties are determined by means of laboratory testing. However, there is an important difference between intact rock material and rock mass characteristics. It is compulsory to determine representative physical and mechanical properties of the rock mass instead of intact rock material. Data regarding the physical and mechanical properties of surrounding rock are given in Table 1.

The laboratory tests were carried out on core samples from exploration drilling. Rock blocks were taken directly from the mine. The data presented in Table 1 are representative only of intact rock material. Determination of rock mass strength characteristics is rather difficult. Therefore, it is a common practice to derive rock mass strength from intact rock material properties by using various failure criteria. In this study, intact rock material properties were converted into rock mass data by using RockLab code and empirical relations widely used in the literature, e.g., Hoek and Brown failure criterion, Bieniawski's RMR classification system, and the Geological Strength Index (GSI). Physical and mechanical properties of the rock mass used for numerical modeling by FLAC^{3D} are presented in Table 2.

NUMERICAL MODELING

Modeling Procedure in General

Modeling was carried out with FLAC^{3D}, which is used for stress and deformation analyses around surface and underground structures opened in both soil and rock. This software is based on the finite difference numerical method with the Lagrangian calculation method. The finite difference method can be better applied to modeling of stress distribution around underground mining excavations in comparison to other numerical techniques. FLAC^{3D} is commercially available software that is capable of modeling in 3D. Modeling of longwall caving is performed in five steps:

A. Determination of boundaries and material properties.
B. Formation of the model geometry and meshing. Determination of the model behavior.
C. Determination of the boundary and initial conditions. Initial running of the program and monitoring of the model response.
D. Re-evaluation of the model and necessary modifications.
E. Obtaining of results.

Model geometry and meshing refer to physical conditions of the district to be modeled. Model behavior is the response of a model under a certain loading condition. By means of boundary and initial conditions, physical limits of the model and original conditions are determined. Gate roadways, the face, and other structures were later created in the form of modifications. The modeling process is presented in Figure 9 in a flow sheet (ITASCA, 1997).

Model Geometry and Meshing

The E1 longwall panel of Parvade 1 coal mine with a two-entry system was modeled using FLAC^{3D} software. The E1 panel is the first panel that was extracted using the retreating method. Steps of a true scale 3D modeling of the E1 longwall panel with FLAC^{3D} are given below:

Table 2. The input parameters regarding rock mass used in numerical modeling.*

Rock Definition	Siltstone	Sandy Siltstone	Silty Mudstone	Coal	Mudstone	Sandstone
Definition code	1	2	3	4	5	6
Density (MN/m3)	0.0272	0.0271	0.0268	0.016	0.0263	0.027
Internal Friction angle (φ)	27.42	31.75	22.17	15.76	20.13	43.52
Cohesion *c* (MPa)	0.357	0.443	0.257	0.084	0.231	0.767
Modulus of elasticity *E* (MPa)	2238	2818	1778	749	1995	3548
Tensile strength (MPa)	0.012	0.007	0.005	0.002	0.013	0.017
Poisson's ratio *v*	0.25	0.25	0.28	0.25	0.31	0.25
Bulk modulus [a] (*K*) (MPa)	1492	1878	1347	499	1750	2365
Shear modulus [b] (*G*) (MPa)	895	1127	695	299	761	1419
Uniaxial compressive strength (MPa)	0.273	0.287	0.114	0.015	0.165	1.011

* *These values are obtained from RockLab code.*

[a] $K = E/3(1-2v)$ [b] $G = E/2(1+v)$

1. Face length was 170 m at the E1 longwall panel. Therefore, face length was taken as 170 m on the +x coordinate axis in the model.
2. The actual panel length was 980 m. However, due to computer running time and capacity restrictions, the panel length was taken as 120 m on the +y coordinate axis in the model.
3. In accordance with the actual depth below the surface, this value was taken as 200 m on the -z coordinate axis in the model.
4. There was a solid panel called E2 separated by a 26-m-wide rib pillar.
5. In order to obtain more precise stress distribution results, a smaller mesh size was selected at regions in the vicinity of the production area.
6. Cubic and prismatic (brick) elements were used for model construction. The model was composed of 209,056 elements and 222,557 grid points.

Initial Caving Distance Modeling

In the retreat longwall working, following the excavating of tailgate and headgate entries, the setup room entry will be excavated between the two entries approximately 6.1 to 7.3 meters in width (Peng, 2008). As the coal extraction was beginning, the distance between the end of the longwall shield and the wall was almost 1.5 to 2 m. Therefore, the first step will be modeling of this section (Figure 10a). In the Parvade mine, setup room was excavated about 7 m in width. The layout of E1 face line cross section from headgate in the Tabas coal mine is shown in Figure 10b.

In the initial period, as the mining proceeds, the roof remains intact and the gob is left open (Figure 11a). As the length of the gob increases, the immediate roof begins to bend and sag. Eventually, it separates from the main roof along the bending plane of contact (Figure 11b). After that, the immediate roof splits into two sections, both of which lose support and fall. Also the roof pressure reaches the maximum right before this happens. This is the initial caving distance that has been modeled and is shown in Figure 11c. The layout for the longwall panel consists of various positions of the face line as presented in Figure 12 as well.

Stress Distribution Around the Longwall Face

The model that was made of only solid rock mass not including any openings inside was solved until a state of equilibrium was reached. After this stage, the model was ready for inclusions of underground mine structures such as roadways and the longwall panel. At first, the headgate and tailgate of the E1 panel were formed in the model with their actual dimensions of 4.5 m in width and 3.5 m in height. The location of the headgate and tailgate, together with the rib pillar between the E1 panel and the E2 new working panel and the face are presented in Figure 13. In the mine, the headgate and tailgate were supported by means of wire mesh (a strap), rock bolt systems, and then a frame of joists. It was possible to add such support types in the model prepared by FLAC^{3D}; therefore, it was convenient to represent support in the model. According to the panel length, which was taken as 120 m on the +y coordinate axis in the model, the tailgate and headgate have been excavated and supported at the 30 sections. After the formation of the headgate and tailgate, the setup room was formed. Setup room dimensions were 2 m in height and 7.2 m in width because of zone dimensions.

PRESENTATION OF MODELING RESULTS

Because this modeling study depended on face advance, stress and displacement distributions were found for various conditions.

Horizontal stress distribution on the x- and y-axes and vertical stress distribution on the z-axis are presented in Figure 14 after a face advance of 10.4 m from the face start line.

Horizontal stresses were found at the both ends in the order of 4.18 MPa in the x direction and 2.10 MPa in the y direction. Vertical stress was found to be at maximum at 7 m in front of the face in the order of 7.62 MPa in the z direction. The results revealed that z, x, and y directions corresponded to maximum, intermediate, and minimum principal stress directions, respectively.

By using numerical modeling, the progressive face advance is simulated in stages of 0.8 m until the initial caving is observed

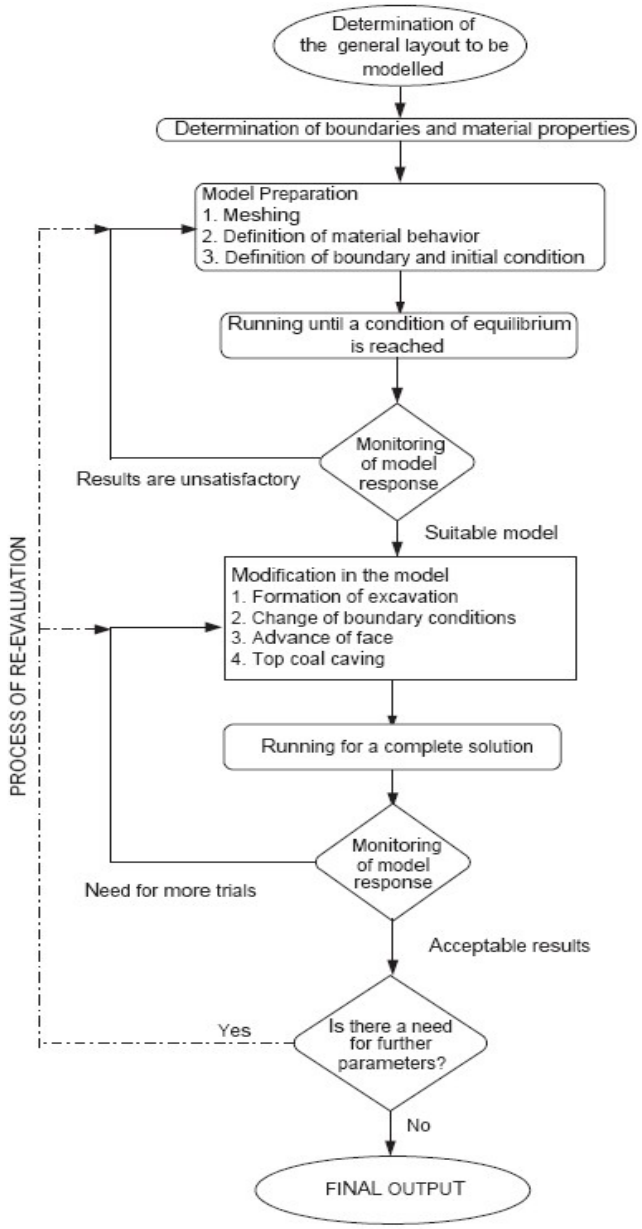

Figure 9. A general flow sheet of the modeling process.

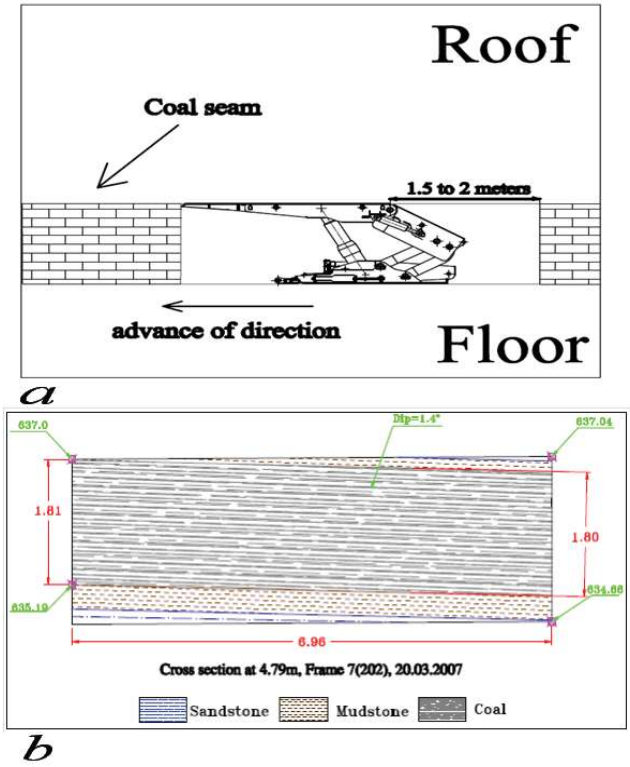

Figure 10. The scheme of the setup room (a), E1 face line cross section from headgate in the Tabas coal mine (b).

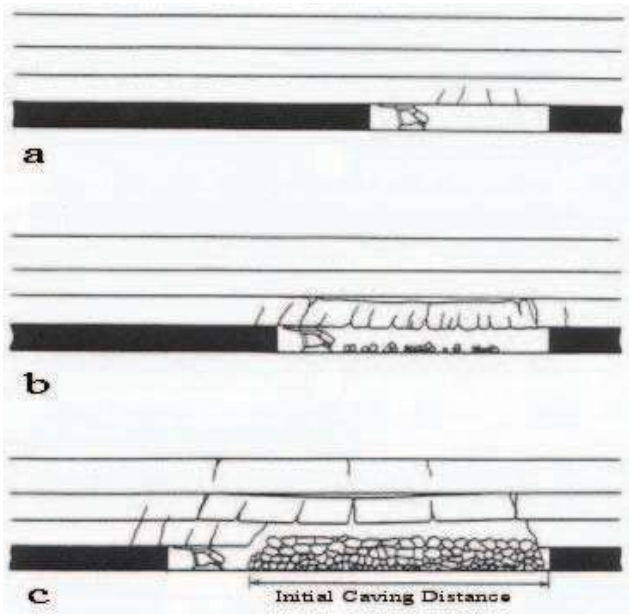

Figure 11. Idealized sequences of roof movements leading to initial caving.

within the 3D modeling limitations. Results of this modeling study revealed that the initial caving distance was 10.4 m.

For estimation of the vertical load variations on the coal production area while the area width was being increased, before the initial caving occurs, pressure arch, beam theory, and Terzaghi methods were employed. Figure 15 presents the distribution of vertical loads above the face at various distances toward the direction of advance from the face line, such as 1.6, 3.2, 4.8, 6.4, 8, 9.6, and 10.4 m. According to the curves in Figure 15, pressure arch and beam theory methods show good agreement with eachother. Also, in the Terzaghi method, vertical load on the tunnel is more than the other methods.

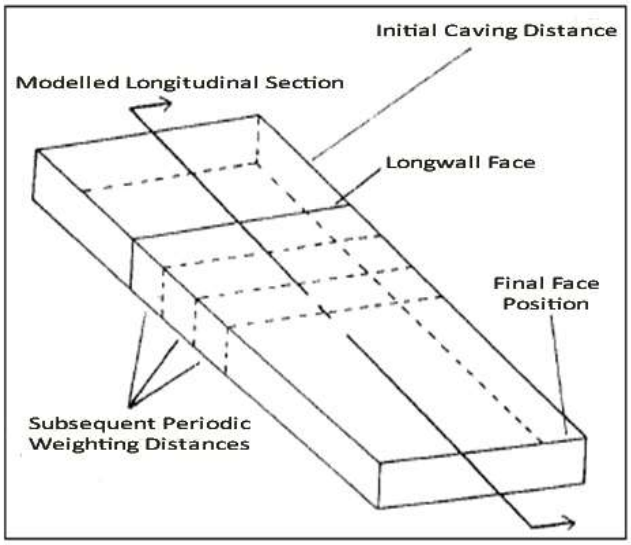

Figure 12. Layout for longwall panel modeling.

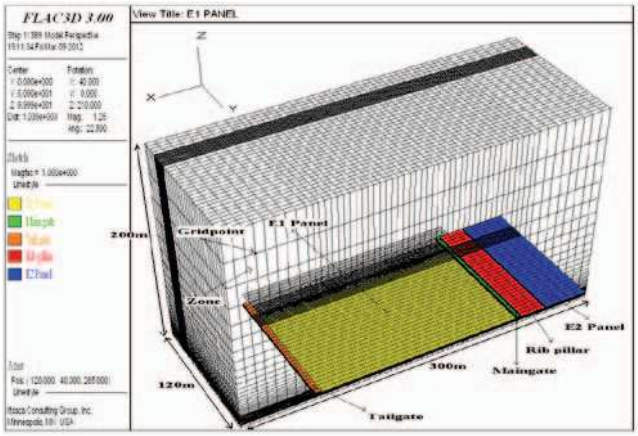

Figure 13. Isometric view of the model created in FLAC3D.

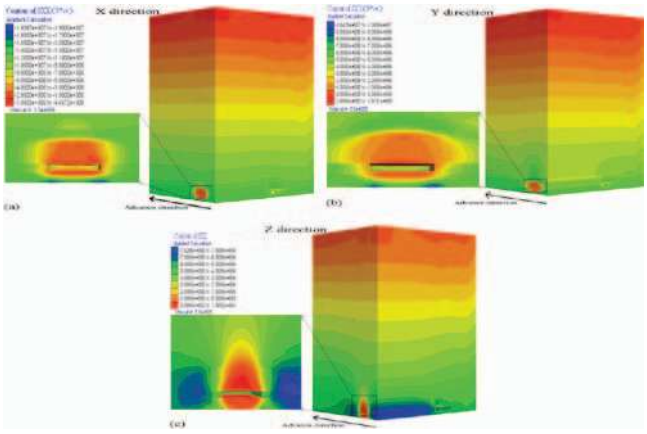

Figure 14. Distribution of horizontal (x- and y-direction) and vertical (z-direction) stresses around longwall panel.

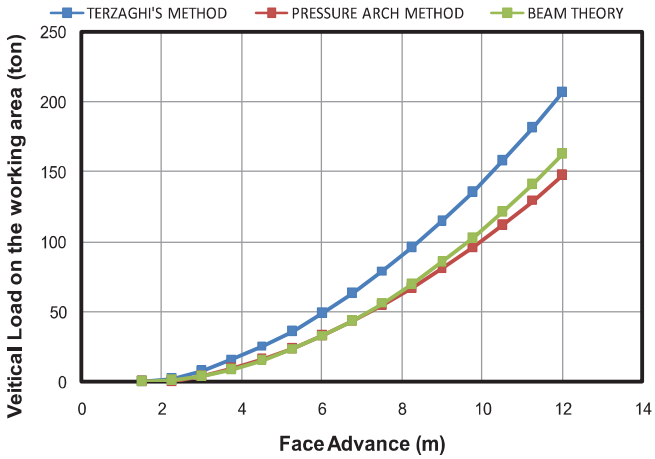

Figure 15. Vertical load variations on the working area with increase in area width before the initial caving.

By using the fixed beam theory and Peng's equation (Equation 13), the initial caving distance was obtained 10.95 m and it also has been reported 12 meters by site observations.

As shown in Figure 16a, the state of displacement distribution has been shown on the z-axis. In this figure red and blue colors indicate the highest and lowest magnitude displacement, respectively. As expected, the displacement progress increases with face width advancing and expands toward its center (Figure 16b).

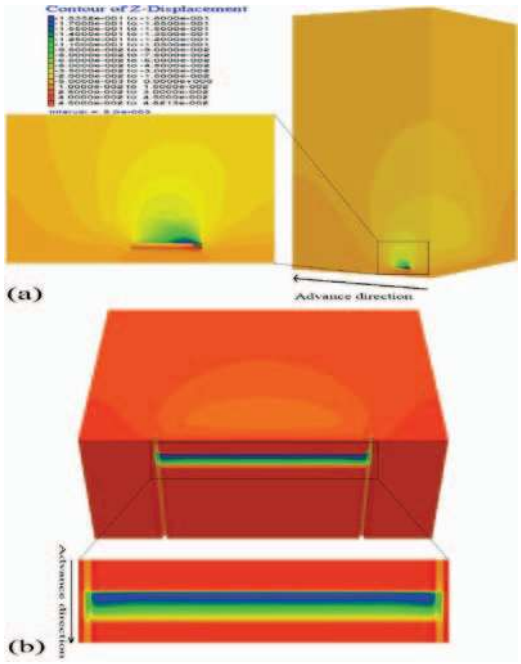

Figure 16. Distribution of z displacement on a longitudinal section through the center, and (a) displacement progress increases with face width advancing and expanding toward its center (b).

CONCLUSIONS

In this study, 3D modeling of the initial caving distance with the longwall caving method applied at the E1 panel of the Parvade1 Underground Mine was carried out by FLAC^{3D}. For realistic modeling, material properties were derived for the rock mass from laboratory data by using the RockLab code, Mohr-Coulomb failure criterion, the RMR, and the GSI systems together with empirical equations. Results of this modeling study revealed that the initial caving distance was 10.4 m. Also the initial caving distance obtained by using an analytical method was 10.95 m. On the other hand, according to the site observations, the initial caving distance was reported to be 12 m. A comparison of the results obtained from numerical approach, analytical calculations, and observed data show good agreement. From the point of view of forces affecting the production area, the vertical load on the area based on pressure arch, beam theory, and Terzaghi methods were compared with each other. All these three methods show a consistent increase in the pressure with increasing the coal face advance before the initial caving occurs. Pressure arch and beam theory methods show better agreement in comparison with the Terzaghi method.

REFERENCES

Beer, F.P., Johnston, E.R. (2005). *Mechanics of Materials*. 4th ed. McGraw Hill, 779 p.

IRITEC (2003). Tabas Coal Mine Project, Detailed Engineering Report, vol. 1, Underground Mine Revision A. IRITEC.

ITASCA. (1997). *User manual for FLAC^{3D}, version. 2.0.* Minnesota: Itasca Consulting Group Inc.

Oraee, K. (2001). *Underground Coal Mining*. Tehran, Iran: Polytechnic University Press.

Oraee, K., Oraee, B., Bangian, A. (2010). "Design optimization of longwall chain pillars." In: *Proceedings of the 29th International Conference on Ground Control in Mining*.

Peng, S.S. (2006). *Longwall Mining,* 2nd ed. Society for Mining, Metallurgy, and Exploration, Inc. (SME).

Peng, S.S. (2008). *Coal Mine Ground Control*, 2nd ed. Morgantown, WV: West Virginia University.

Peng, S.S., Chiang, H.S. (2006). *Longwall mining*. Hoboken, NJ: John Wiley and Sons.

Singh, G.S.P., Singh, U.K. (2009). "A numerical modeling approach for assessment of progressive caving of strata and performance of hydraulic powered support in longwall workings." *Computers and Geotechnics*. *36*(7):1142–1156.

A Review of Effective Parameters on Roof Fall During Retreat Mining in Room and Pillar Coal Mines

Ebrahim Ghasemi
Mohammad Ataei
Department of Mining, Petroleum and Geophysics Engineering
Shahrood University of Technology
Shahrood, Iran

Kourosh Shahriar
Department of Mining and Metallurgical Engineering
Amirkabir University of Technology
Tehran, Iran

ABSTRACT

Problem statement: One of the most challenging safety problems in room-and-pillar coalmines is controlling roof falls during retreat mining. Roof falls not only cause both fatal and non-fatal injuries to miners, stoppages in mining operations, and equipment breakdowns, but also results in the inefficient recovery of coal reserves.

Approach: Sufficient awareness of effective parameters related to roof falls is an important factor in roof control. In this study, the major contributing parameters on roof falls during retreat mining are introduced based upon experience and judgment acquired from extensive retreat mining case histories and a review of relevant literature.

Key findings: The main roof fall parameters in retreat mining can be divided into three categories: geological, design, and operational.

Key conclusions: The design and operational parameters can be controlled by the engineer and/or operator. By the appropriate selection of these parameters in the design and implementation stages of retreat mining, the roof fall risk can be decreased to an acceptable extent.

INTRODUCTION

The room and pillar method is one of the oldest methods used for the extraction of flat and tabular coal seams (Peng 2008). In this method, a series of rooms are driven in the solid coal using a continuous miner (CM) and shuttle cars. Pillars are created during the driving of development panels to support the roof and prevent collapse. To increase the total recovery of the coal resource, the pillars are removed in a later operation known as retreat mining or pillar recovery. Retreat mining is one of the most hazardous activities because it creates an inherently unstable situation. The process of retreat mining removes the main support for overburden and allows the immediate and main roof to cave. As a result, the pillar line is an extremely dynamic and highly stressed environment. The roof at the pillar line is subjected to severe stresses and deformations.

Retreat mining accounts for about 10% of all US underground coal production, yet it is associated with more than 25% of all roof and rib fall fatalities between 1986 and 1996 (Mark et al., 2003). Furthermore, similar statistics are observed in coal mining in Australia and South Africa (Lind, 2005). Between 1995 and 2008 in the US, there were a total of 112 roof and rib fatalities in bituminous underground coal mines, which is 21% of the total fatalities that have occurred during retreat mining (Mark et al., 2009). These statistics and reviews emphasize the need for continuing efforts to reduce roof fall fatalities and injuries.

Unfortunately, there are not many studies about roof falls during retreat mining. Mark, Chase, and Pappas (2003) introduced a set of risk factors associated with retreat mining. They provided a risk factor checklist that can help evaluate the overall level of roof fall risk and identify possible ways to reduce the risk of face line roof falls. Similar studies were carried out for reducing roof fall accidents during retreat mining by Mark et al. (2002), Mark and Zelanko (2005), and Feddock and Ma (2006).

Furthermore, extensive research has recently been conducted to control and assess roof fall risk in coalmines but not during retreat mining. Some of these studies have been carried out by Molinda et al. (2000), van der Merwe et al. (2001), Deb (2003), Duzgun and Einstein (2004), Duzgun (2005), Palei and Das (2009), and Ghasemi et al. (2011).

As a result, roof control is a challenging safety consideration during retreat mining. Awareness of effective parameters on roof falls is helpful for roof control. Controlled roof falls depend on a number of parameters. Uncontrolled falls, can have detrimental effects on miners in the form of injury, disability, or fatality, and on the mining company, due to downtime, interruptions in the mining operations, and equipment breakdowns. In this paper, available literatures about the retreat mining in room and pillar mines have been investigated and based on these case histories, the effective parameters on roof fall have been identified and the role of each one has been discussed.

CONTRIBUTING PARAMETERS ON ROOF FALL

The major contributing parameters on roof fall during retreat mining can be divided into three categories (as shown in Figure 1):

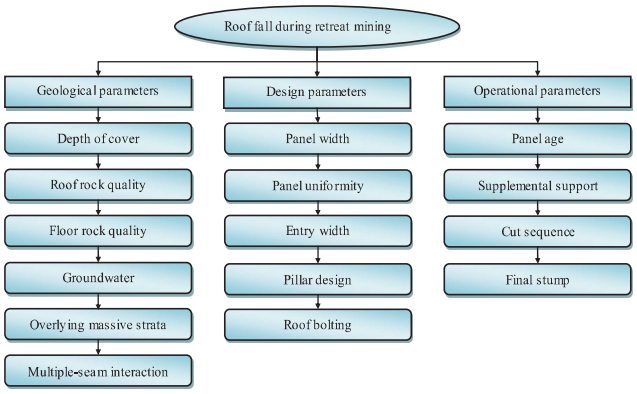

Figure 1. Major contributing parameters on roof fall during retreat mining.

1. Geological parameters: these parameters are related to coalfield geological conditions and features of the coal seam and rib. This category, shown in Figure 1, includes six parameters.
2. Design parameters: this category is related to the design of extraction panel, pillars, and roof support system. This category includes five parameters (as shown in Figure 1).
3. Operational parameters: this category is related to the implementation conditions of retreat mining and, according to Figure 1, includes four parameters.

In the following, each of these parameters and their influence on roof falls are described.

GEOLOGICAL PARAMETERS

Depth of cover: In US coalmines, more than one-third of the retreat mining fatalities have occurred in deep cover(Mark et al., 2003). Increasing depth leads to an increase in virgin stress levels in the rock mass, both vertically and horizontally. Therefore, achieving sufficient stability is harder at high depth, and special precautions are required to ensure ground stability. Of course, the surface effect (the effect of stresses on overburden) on shallow depth panels is an important issue because, in shallow depths (less than 40 m); the surface effect can result in overburden failure in a brittle and unpredictable fashion (Department of Mineral Resources, 1992).

Roof rock quality: Quality of roof rock has an important role in the occurrence of roof falls. Incident reports within retreat mining in the US showed that the weak roof was the main reason in more than one-third of the fatal incidents (Mark et al., 2003). Various methods have been presented for classification and evaluation of roof in coal mines, but one of the most applicable of them is the coal mine roof rating (CMRR) (Mark and Molinda, 2005). The CMRR was developed by Molinda and Mark (1994) and, similar to Bieniawski's RMR, has a single rating between 0 and 100. When the CMRR value is approaching 0, the roof is weaker; whereas a value approaching 100 shows that the roof is stronger. One of the important advantages of this classification method is the consideration of natural causes of roof fall, such as strength of roof rock, bedding, and other discontinuities.

Floor rock quality: Floor, pillar, and roof work as a system in room and pillar mines. Therefore, floor stability plays an important role in the safety and operation of underground coal mines, both in maintaining the access of equipment transportation and in providing a foundation for the floor-pillar-roof system (Santos and Bieniawski, 1989). When the floor rock does not have suitable quality, pillars penetrate into the floor, and this can result in roof convergence and, ultimately, its failure.

Groundwater: Presence of groundwater resources and strata containing water above the extracting panel is one of the causes of roof instability. Retreat mining results in overburden failure and the creation of joints and fractures in it. Water above the panel flows down from these joints and fractures and can cause roof instability, especially in a pillar line.

Overlying massive strata: Safe retreat mining does not mean preventing roof collapse; it means ensuring that it only occurs after the miners have completed their work and have left the area. Roof collapse should occur uniformly and constantly at the active pillar line as the continuous miner moves across the panel. One of the most important influential parameters on roof cavability is the existence of massive strata, over the panel (Lind, 2005). Massive strata can cause a violent roof fall during retreat mining because these strata tend to cantilever and span large distances. However, after exceeding a critical span, they break violently. This violent and unpredictable behavior results in various combinations of loss of life, loss and burial of CM, the associated loss in production, as well as other damage caused by accompanying windblasts.

Multiple-seam interaction: In many coalfields, coal seams are close to each other and form a series of extractable seam that are separated by rock strata (interburden). The mining of two or more adjacent seams is called multiple-seam mining. The ground control problems caused by this mining method are called multiple-seam interaction (Peng, 2008). Interburden thickness and lithology are critical factors in determining the potential for multiple-seam interaction. Ground instability is usually the greatest hazard in multiple-seam interaction, potentially causing roof falls, rib spalling, and floor heave, all of which can seriously disrupt mining operations and threaten the safety of miners. Therefore, identification of potential multiple-seam interaction areas seems essential in the planning stage, i.e.it should be mapped, understood, and supported if it is possible but if not the retreat mining in these areas should avoided.

DESIGN PARAMETERS

Panel width: Panel width affects abutment loads, distribution, and overburden caving mechanism during retreat mining. Based on empirical equations for calculating abutment loads, in a specific depth, the increase of panel width causes increased front abutment load applied on pillars adjacent to the pillar line (Ghasemi and Shahriar, 2012). Increase of load can result in roof instability. Moreover, with increase of panel width, the height of a tensile zone developed in the overburden increases, which may cause violent failure and, eventually, full caving of overburden (Bieniawski 1987).

Panel uniformity: Panel shape and pillars shape and size are important in panel uniformity (Ghasemi et al., 2010). Irregular panel shapes make pillar lines uneven during retreat mining,

causing unpredictable and uncontrollable roof falls. Moreover, panel development consisting of uniformly sized pillars is recommended strongly because non-uniform and unequal-sized pillars cause non-uniform stress distribution reducing roof stability.

Entry width: Between 1997 and 2008, 29 coal miners died from roof fall and coal outbursts while using the retreat mining method (MSHA, 2008). Many of these accidents occurred in intersections. Research has shown that intersections are 8 to 10 times more likely to collapse than the equivalent length of entry or crosscut. Rock load applied on the roof in intersections is proportional to the cube of the span, unlike entries and crosscuts (Molinda et al., 1998). One of the most important methods of decreasing roof instability at intersections is that the entries and crosscuts that create an intersection should be mined to the minimum possible width, in order to make operation of extraction and haulage equipment safer. Increased entry width naturally leads to greater propensity for roof instability. Roof collapse and support problems are likely to be experienced where entry widths are greater than approximately 7 m (Jeffrey, 2002).

Pillar design: As mentioned before, the roof, pillar, and floor work as a system in room and pillar mines. This means that instability of each element leads to instability of other elements. For example, pillar instability during retreat mining can lead to roof instability and, finally, roof falls. Therefore, proper pillar design has a significant role in roof stability. Analysis of the retreat mining pillar stability (ARMPS) program is an effective means for pillar design and the prediction of pillar stability during retreat mining (Mark and Chase, 1997).

Roof bolting: The purpose of roof bolting is to assist the rock to become self-supporting. Accident investigation in US coalmines revealed that roof bolt systems failures have been major factors in one-quarter of the recent pillaring roof fall fatalities because roof bolts are usually the only overhead protection for miners during retreat mining (Mark and Zelanko, 2005). The experimental installation of one roof bolt in one square meter of roof (bolt density=1) in coal mine entries seems to be safe, but this value is not adequate at an intersection because intersections are subjected to more abutment loads during retreat mining. Therefore, intersections require extra roof bolting. Increasing the volume of roof bolt support in many cases, especially in intersections, can be the simplest way to reduce the risk of roof fall.

OPERATIONAL PARAMETERS

Panel age: Panel age is a vital parameter in extracting the pillar inside it because, as time passes, the roof of the mine becomes weaker (rock behavior depends on time). Supplemental bolting is often required, particularly in intersections, to prepare old panels for retreat mining.

Supplemental support: Supplemental roof support is necessary in retreat mining to increase safety and to minimize the risk of injury from roof falls. Timber posts, cable bolts and mobile roof supports (MRS) provide supplemental support for retreat mining. Using MRS is recommended strongly because the use of timber posts as pillar line supports has many disadvantages: the most important of which is that the timber posts are passive supports, and roof convergence would be greater than MRS (Chase et al., 1997; Barczak and Gearhart, 1997). Statistics in US coalmines show that a miner on a timber panel is exposed a risk of fatal injury 1.7 times higher than a miner protected by MRS (Mark and Zelanko, 2005). In comparison with timber posts, MRS reduces the risk for miners because of reduction in miner exposure to roof falls at the pillar line and elimination of material handling. They have high load-bearing capacity and can maintain load over a much greater range of displacement. They increase production because they make the pillar line mechanized and allow for a fluency of mining through greater cutting time.

Of course, MRS have some disadvantages: the main disadvantages being the initial costs, the necessity to recover them if they are trapped by a ground fall, and operating range that is limited to seams thicker than approximately 1m (Mark et al., 2003).

Cut sequence: Mines employ a wide variety of cut sequences to recover pillars, and most of them can be divided into three categories:

1. Left-right (also called Christmas tree or twinning), in which cuts are taken on both sides of the entry, does not require place changes and bolting.
2. Outside lift, which is similar to left-right, except cuts are taken on just one side. It does not require place changes and bolting.
3. Cut sequences requiring cuts to be bolted. This method is usually used when the pillars are so large that they must be split before they are fully recovered. Split-and-fender and pocket-and-wing are two common types of this method.

In US coal mines, almost two-thirds of the retreat mining tonnage are obtained using some type of left-right sequence. Outside lift sequences are used under shallow overburden where smaller pillar widths are possible. Only a few mines employ split-and-fender or other sequences that require roof bolting in the cuts (Mark and Zelanko, 2005).

Mark et al. (2002) evaluated the influence of the cut sequences on ground stability using the boundary element numerical model. They compared four common cut sequences (left-right, outside lift, split-and-fender, and pocket-and-wing) based on actual plans used by mines in southern West Virginia. Results show that outside lift is the most stable method following by the left-right. The two other methods seem unstable. Analysis of the fatalities statistics confirms this fact, too.

Final stump: The final stump (also known as last lift, push out, or stump) is a critical element in roof control during retreat mining because it protects the active intersection. The final stump is the corner of the pillar at the intersection, usually with a wedge-shaped area. Therefore, the final stump provides resistance to the roof and floor displacement. Also, it is a much stiffer support system than either timber post or MRS and, therefore, provides a greater resistance against displacement (Lind, 2002; Mark and Zelanko, 2001). In retreat mining, the roof above the intersection should remain stable until after the pillars have been extracted. Leaving a final stump with proper size can reduce the risk of roof fall. The optimum size of the final stump should be large enough to provide effective support to the roof above the intersection but small enough not to prevent the main roof from caving.

CONCLUSION

Uncontrolled roof falls is the reason behind many hazardous accidents in room and pillar coalmines, especially during retreat mining. There are many parameters that influence roof falls during retreat mining. These parameters can be divided into three categories: geological, design, and operational parameters. To be aware of these parameters and their roles on roof fall can help mining engineers and designers to discover these hazardous circumstances and prevent hazards. These parameters can be divided into the uncontrollable and controllable categories. Uncontrollable parameters, such as geological parameters, reflect the ground conditions and cannot be changed. By applying preventive measures roof fall risk can be controlled to some extent. Controllable parameters, such as design and operational parameters, respond to ground conditions in order to perform the mining operation. These parameters are changeable, and the roof fall risk can be decreased to an acceptable degree by using them in the design and implementation stages of retreat mining.

REFERENCES

Barczak, T.M. and Gearhart, D.F. (1997).“Full-scale performance evaluation of mobile roof supports.” In: *Proceedings of the New Technology for Ground Control in Retreat Mining*. Pittsburgh, PA: NIOSH, pp. 99–126.

Bieniawski, Z.T. (1987). Strata control in mineral engineering. Hoboken, NJ: Wiley, pp. 212.

Chase, F.E., McComas, A., Mark, C., and Goble, C.D. (1997).“Retreat mining with mobile roof supports.” In: *Proceedings of the New Technology for Ground Control in Retreat Mining*. Pittsburgh, PA: NIOSH, pp.74–88.

Deb, D. (2003). “Analysis of coal mine roof fall rate using fuzzy reasoning techniques.”*International Journal of Rock Mechanics and Mining Sciences 40*: 251–257.

Department of Mineral Resources (1992).*Manual on pillar extraction in NSW underground coal mines*. New South Wales, Australia: Department of Mineral Resources, Coal Mining Inspectorate and Engineering Branch, pp. 106.

Düzgün, H.S.B. (2005). “Analysis of roof fall hazards and risk assessment for Zanguldak coal basin underground mines.”*International Journal of Coal Geology 64*(1–2): 104–115.

Düzgün, H.S.B. and Einstein H.H. (2004).“Assessment and management of roof fall risks in underground coal mines.”*Safety Science 42*(1): 23–41.

Feddock, J.E. and Ma, J. (2006).“Safety: a review and evaluation of current retreat mining practices in Kentucky.” In: *Proceedings of the 25th International Conference on Ground Control in Mining*. Morgantown, WV: West Virginia University, pp. 366–373.

Ghasemi, E., Ataei, M., and Shahriar, K. (2011).“Prediction of roof fall rate in coal mines using fuzzy logic.” In: *Proceedings of the 30th International Conference on Ground Control in Mining*. Morgantown, WV: West Virginia University, pp. 186–191.

Ghasemi, E. and Shahriar, K. (2012).“A new coal pillars design method in order to enhance safety of the retreat mining in room and pillar mines.”*Safety Science 50*(3): 579–585.

Ghasemi, E., Shahriar, K., and Sharifzadeh, M. (2010).“A new method for risk assessment of pillar recovery operation.”*Safety Science 48*(10): 1304–1312.

Jeffrey, L.S. (2002). “Impact of geotechnical factors on the secondary extraction of coal in the Witbank and Northern Highveld Coalfields, specifically related to safety.”In: *Proceedings of the Safety in Mines Research Advisory Committee COL810* (April): pp. 1–48.

Lind, G.H. (2002). “Key success elements of pillar extraction in New South Wales.”*Journal of the South African Institute of Mining and Metallurgy May/June*: 199–206.

Lind, G.H. (2005). “Risk management of underground coal pillar extraction in South Africa.”*International Journal of Surface Mining, Reclamation and Environment 19*(3): 218–233.

Mark, C. and Chase F.E. (1997).“Analysis of retreat mining pillar stability (ARMPS).” In: *Proceedings of the New Technology for Ground Control in Retreat Mining*. Pittsburgh, PA: NIOSH IC 9446, pp. 17–48.

Mark, C., Chase, F.E., and Pappas, D.M. (2003).“Reducing the risk of ground falls during pillar recovery.”In: *Proceedings of the Society for Mining, Metallurgy, and Exploration, Inc. Annual Meeting and Exhibit.* Littleton, CO: SME, pp. 1–9.

Mark, C., Karabin, G., Zelanko, J.C., Hoch, M.T., and Chase, F.E. (2002).“Evaluation of pillar recovery in southern West Virginia.” In: *Proceedings of the 21st International Conference on Ground Control in Mining*. Morgantown, WV: West Virginia University, pp. 81–89.

Mark, C. and Molinda, G.M. (2005).“The coal mine roof rating (CMRR)—a decade of experience.”*International Journal of Coal Geology 64*(1–2): 85–103.

Mark, C., Pappas, D.M., and Barczak, T.M. (2009).“Current trends in reducing ground fall accidents in US coal mines.”In: *Proceedings of the Society for Mining, Metallurgy, and Exploration, Inc. Annual Meeting and Exhibit.* Littleton, CO: SME, pp. 1–5.

Mark, C. and Zelanko, J.C. (2001).“Sizing of final stumps for safer pillar extraction.” In: *Proceedings of the 20th International Conference on Ground Control in Mining*. Morgantown, WV: West Virginia University, pp. 59–66.

Mark, C. and Zelanko, J.C. (2005).“Reducing roof fall accidents on retreat mining sections.”*Coal Age 110*(12): 26–31.

Molinda, G.M., Mark, C., Bauer, E.R., Babich, D.R., and Pappas, D.M. (1998).“Factors influencing intersection stability in US coal mines.” In: *Proceedings of the 17th International Conference on Ground Control in Mining*. Morgantown, WV: West Virginia University, pp. 267–275.

Molinda, G.M., Mark, C., and Dolinar, D. (2000).“Assessing coal mine roof stability through roof fall analysis.” In: *Proceedings of the New Technology for Coal Mine Roof Support*. Pittsburgh, PA: NIOSH IC 9453, pp. 53–71.

Molinda, G.M., Mark and C. (1994).*The coal mine roof rating (CMRR): a practical rock mass classification for coal mines*. Washington, D.C.: US Department of Interior, Bureau of Mines: pp. 83.

Mine Safety and Health Administration (MSHA) (2008). Available from: <http://www.msha.gov/S&HINFO/PROP/PROPBulletins/2008/Retreat%20Mini-ng%20 Flyer.pdf>.

Palei, S.K. and Das, S.K. (2009).“Logistic regression model for prediction of roof fall risks in bord and pillar workings in coal mines: an approach.”*Safety Science 47*(1): 88–96.

Peng S.S. (2008). *Coal mine ground control*. 3rd edition. Morgantown, WV: West Virginia University, pp. 750.

Santos, C.F. and Bieniawski, Z.T. (1989).“Floor design in underground coal mines.”*Rock Mechanics and Rock Engineering 22*(4): 249–271.

van der Merwe, J.N., van Vuuren, J.J., Butcher, R., and Canbulat, I. (2001). “Causes of falls of roof in South African collieries.”In: *Proceedings of the Safety in Mines Research Advisory CommitteeCOL613*(March): pp. 1–117.

Application of Neuro–Fuzzy Technique in Mine Support System for Ground Control

Sudhir Kumar Kashyap, Principal Scientist
Support Development & Testing Division
Central Institute of Mining and Fuel Research, CSIR (Ministry of Science & Technology, Govt. of India)
Barwa Road, Dhanbad, India

Dayal Ramakrishna Parhi, Professor
National Institute of Technology
Rourkela, India

Amalendu Sinha, Director
Cimfr, Dhanbad
Central Institute of Mining and Fuel Research
Barwa Road, Dhanbad, India

ABSTRACT

In underground activities ground control is a challenging problem. It affects safety, production, and efficiency. As per statistics of accident data, “fall of roof/sides” is one of the major causes of mine accidents. In many cases, our experiences and understanding of soil and rock behavior still fall short of being able to predict how the ground will behave. Presently, empirical approaches to design are widely used in estimating mine support parameters. Under these circumstances, expert judgment plays an important role, and such accidents can be obviated with accurate measurement and optimization of data and analysis using the neuro-fuzzy technique of artificial intelligence.

Recently, a neuro-fuzzy hybrid approach has become one of the major areas of interest in engineering fields because it gets the benefits of neural networks as well as those of fuzzy logic systems, and it removes the individual disadvantages by combining them on the common features. Neural network and fuzzy logic technologies have common features, such as a distributed representation of knowledge, the ability to handle data with uncertainty and imprecision, etc., like in ground control. Fuzzy logic technique has tolerance for imprecision of data, while neural networks have tolerance for noisy data.

In this paper we have focused an intelligent technique, i.e., neuro-fuzzy technique, to approximate the setting load given to the standing support (props) erected for the purpose of supporting freshly exposed roof during underground mining. We have used twelve input variables of rock parameters, and after having trained using a neural network with a sigmoidal function as an activation function, simulation was done to find the output parameter, i.e., the pre-load (setting load)to be applied on props. Outputs of the neural network were again fed to the fuzzy system together with the twelve parameters, incorporating five triangular membership functions for each parameter. Final optimum output was approximated using the MATLAB program, which was found to be satisfactory. Neuro-fuzzy technique has better performance over individual neural networks or fuzzy logic technique.

INTRODUCTION

Exploitation of coal with proper safety in India has been a big problem for many years. In terms of the method of coal excavation, the share of opencast mining, which was as low as 14% in 1951, increased to current high level of above 80%, whereas the share of underground mining declined from 77% in 1971, to its current 20%. Even so, we can’t ignore the underground mine coal production due to its superior quality of coal as well as for societal causes i.e. rehabilitation of people living in mine surrounding areas. In underground mining, ground control is an important activities affecting safety, production, and efficiency.

In terms of number of mines in India, there are about 595 operating mines, and about 384 are underground mines. In underground coal mining technology, bord and pillar mining is one of the major methods being used in India, accounting for about 91% of the underground coal production and employing about 57% of total work force. As per statistics of accident data, “fall of roof/sides” is one of the major causes of mine accidents. A major consideration in supporting mine roofs is limiting the movement and expansion of the rock strata immediately above the roof. Cause-wise analysis of mine accidents reveals that roof falls continue to remain the single largest killer. As many as 61% of the incidences, which is 28.5% of total fatalities, are due to roof fall. Such accidents can be minimized to a great extent with accurate measurement and optimization of data and its analysis using artificial intelligence. Since artificial intelligence (AI) techniques can make use of heuristic knowledge (rules of thumb), or pattern matching techniques, as opposed to solving a set of mathematical equations, they should be ideally suited for application in the field of geotechnical engineering. Many aspects of mine design are based upon empirical data. The availability of data and knowledge are two important considerations in implementing many engineering and scientific applications.

The techniques of AI that are adopted here include Artificial Neural Network (ANN), Fuzzy Logic Technique, and its hybridization, Neuro-Fuzzy Technique.

DATA SETS

Inputs

- Rock mass rating (RMR)
- Distances of the props from the face (six inputs)
- Working height
- Rock density
- Seam thickness
- Width of gallery
- Charge per blasting hole

Output

- Setting load on prop

Sample data were taken arbitrarily for training the ANN by back propagation neural network (BPNN). In this case, log-sigmoid has been used as transfer function.

Output data, i.e., an appropriate setting load, can be estimated with the available input data after simulation through the neuro-fuzzy hybrid technique. Sample datasets are shown in Table 1.

Table 1. Sample field data for training.

Sl.No.	Parameters	Set 1	Set 2	Set 3	Set 4	Set 5	Set 6	Set 7	Set 8	Set 9	Set 10
1.	RMR	42	55	43	56	42	57	49	38	58	47
2.	Distance of first prop from the face (d1) (m)	0.6	0.8	0.4	0.6	0.4	0.6	0.8	0.8	0.6	0.6
3.	(d2)	1.2	1.4	1.0	1.0	0.8	1.2	1.2	1.2	1.2	1.4
4.	(d3)	1.8	2.0	1.6	1.4	1.2	1.8	1.6	1.6	1.8	2.2
5.	(d4)	2.4	2.6	2.2	1.8	1.6	2.4	2.0	2.0	2.4	3.0
6.	(d5)	3.0	3.2	2.8	2.2	2.0	3.0	2.4	2.4	3.0	3.8
7.	(d6)	3.6	3.8	3.4	2.6	2.4	3.6	2.8	2.8	3.6	4.6
8.	Working Height (m)	2.7	2.6	3.0	2.4	2.6	4.5	3.0	4.5	3.0	3.0
9.	Rock Density(gm/cc)	2.2	3.0	2.4	2.8	2.6	2.2	2.4	3.0	2.3	2.8
10.	Seam Thickness (m)	3.4	4.1	4.8	3.4	3.8	4.8	4.4	6.4	3.6	3.6
11.	Width of Gallery (m)	4.2	4.2	4.5	4.2	4.2	4.2	4.0	4.2	4.2	4.2
12.	Charge per Hole (g)	400	400	450	450	400	500	400	400	500	600
13.	**Target** – Setting load on standing prop (1) (Ton)	09	07	10	06	10	07	08	10	06	08

ARTIFICIAL NEURAL NETWORK

Artificial neural networks analyze data and make predictions based on previous results. Neural networks have advantages over conventional empirical design approaches because they use observable data and knowledge. Past research in this technique establishes that artificial neural networks are effective and efficient computational processors for performing a variety of problems, including pattern recognition, classification, combinatorial problem solving, noise filtering and data compression, modeling, and forecasting.

Neural networks are able to detect similarities in inputs, even though a particular input may never have been seen previously. This property allows for excellent interpolation capabilities, especially when the input data are noisy (not exact). Neural networks, with their remarkable ability to derive a general solution from complicated or imprecise data, can be used to extract patterns and detect trends that are too complex to be noticed by either humans or other computer techniques. A trained neural network can be thought of as an "expert" in the category of information it has been given to analyze. The particular network is a supervised learning, as shown in Figure 1.

A neural network is a parallel-distributed processor comprising several simple computational units known as neurons. Figure 2 shows the model of a neuron. A neuron model can be identified by three basic elements:

- A set of synapses or connecting links, each of which is characterized by a weight or strength of its own. Specifically, a signal x_j at the input of synapse "j" connected to neuron "k" is multiplied by synaptic weight w_{kj}.
- An adder for summing the input signals after they have been weighted by the respective synapses of the neuron.
- An activation function is used for transforming the result of the adder and limiting the amplitude of the output of a neuron. Generally, the normalized amplitude range of the output of a neuron is given as the closed unit interval [0,1] or alternatively [-1,1]

Mathematically, neuron k can be described by the following two equations:

$$u_k = \sum_{j=1}^{p} w_{kj} x_j \quad (1)$$

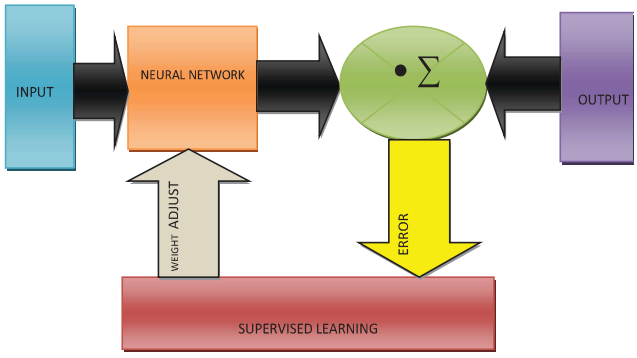

Figure 1. Supervised learning.

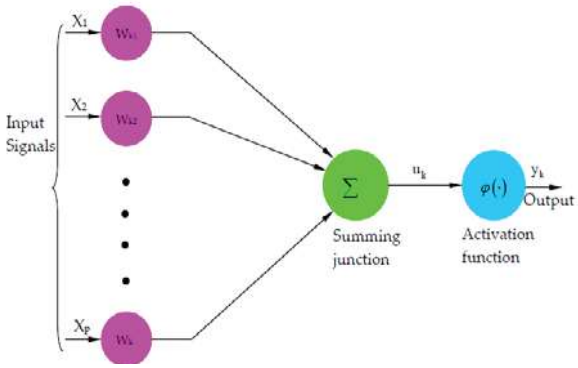

Figure 2. Model of a neuron.

$$x_k = \varphi(u_k) \quad (2)$$

where

$x_1, x_2, \ldots, x_p$ are the input signals;

p is the number of input signals;

$w_{k1}, w_{k2}, \ldots, w_{kp}$ are the synaptic weights of neuron k;

u_k is the output of the adder;

φ(.) is the activation function; and

y_k is the output signal of the neuron.

The activation function, denoted by φ(.), defines the output of a neuron in terms of the activity level at its input. In this research, the activation function that is used is the Sigmoidal function. A neural network resembles the brain in two respects:

- Knowledge is acquired by the network through a learning process.
- Inter-neuron connection strengths known as synaptic weights are used to store the knowledge.

The procedure used to perform learning is called a learning algorithm, the function of which is to modify the synaptic weights of the network in an orderly fashion so as to attain a desired design objective.

The artificial neural network that was used here is six-layers perceptrons. This number of layers has been found to ease the training of the network. The input layer has twelve neurons, each representing one of the parameters specified as an input in the data set. The output layer has single neuron, which produces the setting load. The first, second, third and fourth hidden layer shave30, 14, 7, and 4 neurons, respectively. These numbers of hidden layers were found empirically. Figure 3 depicts the neural network with its input and output signals.

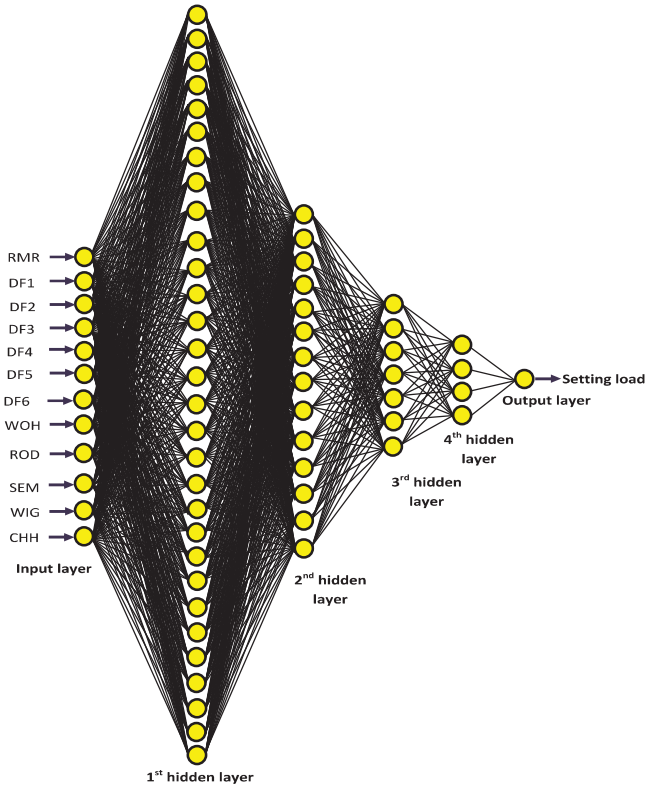

Figure 3. Neural network controller.

The neural network is trained to estimate the setting load to be applied to the respective prop.

In Figure 3 the input parameters are as follows:

1. RMR: Rock mass rating
2. DF1: Distance of 1st prop from the face
3. DF2: Distance of 2nd prop from the face
4. DF3: Distance of 3rd prop from the face
5. DF4: Distance of 4th prop from the face
6. DF5: Distance of 5th prop from the face
7. DF6: Distance of 6th prop from the face

8. WOH: Working height
9. ROD: Rock density
10. SEM: Seam thickness
11. WIG: Width of gallery
12. CHH: Charge per hole

The neural network is trained to estimate the setting load to be applied on the first prop from the face. The amount of setting load to be given can be predicted on other props also. Table 2 shows the setting load applied at the mine and also estimated with the neural network technique in first prop.

Table 2. Setting load obtained after simulation by neural network.

Serial Nos.	Parameters	At mine site (Ton)	By neural network technique (Ton)
1.	Setting load on first prop from face	9	9.7
2.		7	7.1
3.		10	9.1
4.		6	6.0
5.		10	8.9
6.		7	7.0
7.		8	8.4
8.		10	9.3
9.		6	6.0
10.		8	8.0

By simulation it is seen that the setting load obtained from the ANN technique varies by 4.11% with the real mine data.

FUZZY LOGIC THEORY

Professor Lofti Zadeh (1992) of the University of California at Berkeley is the father of fuzzy logic. According to his theory, for all worldly natural systems, a mathematics of fuzzy and cloudy quantities is needed. Fuzzy logic states that fuzzy sets i.e. vague linguistic statements of an activity, whose characteristics have elements belonging to them only to some degree according to a membership function with values between 0 and 1. The fuzzy logic theory is one of the tools to handle any uncertain and unpredictable activities like those in mining. The fuzzy sets can be considered as a more fruitful tool for the modeling of human reasoning to minimize uncertainties.

Many scientific, engineering, and industrial problems have an uncertain nature that cannot be appropriately solved by classical analytical methods in a reasonable way. The reason behind the difficulties often lies in the blurred boundaries of the involved system properties and, therefore, exact mathematical representation. For this, fuzzy sets arethe true alternative. It is represented as follows.

Consider a data set X, which has N number of variables or parameters as follows:

$X = \{X_1, X_2 \ldots\ldots X_N\}$

The fuzzy set is defined by assigning to each individual variable a value between 0 and 1, i.e., a membership function;0 being absolute uncertainty and 1 being complete certainty.

Mathematically,

Fuzzy set $A = \{\mu_A(X_1), \mu_A(X_2) \ldots\ldots \mu_A(X_N)\}$.

Where

$\mu_A(X_i)$ is the membership grade of the variable Xi and is

defined as

$\mu_A(X_i) \rightarrow [0,1]$ I = 1,2……N

Alternatively,

$0 \leq \mu(X_i) \geq 1$

An analysis of mine support data and an estimation of setting load using a fuzzy logic controller is depicted in Figure 4. In this research a triangular membership function is considered. For each of the 12 input parameters5 linguistic variables are considered. Thus, the total number of possible rules is:

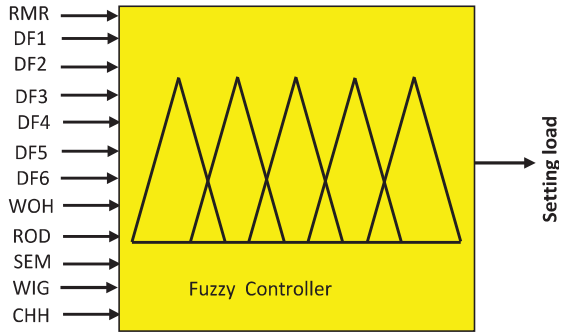

Figure 4. Fuzzy logic controller for estimation of setting load.

5x5x5x5x5x5x5x5x5x5x5x5 = 244140625 = 5^{12}

or,

(Memberslip function)$^{(Nosof\ input\ parameters)}$

With 12 input parameters, the setting load on the first prop, i.e. the output, is estimated.

With 12 inputs, one output, and five membership functions at each input, the total number of rules mentioned above is too large. With so many rules, many may not contribute significantly to the problem. Therefore, good judgment is needed to eliminate unnecessary rules. Some of the rules for the above mentioned 12 parameters are depicted in Table 3. By varying the various input parameters, the required setting load is known for the first prop, which is nearer to the blasting face. The setting loads for the other props may be found in a similar fashion.

Table 3. Fuzzy Rules for simulation by fuzzy logic.

Sl.Nos.	If INPUT parameters												Then OUTPUT parameters
	Rock mass rating (RMR)	Distance of 1st prop (DF1)	Distance of 2nd prop (DF2)	Distance of 3rd prop (DF3)	Distance of 4th prop (DF4)	Distance of 5th prop (DF5)	Distance of 6th prop (DF6)	Working height (WOH)	Rock density (ROD)	Seam thickness (SEM)	Width of gallery (WIG)	Charge per hole (CHH)	
1.	MER	VND	MED	NED	VHD	VND	NED	VLH	HRD	VHT	HIW	MEC	VLS
2.	VHR	VND	VND	VND	VHD	HID	NED	VLH	LRD	VHT	HIW	VHC	MES
3.	VHR	VHD	MED	HID	NED	NED	HID	VLH	HRD	VHT	MEW	VHC	LOS
4.	VLR	VND	MED	MED	HID	HID	HID	MEH	MRD	LOT	MEW	VHC	MES
5.	VLR	MED	VND	VND	MED	MED	MED	MEH	HRD	VHT	VLW	VLC	HIS
6.	VLR	VHD	MED	NED	HID	MED	NED	MEH	VLD	VHT	VHW	VHC	HIS
7.	VLR	VND	VND	VND	VND	VHD	NED	MEH	HRD	LOT	MEW	VHC	HIS
8.	VHR	VND	MED	HID	VHD	NED	MED	VHH	HRD	VHT	MEW	VHC	MES
9.	VLR	VND	VND	VND	VND	VHD	NED	MEH	HRD	LOT	MEW	VHC	HIS
10.	MER	VND	VND	VND	VND	VHD	NED	MEH	HRD	LOT	MEW	VHC	MES

A series of simulation tests were conducted with the different parameters. The fuzzy logic controller successfully gives the result by choosing any number of input parameters out of the 12 variables. A new intelligent controller using fuzzy logic has been proposed for predicting the setting load applied on the prop nearest to the blasting face. It is more efficient than the other traditional reactive behavior controls and also easier to design and implement. Linguistic variables were represented in the fuzzy rules. Setting load on the prop nearest to the blasting face was defuzzified, and the estimated load obtained was compared with the practical setting load that was applied at mine site, as shown in Table 4

Table 4. Setting load obtained after simulation by Fuzzy Logic.

Serial Nos.	Parameters	Setting load applied on prop at mine site (Ton)	Setting load on prop by fuzzy logic technique (Ton)
1.	Twelve nos. of input parameters	9	9.5
2.		7	7.0
3.		10	9.0
4.		6	5.8
5.		10	10
6.		7	7.5
7.		8	8.1
8.		10	9.1
9.		6	5.8
10.		8	8.0

Simulations show that setting load obtained from fuzzy logic technique has an average percentage variation of 3.96 with real mine data.

NEURO-FUZZY TECHNIQUE

A hybrid model employing a combination of an artificial neural network and a fuzzy system produces better results. For a robust intelligent system, various hybridization with the different techniques of artificial intelligence are quite necessary. The neuro-fuzzy model, which involves the integration of ANN and FL techniques, is perhaps the most popular hybrid technique used in engineering problems. The ANN technique is usually used as the learning algorithm for the defuz zification process in FL-based models. Neuro-fuzzy models are able to take advantage of the fuzzy inference mechanism capabilities in fuzzy logic and the learning ability of neural networks. In hybrid the neuro-fuzzy system model, both the learning capabilities of a neural network and the reasoning capabilities of fuzzy logic were combined in order to give enhanced prediction capabilities when compared to using a single methodology alone.

The neuro-fuzzy technique developed here consists of a pre-processor using a back propagation neural network followed by a fuzzy logic controller. Figure 5 depicts the neuro-fuzzy controller and highlights the details of the neurons with its inputs and output signal with a fuzzy controller. The neural network used here is also a back propagation multilayer perceptron, having six layers. The input layer has 12neurons. The output layer has a single neuron meant to produce the setting load on the prop. The output of the neural network (the first estimate of the setting load) is fed to the fuzzy controller along with the information concerning the various mine support geological parameters. The output of the fuzzy controller is to compute the setting load to be applied to the standing prop. From the fuzzy logic controller it was concluded that the triangular membership function is the best among other membership functions for this type of problem. Therefore, the triangular membership function is used in the fuzzy controller. The neuro-fuzzy technique has been demonstrated in simulation mode, which showed that the prop was applied the required load so that it does not dislodge after blasting of the working face. Among the techniques developed, the neuro-fuzzy technique is found to be most efficient for prediction of setting load to be given to the respective prop. Practical data verifications have been done with the simulation results to prove the authenticity of the developed neuro-fuzzy technique.

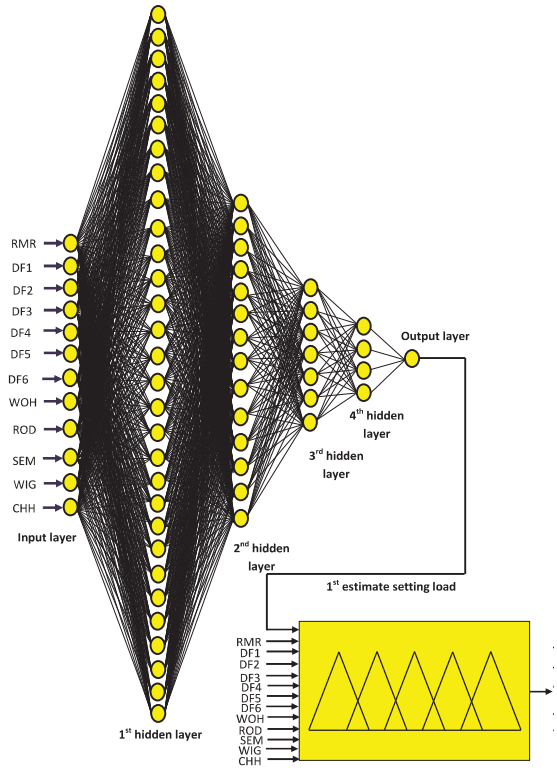

Figure 5. Neuro-fuzzy controller.

Some of the fuzzy rules that contribute significantly are depicted in Table 5 for the 12 parameters. The estimated setting load from the neural network is fed to the fuzzy controller as the 13th input parameter. Thus, the final output setting load is obtained with the neuro-fuzzy controller. By varying the various input parameters, the required setting load is found for the first prop that is nearest to

the blasting face. The setting load to be applied on the other props may be foundi n a similar fashion.

The series of simulation tests were conducted with the different parameters. The neuro-fuzzy controller successfully gives the comparatively better result than that of fuzzy logic alone. Thus, a new intelligent hybrid controller has been proposed for predicting the setting load applied on the nearest prop to the blasting face. It is more efficient than the other traditional reactive behavior control and also easier to design and implement. In this technique, with the help of a trained neural network, fuzzy rules linguistic variables were also represented. Setting load on the prop nearest the blasting face was defuzzified, and the estimated load obtained was compared with the practical setting load that was applied at mine site, as shown in Table 6.

By simulation it is seen that setting load obtained from neuro-fuzzy technique has an average percentage variation of 1.49 with real mine data.

CONCLUSIONS

A hybrid model employing a combination of an artificial neural network and a fuzzy system produces better results for estimating the setting load on a prop. The neuro-fuzzy model, hybridization of neural network and fuzzy logic techniques of artificial intelligence is perhaps the most popular hybrid technique used in engineering problems. The ANN technique uses a learning algorithm for the defuzzification process in FL-based models. In the fuzzy logic technique, human experience is modeled. . In the hybrid neuro-fuzzy system model, both the learning capabilities of neural network and the reasoning capabilities of fuzzy logic were combined in order to give enhanced prediction capabilities when compared to using single methodology alone.

Thus, neuro-fuzzy technique is the most appropriate and efficient technique for simulating parametric data obtained from underground excavations to get optimal solutions i.e. setting load to be applied on the prop near the blasting face. The average percentage variation in simulation through MATLAB in case of ANN was 4.11;fuzzy logic technique had a percentage variation of 3.96; and neuro-fuzzy technique had a percentage variation of 1.49.

ACKNOWLEDGEMENT

The authors are thankful to the Director, CIMFR, Dhanbad, India, for his kind permission to publish this work

REFERENCES

Bieniawski, Z.T.(1989).*Engineering Rock Mass Classifications*. New York: John Wiley & Sons.

Huang, Y., Wanstedt, S.(1997). "The use of artificial neural networks for the delineation of boundaries between ore bodies based on geophysical logging data."*Mineral Resources Engineering*.*6*(1):1–15.

Kashyap, S.K., Parhi, D.R, Sinha, A., Singh, M.K., Singh, B.K. (2008)."Optimisation of mine support parameters using Neural Network approach." Presented at the 12th IACMAG. Goa, India: October1–6.

Kim, Y.S., Kim, B.T.(2007). "Prediction of relative crest settlement of concrete-faced rockfill dam analyzed using an artificial neural network model." *Computers and Geotechnics*.*34*(6):423–434.

Lu,Y.(2005). "Underground blast induced ground shock and its modeling using artificial neural network." *Computers and Geotechnics*.*32*:164–178.

Parhi, D.R.,Kashyap, S.K.,Sinha, A.(2011). "Neuro-fuzzy controller for prediction of setting load for standing support in underground mine."*International Journal of Artificial Intelligence and Computational Research*.*3*(1):39–41.

Simpson, P.K.(1990).*Artificial Neural System—Foundation, Paradigm, Application and Implementation*. New York: Pergamon.

Tettamanzi, A.,Tomassivi, M. (2001).*Soft Computing: Integrating Evolutionary, Neural, and Fuzzy System*.Berlin: Springer, pp. 201–211.

Zadeh, L.A.(1992).*Knowledge Representation in Fuzzy Logic: an Introduction to Knowledge Application in Intelligence Systems*. Boston: Kluwer Academic.

Table 5. Fuzzy rules for simulation through neuro-fuzzy.

Sl.Nos.	If INPUT parameters												Then OUTPUT parameters
	Rock mass rating (RMR)	Distance of 1st prop (DF1)	Distance of 2nd prop (DF2)	Distance of 3rd prop (DF3)	Distance of 4th prop (DF4)	Distance of 5th prop (DF5)	Distance of 6th prop (Df6)	Working height (WOH)	Rock density (ROD)	Seam thickness (SEM)	Width of gallery (WIG)	Charge per hole (CHH)	
1.	MER	VND	MED	NED	VHD	VND	NED	VLH	HRD	VHT	HIW	MEC	VLS
2.	VHR	VND	VND	VND	VHD	HID	NED	VLH	LRD	VHT	HIW	VHC	MES
3.	VHR	VHD	MED	HID	NED	NED	HID	VLH	HRD	VHT	MEW	VHC	LOS
4.	VLR	VND	MED	MED	HID	HID	HID	MEH	MRD	LOT	MEW	VHC	MES
5.	VLR	MED	VND	VND	MED	MED	MED	MEH	HRD	VHT	VLW	VLC	HIS
6.	VLR	VHD	MED	NED	HID	MED	NED	MEH	VLD	VHT	VHW	VHC	HIS
7.	VLR	VND	VND	VND	VND	VHD	NED	MEH	HRD	LOW	MEW	VHC	HIS
8.	VHR	VND	MED	HID	VHD	NED	MED	VHH	HRD	VHT	MEW	VHC	MES
9.	VLR	VND	VND	VND	VND	VHD	NED	MEH	HRD	LOW	MEW	VHC	HIS
10.	MER	VND	VND	VND	VND	VHD	NED	MEH	HRD	LOW	MEW	VHC	MES

Table 6. Setting load obtained after simulation by Neuro-Fuzzy.

Serial Nos.	Parameters	Setting load applied on prop at mine site (Ton)	Setting load on prop by neuro-fuzzy technique (Ton)
1.	Twelve nos. of input parameters	9	9.01
2.		7	7
3.		10	10
4.		6	6.2
5.		10	9.9
6.		7	7.2
7.		8	8
8.		10	9.4
9.		6	5.9
10.		8	8.0

Determination of the Strength of Powered Roof Supports According for Fatigue Life

Monika Patrycja Polak - Micewicz, Master of Science Engineering
Designer, Doctoral Students
Fazos Co. LW Support System The Opole University of Technology, faculty of Mechanical Engineering
Tarnowskie Góry, Poland

Tadeusz Łagoda, Prof.Phd. Eng.
The Opole University of Technology, faculty of Mechanical Engineering
Opole, Poland

Abdul Wahab Khair, Professor Emeritus
Department of Mining Engineering West Virginia University
Morgantown, WV

ABSTRACT

This paper presents an approach for estimating the fatigue life for the base of powered roof supports (shield) manufactured by the FAZOS roof support company. FAZOS's powered roof supports are designed to operate on an inclined coal seam in full caving with a medium, strong roof strength. This shield support is utilized in conjunction with a shearer and face conveyor for a complete longwall mining system. To design shield support, it is essential for contractor to know the physical (hardness, toughness, etc.) and mechanical properties of material (tensile strength, Young's modulus, etc.) used for the shield support as well as the geotechnical properties of the mine site. The fatigue strength of the shield support material depends on the mean stress, alternating stress, cycle frequency, transport dimensions, mine environment and other factors. In order to estimate the fatigue life for a powered roof support system, it is assumed in this paper that the support must keep the roof stable in the mine under variable load cycles. The approach selected in this study contains Goodman's model (Goodman, 1899) for all blocks in the design housing which is subjected to sinusoidal load. On this basis, the degree of fatigue damage was calculated and compared to the results of experimental tests. It will be shown that there is a significant detrimental effect on the fatigue life of the base of the powered roof supports due to geometrical notches. The Ramberg-Osgood model and damage accumulation rule (Palmgren-Miner) (Miner M., 1945) were used and numerical analyses were conducted, utilizing ANSYS finite element software. These analyses play a very important role in longwall casing design. The proposed method allows assessment of the yield state and forecast of the structure cracking, taking plastic strains occurrence into account. The presented method is universal and can be applied for fatigue life estimation of other subassemblies of powered roof supports. The final portion of the paper presents results of variable amplitude loading simulations on the S355N and S690Q steel used to make powered roof supports. The results of the physical tests were compared with the results from finite element methods. The proposed approach to calculate fatigue life gives the best correlation between the experimental results and calculated values of fatigue life for the powered roof support base. Finally, the design process uses a simple approach to predict fatigue life in a short time, reducing design costs and providing longer service life for roof supports.

INTRODUCTION

A designer of powered roof supports should consider many factors that influence optimization of the structure and costs of manufacturing. Each FAZOS-produced powered roof support must obtain a certificate permitting its use in a mine. Thus, it is necessary to perform standard tests in order to control the real state of the structure strength under its overload. A optimum structure design should consider both static and fatigue strength. Computer programs based on the finite element method are irreplaceable for strength calculations and design properties selection for FAZOS powered roof supports (Polak, Łagoda, 2010).

The considered roof support is applied a caving longwall face accompanied by a full roof caving. Service loads acting on the sections are usually variable and cause material fatigue.Fatigue damage develops as two stages, first, the initiation process proceeds in the range of elastic strain of the material, and next the damage propagates in the area of plastic strains.

The problems connected with powered roof support design are widely discussed in literature (Peng, 1978, Barczak, 1992); however, there are some problems which remain unidentified, such as variety of supports related to a correct number of fatigue cycles, and asymmetry of the supports associated with such problems.

This paper presents a new algorithm approach that includes cyclic fatigue tests based on numerical analyses. This paper also contains verification of the results of experiments performed in a certificating unit – the experimental results compared with the results of numerical tests. The comparison was a basis for the calculation method for subassemblies included into the FAZOS powered roof support.

EXPERIMENTS

A powered roof support including a rigid, "catamaran" type base, caving shield (gob shield), canopy and lemniscates linkages (two front and two rear link) was subjected to tests. The section (shield) was tested at the minimum height of expansion (Figure 1). Twenty strain gauges (SGD-6/120-RYB21) were placed in critical pointsas determined by means of numerical simulations. The tests were performed at the Technical Laboratory in Opava,

the Czech Republic; they were performed up to the structure damage stage (European Standards PN-EN 1804-1). When cracks occurred, the tests were completed and the life of the powered roof support was determined. The section of the powered roof support was placed in a stationary steel frame influenced by cyclic loading (Szweda, 1996). Cyclic loading was applied by means of pressure in hydraulic props, and it ranged from 0.25 to 1.05 times the rated shield capacity. A history of legs pressure variation for asymmetric support of the sectionis shown in Figure 2.The results of the experiments were used for determination of elastic and elastic-plastic stresses (Jaszczuk, 2009) according to the following equations:

Figure 1. FAZOS's powered roof support during the experimental test in the Opava (Czech Republic) Technical Laboratories.

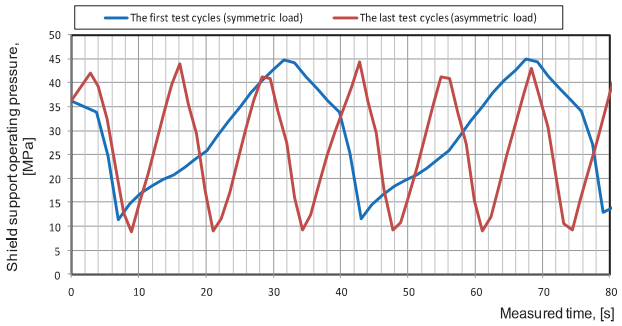

Figure 2. Pressure changes in the hydraulic leg during the test.

$$\varepsilon_{rz} = \varepsilon_{ae} + \varepsilon_{ap} \tag{1}$$

where:

ε_{rz} – amplitude of total strain,

ε_{ae} – amplitude of elastic strain,

ε_{ap} – amplitude of plastic strain.

The cyclic stress-strain curve was determined from the Ramberg-Osgood equation:

$$\varepsilon_{rz} = \frac{\sigma_a}{E} + \left(\frac{\sigma_a}{K'}\right)^{1/n'} \tag{2}$$

where:

ε_{rz} – amplitude of total strain,

σ_a – amplitude of stress,

K' - cyclic strength coefficient,

n' – exponent of the cyclic strain hardening.

The following material properties were assumed: for steel S355N: K'=635[MPa](92,098 psi), n'=0.096, and for steel S690Q: K'=1065[MPa] (15,4465 psi.), n'=0.050. At the next step, the strain range was determined from Equation (3):

$$\Delta\varepsilon_{rz} = \varepsilon_{max} - \varepsilon_{emi}n \tag{3}$$

where:

$\Delta\varepsilon_{rz}$ - total strain range,

ε_{max} - maximum strain,

ε_{min} - minimum strain.

From Equation 2 and 3, Equation (4) can be developed:

$$\Delta\varepsilon_{rz} = \frac{\Delta\sigma_{rz}}{E} + \left(2 \cdot \left(\frac{\Delta\sigma_{rz}}{2 \cdot K'}\right)^{1/n'}\right) \tag{4}$$

where:

n' - cyclic strain hardening exponent,

E - modulus of elastic (Young).

The next step includes a determination of the arithmetic mean of the cycle amplitude and the mean value of the cycle amplitude for particular loading blocks. The transformed amplitude of stress is determined according to the Goodman criterion:

$$\frac{\sigma_a}{\sigma_{af}} + \frac{\sigma_m}{R_m} = 1 \tag{5}$$

where:

R_m – strength of the materials: (690[MPa] and 355[MPa]),

σ_{af} – amplitude of transformed stress.

The basic fatigue characteristic of the considered materials must be known in order to define the fatigue characteristic under random stress states. For this purpose, the Basquin equation was applied:

$$\log N_f = a + b\log \sigma_a \tag{6}$$

where:

N_f - cycles to failure,

a, b - parameters of material

When transformed amplitudes have been defined for all the measuring points, the Palmgren-Miner linear hypothesis (P-M) of fatigue damage accumulation is assumed. This hypothesis assumes that every applied fatigue cycle of defined parameters gives damage equal to total inverse of the number of cycles (Kocańda, 1997). This function can be written as:

$$S_{PM}(T_o) = \begin{cases} \sum_{i=1}^{j} \dfrac{n_i}{N_o \left(\dfrac{\sigma_{af}}{\sigma_{ai}} \right)^m} & \text{dla} \quad \sigma_{ai} \geq \sigma_{af} \\ 0 & \text{dla} \quad \sigma_{ai} < \sigma_{af} \end{cases} \tag{7}$$

where:

$S_{PM}(T_o)$ – degree of the material damage at time T_o

n_i – number of cycles with amplitudes σ_{ai} at T_o,

T_o – time of observation,

m – exponent of the fatigue curve S-N,

N_o – number of cycles corresponding to the fatigue limit σ_{af}.

The fatigue life is being defined up to the moment when it reaches value 1 (Łagoda, et al., 1998). It has been found that after 8,000 cycles, further damage takes place and weakens all the sections of the base. At the next step, the increases of stresses on internal and external braces were considered.

When the damage degree $S(N_{blok})$ is defined for each support block based on the general equation (7), the fatigue life (N_{cal}) is calculated according to the following formula:

$$N_{cal} = \frac{N_{block}}{S(N_{block})} \tag{8}$$

Structure of the powered roof support resisted up to29,000 cycles, and cracked near the holes, and the above calculations should be corrected. Figure 3 shows the crack point at the test stand.The obtained experimental data was applied for the correction of the calculation results; namely, the influence of the notch coefficient was included. Observation of the figure indicated that at the crack point, characteristic fatigue strips can be seen in all the sheet sections of the base. Figure4 presents a fragment of the crack with macroscopically visible strips confirming the fatigue character of the crack. Tables 1 and 2 contain the results of the final calculations for the point located on the lower sheet of the base.

DETERMINATION OF THE FATIGUE LIFE BASED ON NUMERICAL CALCULATIONS

A 3D numerical model of the shield was made using Inventor 2011 software. The result was a geometrical form represented by a network of finite elements (Figure 5). Solid elements of eight nodes were used for discretization. The model contained 17,1827 elements and 68,8515 nodes.

Numerical models were images of real objects, and all dimensions were input according to the technical documentation. A variety of supports, simulations were performed for all the loadings acting on the shield? at the test stand (Polak, Łagoda, 2010). Calculations were performed as static ones, so two analyses were performed for each support of the section (for the minimum and maximum loading). Before simulation in the program ANSYS DesignSpace v.12.1, it was necessary to assume material parameters (Karolczuk, Łagoda, 2002). The following initial properties were introduced before calculations: density, Young modulus, Poisson ratio and limit of elasticity. In the solid model, a simplified simulation of welded joints was applied (Eurocode 3). It insisted in omission of the weld profile. Example results of stress distribution calculations are presented in Figure 6. Simulation of the work shows that the dangerous area for fatigue life occurs near geometric notches and in the points of support. However, there are local stress concentrations (Molski, Glinka, 1981), and from verification with the experimental data it appears they do not strongly influence an increase of the section fatigue life.

The results for the reduced stresses (H-M-H) were drawn from the numerical simulation (Khair, 2004) and their amplitudes were determined. Pseudoelastic stresses (Neuber, 1968) were defined according to the Neuber relationship:

$$\frac{\sigma_{MES}^{\,2}}{2E} = \frac{\sigma_N^{\,2}}{2E} + \frac{\sigma_N}{2}\left(\frac{\sigma_N}{K'}\right)^{1/n'} \tag{9}$$

where:

σ_N – the searched stress value on the assumption of elastic-plastic behavior of the material.

σ_{MES} - the value of stresses read from Ansys (numerical program),

n' - cyclic strain hardening exponent,

E - modulus of elastic (Young).

Table1. Comparison between Analytical Study and Experimental Data for Fatigue Life of the Base, lower sheet.

Transformed Stress (Goodman) [MPa]	Read-out Number of Cycles	Observed Number of Cycles (laboratory)	Load Support According to the European Standard PN-EN 1804-1	Calculated Degree of Damage
425	**1.2000E+04**	**8000**	**A.1.1a lub A.1.2a+A6d lub A.6c**	**0.667**
470	1.8000E+03	2000	A.8	1.1 (crackingstart)
380	1.0400E+05	1000	A.2a+A.3b	0.010
350	5.0000E+05	2000	A.2a+A.3a	0.004
320	2.7740E+06	3000	A.1.1b lub A.1.2b+A.2a	0.001
315	3.7490E+06	1000	A.4a lub A.4c	~0.0
480	1.2000E+03	1000	A.4b lub A.4c	0.833

Table 2. Comparison between Analytical Study and Experimental Data for Fatigue Life of the Base, the inner side sheet.

Transformed Stress (Goodman) [MPa]	Read-out Number of Cycles	Observed Number of Cycles (laboratory)	Load Support According to the European Standard PN-EN 1804-1	Calculated Degree of Damage
4	**1.88307E+38**	**8000**	**A.1.1a lub A.1.2a+A6d lub A.6c**	**~0.0**
21	**1.88307E+38**	**2000**	**A.8**	**~0.0**
37	**2.76301E+34**	**1000**	**A.2a+A.3b**	**~0.0**
67	**9.21711E+27**	**2000**	**A.2a+A.3a**	**~0.0**
150	**1.41207E+19**	**3000**	**A.1.1b lub A.1.2b+A.2a**	**~0.0**
920	732	1000	A.4a lub A.4c	1.3 (crackingstart)
558	49000	1000	A.4b lub A.4c	0.0204

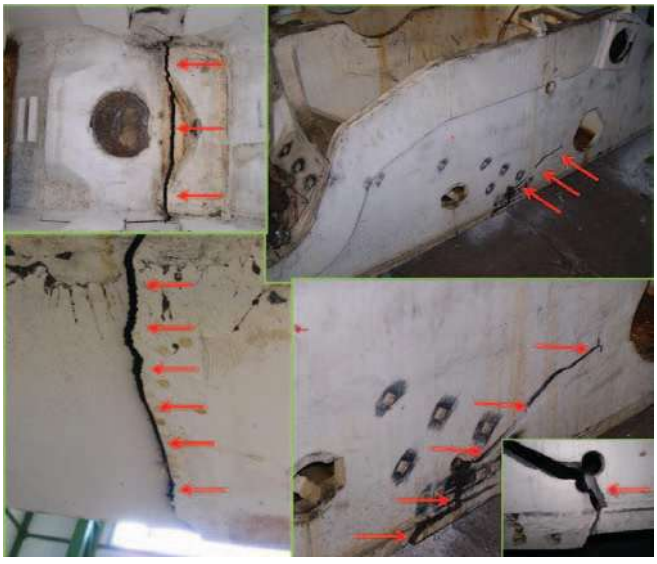

Figure 3. Cracks on the base started from the hole as geometric notch.

Finally, all the results were collected. According to Equation (9), it has been found that in most of the measuring points in the main subassemblies of the powered roof support, the fatigue life was greater than a million cycles. As for the base, the estimated fatigue life was much lower and the first cracks were expected after 6,300 cycles(Table 3).

Figure 4. Fatigue striation on fracture, formed on the lower sheet of the powered roof support base.

In future stages it's connected with further propagation and structure damage. It should be expected that the nucleated crack under cyclic loading will be propagating up to the moment when it reaches its critical dimension. Time of the crack growth to the critical dimension is usually much longer than time of nucleation at the process beginning and time of catastrophic increase at the end of the failure process. Strength calculations did not exceed the limit of elasticity on the braces, so the results obtained with the finite element method (numerical simulation) should be always verified with the experimental results. The other elements of the structure were not damaged and it was substantiated by calculations.

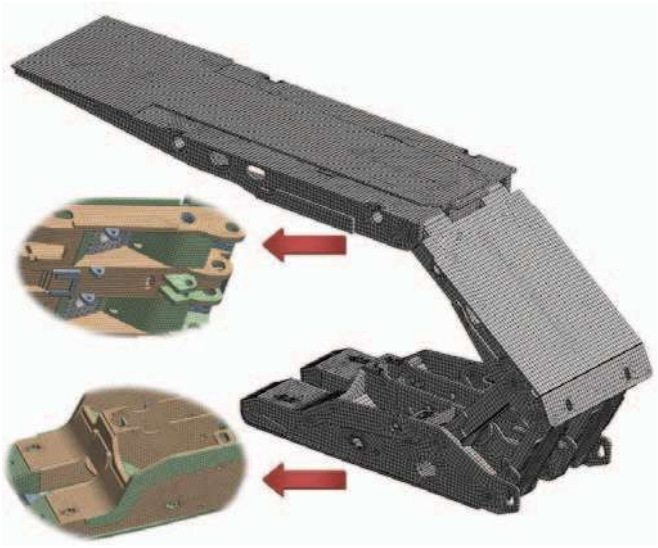

Figure 5. Discrete model of the FAZOS powered roof support section.

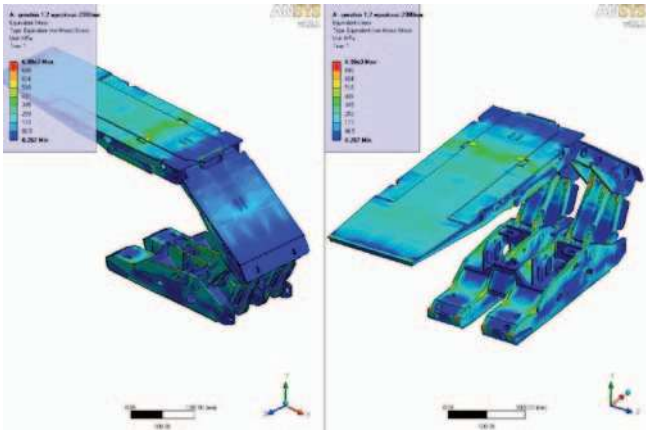

Figure 6. Shows stress contour, according to the Huber-Mises-Hanckyhypothesis.

CONCLUSION

Numerical simulations allow us to analyze the influence of the support on the mine section and to determine the areas where danger can occur. From the performed experiments and numerical simulation, it appears that the base is the element subjected to the greatest stresses. The service results, however, show that shields are the elements most often subjected to breakdown. The other subassemblies were not subjected to any serious deformations or fatigue cracks (Table 4). During tests, special attention was paid to phases of crack development from the microcrack initiation to propagation in the macroscopic scale. Analytical calculations allow us only to estimate approximate fatigue life of a powered roof support, and they must be verified experimentally.

The presented procedure of evaluation of the technical state of the base allows the determination of safety and durability of the structure while it stands tests and operation in the mine. Owing to the modern numerical methods and tests, the proposed method allows an estimation of fatigue life and the influence of important factors (i.e., geometric notches) on its negative changes.

The results from experiments and the finite element method allow for effective determination of stress and strain concentration and to obtain a satisfactory comparison of the fatigue performance of the subassemblies of a powered roof support.

REFERENCES

Barczak T., Gearhart D. “Canopy and base load distribution on a longwall shield.” Report of Investigations 9418. United States Department of the Interior. 1992, pp. 1-23.

Eurocode 3: Design of Steel Structures – Part 1-1: General Rules for Buildings. European Committee for Standardization. Brussels, Belgium.1992. ENV 1993-1-1.

Jaszczuk M., Markowicz J., Szweda S.“Evaluation fort basic elements powered roof section of the various methods of support”. Proceedings- Innovative - safe and effective techniques and technologies for mining:Human - Machine-Environment. Komtech, Gliwice. 2009. pp.347-335.

Table 3. Comparison between Analytical Study and Numerical Calculations (FEM) for Fatigue Life of the Base, lower sheet.

Transformed Stress (Goodman) [MPa]	Read-out Number of Cycles	Observed Number of Cycles (laboratory)	Load Support According to the EuropeanStandard PN-EN 1804-1	Calculated Degree of Damage
440	**6.3000E+03**	**6300**	**A.1.1a lub A.1.2a+A6d lub A.6c**	**1.0**
		2000	A.8	(crackingstart)
		1000	A.2a+A.3b	-
		2000	A.2a+A.3a	-
		3000	A.1.1b lub A.1.2b+A.2a	-
		1000	A.4a lub A.4c	-
		1000	A.4b lub A.4c	-

Table 4.Results of experimental studies for all measuring points.

The Measuring Point	Calculated Fatigue Life (beginning of the crack)
1	**16000**
2	>1000000
3	>1000000
4	**16000**
5	>1000000
6	>1000000
7	>1000000
8	>1000000
9	>1000000
10	**8000**
11	>1000000
12	>1000000
13	>1000000
14	>1000000
15	>1000000
16	>1000000
17	>1000000
18	>1000000
19	>1000000
20	>1000000
BASE	
GOB SHIELD	
CANOPY	

Karolczuk A., Łagoda T., Macha E."Determination of Fatigue Life of 10HNAP and 1208.3 Steels with the Parameter of Strain Energy Density".International. Fatigue Congress, 2002. Stockholm, Sweden, 2002.vol.1, pp. 515-522.

Khair, A.W.,Yu, B."Rock cutting process simulation by Dynamic Finite Element Analysis, Mine Planning and Equipment Selection".Wroclaw, Poland.September 2004. pp.253-256.

Łagoda T., Macha, E."Energy approach to fatigue under combined cyclic bending with torsion of smooth and notched specimens". Materials Science.vol. 34, 1998.pp.630-639.

Łagoda T., Macha E. Generalization of energy multiaxial cyclic fatigue criteria to random loadings. Multiaxial Fatigue and Deformation: Testing and Prediction.ASTM STP 1387. pp.173-190.

Miner. M.A.: Cumulative damage in fatigue. J. Appl. Mech.. Trans. ASME. 1945.

Molski K., Glinka G. A method of elastic-plastic stress and strain calculation at a notch root. Materials Science and Engineering.. vol. 50, 1981. pp. 93-100.

Neuber, H. Taking into account the stress concentration on strength calculations, construction, Academic book, no 7, 1968, pp.245-251.

Peng, Syd S. (1978). Coal Mine Ground Control. West Virginia University, College of Mineral and Energy Resources. pp. 209-240.

PN-EN 1804-1: Machines for underground mines. Safety requirements for hydraulic powered roof supports. Part 1: Support units and general requirements.

Polak-Micewicz M., Łagoda T.: Determination of stresses and strains at critical points of the base of powered roof supports, Opencast Mining, no 3/2010, X International Scientific Conference Computer Aided Engineering, Szklarska Poręba, 2010.pp.25-28

Polak - Micewicz M., Łagoda T.: Methods of study of powered roof support FAZOS including the fatigue life, VII International Conference on Mining Techniques, Krakow - Krynica2011,University of Mining and Metallurgy, Monograph, Modern methods of coal mining and hard rock, pp.182-190.

Miner M.A.: Cumulative damage in fatigue, J. Applied Mechanics, Vol. 12, 1945, pp.159-164

Goodman J.: Mechanics Applied to Engineering, Longmans, Green, and Co., 1899

Strata Management with Ground Behavior Assessment for Mass Exploitation of Coal Deposits: A Case Study of Continuous Miner

Sanjay Kumar Singh, Sr. Manager (Mining)
Coal Mining
S.E.C.L.(A Subsidiary Company of Coal India Limited)
Bishrampur, India

Singam Jayanthu, Professor/Dr.
National Institute of Technology
Rourkela, India

Gopal Singh, Director (P&P)
S.E.C.L.(A Subsidiary Company of Coal India Limited)
Bilaspur, India

ABSTRACT

The mechanics of load transfer in bord-and-pillar mining is not well understood despite the evolution of the art of pillar extraction over the last 20 years via trial and error (empirical) or Rock Mass Rating (RMR), simple monitoring and pillar extraction experiences at neighboring mines. Variations in geologic conditions and pillar extraction methods, along with a lack of comprehensive instrumentation programs for monitoring ground behavior during pillar recovery, are among the factors that make it difficult to predict how strata will respond to pillar extraction.

Efficient and safe use of roof supports depends on the interaction between the designed support and coal strata. Of particular interest in this study is the mechanics of strata deformation as influenced by geologic conditions, pillar extraction methods and optimum support with load-bearing capabilities in strata control during mass exploitation of underground coal deposits required detailed investigation,". To provide a better understanding of the mechanics of strata deformation, as researchers, we have collected data and reviewed measurements of convergence and stress in one mine of South Eastern Coalfields Limited (S.E.C.L.), i. e., in North Chirimiri Pondary Hills (NCPH) and have completed numerical modeling with FLAC software for (Fast Lagrangian Analysis of Continua modeling, Itasca India Consulting Pvt. Ltd.) for two typical pillar extraction plans. Stress distribution in the mine roof above pairs of roof supports was calculated to demonstrate how Resin roof bolt support installed support contributed to roof block movement control. It was shown that overall stress and roof-floor convergence patterns were most influenced by the stiffness of coal measure rocks and by pillar extraction sequences and layouts. Also, resin roof bolts and other support systems play a critical role in controlling stability of both the immediate roof and the main roof for a distance of up to 18 meters (i.e., working coal seam height X three times) above the seam. Installed supports provide unique strata control advantages over other types of secondary support by significantly reducing the time between mining and installation of the secondary support. Although resin roof bolts are similar to posts in stiffness and capacity, they are more effective than posts under static loads because they can yield and still maintain loads at near-peak capacity(Singh, et al., 2006), whereas posts fail and lose their ability to limit mine roof deformation.

INTRODUCTION

Over time, shallow coal deposits in India are being exhausted; hence, the future of coal mining in this country lies with the underground mining of deep-seated deposits. Many problems arise in these deep underground mines, and one of the most important, from a safety point of view, is strata control. The efficacy of control can be ascertained by proper monitoring and analysis of various stratigraphic parameters like convergence, rate of convergence, C_1 / C_2 ratio, (Where C_1= Daily convergence at site in a day N and C_2=Average daily convergence at the site upto the previous day i. e. up to day (N-1), When C_1 / C_2 ratio is equal to or more than 2.0, it means fall indicated) deformation of different immediate roof layers, support load, stress on the pillars including the barriers vis-à-vis roof falls (strata movement), abutment extent and other factors. Performance of underground structures is highly dependent upon two types of stresses: in-situ stress and mining-induced stress. In-situ stress is more or less static in nature for a particular site, but mining-induced stress is highly influenced by strata equilibrium dynamics around the goaf edge, which becomes extremely dangerous when working under strong and massive roof strata. Mining-induced stress is basically the concentrated part of natural stress, perturbed due to mining activities. The strata equilibrium dynamics around the goaf edge is of special interest for Indian coalfields because of frequent encounters of strong and massive roof strata by underground depillaring faces. Vertical load of the rock strata, directly above an opening, shift onto surrounding pillars and leave a de-stressed zone in the roof strata. Tributary area methods for the estimation of mining-induced stresses over the pillar remain valid only for development, such as pillar formation in a coal seam, because the development of pillars adopts symmetrical excavation patterns of a narrow span. Final extraction (depillaring) of pillars adopts a complex shape and experiences extensive overlying strata movements (Figure 1) and failures. Because of this, the tributary area method cannot be applied during final pillar extraction. Calculation of the actual load on a pillar is more complex than the determination of pillar strength. Both the theory of elasticity and the principles of soil mechanics do not completely explain the behavior of coal measure formations and, hence, a reliable simulation of the geo-mining conditions of the field in mathematical or physical models becomes an extremely difficult task. Empirical formulations based on in-situ measurements are an acceptable way to estimate rock mass

behavior. Our study has assessed the stresses during development and extraction of coal pillars by continuous miners and field (underground) investigations to visualize the nature of development of mining-induced stress under varying geo-mining conditions.

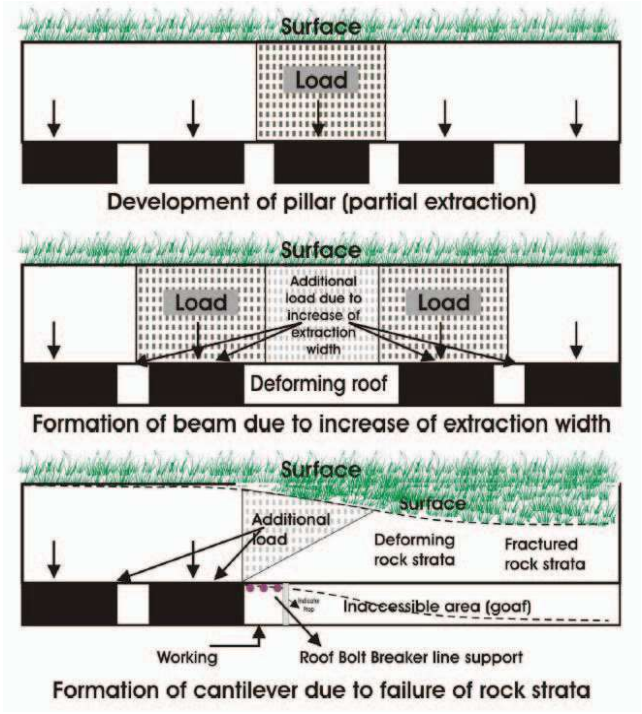

Figure 1. Mechanism of mining induced stress development during depillaring and limitations of the conventional tributary area method.

This study was performed using simulated numerical models. FLAC (Fast Lagrangian Analysis of Continua) modeling software. Itasca India Consulting Pvt. Ltd. Rock Mass properties used for Mohr-coulomb material see in table 1.Vibrating wire stress meters were used for underground monitoring of the stress development, with increases in dimensions of excavation. The quality of the overlying roof strata was assessed in a laboratory through geo-technical logging and testing of physico-mechanical properties of the procured core samples. Attempts were also made for in-situ testing of the rock mass by a borehole rock indenter. As perceived, mining-induced stress (vertical) increased with the increase in dimension of excavation and, generally, its maximum value was observed just before a major roof fall in the panel. During the field monitoring, it is observed that the stress distribution over a pillar/ stook, in and around a depillaring face, depends on a number of factors. It is recognized that the roof span plays a very important role in the strength of the roof strata.

1. Impact of Depth Cover
2. Impact of Overlying Strata
3. Range of Influence

According to the results of this field investigation, the nature of roof strata has considerable impact on the qualitative and quantitative nature of abutment loading of pillars of shallow mines. Incorporating these two important factors together in the analysis, a best fit expression for the range of influence (R) is derived as:

$$R = 0.24\ H + 9.59 \times 10^{-3}\ I \quad (1)$$

$$R = 0.16\ H + 9.63 \times 10^{-3} I \text{ (for } H < 200m) \quad (2)$$

Where, H is depth cover I is Caveability index.

A simple empirical model was developed for abutment loading as the value of the ultimate mining-induced vertical stress, and its range was found to be correlated with the roof rock mass quality and depth of cover. It was observed that the nature and amount of mining-induced stress have considerable influence over the performance of the natural and artificial supports around the goaf edge. Impact of the highly active nature of mining induced stress over the natural supports is observed to be the most serious factor for the safety of working under a hard and massive roof rock mass. Our study has also been helpful to exhibit the role of the mining induced stress for pillar extraction with optimum support requirement.

SITE DESCRIPTION OF NCPH COLLIERY R-6 MINE

The North Chirimiri Pondary Hills (NCPH) Colliery R-6 underground mine is located in the Chirimiri area of South Eastern Coalfields Limited (S.E.C.L.) in the Korea district of the State of Chhattisgarh, India. It is bounded by latitude 23° 11' 20" to 23° 30' 20" N and longitude 82° 19' 40" to 82° 23 ' 08" E, as per Survey of India Topo Sheet no. 64 I/8. The project lies in the eastern part of the Chirimiri coalfield about 1 kilometer from the Anuppur-Chirimiri Railway line of the South Eastern Railway. By rail, it is 90 km from Anuppur on the Bilaspur-Katni main line. An all-weather road connects the project with the key towns of the Korea district. Bilaspur town, the headquarters of SECL, is about 200km away. After 2010-2011, the estimated reserve was approximately 5.112 million tones. The quality of the coal seams is as gross calorific value (GCV) varying from 6,454 Kcal/Kg to 5,597 Kcal/Kg at 5% moisture level. With the present rated production capacity of 1.5 Mtpa, the life of the project will be another nine years, meaning it will be closed by 2017 or 2018.

Boundaries of the Mine

The following features bind the colliery area, or the core zone:

North - West Chirimiri Colliery and forest area
South - Kurasia Colliery
East - North Chirimiri Colliery
West - Forest area land

Topography and Drainage

The core and buffer zones of the colliery are marked by highly undulating topography with the highest Reduce Level (R.L.) being slightly more then 850 m. The colliery area is marked by the presence of a major hillock, and its altitude varies between 510 and 850 m. The general slope of the ground is northwest. The area is drained by a number of first- and second-order drains originating from the hillock and then forming a nallah. This nallah (called Korea nallah) ultimately joins the Hasdeo River near Manendragarh.

Table 1. Rock Mass Properties used for Mohr-Coulomb Material.

Rock Type	Engineering Property	Property of the rock	Property of the rock mass
Coal (RMR=56)	UCS, MPa	28.5	3.16
	Tensile Strength, MPa	3	0.6
	Young's Modulus, GPa	7	1.4
	Poisson's Ratio	0.27	0.27
	Cohesion, MPa	-	0.72
	Friction, Degree	-	41.5°
Fine Grained Sandstone/ Shaly Sandstone (RMR=47)	UCS, MPa	22.59	1.6
	Tensile Strength, MPa	3	0.44
	Young's Modulus, GPa	4	0.6
	Poisson's Ratio	0.41	0.41
	Cohesion, MPa	-	0.69
	Friction, Degree		35°
Medium Grained Sandstone (RMR=65)	UCS, MPa	16.33	2.84
	Tensile Strength, MPa	2	0.55
	Young's Modulus, GPa	7	1.96
	Poisson's Ratio	0.31	0.31
	Cohesion, MPa	-	0.7
	Friction, Degree	-	41°
Coarse Grained Sandstone (RMR=41)	UCS, MPa	9.02	0.47
	Tensile Strength, MPa	1	0.1
	Young's Modulus, GPa	2	0.3
	Poisson's Ratio	0.43	0.43
	Cohesion, MPa	-	0.7
	Friction, Degree	-	37.9°

Geology

The lithostratigraphic units encountered in the colliery leasehold belong to the Karharbaris/Barakars and the Deccan Traps geological formations. The Karharbaris/Barakars deposits are represented by sandstone, shale, carboniferous shale and coal seams. The coal seams outcrop in the depressions and on the ground surface in good condition, and tend to follow the surface counter because of the rather flat dips.

An east-to-west trending fault divides the workings into two parts. The area lying to the north and south of this faulted zone are known as the R-6 workings and the Amajharia and Haldibadi workings, respectively. The fault zone narrows towards the east. The fault throw horizontal is about 30 m towards the south in the areas adjacent to the North Chirimiri Colliery, and increases towards the east. The area forms a part of the shallow basin deposit with rolling dips of 1.43 to 5.71 degrees, the dip is almost flat in the central part of the R-6 workings. Dips up to 1 in 40 were observed near the North Chirimiri Colliery leasehold. The strike in this area is northeast-to-southwest with coal seam dips 1.3 degrees towards the northwest.

Mine Workings

The NCPH colliery is situated near the central Chirimiri coalfield. The colliery is working four coal seams in two parts separated by a major fault. Bord-and-pillar systems with caving and partial extraction have been adopted in all seams; brief details are given below.

Conventional Bord-and-Pillar System

In the conventional bord-and-pillar system, the panels are being developed parallel to the provisions of 1957 coal mine regulations outlining the size of pillars and galleries and an incubation period of about nine months for depillaring life. During development, the coal is extracted by conventional solid blasting as per the directives of the Directorate General of Mines Safety (DGMS). The roof is being supported by 2.4 m-long resin bolts. Depillaring is by a conventional stooking/slicing method with supports per the systematic support system approved by the DGMS.

Continuous Miner Bord and Pillar System For Mass Exploitation

Mass exploitation of coal is referred to as "economical excavation of coal with due method of higher productivity, safety

and conservation." In the panels designed for extraction by the continuous miners, the development had been done by these units and the final extraction is also proposed to be done by these machines. During development and splitting, the roof has been supported by 2.4 m- and 1.8m-long resin bolts.

LITHOLOGICAL CHARACTERS OF ROOF STRATA

Roof litho logy and structure plays an important role in contributing to unstable roof conditions. During mining, abrupt changes in the behavior of roof litho logy and structure may give rise to a complex situation in which strata deformation and creep effects lead to further strata weakness. The knowledge gained by preparing of borehole core samples help in identifying areas prone to roof instability. The primary requisite to study a roof strata's litho logy characteristics is to log the borehole core sample's geotechnical data, furnishing the details of core dips, laminations, fractures, the nature of contact between the litho-units, the average length of core, the percentage of Rock Quality Designation (RQD%) and structural features. The geological succession established in the mining block of the NCPH Colliery R-6 Mine from the borehole exploration data is given in Figure 2, along with the thickness range of each formation within the blocks as interpreted from the borehole's section.

STRATA MONITORING AT THE NCPH R-6 MINE IN CONTINUOUS MINER SECTION DURING EXTRACTION OF COAL

The following specifications have been recorded via data collection and strata monitoring:

Coal Seam: No. 3

Depth of Cover: 60 m to 106 m

Panel No.: S-1

Pillar Size: 22 m x 22 m

Width of gallery: Not exceeding 6 m

Height: Not exceeding 4 m

Panel RMR: 48.07

SYSTEM OF SUPPORT AND STRATA BEHAVIOR

The standard roof bolt used throughout the R-6 Mine was 2.4 m for original gallery and 1.8m for split gallery, and 22mm diameter rebar with a 150 mm thread and a range of 24T-28T in yield strength of the rod. The bolt was installed in a 25mm diameter hole with resin capsules for nominally full encapsulation. A crimped nut and antifriction washer plate was used. Successful installation of the bolt requires the drill operator wait a specified period for the fast resin to set before completing the installation by tightening the nut. Figure 3-1, Figure 3-2, Figure 3-3 shows the systematic support rules during development and depillaring.

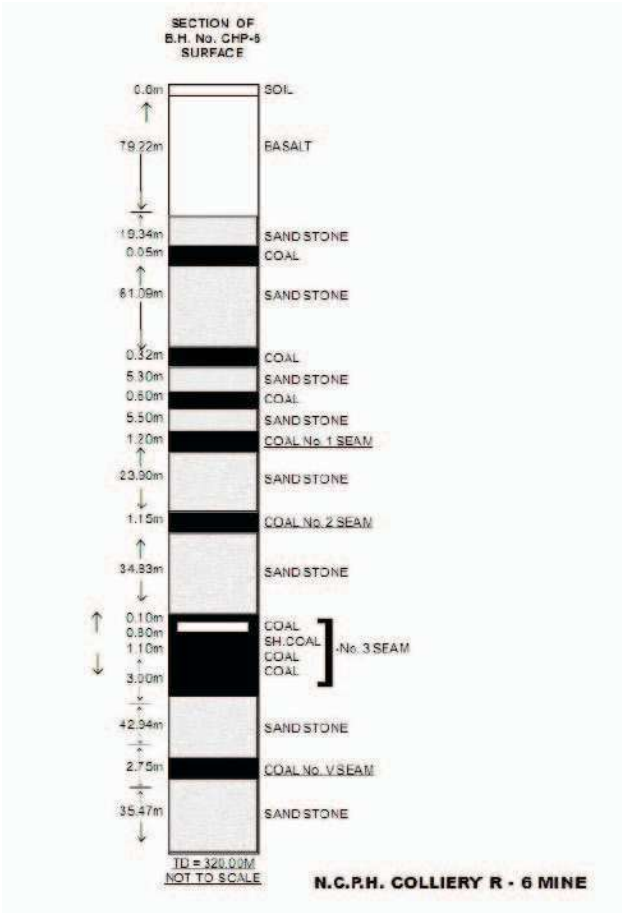

Figure 2. Intersected Geological Succession of NCPH Colliery R-6 Mine.

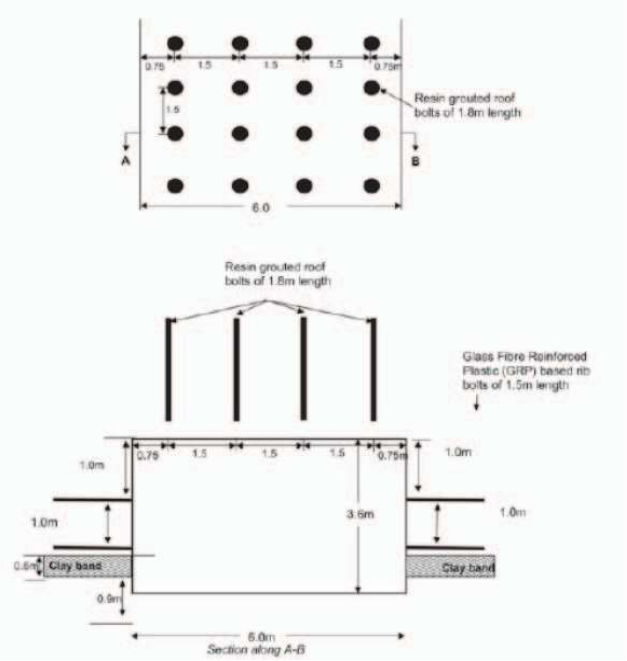

Figure 3-1. Support system in development and split galleries.

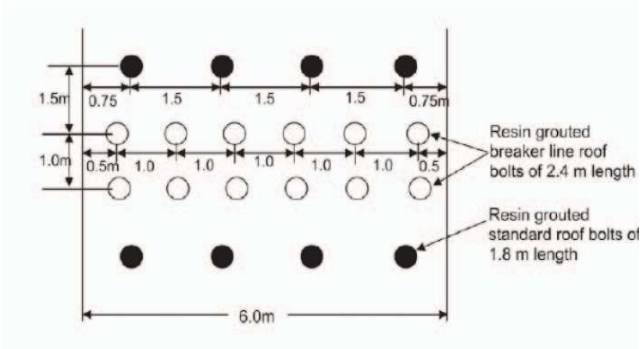

Figure 3-2. Breaker line support system in depillaring galleries.

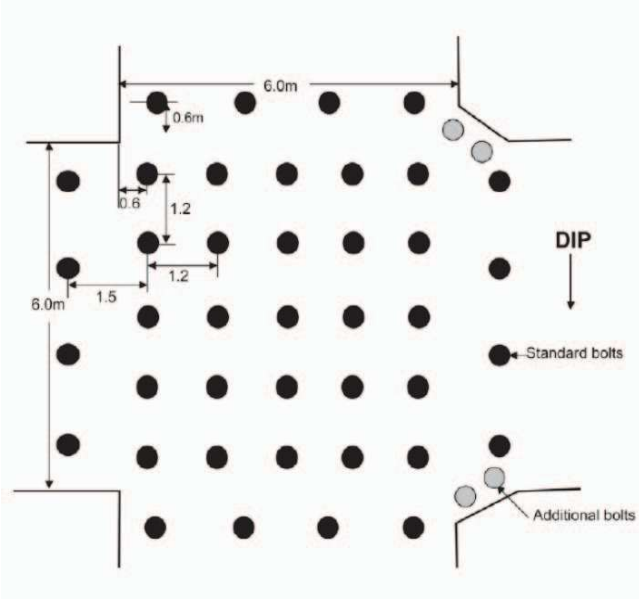

Figure 3-3. Support system at Junctions.

A study of typical installations revealed the following problems:

- The hole was often drilled too long, preventing full encapsulation.
- The resin was not inserted to the top of the hole.
- Mixing was not continued for the specified time.
- The hold period was too short.
- Torturing often resulted in the bolt being pulled down the hole, permanently reducing the bond strength.

It was concluded that correct installation of the system was not taking place. The bolt system used was difficult to install correctly and prone to operator error. (It is authors personal Observations during bolting installation in mine.) The resulting installation was likely to have very low bond strength. In-mine roof bolt systems did not incorporate such features as effective torque nuts and deformable end plates, which provide quality control during installation and information on the development of end loading.

MINE PLAN AND PART PLAN OF INSTRUMENTATION IN PANEL S-1

The instrumentation plan of strata monitoring is shown in Figure 4 referencing points of reading observations during development and pillar extraction.

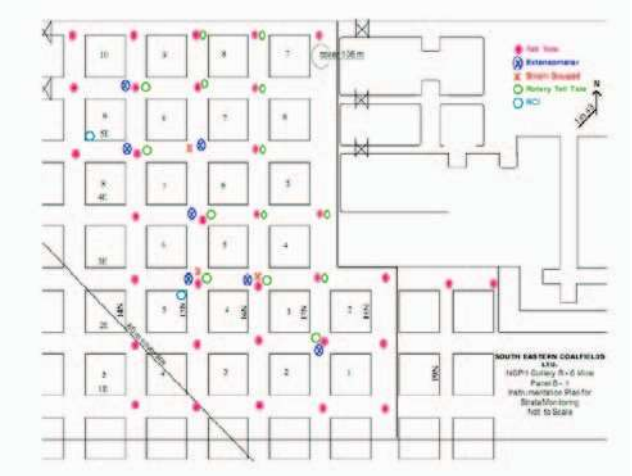

Figure 4. Mines Plan and Part Plan of Instrumentation in Panel S-1.

Instruments Used

- Rotary tell tale/Dual-height tall tale
- (Magna sonic) Extensometers/Rib extensometer
- Strain gauge bolt
- Remote convergence indicator
- Stress meter/Capsule

SYSTEM OF MONITORING

Stress change monitoring was designed to record the stress changes in the roadway roof prior to, during and after excavation. This method overcame the shortcomings of conventional displacement monitoring techniques, which can only monitor the roof response after the excavation of the roadway (and usually after bolting), missing the period when the crucial roadway reaction is occurring.

The in-situ stresses in the coal seam and roof rock were measured in the vicinity of the monitoring sites using the over-coring technique. The in-situ stress measurements were conducted in the pillar between 49 and 50 cutthroughs (SCT, 2002).

- Data input from the instruments were recorded by a researcher or competent person and duly authorized by the mine manager in writing.
- Researcher or strata control personnel recorded the input from the instruments on a weekly basis during development and daily in the case of depillaring.
- Researcher maintained the records of all data and analyses in a bound page book on a regular basis.
- Researcher and panel in charge/Asst. Manager also closely monitored the status of the panel.

- The result of this instrument had interpreted strata performance and ground behavior by its reading.

FREQUENCY OF MONITORING

All instruments lying within two pillars of the pillar under extraction had recorded daily data, except for remote the convergence indicator and stress meter, which recorded on a shift basis. Recording was done on an alternate-day basis.

DATA INTERPRETATION TABLE

A brief summary of the instruments' readings in the S-1 panel of the NCPH Colliery R-6 Mine are referenced taken from first author's research **dissertation work**.

Site Performance As Observed

- **Convergence**: Maximum 4mm convergence at the rib pillar and minimum 1mm at 16m away from the point of continuous miner operation for pillar extraction.
- **Strain development/loading on rock bolts**: Strain development was observed at a maximum 3 mm at the pillar side within 6m distance and a minimum 1mm at the pillar side away from 19 m of pillar extraction in continuous miner operation.
- **Displacement of different rock layers**: Displacement of immediate rock layers has found maximum up to 9mm of roof strata at pillar extraction. This is found vary from 3 mm to 2.5 mm in relation to width of extraction 5.4-6 m and 2.4 m in working height when extraction was performed along the roof at development panel. After sequencing height and floor during recovery, a slight increase of 3mm in increase of working height up 3 meter and more is noted.
- **Stress developed on pillars/ribs**: When the depth of cover is 75 m, stress on the 22 m x 22 m pillars is noticed up to a maximum of 3Mpa and minimum 1.6 Mpa and varying from 2 to 5 Mpa at the time of stooking or final extraction of pillar. Final pillar extraction reduces the pillar size with the diagonal slicing method inducing stress on the rib to a maximum of 6 Mpa and minimum 2 Mpa.

NUMERICAL MODELLING AND PREDICTIONS

Basic Set-up

Three dimensional numerical models were prepared to evaluate stability of roof rock under various conditions and also to make predictions for continuous miner operations under 6 m wide galleries. All litho logical units with their respective rock mass properties were used for the modelling. Corresponding materials, as per the typical litho logs figure 1, have been considered to follow Mohr-Coulomb's elasto-plastic rock failure model with non-associated flow rule. Various rock mass properties and corresponding rock properties are given in Table 1. The prepared models were provided with gravity loading only as initial load conditions due to the reason that the mine is under shallow depth cover of 87m and there is no sign of distress due to in-situ stresses. Model geometry prepared and used for the modelling. Model boundaries are truncated using advantage of symmetric planes. The positions of symmetric planes are explained in Figure 6. Pillar length of 22 m considered to avoid effect of far field boundaries on the simulations. Appropriate roller boundaries are placed at the far field model boundaries. Two categories of models are prepared. The models with 6 m wide gallery were prepared for validation of the modelling while the models with 6.4 m wide gallery were prepared for prediction of roof conditions during continuous miners operations. All simulations have been solved following two stages. Gravitational loads made to settle for initial stage of excavation and thereafter the staged excavation mining steps were incorporated. The models have 38280 zones and 42067 grid points. These zones and grid-points were kept dense surrounding the area of interest, i.e., the mining gallery. Staged excavation with 1m mining step covering 12 mining steps has introduced during the simulations. Models behaviour was evaluated after each simulation through observations of roof rock deformations, material failure state and safety factor contours.

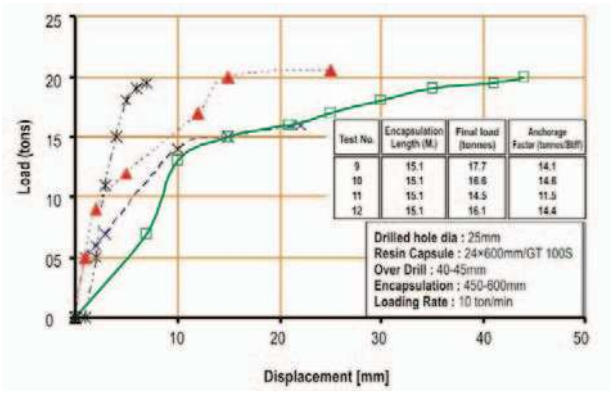

Figure 5. Long Tensioned 1.8-meter Roof Bolt Results.

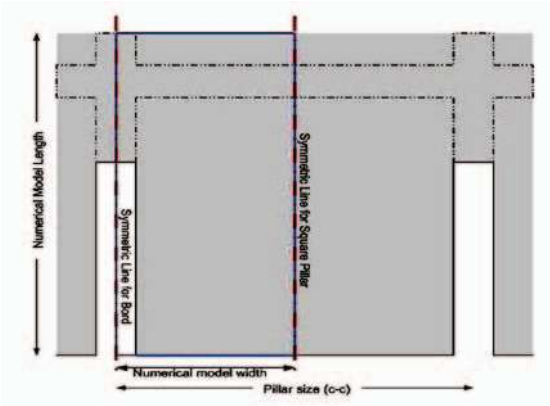

Figure 6. Pillar size and symmetric boundary conditions.

Validation of the Modelling

Numerical modelling results are compared with observed deformations values at 3L/16D by multi-pint borehole extensometers (MPBX, observations shown elsewhere) in the mine. Corresponding predicted deformation values through the modelling and the observed deformation values are compared and shown in Figure 7. Comparison in the deformation values shows a correlation coefficient of 86% with the slope of the trend line as 25.64°. The high correlation coefficient indicates that the prepared numerical models are accurate enough to provide reasonable trends for the mining conditions.

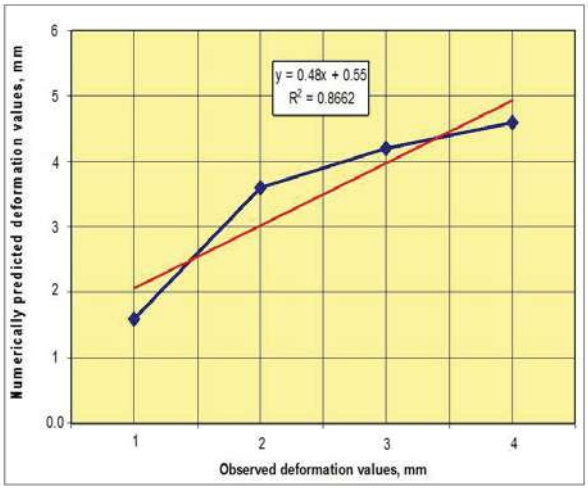

Figure 7. Comparison of numerically predicted and observed roof deformations.

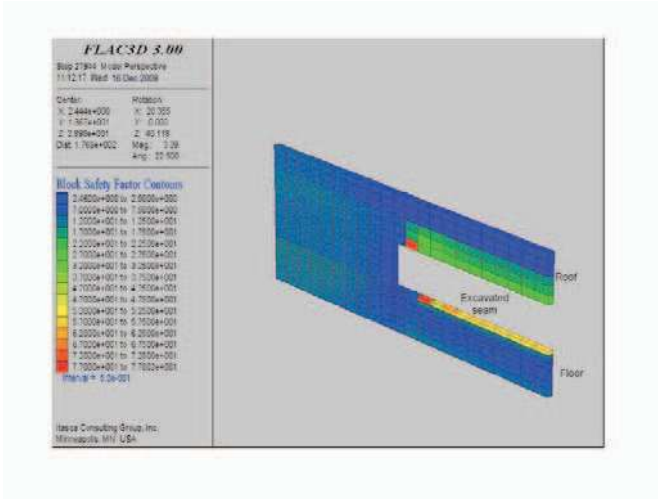

Figure 9. Distribution of safety factor contours in roof, face and floor at the centre of bord for 6m.

Further, no material failure state and corresponding high safety factor contours in the roof strata after 18m of staged excavation simulations (Kindly see Figures 8 and 9, respectively) corroborate to the prevailing general conditions in the mine. The minimum safety factor contour value is obtained as 2.5 as per the face line while roof level have safety factor values more than 10. These corroborative results are also reinforced later through field observations of deformations through MPBX. The MPBX observations demonstrated deformations in the order of a fraction of 2 mm.

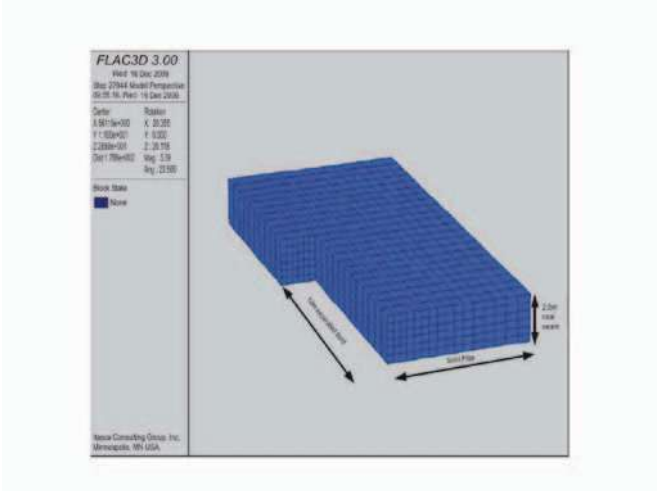

Figure 8. Material Failure State in coal seam for 6m wide gallery.

Predictions of the Numerical Modelling

Material failure state plots (Figure 10) and Safety Factor Contours (Figure 11) are evaluated to make the predictions for the roof behaviour during the continuous miner operations under 6m wide galleries. The minimum safety factor contour value is of 1.97 at the face while roof level has the safety factor value more than 10. Plots illustrated in Figures 11 and 12 do not reflect any material change in conditions for the mine from the gallery width widening from 6 m to 6.4 m even after 18 m of staged excavation simulation steps. Further, comparisons of deformation values and support pressure values between corresponding excavation stages of 6m and 6.4m wide galleries indicate that there will be 26% increase in deformation values and no change in support pressure values. An increase of 26% in deformation means that the deformation values will remain less than 2mm for 6.4 mm wide galleries. This miniscule change in the deformations will not result into any change in support pressure. These observations, like the empirical predictions, predicts that the 6m wide galleries with a cut-out distance limited only by human factor (tendencies to step into unsupported area by CM operator to visualize change in roof strata) and ventilation factor (dust and gas emission) will be safe for the NCPH colliery R-6 mine, SECL, Bilaspur. Impact of solid pillar size reduction on pillar stability can also be evaluated from a comparative observation of the safety factor contours over coal seam and its pillar formed. Such an observation for respective bord size of 6 m is shown in Figure 12.1. Figure 12.2 indicates that the increase in the bord width does not produce an interaction effect on the pillar size. A reduction in safety factor value from 2.98 to 2.69 with the respective increase in the bords width can only be seen on the side of the gallery up to a skin depth of 0.3 m. The remaining pillar sizes are unaffected and safe under the proposed bord width increase.

Strata Management for continuous miner operations is illustrated. The process involves obtaining field and laboratory data for rock mass characterization. The characterization assists in finding out an appropriate gallery width which in turns assists to find out a suitable width for the cutting drum for the continuous miner. Bieniawski's RMR and NIOSH CMRR are required to ascertain requirements of cut-out distance and gallery width. Economical operations for continuous miners dictate that the roadway width should be at least twice the drum width. The process then involves determination of roof deformation characteristics through rock mechanics instrumentation. This valuable data not only decides the length of rock reinforcement measures but also used to simulated numerical models. Thereafter, simulated numerical models are used to predict overall rock mass response as a result of continuous mining operations. The above procedure is applied to NCPH colliery R-6 Mine, Chirimiri Area, SECL and the mine is successfully enjoying the benefits of the

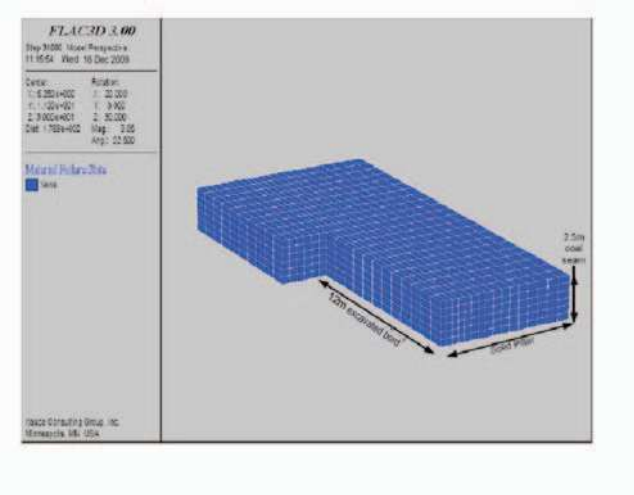

Figure 10. Material Failure State in coal seam for 6.4m wide gallery wide gallery.

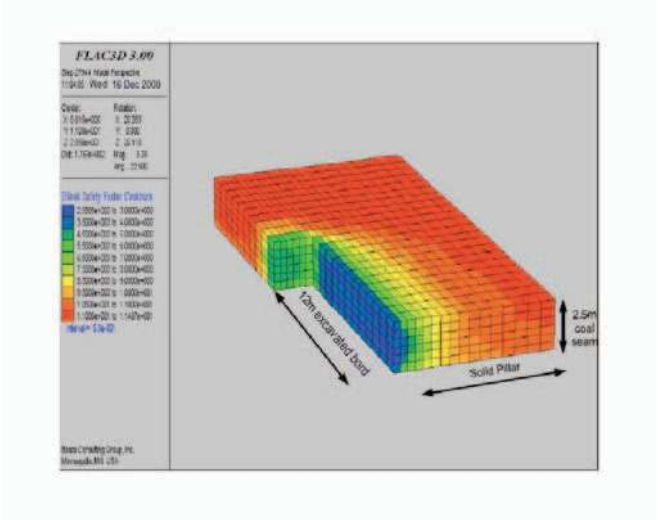

Figure 12.1. Interaction of bord width on pillar size with Safety Factor Contours over coal seam in 6m wide galleries.

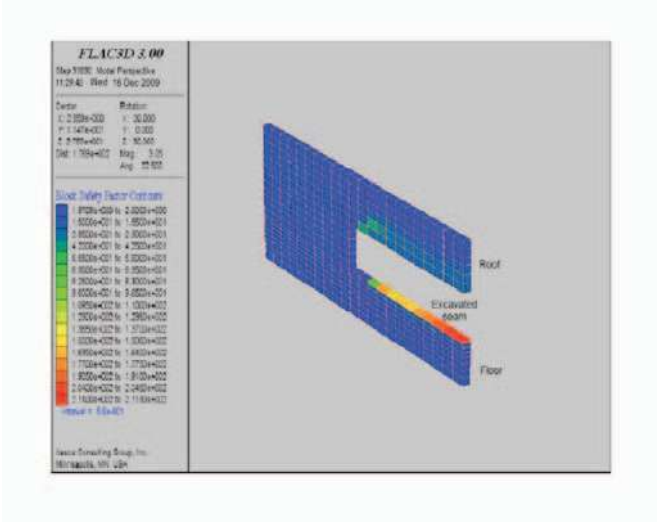

Figure 11. Distribution of safety factor contours in roof, face and floor at the centre of bord for 6m wide gallery.

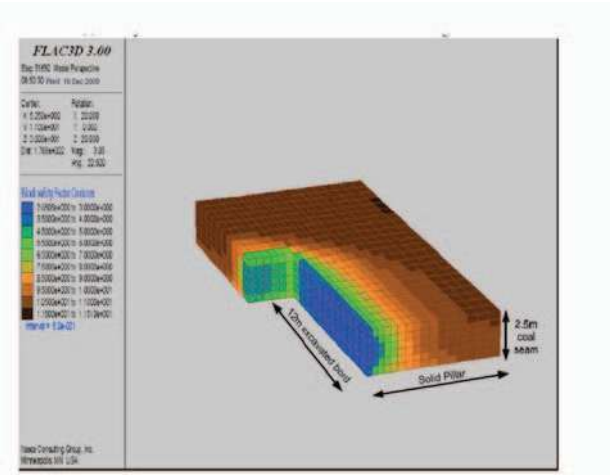

Figure 12.2. Interaction of bord width on pillar size with Safety Factor Contours over coal seam in 6.4m wide galleries.

design model without a single instance of roof fall since inception of panel S-1 to end of coal recovery in this panel.

CONCLUSIONS AND RECOMMENDATIONS

The main objective of this research is to determine the safety standard, with productive and cost-effective ground support strategy, which was done by examining the support density, roof bolt length and, optionally, the type of permitted ground support for the NCPH mine of South Eastern Coalfields Limited (S.E.C.L.). This can be also useful in other similar geo-mining conditions in different coal fields in India for mass exploitation of underground coal deposits. Currently, the ground support system for 6m roadways consists of 19 to 22 mm diameter, 1.8m-length, point-anchored resin rebar on 1.2 m centers with Bureau of Indian Standards (BIS) norms grade-bearing plates with no screen.

The key conclusions drawn from this research include:

1. Roof bolt corrosion has been limited to thin surface rust films on the installed plates and exposed rebar. Case history reflection and empirical estimate references for roof bolt longevity strongly suggest that corrosion will not measurably affect the rock bolt strength until now
2. The elastic beam theory of rock bolt support function is the best general model for the NCPH mine of S.E.C.L. for sandstone roof. Where vertical discontinuities extend through the bolted roof thickness, beam theory may be more appropriate.
3. Wedge support analysis, facilitated with modeling software, has excellent application at the NCPH mine of S.E.C.L. for assessing the capacity of the primary roof support to stabilize roof wedges.
4. Pyramid idealizations of intersection wedge geometry are most appropriate for massive sandstone roof.

5. A critical wedge was determined to be defined by joints angled at 30 degrees above the roof line and a slab of rock formed with a joint angled at 18 degrees based on sandstone roof supported with 1.8 m point-anchored rock bolts on 1.5 m centers. The corresponding critical angles for wedges and slabs supported with 1.8 m point-anchored rock bolts on 1.5 m centers are 27 to 30 degrees, respectively. Wedges and slabs formed by joints angled more steeply will require supplemental support assessment.
6. Empirical estimates of support requirement for the NCPH mine roof suggest a conservative range of rock bolt lengths and pattern support spacing, and a greater support load density and anchorage depth that have successfully been provided by the current installed ground support. Methods based on beam theory require excessive bolt lengths of 2.4 m for 1.5m center-to-center bolt spacing.
7. The analytical support predictions prescribe 1.8 m for split and 2.4 m long roof bolts for original gallery and point-anchored rebar on 1.5 m center-to-center spacing, a design well suited to the roof conditions in NCPH mine of S.E.C.L.
8. Our research observations recommend 1.8m-long roof bolts on 0.75 m and 1.5 m center-to-center support spacing best suited for NCPH mine of S.E.C.L.
9. Resin roof bolts are finding increasing applications in underground coal mines, particularly un-tensioned, forged headed rebar, with lengths of 1.8m being the most accepted.
10. The 1.8 m-long, 22 mm-diameter grade BSI mechanical roof bolts on 1.5 m centers are recommended as primary roof support based on pull tests and the resulting bolt minimum bolt capacity of 20 tonnes at 50 mm displacement. A plan of quality control of strata management with bolt testing is also established for monitoring within the first three months of usage at a minimum rate of 10% of installation or 50 bolts per month, whichever is higher.
11. Reviews of empirical, analytical and numerical modeling roof support design methods recommend either 19-tonne capacity, 1.8 m minimum length point-anchored resin rebar, or mechanical roof bolts on 1.5-meter centers to serve as roof supports for the NCPH mine.
12. It is our knowledge that it is a good match between the sandstone roof and mechanical rock bolts based on underground observations; however, the authors/researcher have cautioned that quality assessment and control must be part of the application, and that they would not be appropriate in structurally controlled/faulted ground.
13. Forged head bolts performed very well in underground pull tests. The average yield load and corresponding displacement for rebar lengths of 1.2, 1.5 and 1.8m are shown in Table 2. The bond strength from a single SEPT (Standard Encapsulation Pull Test) on a 1.8 m length was observed at 50 tonnes/meter. The average bond strength of SEPTs on a 1.8 m torque tension rebar was 45 tonnes/meter at an average yield load of 15.5 tonnes.

Based on the conclusions itemized mentioned 1 to 13 above, recommendations for ground support at the NCPH mine are summarized in Table 3.

The Type B support system recommendation is based on the presented results of other researchers and requires updating to before implementation in the NCPH mine of S.E.C.L or any other mine of the same geo-mining conditions. The material properties of currently available mechanical bolts, including the anchorage capacities of the capsule, should be tested thoroughly before the Type B standard is adopted into the NCPH mine's primary ground support plan. The Roof bolt testing procedure has been implemented, as recommended by DGMS Circular. Tech Sapicom 3 of 1993 and 6 of 1996 should be followed until a site-specific procedure is developed at the NCPH mine for mechanical roof bolts. Supplementary supports for face spalling control, passive support roof stitching with wooden lagging and posts for rib and roof support should be reviewed for inclusion on a case-by-case basis or according to approved design rules. Strata support design at the NCPH mine of S.E.C.L for mass exploitation of underground coal deposits are best suited in application to continuous miner operation panels as outlined in Table 3.

Table 2. Summary of Pull Test Results – Forged Head Bolts.

Bolt's Length (m)	Avg. Yield Load (T)	Avg. Displacement at Yield load (mm)
1.2	13	7
1.5	14	10
1.8	19	5

ACKNOWLEDGEMENT

The authors acknowledge the assistance of management at South Eastern Coalfields Limited and all persons of related collieries directly or indirectly associated in the investigations presented in this paper. The views expressed in the paper are those of the authors and do not necessarily reflect those of the organization.

REFERENCES

Bigharia, J. K., Singh, B. B., Kumar, N. (2001). "Introduction of mass production technology at zero seams (Ajanta Incline) of Chirimiri Colliery at Chirimiri Area (S.E.C.L.)." MGMI, Bilaspur Chapter, India.

Brumby, I. D. (1980). "Continuous Mining with Tavistock Group of Colliery." Journal of the South African Institute of Mining and Metallurgy, January, Issue Pp5-9.

Jayanthu, S., Atul, G., Gupta, R. N. (2000). "Technology management for absorption of innovative trends in roof support of underground coal mines." In: Proc. of the International Conference on Technology Management in Mining Processing and Environment. December 1-3, 2000. IIT Kharagpur, India. Pp35-48.

Jayanthu, S., Singh, T. N. Singh D. P. (2004). "Stress Distribution during Extraction of pillar in a Thick Coal Seam." *Rock Mechanics & Rock Engineering*. 37(3), Pp171-192.

Jay, P.T. (1980).Monitoring rock stress and displacement in underground mines, (Dissertation). W.S. and L.B. Robinson University College,, New South Wales University, Australia.

Saharan, M. R., Jha, B. K., Sazid, M., Kumar, R. (2009). "Designing cut-out distance for continuous miners operations" using numerical modelling and rock mechanics instrumentation *Vis-À-Vis Rock Mass Characterization, Short Term Course on*

Table 3. Strata Support Design – NCPH mine of S.E.C.L.

TYPE A	
Roof bolt material	Tor-steel (IS: 1570/IS: 226-1975)
Yield load/Capacity (tonnes)	19
Bolt type	Fully grouted forged-head resin rebar
Resin capsule	24 x600mm /GT 100S resin or equivalent
Length (m)	1.5
Bolts per row	4.00
Rib-to-rib-side bolt spacing (m)	0.75
Bolt-to-bolt spacing (m)	1.50
Row spacing	1.50
Plate	MS- IS: 226-1975 SZ 150mmTH:6mm
Screen	Not required
TYPE B	
Roof bolt material	Tor-steel (IS: 1786-1985/IS: 226-1975)
Yield load/Capacity (tonnes)	24
Bolt type	Mechanical roof bolt w/ hardened steel dome washer plate
Resin capsule	24 x 600mm /GT 50S resin or equivalent
Length (m)	1.8
Bolts per row	4.00
Rib-to-rib-side bolt spacing (m)	0.75
Bolt-to-bolt spacing (m)	1.50
Row spacing	1.50
Plate	MS- IS: 226-1975 SZ 150mmTH:8mm
Screen	Not required
Table 3(a):Supplemental support: Faulted/Geological Structure Controlled Ground	
Passive support	Cable bolt or rope stitching for deeper suspension
No.9 Gauge wire mesh	Roof sagginess control
Posts	Roof span reduction/support

Strata Control Techniques and Instrumentation for Coal Mines. November 19-22, 2009, Department of Mining Engineering, National Institute of Technology, Rourkela-8, India.

Singh, S. K., Singh, Gopal, Jayanthu, S. (2009). "Strata control problem in S.E.C.L. for mass exploitation of underground coal deposits." In: *Proc. of Geomintech Symposium on New Equipment New Technology and Safety in Mines and Mineral Based Industries*. May 11-12, 2009. Bhubaneswar, India. Pp62-66.

Singh, S. K., Jayanthu, S. (2009). "Mass exploitation of underground coal deposits vis-à-vis strata control." In: *Proceedings of* 21st *National convention of Mining Engineers and National Seminar on Technological Advancements in Mining Industry*. December 4-6, 2009. Pp195-201.

Singh, S. K., Jayanthu, S., Biswal, M.K. (2010). "Mine safety vis-à-vis geotechnical investigations for strata control in coal mines." In: *Proceedings of ISRM National Workshop on Rock Mechanics Tools and Techniques*. January 15-17, 2010. International Society for Rock Mechanics (India) and Central Board of Irrigation and Power, in association with Central Institute of Mining and Fuel Research, eds. Regional Centre, Nagpur (Maharashtra), India.

Singh, S. K., Jayanthu, S. (2010). "Strata control technology of continuous miners for mass exploitation of underground coal deposits: A review of Indian context." In: *Proceedings of National Seminar Mine Tech '10 Mining Technology-Extraction Beneficiation for Safe and Sustainable Development*. May 7-8, 2010. . Bhubaneswar, Orissa, India. Pp62-68.

Singh, S. K., Jayanthu, S. (2010). "Implication of continuous miners in room and pillar mining for mass exploitation of underground coal deposits: An overview." In: *Proceedings of National Conference on Underground Coal Mining-Challenges and Opportunities*. September 24-26, 2010. Kolkata, India.

Singh, S. K., Jayanthu, S. (2011). "Strata control technology vis-à-vis mine safety." In: *Proceedings of National Seminar cum Workshop on Environment and Sustainable Development in Mineral Industry and Solid Waste Management*. March 14-15, 2011. Department of Geology, Andhra University Vishapatnam-530003, eds. Andhra Pradesh, India.

Singh, S. K., Jayanthu, S. (2011). "Implication of continuous miners in room and pillar mining for mass exploitation of underground coal deposits: An overview." *Journal of Mines Metals & Fuels*. Publisher Books & Journals Private Ltd., 6/2, Madan Street (3rd Floor), Kolkata-700072, India, Special Issue on Underground Coal Mining in India-Challenges and Opportunities, March-April 2011, ISSN0022-2755., Pp83-95.

Singh, S. K., Jayanthu, S. (2011). "Ground control technology for mass exploitation of coal deposits with continuous miners: A review of the Indian scenario." In: *Proceedings of the 30th International Conference on Ground Control in Mining (ICGCM),* July 26-28, 2011. Department of Mining Engineering, College of Engineering and Mineral Resources, West Virginia University, eds. Morgantown, West Virginia, U.S.A.

Singh, Sanjay Kumar, M.Tech. (Res), Dissertation Work (Unpublished), National Institute of Technology, Rourkela, India

Van der Merwe, Jacob Nielen. (1998). "Practical coal mining strata control. A guide for managers and supervisors at all levels." Publisher Sasol (PO Box 5486, Second Edition, Jonesburg, South Africa).

APPENDIX-I

Extensometer Reading

Date: 29.08.2009 Shift: I st High: 412 Hz = 1 mm

Low: 262 Hz = 1mm

	Location	Chh	Band	Base Read Htz.	Prev. Read Htz.	Current Reading In Htzs.				Change in Reading Htzs.				Final Reading (mm)				Head Posit. (m)	
						9.15 A.M.	10.30 A.M.	12.15 P.M.	1.30 A.N.	1	2	3	4	1	2	3	4	St.	Hz.
						1	2	3	4										
Goaf	6E/14-15 N	1	L	87870	GOAF EDGE														
			H	141560															
		2	L	87890															
+	3E/15N	3	L	88180		88170	88170	88170	88170	10	10	10	10	0mm	0mm	0mm	0mm		
			H	140930		141000	141000	141000	141000	70	70	70	70	0mm	0mm	0mm	0mm		
		4	L	87430		87420	87420	87420	87420	10	10	10	10	0mm	0mm	0mm	0mm		
Goaf	3E/16N			Goaf edge	GOAF EDGE														
	2E/17N																		
	4E/15N	9	L	87320															
			H	140130															
		10	L	87780															
	5E/14N	13	L	87270															
			H	140460															
		14	L	90910															
	6E/14N	15	L	87860															
			H	141150															
		16	L	87660															
+	14N/4E-3E	17	L	87720		87860	87860	87860	87860	140	140	140	140	0.5mm	0.5mm	0.5mm	0.5mm		
			H	140530		14190	14190	14190	14190	660	660	660	660	1.6mm	1.6mm	1.6mm	1.6mm		
		18	L	87210		87420	87420	87420	87420	210	210	210	210	0.8mm	0.8mm	0.8mm	0.8mm		
Goaf	5E/15N	23	L	87740		GOAF EDGE													
			H	140260															
		24	L	87490															
			H	140570															

Modal Testing and Dynamic Finite Element Analysis of a Roof Bolter's Drilling Boom

Youzhen Zhang, Associate Research Fellow
Zhijun Shi, Researcher
Jianming Zhang, Associate Research Fellow
Drilling Technique and Equipment Research and Invention Center
Xi'an Research Institute of China Coal Technology & Engineering Group Corp
Xi'an, China

ABSTRACT

The drilling boom is the key component of a roof bolter, and it has significant impact on the performance, safety, and reliability of the overall working device. In this paper, the experimental modal parameters of a drilling boom at low frequencies are identified with the Laplace wavelet correlation filtering method. Based on the obtained experimental parameters, a finite element model of the drilling boom is revised using an optimization algorithm to improve its accuracy. The dynamics of the drilling boom are analyzed through its modal and harmonic response. As a result, an improvement for the drilling boom is proposed to fix the weak links and enhance the dynamic performance.

INTRODUCTION

Bolt support is the most economic and effective supporting method in coal mines. It represents the main development trend of coal mine roadway support technology. To improve the current underground support condition in Chinese coal mines, the twin-boom and narrow-bodied, crawler type roof bolter has been developed recently. The drill is the key component of a roof bolter, and it has significant impact on the performance, safety, and reliability of the overall device. The stress state of the drill in a work process is very complicated; therefore, improved structural dynamic characteristics in the roof bolter can not only ensure safe and reliable bolting operation, but also reduce the vibration, noise, and support safer working conditions for the driller. This paper is targeting to improve the reliability and stability of the drilling boom of the newly developed roof bolter based on structural dynamic analysis.

IDENTIFICATION OF MODAL PARAMETERS

The natural frequency of structures can be easily measured, has high anti-noise ability and lower statistical alterability. Therefore, the natural frequency is always measured and analyzed in engineering practice (Wang and He, 2007). Modal parameters are previously extracted based on the double channel Fast Fourier Transform (FFT) method and least square method. It is difficult to extract modal frequency and damping results accurately (Dong et al., 2009; Huang et al., 1998; Freudinger, Lind, and Brenner, 1998). In this paper, Laplace wavelet is used to extract modal parameters by searching for the time, oscillation frequency, and damping ratio of unilateral wave attenuation. Laplace wavelet has very high accuracy in extract the modal parameters such as natural frequency and damping ratio, which serves as the basis for the modal analysis of the drilling boom.

Figure 1 shows the test system, which is composed of a drill, acceleration sensors, and the Sony EX data acquisition instrument. In this experiment, a shock hammer is used to provide the impulse excitation, and the test flow can be found in Figure 2. The energy of vibration and the frequency width are determined by the operator's strength and the hammer's weight, hardness, etc. The input force is close to the Dirac pulse, which means that the striking time is near to zero, while the impulse is 1. The unitized sampling frequency is 200 Hz.

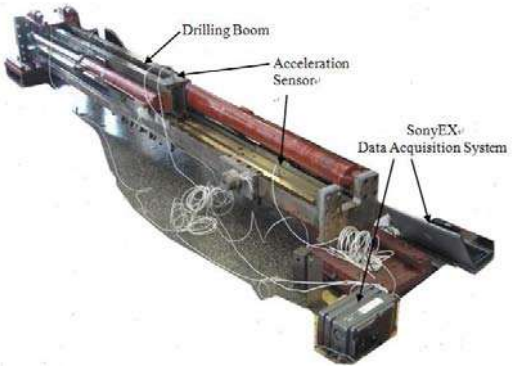

Figure 1. Modal test system of the drill.

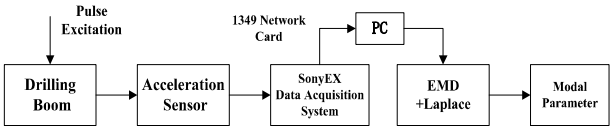

Figure 2. Modal test flow of the drill.

The time domain waveform and frequency spectrum of the measured impulse response signal can be seen in Figure 3. The three obvious peaks of the impulse response signal indicate the first three natural frequencies of the drill, respectively. Meanwhile, the high precision modal parameters extraction method is used to accurately extract modal parameters of a measured signal.

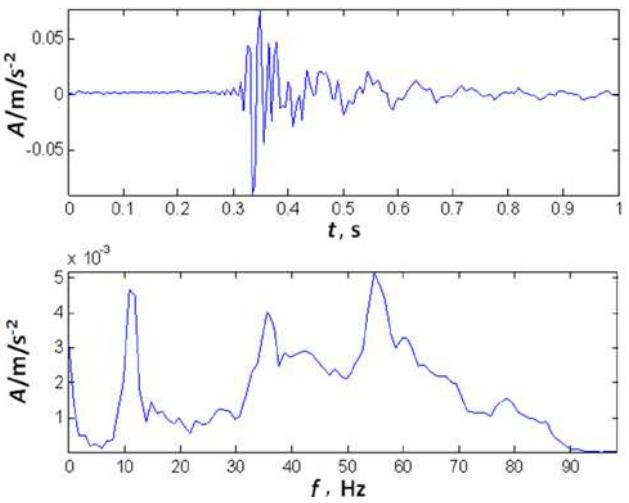

Figure 3. Impulse response signal.

The Empirical Mode Decomposition (EMD) in combination of the Laplace method is adopted in this paper for the modal analysis. First of all, the (EMD) method is used to decompose the drill response signal. As shown in Figure 4, the response signal and decomposition results are found on the left side of the figure; $c_1(t)$ $c_2(t)$ and $c_3(t)$ indicate the first three Intrinsic Mode Functions' (IMF). The right side of the figure shows the corresponding frequency spectrum. Through the EMD method, the impulse response signal is decomposed into the first three modal response signals for ensuring the reliability of the low step, which correspond to the first three IMF.

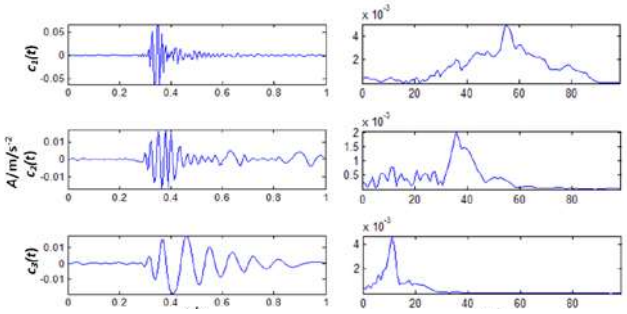

Figure 4. EMD result of impulse response signal.

Next, Laplace wavelet correlation filtering is used to filter IMF. Taking the second order modal parameters as an example, the results are shown in Figure 5. Figure 5(a) shows the second IMF signal, and Figure 5(b) shows the correlation coefficient peak $k(\tau)$ of the moment τ. Figure 5(c) and Figure 5(d) show parameters of the frequency and the damping ratio of Laplace wavelet. From the figure (b), the correlation coefficient $k(\tau)$ of the impulse response signal is near to 1, which means the error is minimized. The frequency curve and the damping ratio curve are relatively stable. This means that a similar Laplace wavelet can be found in the signal. Furthermore, the second modal parameters of f=35.4 Hz, z = 0.11 can be acquired.

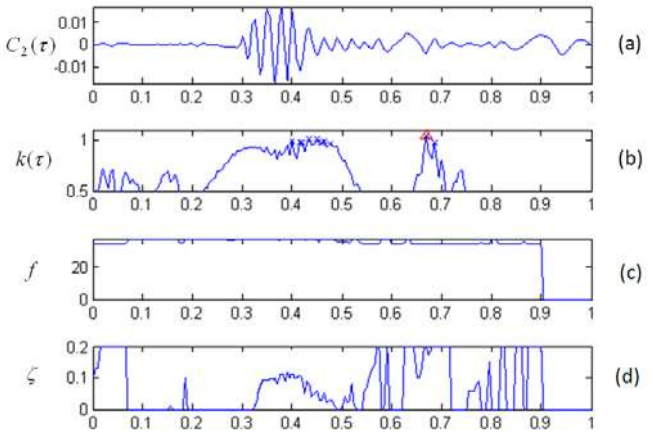

Figure 5. The second IMF signal of Laplace wavelet correlation filtering.

The first three IMF are filtered by Laplace wavelet correlation filtering. The corresponding modal parameters of the drill are shown in Table 1. In this table, f_n(n=1, 2, 3) is the natural frequency of the order n, and ζ_n= 0.11 is the corresponding damping ratio.

Table 1. Modal parameters of the drilling boom.

n	Natural Frequency Hz	Damping Ratio
1	11.53	0.13
2	35.40	0.11
3	56.60	0.04

REVISION OF FINITE ELEMENT MODEL

The accuracy of the finite element model for dynamic structures is an important issue in simulations. Compared with the corresponding actual mechanical structures, the finite element model is usually idealized through simplification. The elastic modulus of the material can be obtained through a table, and the boundary conditions are simplified, which may lead to a calculated error.

In the research of drill structural dynamics, the boundary condition is one of the vital factors. Improper simplification of the boundary condition may lead to a huge difference between the calculated frequency and the measured experimental frequency. However, the size parameters of the drill can be precisely processed and measured, and the physical parameters can be calculated through the relationship among density, mass, and volume. In order to eliminate the frequency error between calculation and

experiment, the boundary optimization algorithm is adopted to revise the finite element model.

The boundary optimization method is used to find the most suitable boundary conditions according to the practical real model. The process is shown in Figure 6.

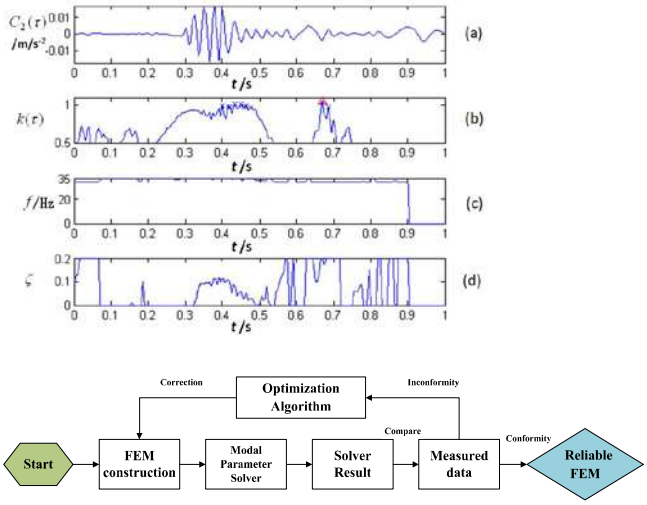

Figure 6. The finite element model revising flow chart.

In the numerical model of the drilling boom, a simplified support condition is regarded as the boundary conditions. The drilling boom's connection and support position in modal extraction experiments are different from the actual working conditions. In the numerical model, the experimental condition is considered. In the case of larger support width, it can be equivalent to more than one spring, whose support stiffness is k_b and support position is located in the support of the lug.

Three steps are adopted to revise the finite element model of the drilling boom. First, the support position is equivalent to the spring support. Second, the natural frequency of the finite element model is obtained through the numerical solution. Finally, the optimization result, which is also the optimal boundary, is obtained by the optimization algorithm whose evaluation function is the difference between the measured natural frequency and the calculated one. The function is shown in Equation 1.

$$F(k_{b1},k_{b2}\ldots;x_1,x_2\ldots)=\sum_{j=1}^{3}W_{rj}\left|\frac{f_{rj}-f_{mj}}{f_{mj}}\right| \quad (1)$$

k_{bi} is equivalent spring stiffness,

x_i is the distribution position of the spring in support plate (i=1,2…),

W_{rj} is the weight coefficient,

f_{mj}(j=1,2,3) is the measured first three natural frequencies of the drilling boom, and

f_{rj}(j=1,2,3) is the calculated first three frequencies of the finite element model.

The goal of optimization is to obtain the minimum of Equation 1.

Through the finite element method, the first three frequencies are 6.13, 20.21, and 46.9, which are different from the natural ones of the drilling boom (they are 11.5, 35.4, and 56.6). This error is caused by simplification in the model and the spring stiffness between structure and ground. With the adjustment of evaluation function and spring stiffness, the final first three frequencies are given as 11.5, 34.5, and 53.8. The fitness function is decreased from 1.09 to 0.07, and a spring stiffness is 2,000 N/mm if we use W_{rj} =1.

STRUCTURAL DYNAMICS ANALYSIS

Model Analysis

Using this more reliable finite element model, the drilling boom modal parameter has been further analyzed. The mode superposition method is adopted in this dynamic analysis, which is based on all modal parameter of the mechanical structure. A frequency extraction analysis step is defined first. Then the structure modal shape and natural frequency can be obtained with the help of ABAQUS/Standard (Zhang, Chang, and Zhang, 2008).

The first ten modals are obtained in this paper, and Figure 7 shows the first two steps of modal shape. Based on the results, the service life of the hydraulic cylinder could be reduced because the top of the second feeding cylinder and the carriage suffered high bending load in the first two step modes. It is the bending swing of the supporting anchor net cylinder and the second feeding cylinder in the third and fourth step modes that could increase the stress of the two lids of the cylinder. In the fifth and sixth step modes, the first feeding cylinder and the supporting anchor net cylinder could produce the bending deformation. In the seventh and eighth step modes, the feeding sliders and the joint between the drilling frame and the second slider could produce the wear and the bending deformation. In the last two step modes, the beams of the drilling crack exist to torsion deformation, and the column could have bending deformation, which could increase torque moment of the drilling boom.

Based on the modal shape analysis, three conclusions are obtained:

1. There are no apparent weaknesses in rigidity and mass on the drilling boom.
2. The minimum natural frequency of drilling boom is 11.5 Hz, and the excitation frequency is 10 Hz, which is less than natural frequency, so the drilling crack will not resonate.
3. The crawler-type roof bolter accepted the inner excitation pulse, which comes from the motor. The motor's rotational speed is 1,480 r/min. So the frequency is 24.67 Hz, which is less than the second natural frequency and not an integer multiple of the minimum natural frequency. Therefore, the risk of resonation is reduced.

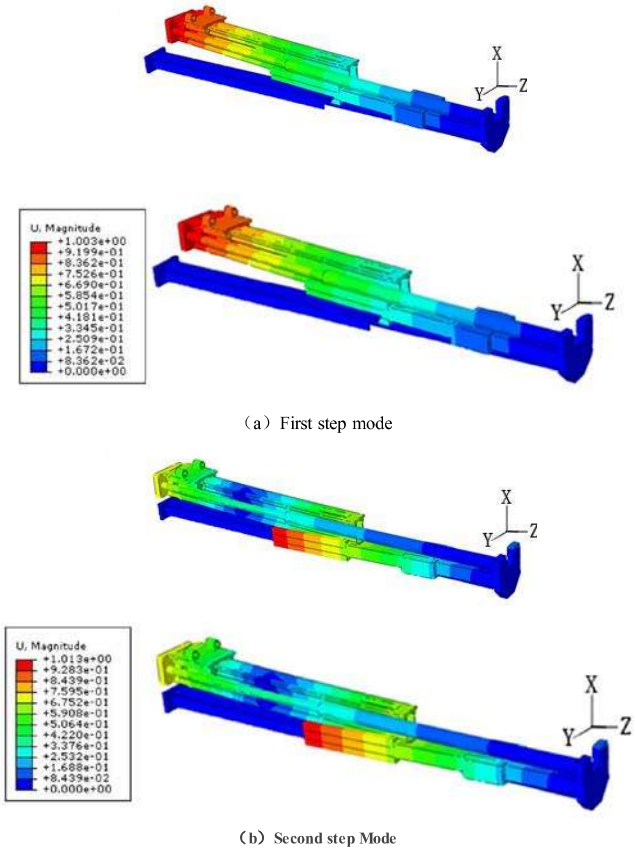

Figure 7. Modal shape.

Harmonic Response Analysis

The dynamic excitation output from the interaction between the tools and coal rock presents a significant sine periodic signal characteristics. For further analysis of dynamic characteristics of the drilling boom during forced vibration and self-excited vibration, harmonic response is studied to calculate displacement under harmonic excitation. The harmonic excitation frequency range is from 0 to 200 Hz. The harmonic response analysis result is shown in Figures 8 and 9.

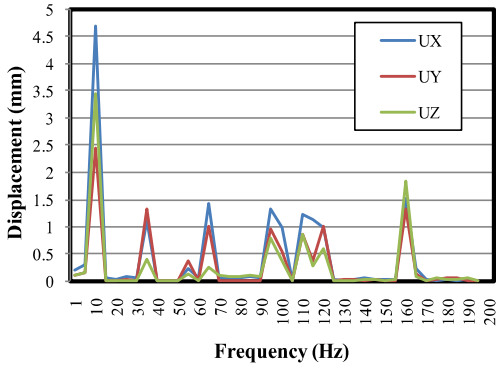

Figure 8. Curve of displacement response.

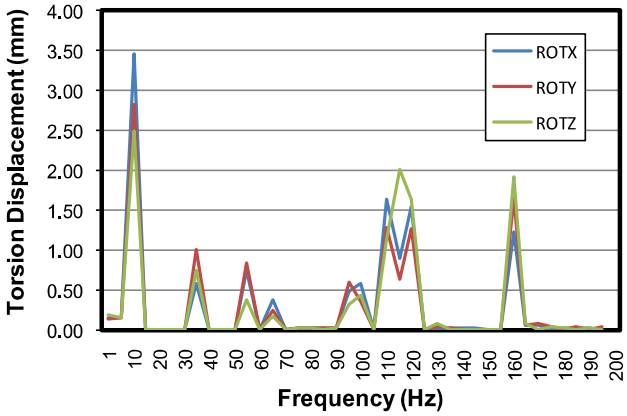

Figure 9. Curve of torsion displacement response.

As shown in Figures 7, 8, and 9, the main vibration direction of drilling boom is the X direction. The macro vibration on this direction is mainly backward and forward swing. The rotation direction around the x-axis is another main vibration direction. As shown in Figures 8 and 9, the second feeding cylinder, the supporting anchor net cylinder, and the drilling frame guider are dangerous parts that have significant vibration on the X direction. The vibration and the rotating vibration on the Z direction are the smallest. When the excitation frequency is relatively large, the vibration and rotating vibration response on the Z direction appear obviously. The vibration and rotating vibration amplitudes on the Y direction are between those on the X and Z directions.

In the structural optimization design, the natural frequency of the roof bolter is considered to avoid resonance. According to the structural dynamics simulation, the following measurements are given to enhance the structural dynamic characteristics of the drill:

1. One weakness is the joint band located between the second drilling crack and the drilling frame guider. It is obvious in dynamic response analysis. We can improve the stiffness of this band by increasing the installation pre-tightening force and improving surface processing quality.
2. The design strength and the safety factor of the second feeding cylinder and supporting anchor net cylinder were increased in order to ensure reliability of the cylinders and their connection.
3. The carriage of power head has relatively big bending vibrations, which directly affect the quality of drilling holes. Therefore, reinforcing of the plate quantity is increased to improve its rigidity.

CONCLUSION

The crawler-type roof bolter is always working in very tough environment, and the drilling boom has a very complicated stress state. In this paper, the finite element model of the drilling boom is revised through the more reliable experiment modal parameters. Using this more reliable finite element model, the dynamics of the drilling boom have been further analyzed by modal and harmonic response analysis. An improvement scheme for the drilling boom is proposed, which can fix the drilling boom's weak joints and enhance its dynamic characteristics.

ACKNOWLEDGEMENTS

This research has been supported by the Natural Science Foundation of Shaanxi Province (Grant No. 2011JM7017).

REFERENCES

Dong, H.B., Chen, X.F., Li, B., Qi, K.Y., He. Z.J. (2009). "Rotor crack detection based on high-precision modal parameter identification method and wavelet finite element model." *Mechanical Systems and Signal Processing*. *23*(3):869–883.

Freudinger, L.C., Lind, R., Brenner, M.J. (1998). "Correlation filtering of modal dynamics using the laplace wavelet." In: *Proceedings of 16th International Modal Analysis Conference*. Society for Experimental Mechanics, pp. 867-877.

Huang, N.E., Shen, Z., Long, S.R., Wu, M.C., Shih, H.H., Zheng, Q., Yen, N.C., Tung, C.C., Liu, H.H. (1998). "The empirical mode decomposition and the Hilbert spectrum for nonlinear and non-stationary time series analysis." *Proceedings of the Royal Society London A*. *454*: 903–995.

Wang, B.S., He, Z.C. (2007). "Crack detection of arch dam using statistical neural network based on the reductions of natural frequencies." *Journal of Sound and Vibration*. *302*(4–5): 1037–1047.

Zhang, Y., Chang, J., Zhang, J. (2008). "Dynamic analysis of feeding body of all hydraulic power head type drilling rig" (in Chinese). *Coal Mine Machinery*. *29*(3): 71–73.